Small molecules for modulating biological targets

Laia Miret Casals

Programa Química Orgànica
Tesi Doctoral

SMALL MOLECULES FOR MODULATING BIOLOGICAL TARGETS

Laia Miret Casals

Dirigida i revisada per:

Dr. Fernando Albericio
(Universitat de Barcelona)

Dr. Antonio Zorzano
(Universitat de Barcelona)

Barcelona, 2014

Tesi Doctoral

SMALL MOLECULES FOR MODULATING BIOLOGICAL TARGETS

Laia Miret Casals

UNIVERSITAT DE BARCELONA

INSTITUTE
FOR RESEARCH
IN BIOMEDICINE

Departament de Química Orgànica
Facultat de Química
Universitat de Barcelona
2014

Als meus avis, pares i a la meva germana

AGRAÏMENTS

Després de 6 anys i mig al laboratori, de treballar moltes hores, d'anar de bòlit, de ruptures, de mudances infinites, de que no surti res, de perdre la gent que estimes, d'excés de feina i d'arribar al final… he de dir que m'ha passat de tot i més i que m'ha encantat. Poca gent pot dir que cada dia s'aixequi amb un somriure a la cara perquè va a treballar amb una cosa que li agrada, que l'omple i a més, amb gent que estima. 5 anys entre dos laboratoris, que podríem dir que en son 4, donen per molta gent. La veritat, és que ha estat un plaer coneixeu-vos a tots, m'he fet una persona més tolerant i oberta pel fet de compartir el dia a dia amb tots vosaltres, amb gent de nacionalitats i cultures diferents! Ha estat genial! Us trobaré a faltar!

Primer de tot les gràcies més formals als capos. **Fernando** t'ho agrairé sempre que m'agafessis sabent que mai tindria beca, encara que em fessis patir al principi i pencar com una burra corregint un llibre. Em va encantar quan em vas preguntar que vols fer de gran i em vas dir que tot era possible. Tu si que saps fer somiar. Sense tu no hauria estat possible! Gràcies per ajudar-me en tot! I molta sort en la nova aventura! Per cert, el Tommaso m'ho va dir que li havies dit que m'agafaves per canyera i per pesada!

Gràcies al meu segon codirector de tesi a l'**Antonio**, per donar sempre ànims, per no veure-li mai una mala cara, per contagiar les ganes de fer ciència, per les idees, per fer-me un forat a la seva apretada agenda i per preocupar-se. Gràcies per tot Antonio!

I a l'**Eduard**, per aquesta col·laboració, per entrar-me en el món dels bacteris, per escoltar-me i atendre'm sempre. Moltes gràcies. Al final ho hem aconseguit!

I també vull donar les gràcies a la **Mercè**, que sempre m'ha obert la porta i ha tingut temps per resoldre'm tots els dubtes que he tingut i fins i tot corregir-me una part de la tesi. I al **Rodolfo**, un gran jefe, gracias por tu tiempo. I als altres dos membres del TAC, a l'**Ernesto** i al **Manuel**. Manuel, eres una joya siempre innovando y preguntando con una sonrisa.

També vull donar les gràcies a la **Mabel** i al **Pepo**, per sentir-me tan acollida al grup de Santiago només començar el projecte i per ensenyar-me tantes coses de HTS.

De la gent del laboratori, m'agradaria començar per la gent que ja no hi és. El **Tommaso** que és el primer que vaig conèixer, un gran amor d'amistat, inseparables durant 2 anys, m'he passat hores i hores amb tu al laboratori, i després de coneixents molt, enfadar-nos molt i acceptar-nos, encara que siguis un stronzo i que faci dos anys que quasi no sé res de tu, et porto al cor! I tu ja ho saps! Gràcies pel dia a dia, pels sopars, les converses, la ciència i per la teva amistat. **Carol,** eres un amor, te hecho mucho de menos y me encantaría que viviéramos más cerca!!! Que bien que nos lo hemos pasado juntas!!! Echo de menos las

cenas, el vino y las risas. Te quiero un montón!!!. L'esbojarrada que també em va fer riure molt és la **Yessi**, espero que tot et vagi molt bé guapa! I com no molta gent que ja no hi és com l'**Albert**, el **Dani Pla** (gràcies per sempre tenir temps per qualsevol dubte i tenir un cor ben gran), el **Carles** i la **Eli**.

A Santiago de Compostel·la vaig tenir l'oportunitat de conèixer la **Isa**, que em va adoptar, quin far de riure que ens vam fer. Isa que bien nos los pasamos, ¿cuándo vienes a verme?.

I començo pel meu lab, pel sector dels desperdigats, per **les tres fantàstiques**, últimament no ens separem. Al meu gran i únic amor, si fos lesbiana sortiria amb tu, quina llàstima… a la **Marta Pelay**, dios fa més de 6 anys que t'aguanto tots els dies, però tots eeehhhh… jajajaja em dures més que un nòvio! Guapa, et trobaré a faltar moltíssim, jo crec que serà difícil que t'oblidis de mi ;). Em sembla que per molt lluny que estiguem i encara que passi molt de temps sense veure'ns tu i jo ja no ens separarem mai. Petarda, gràcies per escoltar-me, per aguantar-me, per fer-me riure, i més que res i el més important per compartir el dia a dia, t'estimo moltíssim. L'altra petarda que m'ha estovat el cor és l'**Ariadna**, la meva nena, gràcies per rejovenir-me, per fer-me riure, per sentir la força i les ganes de la gent que és més jove que jo (encara que no ho sembli, jaja), per aguantar-me i per donar-me aire fresc, ho necessitava! Vagis on vagis, encara que plogui a vots i barrals tots els dies te'n sortiràs!!! Et trobaré molt a faltar guapa, ets un tresor! I per acabar amb el trio calavera, **l'Anna-Iris**, quina tia. Guapa, ets única i irrepetible, estàs com un llum, i encara que m'hagis fet enfadar mil vegades, ets irresistible i em despertes un somriure a la cara, tu sí que saps que és viure el dia a dia, no te'n perds ni una. Que bé que m'ho vaig passar a la teva tesi! La teva filosofia única, bo o dolent gaudeix però aprèn, continua amb el teu positivisme i et desitjo el millor en la teva nova aventura. Continuem per la **Judit** que ens ha aguantat a totes, quina paciència! M'ha encantat conèixer-te, gràcies per escoltar, per preocupar-te, per ajudar-me, per compartir amb tu el dia a dia (la campana ja saps que no, jajajaja) i per apretar-me en l'última etapa, tenies raó!. Tens un aguant i una força infinites. I dos collons també ;). Et trobaré a faltar, muakkk!!! I el **Peter**, que quan no t'ho esperes et diu un disbarat o t'ensenya qualsevol tonteria que t'alegra el dia, gràcies per ajudar-me en qualsevol cosa sempre que t'ho he demanat. Feu molt bona parella amb la **Miriam Royo**, que sempre t'està buscant i fotent canya, ha estat un plaer Miriam conèixer-te, gràcies per aparèixer pel lab i alegrar-nos el dia, per preocupar-te i sobretot per les últimes festes! L'**Edgar** encara s'amaga!jajajaja. Edgar sé que vindràs a la meva tesi, això ja ho tens! Muakkk.

Després tenim el **Juan**, sembla un home serio i callat, però no us deixeu enganyar, que te'n deixa anar cada una… Juan un placer todas las comidas románticas los fines de semana en los microondas jajajaja. Muchas gracias por todo, por las dudas, consultas y tiempo invertido en mi tesis. I el **Jan** que sempre fa ritmes amb el meu nom i últimament persegueix la gent perquè doni i vagi als seminaris, tot un repte! Ja m'ha tornat a enganxar. I com no la desapareguda **Rubí**, tant bella como peligrosa, la única que conozco que se casa dos veces

con la misma persona… pero esto no eras así no? jajaja Espero que te vaya genial y que no pares con tu enganche a la adrenalina, viajes, viajes y viajes… muaaaaa!;) I a les últimes adquisicions al **Markus**, you are always ready to go out ☺, a l'**Helena** i a La **Judit**, sort en aquesta etapa!.

Rodejats tenim el **Bernat**, quin futur ens espera? D'aquí a 2 anys et truco a veure que has fet! El senyor **Miguelin** que estás echo un figurín jajaja siempre me has hecho reír eres míster simpático!! **Xavi Vila**, titi estàs fet un fiesta, jo amb tu me'n vaig a la lluna!

I l'**Esther**, tants anys al laboratori i ja has marxat, set troba a faltar! Sé que has passat i estàs passant per moments difícils, et desitjo tota la fortalesa i felicitat del món perquè te l'ha mereixes. A la **Laura N**. por todos los consejos y ayudas proprcionadas, que no han sido pocas, tu vas a llegar lejos! y a la **Laura M**. que ha estat indispensable en tots els esdeveniments del laboratori, ya nos queda pocoooo!!!!!

I al lab 100, **Adriana**, **Janire**, **Xavi Just, Jesús, Kamil** sou uns catxondos, m'hauria agradat compartir més moments amb vosaltres, gràcies per està sempre disposats a ajudar. **Ximena** ahora ya no salimos a correr sino que corremos para terminar la tesis i la **Marta Paradís**, ets un sol per preocupar-te per tot.

Una de les últimes adquisicions, a part de companya de laboratori, actualment també de pis, gràcies a la **Roberta** per compartir el dia a dia amb mi i fer-me costat en aquesta època d'escriptura. Te voy a echar de menos!!!!

La veritat és que el sopar de Nadal d'aquest any va ser genial, per tots els fiesteros que vau venir al Jamboree un petó molt gran.

I sobretot a l'**Eva Poca** per tenir aquesta santa paciència amb tots nosaltres, per compaginar-ho tot, per escoltar tants problemes i per solucionar-ho! Ets imprescindible.

I després tot un altre desplegament de gent al laboratori de baix. Vull començar pel meu jefe catxondu **David Sebastián**, que mente tan perversa tienes. Gràcies per ensenyar-me i introduir-me al món de la biologia, per ajudar-me, per escoltar-me cada cop que ho he necessitat, per la tesi... Un plaer compartir la pollata i el dia a dia amb tu, ya sé que me estas echando de menos ;).

Seguint pel pasillo catxondu, he de dir que entre el **Sala** (sóc la primera que no et diu becari), l'**Edu** i el **Gonzalo** m'han aixecat l'autoestima diàriament dient-me de tot i més ;), ens hem fet un far de riure. Salaaaaa m'ha encantat conèixer-te, treballar amb tu, que m'expliquessis tot de coses interessants que no fossin ciència…et vinc a veure!!! muakkk. Noguera, ets un personatge, i quina gràcia que em fas! Al final has acabat la tesi abans que jo, quina ràbia!!!

Jajaja un dia d'aquests ho celebrem! Gonzalo, pero aún no has empezado a escribir? ;)Un placer las cenas, esquiadas y las fiestas!!! Tú sí que sabes! Nos vemos en Australia? L'**Elena**, un cul inquiet amb ganes de fer de tot. Guapíssima, m'ha encantat treballar amb tu, quin far de riure i quin munt d'hores a la poiata fins a altes hores! Merci per la companyia! muak!!! Qui més òstia la **Joana**, que posa ordre, un parell de crits i tothom tieso. I l'**Albert**, que sempre és tant simpàtic i em burxa fins a l'infinit. I l'últim que li dóna el toc de glamur amb la seva super barba, el **Nacho**. Nacho voy o vengo? A part de ser primer company de feina, després company de pis i un dels meus millors amics que te voy a decir… que te quiero mucho, que sé que soy la primera catalana en tu vida que ha marcado la diferencia y que siempre me has ayudado y entendido en todo. Muchas gracias!!!! I aquí coloco a mi excompi de piso a la **Laura**, me ha encantado vivir contigo, eres un sol, muchas gracias por todo y por formar una gran familia.

I donant una ullada pel lab tenim a la **Manu**, ets un tresor, a la **Montse**, te veo a tope, al **JP**, eres un pozo de ciencia inacabable, gracias por todo, a la **Paula**, per les últimes converses, la **Saska**, por la compañía en la campana de cultivos, y a la **Laura**, te vas o no? jajajaja, a l'**Anna** que sempre fa companyia a hores impensables, la **Maribel** , la **Natàlia,** i com no als super tècnics del laboratori, al **Jordi** i a la **Susana**, que ens fan la vida més fàcil dia a dia. A l'**Olga** que és una catxonda i cada cop que m'expliques la teva vida flipooo jajajaja, i a la **Natàlia** que al moment et troba una cita amb el gran jefe.

I també donar les gràcies als amics que no formen part de la gran família del laboratori.
A les **Nenes**, un grup d'amigues de 9 ties que són la òstia. A la **Naza** (alias el partidón) que eres más mala con este humor tan negro, como me haces reír! Y tu hermana no es adoptada! Gràcies per tenir sempre temps, sé que puc comptar amb tu!. A l'**Anna** que té un cor que no li cap al pit, per la teva comprensió i la teva paciència, però sobretot per escoltar-me i pels teus consells. A la **Maria**, la més extrovertida i esbojarrada, estàs com una cabra! Però m'encantes i encara més la teva manera de viure i veure la vida! Et veig molt feliç. A la **Sheila**, ets com un forat a la butxaca, m'arruïnes amb les factures de telèfon !!! ☹ Ya lo sabes, muchas gracias por escucharme y por comerte todos estos rollos! Ya sabes que me gusta mucho meterte caña, creo que hacemos un dúo explosivo, te quiero un montón!!!. A la meva **Dome**, la coneix-ho des d'abans de néixer… bufff n'he fet tantes amb tu, ets la meva amiga de tota la vida de veritat (la Torregassa és massa, el Papiolet no n'hi ha ni un de dret i les Cometes al poder, tot això és difícil d'entendre). Espero que volis alt i lluny i ben aviat. La **Cristina**, la cañera, tú las matas todas callando, que flecha estas hecha! Tu pots amb tot, o sigui que aixecat! I després tenim l'**Àngels**, la princeseta juerguista, lluitadora del dia a dia, carinyu vindran temps millors!!!! i l'**Alba**, encara ens recordo al provador del Zara, aquell dia va començar tot, passant per tots els descobriments de l'adolescència i fins avui. Per moments inoblidables com el cap de setmana a Manchester, Eivissa, a Cervera, St Adrian, a Lisboa (x l'Anna), els carnavals, despedides i casaments, els aniversaris, pels somriure i pels plors i sobretot per les amigues invisibles. La veritat és que no acabaria mai... gràcies per ser-

hi sempre, perquè sé que puc comptar amb vosaltres pel que faci falta, per formar part de la meva vida i perquè sé que m'accepteu tal com sóc. Per cert, la meva planta s'ha convertit en la selva de l'Amazones! Us he guanyat! PER SEMPRE NENES!!!!

Després a les meves dues feres particulars que bé que m'ho he passat amb vosaltres, això ha estat inoblidable. La meva **Pentinat**, mira que fa anys que ens coneixem, primer treballant juntes a la Robert Bosch buff fa molt de temps, i després anys i panys sense perdre el contacte. Això és perquè tenim un feeling especial, els millors moments els he passat amb tu, Pamplona, Málaga, Tailàndia, festes, sopars, carnavals… quin far de riure! T'estimo moltíssim. I a l'**Oscar** no li guardo rancor perquè t'hagi robat el cor ☺. A l'altra indomable, a la **Gemma**, quina juerguista estàs feta! Amb tu sí que les hem fet grosses, per tants Benasques i fars de riure, aquella festa a Lisboa, esquiades, Azores, ferrades, barrancs, helicòpters que et vénen a rescatar, caigudes i ressaques infinites… gràcies per donar-me l'adrenalina que necessito !!! Com era allò… les fieres de la muntanya!!! De dia muntanyeres i de nit super fiesteres!!!!

Passant pel sector de la Universitat l'**Anna** i l'**Eva**. M'estic posant melancòlica, quin munt d'anys noies que vam passar juntes. Clar, com que no aprovàvem res, quin percal. I tots els semestres, que sí que aquest és el bo, aquest estudiarem… voluntat 0! I qui ho havia de dir que les tres faríem el doctorat... Anna, tu i jo no ens podem ajuntar que perdem el seny i la vergonya entre el Plataforma i la Boite! Sort que en tenim de l'Eva, que és el nostre equilibri! Que bé que m'ho he passat amb vosaltres! Dos dels meus pilars, gràcies per ser-hi sempre, pels viatges, per les sortides, per escoltar, per animar, per passar-les totes juntes! Us estimo moltíssim! I l'**Alba N** excompanya de pis i de la uni, que ve que ens ho vam passar aquell any amb la **Georgina**, un festival! Ho trobo a faltar! I el **David P**, un gran amic, que sempre té temps per mi, el nostre racó la plaça d'osca, ara el carrer de Blai. Gràcies per tantes trobades i converses, pels consells i per saber escoltar, ets un sol! I al **Marc T**, ets un catxondu, m'encanta trobar-te inesperadament, al **Luca**, dai Luca forza che anche per te il traguardo è ormai vicino, i al **Michel**, gràcies perquè sé que sempre puc comptar amb tu. **Jaume Nin** ets un figurin!!!Quin munt que n'hem fet plegats!

I el meu millor amic el **Toni**, més que amics germans. No m'imagino la meva vida sense tu. Company de filosofades infinites, que em salva el cul cada cop que ho necessito, per aguantar-me, per fer-me riure, per entendre'm tan bé, per fotrens unes festes de bojos, que bé que m'ho vaig passar al Primavera, no espero menys del Tomorrowland i per ser la polla amb vinagre. Ja saps que encara que no t'ho digui mai perquè ets més fred que una pedra t'estimo molt.

També li vull donar les gràcies al **Jordi**, 12 anys junts, un dels pilars de la meva vida, sempre m'has ajudat, a l'institut, a la carrera, al màster, al doctorat, aquesta tesi també és teva. Moltes gràcies per tot i tu ho saps.

I a l'**Osmy**, ha estat curt o no, però molt intens, gràcies per fer-me sentir el que he sentit, no sabia que es podia sentir tant.

I per últim al més important, als que facis el que facis sempre hi son, als incondicionals i als més estimats. A la meva família. Primer de tot a la meva mare, la **Lourdes**, per ser tan entregada, per tenir-ho sempre tot a punt, per comprar-me tot el que necessito i més, per preocupar-se per tot i per ara ser el pilar i fer que ens reunim tots. Al meu pare, el **Josep**, que té una passió infinita pels cavalls que són la seva vida, per les sortides que fem a cavall que són els nostres moments i per la forma que té de pendres la vida. Papes us estimo, gràcies per fer-me com sóc, aquesta fortalesa no ha vingut sola. I a la meva germana, la **Cristina**, bufff la persona que estimo més en aquest món. Per ser com ets, perquè encara que siguis la petita ets la que té més seny, m'encanta la relació que tenim, perquè sempre m'has ajudat i fet costat en tot, i perquè només amb tu aniria a la fi del món. A part del dia a dia mai oblidaré el viatge a Alemanya i a la Índia, quin munt d'aventures, d'anècdotes i confessions. Només desitjo que continuïs igual de feliç que ara, que sé que ho ets i amb la persona que tens el costat. **Cristina P**, per ser la teva cunyada, no et pots queixar que hauria pogut estar pitjor ;P! M'encanta el teu humor negra, gràcies per donar-me un cable i per fer feliç a qui tu ja saps, muaaaa! Osti i el **muxu** que me'l deixava. I també als "tiets", que comparteixen tots els diumenges amb nosaltres. Gràcies al **David**, que a part de ser tiet ha fet de pare i d'amic, i de company de pis, per preocupar-te encara que et digui pesat, pels consells i per sempre ser-hi quan ho he necessitat. I el **Xavi** el banyolí, per donar aquest toc d'alegria, ja saps que em caus genial! I als avis, els que hi són i els que no. A la iaia **Maria** per ser una dona amb les idees tan clares i tan pràctiques, política hauries tingut de ser, amb el gran que ets i no t'estranyes de res. Em pensava que hi series a la tesi, haguessis estat orgullosa iaia. A l'avi **Josep** que ens va deixar ja fa temps, sempre li semblava tot bé, i el recordo sempre feliç i content. A l'avi de Papiolet, al **Joan**, que t'han fet besavi per segona vegada, quin far que t'has fet de treballar (i a mi tbé plantant enciams) i quines ganes de riure que tens ara, tu sempre em dius: mira com riu... que feliç que és, però jo a tu també t'hi veig. I a la iaia **Carmeta**, que ens va deixar fa un any i mig. Més que una iaia també va ser una mare, no saps el que et trobo a faltar, les rialles, els enfados, veure't ballar al mig del menjador, els dinars... tot.

I als tiets i tietes **Xavi**, **Silvia** i **Montse** i als cosins i cosines directes o polítics **Jordi**, **Meritxell**, **Marc**, **Sara**, **Ester** i **Edu**, i als dos petits de la família al **Biel** i al **Quim**. Per les festes i dinars compartits i per estar units.

CONTENTS

CONTENTS

ABBREVIATIONS AND ANNEXES **I-XI**
Annex I. Abbreviations and acronyms I
Annex II. Glossary VIII
Annex III. Natural amino acids X
Annex IV. Coupling reagents XI

CHAPTER 1 - Synthesis of an *N*-hydroxylamine-based library of potential Drugs for the treatment of Respiratory Infectious Diseases (RID)

Abstract **3**

Introduction **7**

1. General introduction 9
    1.1. Antibiotic Resistance Bacteria 10

2. Ribonucleotide Reductase (RNR) system 12

3. Pathogenic bacteria 16
    3.1. Bacteria phenotype: Biofilm formation 16
    3.2. Bacterial types 17
        3.2.1. Pseudomonas aeruginosa 17
        3.2.2. Burkholderia cenocepacia 18
        3.2.3. Staphylococcus aureus 18
        3.2.4. Bacillus anthracis 19

4. Respiratory infections 21
    4.1. Upper and lower respiratory tract infections 21
        4.1.1. Pneumonia 22
    4.2. Opportunistic biofilm infections 23
        4.2.1. Asthma 23
        4.2.2. Chronic Obstructive Pulmonary Disease 23
        4.2.3. Bronchiectasis 24
        4.2.4. Chronic Granulomatous Disease 25
        4.2.5. Cystic Fibrosis 26

References **28**

Objectives **33**

Results and discussion **37**

1. Synthesis of hydroxamic acid derivatives in solid phase 39
1.1. Synthesis of a small library of hydroxamic acid derivatives 41

2. Synthesis of *N*-alkylhydroxylamines 42
2.1. Oxidation of primary amines to *N*-alkylhydroxylamines 42
2.1.1. Catalytic oxidation using urea hydrogen peroxide complex and sodium tungstate 42
2.1.2. Oxidation using oxone 43
2.1.3. Oxidation using benzoyl peroxide 46
2.1.3.1. Synthesis and optimization of *O*-acyl-*N*-alkylhydroxylamine intermediates 49
2.1.3.2 Hydrolysis of the *O*-acyl-*N*-alkylhydroxylamines 51
2.2. Reductive amination of aldehydes to *N*-alkylhydroxylamines 54
2.2.1 Synthesis of *N*-alkylhydroxylamine library 55

3. Compounds activity 58
3.1. Evaluation of the Minimum inhibitory concentration (MIC) 58
3.1.1. Hydroxamic acid derivatives 58
3.1.2. *N*-Hydroxylamine, secondary hydroxylamine, oxime and amide compounds 59
3.2 Evaluation of capacity to inhibit the formation of bacterial biofilms 60
3.3. Evaluation of capacity to reduce already formed bacterial biofilms 62
3.4. Evaluation of cytotoxicity 65

References **67**

Conclusions **69**

Materials and methods of chapter 1 **73**

1. Solvents and reagents 75
1.1. Solvents 75

1.2. Reagents 75

2. Instrumentation 75
2.1. General basic instrumentation 75
2.2. Chromatographic methods 76
2.2.1. Thin layer chromatography (TLC) 76
2.2.2. Flash chromatography 76
2.2.3. Analytical High-performance liquid chromatography photodiode array (HPLC-PDA) 76
2.2.4. Semi-preparative HPLC 76
2.3. High-Performance Liquid Chromatography-Mass Spectometry (HPLC-MS) 77
2.4. Nuclear Magnetic Resonance (NMR) 77

3. Solid phase methodology for the synthesis of hydroxamic acids 78
3.1. General considerations 78
3.2. Colorimetric test 78
3.2.1. Kaiser test 78
3.3. Conditioning of the resin 79
3.4. Incorporation of the *N*-Fmoc-hydroxylamine linker 79
3.5. Elimination of the Fmoc group 79
3.6. Determination of the resin loading by quantification of the Fmoc group 79
3.7. Incorporation of the first amino acid 80
3.8. Acetylation of *N*-terminal function 80
3.9. Mini-cleavage and HPLC/HPLC-MS analysis 81
3.10. Cleavage of the molecule from the resin 81
3.11. Hydroxamic acids purification and characterization 81

4. Hydroxamic acids compounds 82
4.1. Syntheses of hydroxamic acid compounds 82
4.2. Hydroxamic acids characterization 82

5. Oxidation of primary alkyl amines to *N*-alkylhydroxylamines 85
5.1. By Catalytic Oxidation with Hydrogen Peroxide 85
5.2. Using Oxone 85
5.2.1. Standard Procedure with Solvent 85
5.2.2. Standard Solvent-Free Procedure 86
5.2.3. Biphasic Procedure 86
5.3. Using Dibenzoyl Peroxide 86
5.4. *O*-acyl-*N*-alkylhydroxylamine intermediate products 87
5.5. Hydrolysis of the *O*-acyl-*N*-alkylhydroxylamines 87
5.6. *N*-benzoylated-*N*-alkylamine products 88

6. Synthesis of *N*-alkylhydroxylamines by reductive amination 89
6.1. Characteritzation of *N*-alkylhydroxylamines 89

7. Bacterial cell lines used to test the activity of the compounds 93

References **94**

CHAPTER 2- Phenotype screening identifies a new regulatory pathway linking pyrimidine biosynthesis, p53 and mitochondrial morphology

Abstract **99**

Introduction **103**

1. Mitochondrion 105
1.1. Mitochondrial dynamics 106
1.1.1. Mitochondrial fusion 107
1.1.2. Mitochondrial fission 109
1.1.3. Functional impact of mitochondrial dynamics 111
1.1.4. Mitochondrial dynamic proteins involved in metabolic disease 112
1.2. Mitochondrial bioenergetics 113

2. Pyrimidine synthesis is linked to electron transport chain 116

3. p53 pathway is linked to mitochondrial function and pyrimidine biosynthesis 121

4. Development of cell-based reporter assays for screening modulators of gene promoters 123
4.1. Generation of promoter-reporter gene constructs 124
4.1.1. Choice of the promoter 124
4.1.2. Choice of the reporter 124
4.2. Generation and validation of the cellular model 126
4.3. Optimization and miniaturization of conditions for cell-based reporter assays in HTS 127
4.4. Validation of HTS screening 129

References **131**

Objectives 139

Results and discussion 143

1. Generation of several human cell clones that stably expresses luciferase under the control of 2 Kb Mfn2 promoter 145

2. Screening and identification of compounds with capacity to enhance Mfn2 promoter activity 148
2.1. Miniaturization assay 148
2.1.1. Luciferase activity 148
2.1.2. Signal/Noise ratio 149
2.1.3. Data dispersion 149
2.2. High Throughput Screening using Prestwick library 150
2.3. Secondary screening to detect false positives 152

3. Selection of activators of Mfn2 expression 154
3.1. Results in HeLa cells expressing luciferase under the control of Mfn2 promoter 154
3.1.1. Hits confirmation in HeLa cells overexpressing Mfn2 promoter 154
3.1.2. Dose Response curves in HeLa cells that stably express luciferase under the control of Mfn2 promoter 155
3.1.3. Confirmation of selected hits in HeLa cells overexpressing Mfn2 promoter using the optimized concentration 156
3.2. Validation of the activators of the Mfn2 promoter at gene and protein level in HeLa and C2C12 cells 157
3.2.1. Mfn2 gene expression 157
3.2.1.1. Mfn2 gene expression in HeLa cells 157
3.2.1.2. Mfn2 gene expression in C2C12 cells 158
3.2.2. Mfn2 protein expression 159

4. Validation of leflunomide as an activator of Mfn2 expression 160
4.1. Optimal conditions of Leflunomide 160
4.1.1. Dose response study measuring Mfn2 mRNA levels in HeLa cells 160
4.1.2. Time course measuring Mfn2 mRNA levels in HeLa cells 161
4.1.3. Validation of leflunomide in HeLa cells 161
4.2. Validation of Teriflunomide in HeLa cells 162
4.2.1. Transcriptional activity 162
4.2.2. Dose response curve measuring Mfn2 mRNA levels in HeLa cells 163
4.2.3. Time course in HeLa cells 164
4.3. Validation of leflunomide in C2C12 cells 164

4.3.1. Mfn2 protein expression in C2C12 cells 164

5. Leflunomide as specific inhibitor of dihydroorotate dehydrogenase 166
5.1. Assays of cell proliferation in HeLa and C2C12 cells 166
5.1.1. Antiproliferative effects of leflunomide and teriflunomide in HeLa cells 166
5.1.2. Antiproliferative effects of leflunomide in C2C12 cells 168
5.1.3. Uridine reverses Mfn2 mRNA expression in HeLa cells incubated with leflunomide and teriflunomide 169

6. Leflunomide modulates other mitochondrial proteins involved in mitochondrial dynamics 171
6.1. Effects of leflunomide and teriflunomide in Mfn1, OPA1 and Drp1 mRNA levels in HeLa cells 171
6.2. Ellects of leflunomide in Mfn1, OPA1, Drp1, Fis1 and porin protein levels in HeLa and C2C12 cells 172
6.3. Uridine reverses Mfn2 and Mfn1 protein expression in C2C12 cells incubated with leflunomide 173
6.4. Mitochondrial morphology in HeLa and C2C12 cells 174

7. Leflunomide affects mitochondrial function in C2C12 cells 176
7.1. Mitochondrial membrane potential in C2C12 cells 176
7.2. Oxygen consumption in C2C12 cells 176

8. Leflunomide promotes mitochondrial elongation in MEF wt, MEF Mfn2$^{-/-}$ and MEF Mfn1$^{-/-}$ cells 179
8.1. Effects of leflunomide in Mfn2, Mfn1, OPA1, Drp1, Fis1 and porin proteins levels 179
8.2. Mitochondrial morphology in MEF wt, MEF Mfn2$^{-/-}$ and MEF Mfn1$^{-/-}$ cells 181
8.3. Assays of cell proliferation in MEF wt, MEF Mfn2$^{-/-}$ and MEF Mfn1$^{-/-}$ cells 183
8.3.1. Antiproliferative effect of leflunomide in MEFwt cells 183
8.3.2. Antiproliferative effect of leflunomide in MEF Mfn2$^{-/-}$ cells 184
8.3.3. Antiproliferative effect of leflunomide in MEF Mfn1$^{-/-}$ cells 185
8.3.4. Global comparison of antiproliferative effects of leflunomide in MEFwt, MEF Mfn2$^{-/-}$ and MEF Mfn1$^{-/-}$ cells 186

9. Leflunomide affects mitochondrial function in MEF wt, MEF Mfn2$^{-/-}$ and MEF Mfn1$^{-/-}$ cells 188

9.1. Mitochondrial membrane potential in MEF wt, MEF Mfn2$^{-/-}$ and MEF Mfn1$^{-/-}$ cells 188
9.2. Oxygen consumption in MEF wt, MEF Mfn2$^{-/-}$ and MEF Mfn1$^{-/-}$ cells 189

10. Specific inhibitors of complex III inhibit pyrimidine synthesis and increase Mfn2 expression 192
10.1. Dose Response and time course study on the effects of myxothiazol and antimycin A 193
10.2. Validation of myxothiazol and antimycin A in HeLa and C2C12 cells 194
10.3 Assays of cell proliferation in C2C12 cells 196
10.4. External uridine reverses Mfn2 mRNA levels in HeLa cells incubated with specific inhibitors of complex III 197
10.5. Myxothiazol and antimycin A effects in Mfn1, OPA1, and Drp1 proteins in HeLa cells 198
10.6. Myxothiazol and antimycin A effects in Mfn1, OPA1, Drp1 and porin proteins in HeLa cells 199
10.7. Mitochondrial morphology in HeLa cells 201
10.8. Myxothiazol effects in Mfn1, OPA1, Drp1 and porin proteins in C2C12 cells 202
10.9. Mitochondrial morphology in C2C12 cells 203
10.10. Myxothiazol effects in MEFwt cells 204
10.11. Mitochondrial morphology in MEFwt cells 205

11. p53 activation is triggered by inhibition of pyrimidine synthesis in response to leflunomide 206
11.1. Leflunomide and teriflunomide induce p53 expression 207
11.1.1. Leflunomide and teriflunomide induce p53 expression in HeLa cells 207
11.1.1.1. p53 mRNA levels of HeLa cells incubated with leflunomide and teriflunomide ± uridine 207
11.1.1.2. p53 protein levels in HeLa cells incubated with leflunomide 208
11.1.2. Leflunomide induces p53 expression in C2C12 cells 208
11.1.3. Leflunomide induces p53 expression in MEFwt, MEF Mfn2$^{-/-}$ and MEF Mfn1$^{-/-}$ cells 209
11.2. Myxothiazol induces p53 expression 210
11.2.1 Myxothiazol induces p53 expression in HeLa cells 210
12.2.1.1. p53 mRNA levels of HeLa cells incubated with myxothiazol ± uridine 210
12.2.1.2. p53 protein levels in HeLa cells incubated with myxothiazol 211

11.2.2. Myxothiazol induces p53 expression in C2C12 cells 212

12. Leflunomide and myxothiazol activates p53 through phosphorylation of Ser15 213
12.1. p53 protein is activated through phosphorylation of Ser15 by leflunomide and myxothiazol in HeLa cells 213
12.2. p53 protein is activated through phosphorylation of Ser15 by leflunomide and myxothiazol in C2C12 cells 214

13. Pyrimdine biosynthesis links mitochondrial elongation to the p53 pathway 217
13.1. U87MG and T98G human glioma cell lines 217
13.2. p53 overexpression in HeLa cells 218
13.3. Effect of p53 gene silencing in HeLa cells 219
13.4. Effect of p53 gene silencing in C2C12 cells 221

References 223

Discussion 225

1. Identification of a positive modulator of Mfn2 expression 227

2. Leflunomide promotes mitochondrial elongation 228

3. Leflunomide links pyrimidine synthesis and mitochondrial morphology 230

4. Mechanism of action of complex III inhibitors 231

5. Leflunomide and myxothiazol promotes mitochondrial elongation through p53 activation 235

References 239

Conclusions 245

Materials and methods of chapter 2 247

1. Instrumentation 249
1.1. General basic instrumentation 249

2. Cell Culture 249
2.1. Cell lines 250
2.1.1. HeLa cells 250
2.1.2. HeLa M2P clones 250
2.1.3. HeLa cells expressing mtDsRed 250
2.1.4. C2C12 cells 251
2.1.5. C2C12 cells expressing mtDsRed 251
2.1.6. MEFs, Mfn1 KO and Mfn2 KO MEFs cells 251
2.1.7. MEFs, Mfn1 KO and Mfn2 KO MEFs cells expressing mtDsRed 251
2.1.8. U87MG and T98G myoblastoma cell lines 251
2.2. Culture media 252
2.3. Maintenance and subculture 252
2.4. Freezing and defrosting 253
2.5. Cell counting 255
2.6. Mycoplasma test 256
2.7. Cell decontamination 256
2.8. Number of cells for each experiment 257

3. Cell treatments 258
3.1. Transient transfection 258
3.1.1. Definition of N/P ratio 259
3.2. Determination of transfection efficiency by FACS 260
3.3. Stable transfection 260
3.4. siRNA transfection 262
3.5. Cells incubated with chemical compounds 265

4. DNA protocols 266
4.1. General considerations 266
4.2. Firefly Luciferase Reporter Vectors 267
4.3. Bacterial transformation by heat shock and plasmid purification 268
4.4. Cloning of DNA 269
4.5. Agarose gel and electrophoresis 270
4.6. Isolating DNA fragments 270
4.7. Ligation 271

5. RNA protocols 272
5.1. General considerations 272
5.2. RNA purification 272
5.3. RNA quantification 274
5.4. Reverse transcription polymerase chain reaction (RT-PCR) 274
5.5. Quantitative Polymerase Chain Reaction (qPCR) 276

5.5.1. Basis of the qPCR and quantification 276
5.5.2. Quantitative real time PCR assays formats 278
5.5.3. Syber Green qPCR 279
5.5.4. qPCR protocol for SYBR Green 280
5.5.5. qPCR protocol for Taqman 280
5.5.6. Housekeeping genes and negative controls 280
5.5.7. qPCR Quantification 281

6. Transcriptional activity protocol 282

7. Protein protocols 284
7.1. Total protein cell extracts 284
7.2. Protein assays and quantification 284
7.3. Western Blot assay 285
7.3.1. Electrophoresis procedure 285
7.3.1.1. Gel preparation and polymerization 286
7.3.1.2. Protein samples preparation 287
7.3.1.3. Gel electrophoresis 287
7.3.2. Transfer 287
7.3.3. Immunodetection of the target protein 288
7.4. Stripping 290
7.5. Densitometry analysis 291

8. Metabolic studies 291
8.1. Oxygen consumption measurements 291
8.2 Measurement of mitochondrial membrane potential 294

9. Immunochemistry of mitochondria (Immunocytochemistry) 294

10. Microscopy 295
10.1. Visualization at the spectral confocal microscope 295
10.2. Visualization of living cells at the spinning disk confocal microscopy 295
10.3. Automated fluorescence Widefield Microscopy with High Content Screening and TIRF 296

11. High Throughput Screening (HTS) 297
11.1. Miniaturization assay 297
11.2. High Throughput Screening using Prestwick library 298
11.3. Secondary screening to detect false positives 299

References **301**

RESUM **303**
Capítol 1 305
Capítol 2 312

ABBREVIATIONS AND ANNEXES

Annex I. Abbreviations and acronyms

A

aa	Amino acid
ACN	Acetonitrile
AcOH	Acetic acid
ADOA	Autosomal Dominant Optic Atrophy
AdoCbl	S-adenosylcobalamin
ADP	Adenosine diphosphate
AIDS	Acquired immunodeficiency syndrome
APH 3’	Aminoglycoside 3‘-phosphotransferase
APS	Ammonium persulfate
aq	Aqueous
ATCase	Aspartate transcarbamylase
ATCC	American Type Culture Collection
ATP	Adenosine triphosphate
AZT	Zidovudine

B

BCA	Bicinchoninic acid assay
Boc	*tert*-Butyloxycarbonyl
BPO	Benzoyl peroxide
bs	Broad singlet
BSA	Bovine Serum Albumin

C

CAP	Community Acquired Pneumonia
CAT	Chloramphenicol acetyltransferase
C2C12	Mouse myoblast cell line
CCCP	Carbonyl cyanide m-chlorophenyl hydrazone
CCiTUB	Centres Científics i Teconlògics de la Universitat de Barcelona
cDNA	Complementary DNA
CDP	Cystidine diphosphate
CF	Cystic Fibrosis
CFTR	Cystic Fibrosis Transmembrane conductance Regulator
CG	Chronic Granulomatous
CGD	Chronic Granulomatous Disease
CMT	Charcot-Marie-Tooth
CO_2	Carbon dioxide
COPD	Chronic Obstructive Pulmonary Disease

CPEC	Cyclopentenylcytosine
CPS II	Carbamoyl Phosphate Synthetase II
CPT	Camptothecin
CSOM	Chronic Suppurative Otitis Media
Ct	Number of cycles
2-CTC	2-Chlorotrityl chloride Resin
CTP	Cytidine-5'-triphosphate
Cyp A	Cyclophilin A

D

δ	Chemical shift
d	Doublet
dATP	Deoxyadenosine triphosphate
dCDP	Deoxycitidine diphosphate
DCM	Dichloromethane
dCMP	Deoxycytidine monophosphate
dGTP	Deoxyguanosine triphosphate
DHO	Dihydroorotate
DHOase	Dihydroorotase
DHODH	Dihydroorotate dehydrogenase
DIEA	*N,N*-Diisopropylethylamine
DIPCDI	*N,N'*-Diisopropylcarbodiimide
DMARD	Disease Modifying Antirheumatic Drug
DMEM	Dulbecco modified eagle's medium
DMF	*N,N*-Dimethylformamide
DMSO	Dimethyl sulfoxide
DNA	Deoxyribonucleic acid
dNDPs	Deoxynucleotides diphosphates
dNTPs	Deoxynucleotides triphosphates
Drp1	Dynamin-related protein 1
dsDNA	double-stranded DNA
dTMP	Deoxythymidine monophosphate
DTT	Dithiothreitol
dTMP	Deoxythymidine monophosphate
dTTP	Deoxythymidine triphosphate
dUDP	Deoxyuridine diphosphate
dUMP	Deoxyuridine monophosphate
dUTP	Deoxyuridine triphosphate
dUTPase	Deoxyuridine nucleotidohydrolase

E

EF	Edema Factor
ELISA	enzyme-linked immunosorbent assay
EMA	European Medicines Agency
EPS	Extracellular Polymeric Substance
Eq	Equivalents
ERRα	Estrogen-related receptor alpha
ESKAPE	*Enterococcus faecium*, *Staphylococcus aureus*, *Klebsiella pneumoniae*, *Acinetobacter baumannii*, *Pseudomonas aeruginosa* and *Enterobacter spp*
ET	Edema Toxin
ETC	Electron Transport Chain
Et_3N	Triethylamine
EtOAc	Ethyl acetate

F

FACS	Fluorescence-Activated Cell Sorting
FBS	Fetal Bovine Serum
FCCP	Carbonyl cyanide-p-trifluoromethoxyphenyl-hydrazon
FDA	Food and Drug Administration
Fis1	Fission protein 1 homolog
Fmoc	9-Fluorenylmethyloxycarbonyl
FRET	Fluorescence Resonance Energy Transfer

G

GAPDH	Glyceraldehyde-3-Phosphate Dehydrogenase
GBD	Global Burden of Disease
GDAP1	Ganglioside-induced Differentiation-Associated Protein-1
GDP	Guanosine diphosphate
GFP	Green Fluorescent Protein
GHE	Global Health Estimates
GST	Glutathione-S-Transferase
GTP	Guanosine-5'- triphosphate

H

HAIs	Health care associated infections
HD	Huntington's Disease
HeLa	Henrietta Lacks
Hepes	4-(2-hydroxyethyl)-1-piperazineethanesulfonic acid
HIV	Human immunodeficiency virus
HOAt	1-Hydroxy-7-azabenzotriazole

HOBt	1-Hydroxybenzotriazole
HPLC-PDA	High-Performance Liquid Chromatography-Photo Diode Array
HPLC-MS	High-Performance Liquid Chromatography-Mass Spectometry
HPV18	Human papillomavirus 18
HRP	Horse Radish Peroxidase
HTS	High Throughput Screening
HU	Hydroxyurea

I

IBEC	Institute for Bioengineering of Catalonia
IDSA	Infectious Diseases Society of America
IMM	Inner Mitochondrial Membrane
IPA	Isopropyl alcohol
ISP	Iron Sulfur Protein

K

KO	knockout

L

L	Long
LF	Lethal Factor
LPDE	Lithium Perchlorate/Diethyl Ether
LSB	Loading Sample Buffer
LT	Lethal Toxin

M

Mdm2	Murine doble minute 2
MDR	Multidrug resistant
MEF	Mouse Embryonic Fibroblast
MEF Mfn1$^{-/-}$	Mouse Embryonic Fibroblast deficient in Mfn1
MEF Mfn2$^{-/-}$	Mouse Embryonic Fibroblast deficient in Mfn2
MeOH	Methanol
Mfn1	Mitofusin 1
Mfn2	Mitofusin 2
Mfns	Mitofusins
MIC	Minimal inhibitory concentration
MIS	Mitochondrial Import Sequence
MMP	Mitochondrial Membrane Potential
MOM	Mitochondrial Outer Membrane
mRNA	Messenger ribonucleic acid
MRSA	Multi-antibiotic resistant *Staphylococcus aureuss*

mtDNA	Mitochondrial DNA
mtSSB	Mitochondrial single-stranded DNA-binding protein
MTT	3-[4,5-dimethylthiazol-2-yl]-2,5-diphenyltetrazolium bromide

N

NADPH	Nicotinamide dinucleotide phosphate
NDPs	Nucleosides diphosphates
Neo	Neomycin resistance gene
NMR	Nuclear Magnetic Resonance
non	Nonet
NTPs	Nucleosides triphosphates

O

OCR	Oxygen Consumption Rate
OMM	Outer Mitochondrial Membrane
OMP	Orotidine-5'-monophosphate
OPA1	Optic atrophy 1
OXPHOS	Oxidative phosphorylation

P

p53	Cellular tumor antigen p53 or tumor suppressor p53
PA	Protective Antigen
PALA	*n*-Phosphonacetyl-L-aspartate
PBS	Phosphate Buffered Saline
PCD	Primary Ciliary Dyskinesia
PCR	Polymerase Chain Reaction
PEI	Polyethylenimine
PGC-1β	Peroxisome-proliferator-activated receptor gamma coactivator-1β
PGC-1α	Peroxisome-proliferator-activated receptor gamma coactivator-1α
PRPP	Phosphoribosyl pyrophosphate
PVDF	Polyvinylidene difluoride
Pyf	Pyrazofurin

Q

q	Quartet
Q	Ubiquinone
QH_2	Ubiquinol
qPCR	quantitative Polymerase Chain Reaction
QS	Quorum Sensing
qt	Quintuplet/Quintet

R

9-RA	9-cis-retinoic acid
RA	Rheumatoid Arthritis
RAR	Retinoic Acid Receptor
RAREs	Retinoic acid response elements
RC	Respiratory Chain
RCR	Respiratory Control Ratio
RCR_p	Phosphorylation Respiratory Control Ratio
RID	Respiratory Infectious Diseases
RISP	Rieske Iron Sulfur Protein
RNA	Ribonucleic acid
RNR	Ribonucleotide reductase
ROS	Reactive Oxygen Species
Rpm	Revolutions per minute
RT	Room Temperature
RT-PCR	Reverse Transcription polymerase chain reaction
rUMP	Ribonucleotide uridine monophosphate
RXR	Retinoid X Receptor

S

s	Singlet
S	Short
SAM	S-adenosylmethionine
SDS-PAGE	Sodium dodecyl sulfate- Polyacrylamide gel electrophoresis
SEM	Standard Error of the Mean
sex	Sextet
SiO_2	Silicon Dioxide (silica)
siRNA	Small interfering RNA or silencing RNA
SLP2	Stomatin-like protein 2
SM	Starting Material
SPAP	Secreted Placental Alkaline Phosphatase
SQ·	Ubisemiquinone

T

t	Triplet
TA	Transcriptional Activation
TBTU	*N*-[(1*H*-benzotriazol-1-yl)(dimethylamino)methylene]-*N*-methylmethanaminium tetrafluoroborate *N*-oxide
^tBu	*tert*-Butyl
TCA	Tricarboxylic acid
TEA	Triethylamine

TFA	Trifluoroacetic acid
TFAM	Mitochondrial Transcription Factor A
T98G	Human Glioblastoma (TP53 mutant, M237I) cell line
THF	Tetrahydrofuran
TLC	Thin layer chromatography
Tm	Melting temperature
TMRM	Tetramethylrhodamine methyl ester
TNF	Tumor Necrosis Factor
TS	Thymidylate Synthase

U

UDP	Uridine diphospahte
Udk	Uridine kinase
UHP	Urea Hydrogen Peroxide
U87MG	Human Glioblastoma (TP53 wild-type) cell line
UMP	Uridine-5'-monophospate
URTIs	Upper respiratory tract infections
USEF	Unidad de evaluación de actividades farmacológicas de compuestos químicos
UTP	Uridine-5'-triphosphate
UV	Ultraviolet

V

VAP	Ventilator associated pneumonia
VDAC	Voltage-Dependent Anion Channel

W

WHO	World health organization
wt	wild type

Y

YLLs	Years of life lost

Annex II. Glossary

Antimycotic: Any agent that destroys or prevents the growth of fungi.

Bacteraemia: Presence of bacteria in blood.

Bactericidal: A substance able to kill bacteria.

Bacteriostatic: Biological or chemical agent that stops bacteria from dividing, without necessarily harming them.

Biofilm: A community of cells attached to a surface, interface or to each other, and are imbedded in a self-made, protective matrix of extracellular polymeric substances.

Bone marrow: Flexible tissue in the interior of bones.

Celite: Used in chemistry as a filtration aid, to filter very fine particles that would otherwise pass through or clog filter paper.

Endocarditis: Inflammation of the inner layer of the heart, the endocardium.

Fungemia: Presence of fungi or yeasts in the blood.

Horizontal Gene Transfer: Genes in one species of bacteria can be transferred to other species of bacteria, such as for example antibiotic resistance genes.

Kartagener syndrome or primary ciliary dyskinesia (PCD): Rare, ciliopathic, autosomal recessive genetic disorder that causes a defect in the action of cilia lining the respiratory tract and fallopian tube, and also flagella of sperm in males.

Quorum sensing: Process by which bacteria use signalling molecules to monitor bacterial density and coordinate gene expression in a population-density-dependent manner.

Laryngitis: Inflammation of the larynx.

Nosocomial Infections: Hospital acquired infections.

Osteomyelitis: Infection and inflammation of the bone or bone marrow.

Pertussis: Highly contagious bacterial disease caused by *Bordetella pertussis*, commonly called whooping cough.

Pharyngitis: Inflammation of the pharynx, hypopharynx, uvula, and tonsils.

Prophage: Phage (viral) genome inserted and integrated into the circular bacterial DNA chromosome or existing as an extra chromosomal plasmid.

Prophylaxis: Any medical or public health procedure whose purpose is to prevent, rather than treat or cure, a disease or other medical issue.

Rhinitis: Inflammation of the nasal mucosa.

Sepsis: Potentially fatal whole body inflammation (a systemic inflammatory response syndrome) caused by severe infection.

Sinusitis: Inflammation of the nares and paranasal sinuses, including frontal, ethmoid, maxillary, and sphenoid.

Tachypnea: The condition of rapid breathing.

Tonsillitis: Inflammation of the tonsils most commonly caused by viral or bacterial infection.

Tonsils: Collections of lymphoid tissue facing into the aerodigestive tract.

Annex III. Natural amino acids

Amino acid	Code	Structure
L-alanine	Ala	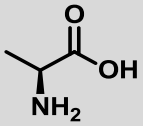
L-Aspartic acid	Asp	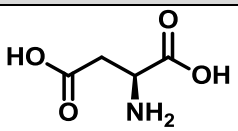
L-Leucine	Leu	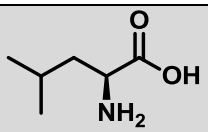
L-Lysine	Lys	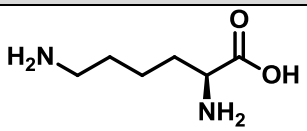
L-Phenylalanine	Phe	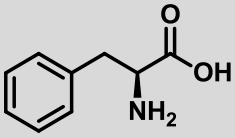

Annex IV. Coupling reagents

Coupling reagent/additive	Symbol	Structure
***N,N*-Diisopropylethylamine**	**DIEA**	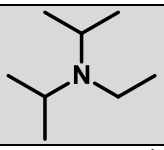
***N,N'*-Diisopropylcarbodiimide**	**DIPCDI**	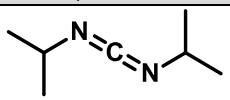
1-Hydroxy-7-azabenzotriazole	**HOAt**	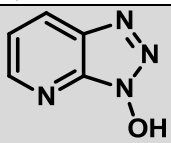
***O*-(Benzotriazol-1-yl)-N,N,N',N'-tetramethyluronium tetrafluoroborate**	**TBTU**	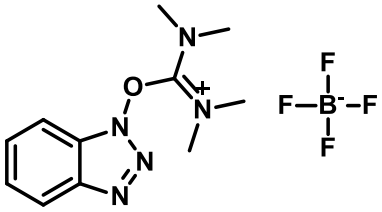

CHAPTER 1

Synthesis of an *N*-hydroxylamine-based library of potential drugs for the treatment of Respiratory Infectious Diseases (RID)

ABSTRACT

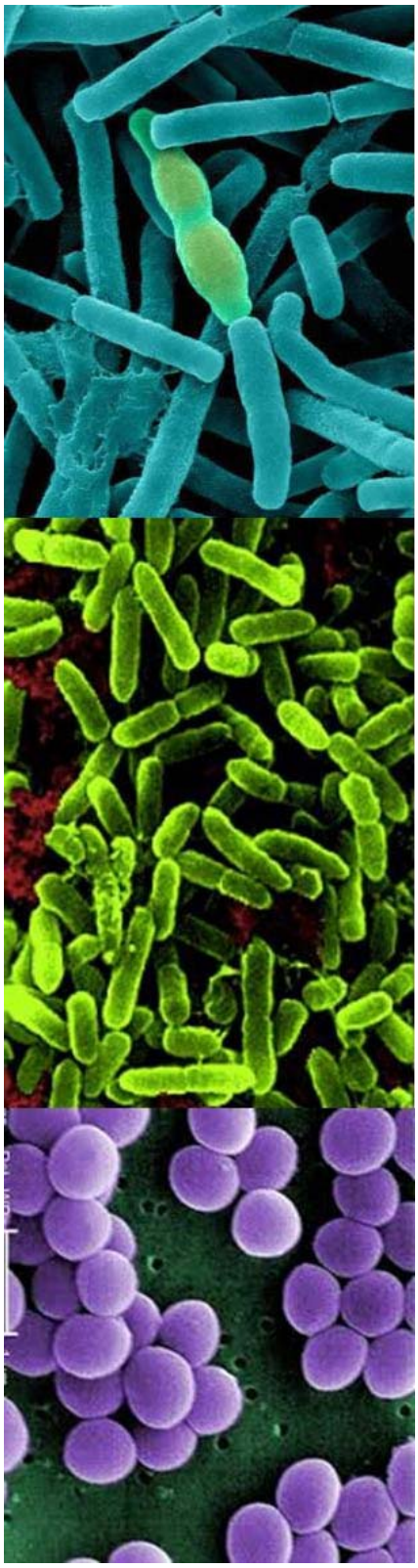

ABSTRACT

Respiratory Infectious Diseases (RID) are diseases affecting the air passages, the bronchi and the lungs. They range from acute infections, such as pneumonia and bronchitis, to chronic conditions such as asthma, cystic fibrosis and chronic obstructive pulmonary disease. Respiratory lung infections are leading causes of morbidity and mortality worldwide with a considerable human, social and financial burden.

RID can be caused by an increasing number of multi resistant bacteria to the existing antibiotics. Bacteria, which normally inhabit the mucus, grow out of control and consequently colonize and infect the lungs. The altered mucus leads to formation of bacterial microenvironments known as biofilms, which are difficult for antibiotics and inmunitary cells to penetrate.

A potential key enzyme of bacteria, associated with chronic lung infections, to be targeted by antiproliferative drugs are ribonucleotide reductase enzymes (RNR). RNR enzyme provides deoxyribonucleotides for DNA synthesis which are needed for growth and spore germination of the pathogen. Inhibition of RNR enzymes could be a valuable therapeutic strategy for the treatment of RID.

In the literature, it has been suggested that hydroxyurea (HU) and *N*-hydroxylamine derivatives can be used as antiproliferative drugs against bacterial lung infections. Therefore, a library of these compounds was synthesized and evaluated against four different bacteria lines: *Pseudomonas aeruginosa*, *Staphylococcus aureus*, *Burkholderia cenocepacia* and *Bacillus anthracis*; all of them are opportunistic infectious pathogens affecting respiratory system.

INTRODUCTION

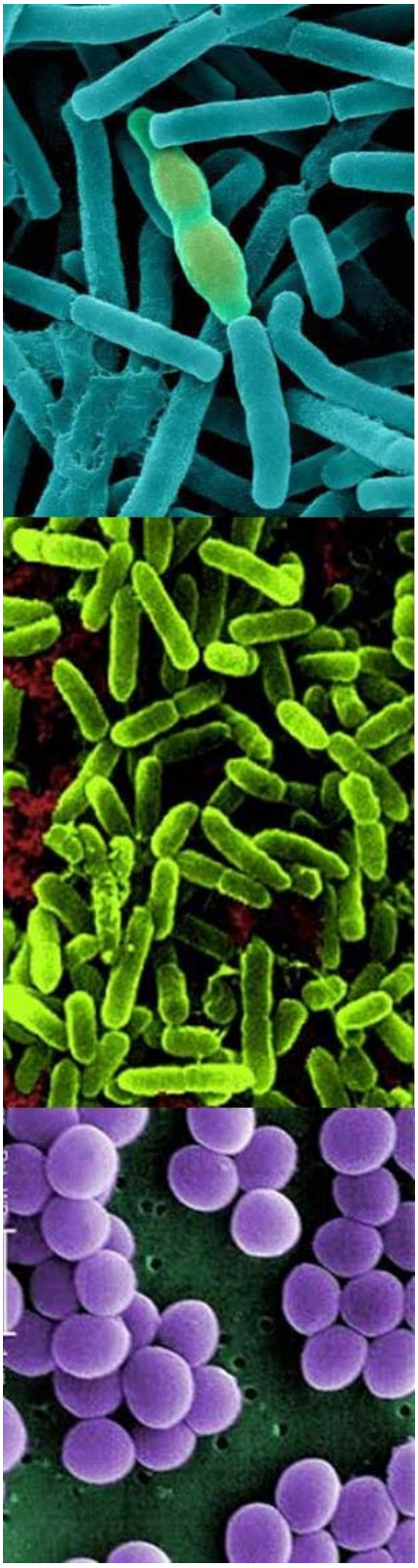

INTRODUCTION

1. General introduction

Respiratory infectious diseases are mainly caused by viruses or bacteria, producing an enormous diversity, both in their epidemiology and severity. These infections may involve the upper respiratory tract (rhinitis, sinusitis, nasopharyngitis, pharyngitis, epiglottitis, laryngitis, laryngothracheitis and tracheitis), the lower respiratory tract (acute bronchitis) or it can be the cause of several serious illnesses involving the lung itself (emphysema, pneumonia and tuberculosis). RID have a major impact on infants, older adults, patients already suffering from chronic illnesses such as those affected by cystic fibrosis (CF), as well as patients with immunodeficiency caused by disease or treatment, such as those affected by acquired immunodeficiency syndrome (AIDS)[1]. Furthermore, chronic respiratory conditions, such as asthma and chronic obstructive pulmonary disease (COPD) can be aggravated by respiratory infections.

The World Health Organization (WHO) Global Health Estimates (GHE) provides the Global Burden of Disease (GBD), a comprehensive and comparable assessment of mortality and loss of health due to diseases and injuries for all regions of the world. COPD and lower respiratory infections are leading causes of morbidity and mortality worldwide counting for almost 12% of total deaths and 9% YLLs (calculated years of life lost due to premature mortality)(Figure 1)[2].

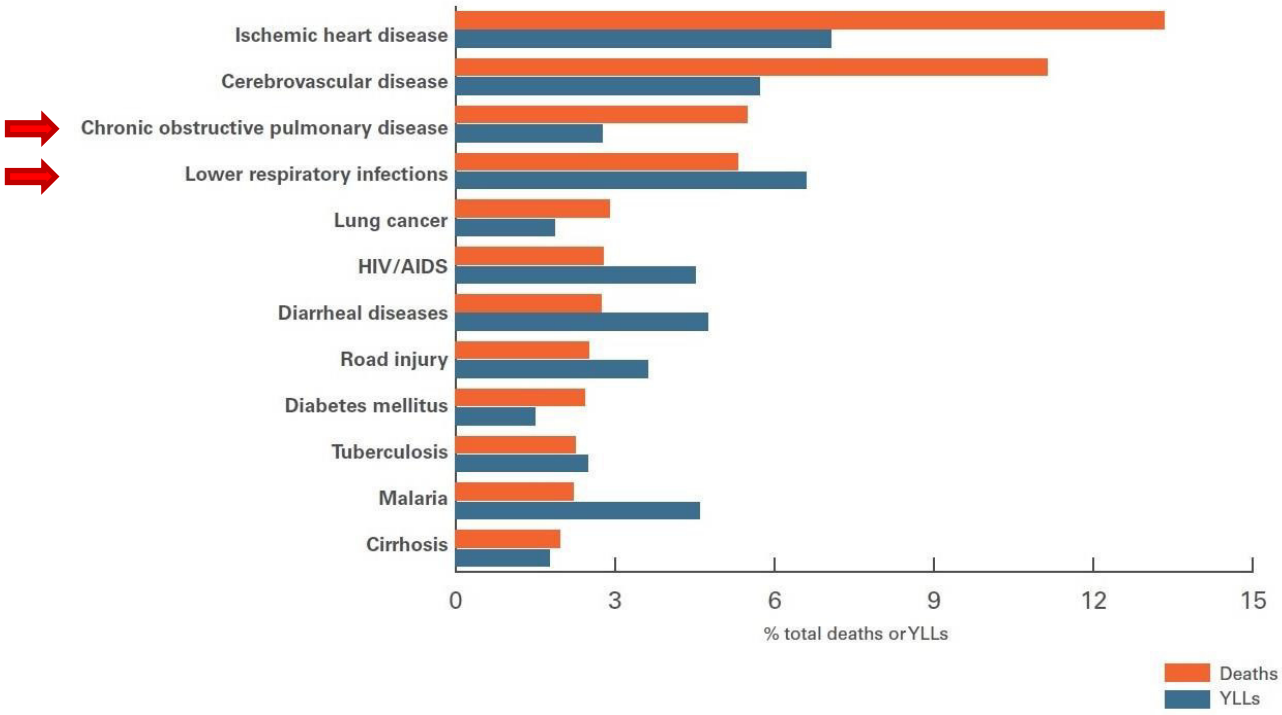

Figure 1. Leading causes of global death and premature death, 2010

RID are common and can be a direct or indirect cause of illness. In particular, there is a diagnostic limitation for respiratory infection, ineffective therapeutic strategies for most viral pathogens, and an increasing number of multi resistant bacteria. Therefore, repeated respiratory infections can produce: antibiotic resistance, resulting in untreatable infections; viral pandemics, such as avian influenza; and bioterrorism, such as anthrax[1].

The current management of acute respiratory infections relies on antibiotic and antiviral use to cover bacterial and viral pathogens. However, antibiotics and antiviral are overprescribed and are used inappropriately producing drug resistance pathogens. There is a need to improve sensitivity and specificity in diagnostic assays and to develop new antibiotics and antivirals for specific respiratory pathogens. Firstly, sensitivity would avoid the incorrect use of antibiotics in viral infections, and secondly, specificity would use specific antibiotics and/or antivirals in the first instance. Therefore, in severe pneumonia, CF and COPD exacerbations[3] the specific antibiotics and/or antivirals will be used at their maximum potential to combat the disease.

In the present chapter we have focused in the study of respiratory infectious disease caused by bacterial pathogens.

1.1. Antibiotic resistance bacteria

Since their clinical introduction in the 1930s, antibiotics have revolutionized life on Earth, allowing advances in medicine, agriculture and industries. However, the excessive uses of antibiotics from clinical use by physicians and patients to agricultural and industrial practice for disease treatment, prophylaxis, livestock grow promotion and food production have applied selective force to bacteria, triggering the growth of antibiotic resistance strains[4]. The two main factors that have expanded global resistance are: the misuse of antibiotics and the spread of resistant microorganisms.

Traditional antibiotics have bactericidal or bacteriostatic activity inhibiting bacterial functions, such as DNA or RNA synthesis, protein synthesis, cell wall synthesis, folate synthesis or depolarizing membrane potential, that are essential for growth. These antiproliferative drug activities impose selective pressure that fosters the growth of drug resistance bacteria[5]. It has been reported that exposure to low concentrations of antibiotics can alter bacterial metabolism and even change behaviour in beneficial signals, such as biofilm formation that increases antibiotic resistance. For example, bacterium *P. aeruginosa* forms biofilms when is incubated at sublethal concentrations of antibiotic tetracycline[6].

The introduction of every novel antibiotic product has been followed by the resistant bacteria against it, producing plenty of classes of antibiotics not useful and approaching the end of the antibiotic era. Consequently, there has been a significant decrease of investments by important pharmaceutical companies towards antibiotics compared to drugs for chronic illness over the last twenty years.

The Infectious Disease Society of America (IDSA) estimates that 70% of hospital-acquired infections are resistant to one or more antibiotics and has selected a group of pathogens: *Enterococcus faecium*, *Staphylococcus aureus*, *Klebsiella pneumoniae*, *Acinetobacter baumannii*, *Pseudomonas aeruginosa*, and *Enterobacter spp*. (the ESKAPE pathogens), with high mutation, transmission, and resistance capacity to escape antibiotics action by biofilm formation[7]. Bacterial infections cause serious and chronic illnesses, disability and death, and an estimated annual bill of €1.5 billion in the EU and US$5 billion in the USA[8].

A significant factor contributing to the pathogenesis and chronic infection to a number of medically important bacterial strains is the ability of bacteria to form a biofilm, conferring antibiotic and host immune system resistance. Biofilm seems to protect bacteria from hostile environmental factors and shows an increased resistance in the penetration barrier to antibiotics than their free-living counterparts. Biofilm is considered to be responsible for 65% of all bacterial infections[9].

There is a need to develop new targets and new compounds for specific respiratory pathogens[10,11]. One potential key enzyme to be targeted by antiproliferative drugs is the Ribonucleotide Reductase (RNR) enzyme family, which are well conserved among species and are essential for viability. RNR enzymes are a promising drug target because catalyses the production of deoxyribonucleotides essentials for DNA synthesis, which essentially prevents bacterial resistance development toward drugs of the radical scavenger type.

2. Ribonucleotide Reductase (RNR) system

During infection, bacteria need to multiply inside the organism and require active DNA synthesis. Ribonucleotide reductases (RNRs) are essential enzymes in all living cells. These proteins are the unique enzymes that catalyse the reduction of nucleotides (NDPs or NTPs where N = C, U, G, or A) to their corresponding deoxynucleotides (dNDPs or dNTPs) via radical chemistry. RNR are responsible for genome replication controlling the relative ratios and absolute concentrations of cellular dNTP pools. For this reason, RNRs play a major role on growth and survival providing the buildings blocks for DNA synthesis and repair[12]. The three known RNR classes (I, II and III) differ in their mechanisms for free radical generation, cofactor requirement, allosteric regulation, quaternary structures, and oxygen dependence[13,14]. Although some amino acid sequences are different, the three-dimensional structure of the catalytic core is preserved and all RNRs reduction is initiated with the generation of a free radical[15-17]. However, different metallocofactors exhibiting different oxygen behaviour are required for radical generation.

Class I RNRs are tetrameric ($\alpha_2\beta_2$) enzymes, composed of two homodimeric proteins: R1 (α_2) containing the catalytic domain (active site) and the complex allosteric domain (responsible for the regulation of the enzyme), and R2 (β_2) carrying a stable tyrosyl radical and an oxygen-linked diiron center required for free radical production. The α_2 protein is controlled by allosteric regulation involving a substrate specificity site that binds ATP, dATP, dTTP, or dGTP and overall activity site, composed by an N-terminal ATP cone, that binds ATP or dATP[12,18]. The specificity site determines which substrate will be reduced in the active site (ribonucleotides diphosphates: CDP, UDP, GDP and ADP) and the overall activity site act as an on/off switch for enzyme activity. The catalysis is inhibited when dATP binds to the ATP cone domain, while binding of ATP activates enzyme catalysis. The same RNR enzyme can reduce the four different substrates. This RNR class only work under aerobic conditions (see Figure 2).

Class I RNRs is further subdivided into classes Ia and Ib, because of significant differences in amino acid sequences, allosteric regulation and gene organization[19]. Class Ia is encoded by the *nrdA* and *nrdB* genes and code for the α_2 protein NrdA and the β_2 protein NrdB, whereas class Ib is encoded by the *nrdE* and *nrdF* genes. This operon code for the α_2 protein NrdE, which lack approximately 50 N-terminal amino acids that constitute the allosteric-activity site compare to NrdA, and for the β_2 protein NrdF. Class Ib RNRs lack the ATP-cone domain and does not have allosteric overall activity site, however encoded for two additional genes: *nrdI*, which encode a flavodoxin-like protein important in radical generation, and *nrdH*, which encodes an electron donor glutaredoxin-like protein[20]. It has been recently shown that class Ib small subunit (NrdF) stabilizes the tyrosyl radical by a dimanganese-oxo center. Class I are oxygen dependent enzymes only functional under

aerobic conditions because the generation of the tyrosyl radical requires oxygen, and they are present in eubacteria, eukaryotes, and some viruses.

Class II RNRs are oxygen-independent enzymes, coenzyme B12-dependent and can be active under both aerobic and anaerobic conditions. Class II RNRs, encoded by the *nrdJ* gene, consist of a single polypeptide chain and exist as a monomeric or homodimeric (α/α_2) enzyme. S-adenosylcobalamin (AdoCbl) (vitamin B12 coenzyme) is required for radical generation. Surprisingly, some class II RNRs reduce ribonucleoside diphosphates and others reduce ribonucleotides triphosphates[21]. This class is mainly found in bacteria, archaea, and a few unicellular eukaryotes[22] (see Figure 2).

Lastly, class III RNRs are oxygen-sensitive enzymes present in anaerobes. Class III RNR are encoded by the *nrdD* and *nrdG* genes, which code for NrdD (α_2) and NrdG (β_2) homodimeric proteins. α_2 contain a stable oxygen-sensitive glycyl radical and require a specific activase β_2 that uses *S*-adenosylmethionine (SAM) to generate the glycyl radical[23,24]. Once the radical has been generated, NrdG is not required for catalysis. Class III RNRs reduce ribonucleoside triphosphates and usually harbors both an allosteric site and an allosteric overall activity site[21]. This class is active only under strict anaerobic conditions, and it is found in eubacteria, archaea, and a few unicellular eukaryotes[22] (Figure 2).

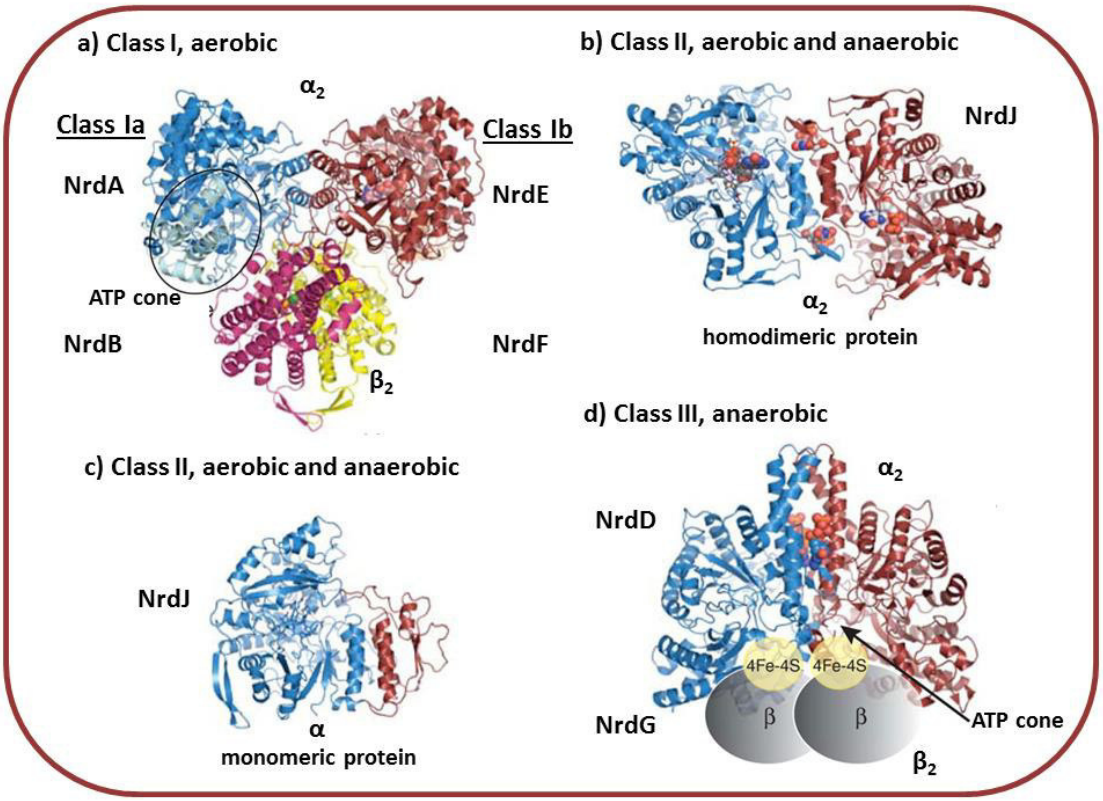

Figure 2. Classes of Ribonucleotide Reductase enzyme (I, II, III)

Despite significant differences in their structures and in cofactor requirements, all three enzymes share similar catalytic mechanisms creating a transient thiyl radical at a

conserved cysteine residue in the active site that initiates the reduction of ribonucleotides for DNA synthesis and repair. The fine-tuning of dNTP levels is achieved by at least two different regulatory mechanisms, transcriptional regulation of the *nrd* genes and allosteric control of the RNR enzyme keeping a balanced formation of each of the four deoxyribonucleotides.

Whereas almost all eukaryotic organisms only encode class Ia RNRs, prokaryotic organisms, such as bacteria, are known to quite often encode more than one class of RNR principally depending on environmental life style[22]. Usually one predominant RNR is responsible for bacterial growth and is regulated depending on the cell cycle to satisfy the changing demands for dNTP synthesis. Other RNR classes that are present in the same genome respond to other regulatory mechanisms that differ from those controlling the predominant RNR class.

Ribonucleotide reductase plays an important role in regulating cell division and cell proliferation since the reaction is rate limiting for DNA synthesis. RNR enzyme has been recognized as a possible target for antiproliferative therapy such as anticancer, antiviral, and antibacterial[25-27]. Since RNR is a complex enzyme under strict regulation different parts of the enzyme can be targeted in drug-design[21]:

- Substrate analogues will usually inhibit irreversibly
- Radical scavengers destroy the tyrosyl radical
- Iron chelators remove the iron needed to form the diiron-radical site
- Peptidomimetics inhibit the protein-protein interactions between NrdA and NrdB
- Antisense techniques, RNA interference and gene therapy manipulate the expression of RNR
- Effectors analogues and other potential inhibitors usually decrease enzyme activity.

The first antiproliferative drug used against RNR was HU, which acts as a radical scavenger reducing the tyrosyl radical in the RNR enzyme. Currently, HU is still a standard drug used in the treatment of many cancers, although is rather inefficient and high concentrations need to be administered with undesired side effects for the patient. Due to the toxicity HU is often combined with other drugs, and frequently used in Human Immunodeficiency Virus (HIV) treatment in combination with zidovudine (AZT) or 2',3'-dideoxyinosine.

Torrents *et al.* carried out a study published in 2005, where they showed that the essential tyrosyl radical of the class Ib RNR protein (NrdF) is a possible target for tailored antibacterial drugs based on radicals scavenging. Hydroxylamine and *N*-methylhydroxylamine were identified as potential inhibitors for treatment of anthrax (*B.*

anthracis) infection, inhibiting the growth of the pathogen at several orders of magnitude lower concentrations compared to HU. Therefore, *N*-methylhydroxylamine inhibited the purified *B. anthracis* NrdF with several hundred-fold higher potency compared to the purified mouse R2/NrdB, which was not inhibited at all[28]. These results demonstrate that is possible to find specific inhibitors targeting bacterial RNR without affecting human RNR. Importantly, *N*-methylhydroxylamine has been shown to be non-toxic to man[29].

Our research is focused on finding specific RNR inhibitors for four different bacterial cell lines: *P. aeruginosa, S. aureus*, *B. cepacia* and *B. anthracis*, which are the most common organisms causing opportunistic infections in patients suffering respiratory diseases. *P. aeruginosa* is one of few bacteria that encodes for all three RNR classes (Ia, II, and III)[30]. Both class Ia and class II enzyme activities were detected in normal growing cells. *S. aureus* relies on the class Ib RNR for aerobic growth and under anaerobic conditions the class III RNR seem to be essential. *B. cenocepacia* encodes a class Ia RNR, for aerobic grow, in combination with class II RNR, which is oxygen independent. Finally, *B. anthracis* genome encodes a class Ib RNR in combination with a class III RNR that is only functional during anaerobiosis. The majority of Gram-positive bacteria rely on class Ib RNR for normal growth during aerobiosis.

3. Pathogenic bacteria

Bacteria have evolved and developed mechanisms to survive over the course of billions of years. The existence of bacteria is perpetuated by their capacity to adapt to various environments and to evade host immune system and antimicrobials, undergoing mutability, horizontal gene transfer, recombination of foreign DNA into the chromosome and formation of biofilm capsules. The bacterial colonization in respiratory disease may be: initial, intermittent, and chronic depending on the quantity of bacteria, the invasive capacity of the bacteria, the antibacterial efficacy and the immune defense system condition showing diverse therapeutic implications.

3.1. Bacterial phenotype: Biofilm formation

Formation of biofilm is initiated upon recognition of surfaces by attachment sites of cell surface, cell-cell interactions, cell signalling, or by exposure to antibiotics. The biofilm life cycle involves several phases; the first two stages are the cellular adhesion of free-floating microorganisms to a surface, followed by cellular attachment using cell adhesion structures. Once colonization has begun, the biofilm grows through a combination of cell division and recruitment. In the fourth stage the cells secrete a matrix of extracellular polymeric substance (EPS) that contains, proteins, nucleic acids, lipids and polysaccharides to form the biofilm, which are embedded with cavities and channels allowing the sequestration of water, the exchange of nutrients, minerals, and waste. The final stage is known as dispersion, once the biofilm is established, dispersal of cells from the biofilm is essential to spread and colonize new surfaces (Figure 3)[31-33].

(4)

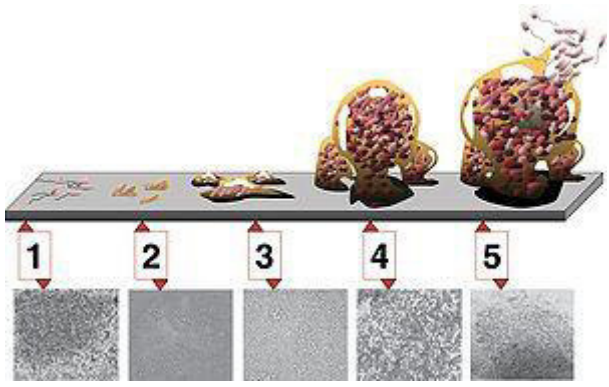

Figure 3. There are five stages of biofilm development: (1) Initial attachment, (2) Irreversible attachment, (3) Maturation I, Maturation (II), and (5) Dispersion

Biofilms are more resistant against host immune system, phagocytosis, antibiotic treatment, fluctuant pH and dehydration than free bacteria, and they become difficult or impossible to eradicate[34-36]. The dense and protected environment of biofilm allows cooperation and interaction through biochemical signals, known as quorum sensing,

hypermutation, and horizontal gene transfer[37,38]. Biofilm may form on living or non-living surfaces in natural, industrial, and hospital environments. There is a shift in behaviour between cells forming part of a biofilm and free cells, and most of the genes are regulated in a different way. Biofilms showing increased resistance to antibiotics, have different mechanism to protect bacteria[32]:

1) The majority of antibiotics are not able to penetrate the biofilm polysaccharide matrix, this phenomenon is known as poor diffusion[39].
2) Biofilm subjected to nutrient and oxygen limitation, leads to zones within the biofilm in which the bacteria enter stationary phase contributing to antibiotic tolerance[40,41].
3) Quorum-sensing, signalling molecules to monitor bacterial growth and gene expression[42].
4) The expression of efflux pumps, which removes toxic substances[43,44].
5) Persister cells: small population of highly resistant bacteria that resist killing when exposed to antimicrobials to rebuild the biofilm. The persistent cells are not mutants[45].

Biofilms have been involved in a high variety of pathogenic implications in the body such as urinary tract infections, middle-ear infections, gingivitis, and more lethal processes such as endocarditis, infections in cystic fibrosis patients, COPD, bronchiectasis and infections of permanent indwelling devices. Biofilm is considered to be responsible for 65% of all bacterial infections[9].

3.2. Bacterial types:

P. aeruginosa, B. cepacia, S. aureus, and *B. anthracis* are the four most common organisms causing infections in patients suffering respiratory disease.

3.2.1. Pseudomonas aeruginosa

P. aeruginosa is a Gram-negative ɣ-proteobacterium well-known for its environmental versatility, ability to cause infection in susceptible individuals, and resistance to antibiotics. This bacterium has the ability to adapt and grow in many ecological environments, from water and soil to plant and animal tissues, as a result of its capacity to use a wide range of organic compounds as food sources[46].

P. aeruginosa is an important cause of hospital acquired infections that affect more than two million patients and cause around 90.000 deaths per year[47,48]. Plenty of these infections are associated with catheterization and intubation such as urinary tract infection. Biofilms strains causing respiratory infection have been found in the ventilators tubes and are associated to ventilator associated pneumonia (VAP)[49]. *P. aeruginosa* has an impressive

ability to cause opportunistic infections in susceptible individuals, such as those affected by cancer, bronchiectasis, CF[50] and COPD[51], as well as burnt, immunocompromised, and elderly patients, causing serious complications in lung infections. Patients with chronic wounds, such as the ones present in diabetic patients, suffer bacterial colonization due to loss of skin and poor circulatory conditions. Most of these infections are difficult to battle due to biofilm formation.

Biofilms seem to protect these bacteria from hostile environmental factors such as the immune system and the antibiotics. The extracellular matrix of biofilms significantly increases their resistance to antibiotics in comparison with their free-living counterparts. Furthermore, multidrug resistant (MDR) pumps also play an important role in antibiotic resistance[52]. *P. aeruginosa* is naturally resistant to a wide range of antibiotics and may show extra resistance after ineffective treatment caused by acquired resistance either by mutation in chromosomally encoded genes or by the horizontal gene transfer.

3.2.2. Burkholderia cenocepacia

B. cenocepacia is an aerobic Gram-negative β-proteobacterium. This plant and human pathogen is highly adaptable, lives under diverse circumstances in nature and can rapidly evolve under *in vitro* stress conditions or during infections.

Most of strains of *B. cenocepacia* are highly transmissible, resistant to almost all antibiotics, with a high capacity to survive and replicate intracellularly in both airway epithelial cells and macrophages. Macrophages play an important role in clearance of infecting bacteria. *B. cenocepacia* causes skin and soft tissue infections, surgical wound infections, genitourinary tract infections, and nosocomial pneumonia. *B. cenocepacia* also is an opportunistic pathogen that causes respiratory infections in those with impaired pulmonary function, such as COPD, chronic granulomatous (CG), immunocompromised and CF patients. Approximately one third of *B. cenocepacia* infected CF patients develop fatal "*cepacia* syndrome", which is characterized by rapid deterioration of pulmonary function[53]. The severity of *B cenocepacia* infection is due in part to its formation of biofilms, which are commonly resistant to antibiotics.

3.2.3. Staphylococcus aureus

S. aureus is a Gram-positive bacterium and a human and animal wound pathogen, causing both hospital and community acquired infections upon the formation of biofilm. *S. aureus* is a common cause of food intoxication, skin and respiratory infections (sinusitis). *S. aureus* uses a wide range of virulence factors and has various survival strategies to invade and survive in mammalian host cells. For example, it is able to replicate in the phagosome or freely in the cytoplasm, escapes the phagosome of phagocytes, overturns autophagy and

induces cell death mechanisms. Therefore, six efflux pumps have been described as a mechanism of resistance in biofilms.

All *S. aureus* genome contain at least one prophage, which is responsible for pathogenesis, such as skin infections and severe life-threatening infections (sepsis, osteomyelitis and endocarditis). *S. aureus* is also an opportunistic pathogen in CG and CF disease and is associated to VAP. Moreover, biofilms also are involved in infections on indwelling medical devices, such as arteriovenous shunts, mechanical heart valves and orthopedic devices[35,54]. The increase of *S. aureus* infection has been connected with an increase in antibiotic-resistant strains in the last 20 years. Multi-antibiotic resistant *S. aureus* (MRSA) has developed resistance to β-lactam antibiotics becoming a crucial problem in many hospitals, where it causes wound infections, bacteraemia and pneumonia[55].

3.2.4. Bacillus anthracis

B. anthracis is a Gram-positive, endospore forming bacterium responsible for anthrax infections and can grow in ordinary nutrient medium under aerobic or anaerobic conditions. *B anthracis* is a human and animal pathogen; often cause livestock disease. *B. anthracis* exists in the environment as a spore and can remain viable in the soil for decades. Spores are highly resilient, surviving extremes of temperature, low-nutrient environments, and harsh chemical treatment.

B. anthracis contains a single circular chromosome and also two circular extrachromosome; pXO1 and pXO2, which causes virulent anthrax strains[56]. The pXO1 plasmid contains genes that encode the protective antigen (PA), the lethal factor (LF), and the edema factor (EF) virulence factors. LF and EF are responsible for tissue necrosis and for severe edema, respectively. PA can bind either LF or EF toxin receptors on the host cell. The PA/LF/EF complex is incorporated into the cell as the lethal toxin (LT) or edema toxin (ET), collectively called the anthrax toxins[57,58]. The pXO2 plasmid encodes for formation of the poly-γ-D-glutamate capsule, which resists phagocytosis, evades the host immune system and is essential for full virulence[59].

After entering the body through the skin, gastrointestinal tract, or by inhalation, the spores germinate to produce the three key factors of anthrax: a capsule, the production of lethal and edema toxins, and achieve high bacterial concentrations in infected hosts[60,61]. *B. anthracis* penetrate into the bloodstream due to lysis of the infected host cells and initiates bacteremia causing edema, hemorrhage and thrombosis, and finally, death of the host. Cutaneous anthrax is the most common form of infection (95%) and it is characterized by inflammatory, black, and necrotic lesion. Gastrointestinal anthrax results from ingestion of spores and can progress to ulceration and severe edema of the gastrointestinal tract, leading to sepsis and death (50%). Inhalational anthrax is the most serious form of anthrax with a mortality rate of near 90%[62-64].

The aim of the present chapter is to find specific inhibitors to fight against resistance bacteria, which are leading causes of respiratory tract infections and opportunistic infections in chronic respiratory disease with high morbidity and mortality impact worldwide. In the following section we will introduce respiratory infections and we will focus in opportunistic biofilm infections.

4. Respiratory infections

The upper respiratory tract hosts a vast range of viruses and bacteria forming a complex microbial community. They may be present in the nasopharynx without causing any respiratory symptoms. However, a disturbance in the equilibrium (acquisition of new bacteria or viruses) may lead to overgrowth and invasion pathogen causing respiratory infections[65,66]. Infections can affect upper and lower respiratory tract of the respiratory system. The upper respiratory tract is composed by nasal cavity, pharynx and larynx and lower respiratory tract refers to the respiratory system: trachea, primary bronchi and lungs (Figure 4).

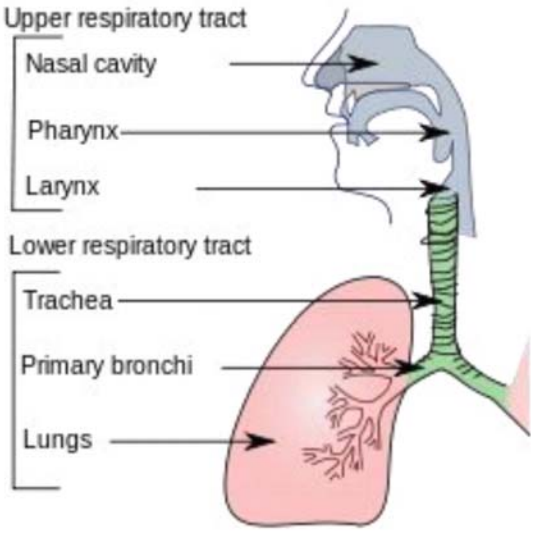

Figure 4. Respiratory tract

The trachea has a membrane that produces a layer of mucus that helps filter waste when an organism breathes. There are also tiny hairs in the lungs called cilia, which act as a filter and control the amount of mucus that enters the lungs. When we cough is because the cilia push up the mucus not to enter the lungs. If cilia does not function properly, there is a risk of a lower respiratory tract infection.

4.1. Upper and lower respiratory tract infections

Upper respiratory tract infections (URTIs) can be caused by viruses (rhinovirus, adenovirus, parainfluenzavirus, influenzavirus, respiratory syncytial virus or coronavirus) and by primary bacterial infections (*Streptococcus pyogenes* (*Streptococcal pharyngitis*) and *Mycolpasma pneumonia*). However, bacteria can also act as secondary pathogens (*Streptococcus pneumoniae*, *Haemophilus influenzae*, *Corynebacterium*

diphtheriae, *Bordetella pertussis*, *B. anthracis*, *S. aureus* and *Moraxella catarrhalis*). These bacterial infections may be localised or extend to involve the lower respiratory tract.

The most common upper respiratory tract infection is the common cold which include rhinitis, pharyngitis, tonsillitis, and laryngitis, and secondary complications are sinusitis or chronic sinusitis and ear infection. Biofilm formation has been demonstrated in different chronic middle ear infectious disease, and *P. aeruginosa*, *Escherichia coli* and *S. aureus* have been identified in chronic suppurative otitis media (CSOM). Other secondary complications affecting the lower respiratory tract are exacerbations of chronic bronchitis or asthma and pneumonia.

The common cold represents a discomfort for a few days without further problems. However, there are high risk individuals suffering from chronic respiratory disease, immunosuppression conditions or immunosuppressive therapy in which URTIs can cause severe complications, affecting de lower respiratory tract and causing illness, and a need for hospitalisation or even death. Our respiratory system is prone developing infections in the lungs.

4.1.1. Pneumonia

Pneumonia, the most common lower respiratory tract infection, is characterized by inflammation of the alveoli in the lungs. Once the air sacs become infected, they fill with pus and mucus causing breathing problems. Pneumonia can be caused primarily by bacteria or viruses and less commonly by fungi and parasites. Viruses also make the body more susceptible to secondary bacterial infections. Pneumonia frequently starts as an upper respiratory tract infection that moves into the lower respiratory tract.

Pneumonia can be classified by how it was acquired, community or hospital acquired. Community acquired pneumonia (CAP) is the most common cause with *Streptococcus pneumoniae* isolated in nearly 50% of cases. Other commonly isolated bacteria include *H. influenzae*, *Chlamydophila pneumoniae*, *M. pneumoniae*, *S. aureus*, *Burkholderia cepacia* and others. Hospital acquired pneumonia is associated with a vast spectrum of pathogens, particularly bacterial pathogens those are usually more resistance and difficult to treat.

Pneumonia affects approximately 450 million people globally per year and results in about 4 million deaths, mostly in third-world countries. Pneumonia is one of the most important causes of death in infants, the elderly and immunodeficiency patients.

4.2. Opportunistic biofilm infections

Airways (bronchi, bronchioles and alveoli) of chronic lung diseases become narrowed and limited air flow, making more difficult to move air in and out of the lung causing shortness of breath. Respiratory infection is a leading cause of acute exacerbations in these diseases. Furthermore, respiratory infection is a major problem due to it remains under recognised as a contributor to the progression of these diseases. Asthma, COPD, bronchiectasis, CGD and CF are major causes of chronic respiratory morbidity.

4.2.1. Asthma

Asthma is an obstructive lung disease, a chronic inflammatory disorder of the airways that causes a reversible restriction in the airflow into the alveoli. The muscles in the walls of bronchi constrict producing episodes of variable airway obstruction. One treatment of asthma is to use a bronchodilator, a drug that relaxes muscles of bronchi.

Asthma patients can have stable asthma for weeks or months and then suddenly develop an increase in the severity of the disease, which is called acute asthma or asthma exacerbation caused by triggering agents such as dust, dander, allergens, viral or bacterial respiratory infection of the upper respiratory tract. Exacerbation attacks affect between 50 to 80% of patients with asthma.

4.2.2. Chronic Obstructive Pulmonary Disease

COPD is a lung disease defined by respiratory failure due to low airflow as a result of breakdown of lung tissue (emphysema), dysfunction of the small airways, and inflammatory mucoid secretions. Primary symptoms are: shortness of breath, cough, and sputum production. Cigarette smoking is a major instigator of COPD and also produces an inflammatory lung response.

Bacterial infection plays a causative role in the pathogenesis of acute exacerbations, increasing airflow obstruction and inflammation, and exacerbations frequency, which contribute to further progression of lung disease[51,67,68]. However, the exact role of bacterial colonization or infection in the initial phase of COPD has not been identified. The most frequently isolated species are *H. influenza* and *P. aeruginosa*, being the last one increasingly accepted as an important pathogen in COPD[69]. Therefore, during episodes of exacerbations other bacteria have been isolated, such as *S. aureus*, *Haemophilus haemolyticus*, *Haemophilus parainfluenzae*[69] and others. Acute COPD exacerbations signs are: shortness of breath, increased hyperinflation, worsening of gas exchange, increase in the quantity and color of phlegm. As bacterial infection may have either a primary or secondary role in 50% of

exacerbations of COPD[68,70], antibiotics are frequently indicated in the management of acute infective exacerbations.

Management involves quitting smoking, vaccinations, rehabilitation, inhaled bronchodilators and long-term oxygen therapy or lung transplantation. In contrast to asthma, COPD is rarely reversible and usually gets worse over time.

Worldwide, COPD ranked as the third leading cause of death in 2010. Mortality is expected to increase due to an increase in smoking rates and an aging population in many countries.

4.2.3. Bronchiectasis

Bronchiectasis is a lung disease characterized by localized, irreversible dilation of the bronchi and bronchioles caused by destruction of the muscle and elastic tissue. Airway obstruction and impaired clearance of secretions is due to dilation, inflammation and failure of the involved bronchi[71].

The disorder often starts with bacterial colonization and infection of the bronchial mucous, which are commonly the causes of the chronic inflammatory process resulting in the destruction and dilation of the bronchial tree. Bacterial colonization is triggered by mucous secretions, which are retained due to disruption of the mucociliary clearance (mechanism against pulmonary infection). The symptoms of many patients having regular exacerbations are: an increase of sputum production with cough, increased dyspnea, raised temperature, increased wheezing, fatigue, deterioration in lung function, and radiological signs of infection[72]. Factors that would point out disease progression are frequent exacerbations, chronic colonization with *P. aeruginosa*, and confirmed systemic inflammation.

P. aeruginosa, which infects 25% of bronchiectasis patients[72], are related to acute exacerbations, poor quality of life, and greater deterioration of lung function leading to no hope of life expectancy.

Bronchiectasis may result from acquired and congenity causes. Acquired causes are more frequent and include recurrent pneumonia, tuberculosis, immunodeficiency, and different respiratory infections such as: pertussis, gram negative bacteria (*P. aeruginosa*, *H. influenza*), gram positive (*Streptococcus pneumonia*) and viruses (HIV, paramyxovirus, adenovirus, and flu). Congenity causes include infections that affect cilia motility (kartagener syndrome) or ion transport (CF).

It has been suggested that the increase in the number of bronchiectasis patients is caused by the greater longevity and the increase in chronic lung disorders. In Europe, bronchiectasis is common in patients with CF and patients with advanced COPD.

The treatment for bronchiectasis is mostly based on experiences gained from the treatment of COPD and CF. The treatment aims are: improving mucociliary clearance, treating infection, airway obstruction and chronic inflammation that leads to disease progression.

4.2.4. Chronic Granulomatous Disease

CGD is an inherited disorder caused by mutations in at least five different genes involved in the assembly and activation of the leukocyte nicotinamide dinucleotide phosphate (NADPH) oxidase enzyme, which oxidizes NADPH and reduces molecular oxygen to produce superoxide anions, reactive oxygen species (ROS)[73,74]. Phagocytes, neutrophils, and macrophages, require ROS production to kill bacterial and fungal microorganisms, which have been digested by phagocytosis. Consequently, phagocytes of CGD patients are unable to destroy ingested microorganisms through ROS, increasing the high risk of CGD patients to suffer severe bacterial and fungal infections and excessive inflammation.

The most frequent sites of infection are skin, lymph nodes, lung, and liver and the most common organisms persisting inside CGD neutrophils causing disease are: bacteria such as *B. cepacia* (necrotising pneumonia +/- sepsis), *Serratia marcescens* (sepsis +/- skin ulcers and osteomyelitis), *S. aureus* (lymphadenitis, liver abscess)*, Nocardia species* and fungi such as *Aspergillus* species (pneumonia +/- dissemination to brain and bone). Pathogens can also cause bacteremia and fungemia[75,76].

CGD affects about 1 in 200,000 people suffering from recurrent infections from the first year of life due to the decreased capacity of their immune system[75,77]. Early diagnosis is important to prevent severe life-threatening infections before they occur, subministrating prophylactic antibiotics and antimycotics. The improvements in bacterial and fungal treatments for CGD patients have increased the average age of survival, most of them reaching adulhood. Interferon-gamma is a drug for prevention of infection in CGD patients, showing a 70% of reduction in infections and a decrease in the severity of the disease. It has the ability to give CGD patients more immune function and improve the microbicidal function. This therapy has been a standard treatment for CGD for several years.

4.2.5. Cystic Fibrosis

Cystic fibrosis is a recessive inheritance disease that affects the body's ability to transport salt and water across epithelial surfaces in the gastrointestinal and hepatobiliary systems, respiratory tract, reproductive system and sweat glands. The disease is caused by genetic mutation in the CF transmembrane conductance regulator (CFTR) gene that encodes a protein that mainly functions as a chloride channel in exocrine epithelia[78,79]. The deficient chloride transport in CF cells causes dehydration of secretions with hyperviscous mucus and leads to pulmonary and gastrointestinal problems. Gastrointestinal symptoms include alterations in liver and defective secretion of pancreatic enzymes, which difficult the digestion and absorption of food nutrients causing intestinal malabsorption. Pulmonary problems caused by chronic airway obstruction include chronic inflammation, fibrosis, and recurrent and chronic infections with *P. aeruginosa*, *B. cepacia*, *S. aureus* and *H. influenza*.

The most common mutation in CF is ΔF508. The gene is missing three nucleotides that lead to a missing phenylalanine at position 508 of the encoded protein. This mutated protein fails to be delivered to the correct location in the cell and is generally destroyed by the proteasome. The small amount that does reach the correct location functions poorly. CF disease has a complex phenotype with variable disease severity and a broad clinical spectrum that reflects the complexity of the CF pathogenesis.

Cystic fibrosis affects 1 in 2500 live births among Caucasians[80] and 80,000 people worldwide. CF is the most common, life-shortening, genetic disorder in western societies and most of CF deaths are due to respiratory failure caused by chronic airway colonization and pulmonary failure, and bronchiectasis.

The main symptoms in the CF respiratory tract are cough, tachypnea and wheezing due to chronic bronchopulmonary infections. Mucus in the paranasal sinuses also cause blockage of the sinus passages, leading to infection and inflammation that can develop nasal polyps and increase breathing difficulties. Recurrent sinonasal (nasal passage and paranasal sinuses) polyps can occur in as many as 15 to 20% of CF patients.

CF respiratory phenotype is characterized by a cycle of mucus obstruction, infection and inflammation of airways that progressively damages the airway tissue leading to respiratory failure and death[81]. Many of these symptoms occur when bacteria that normally inhabit the thick mucus grow out of control and cause chronic bronchitis, pneumonia or promote bronchiectasis caused by recurrent exacerbations.

H. influenzae, *S. aureus*, and *P. aeruginosa* are the three most common organisms causing lung infections in CF patients and appear sequentially with age. Furthermore, *B.*

cepacia has an important repercussion on lung transplantation because of high transmissibility of particular strains. Pulmonary disease is the major cause of morbidity and mortality and the median age of survival is in the late 30s.

Inhaled antibiotics are standard treatment for patients with CF who have been colonized with *P. aeruginosa*. Therefore, lung transplantation is a lifesaving procedure for many patients with CF.

REFERENCES

1 Group, R. I. D. C. (2007).

2 in *Institute for health metrics and evaluation* (ed University of Washington) (2013).

3 Kotsimbos, T. & McCormack, J. Respiratory infectious disease: complacency with empiricism in the age of molecular science. We can do better! *Internal medicine journal* **37**, 432-435, doi:10.1111/j.1445-5994.2007.01424.x (2007).

4 Boucher, H. W. *et al.* Bad bugs, no drugs: no ESKAPE! An update from the Infectious Diseases Society of America. *Clin Infect Dis* **48**, 1-12, doi:10.1086/595011 (2009).

5 Clatworthy, A. E., Pierson, E. & Hung, D. T. Targeting virulence: a new paradigm for antimicrobial therapy. *Nat Chem Biol* **3**, 541-548, doi:10.1038/nchembio.2007.24 (2007).

6 Linares, J. F., Gustafsson, I., Baquero, F. & Martinez, J. L. Antibiotics as intermicrobial signaling agents instead of weapons. *Proc Natl Acad Sci U S A* **103**, 19484-19489, doi:10.1073/pnas.0608949103 (2006).

7 Rice, L. B. Federal funding for the study of antimicrobial resistance in nosocomial pathogens: no ESKAPE. *J Infect Dis* **197**, 1079-1081, doi:10.1086/533452 (2008).

8 Pendleton, J. N., Gorman, S. P. & Gilmore, B. F. Clinical relevance of the ESKAPE pathogens. *Expert review of anti-infective therapy* **11**, 297-308, doi:10.1586/eri.13.12 (2013).

9 Potera, C. Forging a link between biofilms and disease. *Science* **283**, 1837, 1839 (1999).

10 Taubes, G. The bacteria fight back. *Science* **321**, 356-361, doi:10.1126/science.321.5887.356 (2008).

11 Payne, D. J. Microbiology. Desperately seeking new antibiotics. *Science* **321**, 1644-1645, doi:10.1126/science.1164586 (2008).

12 Nordlund, P. & Reichard, P. Ribonucleotide reductases. *Annual review of biochemistry* **75**, 681-706, doi:10.1146/annurev.biochem.75.103004.142443 (2006).

13 Eklund, H., Uhlin, U., Farnegardh, M., Logan, D. T. & Nordlund, P. Structure and function of the radical enzyme ribonucleotide reductase. *Progress in biophysics and molecular biology* **77**, 177-268 (2001).

14 Jordan, A. & Reichard, P. Ribonucleotide reductases. *Annual review of biochemistry* **67**, 71-98, doi:10.1146/annurev.biochem.67.1.71 (1998).

15 Uhlin, U. & Eklund, H. Structure of ribonucleotide reductase protein R1. *Nature* **370**, 533-539, doi:10.1038/370533a0 (1994).

16 Logan, D. T., Andersson, J., Sjoberg, B. M. & Nordlund, P. A glycyl radical site in the crystal structure of a class III ribonucleotide reductase. *Science* **283**, 1499-1504 (1999).

17 Sintchak, M. D., Arjara, G., Kellogg, B. A., Stubbe, J. & Drennan, C. L. The crystal structure of class II ribonucleotide reductase reveals how an allosterically regulated monomer mimics a dimer. *Nature structural biology* **9**, 293-300, doi:10.1038/nsb774 (2002).

18 Aravind, L., Wolf, Y. I. & Koonin, E. V. The ATP-cone: an evolutionarily mobile, ATP-binding regulatory domain. *Journal of molecular microbiology and biotechnology* **2**, 191-194 (2000).

19 Reichard, P. Ribonucleotide reductases: the evolution of allosteric regulation. *Arch Biochem Biophys* **397**, 149-155, doi:10.1006/abbi.2001.2637 (2002).

20 Jordan, A., Aslund, F., Pontis, E., Reichard, P. & Holmgren, A. Characterization of Escherichia coli NrdH. A glutaredoxin-like protein with a thioredoxin-like activity profile. *J Biol Chem* **272**, 18044-18050 (1997).

21 Torrents, E. S., M.; Sjöberg, B.-M. *Ribonucelotide Reductase*. (Nova Science Publishers, Inc., 2008).

22 Torrents, E., Aloy, P., Gibert, I. & Rodriguez-Trelles, F. Ribonucleotide reductases: divergent evolution of an ancient enzyme. *Journal of molecular evolution* **55**, 138-152, doi:10.1007/s00239-002-2311-7 (2002).

23 Tamarit, J., Mulliez, E., Meier, C., Trautwein, A. & Fontecave, M. The anaerobic ribonucleotide reductase from Escherichia coli. The small protein is an activating enzyme containing a [4fe-4s](2+) center. *J Biol Chem* **274**, 31291-31296 (1999).

24 Eliasson, R. *et al.* The anaerobic ribonucleoside triphosphate reductase from Escherichia coli requires S-adenosylmethionine as a cofactor. *Proc Natl Acad Sci U S A* **87**, 3314-3318 (1990).

25 Nocentini, G. Ribonucleotide reductase inhibitors: new strategies for cancer chemotherapy. *Crit Rev Oncol Hematol* **22**, 89-126 (1996).

26 Mayhew, C. N., Phillips, J. D., Cibull, M. L., Elford, H. L. & Gallicchio, V. S. Short-term treatment with novel ribonucleotide reductase inhibitors Trimidox and Didox reverses late-stage murine retrovirus-induced lymphoproliferative disease with less bone marrow toxicity than hydroxyurea. *Antiviral chemistry & chemotherapy* **13**, 305-314 (2002).

27 Tsimberidou, A. M., Alvarado, Y. & Giles, F. J. Evolving role of ribonucleoside reductase inhibitors in hematologic malignancies. *Expert review of anticancer therapy* **2**, 437-448, doi:10.1586/14737140.2.4.437 (2002).

28 Torrents, E., Sahlin, M., Biglino, D., Graslund, A. & Sjoberg, B. M. Efficient growth inhibition of Bacillus anthracis by knocking out the ribonucleotide reductase tyrosyl radical. *Proc Natl Acad Sci U S A* **102**, 17946-17951, doi:10.1073/pnas.0506410102 (2005).

29 Atamna, H., Paler-Martinez, A. & Ames, B. N. N-t-butyl hydroxylamine, a hydrolysis product of alpha-phenyl-N-t-butyl nitrone, is more potent in delaying senescence in human lung fibroblasts. *J Biol Chem* **275**, 6741-6748 (2000).

30 Jordan, A. *et al.* Ribonucleotide reduction in Pseudomonas species: simultaneous presence of active enzymes from different classes. *J Bacteriol* **181**, 3974-3980 (1999).

31 Stowe, S. D. *et al.* Anti-biofilm compounds derived from marine sponges. *Marine drugs* **9**, 2010-2035, doi:10.3390/md9102010 (2011).

32 Soto, S. M. Role of efflux pumps in the antibiotic resistance of bacteria embedded in a biofilm. *Virulence* **4**, 223-229, doi:10.4161/viru.23724 (2013).

33 Garnett, J. A. & Matthews, S. Interactions in bacterial biofilm development: a structural perspective. *Current protein & peptide science* **13**, 739-755 (2012).

34 Costerton, J. W. Introduction to biofilm. *Int J Antimicrob Agents* **11**, 217-221; discussion 237-219 (1999).

35 Costerton, J. W., Stewart, P. S. & Greenberg, E. P. Bacterial biofilms: a common cause of persistent infections. *Science* **284**, 1318-1322 (1999).

36 Fux, C. A., Stoodley, P., Hall-Stoodley, L. & Costerton, J. W. Bacterial biofilms: a diagnostic and therapeutic challenge. *Expert review of anti-infective therapy* **1**, 667-683 (2003).

37 Jayaraman, A. & Wood, T. K. Bacterial quorum sensing: signals, circuits, and implications for biofilms and disease. *Annual review of biomedical engineering* **10**, 145-167, doi:10.1146/annurev.bioeng.10.061807.160536 (2008).

38 Blazquez, J. Hypermutation as a factor contributing to the acquisition of antimicrobial resistance. *Clin Infect Dis* **37**, 1201-1209, doi:10.1086/378810 (2003).

39 Anderl, J. N., Franklin, M. J. & Stewart, P. S. Role of antibiotic penetration limitation in Klebsiella pneumoniae biofilm resistance to ampicillin and ciprofloxacin. *Antimicrob Agents Chemother* **44**, 1818-1824 (2000).

40 Anderl, J. N., Zahller, J., Roe, F. & Stewart, P. S. Role of nutrient limitation and stationary-phase existence in Klebsiella pneumoniae biofilm resistance to ampicillin and ciprofloxacin. *Antimicrob Agents Chemother* **47**, 1251-1256 (2003).

41 Borriello, G. *et al.* Oxygen limitation contributes to antibiotic tolerance of Pseudomonas aeruginosa in biofilms. *Antimicrob Agents Chemother* **48**, 2659-2664, doi:10.1128/AAC.48.7.2659-2664.2004 (2004).

42 Brooun, A., Liu, S. & Lewis, K. A dose-response study of antibiotic resistance in Pseudomonas aeruginosa biofilms. *Antimicrob Agents Chemother* **44**, 640-646 (2000).

43 Gilbert, P., Allison, D. G. & McBain, A. J. Biofilms in vitro and in vivo: do singular mechanisms imply cross-resistance? *J Appl Microbiol* **92 Suppl**, 98S-110S (2002).

44 Lewis, K. Persister cells, dormancy and infectious disease. *Nature reviews. Microbiology* **5**, 48-56, doi:10.1038/nrmicro1557 (2007).

45 Allison, K. R., Brynildsen, M. P. & Collins, J. J. Heterogeneous bacterial persisters and engineering approaches to eliminate them. *Current opinion in microbiology* **14**, 593-598, doi:10.1016/j.mib.2011.09.002 (2011).

46 de Lorenzo, V. Pseudomonas entering the post-genomic era. *Environmental microbiology* **2**, 349-354 (2000).

47 Cross, A. *et al.* Nosocomial infections due to Pseudomonas aeruginosa: review of recent trends. *Reviews of infectious diseases* **5 Suppl 5**, S837-845 (1983).

48 Mulcahy, L. R., Isabella, V. M. & Lewis, K. Pseudomonas aeruginosa Biofilms in Disease. *Microbial ecology*, doi:10.1007/s00248-013-0297-x (2013).

49 Adair, C. G. *et al.* Implications of endotracheal tube biofilm for ventilator-associated pneumonia. *Intensive care medicine* **25**, 1072-1076 (1999).

50 Gibson, R. L., Burns, J. L. & Ramsey, B. W. Pathophysiology and management of pulmonary infections in cystic fibrosis. *Am J Respir Crit Care Med* **168**, 918-951, doi:10.1164/rccm.200304-505SO (2003).

51 Murphy, T. F. *et al.* Pseudomonas aeruginosa in chronic obstructive pulmonary disease. *Am J Respir Crit Care Med* **177**, 853-860, doi:10.1164/rccm.200709-1413OC (2008).

52 Hancock, R. E. Resistance mechanisms in Pseudomonas aeruginosa and other nonfermentative gram-negative bacteria. *Clin Infect Dis* **27 Suppl 1**, S93-99 (1998).

53 Ganesan, S. & Sajjan, U. S. Host evasion by Burkholderia cenocepacia. *Frontiers in cellular and infection microbiology* **1**, 25, doi:10.3389/fcimb.2011.00025 (2011).

54 Otto, M. Staphylococcal biofilms. *Current topics in microbiology and immunology* **322**, 207-228 (2008).

55 Kurlenda, J. & Grinholc, M. Alternative therapies in Staphylococcus aureus diseases. *Acta Biochim Pol* **59**, 171-184 (2012).

56 Uchida, I., Hashimoto, K. & Terakado, N. Virulence and immunogenicity in experimental animals of Bacillus anthracis strains harbouring or lacking 110 MDa and 60 MDa plasmids. *Journal of general microbiology* **132**, 557-559 (1986).

57 Okinaka, R. T. *et al.* Sequence and organization of pXO1, the large Bacillus anthracis plasmid harboring the anthrax toxin genes. *J Bacteriol* **181**, 6509-6515 (1999).

58 Mikesell, P., Ivins, B. E., Ristroph, J. D. & Dreier, T. M. Evidence for plasmid-mediated toxin production in Bacillus anthracis. *Infect Immun* **39**, 371-376 (1983).

59 Barua, S. *et al.* The mechanism of Bacillus anthracis intracellular germination requires multiple and highly diverse genetic loci. *Infect Immun* **77**, 23-31, doi:10.1128/IAI.00801-08 (2009).

60 Friedlander, A. M. Tackling anthrax. *Nature* **414**, 160-161, doi:10.1038/35102660 (2001).

61 Sweeney, D. A., Hicks, C. W., Cui, X., Li, Y. & Eichacker, P. Q. Anthrax infection. *Am J Respir Crit Care Med* **184**, 1333-1341, doi:10.1164/rccm.201102-0209CI (2011).

62 Goldman, D. L. & Casadevall, A. Anthrax-associated shock. *Frontiers in bioscience : a journal and virtual library* **13**, 4009-4014 (2008).

63 Zakowska, D., Bartoszcze, M., Niemcewicz, M., Bielawska-Drozd, A. & Kocik, J. New aspects of the infection mechanisms of Bacillus anthracis. *Annals of agricultural and environmental medicine : AAEM* **19**, 613-618 (2012).

64 Beierlein, J. M. & Anderson, A. C. New developments in vaccines, inhibitors of anthrax toxins, and antibiotic therapeutics for Bacillus anthracis. *Curr Med Chem* **18**, 5083-5094 (2011).

65 Murphy, T. F., Bakaletz, L. O. & Smeesters, P. R. Microbial interactions in the respiratory tract. *The Pediatric infectious disease journal* **28**, S121-126, doi:10.1097/INF.0b013e3181b6d7ec (2009).

66 Bosch, A. A., Biesbroek, G., Trzcinski, K., Sanders, E. A. & Bogaert, D. Viral and bacterial interactions in the upper respiratory tract. *PLoS pathogens* **9**, e1003057, doi:10.1371/journal.ppat.1003057 (2013).

67 Papi, A. *et al.* Infections and airway inflammation in chronic obstructive pulmonary disease severe exacerbations. *Am J Respir Crit Care Med* **173**, 1114-1121, doi:10.1164/rccm.200506-859OC (2006).

68 Zhang, M. *et al.* Relevance of lower airway bacterial colonization, airway inflammation, and pulmonary function in the stable stage of chronic obstructive pulmonary disease. *Eur J Clin Microbiol Infect Dis* **29**, 1487-1493, doi:10.1007/s10096-010-1027-7 (2010).

69 Sethi, S. & Murphy, T. F. Infection in the pathogenesis and course of chronic obstructive pulmonary disease. *N Engl J Med* **359**, 2355-2365, doi:10.1056/NEJMra0800353 (2008).

70 Sethi, S., Maloney, J., Grove, L., Wrona, C. & Berenson, C. S. Airway inflammation and bronchial bacterial colonization in chronic obstructive pulmonary disease. *Am J Respir Crit Care Med* **173**, 991-998, doi:10.1164/rccm.200509-1525OC (2006).

71 Neves, P. C., Guerra, M., Ponce, P., Miranda, J. & Vouga, L. Non-cystic fibrosis bronchiectasis. *Interactive cardiovascular and thoracic surgery* **13**, 619-625, doi:10.1510/icvts.2011.284208 (2011).

72 Rademacher, J. & Welte, T. Bronchiectasis--diagnosis and treatment. *Deutsches Arzteblatt international* **108**, 809-815, doi:10.3238/arztebl.2011.0809 (2011).

73 Kang, E. M. *et al.* Chronic granulomatous disease: overview and hematopoietic stem cell transplantation. *J Allergy Clin Immunol* **127**, 1319-1326; quiz 1327-1318, doi:10.1016/j.jaci.2011.03.028 (2011).

74 Rieber, N., Hector, A., Kuijpers, T., Roos, D. & Hartl, D. Current concepts of hyperinflammation in chronic granulomatous disease. *Clinical & developmental immunology* **2012**, 252460, doi:10.1155/2012/252460 (2012).

75 Segal, B. H., Veys, P., Malech, H. & Cowan, M. J. Chronic granulomatous disease: lessons from a rare disorder. *Biol Blood Marrow Transplant* **17**, S123-131, doi:10.1016/j.bbmt.2010.09.008 (2011).

76 Seger, R. A. Chronic granulomatous disease: recent advances in pathophysiology and treatment. *The Netherlands journal of medicine* **68**, 334-340 (2010).

77 Winkelstein, J. A. *et al.* Chronic granulomatous disease. Report on a national registry of 368 patients. *Medicine* **79**, 155-169 (2000).

78 Kerem, B. *et al.* Identification of the cystic fibrosis gene: genetic analysis. *Science* **245**, 1073-1080 (1989).

79 Rommens, J. M. *et al.* Identification of the cystic fibrosis gene: chromosome walking and jumping. *Science* **245**, 1059-1065 (1989).

80 Cuthbert, A. W. New horizons in the treatment of cystic fibrosis. *Br J Pharmacol* **163**, 173-183, doi:10.1111/j.1476-5381.2010.01137.x (2011).

81 Lubamba, B., Dhooghe, B., Noel, S. & Leal, T. Cystic fibrosis: insight into CFTR pathophysiology and pharmacotherapy. *Clinical biochemistry* **45**, 1132-1144, doi:10.1016/j.clinbiochem.2012.05.034 (2012).

OBJECTIVES

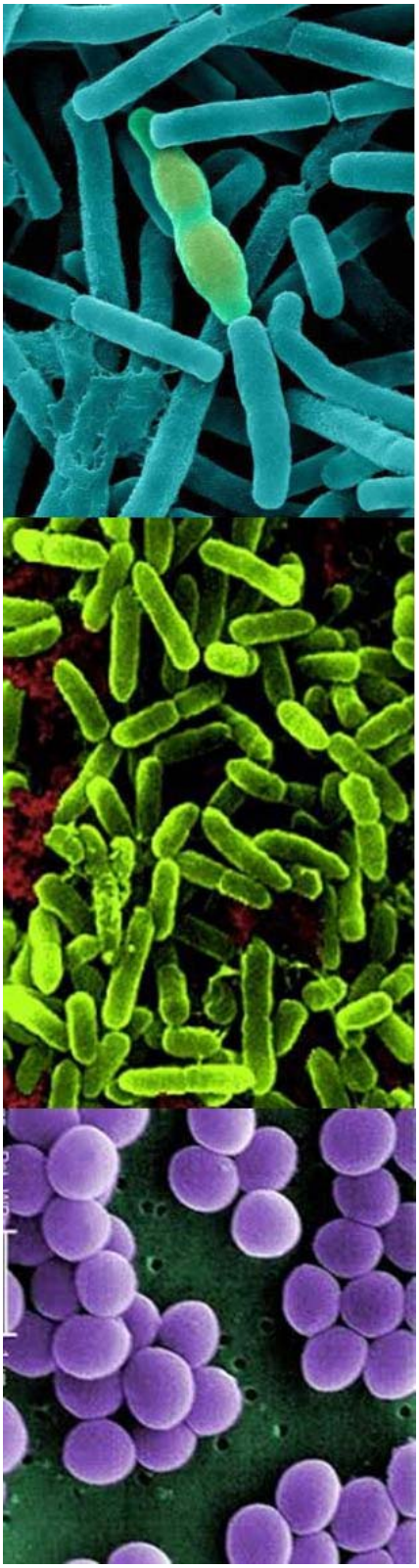

OBJECTIVES

Our group in collaboration with the group of Dr. Torrents leader of the bacterial infections and antimicrobial therapies of the Institute for Bioengineering of Catalonia (IBEC) focused our research in developing a hydroxamic acid and *N*-hydroxylamine-based library of potential drugs, which act as radical scavengers attacking the tyrosil radical in RNR enzyme.

Hydroxamic acids are structurally related to hydroxyurea (HU) that was the first antiproliferative drug used in the cancer treatment acting against RNR as a radical scavenger reducing the tyrosyl radical. Hydroxamic acids have diverse biological activities such as antibacterial, antifungal, antitumor, and anti-inflammatory properties. Therefore, Torrents *et al.* reported that hydroxylamine and *N*-methylhydroxylamine were inhibitors with a greater potential than HU[1]. Consequently, synthesis of hydroxamic acids and *N*-hydroxylamine derivatives was achieved to obtain novel compounds in order to improve antiproliferative properties against bacterial RNR enzyme.

The aim of the study is to find specific inhibitors for class I RNR of bacterial expression without affecting class Ia that is expressed in eukaryotic cells. These inhibitors, with antiproliferative activity against bacteria, could be used as a valuable therapeutic strategy in chronic respiratory infectious disease such as COPD, bronchiectasis, CGD, and CF, as well as immunodeficient patients and chronic wound patients.

The objectives of this chapter are:

1. To prepare a chemical library using several scaffolds based on hydroxamic acid and *N*-hydroxylamine derivatives.

2. To test the compounds in four different bacteria cell lines: *P. aeruginosa, S. aureus*, *B. cenocepacia* and *B. anthracis*, which are the four most common organisms causing opportunistic infections in patients suffering respiratory diseases.

RESULTS AND DISCUSSION

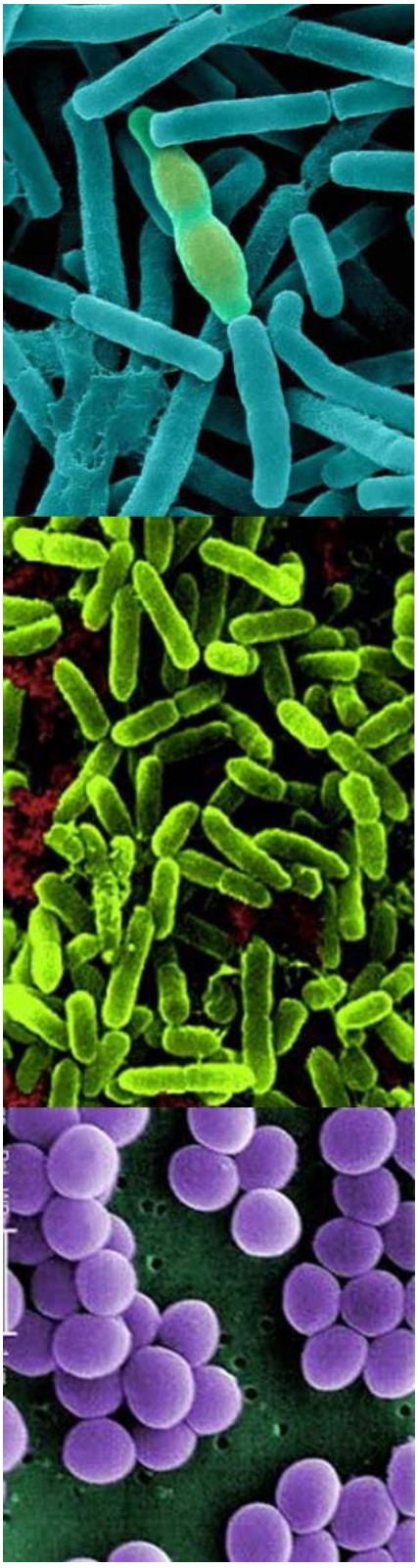

RESULTS AND DISCUSSION

1. Synthesis of hydroxamic acid derivatives in solid phase

Solid phase resin was used to synthesize hydroxamic acid derivatives, because it allows excess of reagents to drive reactions to completion. In addition to this, intermediate purifications steps are avoided and it is a fast method to produce a library of new compounds[2].

Mellor[3] reported a facile method for the production of *N*-Fmoc-aminooxy-2-chlorotrityl polystyrene. Incorporation of the *N*-Fmoc-hydroxylamine linker into 2-CTC is achieved through a nucleophilic attack of the hydroxyl group of the corresponding *N*-Fmoc-hydroxylamine in the presence of DIEA (2 eq) in dichloromethane by stirring for 48 h. Unreacted chloride sites were then "capped" by stirring with methanol (800 μL/g) for 30 minutes. 2-CTC is highly functionalised and has the distinct advantage of being cleaved by mild acidolysis to yield hydroxamic acids.

The loading of commercial 2-CTC is 1.6 mmol/g and it is recommended to work at 0.8 mmol/g to avoid aggregation problems. Thus, to achieve a loading of 0.8 mmol/g resin, 1.5 equivalents of *N*-Fmoc-hydroxylamine and 2 equivalents of DIEA were added. The reaction mixture was shaked for 48 h and then capped with methanol. In our hands, the resulting *N*-Fmoc-aminooxy-2-chlorotrityl resin exhibited a loading of 0.264 mmol/g instead of 0.8 mmol/g reported by Mellor. This value indicates that the introduction of the *N*-Fmoc-hydroxylamine linker was laborious.

Different conditions were tested to optimize the loading of the resin (Table 1). The equivalents of DIEA were increased from 2 to 10 to decrease the reaction time and increase the loading of the resin. The reaction mixture was shaked for 6, 24 and 48 h (Table 1, entry 2, 3 and 4) and the resin loadings were checked. Among all conditions, entry 4 was the best one, using 1.5 eq of *N*-Fmoc-hydroxylamine, 10 eq of DIEA and a reaction time of 48 h, giving a loading of 0.48. The same experiment was performed with 2 eq of *N*-Fmoc-hydroxylamine instead of 1.5 eq giving a resin loading with a slight increase over entry 4. The next step was to use a different base to achieve a better nucleophilic attack of the hydroxyl group of the corresponding *N*-Fmoc-hydroxylamine to the 2-CTC resin. Triethylamine (10 eq) was used instead of DIEA with 2 eq of *N*-Fmoc-hydroxylamine and the reaction was shaked for both 6 and 48 h giving a lowest resin loading compared to entry 5. Consequently, we decided to carry out the synthesis of hydroxamic acids following condition 5, which gave the best results (Table 1).

#	*N*-Fmoc-hydroxylamine	Base		Time	Loading (nnmol/g)
		DIEA	Et_3N		
1	1.5 eq	2 eq	-	48 h	0.26
2	1.5 eq	10 eq	-	6 h	0.11
3	1.5 eq	10 eq	-	24 h	0.46
4	1.5 eq	10 eq	-	48 h	0.48
5	2 eq	10 eq	-	48 h	0.49
6	2 eq	-	10 eq	6 h	0.01
7	2 eq	-	10 eq	48 h	0.25

Table 1. Tested conditions to optimize the loading of the *N*-Fmoc-hydroxylamine into the 2-CTC resin

Once the *N*-Fmoc-hydroxylamine linker was introduced to the resin Fmoc group removal was accomplished by treatment with piperidine/*N*,*N*-dimethylformamdide (DMF) 1:4 (v:v) (2 x 1 min; 2 x 5 min). The coupling of the protected amino acid (Fmoc-aa-OH) was accomplished using TBTU-HOAt-DIEA to form the amide bond. In all cases, using 3 eq. of amino acid, TBTU, HOAt, and 6 eq. of DIEA after one hour of treatment at room temperature, the Kaiser test revealed the absence of free primary amines. The next step was Fmoc-deprotection of the amino acid followed by acetylation (Scheme 1).

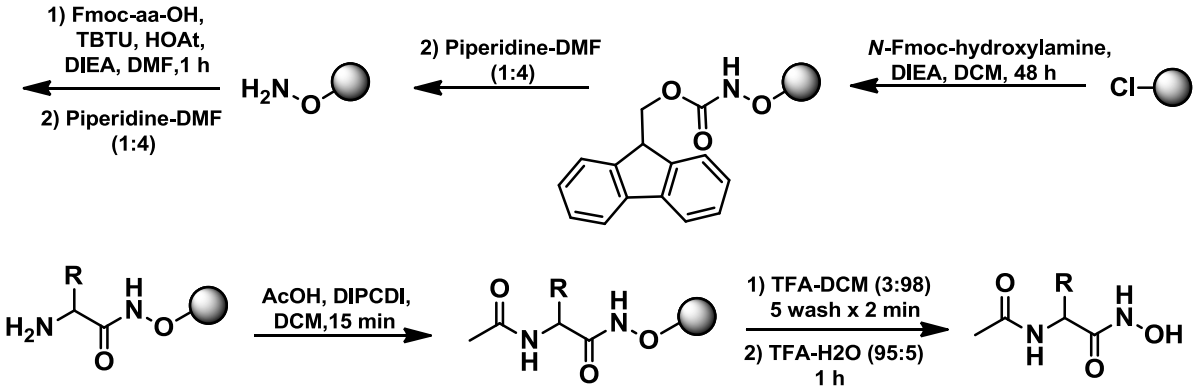

Scheme 1. Synthesis of hydroxamic acid derivatives

Acetylation was performed following a standard protocol of AcOH (6 eq) and DIPCDI (3 eq) in dichloromethane (DCM) for 15 minutes. The acid is activated with DIPCDI for 5 minutes to give the corresponding anhydride, with the formation of a white precipitate (urea), which is removed before adding the mixture into the resin (Scheme 1).

Once the hydroxamic acid derivative was fully assembled, it was cleaved from the resin by acidolytic treatment with a solution of DCM/TFA 97:3 (v:v) (5 x 2min). All the washes were collected in H_2O, which acts as scavenger to avoid side reactions, protecting the hydroxamic acid derivative from carbocations generated during cleavage from the side-chain protecting groups (Boc and ^tBu).

The DCM-TFA solution was evaporated, and finally, all the side-chain protecting groups were eliminated by treatment with TFA/H_2O 95:5 (v:v) for 1 h (Scheme 1). The TFA solution was evaporated, some acetonitrile (ACN) was added to dissolve the crude, and after checking its purity by HPLC-PDA and HPLC-MS analysis, the solution was lyophilized. The crude was purified by reversed-phase semi-preparative HPLC.

1.1. Synthesis of a small library of hydroxamic acid derivatives

A small library of hydroxamic acid derivatives was designed following one principle: different amino acids were introduced to obtain a diverse library with the same scaffold but with different side chain groups (Figure 5).

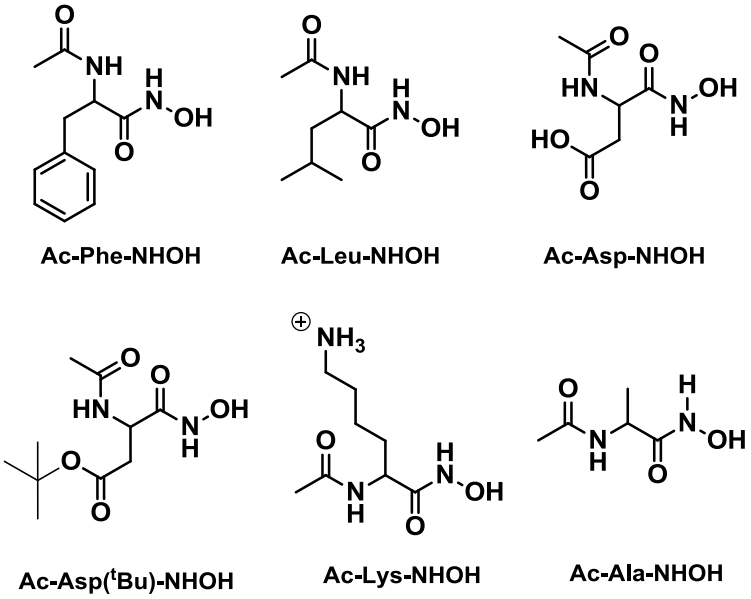

Figure 5. Small library of hydroxamic acid derivatives

The purification process was laborious due to the size and polarity of the compounds. After the acetylation step, secondary products were obtained, and it was really hard to separate them from the hydroxamic acids. The synthesis afforded the hydroxamic acid derivatives after reversed-phase semi-preparative HPLC purification in a very low yield (2%). For those reasons the solid phase strategy to synthesize hydroxamic acid derivatives was discarded, and the main focus was on the synthesis of *N*-hydroxylamine derivatives. However, two hydroxamic acid derivatives were tested against *B. anthracis* (See section 3 of results and discussion).

2. Synthesis of *N*-alkylhydroxylamines

2.1. Oxidation of primary amines to *N*-monoalkylhydroxylamines

The oxidation of an amine initially provides the corresponding amine oxide. If the amine is tertiary, the final product will be an oxide. However, the oxidation of primary and secondary amines gives the corresponding hydroxylamines, which still have a pair of *n* electrons that are vulnerable to further oxidation. For these reasons, the synthesis of *N*-alkylhydroxylamines from primary amines by direct oxidation is complicated due to overoxidation problems leading to nitroso and nitro compounds.

The synthesis of *N*-alkylhydroxylamines from primary amines has been reported in literature. These methods involve the oxidation of the amine with an appropriate oxidation reagent such as hydrogen peroxide, m-chloroperbenzoic acid (associated to overoxidation problems), dimethyldioxirane, oxone on silica or alumina support or benzoyl peroxide. The last method requires treatment of the *O*-benzylated hydroxylamine intermediate with base or acid to obtain the free hydroxylamine.

Several attempts were performed to accomplish the synthesis of *N*-alkylhydroxylamines.

2.1.1. Catalytic oxidation using urea hydrogen peroxide complex and sodium tungstate

Heydari et al.[4] reported that oxidation of primary amines to afford *N*-alkylhydroxylamines is accomplished using Na_2WO_4 in the presence of the urea hydrogen peroxide complex (UHP).

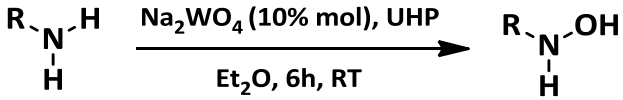

Scheme 2. Synthesis of *N*-alkylhydroxylamines using hydrogen peroxide and sodium tungstate

To a mixture of Na_2WO_4 (0.01 eq, 10 mol%) and UHP (1.2 eq) in ether, R-NH_2 (1 eq) was added and the reaction was stirred at room temperature for 6 h (Scheme 2). The resulting suspension was filtered through a pad of Celite, and the filtrate was concentrated under reduce pressure.

The above procedure was followed for three different primary amines (heptadecafluoroundecylamine, (4-fluorophenyl)methanamine, and 1-Boc-4-(aminomethyl) piperidine). However, it was not possible to obtain the desired *N*-alkylhydroxylamines (Table

2). Although the reaction was set up for both 6 h and overnight, only starting material (SM) was recovered in most of the cases. In entry 4 the starting material underwent overoxidation affording the nitroso compound. In the case of 1-Boc-4-(aminomethyl)piperidine, the equivalents of UHP were increase up to 1.5 and only starting material was recovered. All these products were checked by HPLC-PDA, HPLC-MS and ^{1}H-NMR analysis.

R-NH_2	#	UHP	Time	Obtained Product
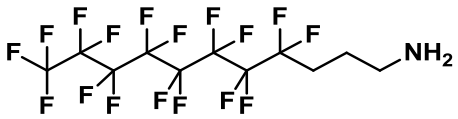 **Heptadecafluoroundecylamine**	1	1.2 eq	6 h	SM
	2	1.2 eq	overnight	SM
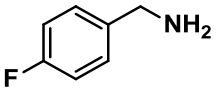 **(4-Fluorophenyl)methanamine**	3	1.2 eq	6 h	SM
	4	1.2 eq	overnight	R-N=O
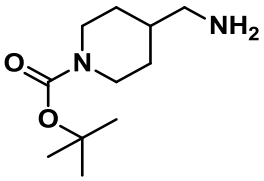 **1-Boc-4-(aminomethyl)piperidine**	5	1.5 eq	6 h	SM
	6	1.5 eq	overnight	SM

Table 2. Tested conditions to afford the oxidation of R-NH_2 using UHP and Na_2WO_4

None of the *N*-alkylhydroxylamines could be obtained using this method, so another procedure was selected to synthesize the desired compounds.

2.1.2. Oxidation using oxone

Oxone, consisting of a 2:1:1 mixture of $2KHSO_5 \cdot 1KHSO_4 \cdot 1K_2SO_4$, over silica gel oxidizes primary amines to the corresponding hydroxylamines. The reaction can be carried out either in the absence of solvent under microwave irradiation (Scheme 3 A) or in the presence of solvent (Scheme 3 B)[5].

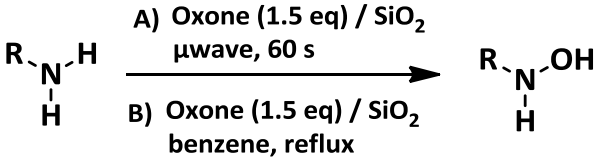

Scheme 3. Synthesis of *N*-alkylhydroxylamines using oxone

Initially, the standard solvent free procedure under microwave irradiation was used to save solvent and time. Silica gel (2.5 g) was equilibrated at 120 ºC for at least 48 h and then was allowed to cool to 25ºC. H_2O was added (0.5 mL) and the adsorbent was turned on a rotary evaporator at atmospheric pressure until uniformly free-flowing. The same protocol was followed for the amine (1 eq), and for oxone (1.5 eq), which were added to the adsorbent and tumbled until free-flowing. The resulting mixture was heated under microwave irradiation for 60 s and then allowed to cool to 25ºC. To release the *N*-alkylhydroxylamines from the silica gel, the mixture was stirred overnight with 100 mL of CH_3OH, filtrated, and concentrated under reduced pressure.

The oxidation of 1-Boc-4-(aminomethyl)piperidine was first attempted by using the free solvent oxidation procedure described above (Scheme 3 A). Even though the reaction was performed under microwave irradiation using several reaction times (from one up to 30 minutes) (Table 3), only starting material was recovered. These experiments were checked by HPLC-PDA and HPLC-MS analysis.

R-NH_2	#	Time	Obtained Product
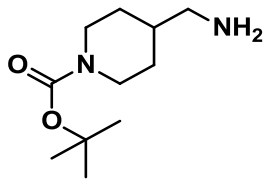 **1-Boc-4-(aminomethyl) piperidine**	**1**	1 min	SM
	2	2 min	SM
	3	5 min	SM
	4	30 min	SM

Table 3. Tested conditions to afford the oxidation of R-NH_2 using oxone and microwave irradiation

In a second attempt the standard procedure with solvent was tested[5]. A 2.5 g portion of the adsorbent was prepared as described above. A solution of the amine (1 eq) in benzene (6 mL) was added to the flask, followed by the addition of oxone (1.5 eq). The slurry was brought to reflux and stirred at 80 ºC for the required amount of time (TLC monitoring). After cooling, the slurry was diluted with 100 mL of CH_3OH, and stirred overnight at 25 ºC. The adsorbent was then removed by vacuum filtration and filtrates were concentrated under reduced pressure.

The standard procedure with solvent was performed with the primary amine 1-Boc-4-(aminomethyl)piperidine at 6, 24, and 48 h. The reaction did not work, and only starting material was recovered (Table 4, entry 1, 2 and 3). However, 2-(4-fluorophenyl)ethanamine and (4-fluorophenyl)methanamine were oxidized at 24 and 6 h, respectively, to give a mixture of oxidized products (Entry 4 and 5). Although the crudes were purified by flash

chromatography, it was not possible to separate them. All these products were checked by HPLC-PDA, HPLC-MS and ^{1}H NMR analysis (Table 4).

R-NH_2	#	Time	Obtained Product
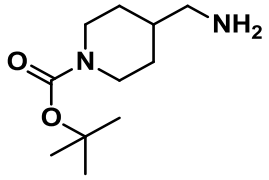 **1-Boc-4-(aminomethyl)piperidine**	1	6 h	SM
	2	24 h	SM
	3	48 h	SM
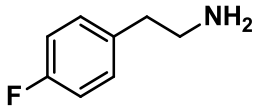 **2-(4-Fluorophenyl)ethanamine**	4	24 h	R-NHOH and R-NO_2
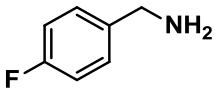 **(4-Fluorophenyl)methanamine**	5	6 h	SM, R-N=O and R-NHOH

Table 4. Tested conditions to afford the oxidation of R-NH_2 with oxone and benzene at 80 ºC

This methodology proved not to be effective for the synthesis of *N*-alkylhydroxylamines. Therefore, a biphasic system composed by H_2O and DCM, providing more solubility to oxone, was tested (Scheme 4). A solution of oxone (1 eq) in water was added to a solution of (4-fluorophenyl)methanamine (1 eq) in DCM. The resulting mixture was stirred at room temperature until TLC monitoring indicated complete consumption of the starting material. Next, the organic phase was extracted with DCM, dried ($MgSO_4$), filtered, and concentrated under reduced pressure. The crude product was analysed by HPLC-PDA, HPLC-MS and ^{1}H-NMR (Table 5).

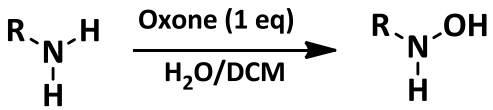

Scheme 4. Synthesis of *N*-alkylhydroxylamines using oxone and a biphasic system

The reaction was performed in a solution of H_2O/DCM 4:1 (v:v) for 1 h providing a mixture of starting material and oxidized products (Table 5, entry 1). In order to only obtain the desired compound, the volume ratio of the solvent mixture was changed to H_2O/DCM 4:3 (v:v). These conditions provided a complete conversion to the nitroso product (Entry 2). As a last attempt to optimize the reaction, the number of equivalents of oxone was

decreased. However, nitro and oxime products were also obtained (Entry 3). All the obtained products were checked by HPLC-PDA, HPLC-MS and ^{1}H NMR analysis.

R-NH_2	#	Oxone	Solvent	Time	Obtained Product
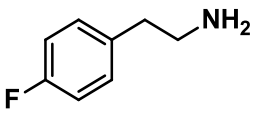 **2-(4-Fluorophenyl) ethanamine**	1	1 eq	H_2O/DCM 4:1 (v:v)	1 h	SM, R-NO_2 and R-NH-OH
	2	1 eq	H_2O/DCM 4:3 (v:v)	1 h	R-NO
	3	0.6 eq	H_2O/DCM 1:1.5 (v:v)	15 min	R-NO_2 and R-CH=N-OH

Table 5. Tested conditions to afford the oxidation of R-NH_2 using oxone with a solution of H_2O/DCM

These methodologies were discarded because of their inefficiency and low selectivity. A mixture of oxidized products was obtained in most of the cases. Moreover, flash chromatography purification turned out to be tedious resulting in low yields.

2.1.3. Oxidation using benzoyl peroxide

Primary amines react with diacyl peroxides such as benzoyl peroxide (BPO) to give *O*-acyl-*N*-alkylhydroxylamines, which upon hydrolysis provide the corresponding *N*-alkylhydroxylamines[6] (Scheme 5). However, this last method also leads to significant formation of the secondary product, *N*-benzoylated-*N*-alkylamine derivatives, as reported in the literature.

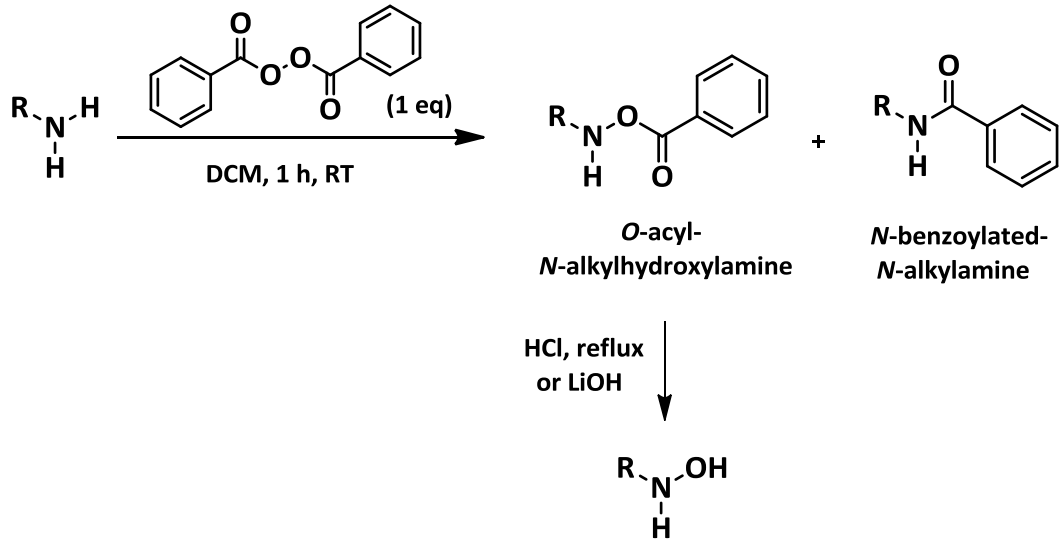

Scheme 5. Synthesis of *N*-alkylhydroxylamines using benzoyl peroxide

BPO (1 eq) was added to a solution of the amine (1 eq) in DCM, and the reaction mixture was stirred at room temperature for 1 h. TLC was used to monitor the consumption of starting material. Once the reaction was complete, the organic layer was washed with

$NaHCO_3$, dried over anhydrous $MgSO_4$, filtered, and concentrated to give the crude product, which was subjected to flash column chromatography.

The above procedure was carried out with (4-fluorophenyl)methanamine, and only the *N*-[2-(4-fluorophenyl)ethyl]benzamide was obtained, thus indicating that the reaction has an important and stable secondary product (Table 6, entry 1). The reaction was then performed under basic conditions, using a saturated aq K_2CO_3 solution. A solution of BPO (1 eq) in tetrahydrofuran (THF) was added to a solution of (4-fluorophenyl)methanamine (1 eq) and saturated aq K_2CO_3 solution 1:1 (v:v). Once the reaction was complete (TLC monitoring), THF was evaporated and DCM was added and extracted twice. The organic layers were combined, washed with a solution of aq HCl (2M), dried with $MgSO_4$, filtered, and evaporated under reduced pressure (Scheme 6).

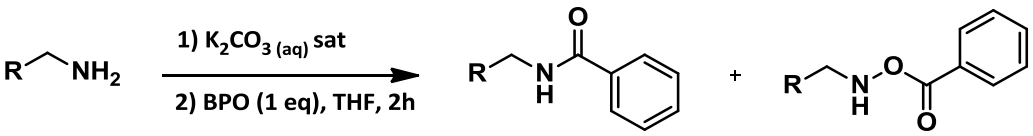

Scheme 6. Synthesis of *O*-acyl-*N*-alkylhydroxylamines using dibenzoyl peroxide in basic conditions

While using these new conditions, the *O*-benzoyl-N-(4-fluorophenethyl)hydroxylamine was obtained in low yields (Table 6, entry 2). In order to improve the yield of the product, the equivalents of BPO were reduced from 1 eq to 0.5, resulting in a slight increased yield from 7 up to 10% (Table 6, entry 3). The proportions of *O*-acyl-*N*-alkylhydroxylamine and *N*-benzoylated-*N*-alkylamine compounds were measured as the area percentatge on the UV chromatogram (λ = 220 nm) for each peak compared to the total area percentatge of the chromatogram (HPLC-PDA analysis). All the products were checked by HPLC-PDA and HPLC-MS analysis (Table 6).

R-NH_2	#	BPO	K_2CO_3	Solvent	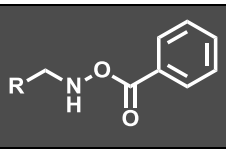	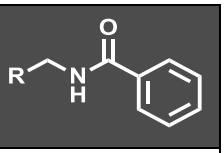
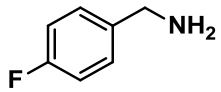 **(4-Fluorophenyl) methanamine**	1	1 eq	-	DCM	-	√
	2	1 eq	√	THF	7%	27.2 %
	3	0.5 eq	√	THF	10%	25.6 %

Table 6. Tested conditions to afford the oxidation of R-NH_2 with dibenzoyl peroxide

This reaction was set up for 4 different primary amines: 2-(4-fluorophenyl)ethanamine, (4-(trifluoromethyl)cyclohexyl)methanamine, 1-Boc-4-(aminomethyl)piperidine, and heptadecafluoroundecylamine. In all the cases the secondary products were obtained in higher yields than the desired products (Table 7). All the crude

products were purified by flash chromatography and checked by HPLC-PDA and HPLC-MS or ^{1}H NMR analysis.

R-NH_2	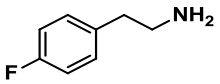 2-(4-Fluorophenyl) ethanamine	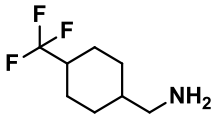 (4-(Trifluoromethyl) cyclohexyl)methanamine	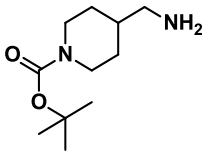 1-Boc-4-(aminomethyl) piperidine	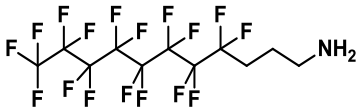 Heptadecafluoro undecylamine
Time	1.5 h	4 h	2 h	3 h
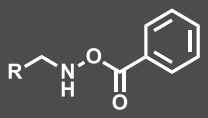	2.6 %	6.7 %	9.5 %	4 %
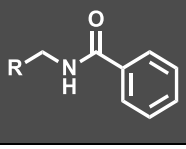	28.6 %	19.4 %	14 %	23.2 %

Table 7. Primary amines tested to afford the *O*-acyl-*N*-alkylhydroxylamines

As it is a common practical in the medicinal chemistry research, the secondary products (*N*-benzoylated-*N*-alkylamine compounds) of the above reaction were also introduced in the library and tested against four different bacterial cell lines (Table 8).

Compound	17	19
Structure	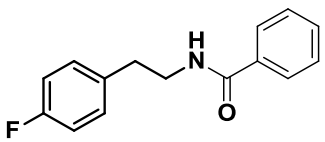	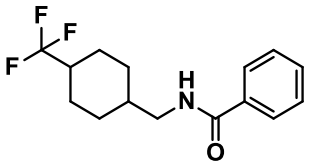
Name	*N*-[2-(4-Fluorophenyl) ethyl]benzamide	*N*-((4-(Trifluoromethyl) cyclohexyl)methyl)benzamide
Compound	**20**	**21**
Structure	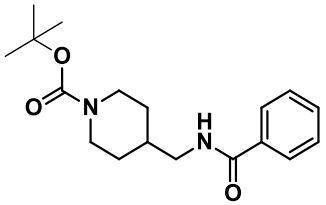	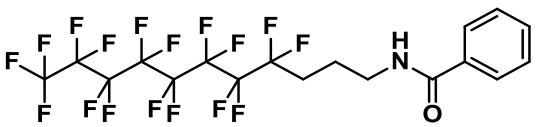
Name	*tert*-Butyl 4{[(phenylcarbonyl) amino]methyl}piperidine-1-carboxylate	*N*-(4,4,5,5,6,6,7,7,8,8,9,9,10,10,11,11,11-Heptadecafluoroundecyl)benzamide

Table 8. Secondary products included in the library.

Although the hydrolysis could have been performed with a small amount of *O*-acyl-*N*-alkylhydroxylamines intermediates, further optimization of the reaction was required.

2.1.3.1. Synthesis and optimization of *O*-acyl-*N*- alkylhydroxylamine intermediates

Different conditions using 2-(4-fluorophenyl)ethanamine were tested to optimize the yield of the reaction (Table 9). All the reactions were performed using 50 mg of starting material and monitored by HPLC-PDA (λ = 220 nm). The proportions of *O*-acyl-*N*-alkylhydroxylamine and *N*-benzoylated-*N*-alkylamine compounds were measured as the area percentage of each peak compared to the total area percentage of the chromatogram. The ratio is calculated as the percentage area of the desired product divided for the percentage area of the secondary product; the higher the ratio, the better results (Table 9).

As a first attempt to optimization, the reaction was performed using LiOH, a stronger base than K_2CO_3. A solution of BPO in THF was added to a mixture of 2-(4-fluorophenyl)ethanamine in an aq LiOH solution (2 M) (1:1) (v:v), providing a high conversion to the secondary product (Table 9, entry 1). Secondly, the reaction was performed at 66 ºC favouring the secondary product formation (Table 9, entry 2). Consequently, the reaction was carried out at low temperatures (4 ºC), and the ratio was slightly improved (Table 9, entry 3).

The effect of the solvent on the reaction yield was evaluated. The reaction was carried out at 4 ºC using different solvents such as isopropyl alcohol (IPA), DCM, ACN, and hexane using both neutral and basic conditions (by the addition of a saturated aq K_2CO_3 solution) (Table 9, entry 4-10). A mixture of a saturated aq K_2CO_3 solution and ACN turned out to be the best reaction condition. The use of basic conditions did not necessarily lead to a better yield as in the case of DCM and IPA. These results suggest that basic conditions are necessary at room temperature, and at low temperature (4ºC) the use of base depends on the solvent employed.

To optimize the desired product yield, the reaction was carried out at -80 ºC using DCM and hexane without basic conditions, resulting in low conversion (Table 9, entry 11 and 12). At this stage, the best result was provided by entry 8. Thus, ACN was used to perform the reaction at 4 ºC. The basic conditions were provided by an aq LiOH solution (2M) instead of K_2CO_3, affording only the *N*-[2-(4-fluorophenyl)ethyl]benzamide (Table 9, entry 13).

At this point of the optimization, the 2-(4-fluorophenyl)ethanamine with or without basic conditions (K_2CO_3) was added dropwise to the dibenzoyl peroxide in ACN (1:1) (v:v) at 4ºC, providing a highly conversion of the desired product (Table 9, entry 14 and 15).

Finally, a method reported by Phanstiel *et al*.[7], which describes how to prepare *O*-acyl-*N*-alkylhydroxilamines from primary amines under biphasic conditions in excellent yields, was carried out. A solution of BPO (1 eq) in DCM (5 mL/mmol BPO) was added quickly to a mixture of the amine (1 eq) in a pH 10.5 buffer solution (5 mL/mmol amine) at room temperature. The pH 10.5 buffer solution was prepared by combining 222 mL of 0.75 N aq $NaHCO_3$ and 70 mL of 1.5 N aq NaOH. After the reaction was complete (TLC monitoring) the aq layer was extracted twice with DCM. The organic layers were combined, dried over anhydrous $MgSO_4$, filtered and concentrated under reduced pressure. The reaction was accomplished with two variables: the temperature and the equivalents of BPO. The reaction was carried out following the above method using 1 and 0.5 eq of BPO and using both room temperature and 4 ºC, providing better results using 1 eq of BPO at 4ºC (Table 9, entry 16-19).

#	Base	Buffer	Solvent	BPO	T (ºC)	*O*-acylhydroxylamines	*N*-benzoylated	Ratio
1	LiOH	-	THF	0.5 eq	RT	0.8 %	15.3 %	0.05
2	K_2CO_3	-	THF	0.5 eq	66 ºC	10.2 %	26.4 %	0.39
3	K_2CO_3	-	THF	0.5 eq	4 ºC	35.7 %	46.2 %	0.77
4	K_2CO_3	-	IPA	0.5 eq	4 ºC	20.4 %	66.7%	0.31
5	-	-	IPA	0.5 eq	4 ºC	33.8 %	55.6 %	0.61
6	K_2CO_3	-	DCM	0.5 eq	4 ºC	32.4 %	45.7 %	0.71
7	-	-	DCM	0.5 eq	4 Cº	38.3 %	49.7 %	0.77
8	K_2CO_3	-	ACN	0.5 eq	4 ºC	36.6 %	40 %	0.92
9	-	-	ACN	0.5 eq	4 ºC	34.7 %	48 %	0.72
10	K_2CO_3	-	Hexane	0.5 eq	4 ºC	1.84 %	33.4 %	0.06
11	-	-	DCM	0.5 eq	-80 ºC	13.4%	35.3 %	0.38
12	-	-	Hexane	0.5 eq	-80 ºC	2.3 %	51.5 %	0.05
13	LiOH	-	ACN	0.5 eq	4 ºC	-	87 %	
14	K_2CO_3	-	ACN	0.5 eq	4 ºC	39.4 %	19.6 %	2
15	-	-	ACN	0.5 eq	4 ºC	32.3 %	17.8 %	1.82
16	-	pH 10.5	DCM	1 eq	RT	22.7 %	16.3 %	1.39
17	-	pH 10.5	DCM	0.5 eq	RT	41.1 %	35.6 %	1.16
18	-	pH 10.5	DCM	1 eq	4 ºC	24.2 %	13.7 %	1.76
19	-	pH 10.5	DCM	0.5 eq	4 ºC	26.8 %	21.7 %	1.25

Table 9. Tested conditions to optimize the formation of the *O*-benzoyl-*N*-(4-fluorophenethyl)hydroxylamine using BPO

Experiments # 14 and 18 provided the highest ratios using different methods and were used to scale up the reaction from 50 mg to 250 mg. This data was compared with the result from table 7, which was obtained before further optimization. The intermediate products were purified by flash chromatography (Table 10).

R-NH_2	#	Base	Buffer	Solvent	T ºC	Yield
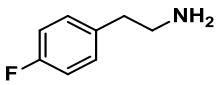 **2-(4-fluorophenyl) ethanamine**	1	K_2CO_3	-	THF	RT	2.6 %
	2	K_2CO_3	-	ACN	4 ºC	15.3 %
	3	-	pH 10.5	DCM	4 ºC	17.3 %

Table 10. Optimized conditions to improve the yield of *O*-benzoyl-*N*-(4-fluorophenethyl)hydroxylamine

In condition 1, the reaction was performed using a saturated aq K_2CO_3 solution in THF (1:1) (v:v) at room temperature resulting in a yield of 2.6 % yields. After optimization steps, the best result was accomplished using saturated aq K_2CO_3 solution in ACN (1:1) (v:v) at 4 ºC providing a 15.3 % yield. Finally, the last method using a buffer of pH 10.5 with DCM at 4 ºC turned out to be the best result providing a 17.3 % yield.

Although the benzoyl peroxide optimized method could not afford good yields of the desired product because of the favourable formation of the secondary product, the hydrolysis of the *O*-acyl-*N*-hydroxylamines was carried out.

2.1.3.2 Hydrolysis of the O-acyl-N-alkylhydroxylamines

Once the synthesis of the *O*-acyl-*N*-alkylhydroxylamines intermediates is accomplished, their hydrolysis provides the corresponding *N*-alkylhydroxylamines[6]. The hydrolysis can be achieved by using either acid or basic conditions (Scheme 7).

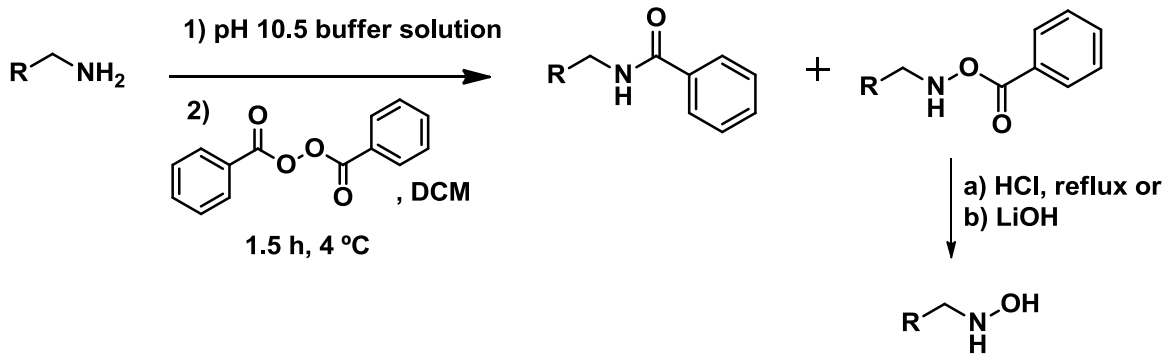

Scheme 7. Synthesis of *N*-alkylhydroxylamnies using dibenzoyl peroxide followed by hydrolysis

Firstly, the hydrolysis of three *O*-acyl-*N*-alkylhydroxylamines intermediates was carried out with aq 37% HCl in THF. The mixture was stirred for 4 h and only starting material was identified. Thus, the reaction was brought to reflux at 100 ºC and stirred for the

required amount of time (TLC monitoring). After the reaction was complete, it was neutralized with an aq NaOH solution (2M) until pH 8 and THF was evaporated under reduced pressure. DCM was then added and extracted twice, combined, and washed with saturated aq $NaHCO_3$ solution. The organic layer was dried ($MgSO_4$), filtered and concentrated by rotary evaporation. Although a mixture of products was observed when the crude products were analysed by HPLC-PDA and HPLC-MS, ^{1}H-NMR analysis showed only one compound (4-chlorobutan-1-ol). This product was produced by the opening of the THF solvent due to the addition of the Cl^- from the HCl (Table 11, entry 1-3).

In order to overcome this problem, the hydrolysis was performed under acid conditions using isopropanol. Following the above procedure, the reaction was brought to reflux at 82.5 ºC and stirred for the required amount of time (TLC monitoring), and again a mixture of products was obtained (Table 11, entry 5).

On the basis of these results, a final attempt was performed by using acid conditions with DCM at room temperature. The reaction was set up overnight and the desired product was obtained. However, after purification by flash chromatography the *N*-hydroxylamine was obtained in a very low yield (Table 11, entry 6).

R-NH2	#	Hydrolysis		Solvent	T ºC	Time	Obtained Product
		HCl 37%	LiOH				
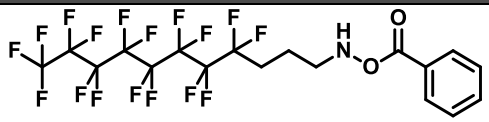 ***O*-benzoyl-*N*-(4,4,5,5,6,6,7,7,8,8,9,9,10,10,11,11,11-heptadecafluoroundecyl)hydroxylamine**	1	√	-	THF	100	4 h	4-chlorobutan-1-ol
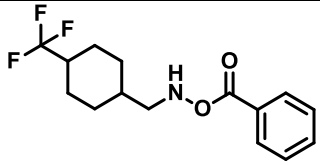 ***O*-benzoyl-*N*-((4-(trifluoromethyl) cyclohexyl)methyl)hydroxylamine**	2	√	-	THF	100	3 h	4-chlorobutan-1-ol
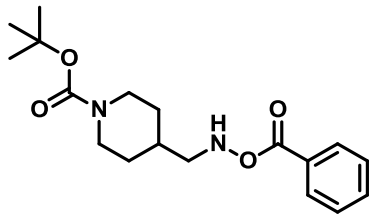 ***tert*-butyl 4-(((benzoyloxy)amino) methyl)piperidine-1-carboxylate**	3	√	-	THF	100	3 h	4-chlorobutan-1-ol
	4	-	√	H_2O/ THF	RT	2 h	Oxime and addition product

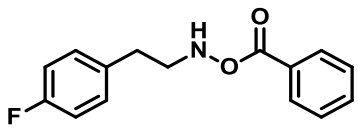 ***O*-benzoyl-*N*-(4-fluorophenetyl)hydroxylamine**	5	√	-	IPA	83	4 h	Mixture of products
	6	√	-	DCM	RT	over night	Product
	7	-	√	H_2O/ THF	RT	2 h	Hydroxylamine and addition product

Table 11. Tested conditions to perform the hydrolysis of the *O*-acyl-*N*-alkylhydroxylamines intermediates

Finally, the reaction was performed in basic conditions using an aq LiOH solution (2M) in THF 3:7 (v:v) for 2 h. After the reaction was complete, an aq 37% HCl solution was added until pH 8 and THF was evaporated under reduced pressure. DCM was then added and extracted twice, and the organic fractions were combined. The organic layer was washed with $NaHCO_3$, dried over anhydrous $MgSO_4$, filtered and concentrated by rotary evaporator (Table 11, entry 4 and 7). In entry 4 two products were obtained, one was the oxime compound and the other initially was not identified, and in entry 7 also two products were obtained, but only *N*-alkylhydroxylamine was identified. The analysis of the crude products by HPLC-PDA, HPLC-MS and ^{1}H-NMR suggested that the unidentified product was an *N*-hydroxyimidate (Scheme 8).

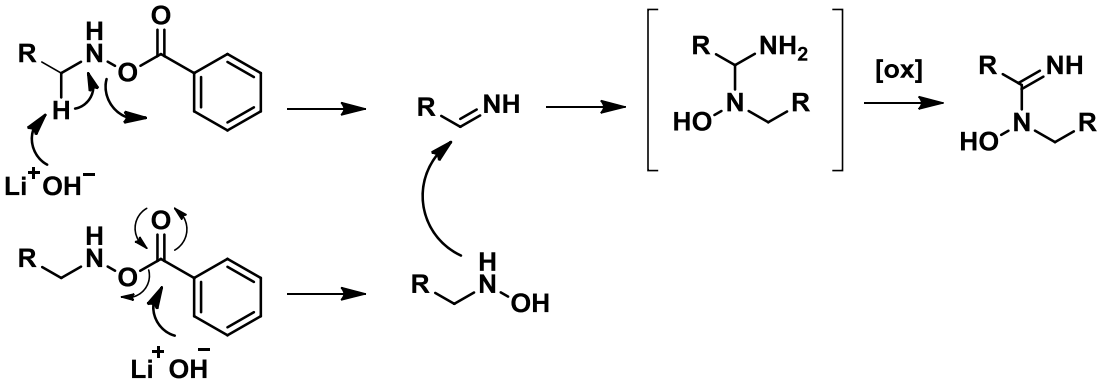

Scheme 8. Hydrolysis in basic conditions using LiOH

Hydrolysis in basic conditions using LiOH, which is a strong base, can provide two products: the desired *N*-alkylhydroxylamine and the imine product. We suggest that the *N*-alkylhydroxylamine acts as a nucleophile and attacks the carbon of the imine group giving an addition product that is oxidized to give *N*-hydroxyimidates.

2.2. Reductive amination of aldehydes to *N*-alkylhydroxylamines

The synthesis of *N*-hydroxylamines products can be accomplished by reductive amination that involves the conversion of a carbonyl group to an amine via an intermediate imine. An attractive method to synthesize mono *N*-alkylhydroxylamines has been reported by Heydari[8]; a general one-pot synthesis for mono *N*-alkylation of hydroxylamines. It has been described that the reaction works with aliphatic, aromatic and hetero-aromatic aldehydes, affording the expected products in good yields.

Treatment of R-aldehyde in 5.0 M LPDE solution with *O*-trimethylsilylhydroxylamine was stirred for 10 min and trimethylsilyl chloride was added. After stirring the mixture for 10 min borane/TEA complex was added and the reaction mixture was reacted for 1-2 h affording mono *N*-alkyl-*O*-trimethylsilylhydroxylamine in good yield (Scheme 9). The reaction was quenched with a saturated aq $NaHCO_3$ solution to obtain the mono *N*-alkylhydroxylamine and then extracted with DCM. The organic extracts were combined, dried ($MgSO_4$) and concentrated. Finally, the crude product was flash chromatographed (SiO_2).

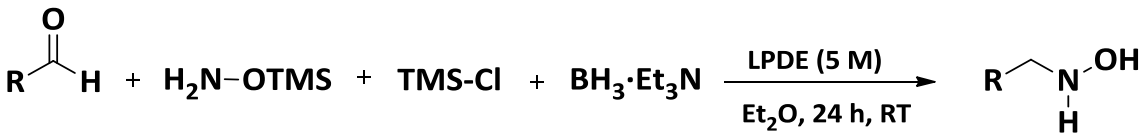

Scheme 9. Synthesis of N-alkylhydroxylamines by reductive amination of aldehydes

The above procedure was carried out with hexanal, and the resulting *N*-hydroxyhexan-1-amine was obtained in 2.3% yield instead of 83% yield as described by Heydari, indicating that the reductive amination of carbonyl group was difficult to achieve. Different conditions were tested to optimize the yield of the reaction (Table 12).

Firstly, the equivalents of the reagents H_2N-OTMS, TMSCl, $BH_3{\cdot}Et_3N$ were increased from 1.1 to 1.5 respect to the aldehyde (1 eq). That resulted in a slight increase in the yield over entry 1. Then, the reaction time was increased up to 3 h obtaining a 7.1 % yield, which is similar to entry 2. To ensure the formation of the protected oxime intermediate, the reaction time before adding the $BH_3{\cdot}Et_3N$ complex was increased up to 4h. That resulted in an improved yield of 19.3% (table 12, entry 4). The same experiment was performed increasing the time before adding $BH_3{\cdot}Et_3N$ up to 8 h and after adding the reductive reagent the reaction mixture was allowed to stir at room temperature overnight, resulting in the best yield (30.5%).

RCHO	#	H_2N-OTMS	TMSCl	Time	$BH_3{\cdot}Et_3N$	Time	Yield
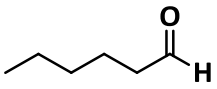 **Hexanal**	**1**	1.1 eq	1.1 eq	10 min	1.1 eq	1.5 h	2.3%
	2	1.5 eq	1.5 eq	10 min	1.5 eq	1.5 h	7.3%
	3	1.5 eq	1.5 eq	10 min	1.5 eq	3 h	7.1%
	4	1.5 eq	1.5 eq	4 h	1.5 eq	4 h	19.3%
	5	1.5 eq	1.5 eq	8h	1.5 eq	overnight	30.5%

Table 12. Yield optimization for mono *N*-alkylhydroxylamines

Consequently, the synthesis of mono *N*-alkylhydroxylamines was carried out following entry 5, which provided the best result (Table 12).

The purification process was laborious due to the size and the polarity of the compounds. In some cases it was extremely challenging to separate them from TEA requiring long gradients with slow increase of EtOAc, from 100% hexane to 100% EtOAc, and long silica columns.

2.2.1 Synthesis of *N*-alkylhydroxylamine library

A small library of mono *N*-alkylhydroxylamines was prepared to obtain novel compounds containing the –NHOH group, which is required to inhibit the RNR enzyme (Figure 2). Some members of this library were commercially available, such as *N*-*tert*-butylhydroxylamine, *N*-benzylhydroxylamine and *N*-cyclohexylhydroxylamine and were purchased from Sigma-Aldrich (Table 13).

When facing the synthesis of compounds 10 and 16 it was found that reduction of the oxime intermediate was not achieved under the reaction conditions. A strong conjugation effect between the aromatic ring and the double bond of the oxime would prevent its reduction. However, these two products, as well as the commercially available ethyl (2*Z*)-cyano(hydroxyimino)ethanoate, were also included in the library as it is a common practical in the medicinal chemistry research. For the same reason, *N,N*-diethylhydroxylamine, HOAt and HOBt, which are secondary instead of primary hydroxylamines, and *N*-hydroxybutyramide, an hydroxamic acid, were also purchased and included in the library (Table 13). These compounds will provide additional information about RNR enzyme. They will prove if oxime (R-HC=NOH), secondary hydroxylamines (RNR'OH) and hydroxamic acids (RCONHOH) compounds will be able to inhibit RNR enzyme, or in contrast the inhibitory activity towards RNR enzyme will be specific for primary hydroxylamines (R-NHOH).

Compound	1	2	3
Structure	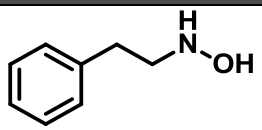	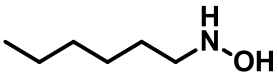	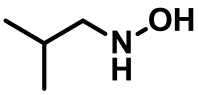
Name	*N*-Hydroxy-2-phenylethanamine	*N*-Hydroxyhexan-1-amine	*N*-Hydroxy-2-methylpropan-1-amine
Yield	45.6%	30.5%	14.8%
Compound	**4**	**5**	**6**
Structure	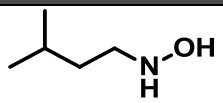	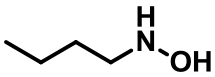	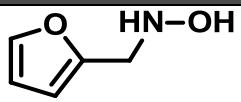
Name	*N*-Hydroxy-3-methylbutan-1-amine	*N*-Hydroxybutan-1-amine	1-Furan-2-yl-*N*-hydroxymethanamine
Yield	56.4%	28.2%	35.4%
Compound	**7**	**8**	**9**
Structure	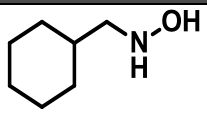	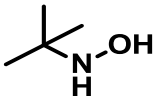	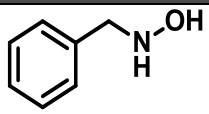
Name	*N*-(Cyclohexylmethyl) hydroxylamine	*N*-Hydroxy-2-methylpropan-2-amine	*N*-Hydroxy-1-phenylmethanamine
Yield	70.2%	Commercial	Commercial
Compound	**10**	**11**	**12**
Structure	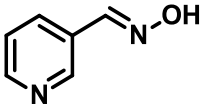	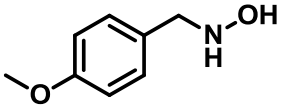	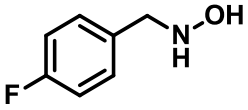
Name	Nicotinaldehyde oxime	*N*-(4-Methoxybenzyl) hydroxylamine	*N*-(4-Fluorobenzyl) hydroxylamine
Yield	20.5%	12.6%	42.4%
Compound	**13**	**14**	**15**
Structure	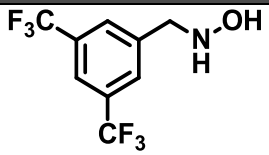	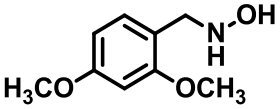	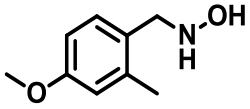
Name	*N*-[3,5-Bis(trifluoromethyl) benzyl]hydroxylamine	*N*-(2,4-Dimethoxybenzyl) hydroxylamine	*N*-(4-Methoxy-2-methylbenzyl)hydroxylamine
Yield	26.4%	22.0%	32.8%

Compound	16	23	24
Structure	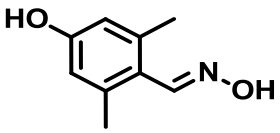	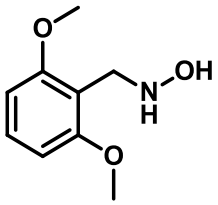	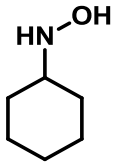
Name	4-Hydroxy-2,6-dimethylbenzaldehyde oxime	*N*-(2,6-Dimethoxybenzyl) hydroxylamine	*N*-Hydroxycyclohexanamine
Yield	25.8%	29.8%	Commercial
Compound	**25**	**26**	**27**
Structure	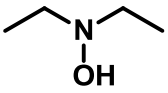	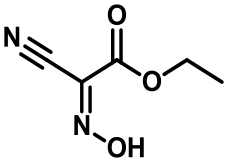	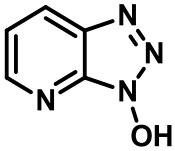
Name	*N,N*-Diethylhydroxylamine	Ethyl (2*Z*)-cyano (hydroxyimino)ethanoate	HOAt
Yield	Commercial	Commercial	Commercial
Compound	**28**	**29**	
Structure	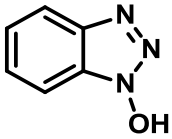	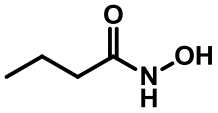	
Name	HOBt	*N*-hydroxybutyramide	
Yield	Commercial	Commercial	

Table 13. N-alkylhydroxylamines library and derivatives

The optimized synthesis afforded the *N*-alkylhydroxylamines and oxime products in a yield from 10% up to 70%. The products were confirmed by ^{1}H NMR, ^{13}C NMR, ^{19}F NMR. In all cases, the purity of the final product was above 95% after flash chromatographed (SiO_2).

N-Hydroxylamine (RNHOH), oxime (RHC=NOH), secondary hydroxylamine (RNR'OH), amides (RNHCOR') and hydroxamic acids (RCONHOH) compounds were tested against four bacterial cell lines by means of an inhibitory concentration (see section 3 of results and discussion).

3. Compounds activity

The biological testing was performed by the group of Eduard Torrents, leader of the bacterial infections and antimicrobial therapies of the Institute for Bioengineering of Catalonia (IBEC). The compounds were tested in four different bacteria cell lines: *P. aeruginosa, S. aureus*, *B. cepacia* and *B. anthracis*, which are the four most common organisms causing opportunistic infections in patients suffering respiratory disease.

3.1. Evaluation of the Minimum inhibitory concentration (MIC)

Minimal inhibitory concentration (MIC) assays were determined by a microtiter broth dilution method described by Cole et al.[9] and modified by Beckloff et al.[10]. The MIC was determined for each compound as the lowest concentration that completely inhibited bacterial growth.

3.1.1. Hydroxamic acid derivatives

B. anthracis was incubated with hydroxamic acid derivatives at different concentrations (0.1, 0.25, 0.5 and 1 mM) at 37 °C for 9 h at 150 rpm. Then, bacterial viability was quantified.

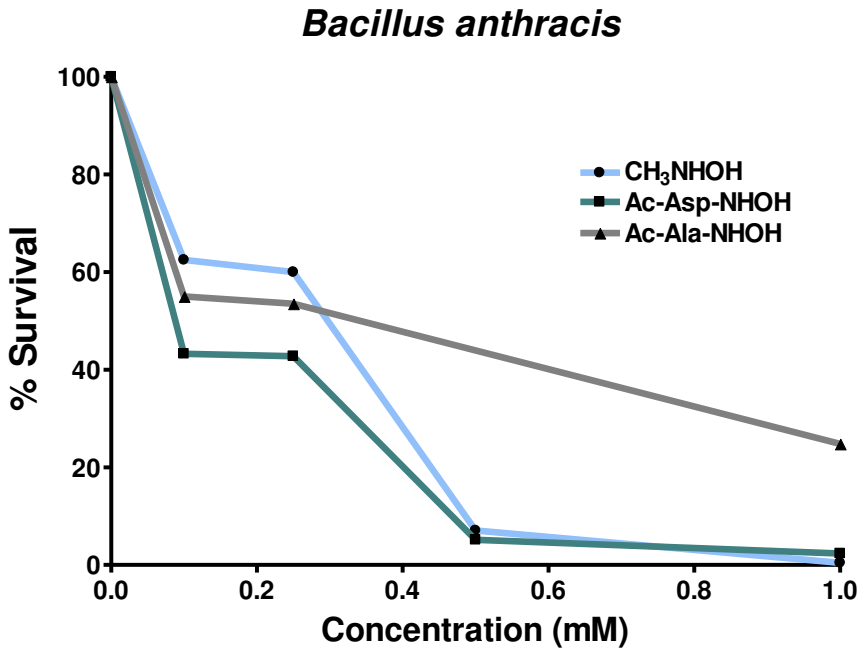

Figure 6. **Inhibitory capacity of two compounds in *B. anthracis* cell line growing in liquid culture**. Data represents mean value. One independent assay was performed per triplicate (n = 1).

N-Methylhydroxylamine was used as a positive control because Torrents *et al.* reported that it is a potential inhibitor against RNR enzyme[1]. Ac-Ala-NHOH compound was

not able to completely inhibit bacterial growth. However, Ac-Asp-NHOH compound inhibited bacterial growth at 0.5 mM, showing the same inhibitory capacity as *N*-Methylhydroxylamine. As it has been mentioned in section 1, we did not carry on the synthesis of hydroxamic acid derivatives due to purification problems and low yields.

3.1.2. *N*-Hydroxylamine, secondary hydroxylamine, oxime and amide compounds

Bacterial cell lines were incubated with the compounds at different concentrations (0.03125, 0.0625, 0.125, 0.25, 0.5, 1, 2 and 4 mM) at 37 °C for 9 h at 150 rpm. Then, bacterial viability was quantified (Table 14).

Compounds	1	2	3	4	5	6	7	8	9	10	11	12	13	14	15
Bacillus anthracis	<0.5	<0.5					<0.5					<0.12	<0.12	<0.25	<0.06
Staphylococcus aureus	<0.5						<0.5					<1	<0.5	<1	
Burkholderia cenocepacea															
Pseudomonas aeruginosa	<1						<0.14					<2	<2	<2	<2

Compounds	16	17	18	19	20	21	22	23	24	25	26	27	28	29	M-HA
Bacillus anthracis	<0.5			<0.25			-								0.25
Staphylococcus aureus	<1						-								<1
Burkholderia cenocepacea							-								-
Pseudomonas aeruginosa	<4						-								<0.5

Table 14. **Inhibitory activity of different compounds in four bacteria cell lines growing in liquid culture.** Data represents mean value. Three independent assays were performed per triplicate (n = 3).

Several promising drug candidates with antibacterial activity against respiratory infections were identified. The most promising ones are compound 1, 7, 12, 13, 14 and 16, all of them showing antiproliferative activity in *B. anthracis*, *S. aureus* and *P. aeruginosa*. Compound 15 showed activity against *B. anthracis* and *P. aeruginosa*. None of the synthesized compounds was active against *B. cenocepacia*. Almost all of the active compounds were *N-a*lkylhydroxylamines, except compound 16 that was an oxime. Neither secondary hydroxylamines nor amides turned out to be active. Thus, we conclude that primary hydroxylamines (R-NHOH) show the highest inhibitory activity towards RNR enzyme.

3.2 Evaluation of capacity to inhibit the formation of bacterial biofilms

To assess the overall cellular effect of the drug candidates with antibacterial activity on biofilms formation, bacterial cell lines were incubated with the compounds at different concentrations at 37 °C for 48 h without agitation. Then, bacterial biofilm formation was quantified.

P. aeruginosa, a Gram-negative bacterium, was treated with compounds 1, 7, 12 and 14 at different concentrations (0.03125, 0.0625, 0.125, 0.25, 0.5, 1, 2 and 4 mM) for 48 h without shaking at 37 °C (Figure 7).

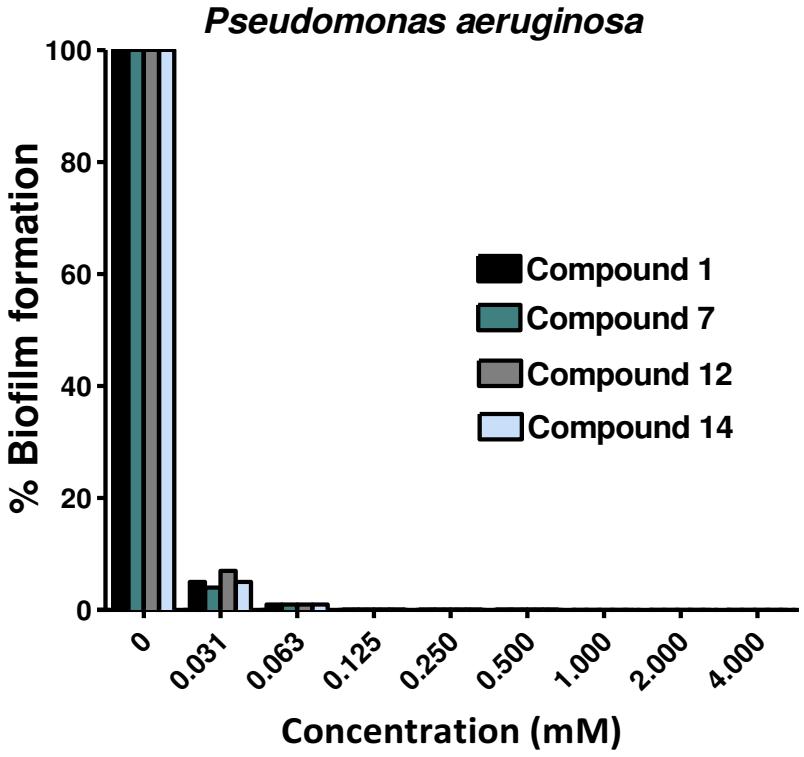

Figure 7. **Inhibitory capacity of biofilm formation by different compounds in *P. aeruginosa*.** Data represents mean value. One independent assays was performed per triplicate (n = 1).

All the compounds at 0.03125 mM inhibited by 95 % *P. aeruginosa* biofilm formation. The inhibition of the compounds at 0.0625 mM was 99 %, and at higher concentrations the inhibition was total.

Moreover, *S. aureus*, a Gram-positive bacterium, was treated with compounds 7, 12 and 14 at different concentrations (0.03125, 0.0625, 0.125, 0.25, 0.5, 1, 2 and 4 mM) for 48 h without shaking at 37 °C (Figure 8).

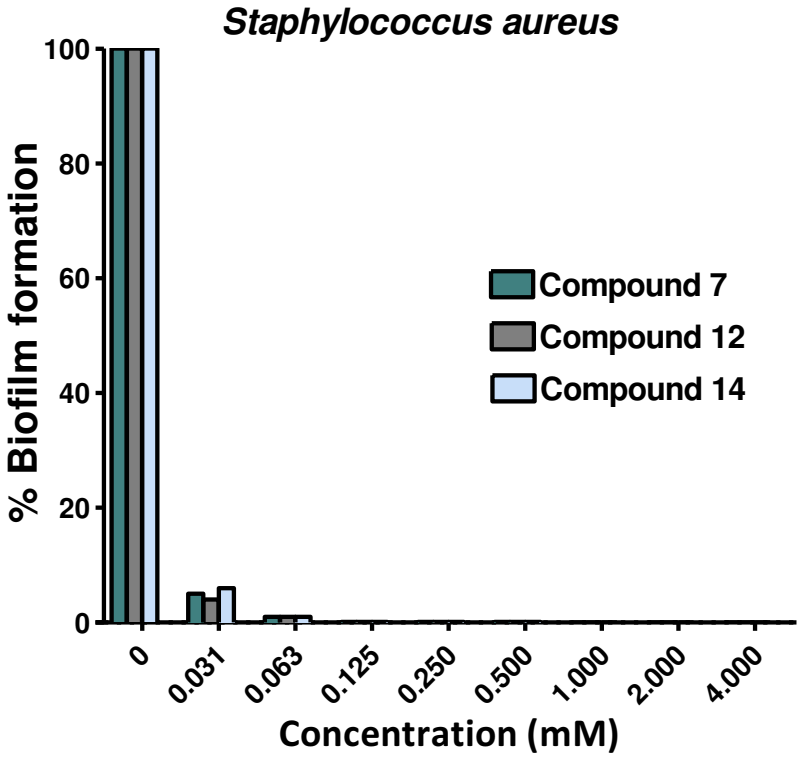

Figure 8. **Inhibitory capacity of biofilm formation by different compounds in *S. aureus***. Data represents mean value. One independent assays was performed per triplicate (n = 1).

All the compounds at 0.03125 mM inhibited by 95 % S*. aureus* biofilm formation. The inhibition of the compounds at 0.0625 mM was 99 %, and at higher concentrations the inhibition was total.

Compound 7, 12 and 14 showed the same antiproliferative activity in *P. aeruginosa* and *S. aureus* biofilm formation.

3.3. Evaluation of capacity to reduce already formed bacterial biofilms

Bacterial biofilms are formed at 37 °C for 24 h or 3 days without shaking. Then, different compound concentrations (0.03125, 0.0625, 0.125, 0.25, 0.5, 1, 2 and 4 mM) dissolved in medium were added to the already formed biofilms and were incubated at 37 °C for 24, 48 or 72 h. Each 24 h the medium of bacterial biofilms is renewed for new medium with compound. Finally, the reduction of the already formed biofilm was quantified.

P. aeruginosa biofilm was treated with compound 7 at different concentrations (0.03125, 0.0625, 0.125, 0.25, 0.5, 1, 2 and 4 mM) for two consecutive day treatment at 37 °C (Figure 9).

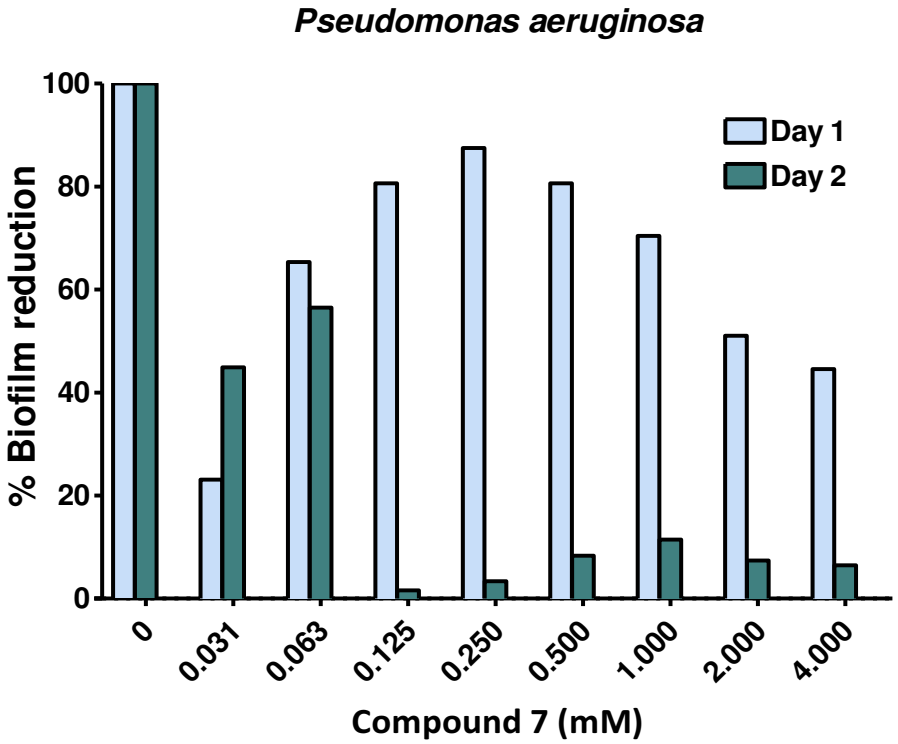

Figure 9. **Compound 7 inhibitory activity in formed *P.aeruginosa* biofilm.** Data represents mean value. One independent assays was performed per triplicate (n = 1).

Compound 7 at different concentrations was not able to inhibit formed biofilm the first day. However, the second day of incubation compound 7 at 0.125 mM was able to inhibit the formed *P. aeruginosa* biofilm. It is of interest to notice that at higher concentrations the inhibitory activity of compound 7 decreases, thus indicating that a consecutive day treatment is necessary to totally inhibit *P. aeruginosa* biofilm.

Furthermore, *S. aureus* biofilm was treated with compounds 7, 12 and 14 at different concentrations (0.03125, 0.0625, 0.125, 0.25, 0.5, 1, 2 and 4 mM) for 24 h at 37 °C (Figure 10).

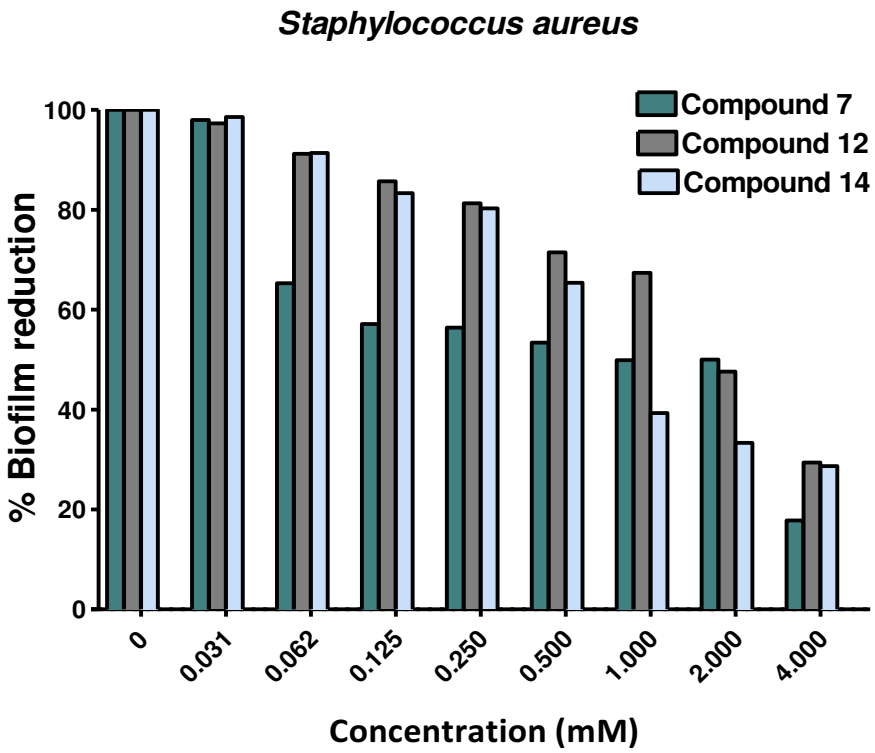

Figure 10. **Compounds 7, 12 and 14 inhibitory activity of already formed *S. aureus* biofilm.** Data represents mean value. Two independent assays were performed per triplicate (n = 2).

Compound 7 showed a higher *S. aureus* biofilm inhibitory activity than compound 12 and 14. The maximum inhibitory activity was achieved at 4 mM for all the compounds. The results obtained suggest that consecutive day treatment of the compounds is required to totally inhibit *S. aureus* biofilm.

Compound 1 was incubated at different concentrations (0.03125, 0.0625, 0.125, 0.25, 0.5, 1, 2 and 4 mM) for three consecutive day treatment at 37 °C with already *s. aureus* formed biofilm (Figure 11).

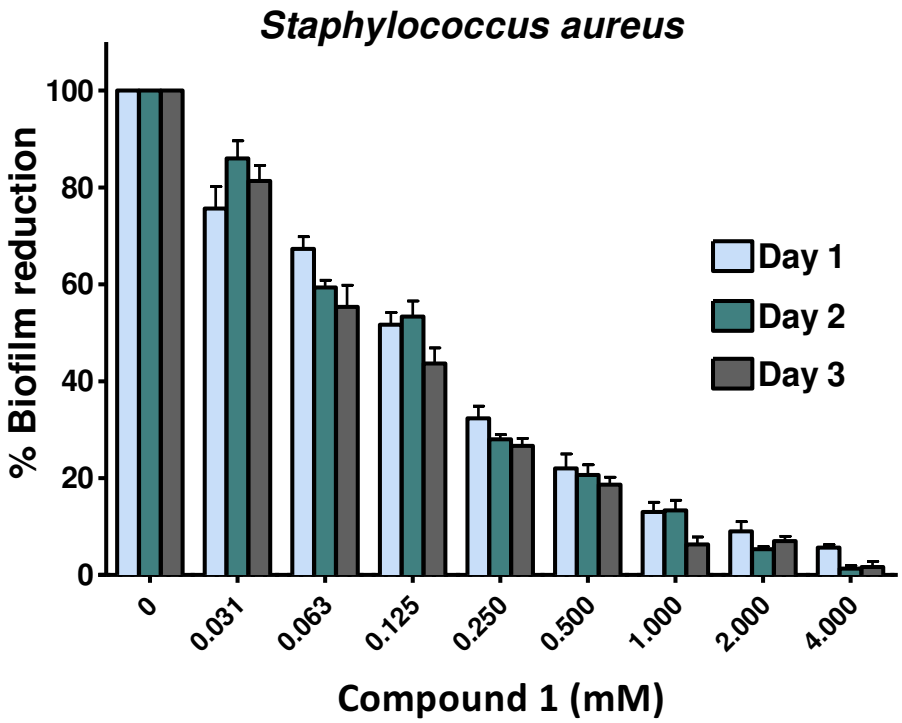

Figure 11. **Compound 1 inhibitory activity of already formed *S.aureus* biofilm.** Data represents mean ± SEM of one representative experiment. Two independent assays were performed per triplicate (n = 2).

Compound 1's activity to reduce already formed biofilm enhances as long as the incubation time and the concentration increases.

Compound 13 was incubated at different concentrations (0.03125, 0.0625, 0.125, 0.25, 0.5, 1, 2 and 4 mM) for three consecutive day treatment at 37 °C with already *S. aureus* formed biofilm (Figure 12).

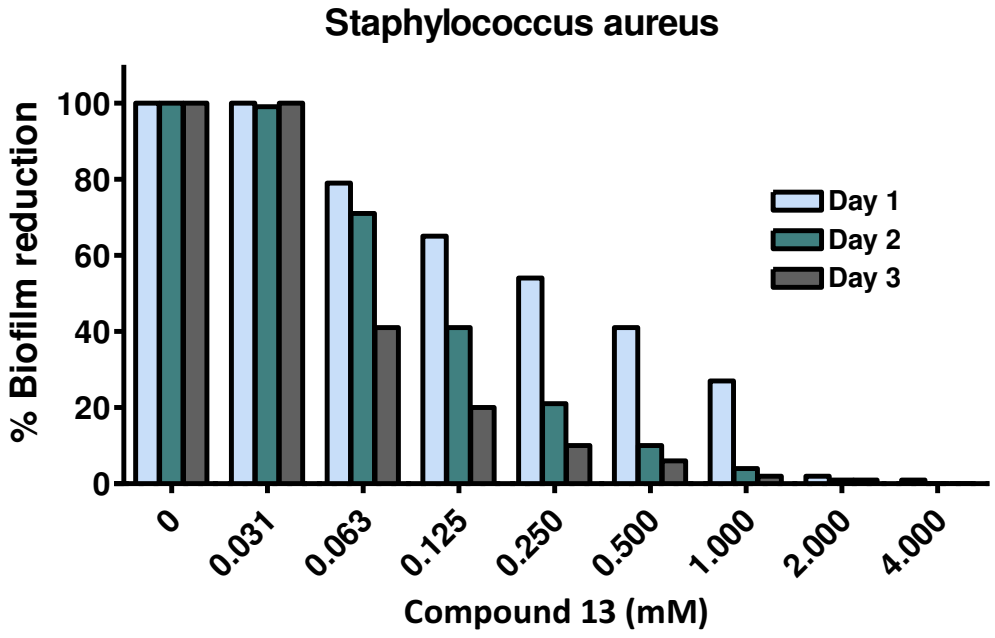

Figure 12. **Inhibitory capacity of already formed *S.aureus* biofilm by compounds 7, 12 and 14**. Data represents mean value. One independent assays was performed per triplicate (n = 1).

Compound 13's activity to reduce already formed biofilm enhances as long as the incubation time and the concentration increases. Moreover, compound 13 showed higher inhibitory *S. aureus* biofilm activity than compound 1.

On the basis of these results, one potential inhibitor against *P. aerugiona* biofilm (compound 7) and two potential inhibitors against *S. aureus* biofilm (compound 1 and 13) have been obtained. Moreover, we need to perform more consecutive day treatment experiments for compounds 7, 12, 14 and 16 in *S. aureus* biofilm, and for compound 1 in *P. aeruginosa* biofilm. These compounds showed antibacterial activity against respiratory infections, and the results suggested that more than 1 day treatment is needed to totally inhibit already formed biofilm.

3.4. Evaluation of cytotoxicity

Once we have obtained several specific inhibitors for class I RNR of bacterial expression, we need to test their inhibitory activity against class Ia RNR that is expressed in eukaryotic cells. If the compounds do not show cytotoxic effects, we can use them as drugs for chronic respiratory infectious diseases. For that reason, murine macrophage J774 cell line was used to perform cytotoxic studies. Macrophages were incubated with the compounds at different concentrations for 24 and 48 h at 37 °C in a humidified atmosphere with 5 % CO_2. Then, cell viability was assessed by using a 3-[4,5-dimethylthiazol-2-yl]-2,5-diphenyltetrazolium bromide (MTT) colorimetric assay (Sigma) (Table 15).

Compound	Cytoxicity (IC_{50}) mM
1	**1.89**
2	**>4**
7	**1.33**
12	**1.30**
13	**2.07**
14	**2.27**
15	**2.18**
16	**>4**
19	**>4**
M-HA	**3.2**

Table 15. Cytotoxic evaluation of the compounds in murine macrophage J774 cell line

The cytotoxic concentrations are higher that the concentrations that exhibited inhibitory activity against biofilm formation and already formed biofilm. We can conclude that these compounds can be used as drugs for chronic respiratory infectious diseases, such as COPD, bronchiectasis, CGD and CF, as well as, immunodeficient patients and chronic wound patients.

The work reported in this chapter has been patented. The patent is in the supplementary information.

PATENT: Primary hydroxylamines and uses thereof
Application Number EP14382032.2
30 January 2014

REFERENCES

1 Torrents, E., Sahlin, M., Biglino, D., Graslund, A. & Sjoberg, B. M. Efficient growth inhibition of Bacillus anthracis by knocking out the ribonucleotide reductase tyrosyl radical. *Proc Natl Acad Sci U S A* **102**, 17946-17951, doi:10.1073/pnas.0506410102 (2005).

2 *The Power of Functional Resins in Organic Synthesis*. (WILEY-VCH Verlag GmbH & Co. KGaA, 2008).

3 Mellor, S. L. M., C; Chan, W. N-Fmoc-aminooxy-2-chlorotrityl polystyrene resin: A facile solid-phase methodology for the synthesis of hydroxamic acids. *Tetrahedron Letters* **38**, 3311-3314 (1997).

4 Heydari, A., Aslanzadeh, S. Oxidation of Primary Amines to N-Monoalkylhydroxylamines using Sodium Tungstate and Hydrogen Peroxide-Urea Complex. *Adv. Synth. Catal.* **347**, 1223-1225 (2005).

5 Fields, J. D. & Kropp, P. J. Surface-mediated reactions. 9. Selective oxidation of primary and secondary amines to hydroxylamines. *The Journal of organic chemistry* **65**, 5937-5941 (2000).

6 Geffken, D. K., M.A. in *Acyclic N-Alkyl- and N,N-Dialkylhydroxylamines, Alkoxyammonium Salts* (Science of Synthesis).

7 Phanstiel, O., Wang, Q. X., Powell, M. P., Ospina, M. P., Leeson, B. A. Synthesis of Secondary Amines via *N*-(Benzyloxy)amines and Organoboranes. *Journal Organic Chemistry* **64**, 803-806 (1999).

8 Heydari, A. A General One-Pot, Three-Component Mono N-Alkylation of Amines and Amine Derivatives in Lithium Perchlorate/Diethyl Ether Solution. *Synthesis* **No. 4**, 627-633 (2005).

9 Cole, A. M., Weis, P. & Diamond, G. Isolation and characterization of pleurocidin, an antimicrobial peptide in the skin secretions of winter flounder. *J Biol Chem* **272**, 12008-12013 (1997).

10 Beckloff, N. *et al.* Activity of an antimicrobial peptide mimetic against planktonic and biofilm cultures of oral pathogens. *Antimicrob Agents Chemother* **51**, 4125-4132, doi:10.1128/AAC.00208-07 (2007).

CONCLUSIONS

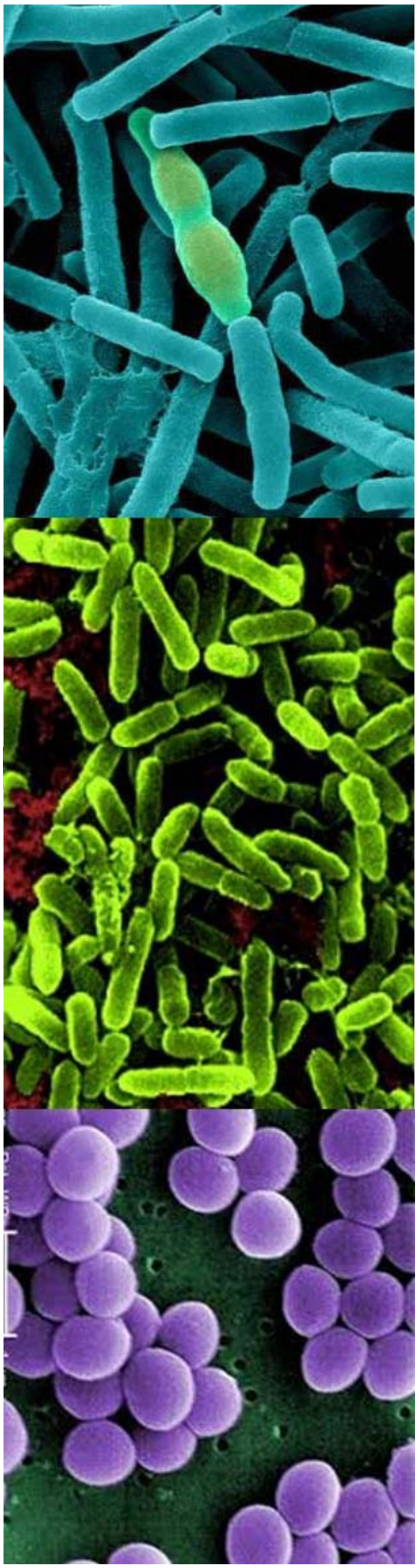

CONCLUSIONS

The principal conclusions that turn out from chapter 1 are:

1. A small library of hydroxamic acid, *N*-hydroxylamine, oxime and secondary hydroxylamine compounds have been designed and collected from mostly synthesis and also purchasing as possible drugs with antibacterial activity against respiratory infections.

2. Several promising drug candidates with antibacterial activity against Gram-positive (*Bacillus anthracis* and *Staphylococcus aureus*) and Gram-negative (*Pseudomonas aeruginosa*) bacteria have been identified. The compounds are able to arrest bacterial growth at relatively low concentrations.

3. Compound 7 is able to inhibit the formation of bacterial biofilms and to reduce the amount of already formed *P. aeruginosa* biofilm. Compounds 1 and 13 are able to inhibit the formation of bacterial biofilms and to reduce the amount of already formed *S. aureus* biofilm. *P. aeruginosa and S. aureus* biofilms are critical in bacterial chronic infections, which can cause chronic opportunistic infections especially in immunodeficient patients and the elderly.

4. The cytotoxic concentrations of the compounds showing antibacterial activity are higher that the concentrations that exhibited inhibitory activity against biofilm formation and already formed biofilm. Thus, these compounds can be used as drugs for chronic respiratory infectious diseases.

MATERIALS AND METHODS

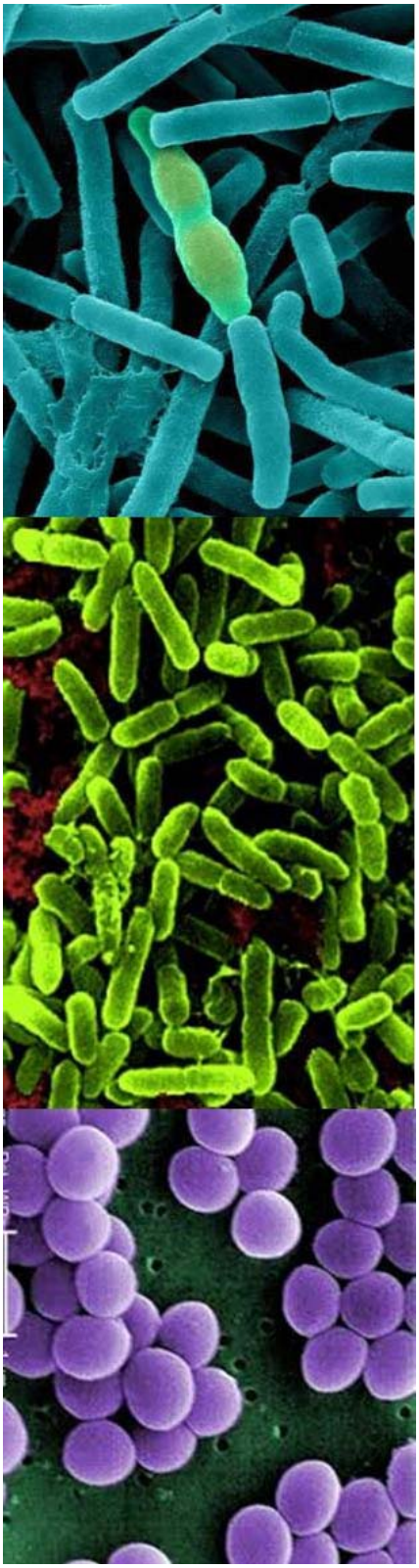

Materials and methods for hydroxamic acids and *N*-alkylhydroxylamines synthesis, purification and evaluation of the activity of the compounds

1. Solvents and reagents

1.1. Solvents

All the solvents used in the present thesis have been purchased to the suppliers Panreac, Scharlau, SDS and Sigma-Aldrich.

1.2. Reagents

Fmoc-protected amino acids were purchased from Iris Biotech GmbH or Bachem. 2-chlorotrityl chloride (CTC) resin was purchased from Iris Biotech GmbH or Novabiochem. HOAt, HOBt and TBTU were obtained from Luxembourg Industries or Novabiochem. Piperidine was purchased from SDS. The rest of reagents employed in the present thesis were purchased from Sigma-Aldrich or Fluka.

2. Instrumentation

2.1. General basic instrumentation

Instrument	Model
MilliQ water	Millipore, Milli-Q A10
Balances	Mettler Toledo, MS 303-S (3 significant digits)
	Mettler Toledo, AB 204-S (4 significant digits)
	Mettler Toledo, AT-261 (5 significant digits)
UV-VIS spectrometer	Shimadzu, mini 1240
Rotatory evaporator	Heidolph, Laborota 4003; connected to a Boc Edwards vacuum pump or to a Vacuubrand MZ 2C vacuum pump
Orbital shakers	Heidolph, Unimax 1010
Vortex mixers	MERCK® eurolab
MW system	CEM corporation, CEM Discover
Lyophilizers	VirTis, Freezemobile 25 EL

Table 16. General basic instrumentation

2.2. Chromatographic methods

2.2.1. Thin layer chromatography (TLC)

Analytical TLC was carried out on Merck Kieselgel 60 F254 plates. Compound spots were visualized by UV light (254 nm) and/or using the following staining solutions:

- Phosphomolibdic acid solution. The spray solution was prepared by dissolving 12 g of phosphomolibdic acid in 100 mL of EtOH. When the TLC plate is sprayed and heated at 110 ºC for 1 min, the presence of compounds is evidenced by the appearance of dark spots.

- Ninhidrine solution. The spray solution was prepared by dissolving 0.5 g of ninhydrine in 100 mL of EtOH. The TLC plate was sprayed and heated at 110 ºC for 1 min. When the TLC plate is sprayed and heated at 110 ºC for 1 min, the presence of primary amine groups is evidenced by the appearance of violet spots.

- Basic $KMnO_4$ solution. The spray solution was prepared by dissolving 3 g of $KMnO_4$ and 20 g of K_2CO_3 in a mixture of 300 mL of H_2O and 5 mL of 5% NaOH (aq.). When the TLC plate is sprayed and heated at 110 ºC for 1 min, the presence of alcohols and/or double bonds is evidenced by the appearance of yellow spots.

2.2.2. Flash chromatography

Flash chromatography was performed on silica gel (60 mesh, 35-70 µm), which was purchased from SDS (Pepypin, France). Separations were performed manually using glass columns of variable size.

2.2.3. Analytical High-Performance Liquid Chromatography PhotoDiode Array (HPLC-PDA)

Analytical HPLC was performed on a Waters instrument comprising a separation module (Waters 2695), an automatic injector, a photodiode array detector (Waters 996 or Waters 2998), and a Millenium ^{32} login system controller. The columns used were a Xbridge™ C18 reversed-phase analytical column (2.5 µm x 4.6 mm x 75 mm) and a SunFire™ C18 reversed-phase analytical column (3.5 µm x 4.6 mm x 100 mm) run with linear gradients of ACN (0.036% TFA) into H_2O (0.045% TFA) over 8 minutes. UV detection was at 220 and 254 nm and the system was run at a flow rate of 1.0 mL/min.

2.2.4. Semi-preparative HPLC

The purification of hydroxamic acids was performed in a semi-preparative RP-HPLC, that is a Waters instrument comprising two solvents delivery pumps (Waters Delta 600), an

automatic injector (Waters 2700 Sample Manager), a Waters 2487 dual wavelength absorbance detector, an automatic sample collector (Waters Fraction collector II), a Masslynx v3.5 system controller and two different columns, obtained also from Waters: a Symmetry® C18 reversed-phase column (5 µm x 30 mm x 100 mm) and SunFire™ Prep C18 OBD™ reversed-phase column (5 µm x 19 mm x 100 mm). Linear gradients of ACN (0.5% TFA) into H_2O (1%TFA) with a flow rate of 10 mL/min or 15mL/min were used.

2.3. High-Performance Liquid Chromatography-Mass Spectometry (HPLC-MS)

HPLC-MS analysis was performed on two different instruments provided with two different columns. The first of them was a Waters instrument comprising a Waters 2695 separation module, an automatic injector, a Waters 2998 photodiode array detector, a Waters ESI-MS Micromass ZQ spectrometer, a Masslynx v4.1 system controller and a SunFire™ C18 reversed-phase analytical column (3.5mm x 2.1mm x 100 mm). UV detection was at 220 and 254 nm, and linear gradients of ACN (0.07% Formic acid) into H_2O (0.1% Formic acid) were run at a 0.3 mL/min flow rate over 8 min. The second instrument comprised a Waters Alliance 2795 separation module, a Waters 2487 Dual λ Absorbance Detector, a MassLynx v4.0 system controller, a Waters ESI-MS Micromass ZQ spectrometer and a Symmetry® C18 reversed-phase analytical column (5 µm x 4.6 mm x 150 mm) run with linear gradients over 15 min and a flow rate of 1mL/min.

2.4. Nuclear Magnetic Resonance (NMR)

^{1}H, ^{13}C and ^{19}F NMR spectra were recorded on a Varian MERCURY 400 (400 MHz for ^{1}H NMR, 101 MHz for ^{13}C NMR and 376 MHZ for ^{19}F NMR) spectrometer. Chemical shifts (δ) are expressed in parts per million downfield from tetramethylsilane and deuterated solvent signal was used as reference. Coupling constants are expressed in Hertz.

3. Solid phase methodology for the synthesis of hydroxamic acids

3.1. General considerations

Solid-phase syntheses were undertaken manually in polypropylene syringes provided with a porous polyethylene filter. All solvents and soluble reagents were removed by suction. Washings between deprotection and coupling were carried out with DMF (3 x 1 min) and DCM (3 x 1 min) using 4 mL solvent/g resin for each wash. All transformations and washes were performed at 25ºC. Short treatments were carried out with manual stirring while longer transformations took place in orbital shakers. All the hydroxamic acids were synthesized in solid phase using the Fmoc protection strategy.

3.2. Colorimetric test

The Kaiser test or ninhydrin test was used to monitor the coupling treatments performed in solid phase.

3.2.1. Kaiser test

The Kaiser test is a colorimetric test that enables qualitative detection of free primary amines. The peptide-resin is washed with DCM and the solvent removed by suction. A small amount of resin beads are transferred to a glass tube and 6 drops of solution A and 2 drops of solution B are added. Then, the tube is incubated at 110ºC for three minutes. A dark blue color in the supernatant and/or on the resin beads reveals de presence of free primary amines, thus, pointing out that the coupling is incomplete (positive test). In contrast, a yellow coloration in the supernatant and/or on the beads means the absence of free primary amines (negative test) ensuring 99.5% of coupling rate.

Solution A: A solution of phenol (400 g) in absolute EtOH (100 mL) is prepared. Some heating is needed for a complete dissolution of the phenol. 20 mL of a 10 mM aqueous KCN solution (65 mg of KCN in 100 mL of H_2O) are added to freshly distilled pyridine (1000 mL). The two solutions are stirred with the ion exchange resin Amberlite MB-3 (40 g) for 45 minutes, then filtered and combined to obtain Solution A for the Kaiser test.

Solution B: Ninhydrin (2.5 g) is dissolved in absolute EtOH (50 mL). The ninhydrin reagent is light sensitive, thus, Solution B is kept in a flash protected from light.

3.3. Conditioning of the resin

2-Chlorotrityl chloride resin (2-CTC) was used to synthesize all the hydroxamic acids in the present thesis. *N*-Fmoc hydroxylamine linker was attached to the resin following Fmoc deprotection, coupling of the first amino acid, then Fmoc deprotection, and finally acetylation. Molecule cleavage from the resin provides the hydroxamic acid. In all cases Fmoc protection strategy was used.

Conditioning of the resin consist on washes with DMF (5 x 1 min) to eliminate hydrochloric acid traces for the extremely labile 2-CTC resin and with DCM (5 x 1min) to obtain an optimal swollen of the resin before incorporation of the *N*-Fmoc-hydroxylamine linker.

3.4. Incorporation of the *N*-Fmoc-hydroxylamine linker

Incorporation of the *N*-Fmoc-hydroxylamine linker into 2-CTC resin is achieved through a nucleophilic attack of the hydroxyl group of the corresponding *N*-Fmoc-hydroxylamine. The loading of commercial 2-CTC resin is 1.6 mmol/g and is necessary to work at 0.8 mmol/g to avoid aggregation problems. Thus, to achieve a loading of 0.8 mmol/g resin, 1.5 equivalents of *N*-Fmoc-hydroxylamine and 10 equivalents of DIPEA are dissolved in DCM and the solution is added into the resin. The resulting mixture is shaked for 48 hours. Unreacted chloride sites were then “capped” by stirring with methanol (800 µL of MeOH/g resin) for 30 minutes. Then, the solvents are removed by suction, and the resin washed with DCM (3 x 1 min), DMF (3 x 1 min) and DCM (3 x 1 min). The resulting *N*-Fmoc-aminooxy-2-chlorotrityl resin exhibited loadings which were typically 0.5 mmol/g indicating that the introduction of the *N*-Fmoc-hydroxylamine linker was laborious. It was impossible to improve the loading of the 2-CTC resin.

3.5. Elimination of the Fmoc group

The Fmoc group is removed from a primary amine by treatment with a solution of piperidine/DMF 1:4 (v:v) (2 x 1 min, 2 x 5 min). After the basic treatments the resin was washed with DMF (3 x 1 min) and DCM (3 x 1 min).

3.6. Determination of the resin loading by quantification of the Fmoc group

The loading capacity of the resin can be found by quantifying the Fmoc group after removal from the incorporation of the *N*-Fmoc-hydroxylamine linker into the resin. Thus,

when deprotecting, all the treatments with piperidine-DMF and the washes with DMF (3 x 1 min) are collected in a volumetric flask, and the UV absorbance at 290 nm of the resulting solution is measured. The loading capacity is calculated as follows:

$$Z = (A \cdot V)/ \varepsilon \cdot Y \cdot l$$

Where:

A: Absorbance

V: Volume of the solvent (mL).

ε: Molar absorbance coefficient ($5800 L \cdot mol^{-1} \cdot cm^{-1}$)

Y: Resing weight (g)

l: length of the cell (cm)

Z: loading of the resin

3.7. Incorporation of the amino acid

The assembly of one amino acid can be achieved by using different coupling conditions. In the present thesis, all the hydroxamic acids have been synthesized using the following protocol:

Step	Treatment	Conditions
1	Washes	DCM (3 x 1 min), DMF (3 x 1min), DCM (3 x 1 min)
2	Deprotection	Piperidine:DMF (1:4) (2 x 1 min, 2 x 5 min)
3	Washes	DMF (3 x 1min), DCM (3 x 1 min)
4	Coupling	Fmoc-AA-OH-TBTU-HOAt-DIEA (5:5:5:10) in DMF (1h)
5	Washes	DMF (3 x 1min), DCM (3 x 1 min)
6	Colorimetric test	Kaiser test

Table 17. Protocol for the incorporation of the amino acid

All the coupling treatments were performed at 25 ºC and lasted 1h. After 3 minutes of manual stirring, they were kept in an orbital shaker. The couplings were checked by Kaiser test. If the test was positive (uncomplete coupling), then recoupling was required, and the procedure was repeated from step 3. If the test was negative (complete coupling), then deprotection of Fmoc group and acetylation of *N*-terminal function was performed.

3.8. Acetylation of *N*-terminal function

Once the amino acid was incorporated followed by Fmoc group deprotection acetylation is achieved following a standard protocol of AcOH (6 equiv) and DIPCDI (3 equiv)

in DCM for 15 minutes. The acid is activated with DIPCDI for 5 minutes giving a white precipitate (urea). Urea is removed before adding the mixture into the resin. Then, the resin was washed with DCM (3 x 1 min), DMF (3 x 1min), and DCM (3 x 1 min).

3.9. Mini-cleavage and HPLC/HPLC-MS analysis

The progress of solid-phase reactions can be monitored by HPLC-PDA and HPLC-MS. A small amount of resin (1-2 mg) was cleaved with a solution of 2% TFA in DCM, the filtrate was concentrated under a stream of N_2, dissolved in ACN/H_2O 1:1 (v:v) and injected into the chromatographic instrument.

3.10. Cleavage of the molecule from the resin

Cleavage from 2-CTC resin is achieved by acidolytic treatment in very mild TFA conditions. After washing the resin with DCM (3 x 1 min), it is treated with a DCM/TFA 97:3 (v:v) solution (5 x 2 min) and then washed again with DCM until the resin colour changes from red to the original yellow. All washes collected in a H_2O-containing flask (15 mL H_2O/200 mg resin) and the TFA and DCM removed by means of a N_2 stream or under reduced pressure. ACN is added and the resulting solution is lyophilized.

Cleavage from the resin and complete side-chain deprotection could be performed in one step increasing the TFA percentage and using the appropriate scavengers according to the molecule. Nevertheless, is better recommended carrying out the two treatments stepwise to obtain cleaner crudes.

3.11. Hydroxamic acids purification and characterization

All compounds were purified using a reverse-phase HPLC equipment. The instrument and the column were chosen depending on the amount of crude, the degree of purity and the complexity of the chromatographic profile of the crude. All the samples were dissolved in the minimum amount of a H_2O/ACN solution, whose ACN percentage depended on the solubility of the hydroxamic acid crude, and filtered through a 0.45 mm nylon filter. The fractions were combined, lyophilized and finally hydroxamic acids products were analyzed by HPLC-PDA, HPLC-MS and ^{1}H-NMR.

4. Hydroxamic acids compounds

4.1. Synthesis of hydroxamic acids compounds

2-CTC resin (500 mg, 1.60 mmol/g) was placed in a 20 mL polypropylene syringe provided with a porous polyethylene filter and attached to a vacuum manifold. The resin was then conditioned by washings and the *N*-Fmoc hydroxylamine linker was attached to the resin. The excess of reactive positions of the resin were capped as it has been described in the general procedures (see section 3.4). The next steps were Fmoc deprotection and amino acid incorporation, which were performed under the conditions described in section 3.7. Then, Fmoc amino acid deprotection was followed by acetylation of the *N*-terminal function as it has been established in section 3.8. Finally, the resulting compound was cleaved using the conditions specified in section 3.10. The product was lyophilized and purified by semi-preparative RP-HPLC. The fractions were again lyophilized and analysed by HPLC-PDA, HPLC-MS and ^{1}H NMR. ^{13}C NMR analysis was performed when hydroxamic acids were obtained in a considerable quantity.

4.2. Hydroxamic acids characterization[1]

Ac-Phe-NHOH

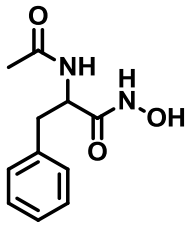

Column: SunFire™ C18 (3.5 µm × 4.6 mm × 100 mm)
HPLC-PDA, t_R (5% to 100% of ACN over 8 min): 3.84 min
m/z calculated for $C_{11}H_{15}N_2O_3$ $[M+H]^+$: 223.10 Da
HPLC-MS(+), $[M+H]^+$: 223.01 Da

Purification column: Symmetry semi-preparative C18 (5 µm x 30 mm x 100 mm)
Purification gradient: 0% to 30% of ACN over 40 min with a flow of 15 mL/min

^{1}H NMR (400 MHz, ($DMSO_{d6}$) δ ppm 10.66 (s, 1H, NH), 8.18 (d, *J* = 8.4 Hz, 1H, NH), 7.28-7.17 (5H, m, ArH), 4.40-4.34 (m, 1H, CH), 3.83 (bs, 1H, OH), 2.91 (dd, *J* = 13.5, 5.3 Hz, 1H), 2.75 (dd, *J* = 13.5, 9.5 Hz, 1H), 1.75 (s, 3H, $COCH_3$).

[1] Low yields were obtained for hydroxamic acids

Ac-Leu-NHOH

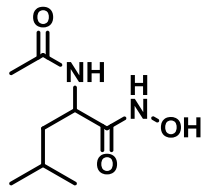

Column: SunFire™ C18 (3.5 µm × 4.6 mm × 100 mm)
HPLC-PDA, t_R (5% to 100% of ACN over 8 min): 3.49 min
m/z calculated for $C_8H_{17}N_2O_3$ $[M+H]^+$: 189.12 Da
HPLC-MS(+), $[M+H]^+$: 189.07 Da

Purification column: Symmetry semi-preparative C18 (5 µm x 30 mm x 100 mm)
Purification gradient: 0% to 30% of ACN over 40 min with a flow of 15 mL/min

^{1}H NMR (400 MHz, ($DMSO_{d6}$) δ ppm 10.65 (s, 1H, NH), 7.98 (d, *J* = 8.4 Hz, 1H, NH), 4.21-4.16 (m, 1H, CH), 3.44 (bs, 1H, OH), 1.81 (s, 3H, $COCH_3$), 1.57-1.47 (m, 1H, CH), 1.45-1.34 (m, 2H, CH_2), 0.87 (d, *J* = 6.6 Hz, 3H, CH_3), 0.82 (d, *J* = 6.5 Hz, 3H, CH_3).

Ac-Asp-NHOH

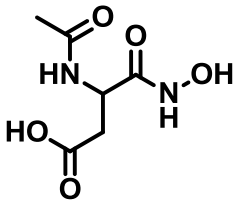

Column: SunFire™ C18 (3.5 µm × 4.6 mm × 100 mm)
HPLC-PDA, t_R (5% to 100% of ACN over 8 min): 1.42 min
m/z calculated for $C_6H_{11}N_2O_5$ $[M+H]^+$: 191.06 Da
HPLC-MS(+), $[M+H]^+$: 190.97 Da

Purification column: Symmetry semi-preparative C18 (5 µm x 30 mm x 100 mm)
Purification gradient: 0% to 30% of ACN over 40 min with a flow of 15 mL/min

The product was obtained as a mixture of rotamers in a ratio 61:39.
Rotamer 1: ^{1}H NMR (400 MHz, ($DMSO_{d6}$) δ ppm 10.75 (bs, 1H, -COOH), 10.19 (s, 1H,NH), 8.56 (d, *J* = 7.5 Hz, 1H, NH), 4.50 (bs, 1H, OH), 4.39 (ddd, *J* = 8.9, 7.6, 4.8 Hz, 1H, CH), 2.92 (dd, *J* = 17.2, 9.0 Hz, 1H), 2.49 (dd, *J* = 17.2, 4.8 Hz, 1H), 1.84 (s, 3H, $COCH_3$).
Rotamer 2: ^{1}H NMR (400 MHz, ($DMSO_{d6}$) δ ppm 10.75 (bs, 1H, -COOH), 10.19 (s, 1H, NH), 8.19 (d, *J* = 8.0 Hz, 1H), 4.50 (bs, 1H, OH), 4.54-4.46 (m, 1H, CH), 2.66 (dd, *J* = 16.5, 5.7 Hz, 1H), 2.55 (dd, *J* = 16.5, 7.3 Hz,1H), 1.83 (s, 3H, $COCH_3$).

Ac-Asp(^{t}Bu)-NHOH

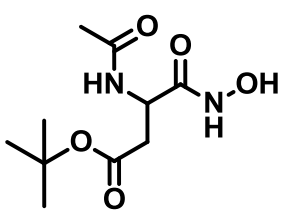

Column: SunFire™ C18 (3.5 µm × 4.6 mm × 100 mm)
HPLC-PDA, t_R (0% to 100% of ACN over 8 min): 3.71 min
m/z calculated for $C_{10}H_{18}N_2O_5$ $[M+H]^+$: 247.12 Da
HPLC-MS(+), $[M+H]^+$: 247.11 Da

Purification column: Symmetry semi-preparative C18 (5 µm x 30 mm x 100 mm)
Purification gradient: 0% to 30% of ACN over 40 min with a flow of 15 mL/min

^{1}H NMR (400 MHz, ($DMSO_{d6}$) δ ppm 10.64 (s, 1H, NH), 8.13 (d, *J* = 8.4 Hz, 1H, NH), 4.54-4.48 (m, 1H, CH), 2.58 (dd, *J* = 15.6, 6.4 Hz, 1H), 2.39 (dd, *J* = 15.6, 6.4 Hz, 1H), 1.80 (s, 3H, $COCH_3$), 1.37 (s, 9H, ^{t}Bu). ^{13}C NMR (101 MHz, ($DMSO_{d6}$) δ ppm 169.1 (s), 168.9 (s), 167.0 (s), 80.1 (s), 47.3 (d), 37.7 (t), 27.6 (q), 22.5 (q).

Ac-Lys-NHOH

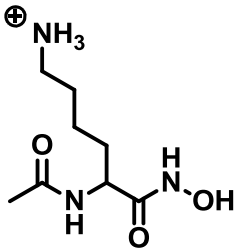

Column: SunFire™ C18 (3.5 µm × 4.6 mm × 100 mm)
HPLC-PDA, t_R (5% to 100% of ACN over 8 min): 1.42 min
m/z calculated for $C_8H_{18}N_3O_3^+$ $[M]^+$: 204.13 Da
HPLC-MS(+), $[M+H]^+$: 204.10 Da

Purification column: Symmetry semi-preparative C18 (5 µm x 30 mm x 100 mm)
Purification gradient: 0% to 30% of ACN over 40 min with a flow of 15 mL/min

The product was obtained as a mixture of rotamers in a ratio 78:22.
Rotamer 1: ^{1}H NMR (400 MHz, ($DMSO_{d6}$) δ ppm 10.34 (bs, 1H, NH), 8.03 (d, *J* = 8.3 Hz, 1H, NH), 7.84 (bs, 3H, NH_3), 4.16-4.07 (m, 1H, CH), 3.41 (bs, 1H, OH), 2.80-2.71 (m, 2H, CH_2), 1.82 (s, 3H, $COCH_3$), 1.59-1.44 (m, 4H, CH_2), 1.35-1.13 (m, 2H, CH_2).
Rotamer 2: ^{1}H NMR (400 MHz, ($DMSO_{d6}$) δ ppm 10.65 (s, 1H, NH), 8.84 (bs, 3H, NH_3), 8.11 (d, *J* = 7.8 Hz, 1H, NH), 4.16-4.07 (m, 1H, CH), 3.41 (bs, 1H, OH), 2.80-2.71 (m, 2H, CH_2), 1.84 (s, 3H, $COCH_3$), 1.59-1.44 (m, 4H, CH_2), 1.35-1.13 (m, 2H, CH_2).

Ac-Ala-NHOH

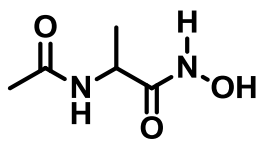

Column: SunFire™ C18 (3.5 µm × 4.6 mm × 100 mm)
HPLC-PDA, t_R (0% to 100% of ACN over 8 min): 1.51 min
m/z calculated for $C_5H_{11}N_2O_3$ $[M+H]^+$: 147.07 Da
HPLC-MS(+), $[M+H]^+$: 147.04 Da

Purification column: Symmetry semi-preparative C18 (5 µm x 30 mm x 100 mm)
Purification gradient: 0% to 30% of ACN over 40 min with a flow of 15 mL/min

The product was obtained as a mixture of rotamers in a ratio 60:40.

Conformer: ^{1}H NMR (400 MHz, ($DMSO_{d6}$) δ ppm 10.58 (bs, 1H, NH), 8.14 (d, *J* = 6.9 Hz, 1H, NH), 4.45 (bs, 1H, OH), 4.36-3.96 (m, 1H, CH), 1.82 (s, 3H, $COCH_3$), 1.24 (d, *J* = 7.3 Hz, 3H, CH_3).
Conformer: ^{1}H NMR (400 MHz, ($DMSO_{d6}$) δ ppm 10.21 (s, 1H, NH), 8.04 (d, *J* = 7.7 Hz, 1H, NH), 4.45 (bs, 1H, OH), 4.36-3.96 (m, 1H, CH), 1.81 (s, 3H, $COCH_3$), 1.15 (d, *J* = 7.1 Hz, 3H, CH_3).

5. Oxidation of primary alkyl amines to *N*-alkylhydroxylamines

Oxidation of primary amines to hydroxylamines derivatives constitutes a common synthetic transformation that may be achieved with a variety of oxidants such as hydrogen peroxide, peroxy acids, oxone, diacyl peroxides…

5.1. By Catalytic Oxidation with Hydrogen Peroxide

To a mixture of Na_2WO_4 (0.032 g, 0.01 mmol, 10 mol%) and 1.2 mmol of hydrogen peroxide-ura complex (UHP) in 15 mL of ether was added 1 mmol of R_1-NH_2. After stirring for 6 h at room temperature, the resulting suspension was filtered through a pad of celite, and the filtrate concentrated on a rotary evaporator[1]. Purification of the residue by flash column chromatography on silica gel (50% ethyl acetate in hexanes) gave the desired *N*-monoalkylhydroxylamine.

5.2. Using Oxone

Oxone on silica gel oxidizes primary amines selectively to the corresponding *N*-alkylhydroxylamines. It has been described that the reactions can be performed either in a solution at 80 ºC or without solvent under microwave irradiation[2].

5.2.1. Standard Procedure with Solvent

Into a 25 mL round-bottomed flask was weighed silica gel (2.5 g) that had been equilibrated with the atmosphere at 120 ºC for at least 48 h. The flask was stoppered and the contents were allowed to cool down to 25 ºC. H_2O (0.5 mL) was added and the adsorbent was tumbled on a rotary evaporator at atmospheric pressure until uniformly free-flowing. A solution of R_1-NH_2 (1 mmol) in benzene (5 mL) was added to the flask, with stirring, followed by oxone (1.5 mmol of $KOSO_2OOH$). The slurry was brought to reflux and stirred at 80 ºC for the specified period of time. After cooling down to 25 ºC, the slurry was transferred to a 200 mL round-bottomed flask, diluted with MeOH (100 mL), and stirred overnight at 25 ºC. The adsorbent was then removed by filtration under reduced pressure

and washed with additional MeOH (50 mL). The combined filtrates were concentrated under reduced pressure.

5.2.2. Standard Solvent-Free Procedure

A 2.5 g portion of the adsorbent was prepared as described above. The amine was added without solvent and the resulting mixture tumbled until uniformly free-flowing. The oxidant was then added and the mixture again tumbled. The resulting mixture was heated under microwave irradiation for 60 s and allowed to cool down to 25ºC. Then, the mixture was stirred overnight with 100 mL of MeOH. The adsorbent was collected by vacuum filtration and washed with an additional 50 mL of MeOH, and the combined filtrates were concentrated under reduced pressure.

5.2.3. Biphasic Procedure

A solution of oxone (1 eq) in H_2O was added to a solution of the amine (1 eq) in DCM 4:1 (v:v). The resulting mixture was stirred at room temperature until TLC monitoring indicated complete consumption of the starting material. Next, the organic phase was extracted with DCM, dried ($MgSO_4$), filtered and concentrated under reduced pressure.

5.3. Using Dibenzoyl Peroxide

Primary amines react with diacyl peroxides such as dibenzoyl peroxide to give *O*-acyl-*N*-alkylhydroxylamines, which upon hydrolysis provide the corresponding *N*-alkylhydroxylamines[3].

The synthesis of *O*-acyl-*N*-alkylhydroxylamines was optimized and two methods were selected giving the best results:

1) A solution of R-NH_2 (1 eq) with saturated aq K_2CO_3 solution was added dropwise to a solution of dibenzoyl proxide (1 eq) in ACN (1:1) (v:v), and the reaction mixture was stirred at 4 ºC. TLC was used to monitor the consumption of starting material. After the reaction was complete, ACN was evaporated and DCM was added and extracted two times. The organic layer was washed with saturated aq $NaHCO_3$ solution and aq HCl (2M), dried over anhydrous $MgSO_4$, filtered, concentrated under reduced pressure. The crude product was purified by flash column chromatography.

2) A solution of dibenzoyl peroxide (BPO, 1 eq) in DCM (5 mL/mmol BPO) was added quickly to a mixture of the amine (1 eq) in a buffer solution at pH 10.5 (5 mL/mmol amine). The pH 10.5 buffer solution was prepared by combining 222 mL of 0.75 N aqueous $NaHCO_3$ and 70 mL of 1.5 N aq NaOH. The resulting mixture was stirred at 4 ºC and monitored by TLC. After

the reaction was complete the aqueous layer was extracted twice with DCM. The organic layers were combined, dried over anhydrous $MgSO_4$, filtered and concentrated under reduced pressure. The crude product was purified by flash column chromatography.

5.4. *O*-Acyl-*N*-alkylhydroxylamine intermediate products

_O_-Benzoyl-_N_-((4-(trifluoromethyl)cyclohexyl)methyl)hydroxylamine

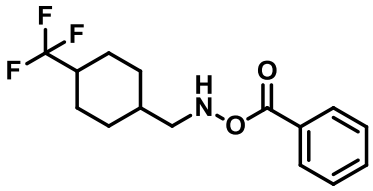

The product was synthesized as it has been described in section 5.3. The residue was purified by flash column chromatography (hexane-EtOAc = 1:0 to 1:2) to give 6.8 % yield of the product: ^{1}H NMR (400 MHz, $CDCL_3$) δ ppm 8.01 (d, *J* = 7.5 Hz, 2H, ArH), 7.97 (bs, 1H, NH), 7.58 (t, *J* = 7.5 Hz, 1H, ArH), 7.46 (t, *J* = 7.5 Hz, 2H, ArH), 3.13 (d, *J* = 7.3 Hz, 1H), 3.00 (d, *J* = 6.6 Hz, 1H), 2.14-2.07 (m, 1H, CH), 2.05-1.99 (m, 2H), 1.80-1.54 (m, 5H), 1.42-1.00 (m, 2H).

5.5. Hydrolysis of the *O*-acyl-*N*-alkylhydroxylamines

The hydrolysis of *O*-acyl-*N*-hydroxylamines was performed using acid and basic conditions. However, using basic condition such as LiOH a mixture of the addition product (*N*-hydroxyimidate) and the desired product were obtained, and were difficult to separate by flash chromatography. Then, using acid conditions (HCl) overnight at room temperature the final product was obtained in a very low yield.

_N_-(*tert*-Butoxycarbonyl)piperidine-4-carbaldehyde oxime

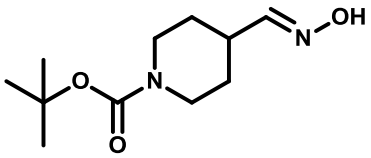

In this case the oxime was obtained instead of the *N*-hydroxlyamine. The product was obtained in a 26.3 % yield and a mixture of ismoers (cis and trans) in a ratio 81:19 were identified. **Isomer 1:** ^{1}H NMR (400 MHz, CD_3OD) δ ppm 9.20 (bs, 1H, OH), 7.27 (1H, dd, *J* = 5.8, 2.6 Hz, 1H, HC=N), 4.10-3.90 (m, 2H), 2.78-2.64 (m, 2H), 2.37-2.21 (m, 1H, CH), 1.68 (m, 2H), 1.38 (d, *J* = 2.0 Hz, 9H, ^{t}Bu), 1.57-1.11 (m, 2H). **Isomer 2:** ^{1}H NMR (400 MHz, CD_3OD) δ ppm 9.20 (bs, 1H, OH), 6.47 (1H, dd, *J* = 6.9, 2.1 Hz, 1H, HC=N), 4.10-3.90 (m, 2H), 3.11-3.00 (m, 1H, CH), 2.78-2.64 (m, 2H), 1.57-1.54 (m, 2H), 1.35-1.11 (m, 11H). ^{13}C NMR (101 MHz, $CDCL_3$) δ ppm 154.7 (s), 153.6 (d), 79.6 (s), 36.6 (2t), 32.0 (d), 29.0 (2t), 28.3 (3q).

5.6. *N*-Benzoylated-*N*-alkylamine products

All the *N*-benzoylated products were obtained as secondary products from the oxidation of primary amines using dibenzoyl peroxide.

_N_-[2-(4-Fluorophenyl)ethyl]benzamide

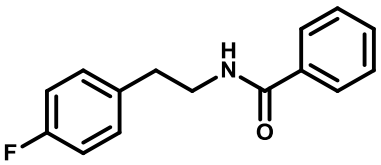

28.6 % yield. ^{1}H NMR (400 MHz, $CDCL_3$) δ ppm 7.71-7.68 (m, 2H, ArH), 7.51-7.46 (m, 1H, ArH), 7.43-7.39 (m, 2H, ArH), 7.22-7.16 (m, 2H, ArH), 7.03-6.98 (m, 2H, ArH), 6.18 (bs, 1H, NH), 3.71-3.66 (m, 2H, CH_2), 2.91 (t, *J* = 7.0 Hz, 2H, CH_2). ^{13}C NMR (101 MHz, $CDCL_3$) δ ppm 167.5 (s), 162.9 (d), 160.5 (s), 134.5 (s), 131.5 (d), 130.2 (d), 130.1 (d), 128.6 (2d), 126.8 (2 d), 115.6 (d), 115.4 (d), 41.2 (t), 34.9 (t). ^{19}F NMR (376 MHz, $CDCL_3$) δ ppm -116.5 (m, 1F, CF).

***tert*-Butyl 4-{[(phenylcarbonyl)amino]methyl}piperidine-1-carboxylate**

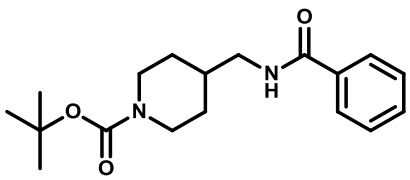

14 % yield.^{1}H NMR (400 MHz, $CDCL_3$) δ ppm 7.71-7.67 (m, 2H, ArH), 7.51 (t, *J* = 5.9 Hz, 1H, NH), 7.33-7.29 (m, 1H, ArH), 7.21 (t, *J* = 7.6 Hz, 2H, ArH), 3.97-3.82 (m, 2H), 3.22-3.03 (m, 2H), 2.56-2.35 (m, 2H, CH_2), 1.67-1.55 (m, 1H, CH), 1.55-1.47 (m, 2H), 1.30 (s, 9H, ^{t}Bu), 0.95 (m, 2H). ^{13}C NMR (101 MHz, $CDCL_3$) δ ppm 167.6 (s), 154.3 (s), 134.2 (s), 130.9 (d), 127.9 (2d), 126.7 (2d), 78.9 (s), 44.9 (2t), 35.9 (2t), 29.4 (t), 28.0 (d, 3q).

_N_-{[4-(Trifluoromethyl)cyclohexyl]methyl}benzamide

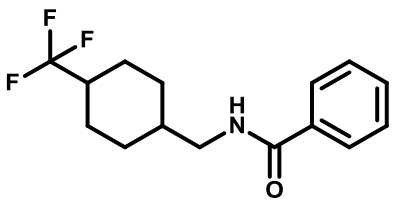

19.4 % yield.^{1}H NMR (400 MHz, $CDCL_3$) δ ppm 7.77-7.75 (m, 2H, ArH), 7.51-7.46 (m, 1H, ArH), 7.44-7.38 (m, 2H, ArH), 6.41 (bs, 1H, NH), 3.44 (dd, *J* = 7.4, 6.3 Hz, 1H), 3.31 (t, *J* = 6.5 Hz, 1H), 2.15-1.90 (m, 3H), 1.70-1.51 (m, 5H), 1.34-1.25 (m, 1H), 1.06-0.97 (m, 1H). ^{13}C NMR (101 MHz, $CDCL_3$) δ ppm 167.7 (s), 134.6 (s), 131.4 (d), 128.5 (2d), 126.8 (2d, q), 45.7 (t), 42.2 (d), 37.4 (d), 29.2 (2t), 26.2 (2t). The product was obtained as a mixture of rotamers in the ^{19}F NMR in a ratio (83:13:4). ^{19}F NMR (376 MHz, $CDCL_3$) δ ppm -73.8 (d, *J* = 8.1 Hz, 3F, CF_3), -73.9 (d, *J* = 8.1 Hz, 3F, CF_3), -74.0 (d, *J* = 8.2 Hz, 3F, CF_3).

***N*-(4,4,5,5,6,6,7,7,8,8,9,9,10,10,11,11,11-heptadecafluoroundecyl)benzamide**

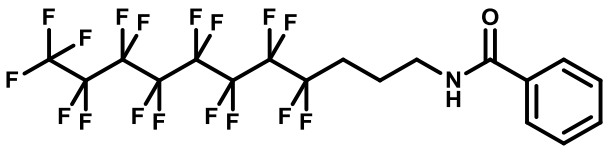

23.2 % yield. ^{1}H NMR (400 MHz, $CDCL_3$) δ ppm 7.76 (d, *J* = 7.5 Hz, 2H, ArH), 7.47 (t, *J* = 7.5 Hz, 1H, ArH), 7.38 (t, *J* = 7.5 Hz, 2H, ArH), 6.87 (bs, 1H, NH), 3.50 (q, *J* = 6.7 Hz, 2H, CH_2), 2.20-2.07 (m, 2H, CH_2), 1.95-1.87 (m, 2H, CH_2). ^{13}C NMR (101 MHz, $CDCL_3$) δ ppm 168.1 (s), 134.3 (s), 131.5 (d), 128.5 (4d, t, q), 126.9 (6t), 39.1 (t), 28.4 (t), 20.8 (t). ^{19}F NMR (376 MHz, $CDCL_3$) δ ppm -81.1 (t, *J* = 10.0 Hz, 3F, CF_3), -114.3 (qt, *J* = 16.6 Hz, 2F, CF_2), -121.9 (bs, 2F, CF_2), -122.1 (bs, 4F, CF_2), -123.0 (bs, 2F, CF_2), -123.5 (bs, 2F, CF_2), -126.4 (bs, 2F, CF_2).

6. Synthesis of *N*-alkylhydroxylamines by reductive amination

The synthesis of hydroxylamines products can be accomplished by reductive amination which involves the conversion of a carbonyl group to an amine via an intermediate imine.

To a mixture of aldehyde (1 g, 1 eq) in a solution of 5 M $LiClO_4/Et_2O$ (10 mL) was added *o*-(trimethylsilyl)hydroxylamine (1.5 eq) at room temperature. The mixture was stirred for 10 minutes and $(CH_3)_3SiCl$ (1.5 eq) was added. After stirring the mixture for 8 hours $BH_3.NEt_3$ (1.5 eq) was added and the mixture was allowed to stir at room temperature overnight.

The reaction was set up for 24 hours and was quenched with aq saturated $NaHCO_3$ solution, and the product was extracted with DCM. The organics extracts were combined, dried with $MgSO_4$ and concentrated. The crude product was flash chromatographed (SiO_2) using a hexane-EtOAc gradient from 1:0 to 0:1.

6.1. Characteritzation of *N*-alkylhydroxylamines

All the products were synthesized following the general procedure described in section 6. The separation of the product from TEA was laborious and long columns and long gradients were required.

***N*-Hydroxy-2-phenylethanamine**

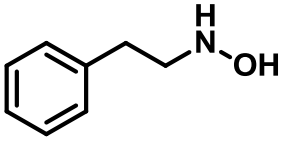

45.6 % yield. ^{1}H NMR (400 MHz, $CDCL_3$) δ ppm 7.33-7.26 (m, 2H, ArH), 7.26-7.18 (m, 3H ArH), 4.22-3.92 (m, 2H, NHOH), 3.21 (t, *J* = 7.1 Hz, 2H, CH_2), 2.90 (t, *J* = 7.1 Hz, 2H, CH_2). ^{13}C NMR (101 MHz, $CDCL_3$) δ ppm 139.0 (s), 128.8 (2d), 128.6 (2d), 126.4 (d), 54.8 (t), 33.1 (t).

_N_-Hydroxyhexan-1-amine

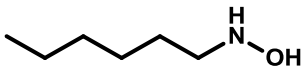

30.5 % yield. ^{1}H NMR (400 MHz, $CDCL_3$) δ ppm 2.80-2.74 (m, 2H, CH_2), 1.65-1.48 (m, 2H, CH_2), 1.34-1.25 (m, 6H, CH_2), 0.90-0.86 (m, 3H, CH_3). ^{13}C NMR (101 MHz, $CDCL_3$) δ ppm 60.2 (t), 31.6 (t), 26.9 (t), 26.2 (t), 22.5 (t), 14.0 (q).

_N_-Hydroxy-2-methylpropan-1-amine

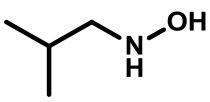

14.8 % yield. ^{1}H NMR (400 MHz, $CDCL_3$) δ ppm 5.13 (bs, 2H, NHOH), 2.80 (d, *J* = 6.9 Hz, 2H, CH_2), 2.01-1.88 (m, 1H, CH), 0.95 (d, *J* = 6.7 Hz, 6H, CH_3). ^{13}C NMR (101 MHz, $(CD_3)_2SO$) δ ppm 45.7 (t), 26.4 (d), 19.6 (2q).

_N_-Hydroxy-3-methylbutan-1-amine

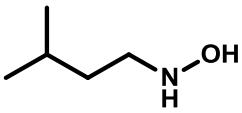

56.4 % yield. ^{1}H NMR (400 MHz, $CDCL_3$) δ ppm 6.48 (bs, 2H, NHOH), 2.93-2.89 (m, 2H, CH_2), 1.65-1.52 (m, 1H, CH), 1.41-1.35 (m, 2H, CH_2), 0.87 (d, *J* = 6.6 Hz, 6H, CH_3). ^{13}C NMR (101 MHz, $(DMSO_{d6})$ δ ppm 58.9 (1C, s , C_1), 37.7 (1C,s, C_2), 27.5 (1C, s, C_3), 23.6 (1C, s, $C_{4,5}$).

_N_-Hydroxybutan-1-amine

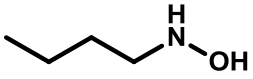

28.2 % yield. ^{1}H NMR (400 MHz, $CDCL_3$) δ ppm 6.14 (bs, 2H, NHOH), 2.95 (t, *J* = 7.3 Hz, 2H, CH_2), 1.53 (qt, *J* = 7.4 Hz, 2H, CH_2), 1.36 (sex, *J* = 7.4 Hz, 2H, CH_2), 0.93 (t, *J* = 7.3 Hz, 1H, CH_3). ^{13}C NMR (101 MHz, $CDCL_3$) δ ppm 53.4 (t), 28.7 (t), 20.2 (t) 13.9 (q).

1-Furan-2-yl-_N_-hydroxymethanamine

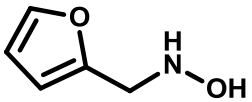

35.4 % yield. ^{1}H NMR (400 MHz, $CDCL_3$) δ ppm 7.36 (d, *J* = 1.8 Hz, 1H, ArH), 6.43 (bs, 2H, NHOH), 6.31 (dd, *J* = 3.2, 1.8 Hz, 1H, ArH), 6.25 (d, *J* = 3.2 Hz, 1H, ArH), 3.97 (s, 2H, CH_2). ^{13}C NMR (101 MHz, $CDCL_3$) δ ppm 151.0 (s), 142.1 (d), 110.3 (d), 108.5 (d), 50.3 (t).

_N_-(Cyclohexylmethyl)hydroxylamine

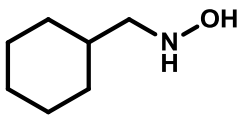

70.2 % yield. ^{1}H NMR (400 MHz, $CDCL_3$) δ ppm 6.35 (bs, 2H, NHOH), 2.77 (d, *J* = 6.6 Hz, 2H, CH_2), 1.75-1.53 (m, 6H), 1.30-1.09 (m, 3H), 0.97-0.87 (m, 2H). ^{13}C NMR (101 MHz, $CDCL_3$) δ ppm 60.5 (t), 35.1 (d), 31.3 (2t), 26.5 (t), 25.9 (2t).

Nicotinaldehyde oxime

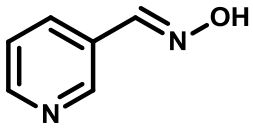

The product was obtained in a 20.5 % yield and a mixture of isomers (cis and trans) in a ratio 90:10 were identified in the ^{1}H NMR.

Isomer 1: ^{1}H NMR (400 MHz, $CDCL_3$) δ ppm 8.80 (d, *J* = 1.9 Hz, 1H, ArH), 8.61 (dd, *J* = 4.9, 1.9 Hz, 1H, ArH), 8.16 (s, 1H, HC=N), 7.96 (dt, *J* = 7.9, 1.9 Hz, 1H, ArH), 7.34 (dd, *J* = 7.9, 4.9 Hz, 1H, ArH). **Isomer 2:** ^{1}H NMR (400 MHz, $CDCL_3$) δ ppm 9.07 (d, *J* = 1.8 Hz, 1H ArH), 8.64 (dd, *J* = 7.4, 1.8 Hz, 1H, ArH), 8.44 (dt, *J* = 8.1, 1.8 Hz, 1H, ArH), 8.16 (s, 1H, HC=N), 7.41-7.38 (m, 1H, ArH). ^{13}C NMR (101 MHz, $CDCL_3$) δ ppm 150.2 (d), 148.3 (d), 146.8 (d), 133.8 (d), 128.8 (s) 123.7 (d).

_N_-(4-Methoxybenzyl)hydroxylamine

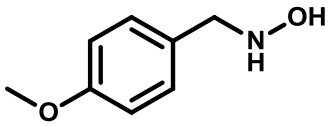

12.6 % yield. ^{1}H NMR (400 MHz, $CDCL_3$) δ ppm 7.20 (d, *J* = 8.7 Hz, 2H, ArH), 6.83 (d, *J* = 8.7 Hz, 2H, ArH), 6.30 (bs, 2H, NHOH), 3.88 (s, 2H, CH_2), 3.74 (s, 3H, CH_3). ^{13}C NMR (101 MHz, $CDCL_3$) δ ppm 159.2 (s), 130.4 (2d), 128.8 (s), 113.9 (2d), 57.5 (q), 55.2 (t).

_N_-(4-Fluorobenzyl)hydroxylamine

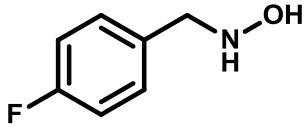

42.4 % yield. ^{1}H NMR (400 MHz, $CDCL_3$) δ ppm 7.34-7.29 (m, 2H, ArH), 7.06-7.00 (m, 2H, ArH), 4.01 (s, 2H, CH_2). ^{13}C NMR (101 MHz, $CDCL_3$) δ ppm 163.5 (d), 161.1 (s), 130.8 (d), 130.8 (d), 115.38 (d), 115.2 (d), 57.2 (t). ^{19}F NMR (376 MHz, $CDCL_3$) δ ppm -114.8 (tt, *J* = 8.8, 5.4 Hz, 1F, CF)

_N_-[3,5-Bis(trifluoromethyl)benzyl]hydroxylamine

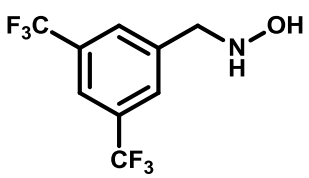

26.4 % yield. ^{1}H NMR (400 MHz, $CDCL_3$) δ ppm 7.83 (s, 2H, ArH), 7.82 (s, 1H, ArH), 5.58 (bs, 2H, NHOH), 4.13 (s, 2H, CH_2). ^{13}C NMR (101 MHz, $CDCL_3$) δ ppm 140.3 (2s), 131.7 (2q), 129.0 (2d), 124.7 (s), 121.5 (d), 56.9 (t). ^{19}F NMR (376 MHz, $CDCL_3$) δ ppm -62.9 (6F, s, F).

_N_-(2,4-Dimethoxybenzyl)hydroxylamine

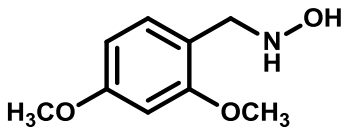

The product was obtained in a 22 % yield. ^{1}H NMR (400 MHz, $CDCL_3$) δ ppm 7.16 (d, *J* = 7.9 Hz, 1H, ArH), 6.46-6.43 (m, 2H, ArH), 4.03 (s, 2H, CH_2), 3.82 (s, 3H, CH_3), 3.80 (s, 3H, CH_3). ^{13}C NMR (101 MHz, $CDCL_3$) δ ppm 160.6 (s), 158.8 (s), 131.8 (d), 116.9 (s), 103.8 (d), 98.37 (d), 55.2 (q), 55.1 (q), 53.4 (t).

_N_-(4-Methoxy-2-methylbenzyl)hydroxylamine

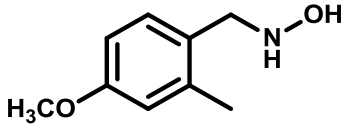

The product was obtained in a 32.8 % yield. ^{1}H NMR (400 MHz, $CDCL_3$) δ ppm 7.18 (d, *J* = 8.2 Hz, 1H, ArH), 6.73 (d, *J* = 2.7 Hz, 1H, ArH), 6.70 (dd, *J* = 8.2, 2.7 Hz, 1H, ArH), 4.01 (s, 2H, CH_2), 3.78 (s, 3H, CH_3), 2.35 (s, 3H, CH_3). ^{13}C NMR (101 MHz, $CDCL_3$) δ ppm 158.9 (s), 138.4 (s), 131.3 (d), 126.6 (s), 115.8 (d), 110.8 (d), 54.9 (q), 54.9 (t), 19.1 (q).

4-Hydroxy-2,6-dimethylbenzaldehyde oxime

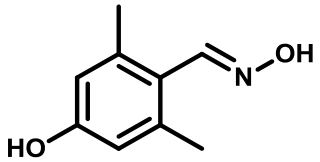

The product was obtained in a 25.8 % yield and a mixture of isomers (cis and trans) in a ratio 75:25 were identified in the ^{1}H NMR and ^{13}C NMR.

Isomer 1: ^{1}H NMR (400 MHz, CD_3OD) δ ppm 8.25 (s, 1H, HC=N), 6.53 (s, 2H, ArH), 2.13 (s, 6H, CH_3). ^{13}C NMR (101 MHz, CD_3OD) δ ppm 163.1 (s), 157.0 (d), 137.7 (2s), 125.8 (s), 115.4 (2d), 18.48 (2q). **Isomer 2:** ^{1}H NMR (400 MHz, CD_3OD) δ ppm 8.25 (s, 1H, HC=N), 6.55 (s, 1H, ArH), 6.48 (s, 1H, ArH), 2.26 (s, 3H, CH_3), 2.18 (s, 3H, CH_3). ^{13}C NMR (101 MHz, CD_3OD) δ ppm 163.1 (s), 158.1 (d), 138.4 (s), 136.6 (s), 125.8 (s), 115.7 (d), 114.9 (d), 19.4 (q), 18.6 (q).

_N_-(2,6-Dimethoxybenzyl)hydroxylamine

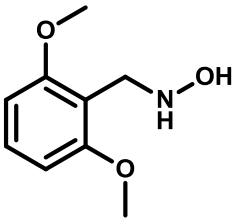

The product was obtained in a 29.8 % yield. ^{1}H NMR (400 MHz, $CDCL_3$) δ ppm 7.19 (t, *J* = 8.4 Hz, 1H, ArH), 6.52 (d, *J* = 8.4 Hz, 2H, ArH), 6.33 (bs, 2H, NHOH), 4.22 (s, 2H, CH_2), 3.80 (s, 6H, CH_3). ^{13}C NMR (101 MHz, $CDCL_3$) δ ppm 159.4 (2s), 128.6 (d), 114.4 (s), 103.9 (2d), 55.8 (2q), 47.9 (t).

7. Bacterial cell lines used to test the activity of the compounds

All the compounds were tested in four different bacterial cell lines: *bacillus anthracis*, *staphylococcus aureus*, *burkholderia cenocepacia* and *pseudomonas aeruginosa* (see table 14). This project has been accomplished in collaboration with the group of Eduard Torrents. All the biological experiments were performed by Eduard Torrents.

Bacterial cell lines	ATCC	CECT	Nomenclature
Bacillus anthracis	**-**	**-**	Sterne 7700 $pXO1^-/pXO2^-$
Staphylococcus aureus	12600	86T	
Burkholderia cenocepacea	J2315		
Pseudomonas aeruginosa	15692	4122	PAO 1

Table 18. Bacterial strains used to test the activity of the compounds

REFERENCES

1 Heydari, A., Aslanzadeh, S. Oxidation of Primary Amines to N-Monoalkylhydroxylamines using Sodium Tungstate and Hydrogen Peroxide-Urea Complex. *Adv. Synth. Catal.* **347**, 1223-1225 (2005).

2 Fields, J. D. & Kropp, P. J. Surface-mediated reactions. 9. Selective oxidation of primary and secondary amines to hydroxylamines. *The Journal of organic chemistry* **65**, 5937-5941 (2000).

3 Geffken, D. K., M.A. in *Acyclic N-Alkyl- and N,N-Dialkylhydroxylamines, Alkoxyammonium Salts* (Science of Synthesis).

CHAPTER 2

Phenotype screening identifies a new regulatory pathway linking pyrimidine biosynthesis, p53 and mitochondrial morphology

ABSTRACT

ABSTRACT

Mitofusin-2 (Mfn2) participates in mitochondrial fusion and moreover, regulates mitochondrial metabolism. We have previously reported that Mfn2 is down regulated in muscle from obese or type 2 diabetic patients, and recently we have demonstrated that Mfn2 deficiency in liver or muscle leads to glucose intolerance and insulin resistance in mice. Therefore, activators of Mfn2 expression could be used as a valuable potential therapeutic strategy for the treatment of type 2 diabetes and obesity.

For this purpose, we decided to search activators of Mfn2 expression by High Throughput Screening using a FDA-approved library of 1120 compounds (Prestwick). HeLa cells stably expressing luciferase under the control of 2 kb of human Mfn2 promoter, were incubated with the library and leflunomide was identified as a potent activator of Mfn2 transcriptional activity. Importantly, leflunomide also increased Mfn2 mRNA and protein levels in HeLa and C2C12 cells. Furthermore, leflunomide also induced the expression of the mitochondrial fusion protein Mfn1 and repressed the mitochondrial fission protein Drp1 in both cell lines. Leflunomide increased the mitochondrial fusion proteins such as Mfn2 and Mfn1, and decreases the mitochondrial fission protein Drp1, leading to elongation of mitochondrial network. In addition, leflunomide was able to increase Mfn2, Mfn1 and Opa1 protein levels and promoted mitochondrial elongation in MEFwt, MEF $Mfn2^{-/-}$ and MEF $Mfn1^{-/-}$ cells. However, mitochondrial elongation is more dependent of Mfn1 than Mfn2 due to the higher mitochondrial elongation of MEF $Mfn2^{-/-}$ compared to MEF $Mfn1^{-/-}$ cells.

Leflunomide decreases the synthesis of pyrimidines by inhibiting dihydroorotate dehydrogenase (DHODH), which causes cell stress and p53 activation by phosphorylation at Ser15. p53 triggers Mfns up-regulation promoting mitochondrial elongation. The addition of external uridine, which reverses the deficiency in pyrimidines synthesis, prevents p53 and Mfns increase in C2C12 cells. Moreover, myxothiazol, an inhibitor of complex III that indirectly inhibit DHODH, and consequently pyrimidine synthesis, also up-regulates p53 producing an increase in Mfns protein expression. Myxothiazol also promotes mitochondrial elongation in HeLa, C2C12 and MEFwt cells.

We conclude that the depletion of pyrimidine pools, by complex III or DHODH inhibitors, cause cell stress, and trigger p53 accumulation and activation by p53 phosphorylation at Ser15. Cell cycle arrest, up-regulation of Mfns and down-regulation of Drp1 is triggered by p53. The modulation of mitochondrial proteins involved in fusion and fission events promotes mitochondrial elongation to confer stress resistance on cells. Therefore, mitochondrial elongation represents an adaptive response against cell stress caused by leflunomide and myxothiazol.

INTRODUCTION

INTRODUCTION

1. Mitochondrion

Mitochondria, in Greek means thread grain, are dynamic, essential and double membrane organelles, and they are found in most eukaryotic cells. Mitochondrion generates most of the cell's energy derived from carbohydrates and fatty acids degradation, which are converted to adenosine triphosphate (ATP) by oxidative phosphorylation. In addition to supplying cellular energy, mitochondria are involved in many cellular functions such as Ca^{2+} signaling[1], cellular differentiation, apoptosis[2], substrates oxidation, as well as the control of the cell cycle and cell growth[3,4].

The compartments that carry out specialized functions include the outer mitochondrial membrane (OMM), the intermembrane space (the space between the outer and the inner membranes), the inner mitochondrial membrane (IMM), the cristae space (formed by infoldings of the inner membrane), and the matrix (space within the inner membrane).

The OMM encloses the entire organelle and is composed of phospholipids bilayers and proteins with the same ratio. In addition, it contains large numbers of porin proteins that form channels allowing molecules up to 5 KDa to freely diffuse from one side of the membrane to the other[5]. OMM mediates exchange between cytosol and intermediate space[6]. Disruption of the outer membrane permits proteins in the intermembrane space to leak into the cytosol, as for example cytochrome c, leading to apoptosis signal.

The IMM has a higher content of proteins than phospholipids, and also is rich in cardiolipin, which makes the inner membrane more impermeable. Unlike the outer membrane, the inner membrane is highly impermeable to all molecules and is compartmentalized into numerous cristae junctions. Cristae expand the surface area of the inner mitochondrial membrane on which the oxidative phosphorylation (OXPHOS) takes places, producing a membrane potential across the inner membrane to produce ATP. The high surface area allows greater capacity to produce ATP.

The matrix is the space enclosed by the inner membrane with high protein content, on which pyruvate oxidation, fatty acid β-oxidation and the citric acid cycle (Krebs cycle) take place. Moreover, the matrix contains the mitochondria genetic material, and the machinery to manufacture their RNAs and proteins. Mitochondria have circular double-stranded DNA and encode 37 genes: 22 tRNA, 2 rRNA, and 13 mitochondrial proteins[7]. The mitochondrial proteins in humans are integrated into the inner mitochondrial membrane

and are implicated in the electron transport and in the OXPHOS system, along with other proteins encoded by genes that reside in the cell nucleus.

1.1. Mitochondrial dynamics

Mitochondrial dynamics is used to describe the movement of mitochondria along the cytoskeleton, the morphology and distribution of mitochondria and connectivity mediated by tethering or fusion and fission events[8].

Mitochondrial morphology and function is dependent on the balance between fusion and fission processes. Increased mitochondrial fusion can be achieved by increasing mitochondrial proteins involved in fusion or decreasing proteins involved in fission, and viceversa. Moreover, when both processes are inhibited mitochondrial morphology is similar to the basal state, indicating that mitochondrial morphology is a consequence of the balance between fusion and fission events[9]. However, mitochondrial morphology depends on mitochondrial dynamics and also on other proteins or mediators, such as cytoskeleton-based transport[10].

Mammalian proteins involved in mitochondrial fission are dynamin-related protein 1 (Drp1), fission protein 1 homolog (Fis1), mitochondrial fission factor (Mff), mitochondrial dynamics proteins of 49 and 51 kDa (MiD49 and MiD51, respectively), and ganglioside-induced differentiation-associated protein 1 (GDAP1). Similarly, Mitofusin 1 (Mfn1), Mitofusin 2 (Mfn2) and Optic Atrophy gene 1 (Opa1) are proteins that participate in mitochondrial fusion in mammals (Figure 1).

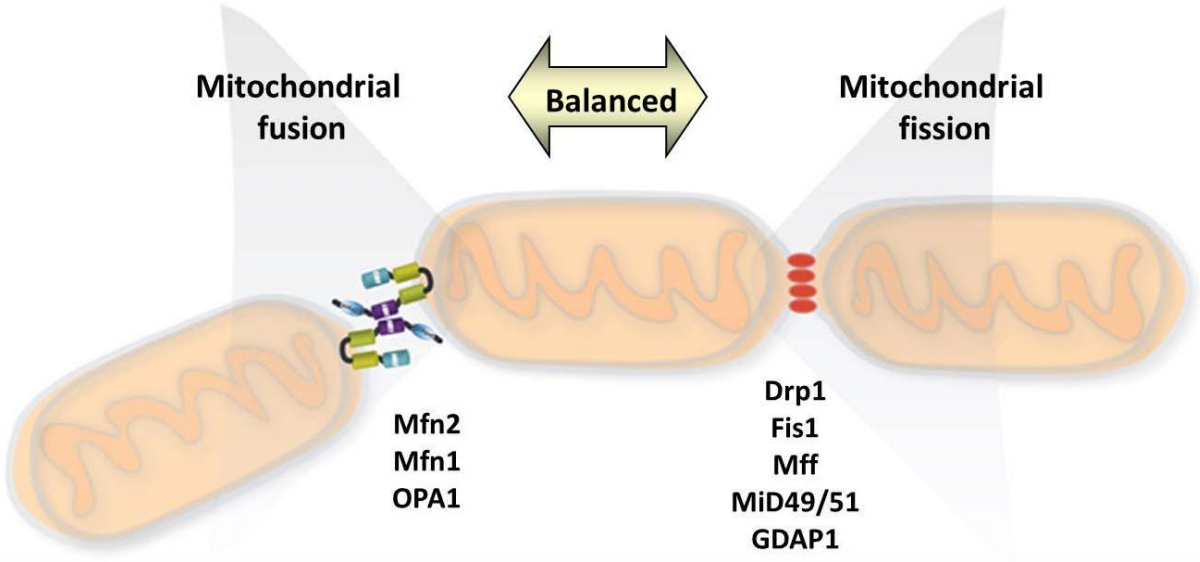

Figure 1. Mitochondrial dynamics

Mitochondrial dynamics regulates mitocondrial morphology, mitophagy, apoptosis, oxphos, Ca^{2+} signaling, mitochondrial DNA (mtDNA) stability, mitochondrial quality, ROS generation and cellular stress response.

1.1.1. Mitochondrial fusion

Mitochondrial fusion is a two-step process, where the outer and inner mitochondrial membranes fuse separately. The most important proteins involved in fusion are the two highly conserved dynamin-related GTPases Mfn2 and Mfn1[11], localized in the OMM, and Opa1[12], localized in the IMM (Figure 2). Mitochondrial fusion mediates molecular exchanges[13], is required to facilitate the intercomplementation of mitochondrial DNA[14], and protects mitochondria under different kinds of cellular stress.

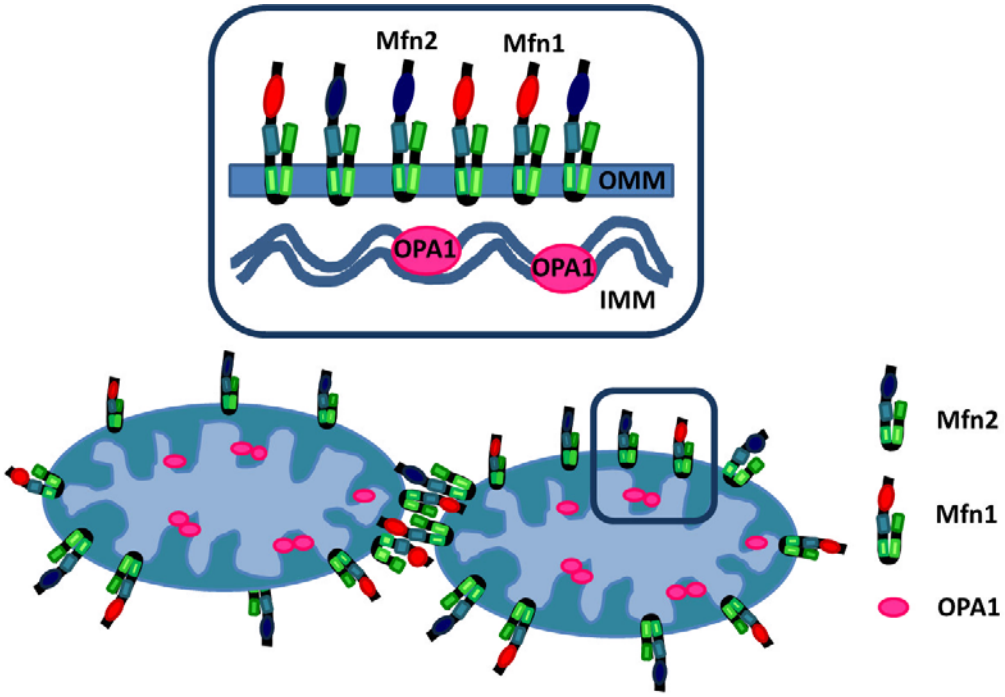

Figure 2. Mitochondrial proteins involved in fusion process.

Human Mfn1 and Mfn2 have 63% of identity and are transmembrane GTPases proteins. The most obvious conserved domains are: two transmembrane domain and a coiled-coil domain (also called heptad-repeat domain, HR2) located in the C-terminal part; and the GTP-binding domain and another coiled-coil domain (HR1) located in the N-terminal part. The transmembrane domains confer upon Mfns a U-shaped structure. As a result, both the HR2 and GTPase domain are exposed to the cytosol. The tethering of two adjacent mitochondria is accomplished through assembling a dimeric antiparallel coiled-coil structure (HR2)[15], which can be homotypic (Mfn1-Mfn1 or Mfn2-Mfn2) or heterotypic (Mfn1-Mfn2)[9] (Figure 2).

Fusion activity of Mfn1 and Mfn2 depends on the GTPase activity and HR2 domain. The functionality of the GTPase domain is crucial for Mfns fusion activity, and HR2 domain is important for mitochondrial membrane tethering[15-17]. Fusion starts with the tethering of two different mitochondrial membranes by Mfns dimerization, followed by a GTP hydrolysis, and consequently producing conformation changes that leads to the final fusion between mitochondria. Moreover, mitochondrial fusion is higher overexpressing Mfn1 than Mfn2 which could be due to increased GTPase activity of Mfn1 than Mfn2[18]. These findings were further confirmed by Cipolat et al. suggesting that Opa1 can elongate mitochondria in the absence of Mfn2 but not Mfn1[19]. On the other hand, overexpression of Mfn1 or Mfn2 causes mitochondrial aggregation. This effect is dependent of the HR2 that mediates mitochondrial tethering, and is not dependent of the GTPase domain[15,16,20,21].

Chen et al[9]. reported that Mfn1 and Mfn2 knockout mice die during gestation due to a lethal placental defect. Moreover, mouse embryonic fibroblasts (MEFs) from Mfn1 KO mice showed a dramatic mitochondrial fragmentation, which is more severe than *mfn2* ablation. Moreover, overexpression of Mfn1 in Mfn2-deficient cells or Mfn2 in Mfn1-deficient cells is sufficient to rescue mitochondrial morphology[9]. However, the former rescued the mitochondrial morphology in 75-80%, whereas the latter restored mitochondrial tubules in 25%, indicating that mitochondrial elongation is more dependent of Mfn1 than Mfn2. In addition, double knockout Mfn1/Mfn2$^{-/-}$ cells lack any detectable fusion activity in vivo.

Moreover, de Brito et al. reported that Mfn2 is enriched at the ER-mitochondria interface, promoting tethering between both organelles. In addition, Mfn2 ablation or silencing disrupts ER morphology and its tethering to mitochondria[22].

Opa1 is a dynamin-related GTPase localized in the mitochondrial intermembrane space in soluble forms or attached to the inner membrane[23], and controls mitochondrial fusion and cristae remodelling[19,24,25]. Mitochondrial fusion mediated by the OMM and IMM is possibly accomplished by interaction between Opa1 C-terminus and Mfn U-shaped topology[19]. Like mitofusins, Opa1 is also involved in maintaining mitochondrial function, calcium homeostasis[26], apoptosis by regulating cytochrome c release[27], mtDNA level[28,29], mitophagy[29], respiratory capacity[30], and maintenance of mitochondrial membrane potential (MMP).

Opa1 protein contains a NH_2-terminal mitochondrial import sequence (MIS), which confers mitochondrial localization, a transmembrane domain (associate Opa1 to the IMM), a coiled-coil domain (involved in protein-protein interactions), a GTPase and middle domain, and a second coiled-coil domain in the COOH terminal part[31].

The GTPase domain of Opa1 is crucial for the activity of Opa1. Moreover, Opa1 exists in several different isoforms as a result of post-transcriptional and post-translational regulation. In humans, alternative splicing generates at least eight mRNA isoforms of Opa1, and in mice four different variants are generated. In addition, Opa1 is regulated by proteolytic cleavage, which causes reduction in the abundance of the long (L)-Opa1 isoforms, and enhances the abundance of the short (S) isoforms increase. It has been suggested that Opa1 mediates mitochondrial fusion through the long isoforms, and short isoforms are required by long isoforms to mediate fusion. The induction of apoptosis and the specific dissipation of mitochondria membrane potential induce the cleavage of L-Opa1 isoforms to S-Opa1 isoforms[32-34].

Opa1 knock-down results in mitochondrial fragmentation and a loss of mitochondrial fusion[19,25]. Opa1 repression activates apoptosis, and decreases cell growth and oxygen consumption[12,34]. In addition, Opa1 participates in the elimination of damaged mitochondria by autophagy[29].

1.1.2. Mitochondrial fission

Mitochondrial fission is necessary to drive old or damaged mitochondria from the cell through an autophagic process called mitophagy. The most relevant proteins in mitochondrial fission are Drp1, Fis1, and Mff that are located in the OMM (Figure 3). These proteins are also found in peroxisomes and regulate their fission[35-38]. Drp1 is also involved in the induction of apoptosis, given that the sensitivity of the cell to enter programmed cell death decreases when Drp1 is inhibited[39], in neuronal function, cardiac and muscle differentiation, and cell cycle. Moreover, Drp1 is expressed in all tissues.

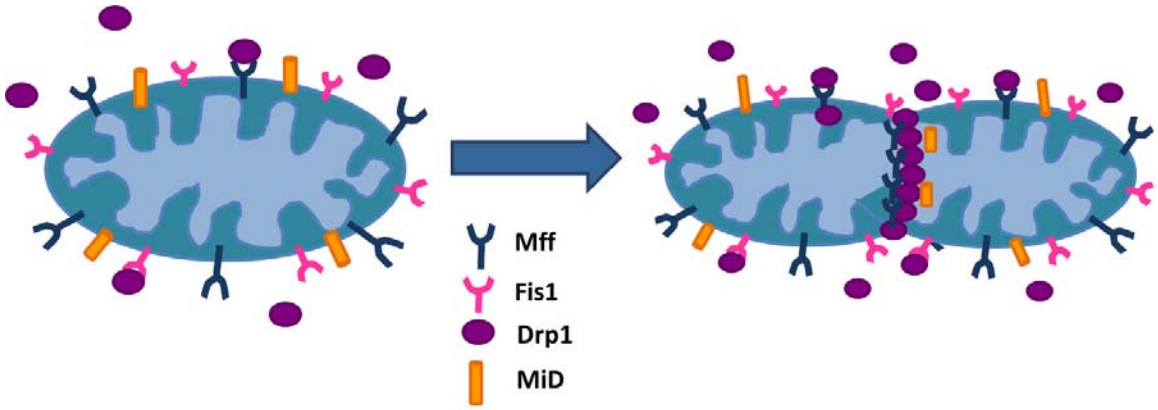

Figure 3. Mitochondrial proteins involved in fission process.

Drp1 contains a GTPase domain, a middle domain and the GED or assembly domain[40]. GTPase domain, middle and GED domain are rearranged by GTP, producing mitochondrial membrane constriction[41]. Drp1 dimer or tetramer, localized in the cytoplasm, assembles into larger oligomeric structures during mitochondrial fission at the mitochondrial

fission sites. These oligomeric structures that depend on GTP binding, surround the mitochondria, and form a spiral ring around the scission site. Finally, the mitochondria membrane is divided by GTP hydrolysis[42-44]. Mutations in GTP-binding generate long and interconnected mitochondria by inhibiting mitochondrial division, as well as Drp1 knockdown cells[45,46].

Dynamin related protein Drp1 mostly localizes to the cytoplasm and is recruited by several Mitochondrial Outer Membrane (MOM) proteins, such as Fis1, Mff, MiD49, and MiD51 to be located on the mitochondria and to regulate mitochondrial fission[43,46,47].

Fis1 is a small protein of 17 KDa and is composed by an NH_2- and COOH- terminal part. The former contains four differentiated regions with five α-helices[48,49], whereas the latter is composed by an α-helix, a transmembrane domain, and a COOH-terminal tail exposed to the intermembrane space[50]. The COOH terminal part of Fis1 is responsible for its uniform localization on the OMM[51], and the first α-helix from the NH_2-terminal part that is charged is crucial for mitochondrial fission activity and for Fis1 oligomerization[50]. It has been described that Drp1 functionally interact with Fis1[52]. The overexpression of Fis1 causes mitochondrial fragmentation, and its repression leads to mitochondrial elongation[53,54]. Moreover, Fis1 also plays a key role in apoptosis.[55]

The Mff protein contains a short amino-terminal, a middle segment with strong coiled coil forming propensity, and a carboxy-terminal hydrophobic segment[37]. Mff1 is a C-tail anchored protein linked to the mitochondrial fission[37]. Mff1 knockdown causes mitochondrial elongation[37] and decreases Drp1 mitochondrial levels[56]. In addition, Mff1 overexpression produces mitochondrial fragmentation with increased Drp1 recruitment to mitochondria[51,56,57]. Furthermore, Mff colocalizes with the Drp1 foci on the MOM[51], and in the absence of Drp1, Mff dotted structure disperses throughout the MOM[47], indicating that Drp1 affects oligomerization of Mff[47].

MiD49 and MiD51 (MiDs) are transmembrane proteins with C-terminal cytosolic domains that bind to the OMM by the N-terminus[58]. MiDs can mediate Drp1 recruitment and mitochondrial fission independently of Fis1 and Mff1[58-60]. Interestingly, overexpression of MiD49/MiD51 causes increase in Drp1-MiD51 interaction enhancing Drp1 recruitment to mitochondria. However, Drp1-MiD51 interaction affects the binding of GTP to Drp1, decreasing the fission activity of Drp1[61], and increasing the elongation of mitochondria[58,60,61]. Moreover, double MiD49/51 knockdown causes mitochondrial elongation and reduces Drp1 recruitment[58].

In addition, there are other proteins involved in mitochondrial dynamics, such as GDAP1. GDAP1 is localized in the OMM, and is expressed mainly in nerve tissue[62,63]. GDAP1 is composed by two separate glutathione-S-transferase (GST) domains and a COOH-terminal

bipartite hydrophobic domain. Niemann *et al*. reported that GDAP1 depletion causes mitochondrial elongation and GDAP1 overexpression produces mitochondrial fragmentation[62].

1.1.3. Functional impact of mitochondrial dynamics

Mitochondrial proteins involved in mitochondrial dynamics, such as Mfn2, Mfn1, Opa1, Drp1, and Fis1 regulate mitochondrial function, and consequently cell metabolism. Mitochondrial fusion and fission events allow mitochondria to exchange lipid membranes and intramitochondrial content to sustain mitochondrial population health. Fusion provides a pathway to recover defective mitochondria caused by the loss of essential components such as substrates, metabolites, specific lipids or mitochondrial DNA (mtDNA)[64]. mtDNA is essential for mitochondrial function given that encodes essential subunits of the respiratory complexes I, III and IV, which are indispensable for oxidative phosphorylation. Chen et al. described that mitochondria lose their mtDNA when mitochondrial fusion is abolished[65]. Moreover, Opa1-deficient MEF cells lacked mtDNA nucleoids[65]. On the other hand, fission produces mitochondrial fragmentation and facilitates apoptosis by releasing intermembrane-space proteins, such as cytochrome *c*, into the cytosol. Previous studies have reported that inhibition of fission activity blocks mitochondrial fragmentation, reduces cytochrome *c* release, and can reduce cell death[39,55].

A considerable amount of literature has been published on the relation between alterations in mitochondrial dynamics proteins and mitochondrial function. MEFs cells lacking Mfn2 or Mfn1 show a reduction in mitochondrial membrane potential[9]. Moreover, the same results were obtained in L6E9 lacking Mfn2, and glucose transport and lactate production are increased in these cells[66,67]. Mfn2-knockdown fibroblasts show reduced glucose oxidation and oxygen consumption[67]. Furthermore, fibroblasts that lack both Mfn1 and Mfn2 have reduced endogenous respiratory capacity, poor cell growth, inability to enhance respiration by the addition of the ionophore 2,4-dinitrophenol, and mitochondria show great heterogeneity in shape and membrane potential[25]. Cells that lack Opa1 show similar defects. Likewise, Opa1 deletion in cells causes a reduced mitochondrial membrane potential and cell respiration, disorganization of mitochondria cristae, and apoptosis[12,19,25,27]. Together, these studies outline that down-regulation of mitochondrial protein fusion reduces mitochondrial membrane potential and respiration. Knockdown of Drp1 fission protein in HeLa cells causes reduced basal and coupled respiration, and a lower rate of ATP synthesis[68]. These results were confirmed, and moreover Drp1 ablation causes a loss of mtDNA in mitochondria[69]. INS1 rat insulinoma Fis1 knockdown cells exhibit a reduction in maximal respiratory activity[29]. Furthermore, there is a large volume of literature describing that the ablation of mitochondrial fusion proteins causes a down-regulation of the expression of the OXPHOS components[25,66]. To better understand the relation between mitochondrial dynamics proteins and mitochondrial function Mfn2 was overexpressed in

HeLa cells. Mfn2 overexpression causes perinuclear aggregation of mitochondria, and an increase in mitochondrial membrane potential and glucose oxidation unrelated to Mfn2 mitochondrial fusion activity[66]. Furthermore, Mfn2 overexpression increased the expression of complexes I, IV and V in L6E9 cells[66].

Together, these studies outline that cells with Mfn2 loss-of-function reduce the activity of krebs cycle and the electron transport chain, and they try to supply the energy deficiency by increasing the rate of glucose uptake and glycolysis and decreasing the rate of glycogen synthesis[8]. Mfn2 gain-of-function shows the opposite effect, it activates mitochondrial metabolism and increases the expression of subunits of the OXPHOS system.

1.1.4. Mitochondrial dynamic proteins involved in metabolic disease

In addition to the relation between alterations in mitochondrial dynamics proteins and mitochondrial function, several human diseases are caused by mutations in genes involved in mitochondrial dynamics.

Heterozygous mutations in Opa1 cause autosomal dominant optic atrophy (ADOA), and is the most common form of inherited optic neuropathy[70,71]. ADOA is characterized by visual impairment as a result of a primary degeneration of retinal ganglion cells, and consequently and increasing atrophy of the optic nerve. ADOA is diagnosed in a range of 1 to 12,000 or 50,000.[72,73] More than 100 pathogenic Opa1 mutations have been identified, with most occurring in the GTPase domain[74], and causing a premature truncation of the Opa1 protein. In addition, Opa1 mutations have been associated with reduced ATP production and reduced mtDNA content[75,76].

Charcot-Marie-Tooth (CMT) disease, one of the most common hereditary neuropathies, is caused by mutations in at least 30 different genes[77]. Affected individuals have progressive distal motor and sensory impairments, which cause weakness and distal muscle atrophy. CMT is diagnosed in 1 of 2,500 individuals[78]. CMT2A is an axonopathy that is caused by a defect in the neurons, and produces loss of peripheral nerve function. CMT2A presents an autosomal dominant neurodegenerative inheritance pattern, and it has been associated with more than 40 mutations in Mfn2, most occurring near the GTPase domain. A subset of patients with CMT2A have optic atrophy, suggesting that Opa1 and Mfn2 mutations can overlap clinical results[79,80]. Another form of CMT is CMT4A where GDAP1, an integral outer membrane protein that probably affects mitochondrial division[62], is mutated. This disease is caused by a primary defect in the Schwann cells that myelinate the peripheral nerves, and by a defect in the neurons.

Both type 2 diabetes and obesity are characterized by insulin resistance. A reduced expression of Mfn2 has been found in skeletal muscle from obese nondiabetic subjects and

in obese or nonobese type 2 diabetic patients[67,81]. Moreover, mitochondrial number and size are reduced in the skeletal muscle of obese and type 2 diabetic patients compared with lean subjects[82,83]. Metabolic inflexibility, i.e., a higher capacity to oxidize lipids instead of glucose in insulin-stimulated conditions, is characterized by dysregulation of OXPHOS activity[84] and by reduction in the expression of OXPHOS subunits genes in muscle from type 2 diabetic patients[85,86]. Our laboratory has reported that tumor necrosis factor (TNF)-α and interleukin-6, which are involved in insulin resistance, inhibit Mfn2 gene expression in cells[81]. Likewise, a negative linear relationship between Mfn2 mRNA levels and body mass index, and a positive correlation between Mfn2 expression in skeletal muscle and insulin sensitivity have been detected in healthy control subjects, and in obese or type 2 diabetic patients[81]. Furthermore, our group has reported that Mfn2 deficiency in liver or muscle leads to glucose intolerance and insulin resistance in mice[87].

1.2. Mitochondrial bioenergetics

Mitochondrion accommodates most of the cellular energy systems to complete the oxidation of sugars, fatty acids and proteins to produce ATP by oxidative phosphorylation[88]. Each of these three substrates can be catabolized to acetyl-CoA, and can enter the citric acid cycle, also known as the tricarboxylic acid (TCA) or Krebs cycle, which takes place in the mitochondrial matrix (Figure 4).

Glycolysis is the metabolic pathway that converts glucose (sugars) into pyruvate in the cytosol of the cell, and then pyruvate is converted to acetyl-CoA by pyruvate dehydrogenase in the mitochondria. Beta oxidation converts fatty acids to acetyl-CoA inside the mitochondria, and diverse enzymes transform specific amino acids into pyruvate, acetyl-CoA or into specific citric acid cycle intermediates[89,90].

The citric acid cycle is used by all aerobic organisms to generate energy through the oxidation of acetate derived from carbohydrates, fatty acids and proteins. The cycle begins with the transfer of a two-carbon acetyl group from acetyl-CoA to the four-carbon oxaloacetate, to produce the six-carbon molecule citrate. Then, citrate undergoes a series of seven subsequent enzymatic steps, providing precursors of certain amino acids, two molecules of carbon dioxide, and finally oxaloacetate. The oxaloacetate is free to enter in the cycle again. Most of the energy liberated in the enzymatic reactions of the citric acid cycle is transferred as electrons to the mitochondrial electron transport chain by the cofactors nicotinamide adenine dinucleotide (NADH) and flavin adenine dinucleotide ($FADH_2$).

The electron transport chain (ETC), also known as the respiratory chain, is composed of four multisubunit protein complexes (I–IV) embedded in the inner mitochondrial

membrane (Figure 4). Complexes I, or NADH dehydrogenase, and complex II, or succinate dehydrogenase, oxidize NADH and $FADH_2$ respectively through transferring the resulting electrons to ubiquinone, also known as coenzyme Q, which is reduced to ubiquinol. Simultaneously, four protons, linked to the transport of electrons from NADH through complex I, translocate from the matrix to the inner mitochondrial membrane. It is of interest to notice that the enzyme catalyzing the reduction of FAD to $FADH_2$ in the citric acid cycle, is itself part of the ETC and it does not pump protons from the matrix to the intermembrane space. Ubiquinol diffuses through the IMM and carries electrons to complex III, or cytochrome *c* reductase. Complex III oxidizes ubiquinol to ubiquinone and passes the electrons across the intermembrane space to two molecules of cytochrome c, and four protons (two from the mitochondrial matrix) are translocated to the intermembrane space[91]. This process is called the Q cycle. Cytochrome *c*, a mobile protein in the intermembrane space, brings electrons to complex IV, also called cytochrome *c* oxidase, which uses the electrons to reduce oxygen to water. Alongside to this reaction four protons are pumped from the matrix to the intermembrane space. All the electrons provided by NADH and $FADH_2$, from the Krebs cycle, are used to transfer the protons from the matrix to the intermembrane space to generate a mitochondrial membrane potential difference across the IMM. This potential difference is used by complex V, or ATP synthase, to fuse free phosphate with adenosine diphosphate (ADP) to synthesize ATP in the final step of oxidative phosphorylation. Typically, three ATP molecules per molecule of NADH, and two ATP molecules per molecule of $FADH_2$ are produced by oxidative phosphorylation.

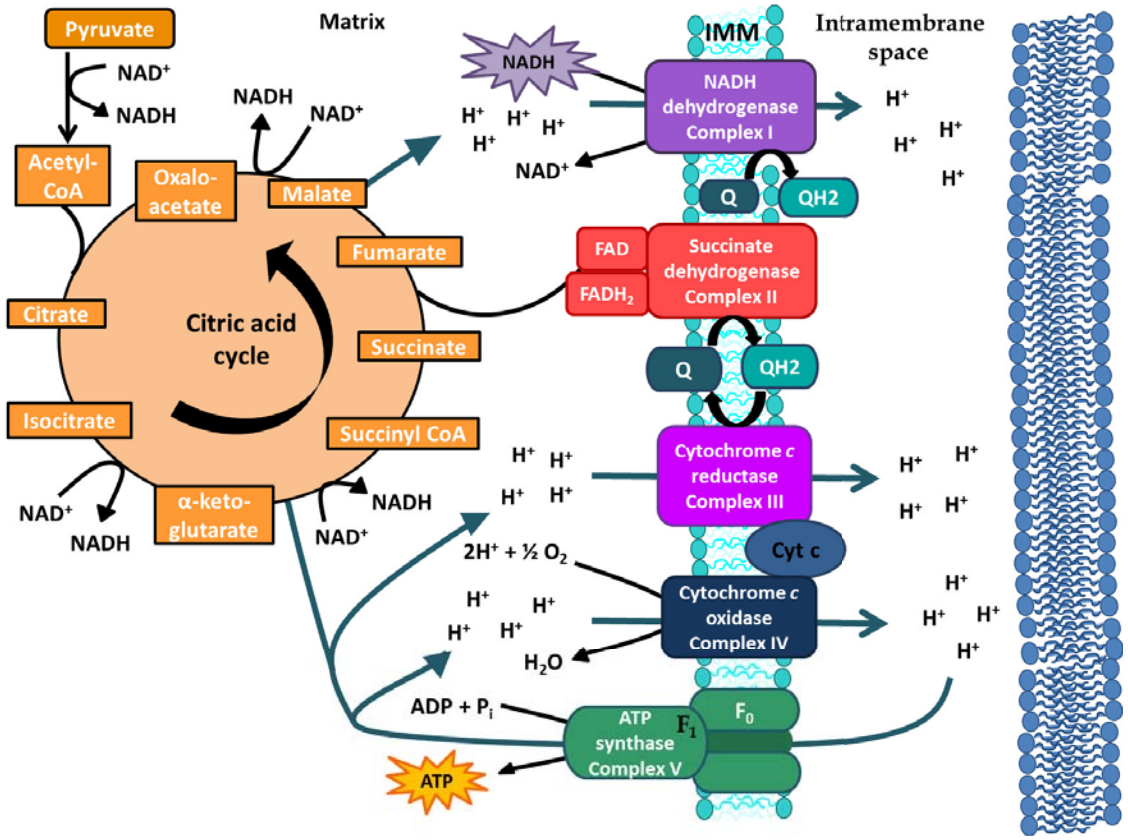

Figure 4. Bioenergetic of the electron transport chain and the citric acid cycle.

Protons are able to leak across the mitochondrial membrane, and this process is known as uncoupling, because the membrane potential is not coupled to ATP production. Uncoupling protein is a mitochondrial inner membrane protein that can dissipate the proton gradient to generate heat instead of ATP. In addition to protons, electrons are also able to leak from the electron transport chain complexes. Premature leakage of electrons allows their reaction directly to oxygen producing superoxide, which is highly reactive and produces oxidative stress to cells[92,93].

Complexes I and II generate reactive oxygen species (ROS) within the mitochondrial matrix while complex III generates superoxide anion into either the matrix or the intermembrane space[94,95,96]. Superoxide generated in the intermembrane space can escape into the cytoplasm through voltage-dependent anion channels[97]. ROS induces cellular machinery dysfunction, and can lead to mitochondrial damage and apoptosis[98,99].

Furthermore, it has been described that the OXPHOS complexes of the electron transport chain differ in abundance[92] and associate into supramacromolecular assemblies to give stability to the individual complexes, to prevent oxygen radical formation, and to facilitate efficient electron flow[100,101]. The complexes I, III, and IV were found to form different types of supercomplexes[102], whereas complex II was never found to be part in none of them. It has been accepted that OXPHOS supercomplexes and single OXPHOS complexes coexist as a dynamic process within the inner mitochondrial membrane[102].

2. Pyrimidine synthesis is linked to electron transport chain

Nucleotides are composed of a nitrogenous base, a five-carbon sugar (ribose or deoxyribose), and can contain up three phosphate groups. Nucleotides have diverse roles in the cell as to transport energy, such as nucleosides triphosphates (ATP, GTP, CTP and UTP), signalling molecules, metabolic regulation, and precursors to informational macromolecules such as DNA and RNA. Deoxynucleoside triphosphates (dNTPs) and nucleosides triphosphates (NTPs) are the substrates for DNA and RNA biosynthesis, respectively. The former is indispensable for cell division, whereas the latter is essential for protein synthesis. If the supply of nucleotides becomes limiting, cells can not synthesize DNA or RNA.

Almost all organisms can make the purine and pyrimidine nucleotides via *de novo* biosynthetic pathway, which form complex end products from simple precursors. Many organisms also have salvage pathways to recover purine and pyrimidine compounds obtained in the diet or released during nucleic acid turnover and degradation. Two purines and three pyrimidines are the building block of nucleic acids. Purines consist of a six-membered and a five-membered nitrogen-containing ring, fused together, whereas pyrimidines have a six-membered nitrogen-containing ring. The purines that are found in RNA and DNA are adenine and guanine, and the pyrimidines are cytosine, uracil, and thymine. Cytosine is found in RNA and DNA, uracil in RNA, and thymine in DNA. We will focus in the synthesis of pyrimidines substrates.

Uridine-5'-monophosphate (UMP) synthesis starts with the assembly of the pyrimidine ring system, and then a ribose-5-P moiety is attached (Figure 5). Starting with ATP and glutamine, UMP synthesis is initiated by the enzyme carbamoyl phosphate synthetase II (CPS II), a cytosolic enzyme that produces carbamoyl phosphate. Then, aspartate transcarbamylase (ATCase) catalyses the condensation of carbamoyl phosphate with aspartate, to form carbamoyl-aspartate. The next step is ring closure and dehydration by an intramolecular condensation catalysed by the enzyme dihydroorotase (DHOase). The product of this reaction give a six-membered heterocyclic ring characteristic of pyrimidines, called dihydroorotate (DHO). The enzyme dihydroorotate dehydrogenase (DHODH) is located in the inner mitochondrial membrane in eukaryotic organisms, and catalyses the oxidation of dihydroorotate into orotate using ubiquinone as co-substrate electron acceptor. DHODH enzyme has two binding sites, dihydroorotate binds to the first site and is oxidized via a cosubstrate electron acceptor, and after the release of orotate, ubiquinone binds to a second site and receives an electron from the cosubstrate. Ubiquinone is converted to ubiquinol, which is a substrate for Complex III in the respiratory chain. Thus, the *de novo* synthesis of pyrimidine nucleotides is coupled to the mitochondrial respiratory chain (RC) via DHODH. The fifth reaction in the *de novo* synthesis of pyrimidines is the bound between the ribose-5-phosphate moiety to the N-1 of orotate catalysed by the enzyme orotate phosphoribosyltransferase to give the orotidine-5'-monophosphate (OMP), a primary

nucleotide. Phosphoribosyl pyrophosphate (PRPP) is the donor of the ribose phosphate. Finally, decarboxylation of OMP gives UMP, one of the common pyrimidine ribonucleotides. All the process described above is known as the *de novo* UMP biosynthesis. However, external uridine also can be taken up by the cells and enter the metabolic pathway, this process is known as the salvage pathway. This is achieved by conversion of uridine to UMP by uridine kinase (udk)[103].

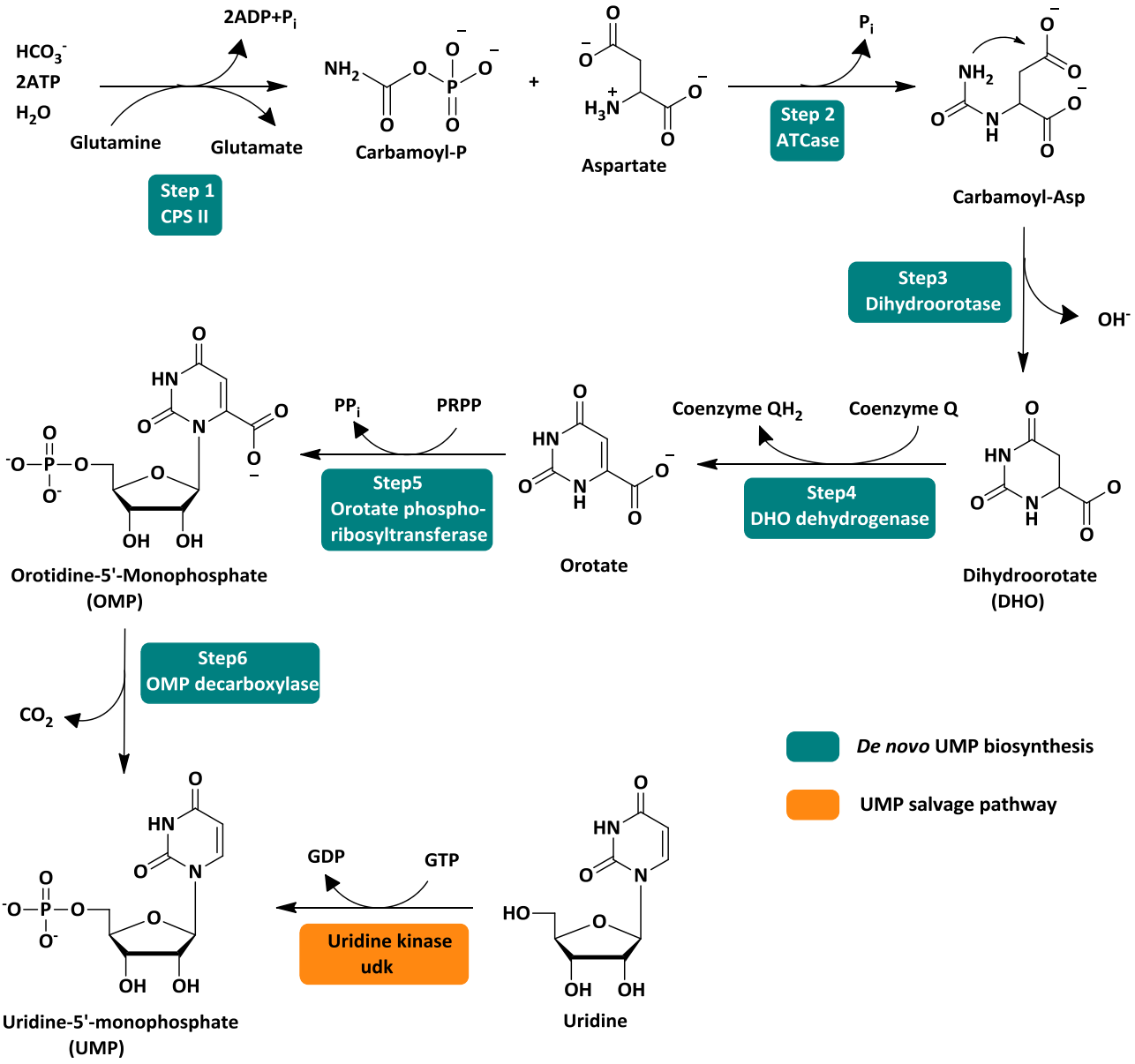

Figure 5. The *de novo* pyrimidine biosynthetic pathway.

The synthesis of the ribonucleotides uridine-5'-triphosphate (UTP) and cytidine-5'-triphosphate (CTP), which are substrates for the RNA polymerase, come from UMP via the same pathway (Figure 6). Moreover, UTP is the source of energy for activating glucose and galactose, and CTP is an energy source in lipid metabolism. In the first step UMP undergoes to UDP via an ATP-dependent nucleoside monophosphate kinase. Secondly, UTP, which is a

precursor of CTP, is formed from UDP by a nucleoside diphosphate kinase. Finally, the enzyme cytidylate synthetase catalyzes the amination of the 4-position of the UTP pyrimidine ring to provide CTP.

The enzyme DNA polymerase, which uses deoxynucleosides triphosphates as substrates, produces DNA. To ensure enough precursors for DNA synthesis, two reactions must occur. First, the 2' position of the ribose ring of ribonucleotides must be reduced from a C-OH to a C-H before the nucleotides can be used for DNA synthesis. Secondly, the thymine ring must be manufactured by addition of a methyl group to uridine.

In most organisms, ribonucleoside diphosphates (NDPs) are the substrates for deoxyribonucleotides formation. The enzymes ribonucleotide reductases (RNRs) are the unique enzymes that catalyze the reduction of nucleotides (ADP, GDP, CDP, and UDP) to their corresponding deoxynucleotides via radical chemistry. RNRs control the relative ratios and absolute concentrations of cellular dNTP pools, and are responsible for genome replication. The deoxyribonucleotides deoxycytidine monophosphate (dCMP) and deoxythymidine monophosphate (dTMP) are precursors for DNA synthesis.

The synthesis of thymine nucleotides proceeds from other pyrimidine deoxyribonucleotides. dTMP production is dependent on deoxyuridine monophosphate (dUMP) formation, a deoxyribonucleotide intermediate in pyrimidine biosynthesis. dUMP can be produced from CTP or deoxyuridine diphosphate (dUDP).

In the first route, dUMP is produced by phosphorylation of dUDP to form deoxyuridine triphosphate (dUTP). Then, dUTP is quickly cleaved in cells by deoxyuridine nucleotidohydrolase (dUTPase) to yield dUMP. dUTP fast removal is important in cells, given that uracil base can be incorporated into DNA. In the second route cystidine diphosphate (CDP), a component of CDP-diacylglycerol, which is an important intermediate in glycerophospholipid biosynthesis, is formed metabolically from CTP by a phosphatase enzyme. Then, CDP is converted to deoxycitidine diphosphate (dCDP) by RNR enzyme, and subsequent dephosphorylation is accomplished to provide deoxycytidine monophosphate (dCMP). Finally, dCMP is converted to dUMP by the dCMP deaminase enzyme.

Once the dUMP has been synthesized, dUMP is methylated by the enzyme thymidylate synthase (TS) to give dTMP. These routes are part of the *de novo* synthetic pathway for dTTP production.

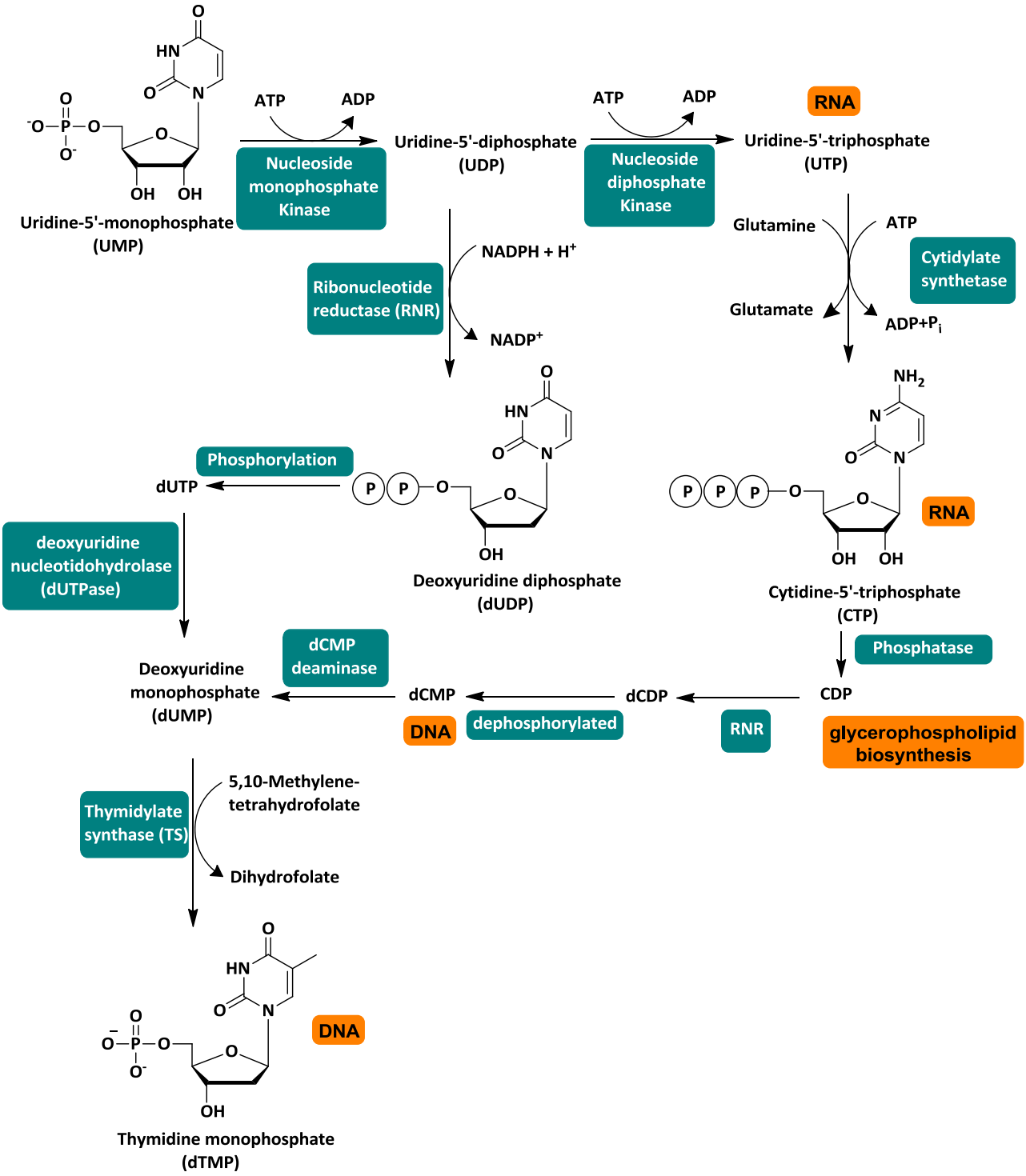

Figure 6. Synthesis of ribonucleotides UTP and CTP, and dTMP.

It is of interest to notice the link and relation between pyrimidine biosynthesis, DHODH and the functional respiratory chain in mammals. The enzyme DHODH is located in the inner mitochondrial membrane, whereas the other five enzymes of the biosynthetic pathway are present as multifunctional proteins in the cytosol. The first three enzymes of the *de novo* pyrimidine pathway (CPS II, ATCase, and DHOase) physical associate to form a polypeptide called CAD, and the last two steps of *de novo* pyrimidine biosynthesis are catalyzed by UMP synthase, which is a bifunctional protein. Any dysfunction of the

respiratory chain, such as lack of oxygen, presence of inhibitors, as well as, complex III defects, automatically would cause impairments of UMP synthesis, a decrease in the nucleotides pools, substantial effects on DNA and RNA synthesis, and protein turnover causing cell cycle arrest. In this sense, it has been reported that DHODH function requires active complex III of the respiratory chain[104], and impairment of DHODH affect the respiratory chain function inhibiting complex III[105]. Moreover, DHODH physically interacts with complex III[105].

3. p53 pathway is linked to mitochondrial function and pyrimidine biosynthesis

The p53 tumor suppressor plays a key role in genetic stability regulating quality control functions to repair processes or to initiate cell death programs by limiting proliferation, motility and viability of abnormal or damaged cells. p53 acts as a transcription factor, which activates or represses several genes to accomplish several functions such as DNA repair, metabolism regulation, cell cycle progression, senescence, and apoptosis. The p53 pathway responds to various cellular stress signals including DNA damage, such as γ-radiation, UV, genotoxic drugs, as well as to conditions that indirectly damage genome integrity, such as oxidative and nutritional stress, defective cytoskeleton, altered cell adhesion, ribonucleotide depletion, and oncogene activation[106,107-109].

Mitochondria are critically important for the p53-mediated cell death, because p53-dependent apoptosis leads to mitochondrial apoptotic changes by release of mitochondrial cytochrome *c* and activation of the caspase cascade[110]. In addition, p53 can induce a transcription-independent apoptosis through the direct interaction with Bcl-2 family proteins[111]. On the other hand, p53 also controls mtDNA regulating the nuclear DNA-encoded mitochondrial transcription factor A (TFAM)[112], and interacts with the repair enzymes mitochondrial single-stranded DNA-binding protein (mtSSB)[113] and TFAM[114] forming p53/TFAM/mtDNA complexes[115] to protect mitochondrial genome. Moreover, p53 interacts with mitochondrial DNA polymerase[116] to promote replication and repair of mtDNA[117]. p53R2, one of the two small subunits comprising ribonucleotide reductase, is transcriptionally induced by p53 upon DNA damage[118], and is reduced in p53 knockdown cells[118,119]. p53 also interacts with an F1F0 ATP synthase subunit to set up the assembly of the ATP synthase complex[120]. Altogether these results confirm that p53 protects mitochondrial genome and supports mitochondrial biogenesis and function.

PGC-1α (peroxisome-proliferator-activated receptor gamma coactivator-1α) is a co-transcriptional co-activator of mitochondrial biogenesis involved in the regulation of genes of energy metabolism[121,122]. In p53 knockout mice mitochondrial content and the levels of PGC-1α in skeletal muscle tissue are reduced[123]. Interestingly, PGC-1α binds to p53 and regulates p53 transcriptional activity promoting pro-cell cycle arrest and pro-metabolic target genes under conditions of metabolic stress[124].

Recent studies suggest that p53 is implicated in the regulation of mitochondrial dynamics by modulating the expression and activity of mitochondrial proteins involved in fusion and fission events[125]. It has been described that the process of fission is a prerequisite for mitophagy[29,126], whereas fusion is required for maintenance of mtDNA[127]. Mfn2 is a direct target of p53, and Mfn2 expression is up-regulated in a p53-dependent manner in HepG2 hepatocellular carcinoma cells[128]. Moreover, p53 induces Drp1 in cardiomyocytes

undergoing apoptosis[129]. In addition, p53 can cause mitochondrial fission in HeLa cells by promoting the translocation of Drp1 to mitochondria[130]. Recently, it has been described that p53, which is involved in Huntington's disease (HD) pathogenesis, binds to Drp1 and mediates Drp1-induced mitochondrial and neuronal damage[131]. However, Wang et al. described that treatment of cultured postnatal cortical neurons with camptothecin (CPT), a DNA damaging agent, results in elongated mitochondria as a result of posttranscriptional suppression of Drp1 by p53[132].

A relationship exists between p53 and pyrimidine synthesis. Linke et al.[133] described that ribonucleotide biosynthesis inhibitors, such as *n*-phosphonacetyl-L-aspartate (PALA), pyrazofurin (Pyf), and cyclopentenylcytosine (CPEC), causing depletion of ribonucleotide pools, induce a strong p53 response in the absence of DNA damage. In normal fibroblasts depletion of ribonucleotides results in a p53-dependent arrest at the G_o/G_1 phase of the cell cycle. They showed that CTP, GTP, or UTP depletion was sufficient to induce p53 arrest. Addition of external uridine, which restored nucleotides levels through salvage pathways, reversed p53 up-regulation. They suggested that p53 can maintain genetic stability by preventing DNA replication during metabolic depletion. Moreover, Khutornenko et al.[134] reported that strong p53 response is induced specifically after an inhibition of the mitochondrial cytochrome bc1 (the electron chain complex III) but not by the impairment of the ETC itself. The p53 response is triggered by the deficiency in pyrimidines that is developed through the uncoupling of complex III and inner mitochondrial membrane-bound DHODH enzyme. DHODH converts dihydroorotate to orotate using ubiquinone as a direct electron acceptor. Ubiquinone is converted to ubiquinol, which carries electrons to complex III. Specific complex III inhibitors, as myxothiazol and antimycin A, and DHODH inhibitors, as leflunomide, up-regulate p53 by blocking directly or indirectly the DHODH enzyme and consequently the pyrimidine biosynthesis.

4. Development of cell-based reporter assays for screening modulators of gene promoters.

In recent years, the use of HTS technologies has emerged as a powerful tool for drug discovery as a result of the growing number of potential therapeutic targets and the development of large compound libraries[135-137]. This has stimulated the development and optimization of valid assays for HTS. Many factors influence the format of the assays used in HTS, such as the type of the pharmacological information for the target class, throughput, cost of the assay and other logistical considerations. However, the use of a cell-based assay is crucial in the process, because it is unlikely that any lead will progress to become a drug candidate without first having demonstrated activity in an appropriate cell model.

Cell based-assays can be classified into three broad categories: second messenger assays, which monitor signal transduction after the activation of cell-surface receptors; reporter gene assays, which monitor cellular responses at transcriptional level; and cell proliferation assays, which monitor the cellular growth or no growth in response to external stimuli[138]. In this section we will focus on cell-based reporter gene assays.

In the development of cell-based reporter gene assays to identify modulators of gene promoter activity, there are several aspects that should be considered, such as the generation of the promoter-reporter gene construct, the choice of the promoter and the reporter gene, the cellular model used, the miniaturization of the assay, the HTS screening itself and the validation of the potential modulators (Figure 7). In this section we will explain all these issues in more detail.

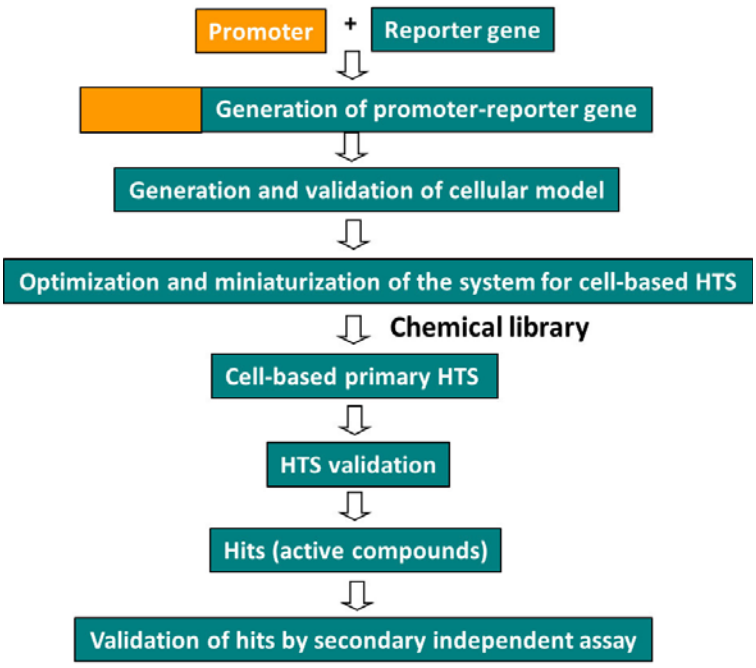

Figure 7 . Schematic process of cell-based reporter gene assay for High Throughput Screening of modulators of gene promoter activity.

4.1. Generation of promoter-reporter gene constructs

Reporter-gene assays are used as indicators of transcriptional activity or activation of particular signaling pathways within the cell. These assays consist of a reporter gene unit that is expressed in a selected cell line. This unit is comprised of the promoter of the target gene and a reporter gene, so that after the activation of the target gene the reporter gene product is also expressed. A critical issue in the establishment of a useful assay system is the choice of a suitable combination of promoter and reporter gene. In this section we will discuss the considerations to be made when defining this optimum combination.

4.1.1. Choice of the promoter

The choice of the promoter depends on the nature of the signaling pathway under study. Relevant parameters to consider are the basal activity of the promoter and the degree of stimulation that can be measured. Promoters can be operationally classified into the following two categories: natural or endogenous promoters, and synthetic promoter elements. Natural promoters contain in their sequence response elements for different transcription factors and therefore the regulation of these promoters is under the control of a complex range of signal transduction pathways [139]. This implies that a careful analysis of the results is required because of the diversity of transcription factors that could be involved in the control of the promoter. In this regard, it is possible to reduce potential interferences by using synthetic promoters that contain a single transcription factor binding site. However, these promoters are still subjected to the regulation of intracellular signaling pathways. Another option is a synthetic promoter that is unable to bind transcription factors native to the cellular model used.

4.1.2. Choice of the reporter

The first important consideration in the choice of the reporter gene is that its product must have unique enzymatic activity that is easily identified and detectable from the mixture of intra- and extra-cellular proteins. Moreover, the product should have a physical property that makes it straightforward to measure by simple, inexpensive and sensitive methods, such as colorimetry, luminescence and fluorescence. Suitable reporters include enzymes that provide cells with new enzymatic capacity, existing enzymes but with higher thermal stability, products secreted by the cell that are easily measurable in the media, fluorescent proteins and bioluminescent proteins. Reporter genes can currently be classified into two groups: intracellular or extracellular [140]. The former are those whose products are generated and retained inside the cell, while the latter are secreted into the culture medium, thereby allowing the detection of the reporter protein activity in culture medium without disturbing the cell. Intracellular reporter genes used in cell-based assays include chloramphenicol acetyltransferase (CAT), β-galactosidase, aequorin, green fluorescent protein (GFP) and

luciferase, whereas extracellular reporter genes comprise secreted placental alkaline phosphatase (SPAP) and β-lactamase (Table 1).

Reporter gene	Advantages	Disadvantages
Chloramphenicol acetyltransferase (CAT)	No endogenous activity. Inexpensive. Automated ELISA available.	High stability. Use of radioisotopes. Insensitive. Narrow linear range.
β-galactosidase	Well characterized. Simple. Colorimetric and bio-or chemiluminescent assays available.	Endogenous activity (mammalian cells).
Aequorin	High sensitivity. Low background.	Requirement of cofactor and calcium.
Green Fluorescent Protein (GFP)	Autofluorescent (no substrate needed). No cell lysis is necessary. No endogenous activity. Mutants with altered spectral qualities available.	Requires post-translational modification. High stability. High background due to accumulation in the cell.
Luciferase (Firefly)	High sensitivity and low stability. Broad linear range. No endogenous activity in mammalian cells.	The assay requires the presence of substrate (luciferine), O_2 and ATP.
Luciferase (Renilla)	High sensitivity and low stability. Broad linear range. No endogenous activity in mammalian cells. No cell lysis is necessary.	The assay requires the presence of substrate (coelenterazine), O_2 and ATP.
Secreted Placental Alkaline Phosphatase (SPAP)	Secreted protein. Inexpensive colorimetric and highly sensitive luminescent assays available.	Endogenous activity in some cells. Possible interference with compounds being screened.
β-lactamase	Secreted protein. No endogenous activity. Sensitive and robust colorimetric and fluorogenic assays available.	Possible interference with compounds being screened.

Table1. Summary of commonly used reporter genes.

The choice of the reporter gene will also depend on the suitability of the assay for a particular study (i.e. sensitivity, reliability, detection limits, and reporter dynamics) [141]. For transcriptional kinetic research or HTS, a reporter gene with low stability and high sensitivity (such as luciferase, with a half-life of 5-6 h) will be the best option. In contrast, reporter genes with high stability and low sensitivity (such as GFP or CAT) will be less effective for these purposes.

All these reporter genes can also be used in combination. For example, SPAP has been used together with luciferase and β-galactosidase to normalize transfection efficiency, and β-galactosidase and Renilla luciferase have been used in conjunction with firefly luciferase for multiple readouts from a single sample[142] and dual detection of gene transcription[143]. These dual reporter assays allow minimization of the experimental variability caused by cell viability, cell number, and cell transfection efficiency in the case of transiently transfected cell lines.

In the present thesis we decided to choose the Luciferase enzyme to perform the HTS. Luciferase refers to a family of enzymes that catalyzes the oxidation of various substrates (e.g. luciferin and coelenterzine), producing light emission. Genes encoding luciferase have been cloned from various species of firefly, beetle, crustaceans, bacteria and the sea pansy. However, the most commonly used in mammalian cells are those from the firefly (*Photinus pyralis*) and the bioluminescent sea pansy *Renilla reniformis*[142]. Firefly luciferase catalyzes the oxidation of luciferin, producing a short-lived flash of light that decays within a few seconds. It has a high sensitivity and a broad linear range (up to 7-8 orders of magnitude). Moreover, the amount of light emitted is proportional to the activation of the promoter and therefore to the transcriptional activity of the target gene. The main disadvantages of firefly luciferase in the original assay are the requirement for cell lysis prior the addition of the substrate luciferin and the difficulty in the detection of the short flash of light. However, these problems have been solved by the use of membrane-permeable and photolysable firefly luciferin esters [144,145], which circumvent the requirement for cell disruption, and the development of "glow" reagents that prolong the half-life of the flash of light to several hours[146]. A common alternative to firefly luciferase is the sea pansy *R. reniformis* enzyme, which catalyzes the oxidation of coelenterazine to produce light. Its sensitivity and detection range are similar to the firefly luciferase, as is the half-life of the flash of light emitted. Moreover, the substrate coelenterazine is membrane-permeable. Therefore Renilla luciferase is appropriate for reporter assays in intact cells[147]. Recently, dual-color and tricolor luciferase reporter assays have been developed [148]. These systems are based on luciferase mutants that emit different colors but react with the same luminescent substrate. These assays allow measurement of the activity of the three reporter genes in a one-step reaction, dividing each emission by an optical filter.

4.2. Generation and validation of the cellular model

The selection of the correct cellular model also has a large impact on the success of the assay. Several aspects should be taken into consideration when choosing a cellular model. First of all, the absence of endogenous background for the reporter gene used is crucial. In this regard, luciferases allow the use of mammalian cells because they do not have any internal background. However, when using β-galactosidase or β-lactamase as reporter genes, this is not the case, because mammalian cells possess endogenous intrinsic fluorescent background, thereby making this technique less sensitive.

A relevant consideration is that the assay can be done using primary cell cultures or immortalized cell lines. Primary human cells are closer to *in vivo* conditions and therefore more physiologically relevant than immortalized cell lines. In addition, several selected primary cell types from humans and other species are now commercially available. However, primary cells are difficult to obtain at the scale required for HTS, and therefore are more

useful for low-throughput assays. Transformed cell lines are the most used for HTS purposes, and they can be useful for screening target genes endogenously expressed in cells.

Finally, assays can involve native and engineered cell lines. The former are used for the determination of endogenously expressed gene targets, whereas the latter are designed to express or overexpress a target gene. Expression can be either transient or stable and several expression systems can be used depending on the nature of the cell line and target. Stable cell lines are generated by transfection or transduction (by retrovirus or lentivirus infection) of a plasmid encoding for the promoter-reporter gene unit and a selection marker that will allow the selection of clones that integrate the construct. The selection can be performed by means of culture medium supplemented with antibiotics such as puromycin or neomycin. Therefore only cells expressing the gene conferring resistance to these antibiotics will survive in the selection medium. Another way to select positive clones is by using the activity of the fluorescent reporter gene itself. Cells are incubated with a compound known to activate the expression of the target gene, and the cells showing enhanced reporter gene activity are then selected by fluorescence activated cell sorting (FACS) or by fluorescence microscopy [149].

The final step after generating engineered cell lines is the validation of the cellular model produced. After transfection/transduction of the plasmid, the gene promoter-reporter gene unit can be integrated in any place of the cell genome, and in some cases this could affect the expression of the target promoter-reporter gene construct, alter the expression of other genes, or even induce changes in the phenotype of the cell. To ensure that the engineered cell line generated will respond adequately in terms of the expression of the target promoter-reporter gene unit, it is necessary to validate the clones obtained. This procedure can be done by using a compound that is known to be an activator of the target gene (a positive control). Each clone is incubated with the compound and the activity of the reporter gene is measured. Only those clones presenting an increase in reporter gene activity upon incubation with the positive control are selected. Furthermore, from the clones selected, it is possible to choose between those that show different levels of either basal or stimulated reporter gene activity.

4.3. Optimization and miniaturization of conditions for cell-based reporter assays in HTS

Given the increases in the number of compounds included in chemical libraries and in the number of molecular targets for lead fitting and sensitivity assays, the miniaturization and automation of HTS systems is required. Assays developed for HTS can be divided in two categories: biochemical and cell-based. The former are simple, direct and specific to the target of interest, allowing structure–activity relationships for weak inhibitors. However, the

activity of a molecule in an *in vitro* assay does not always show the same activity as in a cellular environment. This difference is attributed to diverse *in vivo* effects, such as plasma membrane permeability, cytotoxicity and off-target effects. In contrast to biochemical assays, cell-based assays attempt to identify modulators of a pathway of interest without previous knowledge of the specific target. These assays allow the selection of a compound with activity and capacity to cross cell membrane but without cytotoxic effects. Generally, gene reporter cell-based assays are used to study the regulation of a gene of interest in primary HTS and biochemical assays are used in a secondary screen to identify false positives.

The most important formats for compound testing are standard 384, low volume 384[150] and the 1536 well microtiter plates (w-MTP). These formats require several steps of optimization, such as the nature of the response assay, the duration of the response and whether the compound activity can be conditioned by other stimuli. The best approach is optimized under miniaturized conditions in terms of time, cost and quality of the process. A secondary screen or counter screen using a different methodology or biological readout of target activity should be done to discard compounds that generate a positive signal via other mechanisms.

For cell-based assays, the following parameters should be optimized: sensitivity, reproducibility, accuracy of the positive and negative controls and economy. Sensitivity optimization includes determining the optimal cell density for the assay, the reagent amounts, the optimal concentration of compounds, and determination of cell incubation time with compounds to maintain robust signal detection and acceptable signal-to-background levels. Sensitivity to compound solvent (usually dimethylsulfoxide (DMSO)) should also be determined for cell-based assays. DMSO at 1% or greater can interfere in these kinds of assays. The reproducibility and stability of the reagents and biological response over the time course of an assay and also among well-to-well, plate-to-plate, day-to-day, and batch-to-batch variations should be determined using positive and negative controls. Reproducibility is dependent on assay reagents and instrument settings, such as dispensers (volume, speed, height and position of the pins/tips to be adjusted to avoid damaging adherent cells), incubators and detectors. Positive and negative controls must be included in each plate of the assay to provide diagnostic information. Ideally, controls should be located randomly among the 96, 384, 1536 wells of each plate, but usually the first and the last columns are used for controls. The best option is to place positive and negative controls alternately in order to achieve the same distribution on each row and each of the two columns [151]. This control plate can be used for replicate assay plates on two consecutive days to evaluate well-to-well, plate-to-plate, and day-to-day variations of the assay.

In assay development, the time required for readout of a single well is a critical parameter for successful HTS, which analyses hundreds to thousands of compounds. The

main time-consuming steps of screening are assay development and adaptation, data analysis and interpretation, hit validation and secondary assays. HTS is costly and time should be devoted in advance in order to ensure valuable data from the HTS output.

4.4. Validation of HTS screening

The last step of HTS comprises validation. When validating an assay protocol, it is important to consider performance and sensitivity. The evaluation of the performance is composed by two parameters: signal window and Z' factor, the former evaluating the fold response between maximum and minimum signals and the latter evaluating the precision of this response within a plate and across plates. The signal window measures the statistically significant difference between the maximum (positive activity) and minimum signal (background):

$$SW = (\mu_{max} - \mu_{min} - 3(\sigma_{max} + \sigma_{min}))/\sigma_{max}$$

Given that the activity of a compound in primary HTS is measured in a single well at only one concentration, without replicates, the signal window has to provide adequate separation to enable differentiation between the active compound and the background variability (noise) [152].

The standard measurement to compare the quality of biological assays is the Z' factor, which quantifies from 0 to 1 the separation of a positive control and background control in the absence of test compounds:

$$Z' = 1 - (3(\sigma_{max} + \sigma_{min})/ |\mu_{max} - \mu_{min}|)$$

where σ_{max} and σ_{min} are the standard deviations of the positive and background control, respectively, and μ_{max} and μ_{min} are the means of positive and negative control, respectively. The assay is acceptable when $Z' \geq 0.5$. An assay with $0 < Z' < 0.5$ requires further optimization and a value of $Z' \leq 0$ implies that the assay is not appropriate for HTS.

Assay sensitivity is measured using the minimum significance ratio (MSR), which measures the reproducibility of potency values and defines the statistically significant potency range that can be measured in an assay:

$$MSR = 10^{2\sigma d}$$

where σd is the standard deviation of the difference in log potency. Several statistical parameters have been described to evaluate process validation and reproducibility[153,154].

The hits obtained with the screening also require validation. For this purpose, the effect of chemical compounds on biological targets using a particular assay technology has to be evaluated by independent (orthogonal) readouts, such as counter screens or secondary assays to minimize compound related artefacts. Counter screens are used to remove spectroscopic artefacts that cause interferences in the readout of the assay. Only positive compounds that interact specifically with a particular target and are confirmed by an orthogonal secondary assay with an independent format of primary screening should be considered as starting points for drug discovery. Moreover, the discovery of compounds that activate or inhibit a gene promoter region in cell-based assays will require additional studies to determine the precise mechanism of action, which may be a demanding task.

REFERENCES

1 Rutter, G. A. & Rizzuto, R. Regulation of mitochondrial metabolism by ER Ca2+ release: an intimate connection. *Trends in biochemical sciences* **25**, 215-221 (2000).

2 Wang, X. The expanding role of mitochondria in apoptosis. *Genes & development* **15**, 2922-2933 (2001).

3 McBride, H. M., Neuspiel, M. & Wasiak, S. Mitochondria: more than just a powerhouse. *Curr Biol* **16**, R551-560, doi:10.1016/j.cub.2006.06.054 (2006).

4 Scheffler, I. E. A century of mitochondrial research: achievements and perspectives. *Mitochondrion* **1**, 3-31 (2001).

5 Bay, D. C. & Court, D. A. Origami in the outer membrane: the transmembrane arrangement of mitochondrial porins. *Biochemistry and cell biology = Biochimie et biologie cellulaire* **80**, 551-562 (2002).

6 Frey, T. G. & Mannella, C. A. The internal structure of mitochondria. *Trends in biochemical sciences* **25**, 319-324 (2000).

7 Fernandez-Silva, P., Enriquez, J. A. & Montoya, J. Replication and transcription of mammalian mitochondrial DNA. *Experimental physiology* **88**, 41-56 (2003).

8 Liesa, M., Palacin, M. & Zorzano, A. Mitochondrial dynamics in mammalian health and disease. *Physiol Rev* **89**, 799-845, doi:10.1152/physrev.00030.200889/3/799 [pii] (2009).

9 Chen, H. *et al.* Mitofusins Mfn1 and Mfn2 coordinately regulate mitochondrial fusion and are essential for embryonic development. *J Cell Biol* **160**, 189-200, doi:10.1083/jcb.200211046 (2003).

10 Anesti, V. & Scorrano, L. The relationship between mitochondrial shape and function and the cytoskeleton. *Biochim Biophys Acta* **1757**, 692-699, doi:10.1016/j.bbabio.2006.04.013 (2006).

11 Rojo, M., Legros, F., Chateau, D. & Lombes, A. Membrane topology and mitochondrial targeting of mitofusins, ubiquitous mammalian homologs of the transmembrane GTPase Fzo. *J Cell Sci* **115**, 1663-1674 (2002).

12 Olichon, A. *et al.* Loss of OPA1 perturbates the mitochondrial inner membrane structure and integrity, leading to cytochrome c release and apoptosis. *J Biol Chem* **278**, 7743-7746, doi:10.1074/jbc.C200677200 (2003).

13 Legros, F., Malka, F., Frachon, P., Lombes, A. & Rojo, M. Organization and dynamics of human mitochondrial DNA. *J Cell Sci* **117**, 2653-2662, doi:10.1242/jcs.01134 (2004).

14 Meeusen, S., McCaffery, J. M. & Nunnari, J. Mitochondrial fusion intermediates revealed in vitro. *Science* **305**, 1747-1752, doi:10.1126/science.1100612 (2004).

15 Koshiba, T. *et al.* Structural basis of mitochondrial tethering by mitofusin complexes. *Science* **305**, 858-862, doi:10.1126/science.1099793 (2004).

16 Santel, A. *et al.* Mitofusin-1 protein is a generally expressed mediator of mitochondrial fusion in mammalian cells. *J Cell Sci* **116**, 2763-2774, doi:10.1242/jcs.00479 (2003).

17 Eura, Y., Ishihara, N., Yokota, S. & Mihara, K. Two mitofusin proteins, mammalian homologues of FZO, with distinct functions are both required for mitochondrial fusion. *Journal of biochemistry* **134**, 333-344 (2003).

18 Ishihara, N., Eura, Y. & Mihara, K. Mitofusin 1 and 2 play distinct roles in mitochondrial fusion reactions via GTPase activity. *J Cell Sci* **117**, 6535-6546, doi:10.1242/jcs.01565 (2004).

19 Cipolat, S., Martins de Brito, O., Dal Zilio, B. & Scorrano, L. OPA1 requires mitofusin 1 to promote mitochondrial fusion. *Proc Natl Acad Sci U S A* **101**, 15927-15932, doi:10.1073/pnas.0407043101 (2004).

20 Huang, P., Yu, T. & Yoon, Y. Mitochondrial clustering induced by overexpression of the mitochondrial fusion protein Mfn2 causes mitochondrial dysfunction and cell death. *European journal of cell biology* **86**, 289-302, doi:10.1016/j.ejcb.2007.04.002 (2007).

21 Santel, A. & Fuller, M. T. Control of mitochondrial morphology by a human mitofusin. *J Cell Sci* **114**, 867-874 (2001).

22 de Brito, O. M. & Scorrano, L. Mitofusin 2 tethers endoplasmic reticulum to mitochondria. *Nature* **456**, 605-610, doi:10.1038/nature07534 (2008).

23 Akepati, V. R. *et al.* Characterization of OPA1 isoforms isolated from mouse tissues. *Journal of neurochemistry* **106**, 372-383, doi:10.1111/j.1471-4159.2008.05401.x (2008).

24 Ishihara, N., Fujita, Y., Oka, T. & Mihara, K. Regulation of mitochondrial morphology through proteolytic cleavage of OPA1. *EMBO J* **25**, 2966-2977, doi:10.1038/sj.emboj.7601184 (2006).

25 Chen, H., Chomyn, A. & Chan, D. C. Disruption of fusion results in mitochondrial heterogeneity and dysfunction. *J Biol Chem* **280**, 26185-26192, doi:10.1074/jbc.M503062200 (2005).

26 Kushnareva, Y. E. *et al.* Loss of OPA1 disturbs cellular calcium homeostasis and sensitizes for excitotoxicity. *Cell Death Differ* **20**, 353-365, doi:10.1038/cdd.2012.128 (2013).

27 Frezza, C. *et al.* OPA1 controls apoptotic cristae remodeling independently from mitochondrial fusion. *Cell* **126**, 177-189, doi:10.1016/j.cell.2006.06.025 (2006).

28 Elachouri, G. *et al.* OPA1 links human mitochondrial genome maintenance to mtDNA replication and distribution. *Genome Res* **21**, 12-20, doi:10.1101/gr.108696.110 (2011).

29 Twig, G. *et al.* Fission and selective fusion govern mitochondrial segregation and elimination by autophagy. *EMBO J* **27**, 433-446, doi:10.1038/sj.emboj.7601963 (2008).

30 Chan, D. C. Fusion and fission: interlinked processes critical for mitochondrial health. *Annual review of genetics* **46**, 265-287, doi:10.1146/annurev-genet-110410-132529 (2012).

31 Olichon, A. *et al.* The human dynamin-related protein OPA1 is anchored to the mitochondrial inner membrane facing the inter-membrane space. *FEBS Lett* **523**, 171-176 (2002).

32 Duvezin-Caubet, S. *et al.* Proteolytic processing of OPA1 links mitochondrial dysfunction to alterations in mitochondrial morphology. *J Biol Chem* **281**, 37972-37979, doi:10.1074/jbc.M606059200 (2006).

33 Song, Z., Chen, H., Fiket, M., Alexander, C. & Chan, D. C. OPA1 processing controls mitochondrial fusion and is regulated by mRNA splicing, membrane potential, and Yme1L. *J Cell Biol* **178**, 749-755, doi:10.1083/jcb.200704110 (2007).

34 Arnoult, D., Grodet, A., Lee, Y. J., Estaquier, J. & Blackstone, C. Release of OPA1 during apoptosis participates in the rapid and complete release of cytochrome c and subsequent mitochondrial fragmentation. *J Biol Chem* **280**, 35742-35750, doi:10.1074/jbc.M505970200 (2005).

35 Koch, A. *et al.* Dynamin-like protein 1 is involved in peroxisomal fission. *J Biol Chem* **278**, 8597-8605, doi:10.1074/jbc.M211761200 (2003).

36 Koch, A., Yoon, Y., Bonekamp, N. A., McNiven, M. A. & Schrader, M. A role for Fis1 in both mitochondrial and peroxisomal fission in mammalian cells. *Molecular biology of the cell* **16**, 5077-5086, doi:10.1091/mbc.E05-02-0159 (2005).

37 Gandre-Babbe, S. & van der Bliek, A. M. The novel tail-anchored membrane protein Mff controls mitochondrial and peroxisomal fission in mammalian cells. *Molecular biology of the cell* **19**, 2402-2412, doi:10.1091/mbc.E07-12-1287 (2008).

38 Kobayashi, S., Tanaka, A. & Fujiki, Y. Fis1, DLP1, and Pex11p coordinately regulate peroxisome morphogenesis. *Exp Cell Res* **313**, 1675-1686, doi:10.1016/j.yexcr.2007.02.028 (2007).

39 Frank, S. *et al.* The role of dynamin-related protein 1, a mediator of mitochondrial fission, in apoptosis. *Developmental cell* **1**, 515-525 (2001).

40 Smirnova, E., Shurland, D. L., Ryazantsev, S. N. & van der Bliek, A. M. A human dynamin-related protein controls the distribution of mitochondria. *J Cell Biol* **143**, 351-358 (1998).

41 Chappie, J. S., Acharya, S., Leonard, M., Schmid, S. L. & Dyda, F. G domain dimerization controls dynamin's assembly-stimulated GTPase activity. *Nature* **465**, 435-440, doi:10.1038/nature09032 (2010).

42 Hoppins, S., Lackner, L. & Nunnari, J. The machines that divide and fuse mitochondria. *Annual review of biochemistry* **76**, 751-780, doi:10.1146/annurev.biochem.76.071905.090048 (2007).

43 Ingerman, E. *et al.* Dnm1 forms spirals that are structurally tailored to fit mitochondria. *J Cell Biol* **170**, 1021-1027, doi:10.1083/jcb.200506078 (2005).

44 Chen, Y. J., Zhang, P., Egelman, E. H. & Hinshaw, J. E. The stalk region of dynamin drives the constriction of dynamin tubes. *Nat Struct Mol Biol* **11**, 574-575, doi:10.1038/nsmb762 (2004).

45 Yoon, Y., Pitts, K. R. & McNiven, M. A. Mammalian dynamin-like protein DLP1 tubulates membranes. *Molecular biology of the cell* **12**, 2894-2905 (2001).

46 Smirnova, E., Griparic, L., Shurland, D. L. & van der Bliek, A. M. Dynamin-related protein Drp1 is required for mitochondrial division in mammalian cells. *Molecular biology of the cell* **12**, 2245-2256 (2001).

47 Otera, H., Ishihara, N. & Mihara, K. New insights into the function and regulation of mitochondrial fission. *Biochim Biophys Acta* **1833**, 1256-1268, doi:10.1016/j.bbamcr.2013.02.002 (2013).

48 Dohm, J. A., Lee, S. J., Hardwick, J. M., Hill, R. B. & Gittis, A. G. Cytosolic domain of the human mitochondrial fission protein fis1 adopts a TPR fold. *Proteins* **54**, 153-156, doi:10.1002/prot.10524 (2004).

49 Suzuki, M., Jeong, S. Y., Karbowski, M., Youle, R. J. & Tjandra, N. The solution structure of human mitochondria fission protein Fis1 reveals a novel TPR-like helix bundle. *J Mol Biol* **334**, 445-458 (2003).

50 Jofuku, A., Ishihara, N. & Mihara, K. Analysis of functional domains of rat mitochondrial Fis1, the mitochondrial fission-stimulating protein. *Biochem Biophys Res Commun* **333**, 650-659, doi:10.1016/j.bbrc.2005.05.154 (2005).

51 Otera, H. *et al.* Mff is an essential factor for mitochondrial recruitment of Drp1 during mitochondrial fission in mammalian cells. *J Cell Biol* **191**, 1141-1158, doi:10.1083/jcb.201007152 (2010).

52 James, D. I., Parone, P. A., Mattenberger, Y. & Martinou, J. C. hFis1, a novel component of the mammalian mitochondrial fission machinery. *J Biol Chem* **278**, 36373-36379, doi:10.1074/jbc.M303758200 (2003).

53 Stojanovski, D., Koutsopoulos, O. S., Okamoto, K. & Ryan, M. T. Levels of human Fis1 at the mitochondrial outer membrane regulate mitochondrial morphology. *J Cell Sci* **117**, 1201-1210, doi:10.1242/jcs.01058 (2004).

54 Yoon, Y., Krueger, E. W., Oswald, B. J. & McNiven, M. A. The mitochondrial protein hFis1 regulates mitochondrial fission in mammalian cells through an interaction with the dynamin-like protein DLP1. *Mol Cell Biol* **23**, 5409-5420 (2003).

55 Lee, Y. J., Jeong, S. Y., Karbowski, M., Smith, C. L. & Youle, R. J. Roles of the mammalian mitochondrial fission and fusion mediators Fis1, Drp1, and Opa1 in apoptosis. *Molecular biology of the cell* **15**, 5001-5011, doi:10.1091/mbc.E04-04-0294 (2004).

56 Otera, H. & Mihara, K. Discovery of the membrane receptor for mitochondrial fission GTPase Drp1. *Small GTPases* **2**, 167-172, doi:10.4161/sgtp.2.3.16486 (2011).

57 Otera, H. & Mihara, K. Molecular mechanisms and physiologic functions of mitochondrial dynamics. *Journal of biochemistry* **149**, 241-251, doi:10.1093/jb/mvr002 (2011).

58 Palmer, C. S. *et al.* MiD49 and MiD51, new components of the mitochondrial fission machinery. *EMBO Rep* **12**, 565-573, doi:10.1038/embor.2011.54 (2011).

59 Loson, O. C., Song, Z., Chen, H. & Chan, D. C. Fis1, Mff, MiD49, and MiD51 mediate Drp1 recruitment in mitochondrial fission. *Molecular biology of the cell* **24**, 659-667, doi:10.1091/mbc.E12-10-0721 (2013).

60 Palmer, C. S. *et al.* Adaptor proteins MiD49 and MiD51 can act independently of Mff and Fis1 in Drp1 recruitment and are specific for mitochondrial fission. *J Biol Chem* **288**, 27584-27593, doi:10.1074/jbc.M113.479873 (2013).

61 Zhao, J. *et al.* Human MIEF1 recruits Drp1 to mitochondrial outer membranes and promotes mitochondrial fusion rather than fission. *EMBO J* **30**, 2762-2778, doi:10.1038/emboj.2011.198 (2011).

62 Niemann, A., Ruegg, M., La Padula, V., Schenone, A. & Suter, U. Ganglioside-induced differentiation associated protein 1 is a regulator of the mitochondrial network: new implications for Charcot-Marie-Tooth disease. *J Cell Biol* **170**, 1067-1078, doi:10.1083/jcb.200507087 (2005).

63 Pedrola, L. *et al.* GDAP1, the protein causing Charcot-Marie-Tooth disease type 4A, is expressed in neurons and is associated with mitochondria. *Hum Mol Genet* **14**, 1087-1094, doi:10.1093/hmg/ddi121 (2005).

64 Detmer, S. A. & Chan, D. C. Functions and dysfunctions of mitochondrial dynamics. *Nature reviews. Molecular cell biology* **8**, 870-879, doi:10.1038/nrm2275 (2007).

65 Chen, H., McCaffery, J. M. & Chan, D. C. Mitochondrial fusion protects against neurodegeneration in the cerebellum. *Cell* **130**, 548-562, doi:10.1016/j.cell.2007.06.026 (2007).

66 Pich, S. *et al.* The Charcot-Marie-Tooth type 2A gene product, Mfn2, up-regulates fuel oxidation through expression of OXPHOS system. *Hum Mol Genet* **14**, 1405-1415, doi:10.1093/hmg/ddi149 (2005).

67 Bach, D. *et al.* Mitofusin-2 determines mitochondrial network architecture and mitochondrial metabolism. A novel regulatory mechanism altered in obesity. *J Biol Chem* **278**, 17190-17197, doi:10.1074/jbc.M212754200 (2003).

68 Benard, G. *et al.* Mitochondrial bioenergetics and structural network organization. *J Cell Sci* **120**, 838-848, doi:10.1242/jcs.03381 (2007).

69 Parone, P. A. *et al.* Preventing mitochondrial fission impairs mitochondrial function and leads to loss of mitochondrial DNA. *PLoS One* **3**, e3257, doi:10.1371/journal.pone.0003257 (2008).

70 Alexander, C. *et al.* OPA1, encoding a dynamin-related GTPase, is mutated in autosomal dominant optic atrophy linked to chromosome 3q28. *Nat Genet* **26**, 211-215, doi:10.1038/79944 (2000).

71 Delettre, C. *et al.* Nuclear gene OPA1, encoding a mitochondrial dynamin-related protein, is mutated in dominant optic atrophy. *Nat Genet* **26**, 207-210, doi:10.1038/79936 (2000).

72 Kjer, B., Eiberg, H., Kjer, P. & Rosenberg, T. Dominant optic atrophy mapped to chromosome 3q region. II. Clinical and epidemiological aspects. *Acta ophthalmologica Scandinavica* **74**, 3-7 (1996).

73 Olichon, A. *et al.* Mitochondrial dynamics and disease, OPA1. *Biochim Biophys Acta* **1763**, 500-509, doi:10.1016/j.bbamcr.2006.04.003 (2006).

74 Ferre, M., Amati-Bonneau, P., Tourmen, Y., Malthiery, Y. & Reynier, P. eOPA1: an online database for OPA1 mutations. *Hum Mutat* **25**, 423-428, doi:10.1002/humu.20161 (2005).

75 Kim, J. Y. *et al.* Mitochondrial DNA content is decreased in autosomal dominant optic atrophy. *Neurology* **64**, 966-972, doi:10.1212/01.WNL.0000157282.76715.B1 (2005).

76 Lodi, R. *et al.* Deficit of in vivo mitochondrial ATP production in OPA1-related dominant optic atrophy. *Annals of neurology* **56**, 719-723, doi:10.1002/ana.20278 (2004).

77 Zuchner, S. & Vance, J. M. Mechanisms of disease: a molecular genetic update on hereditary axonal neuropathies. *Nature clinical practice. Neurology* **2**, 45-53, doi:10.1038/ncpneuro0071 (2006).

78 Skre, H. Genetic and clinical aspects of Charcot-Marie-Tooth's disease. *Clinical genetics* **6**, 98-118 (1974).

79 Zuchner, S. *et al.* Axonal neuropathy with optic atrophy is caused by mutations in mitofusin 2. *Annals of neurology* **59**, 276-281, doi:10.1002/ana.20797 (2006).

80 Chung, K. W. *et al.* Early onset severe and late-onset mild Charcot-Marie-Tooth disease with mitofusin 2 (MFN2) mutations. *Brain : a journal of neurology* **129**, 2103-2118, doi:10.1093/brain/awl174 (2006).

81 Bach, D. *et al.* Expression of Mfn2, the Charcot-Marie-Tooth neuropathy type 2A gene, in human skeletal muscle: effects of type 2 diabetes, obesity, weight loss, and the regulatory role of tumor necrosis factor alpha and interleukin-6. *Diabetes* **54**, 2685-2693 (2005).

82 Kelley, D. E., He, J., Menshikova, E. V. & Ritov, V. B. Dysfunction of mitochondria in human skeletal muscle in type 2 diabetes. *Diabetes* **51**, 2944-2950 (2002).

83 Toledo, F. G., Watkins, S. & Kelley, D. E. Changes induced by physical activity and weight loss in the morphology of intermyofibrillar mitochondria in obese men and women. *J Clin Endocrinol Metab* **91**, 3224-3227, doi:10.1210/jc.2006-0002 (2006).

84 Simoneau, J. A. & Kelley, D. E. Altered glycolytic and oxidative capacities of skeletal muscle contribute to insulin resistance in NIDDM. *Journal of applied physiology* **83**, 166-171 (1997).

85 Mootha, V. K. *et al.* PGC-1alpha-responsive genes involved in oxidative phosphorylation are coordinately downregulated in human diabetes. *Nat Genet* **34**, 267-273, doi:10.1038/ng1180 (2003).

86 Patti, M. E. *et al.* Coordinated reduction of genes of oxidative metabolism in humans with insulin resistance and diabetes: Potential role of PGC1 and NRF1. *Proc Natl Acad Sci U S A* **100**, 8466-8471, doi:10.1073/pnas.1032913100 (2003).

87 Sebastian, D. *et al.* Mitofusin 2 (Mfn2) links mitochondrial and endoplasmic reticulum function with insulin signaling and is essential for normal glucose homeostasis. *Proc Natl Acad Sci U S A* **109**, 5523-5528, doi:10.1073/pnas.1108220109 (2012).

88 Ryan, M. T. & Hoogenraad, N. J. Mitochondrial-nuclear communications. *Annual review of biochemistry* **76**, 701-722, doi:10.1146/annurev.biochem.76.052305.091720 (2007).

89 Bartlett, K. & Eaton, S. Mitochondrial beta-oxidation. *Eur J Biochem* **271**, 462-469 (2004).

90 Maechler, P., Carobbio, S. & Rubi, B. In beta-cells, mitochondria integrate and generate metabolic signals controlling insulin secretion. *Int J Biochem Cell Biol* **38**, 696-709, doi:10.1016/j.biocel.2005.12.006 (2006).

91 Crofts, A. R. The cytochrome bc1 complex: function in the context of structure. *Annual review of physiology* **66**, 689-733, doi:10.1146/annurev.physiol.66.032102.150251 (2004).

92 Lenaz, G. & Genova, M. L. Structure and organization of mitochondrial respiratory complexes: a new understanding of an old subject. *Antioxid Redox Signal* **12**, 961-1008, doi:10.1089/ars.2009.2704 (2010).

93 Osellame, L. D., Blacker, T. S. & Duchen, M. R. Cellular and molecular mechanisms of mitochondrial function. *Best practice & research. Clinical endocrinology & metabolism* **26**, 711-723, doi:10.1016/j.beem.2012.05.003 (2012).

94 Brand, M. D. The sites and topology of mitochondrial superoxide production. *Experimental gerontology* **45**, 466-472, doi:10.1016/j.exger.2010.01.003 (2010).

95 Muller, F. L., Liu, Y. & Van Remmen, H. Complex III releases superoxide to both sides of the inner mitochondrial membrane. *J Biol Chem* **279**, 49064-49073, doi:10.1074/jbc.M407715200 (2004).

96 Murphy, M. P. How mitochondria produce reactive oxygen species. *Biochem J* **417**, 1-13, doi:10.1042/BJ20081386 (2009).

97 Han, D., Antunes, F., Canali, R., Rettori, D. & Cadenas, E. Voltage-dependent anion channels control the release of the superoxide anion from mitochondria to cytosol. *J Biol Chem* **278**, 5557-5563, doi:10.1074/jbc.M210269200 (2003).

98 Sun, J. & Trumpower, B. L. Superoxide anion generation by the cytochrome bc1 complex. *Arch Biochem Biophys* **419**, 198-206 (2003).

99 Raha, S. & Robinson, B. H. Mitochondria, oxygen free radicals, and apoptosis. *American journal of medical genetics* **106**, 62-70, doi:10.1002/ajmg.1398 (2001).

100 Cruciat, C. M., Brunner, S., Baumann, F., Neupert, W. & Stuart, R. A. The cytochrome bc1 and cytochrome c oxidase complexes associate to form a single supracomplex in yeast mitochondria. *J Biol Chem* **275**, 18093-18098, doi:10.1074/jbc.M001901200 (2000).

101 Lenaz, G. & Genova, M. L. Structural and functional organization of the mitochondrial respiratory chain: a dynamic super-assembly. *Int J Biochem Cell Biol* **41**, 1750-1772 (2009).

102 Dudkina, N. V., Heinemeyer, J., Sunderhaus, S., Boekema, E. J. & Braun, H. P. Respiratory chain supercomplexes in the plant mitochondrial membrane. *Trends Plant Sci* **11**, 232-240, doi:10.1016/j.tplants.2006.03.007 (2006).

103 Schwartsmann, G. P., G.J.; Laurensse, E.; De Wall, F.C.; Pinedo, H.M. Schedule-dependency of growth-inhibitory and antipyrimidine effects. *Biochem. Pharmacol.* **37**, 3257-3266 (1988).

104 Loffler, M., Jockel, J., Schuster, G. & Becker, C. Dihydroorotat-ubiquinone oxidoreductase links mitochondria in the biosynthesis of pyrimidine nucleotides. *Mol Cell Biochem* **174**, 125-129 (1997).

105 Fang, J. *et al.* Dihydro-orotate dehydrogenase is physically associated with the respiratory complex and its loss leads to mitochondrial dysfunction. *Biosci Rep* **33**, e00021, doi:10.1042/BSR20120097 (2013).

106 Lavin, M. F. & Gueven, N. The complexity of p53 stabilization and activation. *Cell Death Differ* **13**, 941-950, doi:10.1038/sj.cdd.4401925 (2006).

107 Chumakov, P. M. Versatile functions of p53 protein in multicellular organisms. *Biochemistry (Mosc)* **72**, 1399-1421 (2007).

108 Horn, H. F. & Vousden, K. H. Coping with stress: multiple ways to activate p53. *Oncogene* **26**, 1306-1316, doi:10.1038/sj.onc.1210263 (2007).

109 Vlatkovic, N., Boyd, M. T. & Rubbi, C. P. Nucleolar control of p53: a cellular Achilles' heel and a target for cancer therapy. *Cell Mol Life Sci* **71**, 771-791, doi:10.1007/s00018-013-1361-x (2014).

110 Vousden, K. H. p53: death star. *Cell* **103**, 691-694 (2000).

111 Moll, U. M., Wolff, S., Speidel, D. & Deppert, W. Transcription-independent pro-apoptotic functions of p53. *Curr Opin Cell Biol* **17**, 631-636, doi:10.1016/j.ceb.2005.09.007 (2005).

112 Park, J. Y. *et al.* p53 improves aerobic exercise capacity and augments skeletal muscle mitochondrial DNA content. *Circ Res* **105**, 705-712, 711 p following 712, doi:10.1161/CIRCRESAHA.109.205310 (2009).

113 Wong, T. S. *et al.* Biophysical characterizations of human mitochondrial transcription factor A and its binding to tumor suppressor p53. *Nucleic Acids Res* **37**, 6765-6783, doi:10.1093/nar/gkp750 (2009).

114 Wong, T. S. *et al.* Physical and functional interactions between human mitochondrial single-stranded DNA-binding protein and tumour suppressor p53. *Nucleic Acids Res* **37**, 568-581, doi:10.1093/nar/gkn974 (2009).

115 Saleem, A. & Hood, D. A. Acute exercise induces tumour suppressor protein p53 translocation to the mitochondria and promotes a p53-Tfam-mitochondrial DNA complex in skeletal muscle. *J Physiol* **591**, 3625-3636, doi:10.1113/jphysiol.2013.252791 (2013).

116 Achanta, G. *et al.* Novel role of p53 in maintaining mitochondrial genetic stability through interaction with DNA Pol gamma. *EMBO J* **24**, 3482-3492, doi:10.1038/sj.emboj.7600819 (2005).

117 de Souza-Pinto, N. C., Harris, C. C. & Bohr, V. A. p53 functions in the incorporation step in DNA base excision repair in mouse liver mitochondria. *Oncogene* **23**, 6559-6568, doi:10.1038/sj.onc.1207874 (2004).

118 Tanaka, H. *et al.* A ribonucleotide reductase gene involved in a p53-dependent cell-cycle checkpoint for DNA damage. *Nature* **404**, 42-49, doi:10.1038/35003506 (2000).

119 Lebedeva, M. A., Eaton, J. S. & Shadel, G. S. Loss of p53 causes mitochondrial DNA depletion and altered mitochondrial reactive oxygen species homeostasis. *Biochim Biophys Acta* **1787**, 328-334, doi:10.1016/j.bbabio.2009.01.004 (2009).

120 Bergeaud, M. *et al.* Mitochondrial p53 mediates a transcription-independent regulation of cell respiration and interacts with the mitochondrial F(1)F0-ATP synthase. *Cell Cycle* **12**, 2781-2793, doi:10.4161/cc.25870 (2013).

121 Austin, S. & St-Pierre, J. PGC1alpha and mitochondrial metabolism--emerging concepts and relevance in ageing and neurodegenerative disorders. *J Cell Sci* **125**, 4963-4971, doi:10.1242/jcs.113662 (2012).

122 Wenz, T. Regulation of mitochondrial biogenesis and PGC-1alpha under cellular stress. *Mitochondrion* **13**, 134-142, doi:10.1016/j.mito.2013.01.006 (2013).

123 Saleem, A., Adhihetty, P. J. & Hood, D. A. Role of p53 in mitochondrial biogenesis and apoptosis in skeletal muscle. *Physiol Genomics* **37**, 58-66, doi:10.1152/physiolgenomics.90346.2008 (2009).

124 Sen, N., Satija, Y. K. & Das, S. PGC-1alpha, a key modulator of p53, promotes cell survival upon metabolic stress. *Mol Cell* **44**, 621-634, doi:10.1016/j.molcel.2011.08.044 (2011).

125 Wang, D. B., Kinoshita, C., Kinoshita, Y. & Morrison, R. S. p53 and mitochondrial function in neurons. *Biochim Biophys Acta*, doi:10.1016/j.bbadis.2013.12.015 (2014).

126 Gomes, L. C. & Scorrano, L. Mitochondrial morphology in mitophagy and macroautophagy. *Biochim Biophys Acta* **1833**, 205-212, doi:10.1016/j.bbamcr.2012.02.012 (2013).

127 Chen, H. *et al.* Mitochondrial fusion is required for mtDNA stability in skeletal muscle and tolerance of mtDNA mutations. *Cell* **141**, 280-289, doi:10.1016/j.cell.2010.02.026 (2010).

128 Wang, W. *et al.* Mitofusin-2 is a novel direct target of p53. *Biochem Biophys Res Commun* **400**, 587-592, doi:10.1016/j.bbrc.2010.08.108 (2010).

129 Li, J. *et al.* miR-30 regulates mitochondrial fission through targeting p53 and the dynamin-related protein-1 pathway. *PLoS Genet* **6**, e1000795, doi:10.1371/journal.pgen.1000795 (2010).

130 Wang, J. X. *et al.* miR-499 regulates mitochondrial dynamics by targeting calcineurin and dynamin-related protein-1. *Nature medicine* **17**, 71-78, doi:10.1038/nm.2282 (2011).

131 Guo, X. *et al.* Inhibition of mitochondrial fragmentation diminishes Huntington's disease-associated neurodegeneration. *J Clin Invest* **123**, 5371-5388, doi:10.1172/JCI70911 (2013).

132 Wang, D. B. *et al.* Declines in Drp1 and parkin expression underlie DNA damage-induced changes in mitochondrial length and neuronal death. *J Neurosci* **33**, 1357-1365, doi:10.1523/JNEUROSCI.3365-12.2013 (2013).

133 Linke, S. P., Clarkin, K. C., Di Leonardo, A., Tsou, A. & Wahl, G. M. A reversible, p53-dependent G0/G1 cell cycle arrest induced by ribonucleotide depletion in the absence of detectable DNA damage. *Genes & development* **10**, 934-947 (1996).

134 Khutornenko, A. A. *et al.* Pyrimidine biosynthesis links mitochondrial respiration to the p53 pathway. *Proc Natl Acad Sci U S A* **107**, 12828-12833, doi:10.1073/pnas.0910885107 (2010).

135 Fernandes, P. B. Technological advances in high-throughput screening. *Curr Opin Chem Biol* **2**, 597-603, doi:S1367-5931(98)80089-6 [pii] (1998).

136 Hertzberg, R. P. & Pope, A. J. High-throughput screening: new technology for the 21st century. *Curr Opin Chem Biol* **4**, 445-451, doi:S1367-5931(00)00110-1 [pii] (2000).

137 Moore, K. & Rees, S. Cell-based versus isolated target screening: how lucky do you feel? *J Biomol Screen* **6**, 69-74, doi:10.1089/108705701750160200 (2001).

138 Sundberg, S. A. High-throughput and ultra-high-throughput screening: solution- and cell-based approaches. *Curr Opin Biotechnol* **11**, 47-53, doi:S0958-1669(99)00051-8 [pii] (2000).

139 Hill, S. J., Baker, J. G. & Rees, S. Reporter-gene systems for the study of G-protein-coupled receptors. *Curr Opin Pharmacol* **1**, 526-532, doi:S1471-4892(01)00091-1 [pii] (2001).

140 New, D. C., Miller-Martini, D. M. & Wong, Y. H. Reporter gene assays and their applications to bioassays of natural products. *Phytother Res* **17**, 439-448, doi:10.1002/ptr.1312 (2003).

141 Wood, K. V. Marker proteins for gene expression. *Curr Opin Biotechnol* **6**, 50-58, doi:0958-1669(95)80009-3 [pii] (1995).

142 Bronstein, I., Fortin, J., Stanley, P. E., Stewart, G. S. & Kricka, L. J. Chemiluminescent and bioluminescent reporter gene assays. *Anal Biochem* **219**, 169-181, doi:S0003-2697(84)71254-1 [pii]10.1006/abio.1994.1254 (1994).

143 Martin, C. S., Wight, P. A., Dobretsova, A. & Bronstein, I. Dual luminescence-based reporter gene assay for luciferase and beta-galactosidase. *Biotechniques* **21**, 520-524 (1996).

144 Craig, F. F., Simmonds, A. C., Watmore, D., McCapra, F. & White, M. R. Membrane-permeable luciferin esters for assay of firefly luciferase in live intact cells. *Biochem J* **276 (Pt 3)**, 637-641 (1991).

145 Yang, J. & Thomason, D. B. An easily synthesized, photolyzable luciferase substrate for in vivo luciferase activity measurement. *Biotechniques* **15**, 848-850 (1993).
146 George, S. E., Bungay, P. J. & Naylor, L. H. Functional coupling of endogenous serotonin (5-HT1B) and calcitonin (C1a) receptors in CHO cells to a cyclic AMP-responsive luciferase reporter gene. *J Neurochem* **69**, 1278-1285 (1997).
147 Lorenz, W. W. *et al.* Expression of the Renilla reniformis luciferase gene in mammalian cells. *J Biolumin Chemilumin* **11**, 31-37, doi:10.1002/(SICI)1099-1271(199601)11:1<31::AID-BIO398>3.0.CO;2-M (1996).
148 Nakajima, Y. O., Y. Bioluminescence assays: multicolor luciferase assay, secreted luciferase assay and imaging luciferase assay. *Expert opinion in Drug Discovery* **5**, 835-849 (2010).
149 Kotarsky, K., Nilsson, N. E., Olde, B. & Owman, C. Progress in methodology. Improved reporter gene assays used to identify ligands acting on orphan seven-transmembrane receptors. *Pharmacol Toxicol* **93**, 249-258 (2003).
150 Mayr, L. M. & Bojanic, D. Novel trends in high-throughput screening. *Curr Opin Pharmacol* **9**, 580-588, doi:S1471-4892(09)00128-3 [pii]10.1016/j.coph.2009.08.004 (2009).
151 Malo, N., Hanley, J. A., Cerquozzi, S., Pelletier, J. & Nadon, R. Statistical practice in high-throughput screening data analysis. *Nat Biotechnol* **24**, 167-175, doi:nbt1186 [pii]10.1038/nbt1186 (2006).
152 Johnston, P. A. Cellular platforms for HTS: three case studies. *Drug Discov Today* **7**, 353-363 (2002).
153 Inglese, J. *et al.* High-throughput screening assays for the identification of chemical probes. *Nat Chem Biol* **3**, 466-479, doi:10.1038/nchembio.2007.17 (2007).
154 Coma, I. *et al.* Process validation and screen reproducibility in high-throughput screening. *J Biomol Screen* **14**, 66-76, doi:14/1/66 [pii]10.1177/1087057108326664 (2009).

OBJECTIVES

OBJECTIVES

Mitofusin-2 (Mfn2) participates in mitochondrial fusion, endoplasm reticulum morphology, and regulates mitochondrial metabolism. Our group has previously reported that Mfn2 is down regulated in muscle from obese or type 2 diabetic patients[1], and recently we have demonstrated that Mfn2 deficiency in liver or muscle leads to glucose intolerance and insulin resistance in mice[2]. Therefore, activators of Mfn2 expression could be used as a valuable potential therapeutic strategy for the treatment of Charcot Marie Tooth type 2A, as well as, metabolic disorders such as type 2 diabetes or obesity. Thus, the main objective of this chapter was to identify a compound with capacity to enhance human Mfn2 expression for the potential treatment of metabolic disorders such as type 2 diabetes or obesity.

The specific objectives of this chapter are:

1. Generation of several human cell clones that stably express luciferase under the control of 2 Kb of the human MFN2 promoter

2. Identification of compounds with capacity to enhance Mfn2 promoter activity by carrying out a High Throughput Screening (HTS) using the Prestwich Chemical Library®

3. Validation of the activators of the Mfn2 promoter at cellular level in different cell types by measuring Mfn2 mRNA and protein levels

4. Identification of the mechanism of action of the compound

RESULTS AND DISCUSSION

RESULTS AND DISCUSSION

1. Generation of several human cell clones that stably expresses luciferase under the control of 2 Kb Mfn2 promoter.

HeLa cell line that expresses endogenous Mfn2 was selected as a cellular model to perform the screening process since is of human origin, is an immortalized cell line and easily grown in culture which makes screening a feasible task. Then, engineered stable cell lines were generated by co-transfecting pGL3Mfn2P and pGFP (See section 3 and 4 in materials and methods). The former contains the Mfn2 promoter, the luciferase reporter gene, and a selection marker that will allow the selection of clones that integrate the construct, whereas the latter is used to determine the transfection efficiency by flux cytometry (Figure 8). The cells overexpressing pGL3Mfn2P are called HeLa Mfn2P clones and express the luciferase reporter gene when Mfn2 promoter is activated. HeLa Mfn2P cells do not have luciferase endogenous background and they are useful for HTS assays.

In the laboratory several human cell clones that stably expresses luciferase under the control of 2 kb (region -1982/+54) of the human Mfn2 promoter were generated (See section 3.3 in Materials and Methods), and ten clones were selected providing a broad range of Mfn2 transcriptional activity.

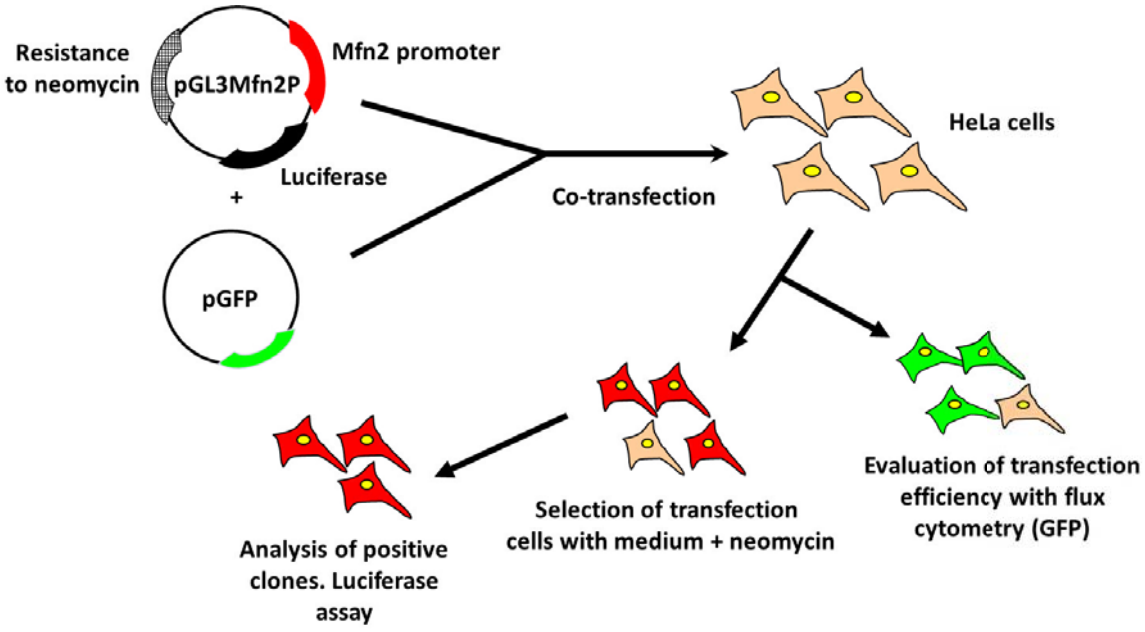

Figure 8. **Generation of several human cell clones that stably expresses luciferase under the control of 2 Kb Mfn2 promoter.** The pGL3Mfn2P encodes a resistance neomycin gene that allows the clone selection.

The final step after generating engineered cell lines is the validation of the cellular model produced. After transfection of the plasmid, the promoter-reporter gene unit can be integrated in any place of the cell genome, and in some cases this could affect the

expression of the reporter gene. To ensure that the engineered cell line generated will respond adequately in terms of the expression of the reporter gene unit, it is necessary to validate the clones obtained.

9-cis-retinoic acid (9-RA) acts by binding to heterodimers of the retinoic acid receptor (RAR) and the retinoid X receptor (RXR). RAR-RXR complex binds to retinoic acid response elements (RAREs) in the regulatory regions of direct targets, thereby activating gene transcription. Mfn2 promoter responds to 9-RA, which acts as a positive control generating luciferase enzyme.

To validate the cellular clones obtained, they were incubated with 9-RA for 16 h and the luminescence levels were measured (See section 6 in materials and methods). The clones incubated with 9-RA exhibited a higher transcriptional activity in relation to the control groups (Figure 9).

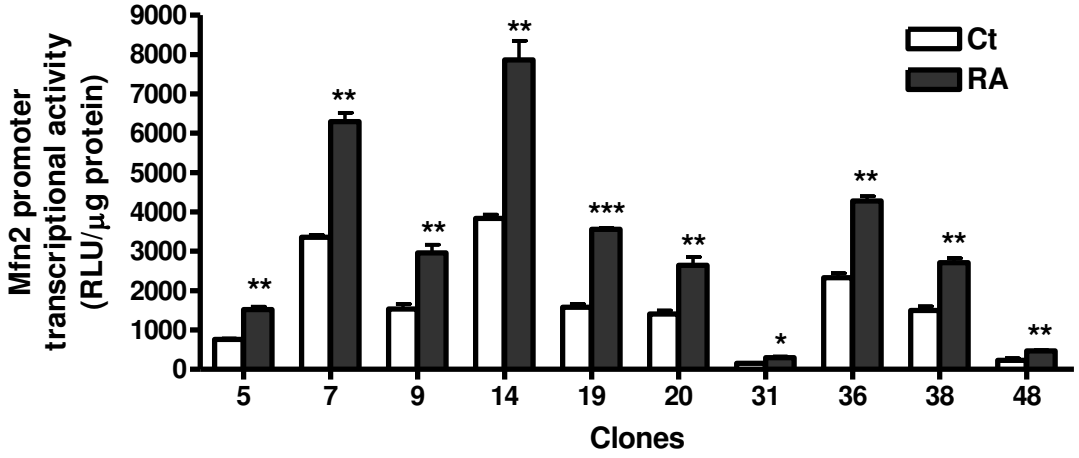

Figure 9. **Tanscriptional activity of the Mfn2 promoter clones increased with 9-RA.** HeLa Mfn2P clones were incubated ±RA (10 µM) for 16 h and the transcriptional activity of Mfn2 promoter was measured by luciferase reporter gene. Data represent the mean ± SEM of one experiment of Mfn2 transcriptional activity relative to µg of protein. *P < 0.05 vs Ct, **P < 0.01 vs Ct, *** < 0.001 vs Ct. One assay was performed per triplicate (n = 1).

As it has already been mentioned above, the promoter-reporter gene unit can be integrated in any place of the cell genome affecting the expression of the reporter gene. Thus, the clones show different basal Mfn2 promoter activities. However, all the clones respond positively to 9-RA. The three clones (9, 14 and 19) providing higher fold inductions with 9-RA were selected for further experiments.

It has been demonstrated previously in our group that peroxisome proliferator-activated receptor ɣ coactivator 1β (PGC-1β), which is a transcriptional co-activator involved in the regulation of genes related to energy metabolism, stimulates Mfn2 gene expression. Mfn2 promoter contains two elements that bind Estrogen Related Receptor alpha (ERRα)[3]. ERRα is a key transcription factor that regulates the expression of genes of the OXPHOS system

mediated by PGC-1β. This regulatory pathway is characterised by a stimulatory action of PGC-1β on the transcription of Mfn2, via co-activation of ERRα.

On the basis of these results, the three stable clones (9, 14 and 19) were transfected with PGC-1β plasmid (See section 3.1 in materials and methods) and luciferase reporter gene was measured (Figure 10).

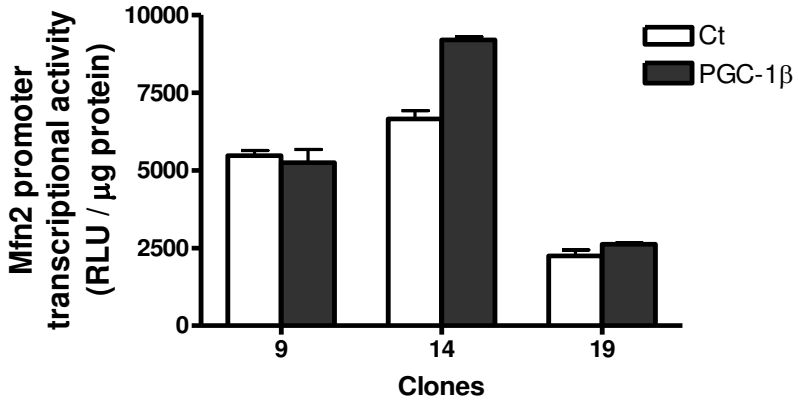

Figure 10. **Tanscriptional activity of the Mfn2P 14 clone increased with PGC-1β transfection.** HeLa Mfn2P clones 9, 14 and 19 were transfected with PGC-1β and the transcriptional activity of Mfn2 promoter was measured by luciferase reporter gene. Data represent the mean ± SEM of one representative experiment and are expressed per µg of protein. Two assays were performed per triplicate (n = 2).

Only clone 14 showed an increase in Mfn2 transcriptional activity upon transfection with PGC-1β. Based on this, clone 14 was selected to perform the High Throughput screening (HTS).

2. Screening and identification of compounds with capacity to enhance Mfn2 promoter activity

The High Throughput Screening (HTS) of the Prestwick Chemical Library® was done in collaboration with Dr. Mabel Loza at the University of Santiago de Compostela since they have operative HTS facilities (Unidad de evaluación de actividades farmacológicas de compuestos químicos (USEF)). The Prestwick Chemical Library® contains 1.120 small molecules, 90% being marketed drugs, and 10% bioactive alkaloids or related substances, thus it presents a high degree of drug-likeliness. The high number of diverse molecules in the Prestwick Chemical Library requires the use of robust assays with good sensitivity and a good dynamic range to maximize reliability and reproducibility for its use in our HTS program.

2.1. Miniaturization assay

The assay for the regulation of Mfn2 gene expression was run in a miniaturized, 96-well plate format. This format requires validation and optimization of the luciferase assay using HeLa Mfn2P 14 clone. Miniaturization process consists in evaluate the luciferase response over time with the substrate luciferine, the signal in relation to noise (background) and the data dispersion.

2.1.1.Luciferase activity

HeLa cells from Mfn2P 14 clone were seeded in a 96-well plate (20,000 cells/well) and incubated at 37 °C in a humidified atmosphere of 5% CO_2/95% air. After 24 h the cells were incubated with 9-RA (control activator) at 10 µM for 16 h. Then luciferase assay was performed and luminescence was measured at different times (1, 3, 4, 5, 11, 12, 13, 15, 17, and 20 min) using an integration time of 100 ms and using a Tecan Ultra Evolution detector (Figure 11).

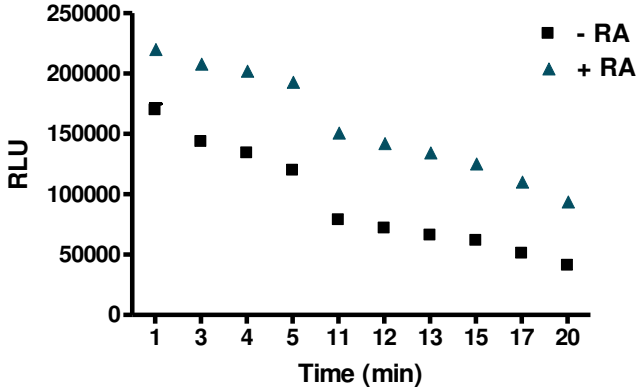

Figure 11. **Luciferase activity was tested at different times.** Tanscriptional activity of the Mfn2 promoter in HeLa Mfn2P 14 clone incubated ± 9-RA (10 µM) for 16 h was measured at different times of luciferine incubation.

The luciferase activity decreases with the incubation time and after 5 minutes there is a notable reduction.

2.1.2. Signal/Noise ratio

The specific activity has been calculated as the signal/noise ratio at different times of luciferine-luciferase incubation. The signal is the luminescence obtained with 9-RA and the noise (or background) is the luminescence obtained without 9-RA along time (Figure 12).

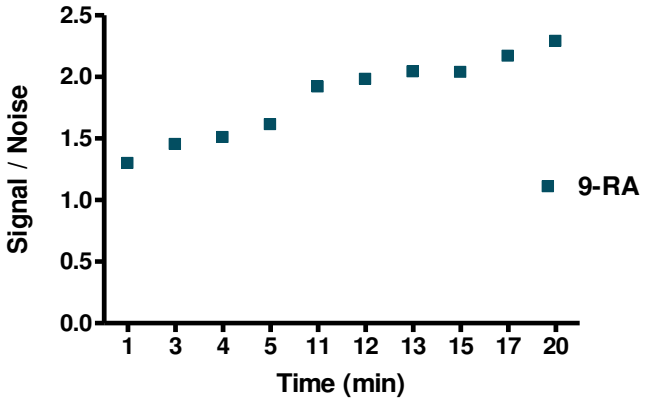

Figure 12. **Specific activity calculated as signal/noise ratio.** HeLa Mfn2P 14 clone was incubated ± 9-RA (10 μM) for 16 h and luminescence was measured.

The specific activity increases with the incubation time. This increase is due to a stronger decrease of the luciferase activity in the experimental data without 9-RA. After 5 minutes the ratio reaches a value superior to 1.5, validating the conditions to carry out the HTS.

2.1.3. Data dispersion

The standard measurement to compare the quality of biological assays is the Z' factor, which quantifies from 0 to 1 the separation of 9-RA (positive control) and background of DMSO (negative control) in the absence of test compounds:

$$Z' = 1 - (3(\sigma_{max} + \sigma_{min}) / |\mu_{max} - \mu_{min}|)$$

where σ_{max} and σ_{min} are the standard deviations of the positive and background control, respectively, and μ_{max} and μ_{min} are the means of positive and negative control, respectively. The assay is acceptable when $Z' \geq 0.5$ (Figure 13).

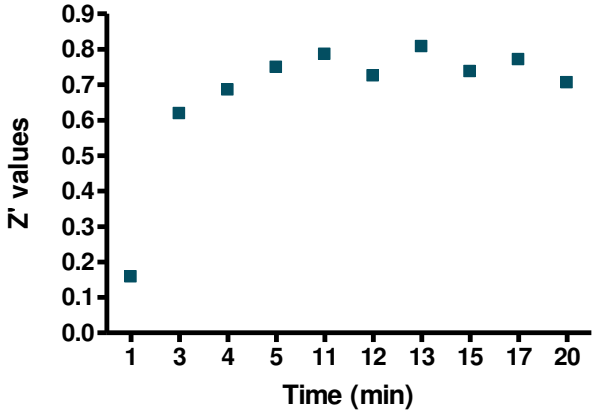

***Figure 13.* Z' factor values for luciferase reporter assay.** This measure is used to compare the quality of the biological assay.

The data dispersion (Z') also improved with 5 min incubation time achieving values superiors to 0.7, validating the luciferase reporter assay. On the basis of these results, the best condition to measure luciferase activity is 5 min after the addition of the luciferine substrate.

2.2. High Throughput Screening using Prestwick library

HeLa Mfn2P 14 clone cells were plated in a 96-well plate (20,000 cells/well) and incubated at 37 ^{o}C in a humidified atmosphere of 5% CO_2/95% air. The next day the cells were incubated with the compounds of the Prestwick Chemical Library® at a concentration of 10 µM for 16 hours. Cells were incubated in parallel with 9-RA (10 µM) and 1% DMSO (v:v), which were used as a positive and negative control, respectively. Positive and negative controls were run as an integral part of each assay to ensure the validity of the obtained results (Figure 14). Each molecule was screened at a single dose of 10 µM and positive hit compounds were defined as those ones that induce an increase in the luciferase activity ≥ 1.6-fold, compared to vehicle (DMSO) treated cells (negative controls) (See section 11 in materials and methods).

The results of the screening were expressed as the activity percentage compared to 10 µM 9-RA, which has been considered as 100 % activity. Regulation of Mfn2 expression induced by tested compounds ranged from compounds that inhibited Mfn2 expression to compounds that increased 2-fold Mfn2 expression compared to 9-RA activity. Compounds showing an activity higher than 60% compared to 9-RA were considered as hits and were confirmed in an independent assay. Finally, twelve compounds were considered possible activators of the human Mfn2 promoter (Table 2).

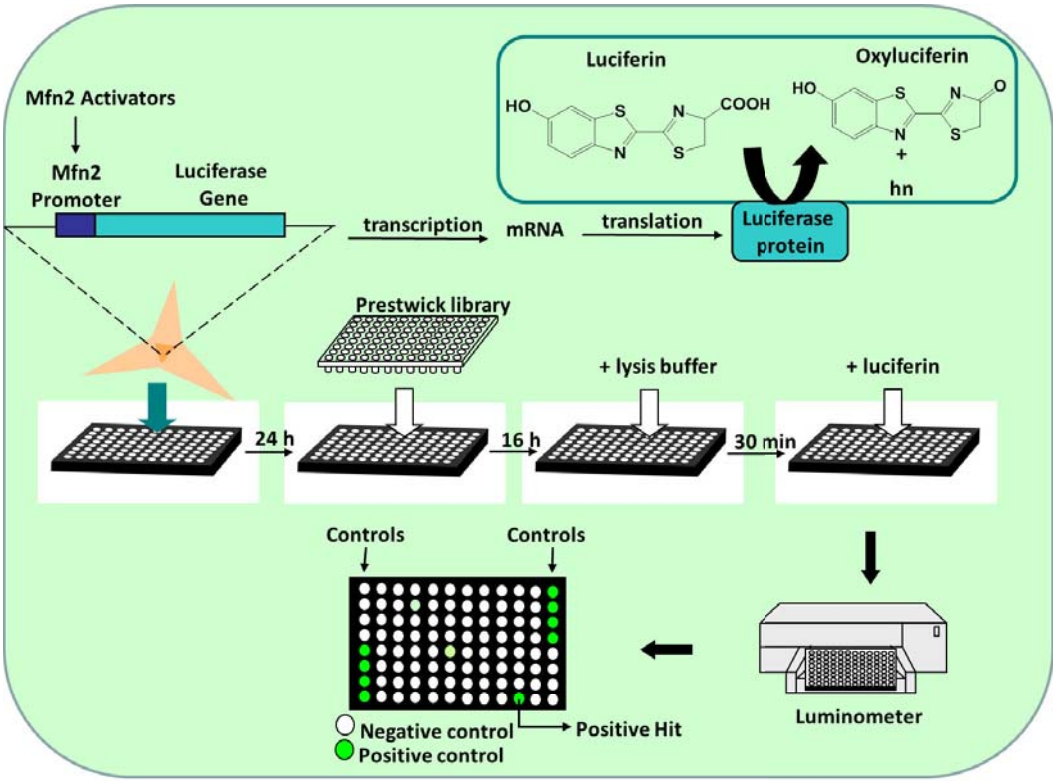

Figure 14. **Prestwick library compounds were screened by HTS using HeLa Mfn2P 14 clone cells.** The cells were incubated with the compounds at 10 µM for 16 h and luciferase reporter gene was measured to identify possible activators of the the human Mfn2 promoter.

USEF #	Compound code	Thesis code	DCI	% Activity (10 µM) assay 1	% Activity (10 µM) assay 2	Mean±eem
CBG000109	Prestw-124	C11	Hesperetin	66.2	70.4	68.3±2.1
CBG000347	Prestw-344	C10	Clorgyline hydrochloride	66.6	70.3	68.5±1.85
CBG000432	Prestw-474	C1	Piperine	112.6	114.7	13.7±1.0
CBG000509	Prestw-524	C9	Tiabendazole	124.8	101.4	113.1±11.7
CBG000539	Prestw-508	C4	Resveratrol	188.2	149.5	168.9±19.3
CBG000725	Prestw-761	C3	Butamben	62.7	63.9	63.3±0.6
CBG000732	Prestw-752	C2	Phenazopyridine hydrochloride	121.6	93.4	107.5±14.1
CBG000734	Prestw-772	C6	Leflunomide	157.8	120.4	139.1±18.7
CBG000844	Prestw-836	C8	Indoprofen	164.0	139.0	151.5±12.5
CBG000947	Prestw-909	C7	Nabumetone	117.7	131.1	124.4±6.7
CBG001052	Prestw-1072	C5	Lansoprazole	60.1	54.9	57.5±2.6
CBG001119	Prestw-1110	C12	Parbendazole	166.7	122.4	144.6±22.2

Table 2. **Possible activators of the human Mfn2 promoter.** Twelve hits showing an activity higher than 60 % compared to 9-RA were identified in the HTS.

2.3. Secondary screening to detect false positives

Generally, gene reporter cell-based assays are used to study the regulation of a gene of interest in primary HTS. Biochemical assays, which are an in *vitro* assays, are used in a secondary screen to identify false positives.

Once the HTS was done, a secondary screen using a different methodology was performed to discard compounds that generate a positive signal via other mechanisms. The objective of the secondary screening was to evaluate the direct effect of the compounds to purified luciferase activity to identify possible false positives.

The test was done in collaboration with Dr. Mabel Loza at the University of Santiago de Compostela following a protocol similar to the one described by the NIH Chemical Genomics Center for the identification of luciferase modulators (Pubchem Bioassay 411), which measures the luciferase capacity to generate light by using luciferine and ATP as substrates. The kit used to perform the secondary assay was PKLight® Assay Kit (Lonza #L07-500) (See section 11 in materials and methods).

Compounds at 10 µM final concentration (10 µL from a stock solution of 1 mM in DMSO) were added to 60 µL of the assay buffer (Imidazol 50 mM, KCl 50 mM, $MgCl_2$ 7 mM, ATP 10 µM, Tween 20 0.01%, BSA 0.05%, pH = 7.2). Then, 30 µL of the luciferase detection mixture was added and the mixture was incubated for 8 min at room temperature. Once the compounds were incubated the luminescence signal was measured using a lector Ultra Evolution (Tecan) using an integration time of 100 µs.

None of the evaluated compounds behaved as positive modulators of the luciferase activity. However, resveratrol (one of our putative hits) at 10 µM inhibited luciferase activity (42±1% reduction). The rest of the compounds did not show any negative modulator behavior by decreasing the activity of purified luciferase. It has been proposed that inhibitors of the luciferase activity can be identified as activators in *in vivo* assays based on luciferase reporter, because they can stabilize the enzyme forming a luciferase-inhibitor complex[4-6].

The results obtained match with the NIH Chemical Genomics Center's results with the same luciferase kit used in the assay USEF (Pubchem Bioassay 411) where the Prestwick library was evaluated among others and the resveratrol exhibited an IC50 = 6.9 µM against the purified luciferase. In the same assay it is described that none of the Prestwick library compounds act as luciferase activators. In other assay, which was performed in San Diego Chemical Genomics Center and using a different luciferase, was described that indoprofen causes 61% reduction in luciferase activity at a concentration of 10 µM.

From the twelve compounds identified as putative activators of Mfn2 expression, which stimulate the transcriptional activity of human Mfn2 promoter, only resveratrol could be identified as a false activator by stabilizing the luciferase enzyme. The rest of the compounds do not seem to be false positive by directly modulating luciferase activity. On the basis of these results we decided to go one step further with all the compounds taking in consideration that resveratrol can be a false positive.

3. Selection of activators of Mfn2 expression

The possible activators of Mfn2 expression obtained from the HTS were commercially available and were purchased to test their activities. Different cellular assays, such as transcriptional activity assay based on luciferase reporter, messenger RNA (mRNA) and protein levels assays were performed to confirm the compounds capability to increase the expression of the Mfn2 protein.

3.1. Results in HeLa cells expressing luciferase under the control of Mfn2 promoter

The possible activators of Mfn2 expression were confirmed by measuring transcriptional activity of the human Mfn2 promoter using the luciferase reporter assay. Moreover, dose-response curves were performed to obtain the optimal concentration of each compound, and finally, the compounds were re-tested again measuring their transcriptional activity at the optimized concentration.

3.1.1. Hits confirmation in HeLa cells overexpressing Mfn2 promoter

The compounds were re-tested in 5 independent luciferase reporter assays and each condition was set up per triplicate in our laboratory.

HeLa Mfn2P 14 clone cells were seeded in 24-well plate (90,000 cells/well). The next day the cells were incubated with the compounds at 10 µM for 16 h, and then luciferase assay was performed (Figure 15).

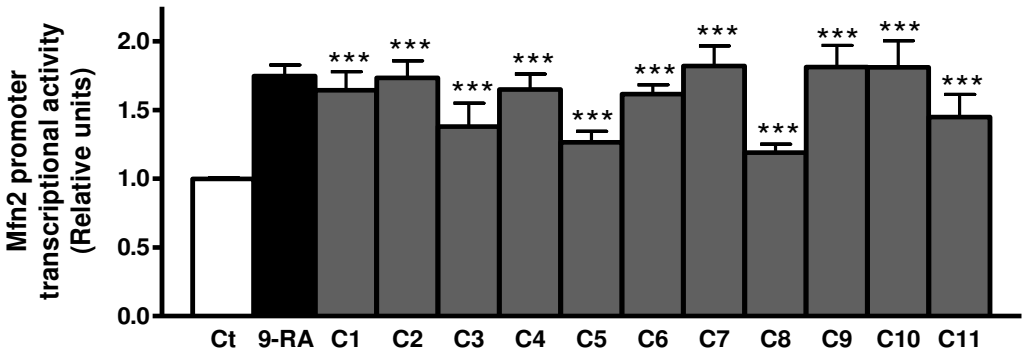

Figure 15. Positive hits from HTS were re-tested in our laboratory. Mfn2 promoter transcriptional activity in HeLa Mfn2P 14 cells incubated with 9-RA and the compounds at 10 µM for 16 h was measured by luciferase reporter gene. Data represent the mean ± SEM expressed relative to the control (Ct) group. ***P < 0.001 vs Ct. Ct, control; 9-RA, 9-cis retinoic acid. Five independent assays were performed per triplicate (n = 5).

Parabendazole (C12) was incubated at 50 nM, 100 nM, 1 µM, 2 µM, 5 µM and 10 µM in HeLa Mfn2P 14 cells, and all the cells died because of toxicity effect. Thus, parabendazole was discarded as possible activator of Mfn2 promoter.

Finally, seven compounds, which gave the highest activation and the better reproducibility, were selected for further studies. The selected compounds were C1 (piperine), C2 (phenazopyridine hydrochloride), C4 (resveratrol), C6 (leflunomide), C7 (nabumetone), C9 (tiabendazole) and C10 (clorgyline hydrochloride).

3.1.2. Dose Response curves in HeLa cells that stably express luciferase under the control of Mfn2 promoter

A dose response study for each compound was performed to determine the optimal concentration at which the compound showed the maximum effect to activate Mfn2 promoter.

HeLa Mfn2P 14 cells were seeded in a 24-well plate (90,000 cells/well) and the next day the cells were incubated with compounds at different concentrations (100 nm, 1 µM, 10 µM, 50 µM and 100 µM) for 16 h. The transcriptional activity of the Mfn2 promoter for each compound at different concentrations was measured using the luciferase reporter assay, and the optimal concentrations were determined (Figure 16).

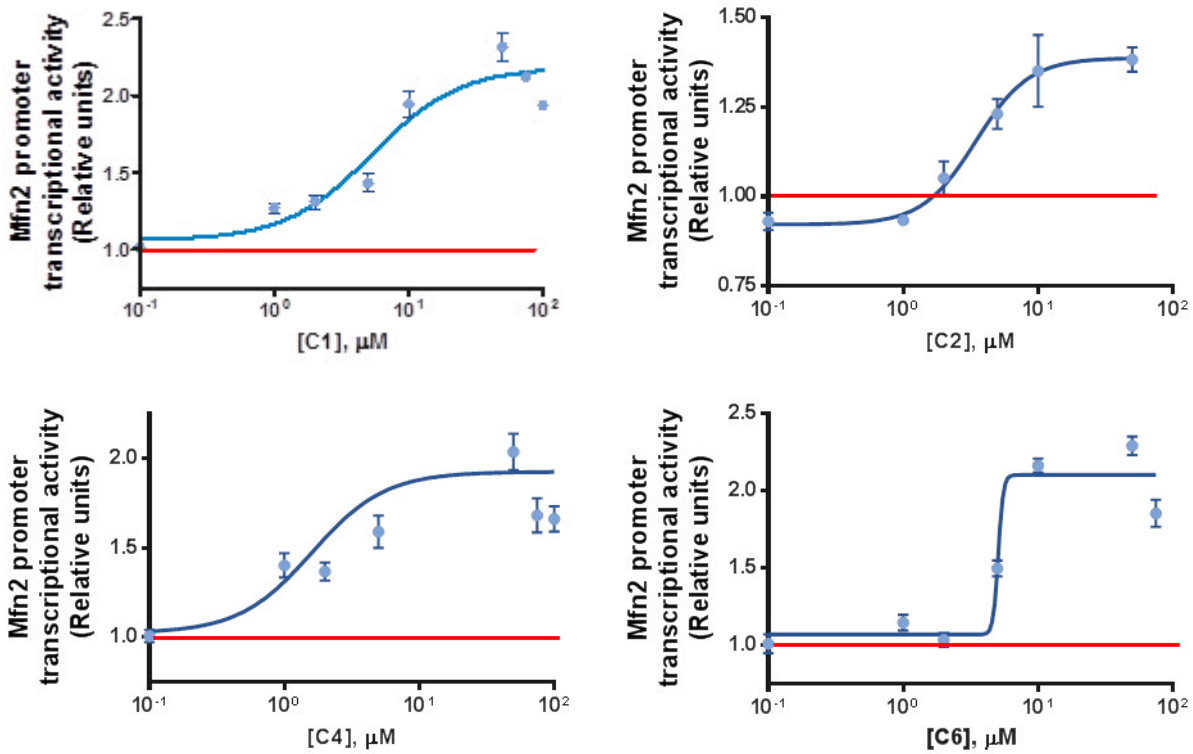

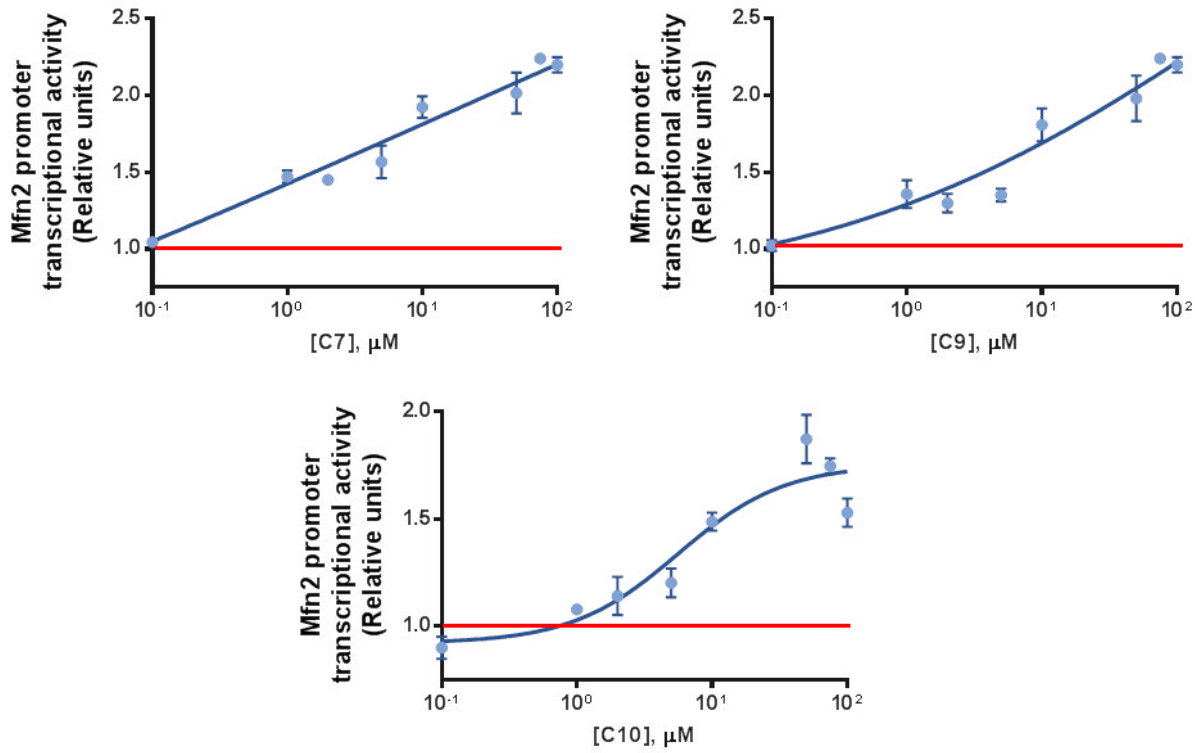

Figure 16. **Dose-Response curves of compounds in HeLa Mfn2P 14 cells.** Mfn2 promoter transcriptional activity in HeLa Mfn2P 14 incubated with the compounds at different concentrations for 16 h was measured by luciferase reporter gene. The points of the graphic show the mean ± error expressed relative to control group (value 1) of one representative experiment. Two assays were performed per triplicate (n = 2).

The dose-response study assigned the optimal concentrations producing the maximum effect to activate Mfn2 promoter in HeLa Mfn2P 14 cells. Compound 1 at 50 µM caused a 2.3-fold stimulation. Compound 2 and 4 at 10 µM produced a 1.5- and 2.5-fold increase, respectively. Compound 6 at 100 µM showed higher activity than 50 µM. However, C6 at 100 µM was discarded because the cells exhibited toxic problems. Thus, C6 at 50 µM was selected producing a 2 fold increase. Compound 7 and 9 at 75 and 100 µM produced higher luminescence increase than 50 µM, but those concentrations were discarded due to toxicity problems. Thus, C7 and C9 at 50 µM producing a 2 fold increase were selected. Compound 10 at 50 µM produced a 1.8 fold increase.

3.1.3. Confirmation of selected hits in HeLa cells overexpressing Mfn2 promoter using the optimized concentration

HeLa Mfn2P 14 cells were seeded in a 24-well plate (90,000 cells/well) and the next day the cells were incubated with the compounds at the optimized concentration. Then, transcriptional activity of Mfn2 promoter was measured using the luciferase reporter gene (Figure 17).

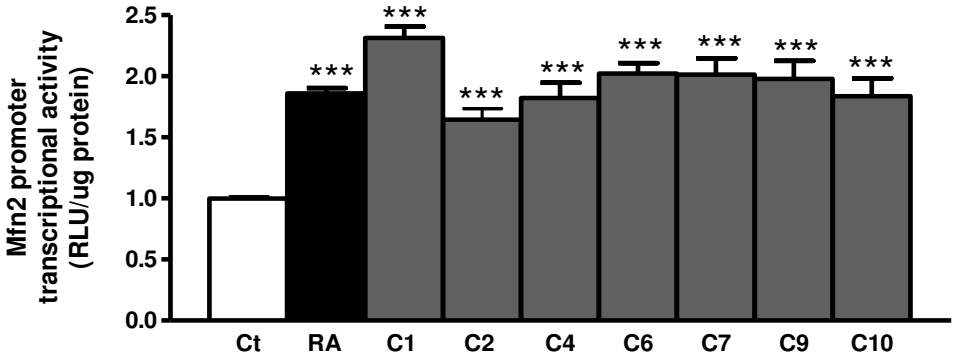

Figure 17. **Trancriptional activity of the human Mfn2 promoter in HeLa Mfn2P 14 cells.** The cells were incubated with the selected compounds at the optimized concentration for 16 h and luciferase reporter gene was measured. Data represent the mean ± SEM expressed relative to the control (Ct) group. ***P < 0.001 vs Ct. Ct, control; 9-RA, 9-cis retinoic acid. Three assays were performed per triplicate (n = 3).

Once the possible activators of Mfn2 expression had been validated in HeLa Mfn2P 14 cells, which overexpress Mfn2 promoter, the next step was to validate these compounds in HeLa and C2C12 cells, which endogenously express Mfn2.

3.2. Validation of the activators of the Mfn2 promoter at gene and protein level in HeLa and C2C12 cells

The possible activators of Mfn2 promoter were tested in HeLa and C2C12 cell lines, and Mfn2 mRNA and Mfn2 protein levels were measured.

3.2.1. Mfn2 gene expression

The compounds were incubated in HeLa and C2C12 for 48 h at the optimized concentration and Mfn2 mRNA levels were measured by quantitative Polymerase Chain Reaction (qPCR).

3.2.1.1. Mfn2 gene expression in HeLa cells

Hela cells that endogenously express Mfn2 were seeded in a 12-well plate (70,000 cells/well) and the next day the cells were incubated with the compounds at the optimized concentration for 48 h. Then, Mfn2 mRNA levels were measured by qPCR (Figure 18).

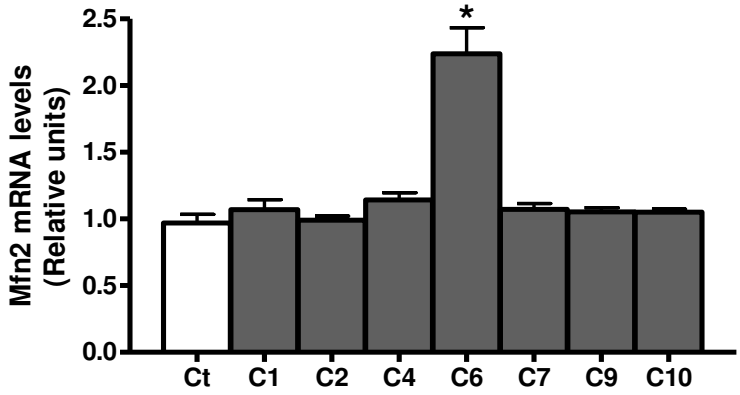

Figure 18. **Mfn2 mRNA levels of HeLa cells incubated with the compounds.** Mfn2 mRNA levels in HeLa cells incubated with the compounds at the optimized concentration were measured by qPCR. The housekeeping gene used was cyclophilin A (Cyp A). Both probes, Mfn2 and Cyp A, were TaqMan. Data represent the mean ± SEM expressed relative to the control (Ct) group of one representative experiment. *P < 0.05 vs Ct. Two independents assays were performed per triplicate (n = 2).

Only compound 6 at a concentration of 50 µM produced a 2.1 fold increase in Mfn2 mRNA levels in HeLa cells.

3.2.1.2. Mfn2 gene expression in C2C12 cells

The effect of the compounds was analysed in a mouse muscle cell line (C2C12), which have a higher expression of endogenous Mfn2 than HeLa cells. C2C12 cells were seeded in a 12-well plate (45,000 cells/well), and the next day the cells were incubated with the compounds at the optimized concentration for 48 h. Then, Mfn2 mRNA levels were measured by qPCR (Figure 19).

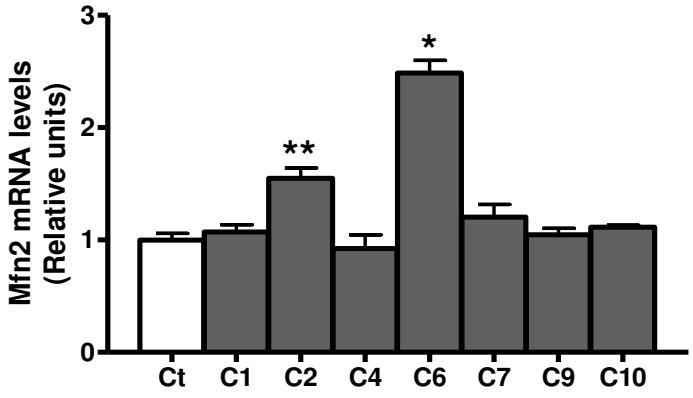

Figure 19. **C2 and C6 increase Mfn2 mRNA levels in C2C12 cells.** Mfn2 mRNA levels in C2C12 cells incubated with the compounds at the optimized concentration were quantified by qPCR. The housekeeping gene used was β-actin. Mfn2 probe was TaqMan and β-actin dye was SYBR. Data represent mean ± SEM expressed relative to the control (Ct) group of one representative experiment. *P < 0.05 vs Ct, **P < 0.01 vs Ct. Two independent assays were performed per triplicate (n = 2).

Compound 2 and 6 at a concentration of 10 and 50 µM produced a 1.6 and 2.5 fold increase, respectively, in Mfn2 mRNA levels in C2C12 cells.

Once the effect of compounds was analysed measuring Mfn2 mRNA levels in HeLa and C2C12 cells, the next step was to measure Mfn2 protein levels in HeLa cells.

3.2.2. Mfn2 protein expression

Mfn2 protein levels in HeLa cells were measured by western blot assay (See section 7 in materials and methods). HeLa cells were seeded in 6-well plate (140,000 cells/well) and the next day the cells were incubated with the compounds at the optimized concentration for 48 h. DMSO was used as a negative control (Figure 20).

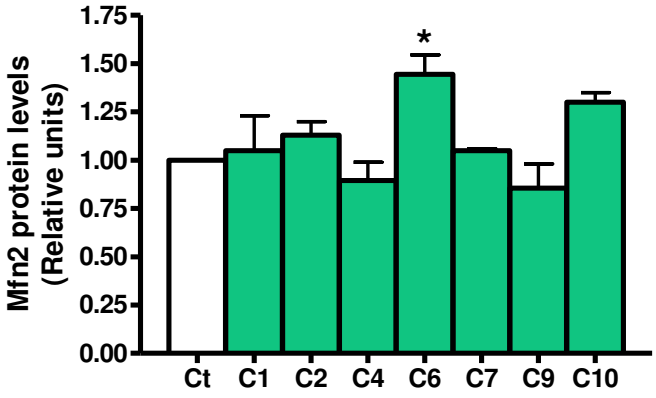

Figure 20. **Mfn2 protein levels in HeLa cells incubated with the compounds.** Mfn2 and tubulin protein levels in total lysates were analysed by western blot. Data represents mean ± SEM expressed relative to control group (Ct) of one representative experiment. Mfn2 protein was normalized by tubulin. Two independent assays were performed (n = 2) per dulpicate.

Compound 6 (leflunomide) at a concentration of 50 µM produced a 45 % increase in Mfn2 protein levels in HeLa cells.

On the basis of these results C6 was selected as activator of Mfn2 expression showing the highest increase in Mfn2 mRNA levels in HeLa and C2C12 cells, and the highest increase in Mfn2 protein levels in HeLa cells. However, C2 showing an increase in Mfn2 mRNA levels in C2C12 was discarded because it was not able to increase Mfn2 expression in HeLa cells. C10 showing a slight increase of Mfn2 protein expression in HeLa cells was also discarded. The possible activator of Mfn2 expression has to be active in different cell lines to be validated as a hit, and C6 (leflunomide) accomplishes this feature.

4. Validation of leflunomide as an activator of Mfn2 expression

4.1. Optimal conditions of Leflunomide

Once leflunomide was selected as an activator of Mfn2 expression, exhibiting a high transcriptional activity in HeLa Mfn2P 14, and a high Mfn2 mRNA and protein levels in HeLa and C2C12 cells, a deeper study for leflunomide validation was performed.

4.1.1. Dose Response study measuring Mfn2 mRNA levels in HeLa cells

A dose response study was performed for leflunomide to determine the concentration with maximum effect to activate Mfn2 promoter measuring Mfn2 mRNA levels in HeLa cells. Previously in section 3.1.2 the same experiment was carried out measuring Mfn2 transcriptional activity. HeLa cells that endogenously express Mfn2 were incubated with leflunomide at 10, 50 and 75 µM for 48 h and Mfn2 mRNA levels were measured by qPCR (Figure 21).

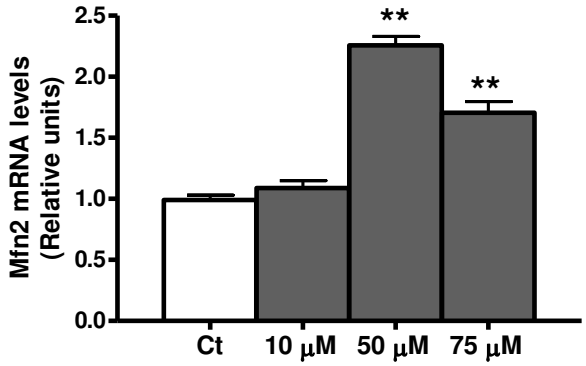

Figure 21. **Dose response study of leflunomide.** Mfn2 mRNA levels in HeLa cells incubated with leflunomide at different concentrations for 48 h were measured by qPCR. The housekeeping gene used was cyclophilin A (Cyp A). Both probes, Mfn2 and Cyp A, were TaqMan. Data represents mean ± SEM expressed relative to control (Ct) group of one representative experiment. **P < 0.01 vs Ct. Two independent assays were performed per triplicate (n = 3).

The dose response curve showed that the concentration providing the maximum effect to activate Mfn2 mRNA levels in two fold increase was 50 µM. Thus, leflunomide was always incubated at 50 µM for further experiments.

4.1.2. Time course measuring Mfn2 mRNA levels in HeLa cells

HeLa cells were incubated with leflunomide at 50 µM at different times of incubation (8, 20, 24, 36 and 48 h) and Mfn2 mRNA levels were measured by qPCR (Figure 22).

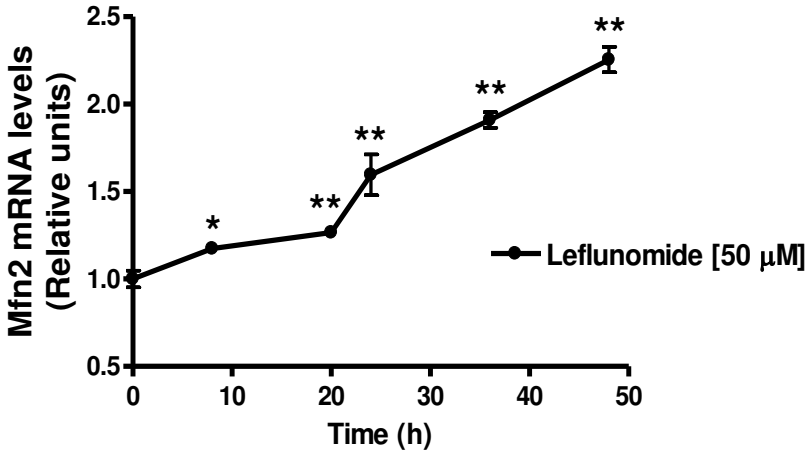

Figure 22. **Time course of Leflunomide in HeLa cells.** Mfn2 mRNA levels in HeLa cells incubated with leflunomide at 50 μM at different incubations times were measured by qPCR. The housekeeping gene used was cyclophilin A (Cyp A). Both probes, Mfn2 and Cyp A, were TaqMan. Data represents the mean ± SEM expressed relative to the control group of one representative experiment. *P < 0.05 vs Ct, **P < 0.01 vs Ct. Two independents assays were performed per triplicate (n = 2).

The best condition achieving two fold increase in Mfn2 mRNA levels was incubating HeLa cells with leflunomide at 50 μM for 48 h. On the basis of these results the selected conditions to obtain the highest leflunomide activity was incubating the HeLa cells at 50 μM for 48 h.

4.1.3. Validation of leflunomide in HeLa cells

HeLa cells were incubated with leflunomide at 50 μM for 48 h and Mfn2 mRNA and protein levels were measured and quantified by qPCR and western blot, respectively.

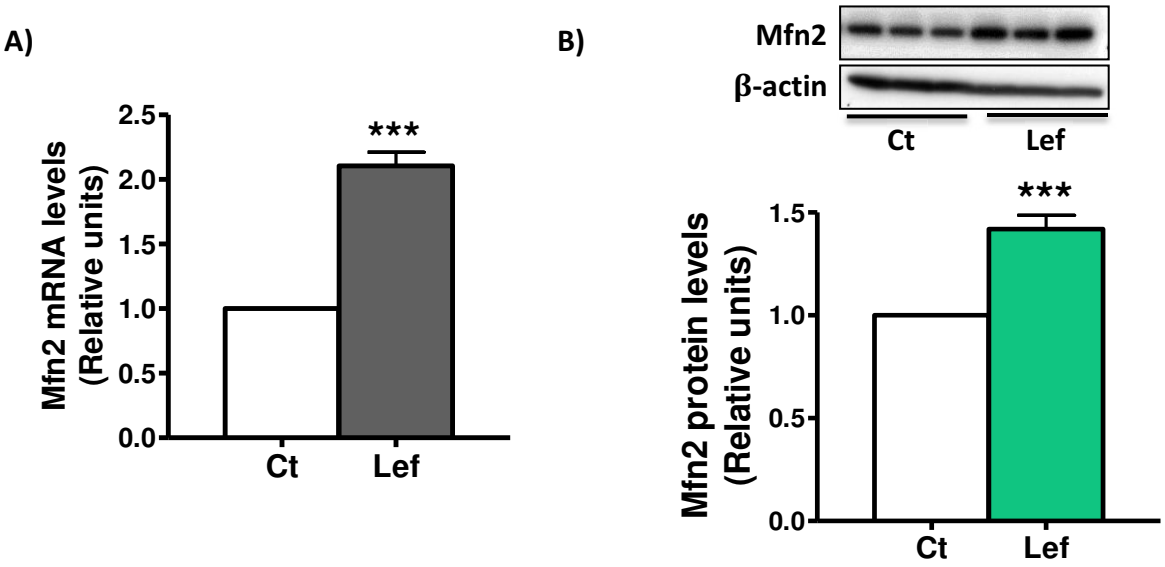

Figure 23. **Leflunomide increases Mfn2 expression.** (A) Mfn2 mRNA levels in HeLa cells incubated with leflunomide at 50 μM for 48 h were quantified by qPCR. Both probes, Mfn2 and Cyp A, were TaqMan (B) Mfn2 and β-actin protein levels in HeLa cells incubated with leflunomide at 50 μM for 48 h were analysed by western blot. Data represent the mean ± SEM expressed relative to the control (Ct) group. ***P < 0.001 vs Ct. Ct,

control; Lef, leflunomide. A) Five independents assays were performed per triplicate (n = 5). B) Seven independent assays were performed per triplicate (n = 7).

Leflunomide was validated as an activator of Mfn2 expression in HeLa cells showing 2.1-fold increase in Mfn2 mRNA levels and 1.4-fold increase in Mfn2 protein levels.

4.2. Validation of Teriflunomide in HeLa cells

Leflunomide (Arava) is indicated for the treatment of active Rheumatoid Arthritis (RA) as a disease-modifying antirheumatic drug (DMARD), and was launched in United States in 1998[7]. Leflunomide, an isoxazol derivative, once administrated is rapidly converted to a malononitril amide (A771726), termed teriflunomide, through an isoxazole ring-opening reaction (Scheme 1). The reaction is nonenzymatic and takes place in plasma and intestinal mucosa.

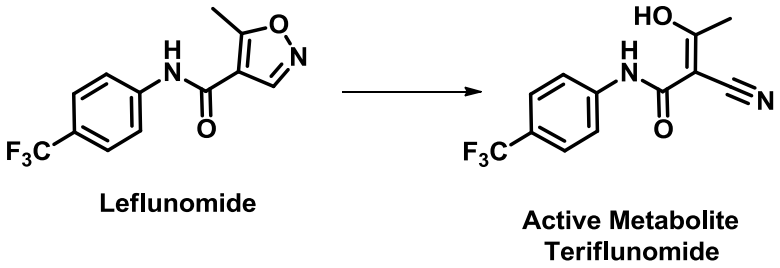

Leflunomide **Active Metabolite Teriflunomide**

Scheme 1. **Leflunomide is rapidly converted to teriflunomide in the body.**

Although leflunomide is effective for the treatment of active RA, has significant diverse secondary effects and therefore, it was discarded for the treatment of diseases related with alterations in Mfn2 expression. However, modulation of proteins involved in fusion and fission events can potentially constitute a molecular target to modulate mitochondrial function for the treatment of mitochondrial-related diseases. For that reason, a profound study of these proteins and their regulation could elucidate new therapeutic opportunities.

Teriflunomide, the active form of leflunomide, was incubated in HeLa Mfn2P 14 and in HeLa cells to confirm that has the same activity as leflunomide.

4.2.1. Transcriptional activity

HeLa Mfn2P 14 cells were seeded in 24-well plate (90,000 cells/well). The next day the cells were incubated with teriflunomide at 50 µM for 16 h and, then luciferase assay was performed (Figure 24 and see section 6 in materials and methods).

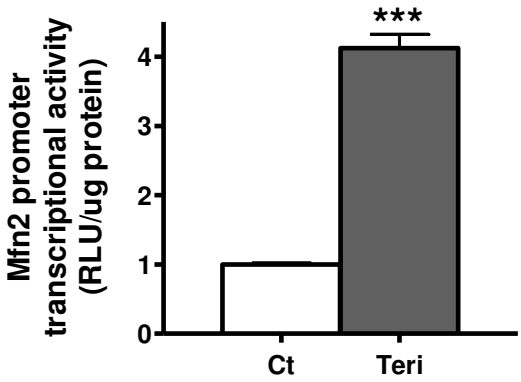

Figure 24. **Teriflunomide increases Mfn2 promoter transcriptional activity in HeLa Mfn2P 14 cells**. Mfn2 promoter transcriptional activity in HeLa Mfn2P 14 incubated with teriflunomide at 50 µM for 16 h was quantified by luciferase gene reporter. Data represent the mean ± SEM expressed relative to the control (Ct) group. ***P < 0.001 vs Ct. Ct, control; Teri, teriflunomide. Three assays were performed per triplicate (n = 3).

Teriflunomide increased Mfn2 promoter transcriptional activity in 4.1-fold increase compared to the control; showing higher Mfn2 promoter transcriptional activity than leflunomide, for the reason that transcriptional activity of teriflunomide was measured at 50 µM and leflunomide was measured at 10 µM.

4.2.2. Dose response curve measuring Mfn2 mRNA levels in HeLa cells

A dose response study was performed for teriflunomide to determine if the concentration with maximum effect to activate Mfn2 promoter measuring Mfn2 mRNA levels in HeLa cells was the same as leflunomide. HeLa cells that endogenously express Mfn2 were incubated with teriflunomide at 1, 10 and 50 µM for 48 h and Mfn2 mRNA levels were measured by qPCR (Figure 25).

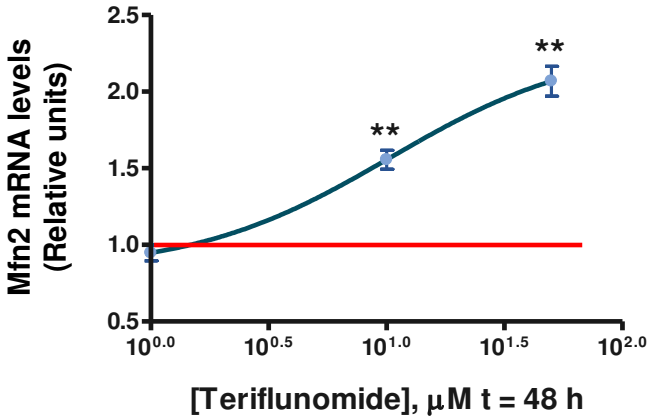

Figure 25. **Dose response curve of teriflunomide.** Mfn2 mRNA levels in HeLa cells at different concentrations of teriflunomide for 48 h were determined by qPCR. The housekeeping gene used was cyclophilin A (Cyp A). Both probes, Mfn2 and Cyp A, were TaqMan. Data represent mean ± SEM expressed relative to the control (Ct) group of one representative experiment. **P < 0.01 vs Ct. Two independent assays were performed per triplicate (n = 2).

The dose response curve showed that the concentration providing the maximum effect to activate Mfn2 mRNA levels in two fold increase was 50 µM. Thus, teriflunomide exhibited the same activity as leflunomide.

4.2.3. Time course in HeLa cells

HeLa cells were incubated with teriflunomide at 50 µM at different times of incubation (8, 24 and 48 h) and Mfn2 mRNA levels were measured by qPCR.

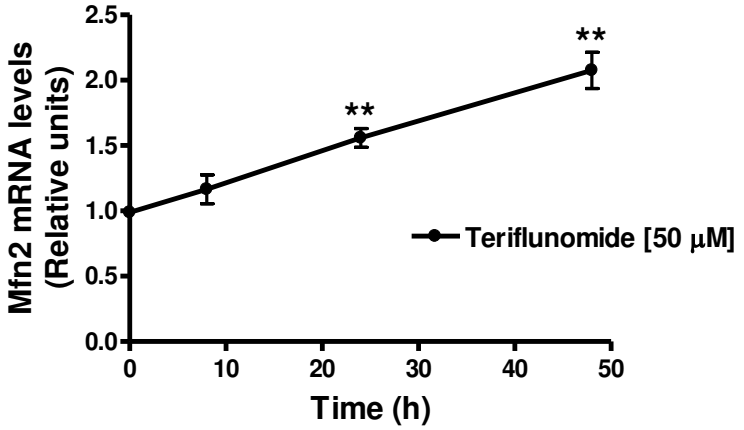

Figure 26. **Time course of teriflunomide in HeLa cells.** Mfn2 mRNA levels in HeLa cells incubated with teriflunomide (50 µM) at different incubations times. The housekeeping gene used was cyclophilin A (Cyp A). Both probes, Mfn2 and Cyp A, were TaqMan. Data represent mean ± SEM expressed relative to control of one representative experiment. **P < 0.01 vs Ct. Two independents assays were performed per triplicate (n = 2).

Teriflunomide at 50 µM produced the maximal activity in Mfn2 mRNA levels at 48 h of incubation as leflunomide. These results confirmed that teriflunomide is an activator of Mfn2 expression.

4.3. Validation of leflunomide in C2C12 cells

Once leflunomide was selected and validated as an activator of Mfn2 expression in HeLa cells, we further explore leflunomide activity in C2C12 cells.

4.3.1. Mfn2 protein expression in C2C12 cells

The effect of leflunomide was analysed in C2C12 cells. The cells were seeded in a 6-well plate (90,000 cells/well) and the next day the cells were incubated with leflunomide at 50 µM for 48 h, and Mfn2 protein levels were analysed by western blot (Figure 27).

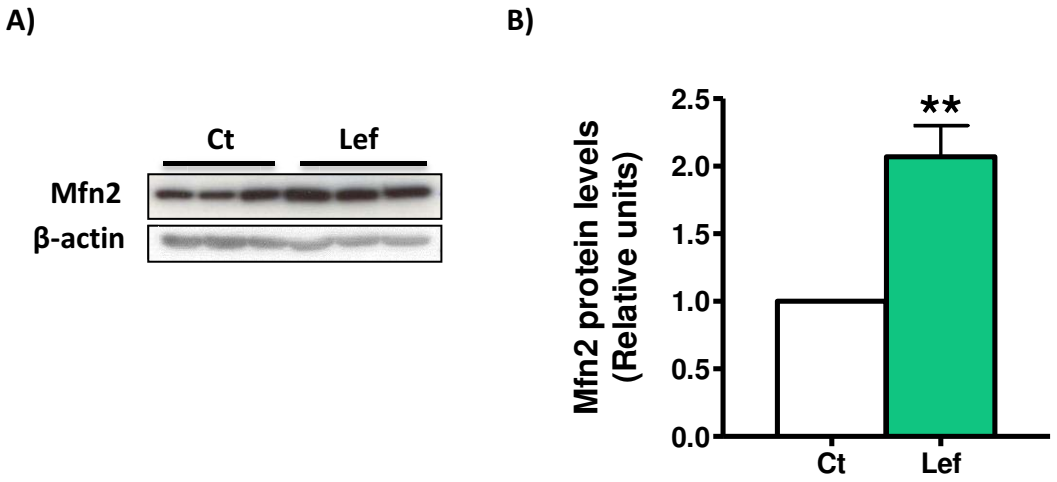

Figure 27. **Leflunomide increases Mfn2 protein levels in C2C12 cells.** The Mfn2 and β-actin protein levels in total lysates from C2C12 cells were analysed by western blot (A) and quantified by densiometry using β-actin as a control (B). Data represents mean ± SEM expressed relative to the control group. **P < 0.01 vs Ct. Ct, control; Lef, leflunomide. Six independent assays were performed per triplicate (n = 6).

Leflunomide increased Mfn2 protein levels by 2.1-fold in C2C12 cells. These results confirm its activity as an activator of Mfn2 expression in C2C12 cells.

5. Leflunomide as specific inhibitor of dihydroorotate dehydrogenase

Dihydroorotate dehydrogenase (DHODH), a flavin mononucleotide containing mitochondrial enzyme, catalyses the fourth reaction of the *de novo* biosynthesis of pyrimidines. DHODH is an enzyme located in the inner mitochondrial membrane and catalyses the oxidation of dihydroorotate into orotate by using ubiquinone as an electron acceptor through an enzyme-bound redox cofactor, FMN.

Leflunomide, a drug approved for the treatment of rheumatoid arthritis[7], is an inhibitor of DHODH. Leflunomide inhibits DHODH by binding to the ubiquinone binding channel, and prevents the production of the pyrimidine ribonucleotide uridine monophosphate (UMP). UMP is a source for pyrimidine nucleotides, which are important precursors used in DNA (thymine and cytosine), RNA (uracil and cytosine), glycoproteins and phospholipids biosynthesis. Pyrimidine bases are essential for cellular metabolism and cell growth.

5.1. Assays of cell proliferation in HeLa and C2C12 cells

Leflunomide shows anti-proliferative effects through inhibition of DHODH, and consequently the *de novo* synthesis of pyrimidines. It has been described that external uridine antagonises the ability of leflunomide and teriflunomide to inhibit cell proliferation[8,9]. Exogenous uridine is immediately metabolised by the cells to uridine monophosphate (UMP) by uridine kinase[10], an enzyme of the salvage pathway. UMP is an essential prerequisite of pyrimidine diphosphate and triphosphate formation[11].

5.1.1. Antiproliferative effects of leflunomide and teriflunomide in HeLa cells

To assess the overall cellular effect of leflunomide and teriflunomide on cell viability, the number of living cells during treatment with both compounds was monitored. HeLa cells were seeded in 12-well plate (70,000 cells/well). Then, the next days the cells were incubated with leflunomide and teriflunomide at 50 M for 6, 24 and 48 h and the antiproliferative activity was visualized by optical microscope (Figure 28).

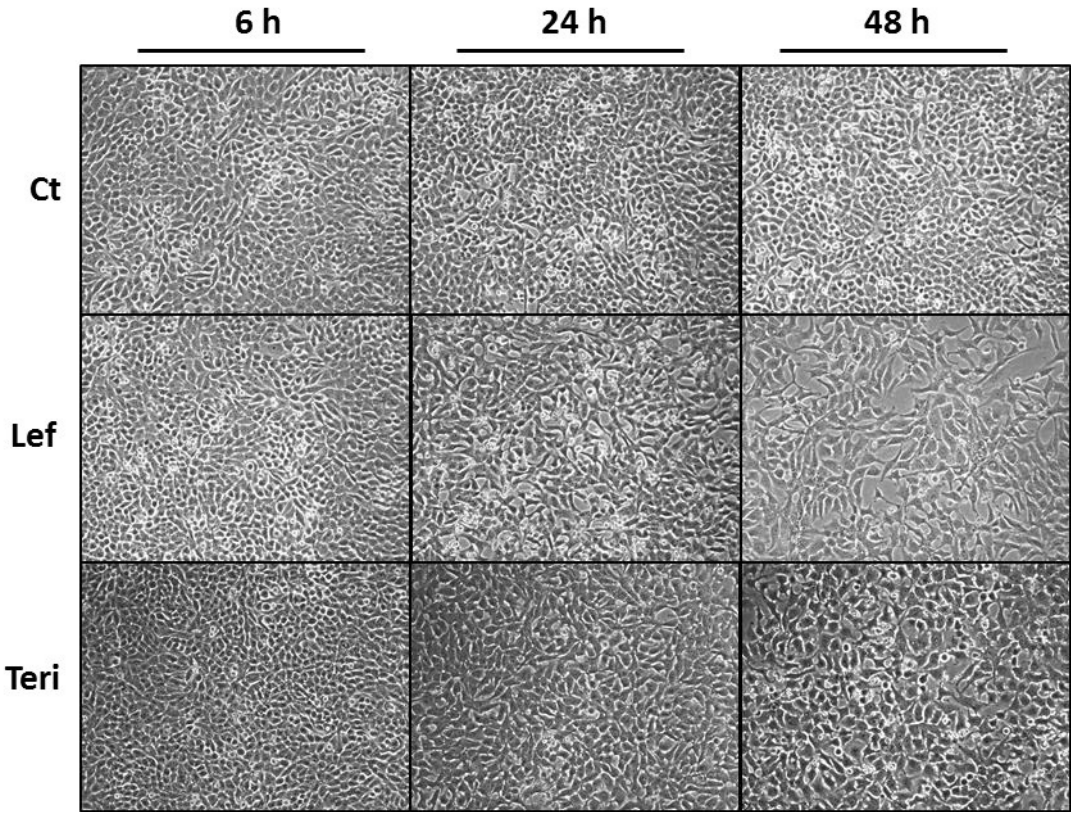

Figure 28. **Antiproliferative effect of HeLa cells incubated with leflunomide and teriflunomide at 6, 24 and 48 h was visualized by optical microscope.** Ct, control; Lef, leflunomide; Teri, teriflunomide.

Leflunomide and its active metabolite showed antiproliferative effects at 24 h, and the effects were even more dramatic after 48 h of exposure. On the basis of these results, we can conclude that leflunomide and teriflunomide have antiproliferative effects by inhibiting the DHODH enzyme, and consequently the *de novo* synthesis of pyrimidines in HeLa cells.

In order to elucidate the antiproliferative activity of leflunomide and teriflunomide in more detail, external uridine (an intermediate of pyrimidine biosynthesis) was added to cells expecting a reversible antiproliferative effect. HeLa cells were incubated with leflunomide and teriflunomide at 50 µM ± uridine at 50 µM for 48 hours and the number of cells was monitored (Figure 29).

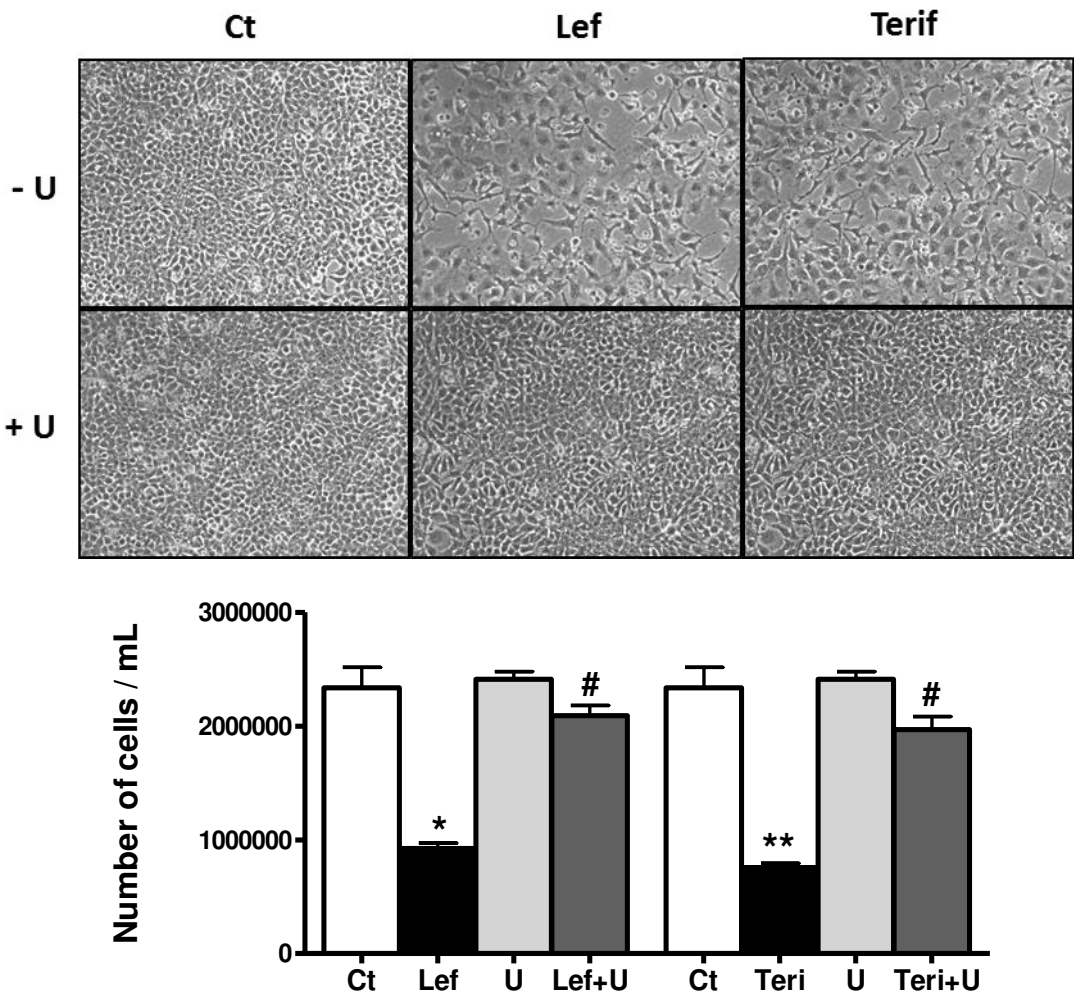

Figure 29. **Uridine is able to reverse the antiproliferative effects of leflunomide and teriflunomide.** The number of HeLa cells incubated with leflunomide and teriflunomide at 50 µM ± uridine at 50 µM were visualized by optical microscope and counted. Data represents the mean ± SEM of one representative experiment. *P < 0.05 vs Ct, **P < 0.01 vs Ct, #P < 0.05 vs Lef or Teri. Ct, control; Lef, leflunomide; Teri, teriflunomide; U, uridine. Two experiments were performed per triplicate (n = 2).

The addition of exogenous uridine to the cells was able to reverse the antiproliferative effects of leflunomide and teriflunomide, suggesting that depletion of pyrimidine ribonucleotides is the mechanism of action of the compounds by DHODH inhibition.

5.1.2. Antiproliferative effects of leflunomide in C2C12 cells

Once the antiproliferative effect of leflunomide and teriflunomide was validated in HeLa cells, the same experiment was performed in C2C12. C2C12 cells were seeded in 12-well plate (45,000 cells/well), and the next day the cells were incubated with leflunomide at 50 µM ± uridine at 50 µM (Figure 30).

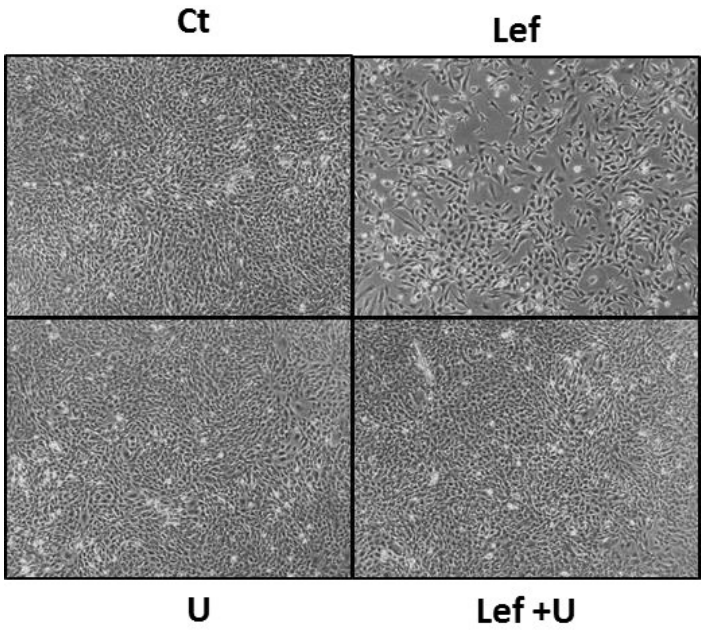

Figure 30. **Antiproliferative effect of C2C12 cells incubated with leflunomide was visualized by optical microscope.** Ct, control; Lef, leflunomide; U, uridine.

Leflunomide showed antiproliferative effects at 48 h in C2C12 cells. The addition of exogenous uridine to the cells was able to reverse the antiproliferative effects of leflunomide, suggesting that depletion of pyrimidine ribonucleotides is the mechanism of action of the compound by DHODH inhibition.

These results confirm the antiproliferative effects of leflunomide in two different cell lines (HeLa and C2C12 cells). Leflunomide and teriflunomide inhibits the synthesis of pyrimidines by DHODH inhibition.

5.1.3. Uridine reverses Mfn2 mRNA expression in HeLa cells incubated with leflunomide and teriflunomide

To address whether the increase in Mfn2 gene expression produced by leflunomide and teriflunomide was a consequence of its antiproliferative activity by DHODH inhibition and consequently, the *de novo* synthesis of pyrimidines, uridine was added expecting a reverse effect in the levels of Mfn2 mRNA.

HeLa cells were incubated with leflunomide and teriflunomide at 50 µM ± uridine at 50 µM for 48 h and Mfn2 mRNA levels were measured by qPCR (Figure 31).

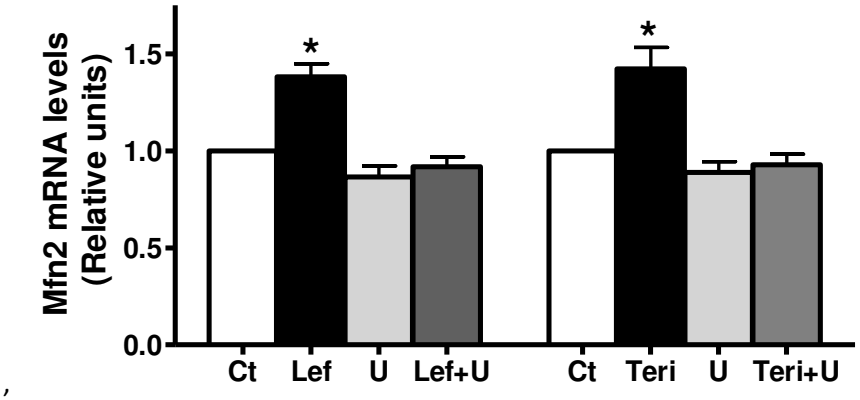

Figure 31. **External uridine reverses the increase of Mfn2 mRNA levels induced by leflunomide and its active metabolite.** Mfn2 mRNA levels in HeLa cells incubated with leflunomide and teriflunomide at 50 µM ± uridine at 50 µM for 48 h were measured by qPCR. The housekeeping gene used was GAPDH. Both dyes, Mfn2 and GAPDH, were SYBR[1]. Data represents mean ± SEM expressed relative to control group. *P < 0.05 vs Ct. Ct, control; Lef, leflunomide; Teri, teriflunomide; U, uridine. Four independent assays were performed per triplicate (n = 4).

The addition of external uridine, which reverses the deficiency in pyrimidine biosynthesis, reversed the increase in Mfn2 gene expression and the antiproliferative activity induced by leflunomide and teriflunomide. These results suggest that Mfn2 up-regulation is triggered by the deficiency in pyrimidines, indicating that the mechanism of action of these compounds is related with the inhibition of the enzyme DHODH.

[1] GAPDH was used as a housekeeping gene instead of Cyp A because it was more stable for normalization.

6. Leflunomide modulates other mitochondrial proteins involved in mitochondrial dynamics

Previous results in section 3 and 4 validated leflunomide as an activator of Mfn2 expression in HeLa and C2C12 cells. Mfn2 protein participates in mitochondrial fusion and moreover, regulates mitochondrial metabolism[12]. Mitochondria are dynamic organelles whose morphology is regulated by fusion and fission processes, which are involved in the control of mitochondrial activity and cell metabolism.

In order to elucidate the capacity of leflunomide to shift the balance between mitochondrial fusion and fission events, other mammalian mitochondrial proteins involved in fusion such as as Mfn1 and Opa1, and mitochondrial proteins involved in fission such as Drp1 and Fis1, were measured. Porin, also called outer membrane-localized voltage-dependent anion channel (VDAC), is the most abundant protein in the outer mitochondrial membrane (OMM), and was also measured as a control for mitochondrial mass.

6.1. Effects of leflunomide and teriflunomide in Mfn1, Opa1 and Drp1 mRNA levels in HeLa cells

First of all, the gene expression of the mitochondrial proteins involved in fusion and fission events were measured. HeLa cells were incubated with leflunomide and teriflunomide at 50 µM in the presence or absence of uridine at 50 µM for 48 h and Mfn1, Opa1 and Drp1 mRNA levels were measured by qPCR (Figure 32).

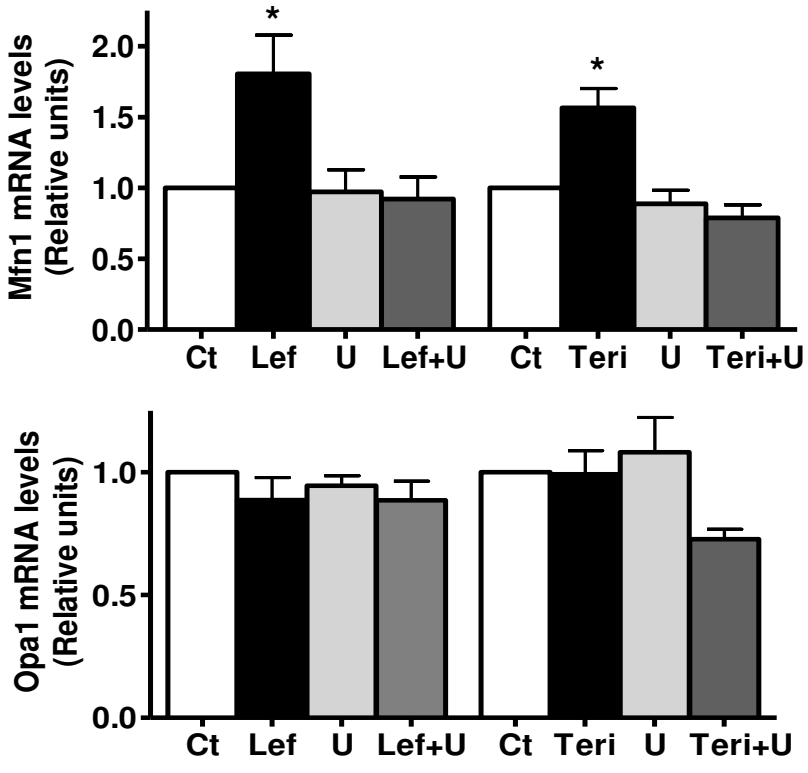

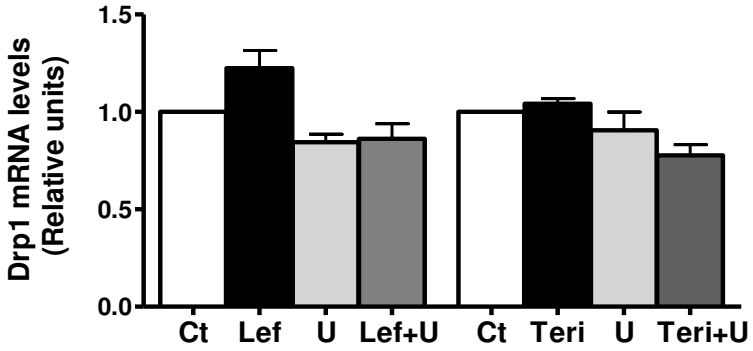

Figure 32. **Mfn1, Opa1 and Drp1 mRNA levels in HeLa cells incubated with leflunomide and teriflunomide.** Mfn1, Opa1 and Drp1 mRNA levels in HeLa cells incubated with leflunomide and teriflunomide at 50 µM ± uridine at 50 µM for 48 h were measured by qPCR. The housekeeping gene used was GAPDH. Mfn1, Opa1 and Drp1 were TaqMan probes and GAPDH was SYBR. Data represents mean ± SEM expressed relative to control group. *P < 0.05 vs Ct;. Ct, control; Teri, teriflunomide; Lef, leflunomide; U, uridine. Three independent assays were performed per triplicate (n = 3).

Leflunomide and teriflunomide induce Mfn1 mitochondrial gene expression and addition of external uridine is able to reverse the increase of Mfn1 mRNA levels. No changes were observed for Opa1 and Drp1 mRNA levels. The results obtained for Mfn1 agreed with Mfn2 data (see section 5.1.3), suggesting that Mfn1 up-regulation, is triggered by the deficiency in pyrimidines caused by leflunomide and teriflunomide through DHODH inhibition.

6.2. Effects of leflunomide in Mfn1, Opa1, Drp1, Fis1 and porin proteins levels in HeLa and C2C12 cells

The next step was to measure the abundance of mitochondrial proteins involved in fusion and fission events. HeLa and C2C12 cells were incubated with leflunomide at 50 µM for 48 h and Mfn1, Opa1, Drp1, Fis1 and porin protein levels were analyzed by western blot (Figure 33).

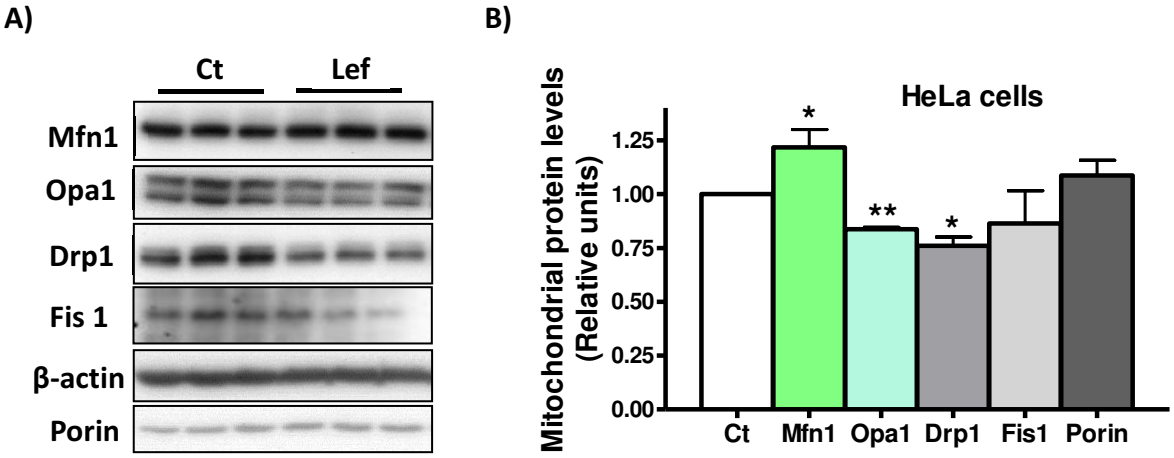

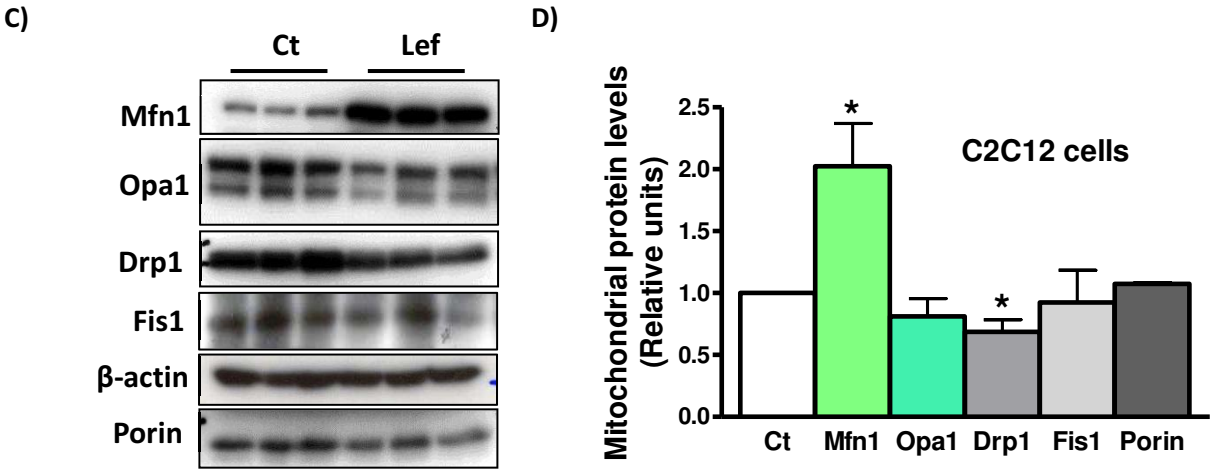

Figure 33. **Mitochondrial protein levels in HeLa and C2C12 cells.** Mfn1, Opa1, Drp1, Fis1, β-actin and porin protein levels in total lysates from HeLa (A) and C2C12 (C) cells were analysed by western blot. Quantification by densitometry was performed for mitochondrial proteins in HeLa (B) and C2C12 (D) cells using β-actin as a control. Data represents mean ± SEM expressed relative to the control (Ct) group. *P < 0.05 vs Ct. A) Three independent assays were performed per triplicate in HeLa cells (n = 3). B) Five independent assays were performed per triplicate in C2C12 cells (n = 5).

Leflunomide up-regulated Mfn1 and decreased Opa1 and Drp1 expression in HeLa cells. No changes were observed for Fis1 and porin proteins. The increase in Mfn1 levels induced by leflunomide was higher in C2C12 cells than in HeLa cells, and Drp1 is down-regulated as in HeLa cells. No changes were observed for Opa1, Fis1 and porin proteins. The changes in mitochondrial proteins are not a consequence of an increase in total mass of mitochondria because porin levels did not change.

These results suggest that leflunomide, up-regulates Mfn2 (see section 4.1.3 and 4.3.1) and Mfn1 fusion proteins and down-regulates Drp1 fission protein. This suggests a displacement of the balance between mitochondrial fusion and fission towards mitochondrial fusion promoting the elongation of mitochondria.

6.3. Uridine reverses Mfn2 and Mfn1 protein expression in C2C12 cells incubated with leflunomide

A further study to confirm that Mfn2 and Mfn1 up-regulation is triggered by the deficiency in pyrimidines caused by leflunomide through DHODH inhibition was performed. C2C12 cells were incubated with leflunomide at 50 µM ± uridine at different concentrations for 48 h and Mfn2 and Mfn1 were analysed by western blot (Figure 34).

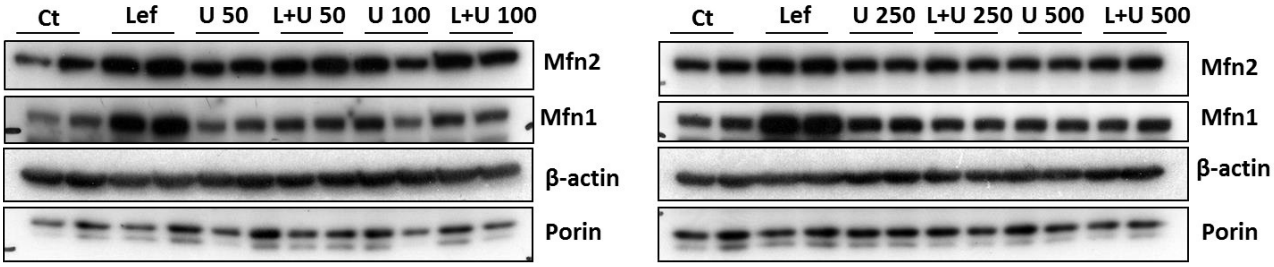

Figure 34. **Mitochondrial protein levels in C2C12 cells incubated with leflunomide and uridine.** The Mfn2, Mfn1, β-actin and porin protein levels in total lysates C2C12 cells were analysed by western blot. One independent assays was performed per duplicate (n = 1).

Leflunomide induced Mfn2 and Mfn1 protein expression. The addition of external uridine at 250 µM was able to prevent Mfn2 up-regulation. Moreover, uridine at 50 µM was able to prevent the increase of Mfn1 protein levels. The changes in mitochondrial proteins are not a consequence of an increase in total mass of mitochondria because porin did not change. On the basis of these results, we propose that Mfn1 and Mfn2 show a differential sensitivity to pyrimidine availability.

These results suggest that leflunomide, which caused a deficiency in pyrimidines through DHODH inhibition, up-regulated Mfn2 and Mfn1 fusion proteins. The addition of external uridine, which reversed the deficiency in pyrimidine biosynthesis, was able to prevent Mfns up-regulation. These results suggest a displacement of the balance between mitochondrial fusion and fission towards mitochondrial fusion promoting the elongation of mitochondria when the cells are exposed to pyrimidine deficiency.

6.4. Mitochondrial morphology in HeLa and C2C12 cells

In order to elucidate the mitochondrial network of HeLa and C2C12 myoblasts cells, HeLa and C2C12 cells stably expressing mtDsRed were seeded on coverslips in 6-well plate, and the next day were incubated with leflunomide (50 µM) for 48 h. HeLa cells were fixed and visualized at the spectral confocal microscopy (Figure 35 and see section 9 and 10 in materials and methods). C2C12 living cells were visualized at the spinning disk confocal microscopy (Figure 35). Moreover, C2C12 cells treated with leflunomide were recorded at the spinning disk confocal microscopy (See section 9 in materials and methods). The videos are in the supplementary information.

A) HeLa cells

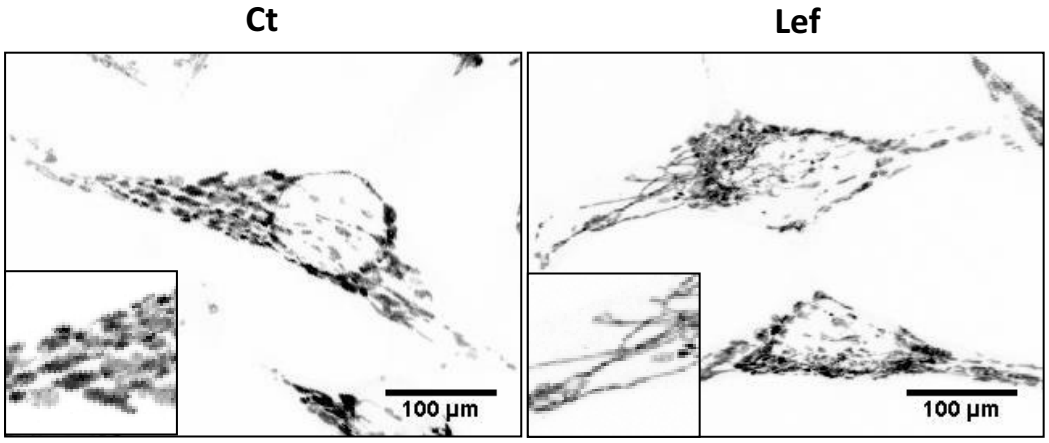

B) C2C12 cells

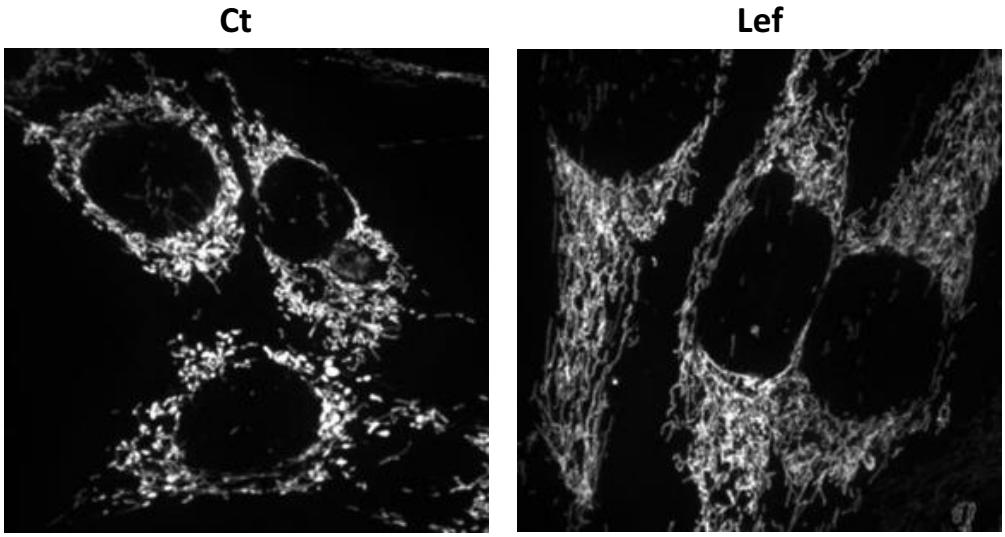

Figure 35. **Representative confocal images of mitochondrial morphology in mtDsRed expressing HeLa (A) and C2C12 (B) myoblasts cells incubated with leflunomide.**

HeLa and C2C12 cells incubated with leflunomide showed an elongated mitochondrial network compared to the control cells demonstrating that leflunomide is able to promote the elongation of mitochondria.

7. Leflunomide affects mitochondrial function in C2C12 cells

Leflunomide modulates mitochondrial proteins involved in mitochondrial dynamics promoting mitochondrial elongation and could affect mitochondrial function. To test this hypothesis, alterations in mitochondrial metabolism were examined measuring the mitochondrial membrane potential and the oxygen consumption in C2C12 cells.

7.1. Mitochondrial membrane potential in C2C12 cells

C2C12 cells were seeded in a 6-well plate (90,000 cells/well) and the next day the cells were incubated with leflunomide at 50 µM for 48 h. Then, the treatment with CCCP and TMRM (See section 8.2 in materials and methods) to measure mitochondrial membrane potential was performed and evaluated by flow cytometry (Figure 36).

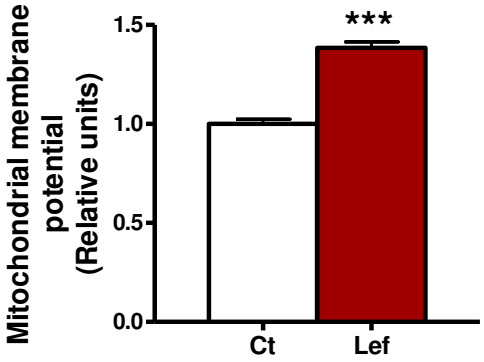

Figure 36. **Leflunomide increases mitochondrial membrane potential in C2C12 myoblasts cells.** C2C12 cells, incubated with leflunomide at 50 µM for 48 h, were stained with tetramethylrhodamine methyl ester (TMRM), which accumulates in mitochondria in a potential-dependent manner and emits fluorescence at 573 nm when it is excited at 540 nm. TMRM positive cells can be quantified using flow cytometry. Data represents mean ± SEM expressed relative to the control (Ct) group. ***P < 0.001 vs Ct. Three independent assays were performed per triplicate in C2C12 cells (n = 3).

Leflunomide produced a 1.4 fold increase in mitochondrial membrane potential in C2C12 cells.

7.2. Oxygen consumption in C2C12 cells

C2C12 cells were plated in SeaHorse Bioscience XF24 plates and the next day the cells were incubated with leflunomide at 50 µM for 48 h. Then, plates were immediately placed into the calibrated Seahorse Bioscience XF24 extracellular flux analyzer to measure oxygen consumption (Figure 37 and see section 8.1 in materials and methods).

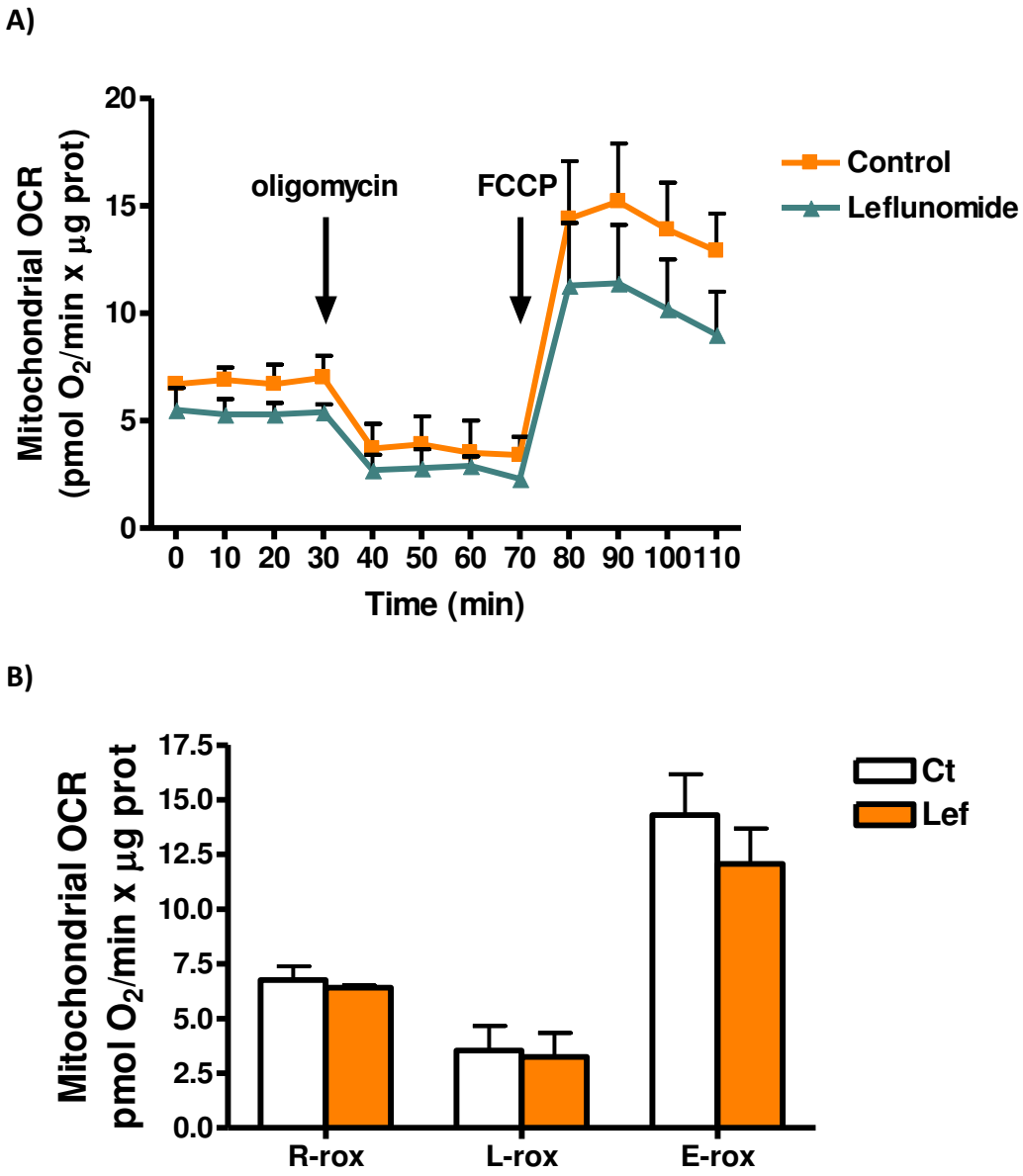

Figure 37. **Mitochondrial oxygen consumption (OCR) was measured in C2C12 cells incubated with leflunomide.** A) Representative experiment in C2C12 cells treated with leflunomide at 50 µM for 48 h. B) The following parameters were measured: oxygen consumption under routine conditions (DMEM with 5.5mM glucose), respiratory leak, measured after inhibition of ATP synthase with oligomycin, and maximal respiratory capacity reached after uncoupling with FCCP. Data are mean ± SEM. Three independent assays were performed per sixtuplicate in C2C12 cells (n = 3).

The oxygen consumption rates (OCRs) are expressed as mitochondrial oxygen consumption rates subtracting the oxygen consumption rate of the rox state to the other states (see materials and methods 8.1).

C2C12 cells treated with leflunomide showed less oxygen consumption in routine state, in leak state, when ATP synthase is inhibited by oligomycin, and in maximal uncoupled respiration, when the respiratory chain is decoupled from the synthesis of ATP by FCCP addition. Although the differences were not statistically significant, our data indicate that maximal mitochondrial respiration was moderately repressed in response to leflunomide.

Two control ratios, the Respiratory Control Ratio (RCR) and the Phosphorylation Respiratory Control Ratio (RCR_p), were calculated from the OCRs values. The former is the quotient between the respiration in state E and state L (E/L) and measures the coupling between ETC and oxidative phosphorylation, whereas the latter is the quotient ((R-L)/E) and indicates the percentage of maximum respiratory capacity used for the cells linked to ATP synthesis (Figure 38).

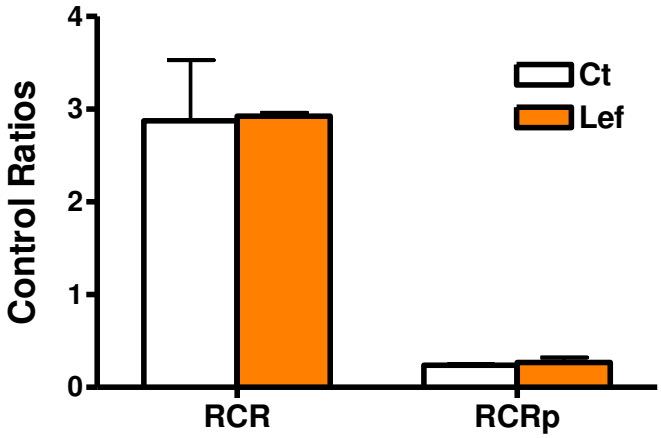

Figure 38. **Control ratios in C2C12 treated with leflunomide.** The following parameters were measured: Respiratory Control Ratio (E/L) and Phosphorylation Respiratory Control Ratio ((R-L)/E). Data are mean ± SEM. Three independent assays were performed per sixtuplicate in C2C12 cells (n = 3).

No differences were observed in RCR and RCRp ratios in C2C12 treated or not with leflunomide.

Leflunomide modulates mitochondrial proteins related in mitochondrial dynamics, morphology, and mitochondrial function in C2C12 cells. Leflunomide promotes mitochondrial elongation, increases mitochondrial membrane potential and moderately represses mitochondrial respiration.

8. Leflunomide promotes mitochondrial elongation in MEF wt, MEF Mfn2$^{-/-}$ and MEF Mfn1$^{-/-}$ cells

Mitochondrial fusion consists in two processes in which the outer and inner mitochondrial membranes (OMM and IMM, respectively) fuse separately[13]. The main components of the fusion machinery are the OMM proteins (Mfn2 and Mfn1) and the IMM protein (Opa1). Mitofusins, Mfn1 and Mfn2, regulate mitochondrial fusion and are essential for embryonic development[14,15]. Embryonic fibroblasts lacking Mfn1 or Mfn2 display different types of fragmented mitochondria, due to a severe reduction in mitochondrial fusion. It has been reported that Mfn1 and Mfn2 have both redundant and distinct functions to promote mitochondrial fusion.

To test whether the key molecular components of the mitochondrial fusion machinery are necessary for mitochondrial elongation in response to leflunomide, MEFwt, and MEFs deficient in Mfn1 (Mfn1$^{-/-}$) and Mfn2 (Mfn2$^{-/-}$) were used.

8.1. Effects of leflunomide in Mfn2, Mfn1, Opa1, Drp1 and porin proteins levels

Mitochondrial proteins involved in fusion and fission events were measured in MEFwt, MEF Mfn2$^{-/-}$ and MEF Mfn1$^{-/-}$ incubated with leflunomide at 50 µM for 48 h by western blot (Figure 39).

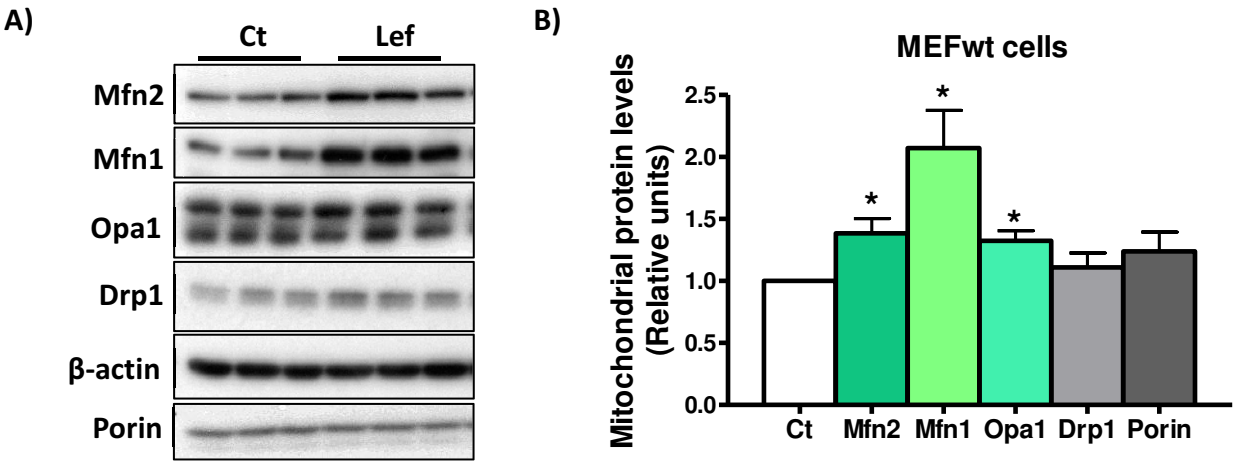

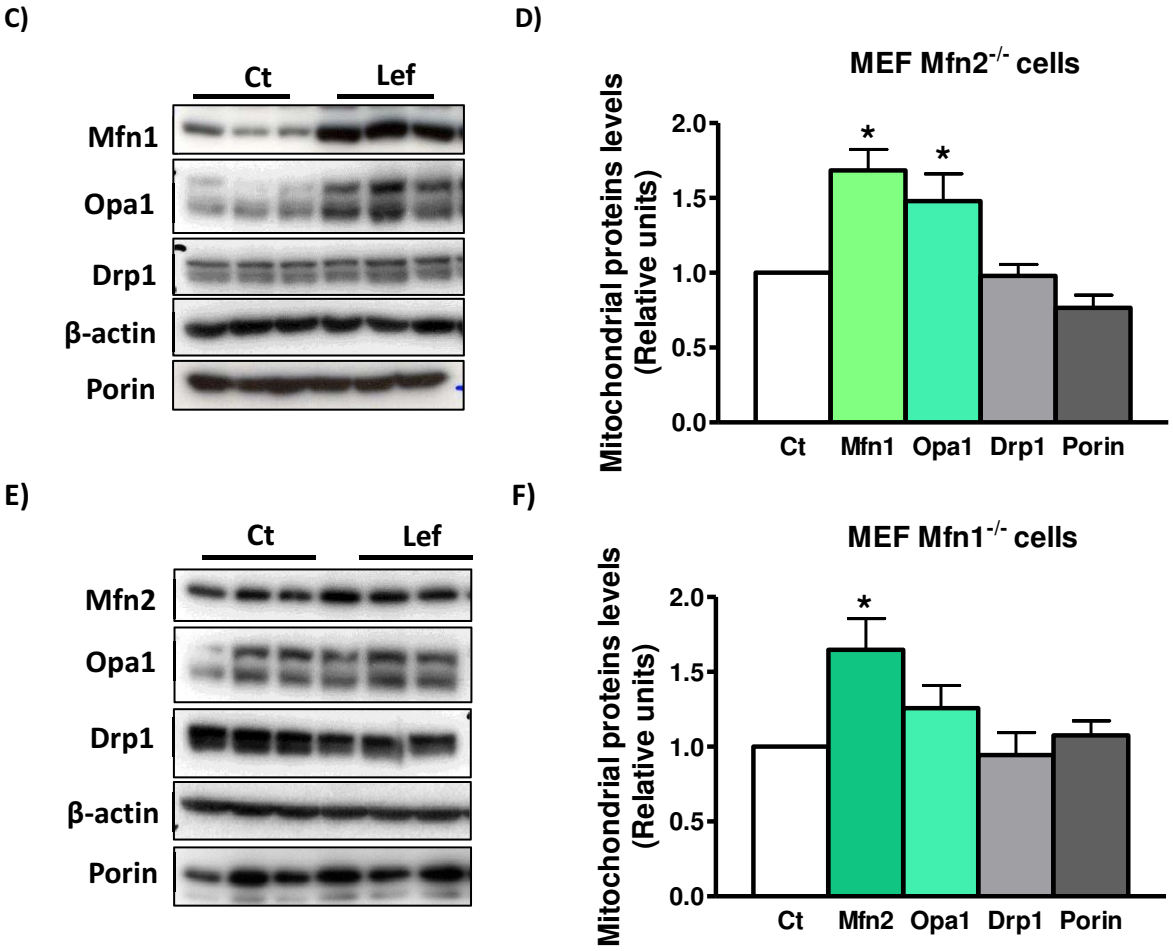

Figure 39. **Mitochondrial protein levels in MEF wt, MEF Mfn2$^{-/-}$ and MEF Mfn1$^{-/-}$ cells.** The Mfn2, Mfn1, Opa1, Drp1, β-actin and porin protein levels in total lysates from MEFwt (A), MEF Mfn2$^{-/-}$ (C) and MEF Mfn1$^{-/-}$ (E) cells were analysed by western blot. Quantification by densitometry was performed for mitochondrial proteins using β-actin as a control in MEF wt (B), MEF Mfn2$^{-/-}$ (D) and MEF Mfn1$^{-/-}$ (F) cells. Data represents mean ± SEM expressed relative to the control (Ct) group. *P < 0.05 vs Ct. Three independent assays were performed per triplicate in each cell line (n = 3).

Leflunomide up-regulated Mfn2, Mfn1, and Opa1 protein expression in MEFwt cells. No changes were observed for Drp1 and porin proteins. Moreover, leflunomide increased Mfn1 and Opa1 protein levels in MEF lacking Mfn2 and no changes were observed for Drp1 and porin proteins. Leflunomide increased Mfn2 protein expression in MEF cells lacking Mfn1, and there was a tendency to increase Opa1. No changes were observed for Drp1 and porin protein expression. The changes in mitochondrial proteins were not a consequence of an increase in total mass of mitochondria because porin did not change.

Leflunomide is able to increase Mfn2, Mfn1 and Opa1 in MEFwt and in MEF cells lacking Mfn1 and Mfn2, respectively. These results suggest that the absence of either Mfn2 or Mfn1 does not affect the effects of leflunomide on Mfn2 or Mfn1 expression. However, the increase of Mfn1 protein levels is higher than Mfn2 indicating that Mfn1 may have a marked role in mitochondrial elongation.

8.2. Mitochondrial morphology in MEFwt, MEF Mfn2$^{-/-}$ and MEF Mfn1$^{-/-}$ cells

Chen et al.[14] described that MEF Mfn1 and Mfn2 deficient cells show aberrant mitochondrial morphology. To examine if leflunomide was able to rescue the mitochondrial morphology in mitofusins deficient cells, MEFwt, MEF Mfn2 $^{-/-}$ and MEF Mfn1 $^{-/-}$ stably expressing mtDsRed were treated with leflunomide at 50 µM for 48 h (Figure 40). Moreover, MEFwt, MEF Mfn2$^{-/-}$ and MEF Mfn1$^{-/-}$ cells treated with leflunomide were recorded at the spinning disk confocal microscopy. The videos are in the supplementary information.

Loss of either Mfn1 or Mfn2 results in fragmentation of mitochondrial tubules. However, loss of Mfn1 leads to a greater degree of fragmentation, resulting in very small spheres that are uniform in size. In contrast, many Mfn2 mutant cells exhibit mitochondrial spheres of widely varying sizes and tubules.

Wild type MEFs showed two different mitochondrial morphologies. The major morphological class was characterized by a network of extended wavy tubules distributed around the nucleus, with no or only a few spherical mitochondria. A much smaller morphological class had mitochondria that were mostly spherical and were termed as fragmented. Leflunomide treatment of MEFwt cells caused mitochondrial elongation in almost all the cells. However, the elongation of mitochondria was not quantified as a result of the difficulty to measure the length of mitochondrial tubules (Figure 40 (A)).

Mfn2 deficient fibroblasts showed a small portion (10%) of spheres or ovals. The majority of the population (82%) contained a mixture of ovals and tubules. The length of these mitochondrial tubules ranged from several microns to 9 µm. A minority class, which contained 8% of cells, had elongated mitochondria network comprising tubules longer than 9 µM. Leflunomide treatment of MEF Mfn2$^{-/-}$ increased up to 53% the cells containing elongated mitochondria network (Figure 40).

In contrast, Mfn1 deficient MEFs had dramatically fragmented mitochondria. Cells with fragmented mitochondria represented 88% of the population, whereas 12% of cells contained short mitochondria. The length of these mitochondrial tubules ranged from several microns to 5 µm. A much smaller morphological class, which encompassed only 1% of cells, had elongated mitochondria with tubules longer than 5 µm. Leflunomide treatment of MEF Mfn1$^{-/-}$ did not increase as much as MEF Mfn2$^{-/-}$ the cells containing elongated mitochondria. However, cells containing short mitochondria increased up to 34% (Figure 40).

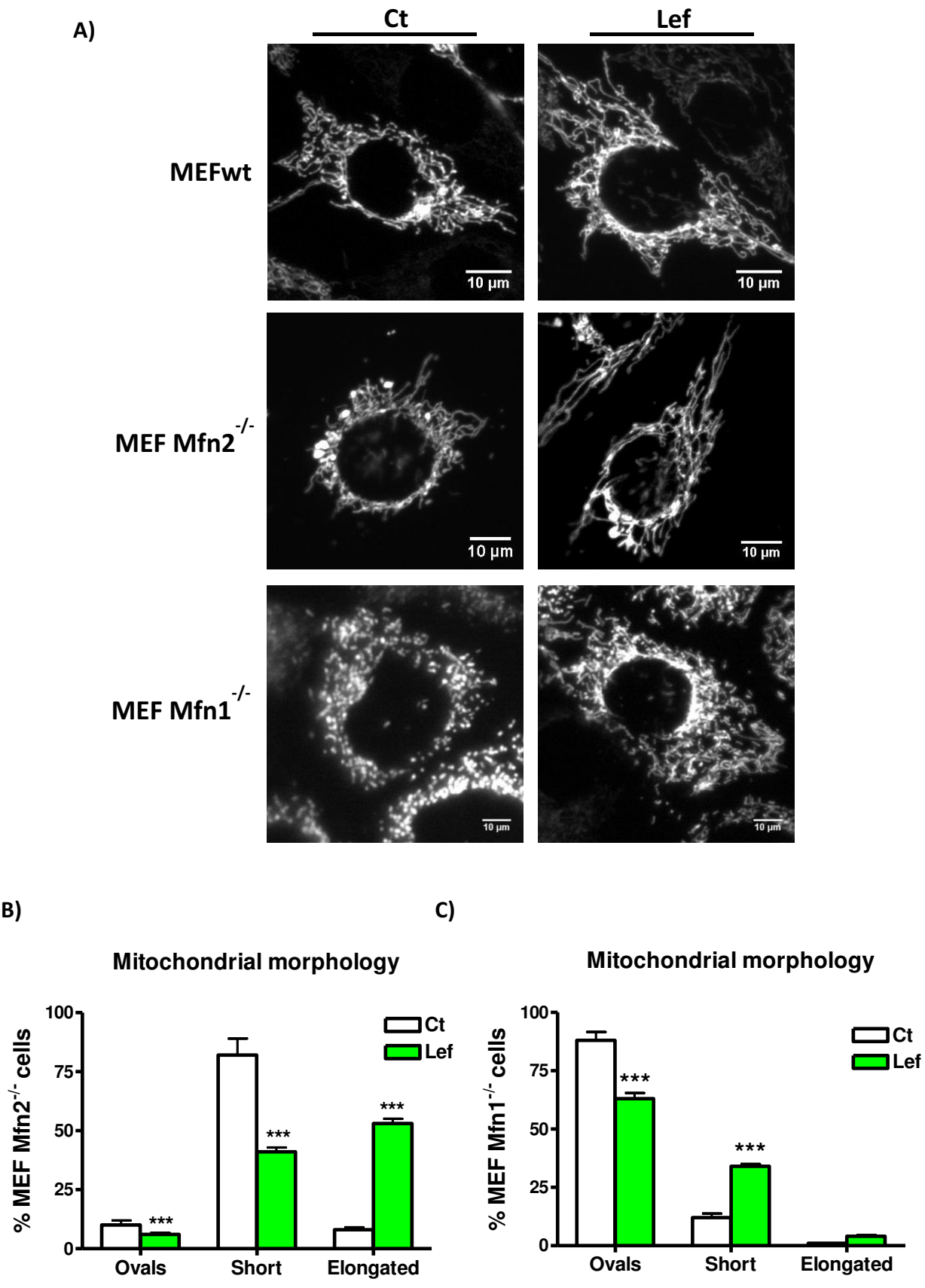

Figure 40. **Mitochondrial morphology in MEFwt, MEF Mfn2$^{-/-}$ and MEF Mfn1$^{-/-}$ cells.** A) Representative images of mitochondrial morphology MEFwt, MEF Mfn2$^{-/-}$ and MEF Mfn1$^{-/-}$ living cells stably expressing mtDsRed incubated with leflunomide. B) Mitochondrial morphology quantification in MEF Mfn2$^{-/-}$. Data represents mean ± SEM expressed relative to the control (Ct) group of one representative experiment. ***P < 0.001 vs Ct. Two

independent assays were performed, and one thousand cells were counted for each condition (n = 2). C) Mitochondrial morphology quantification in MEF Mfn1$^{-/-}$. Data represents mean ± SEM expressed relative to the control (Ct) group. ***P < 0.001 vs Ct. One independent assay was performed, and one thousand cells were counted for each condition (n = 1).

Mfn1 and Mfn2 deficient MEFs cells incubated with leflunomide were able to display the networks of longer extended tubules compared with the control ones. Moreover, MEF Mfn2$^{-/-}$ cells incubated with leflunomide showed long extended tubules similar to wild-type cells incubated with leflunomide. As it has been mentioned before Mfns are outer membrane proteins that induce mitochondrion-mitochondrion contacts through dimerization to undergo fusion. The dimerization of Mfns is controlled by Opa1[16], which is anchored on the inner membrane of mitochondria. We have demonstrated that leflunomide up-regulates Mfn2, Mfn1 and Opa1 protein levels (Section 8.1) and promotes mitochondrial elongation in MEFwt, MEF Mfn2$^{-/-}$ and MEF Mfn1$^{-/-}$. Moreover, the results obtained suggest that mitochondrial elongation is more dependent of Mfn1 than Mfn2 due to the higher mitochondrial elongation of MEF Mfn2$^{-/-}$ compared to MEF Mfn1$^{-/-}$ cells incubated with leflunomide.

8.3. Assays of cell proliferation in MEFwt, MEF Mfn2$^{-/-}$ and MEF Mfn1$^{-/-}$ cells

It has been demonstrated that leflunomide produces anti-proliferative activity inhibiting the DHODH enzyme, and consequently the *de novo* synthesis of pyrimidines. Moreover, external uridine is able to reverse the antiproliferative effect (see section 5.1).

To test whether Mfn2 or Mfn1 mitochondrial fusion proteins are necessary for uridine to reverse the antiproliferative effects caused by leflunomide, MEFwt and MEFs deficient in Mfn1 (Mfn1$^{-/-}$) and Mfn2 (Mfn2$^{-/-}$) were used.

8.3.1. Antiproliferative effect of leflunomide in MEFwt cells

MEFwt cells were seeded in 12-well plate (35,000 cells/well) and the next day the cells were incubated with leflunomide at 50 µM ± uridine at 250 µM for 48 h. Then, the number of living cells during treatment was monitored and antiproliferative activity was visualized by optical microscope (Figure 41).

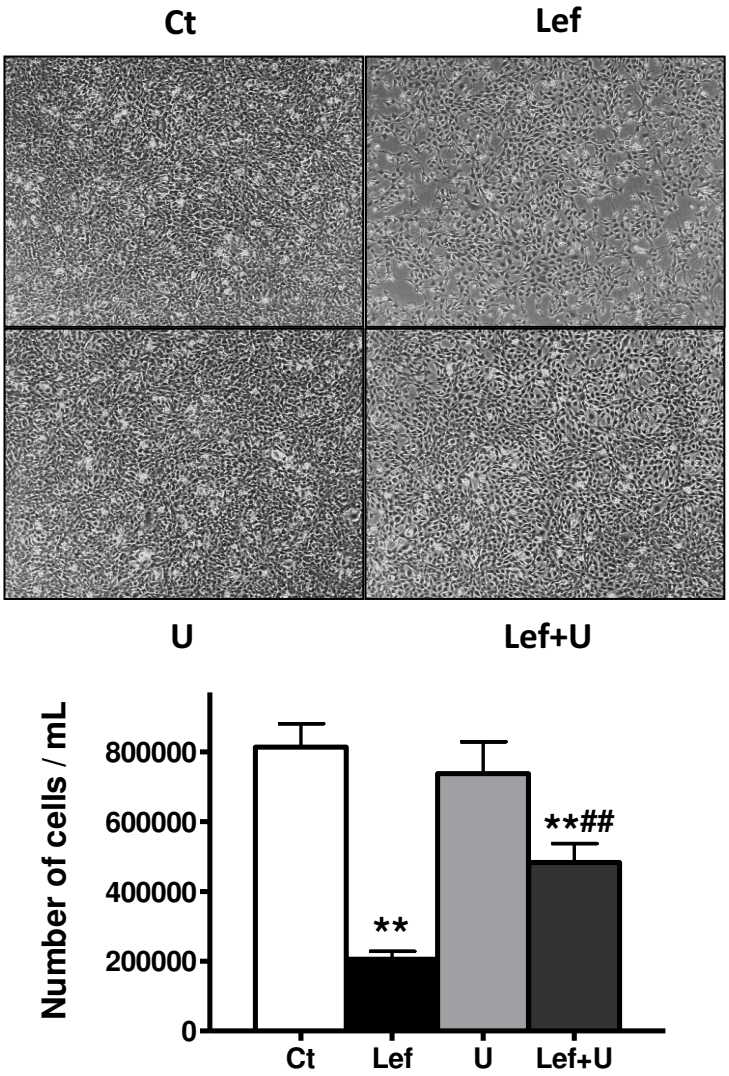

Figure 41. **Antiproliferative effect of MEFwt cells incubated with leflunomide.** Data represents mean ± SEM expressed relative to the control (Ct) group. **P < 0.01 vs Ct; ##P < 0.01 vs Lef. Four independent assays were performed per triplicate (n = 4). Ct, control; Lef, leflunomide; U, uridine.

Leflunomide reduced by 80% the proliferation of MEFwt cells relative to the control group. The addition of exogenous uridine to cells incubated with leflunomide partially recovers the antiproliferative effects of leflunomide, indicating that these cells are more sensitive to DHODH inhibition, and consequently, to pyrimidine deficiency compared with HeLa or C2C12 cells.

8.3.2. Antiproliferative effect of leflunomide in MEF Mfn2$^{-/-}$ cells

MEF Mfn2$^{-/-}$ cells were seeded in 12-well plate (35,000 cells/well) and the next day the cells were incubated with leflunomide at 50 µM ± uridine at 250 µM for 48 h. Then, the number of living cells during treatment was monitored and antiproliferative activity was visualized by optical microscope (Figure 42).

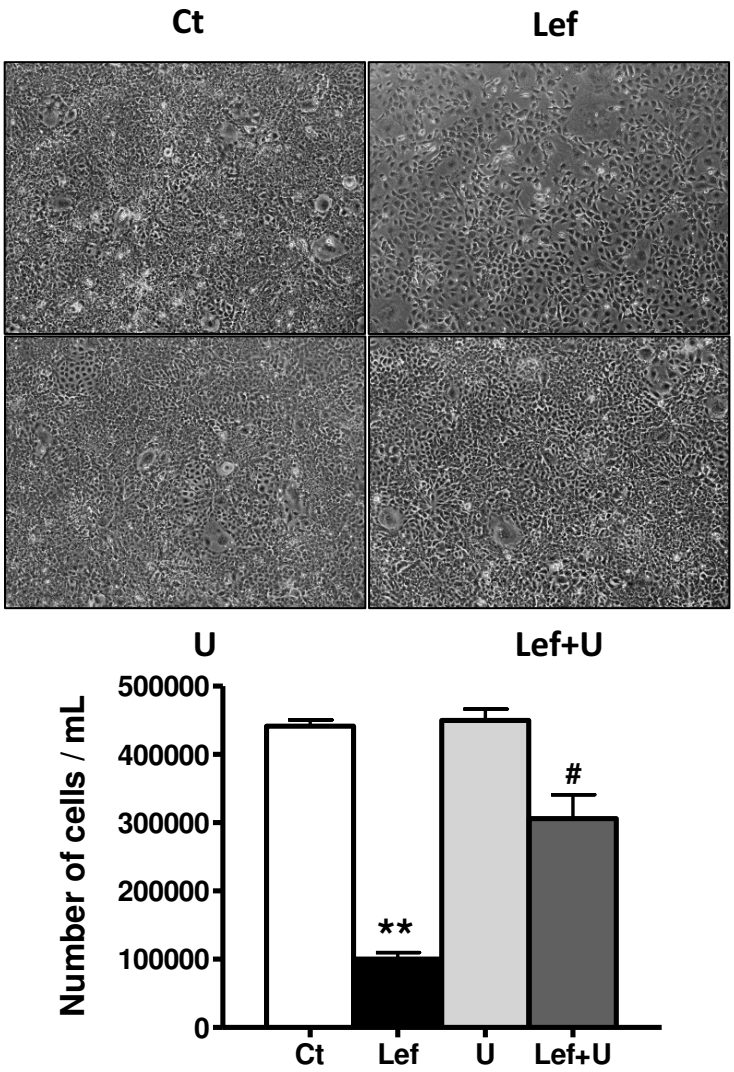

Figure 42. **Antiproliferative effect of MEF Mfn2$^{-/-}$ cells incubated with leflunomide.** Data represents mean ± SEM expressed relative to the control (Ct) group. **P < 0.01 vs Ct; #P < 0.05 vs Lef. Three independent assays were performed per triplicate (n = 3). Ct, control; Lef, leflunomide; U, uridine.

MEF Mfn2$^{-/-}$ cells have a lower proliferation rate than MEFwt cells. Leflunomide reduced by 80% the proliferation of MEF Mfn2$^{-/-}$ cells relative to the control group. The addition of exogenous uridine partially recovers the antiproliferative effects of leflunomide increasing the number of cells three times compared to leflunomide group.

8.3.3. Antiproliferative effect of leflunomide in MEF Mfn1$^{-/-}$ cells

MEF Mfn1$^{-/-}$ cells were seeded in 12-well plate (35,000 cells/well) and the next day the cells were incubated with leflunomide at 50 µM ± uridine at 250 µM for 48 h. Then, the number of living cells during treatment was monitored and antiproliferative activity was visualized by optical microscope (Figure 43).

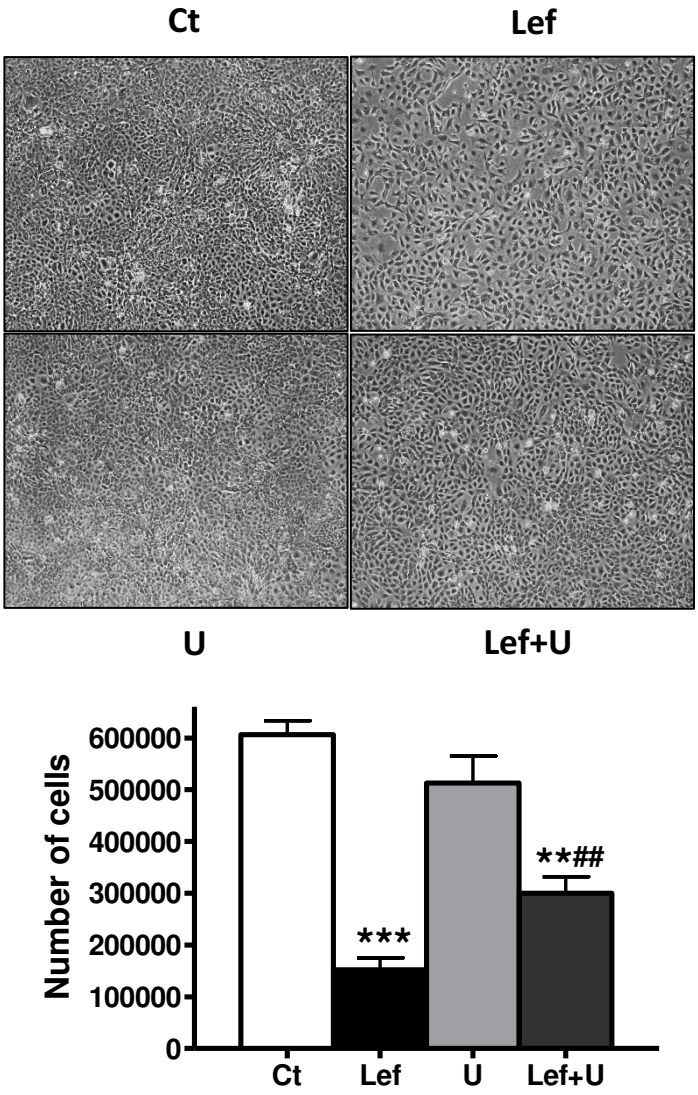

Figure 43. **Antiproliferative effect of MEF Mfn1$^{-/-}$ cells incubated with leflunomide.** Data represents mean ± SEM expressed relative to the control (Ct) group. **P < 0.01 vs Ct, ***P < 0.001 vs Ct; ##P < 0.01 vs Lef. Three independent assays were performed per triplicate (n = 3). Ct, control; Lef, leflunomide; U, uridine.

MEF Mfn1$^{-/-}$ cells have a lower proliferation rate than MEFwt cells. Leflunomide reduced by 80% the proliferation of MEF Mfn1$^{-/-}$ cells relative to the control group, and the addition of exogenous uridine partially recovers the antiproliferative effects of leflunomide increasing the number of cells two times compared to leflunomide group.

8.3.4. Global comparison of antiproliferative effects of leflunomide in MEFwt, MEF Mfn2$^{-/-}$ and MEF Mfn1$^{-/-}$ cells

The antiproliferative effects in MEFwt, MEF Mfn2$^{-/-}$ and MEF Mfn1$^{-/-}$ cells were expressed relative to control group (value 1) and compared among them (Figure 44).

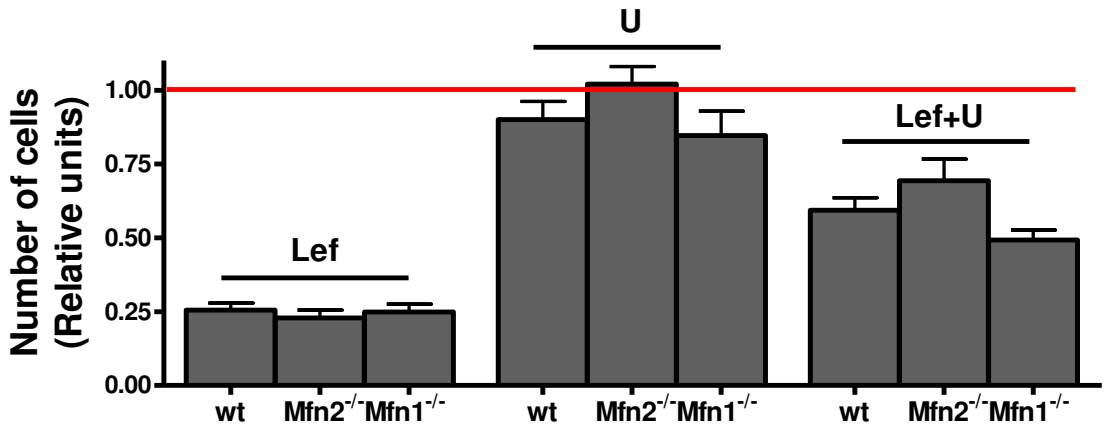

Figure 44. **Comparative of the antiproliferative effects among MEFwt, MEF Mfn2$^{-/-}$ and MEF Mfn1$^{-/-}$ cells incubated with leflunomide.** Data represents mean ± SEM expressed relative to the control (Ct) group. Three independent assays were performed per triplicate (n = 3). Ct, control; Lef, leflunomide; U, uridine.

No significative changes were observed among MEFwt, MEF Mfn2$^{-/-}$ and MEF Mfn1$^{-/-}$ cells in the recovery of the antiproliferative effects by uridine.

9. Leflunomide affects mitochondrial function in MEFwt, MEF Mfn2$^{-/-}$ and MEF Mfn1$^{-/-}$ cells

Leflunomide modulates mitochondrial proteins involved in mitochondrial dynamics promoting mitochondrial elongation and affects mitochondrial function in C2C12. To test if mitochondrial function depends of Mfn2 or Mfn1 expression the mitochondrial membrane potential and the oxygen consumption was measured in MEFwt, MEF Mfn2$^{-/-}$ and MEF Mfn1$^{-/-}$ cells.

9.1. Mitochondrial membrane potential in MEFwt, MEF Mfn2$^{-/-}$ and MEF Mfn1$^{-/-}$ cells

MEFwt, MEF Mfn2$^{-/-}$ and MEF Mfn1$^{-/-}$ cells were seeded in a 6-well plate (90,000 cells/well) and the next day the cells were incubated with leflunomide at 50 µM for 48 h. Then, the treatment with CCCP and TMRM (See section 8.2 in materials and methods) to measure mitochondrial membrane potential was performed and evaluated by flow cytometry (Figure 45).

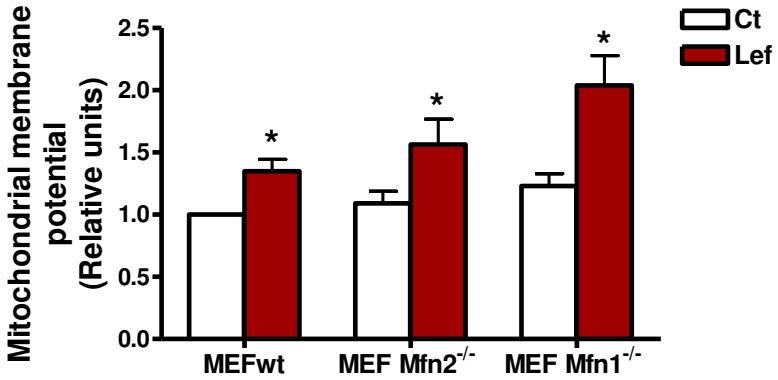

Figure 45. **Leflunomide increases mitochondrial membrane potential in MEFwt, MEF Mfn2$^{-/-}$ and MEF Mfn1$^{-/-}$ cells.** Cells were incubated with leflunomide at 50 µM for 48 h. Then, the cells were stained with tetramethylrhodamine methyl ester (TMRM), which accumulates in mitochondria in a potential-dependent manner and emits fluorescence at 573 nm when it is excited at 540 nm. TMRM positive cells can be quantified using flow cytometry. Data represents mean ± SEM expressed relative to the control (Ct) group. *P < 0.05 vs Ct. Three independent assays were performed per triplicate in each cell line (n = 3).

Leflunomide increased the mitochondrial membrane potential in MEFwt cells, MEF Mfn2$^{-/-}$ and MEF Mfn1$^{-/-}$ cells.

9.2. Oxygen consumption in MEFwt, MEF Mfn2$^{-/-}$ and MEF Mfn1$^{-/-}$ cells

MEFs cells were plated in SeaHorse Bioscience XF24 plates and the next day the cells were incubated with leflunomide at 50 µM for 48 h. Then, plates were immediately placed into the calibrated Seahorse Bioscience XF24 extracellular flux analyzer to measure oxygen consumption (Figure 46).

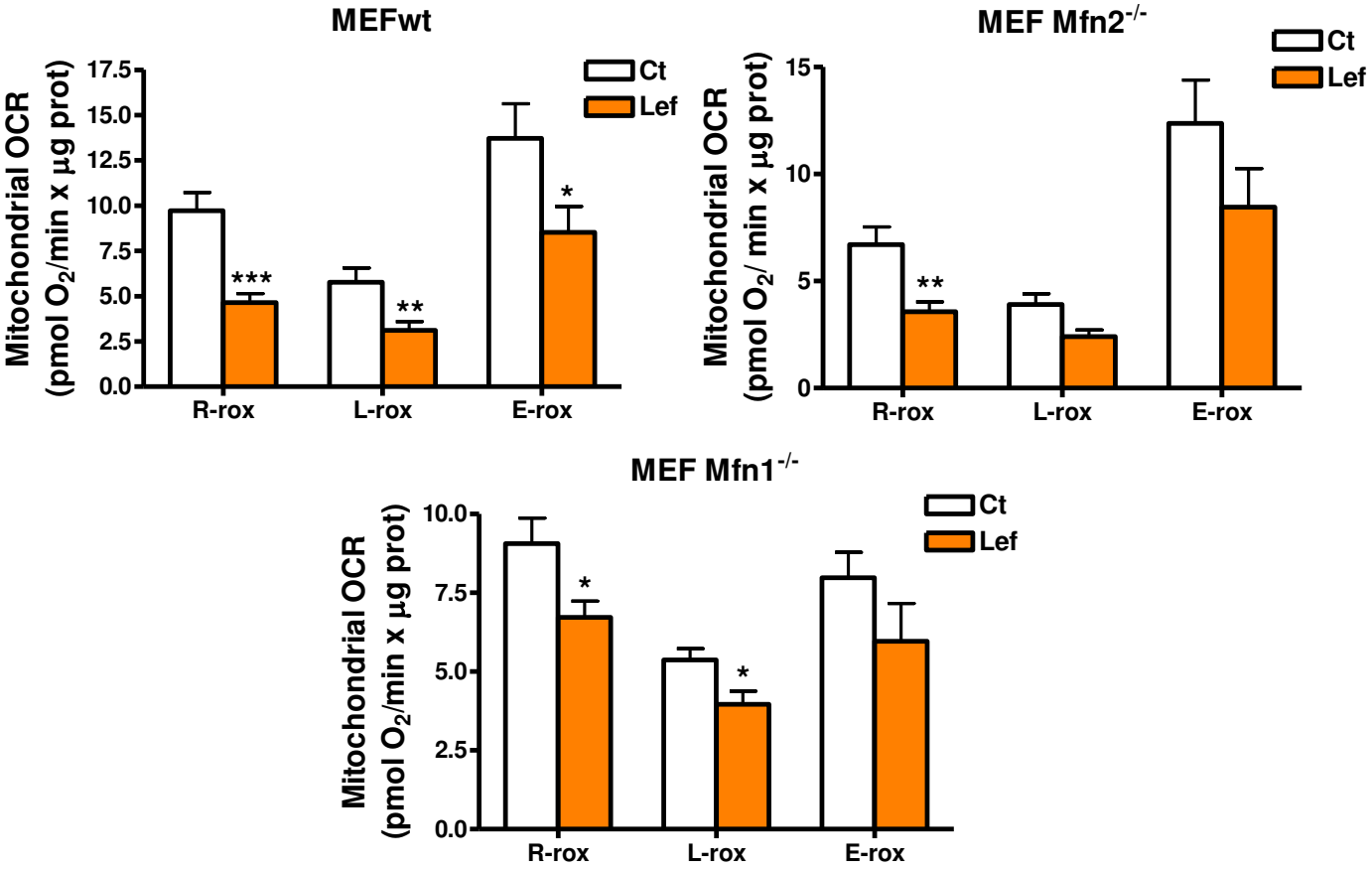

Figure 46. **Mitochondrial oxygen consumption (OCR) was measured in MEFwt, MEF Mfn1$^{-/-}$ and MEF Mfn2$^{-/-}$ cells treated with leflunomide.** The following parameters were measured: oxygen consumption under routine conditions (DMEM with 5.5mM glucose), respiratory leak measured after inhibition of ATP synthase with oligomycin, and maximal respiratory capacity reached after uncoupling with FCCP. Data are mean ± SEM. *P < 0.05 vs Ct, **P < 0.01 vs Ct, ***P < 0.001 vs Ct. Four independent assays were performed per triplicate in each cell line (n = 4).

The oxygen consumption rates (OCRs) are expressed as mitochondrial oxygen consumption rates subtracting the oxygen consumption rate of the rox state to the other states (See section 8.1 in materials and methods).

MEFwt, MEF Mfn1$^{-/-}$ and MEF Mfn2$^{-/-}$ cells treated with leflunomide showed less oxygen consumption in routine state, in leak state, when ATP synthase is inhibited by oligomycin, and in maximal uncoupled respiration, when the respiratory chain is decoupled from the synthesis of ATP by FCCP addition. Our data indicate that mitochondrial respiration was repressed in response to leflunomide. Moreover, MEFs cells treated with leflunomide showed more repression in mitochondrial respiration than C2C12 cells treated with

leflunomide. It is of interest to note that the maximal uncoupled respiratory capacity in MEF Mfn1$^{-/-}$ cells is reduced compared to MEFwt and MEF Mfn2$^{-/-}$ cells.

Two control ratios, the Respiratory Control Ratio (RCR = E/L) that measures the coupling between ETC and oxidative phosphorylation, and the Phosphorylation Respiratory Control Ratio (RCR_p = (R-L)/E) that indicates the percentage of maximum respiratory capacity used for the cells linked to ATP synthesis, were calculated from the OCRs values (Figure 47).

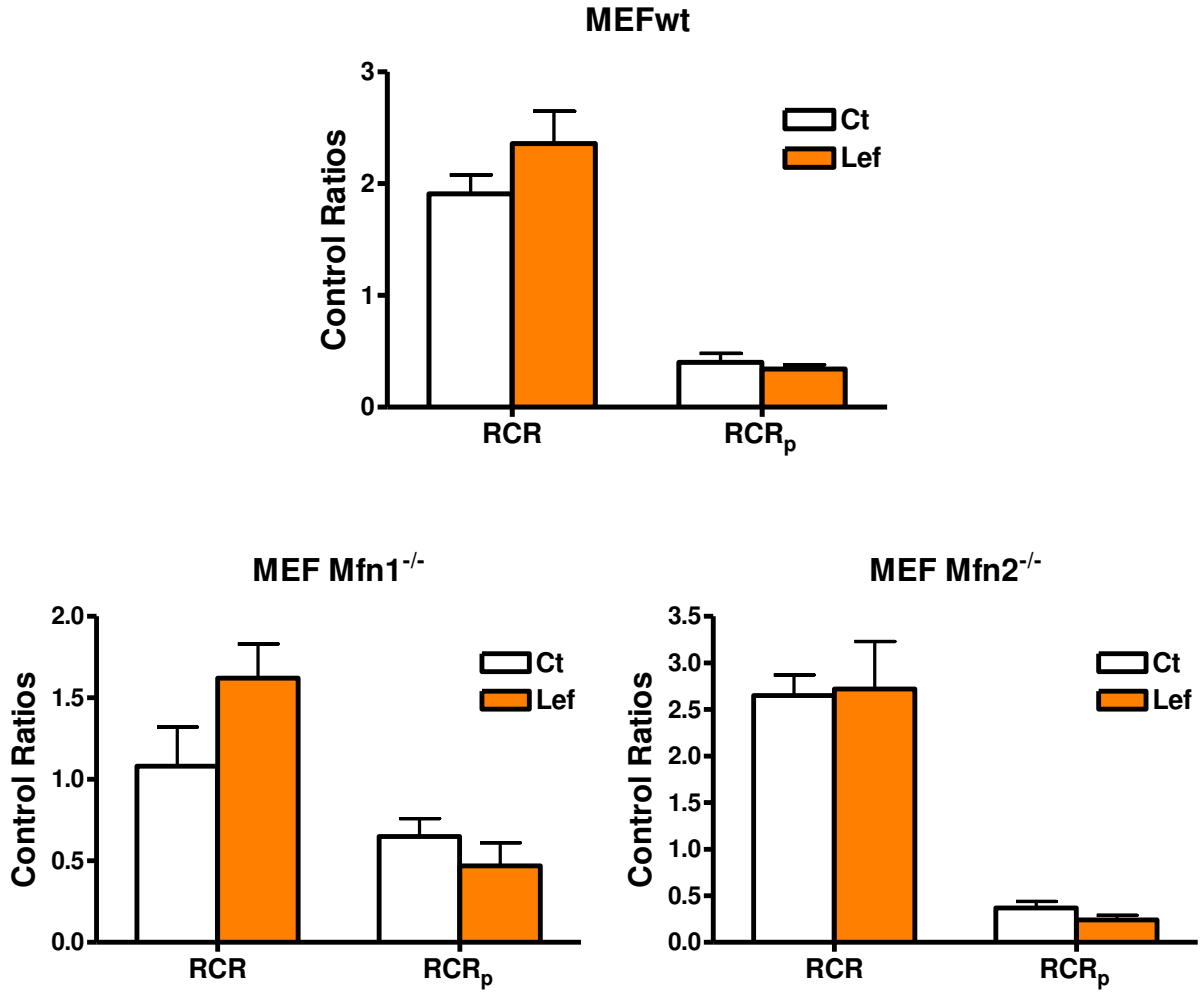

Figure 47. **Control ratios in MEFwt, MEF Mfn1$^{-/-}$ and MEF Mfn2$^{-/-}$ treated with leflunomide.** The following parameters were measured: Respiratory Control Ratio (E/L) and Phosphorylation Respiratory Control Ratio ((R-L)/E). Data are mean ± SEM. Three independent assays were performed per triplicate in each cell line (n = 3).

RCR in MEFwt and MEF Mfn1$^{-/-}$ cells treated with leflunomide showed a tendency to increase compared to control ones, indicating that there is more coupling between ETC and oxidative phosphorylation. No differences were observed for MEF Mfn2$^{-/-}$ cells. RCR_p in MEFs cells treated with leflunomide showed a tendency to reduce compared to control ones, indicating that these cells have less maximum respiratory capacity linked to ATP synthesis.

Leflunomide modulates mitochondrial proteins related in mitochondrial dynamics, morphology, and mitochondrial function in MEFwt, MEF Mfn2$^{-/-}$ and MEF Mfn1$^{-/-}$ cells. Leflunomide promotes mitochondrial elongation, increases mitochondrial membrane potential and represses mitochondrial respiration.

10. Specific inhibitors of complex III inhibit pyrimidine synthesis and increase Mfn2 expression

Dihydroorotate dehydrogenase (DHODH) catalyses the fourth reaction of the *de novo* biosynthesis of pyrimidines. DHODH is an enzyme located in the inner mitochondrial membrane and catalyses oxidation of dihydroorotate into orotate using ubiquinone as co-substrate electron acceptor. Ubiquinone is converted to ubiquinol, which is a substrate for Complex III in the respiratory chain. Thus, the *de novo* synthesis of pyrimidine nucleotides is coupled to the mitochondrial respiratory chain (RC) via DHODH (Figure 48).

In the present thesis it has been demonstrated that leflunomide produces an anti-proliferative activity inhibiting the *de novo* synthesis of pyrimidines (see section 5), and consequently mitochondrial proteins are modulated promoting mitochondrial elongation. Our hypothesis is that respiratory chain dysfunction through complex III, indirectly would inhibit the DHODH enzyme, and would impair pyrimidine synthesis. This alteration would modulate mitochondrial proteins involved in fusion and fission events and would promote mitochondrial elongation.

To test this hypothesis two specific inhibitors of complex III, myxothiazol and antimycin A, which indirectly inhibit DHODH and consequently the synthesis of pyrimidines, were studied.

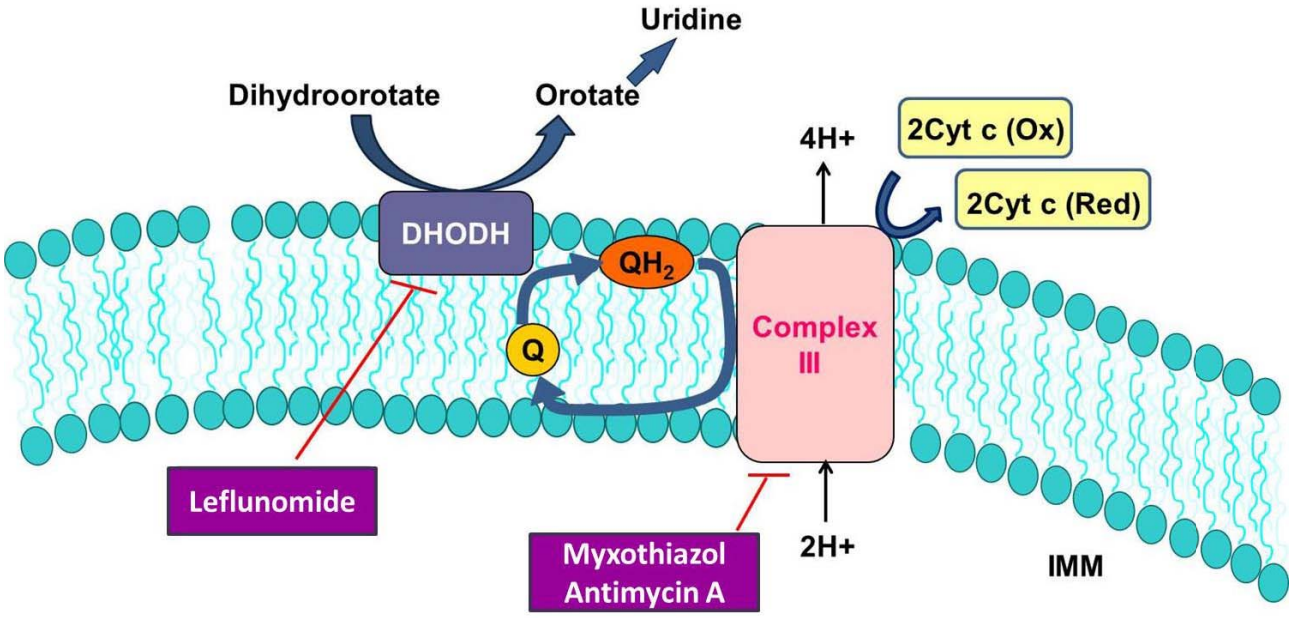

Figure 48. **The *de novo* synthesis of pyrimidine nucleotides is coupled to the mitochondrial respiratory chain (RC) via DHODH.**

10.1. Dose Response and time course study on the effects of myxothiazol and antimycin A

A two dose response study performed at three different times for myxothiazol was used to determine the concentration and the incubation time producing a maximum effect to increase Mfn2 gene expression. HeLa cells that endogenously express Mfn2 were incubated with myxothiazol at 2 and 10 µM for 8, 24 and 48 h and Mfn2 mRNA levels were measured by qPCR (Figure 49).

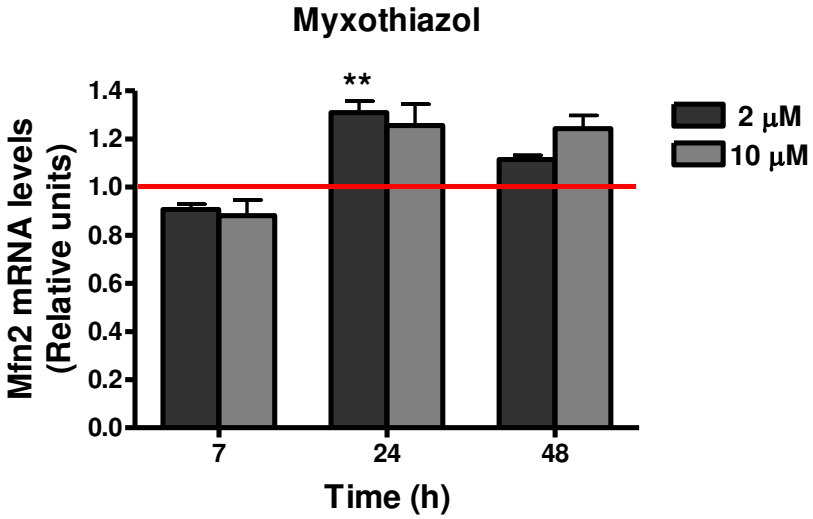

Figure 49. **Dose response and time course for myxothiazol.** Mfn2 mRNA levels in HeLa cells incubated with myxothiazol at two different concentrations for 8, 24 and 48 h were measured by qPCR. The housekeeping gene used was GAPDH. Both dyes, Mfn2 and GAPDH, were SYBR. Data represents mean ± SEM expressed relative to control (Ct) group of one representative experiment. Two independent assays were performed per triplicate (n = 2).

The assay showed that myxothiazol at 2µM for 24 h provided the maximum effect to activate Mfn2 mRNA levels in 1.3 fold increase. Thus, myxothiazol was always incubated at 2 µM for 24 h for further experiments.

Initially, HeLa cells were incubated with antimycin A at 10 and 50 µM for 48 h. However, HeLa cells incubated with antimycin A at 50 µM for 48 h showed cytotoxic effects. Thus, this concentration was discarded for further experiments. Next, a time course study was performed with antimycin A at 10 µM to determine the incubation time producing the maximum effect to increase Mfn2 gene expression. HeLa cells that endogenously express Mfn2 were incubated with antimycin A at 10 µM for 8, 24 and 48 h and Mfn2 mRNA levels were measured by qPCR (Figure 50).

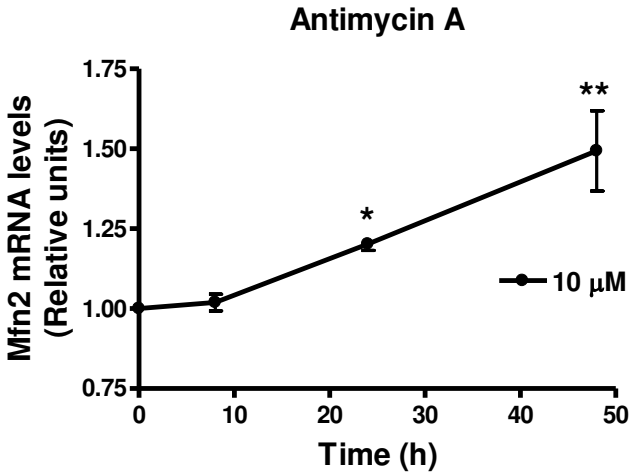

Figure 50. **Time course of antimycin A in HeLa cells.** Mfn2 mRNA levels in HeLa cells incubated with antimycin A at 10 μM at three incubations times were measured by qPCR. The housekeeping gene used was GAPDH. Both dyes, Mfn2 and GAPDH, were SYBR. Data represents the mean ± SEM expressed relative to the control group. *P < 0.05 vs Ct, **P < 0.01 vs Ct. Three independents assays were performed per triplicate (n = 3).

The best conditions were using antimycin A at 10 μM for 48 h, which produced a 1.5-fold increase in Mfn2 mRNA levels. However, HeLa cells showed toxicity problems. On the basis of these results, we decided to incubate HeLa cells with antimycin A at 10 μM for 24 h for further experiments. These conditions afforded a 1.2 fold increase in Mfn2 mRNA levels.

Therefore, inhibitors of complex III, that also impair pyrimidine synthesis by indirect inhibition of DHODH, also produced an increase in Mfn2 gene expression in HeLa cells.

10.2. Validation of myxothiazol and antimycin A in HeLa cells

HeLa cells were incubated with myxothiazol (2 μM) and antimycin A (10 μM) for 24 h and Mfn2 mRNA and protein levels were measured and quantified by qPCR and western blot, respectively (Figure 51).

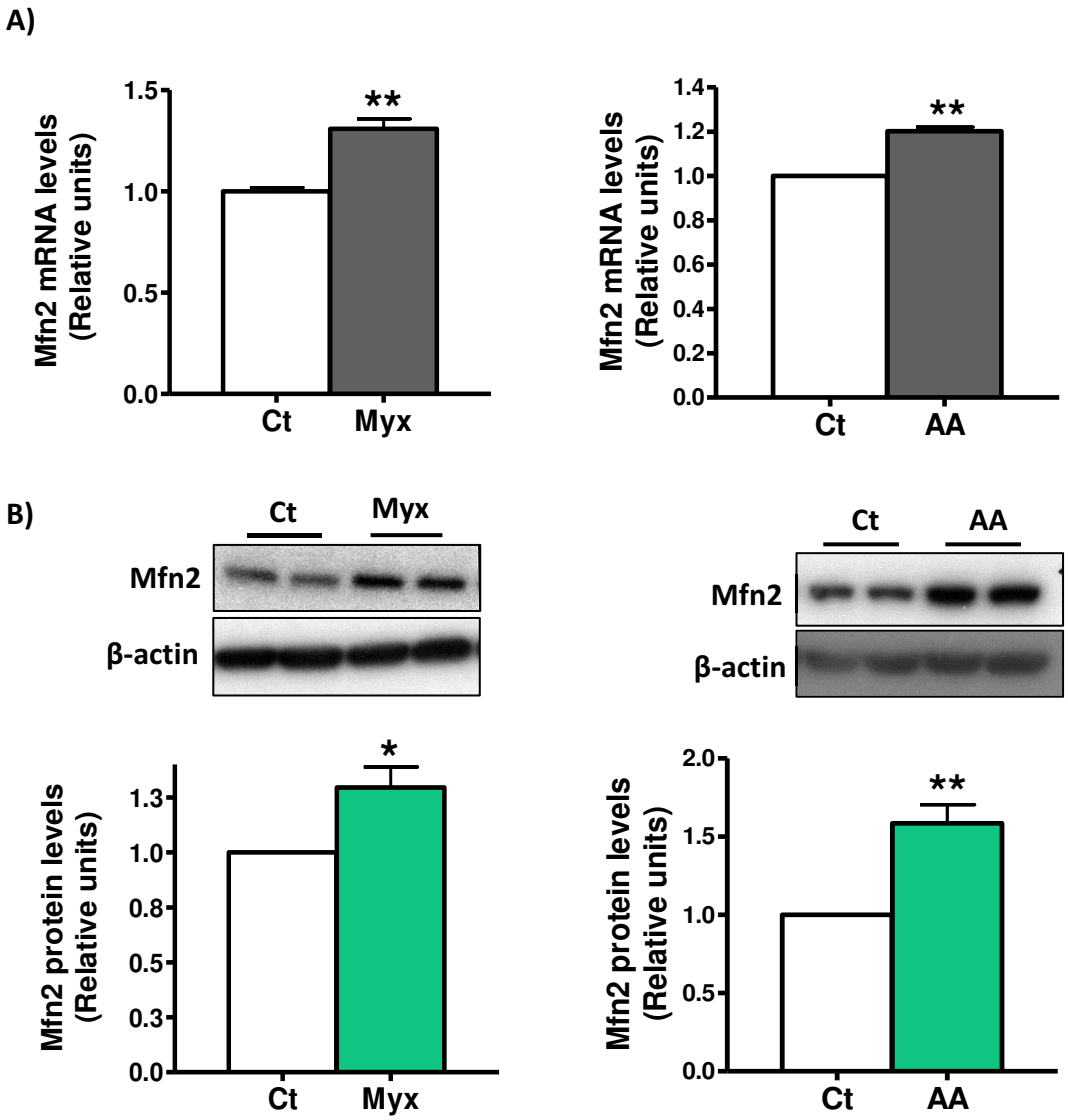

Figure 51. **Myxothiazol and antimycin A increase Mfn2 expression.** Mfn2 mRNA levels (A) and Mfn2 and β-actin protein levels (B) in HeLa cells incubated with myxothiazol (2 µM) and antimycin A (10 µM) for 24 h were quantified by qPCR and analysed by western blot, respectively. Data represent the mean ± SEM expressed relative to the control (Ct) group. *P < 0.05 vs Ct, **P < 0.01 vs Ct. Ct, control; Myx, myxothiazol; AA, antimycin A. (A) The housekeeping gene used was GAPDH. Both dyes, Mfn2 and GAPDH, were SYBR. Two independents assays were performed per triplicate for myxothiazol (n = 2) and three independents assays were performed per triplicate for antimycin A (n = 3). B) Seven independent assays were performed per triplicate for myxothiazol (n = 7) and six were performed per triplicate for antimycin A (n = 6).

Myxothiazol showed 1.3-fold increase in Mfn2 mRNA and protein levels. Antimycin A showed a 1.2-fold increase in Mfn2 mRNA levels and 1.6-fold increase in Mfn2 protein levels. Myxothiazol and antimycin A were validated as activators of Mfn2 expression in HeLa cells.

10.3 Assays of cell proliferation in C2C12 cells

To assess the overall cellular effect of antimycin A and myxothiazol on cell viability, the cells during treatment with both compounds were visualized by optical microscope. C2C12 cells were seeded in 12-well plate (45,000 cells/well), and the next days the cells were incubated with myxothiazol and antimycin A at 2 µM and 10 µM, respectively, for 12, 24 and 48 h (Figure 52).

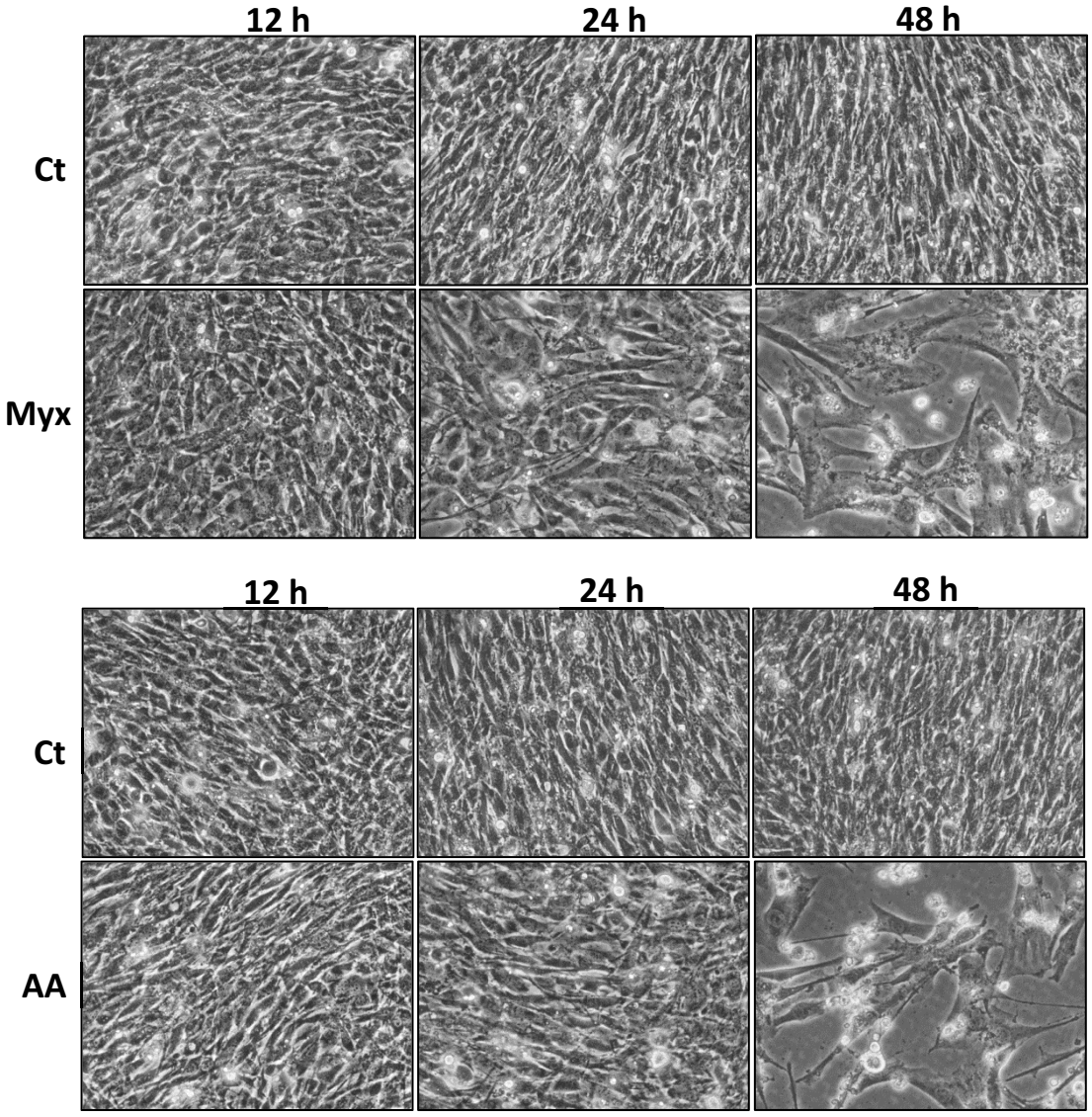

Figure 52. **Antiproliferative effect of C2C12 cells incubated with antimycin A and myxothiazol at 12, 24 and 48 h were visualized by optical microscope.** Ct, control; AA, antimycin A; Myx, myxothiazol.

Myxothiazol and antimycin A showed antiproliferative effects at 24 h, and the effects increased up to 48 h in C2C12 cells. On the basis of these results, we conclude that antimycin A and myxothiazol, specific inhibitors of complex III and indirect inhibitors of DHODH enzyme, impair the *de novo* synthesis of pyrimidines and have antiproliferative effects as leflunomide.

10.4. External uridine reverses Mfn2 mRNA levels in HeLa cells incubated with specific inhibitors of complex III

The results obtained in section 5 confirmed that leflunomide and teriflunomide increase Mfn2 mRNA levels by depleting the *de novo* synthesis of pyrimidines. Addition of external uridine reversed Mfn2 mRNA up-regulation. To be sure that Mfn2 mRNA increase caused by myxothiazol and antimycin A is also due to the inhibition of pyrimidine synthesis, external uridine was added. A reverse effect was expected for the increased levels of Mfn2 mRNA.

HeLa cells were incubated with myxothiazol (2µM) and antimycin A (10 µM) ± uridine at 50 µM for 24 h and Mfn2 mRNA levels were measured by qPCR (Figure 53).

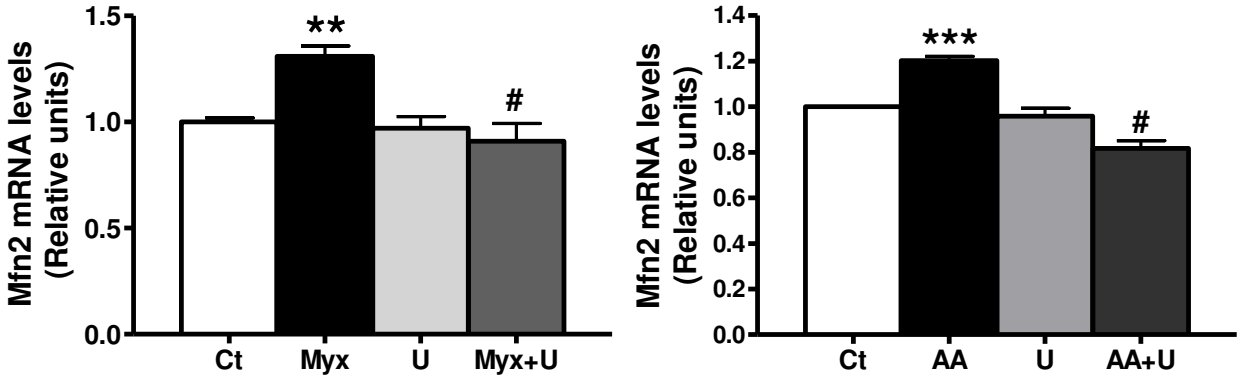

Figure 53. **External uridine reverses the increase of Mfn2 mRNA levels induced by myxothiazol and antimycin A.** Mfn2 mRNA levels in HeLa cells incubated with myxothiazol (2 µM) and antimycin A (10 µM) ± uridine(50 µM) for 24 h were measured by qPCR. The housekeeping gene used was GAPDH. Mfn2 and GAPDH dyes were SYBR. Data represents mean ± SEM expressed relative to control group. **P < 0.01 vs Ct; ***P < 0.001 vs Ct, #P < 0.05 vs Lef. Ct, control; Myx, myxothiazol; AA, antimycin A; U, uridine. One representative experiment was showed for myxothiazol, and two independent assays were performed per triplicate (n = 2). Three independent assays were performed for antimycin A per triplicate (n = 3).

The addition of external uridine, which reverses the deficiency in pyrimidine biosynthesis, reversed the increase in Mfn2 gene expression induced by myxothiazol and antimycin A. These results agreed with the results from section 5 confirming that Mfn2 up-regulation is triggered by the deficiency in pyrimidines.

10.5. Myxothiazol and antimycin A effects in Mfn1, Opa1, and Drp1 mRNA in HeLa cells

In order to elucidate the capacity of myxothiazol and antimycin A to displace the balance between mitochondrial fusion and fission events, Mfn1, Opa1 and Drp1 mRNA levels were measured by qPCR in HeLa cells incubated with myxothiazol (2 µM) and antimycin A (10 µM) ± uridine at 50 µM for 24 h (Figure 54 and 55).

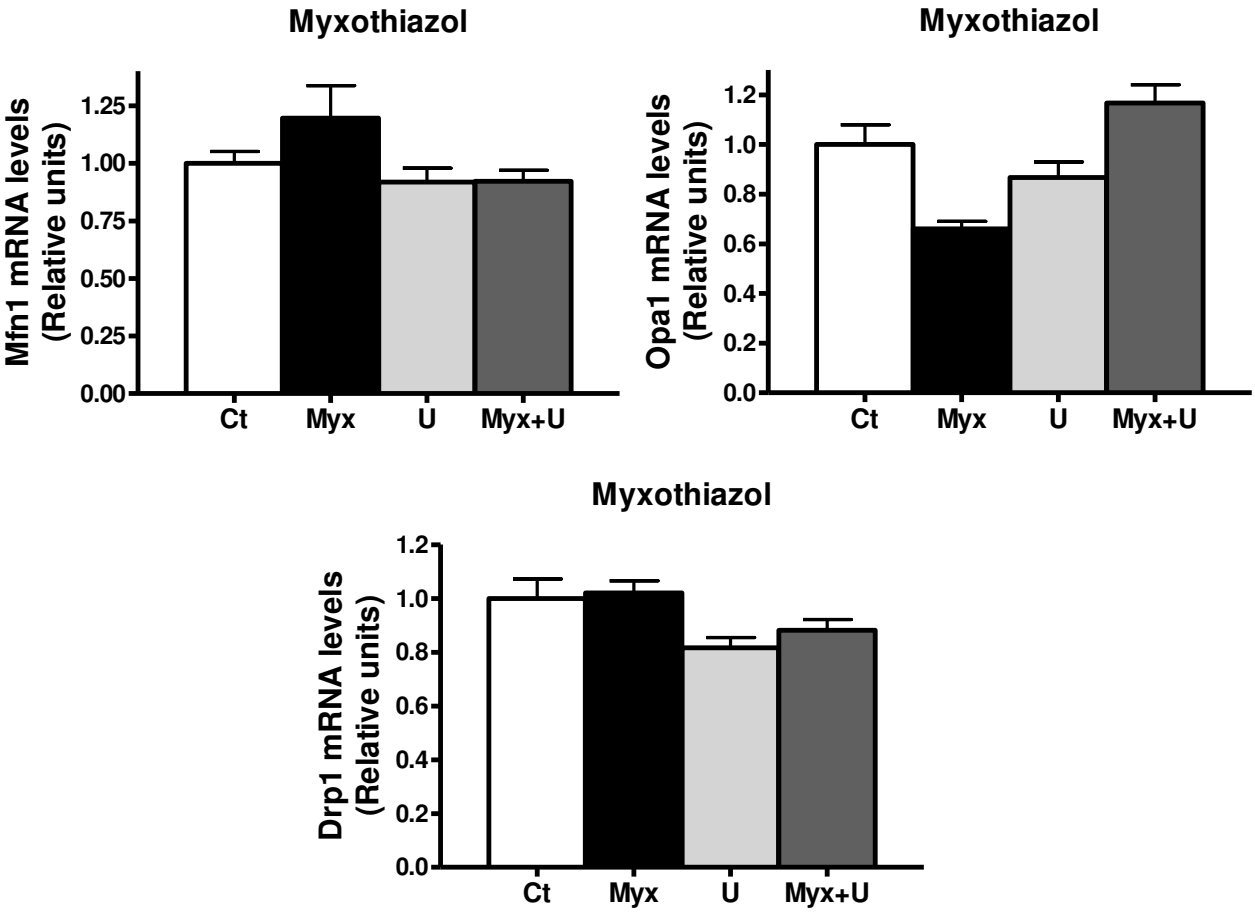

Figure 54. **Mfn1, Opa1, and Drp1 mRNA levels in HeLa cells incubated with myxothiazol.** Mfn1, Opa1, and Drp1 mRNA levels in HeLa cells incubated with myxothiazol (2 µM) ± uridine(50 µM) for 24 h were measured by qPCR. The housekeeping gene used was GAPDH (SYBR). Mfn1, Drp1, and Opa1 probes were TaqMan. Data represents mean ± SEM expressed relative to control group of one representative experiment. Ct, control; Myx, myxothiazol; U, uridine. Two independent assays were performed per triplicate (n = 2).

Myxothiazol showed a tendency to increase Mfn1 and reduce Opa1 gene expression. The addition of external uridine was able to reverse the up and down-regulation of Mfn1 and Opa1, respectively. No changes were observed for Drp1 mRNA levels.

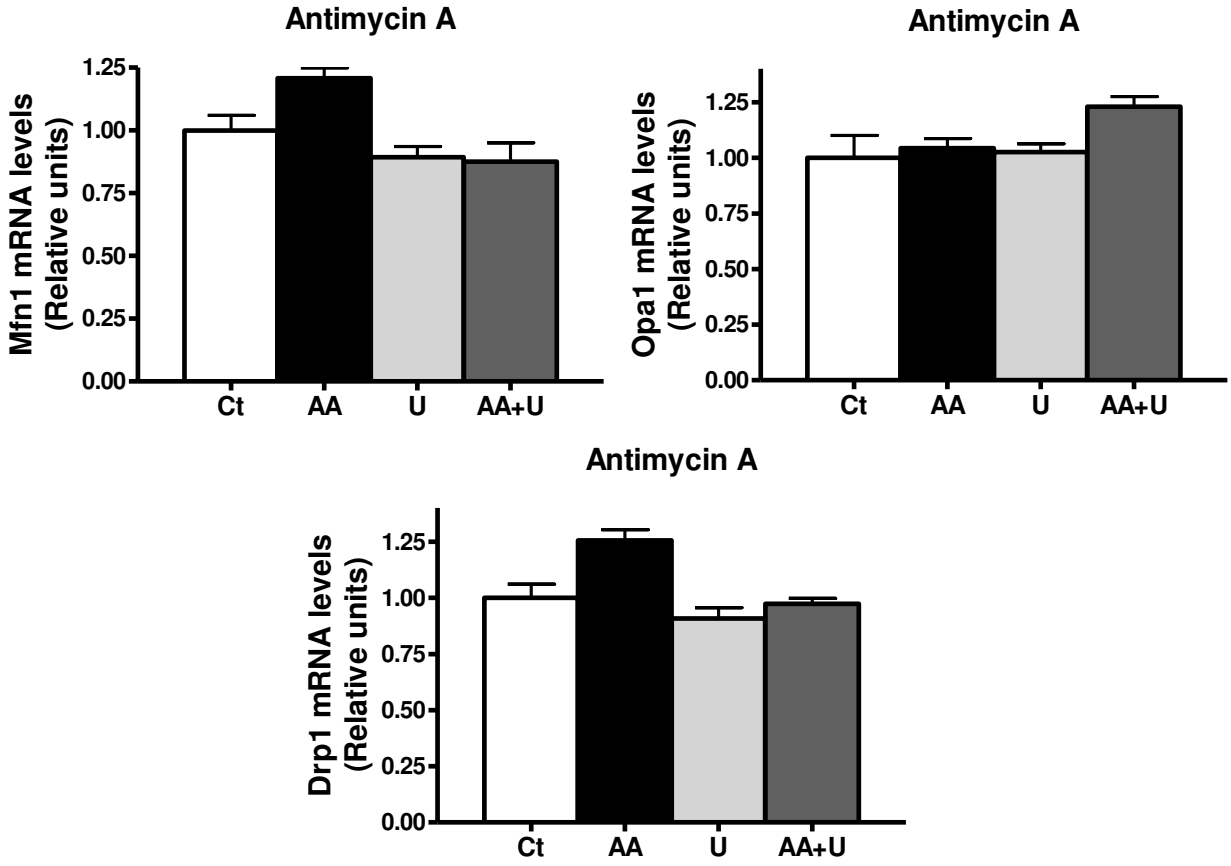

Figure 55. **Mfn1, Opa1, and Drp1 mRNA levels in HeLa cells incubated with antimycin A.** Mfn1, Drp1 and Opa1 mRNA levels in HeLa cells incubated with antimycin A (10 µM) ± uridine(50 µM) for 24 h were measured by qPCR. The housekeeping gene used was GAPDH (SYBR). Mfn1, Drp1 and Opa1 probes were TaqMan. Data represents mean ± SEM expressed relative to control group of one representative experiment. Ct, control; AA, antimycin A; U, uridine. Two independent assays were performed per triplicate (n = 2).

Antimycin A showed a tendency to increase Mfn1 and Drp1 gene expression, and addition of external uridine was able to reverse the increase of Mfn1 and Drp1 mRNA levels. No changes were observed for Opa1 mRNA levels.

10.6. Myxothiazol and antimycin A effects in Mfn1, Opa1, Drp1 and porin proteins in HeLa cells

We have demonstrated that indirect inhibitors of DHODH are able to increase Mfn2 mRNA and protein levels in HeLa cells, and it seems that there is also a tendency to increase Mfn1 gene expression. Thus, the next step was to analyze the levels of mitochondrial proteins related in mitochondrial dynamics as Mfn1, Opa1, Drp1 and porin. HeLa cells were incubated with myxothiazol (2 µM) and antimycin A (10 µM) for 24 h and mitochondrial proteins were analysed by western blot (Figure 56).

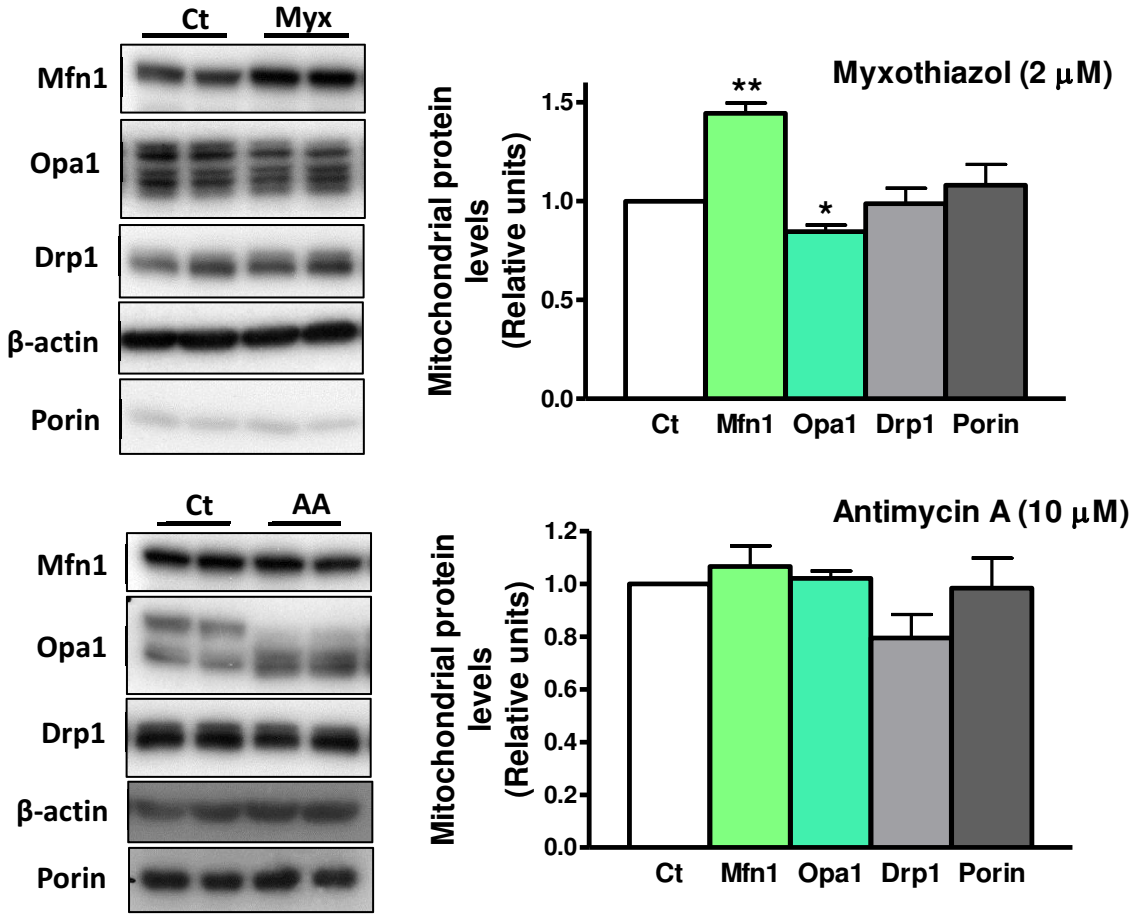

Figure 56. **Mitochondrial protein levels in HeLa cells incubated with myxothiazol and antimycin A.** Mfn1, Opa1, Drp1, β-actin and porin protein levels in HeLa cells incubated with myxothiazol at 2 μM (A) and antimycin A at 10 μM (B) for 24 h were analysed by western blot. Data represent the mean ± SEM expressed relative to the control (Ct) group. *P < 0.05, **P < 0.01. Five independent assays were performed per duplicate for myxothiazol and antimycin A (n = 5).

Myxothiazol up-regulated Mfn1 expression in 1.5-fold increase and down-regulated Opa1 expression in HeLa cells. No changes were observed for Drp1 and porin. The changes in mitochondrial proteins were not a consequence of an increase in total mass of mitochondria because porin did not change. These results suggest that myxothiazol should promote mitochondrial elongation increasing Mfn2 and Mfn1 expression.

Antimycin A did not modulate any mitochondrial protein levels. However, antimycin A was able to modulate the bands of Opa1. It has been described that Opa1 is localized in the mitochondrial intermembrane space, where it facilitates fusion between mitochondria. Human Opa1 exists as eight transcript variants encoding different isoforms. The long L-isoforms activate mitochondrial fusion by interacting with Mfns; the short S-isoforms arrest fusion and generate mitochondrial fragments[17-19]. Apoptosis causes Opa1 release into the cytosol, the long (L) isoforms are proteolytically processed to the short (S) isoforms and mitochondria are fragmented[19].

Western blot analyses showed that antimycin A treatment decreased the size of Opa1 bands, whereas no detectable changes were observed in the Mfn1, Drp1 and porin bands. Antimycin A treatment of cells caused L-isoforms bands to converge into the S-isoforms bands suggesting that mitochondria should be fragmented.

10.7. Mitochondrial morphology in HeLa cells

In order to elucidate the mitochondrial network in HeLa cells, HeLa cells stably expressing mtDsRed were seeded on coverslips in 6-well plate, and the next day were incubated with myxothiazol (2 µM) and antimycin A (10 µM) for 24 h. HeLa cells were fixed and visualized at the spectral confocal microscopy (Figure 57).

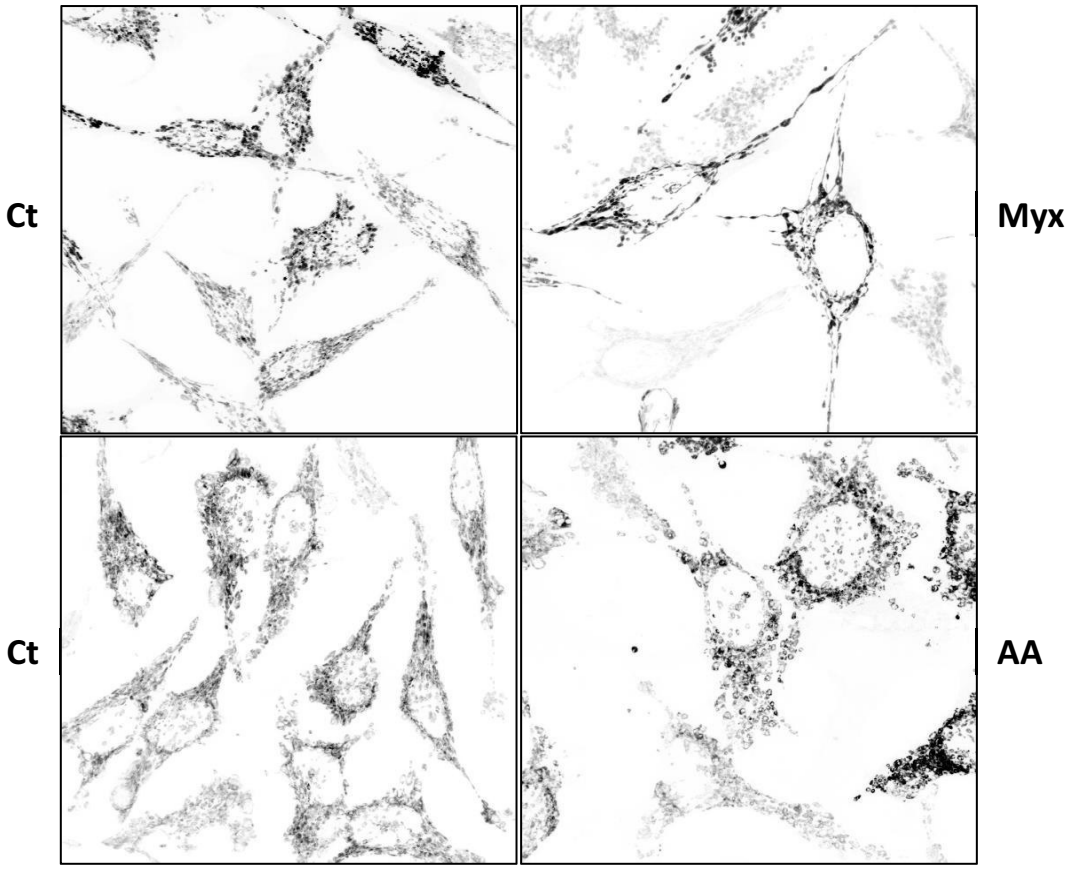

Figure 57. **Representative confocal images of mitochondrial morphology in mtDsRed expressing HeLa cells incubated with myxothiazol and antimycin A.**

HeLa cells incubated with myxothiazol showed an elongated mitochondrial network compared to the control cells demonstrating that myxothiazol by increasing Mfn2 and Mfn1 protein levels is able to promote the elongation of mitochondria. In contrast, antimycin A caused mitochondrial fragmentation. This result suggests that antimycin A accelerates the proteolytic processing of Opa1 L-isoforms to S-isoforms (See section 10.6), and mitochondrial fragmentation is triggered by Opa1 inactivation. We decided to discard the compound antimycin A and only myxothiazol was used for further experiments.

10.8. Myxothiazol effects in Mfn2, Mfn1, Opa1, Drp1 and Fis1 proteins in C2C12 cells

The effect of myxothiazol was analysed in mouse cell lines (C2C12). The cells were seeded in a 6-well plate (200,000 cells/well) and the next day the cells were incubated with myxothiazol at 2 µM for 12 and 24 h. Mfn2 protein levels were analysed by western blot (Figure 58).

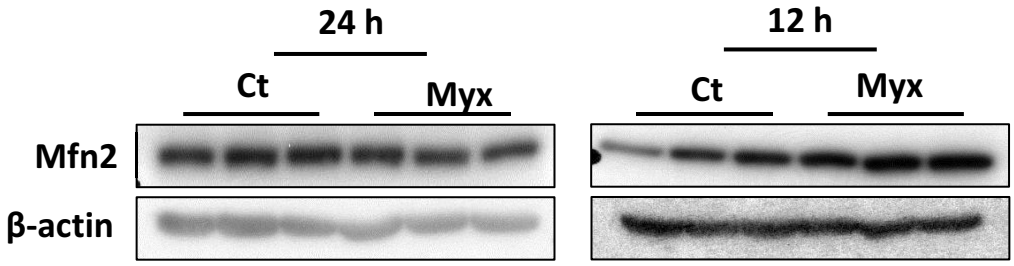

Figure 58. **Mfn2 protein levels in C2C12 cells incubated with myxothiazol.** C2C12 cells were incubated with myxothiazol at 2 µM for 12 and 24 h, and Mfn2 and β-actin protein levels in total lysates from C2C12 cells were analysed by western blot. Two independent assays were performed per triplicate in C2C12 cells (n = 2).

Myxothiazol was not able to increase Mfn2 protein levels at 24 h. However, a notable increase in Mfn2 levels was observed when C2C12 were incubated with myxothiazol for 12 h.

Myxothiazol was validated in C2C12 at 2 µM for 12 h analysing Mfn2 protein levels by western blot (Figure 59).

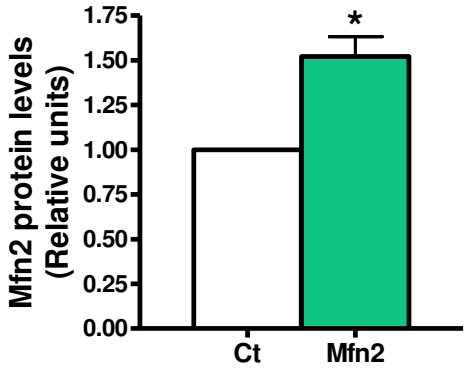

Figure 59. **Myxothiazol increases Mfn2 expression in C2C12 cells.** Mfn2 and β-actin protein levels in total lysates from C2C12 cells incubated with myxothiazol at 2 µM for 12 h were analysed by western blot. Data represent the mean ± SEM expressed relative to the control (Ct) group. *P < 0.05. Three independents assays were performed per triplicate (n = 3).

Myxothiazol produced a 1.5-fold increase in Mfn2 expression in C2C12 cells.

The next step was to measure mitochondrial proteins involved in fusion and fission events. C2C12 cells were incubated with myxothiazol at 2 µM for 12 h and Mfn1, Opa1, Drp1, and porin protein levels were analysed by western blot (Figure 60).

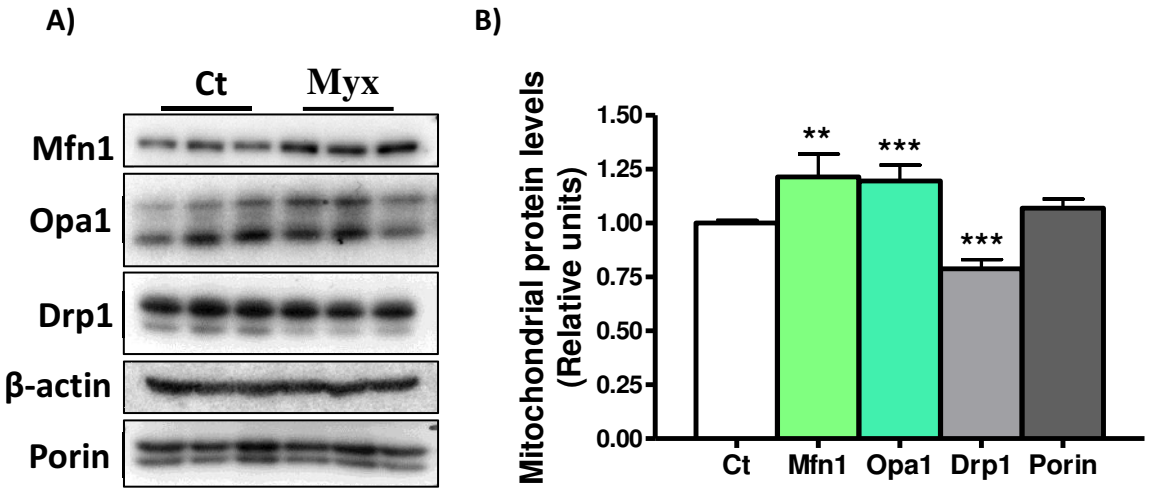

Figure 60. **Mitochondrial protein levels in C2C12 cells incubated with myxothiazol.** Mfn1, Opa1, Drp1, β-actin and porin protein levels in total lysates from C2C12 cells incubated with myxothiazol at 2 µM for 12 h were analysed by western blot (A). Quantification by densitometry was performed for mitochondrial proteins in C2C12 cells using β-actin as a control (B). Data represents mean ± SEM expressed relative to the control (Ct) group of one representative experiment. **P < 0.01, ***P < 0.001. Two independent assays were performed per triplicate in C2C12 cells (n = 2).

Myxothiazol also produced a 1.2-fold increase in Mfn1 and Opa1 expression, and Drp1 expression was reduced by 10% in C2C12 cells. No changes were observed for porin levels. The changes in mitochondrial proteins are not a consequence of an increase in total mass of mitochondria because porin did not change.

These results suggest that myxothiazol, up-regulates Mfn2, Mfn1 and Opa1 fusion proteins and down-regulates Drp1 fission protein. This suggests a displacement of the balance between mitochondrial fusion and fission towards mitochondrial fusion promoting the elongation of mitochondria.

10.9. Mitochondrial morphology in C2C12 cells

In order to elucidate the mitochondrial network of C2C12 cells, C2C12 cells stably expressing mtDsRed were seeded on coverslips in 6-well plate, and the next day were incubated with myxothiazol (2 µM) for 12 h. C2C12 cells were fixed and visualized at the spectral confocal microscopy (Figure 61). Moreover, C2C12 cells treated with myxothiazol were recorded at the spinning disk confocal microscopy. The videos are in the supplementary information.

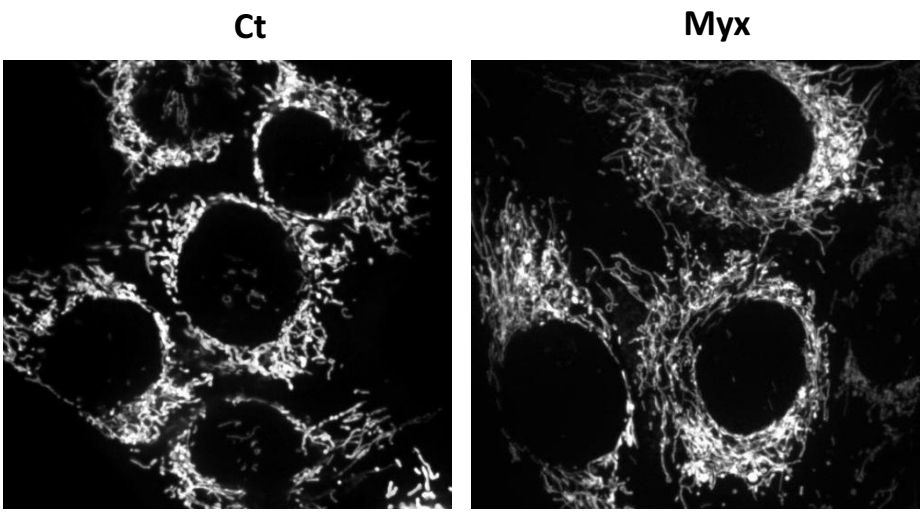

Figure 61. **Representative confocal images of mitochondrial morphology in mtDsRed expressing C2C12 myoblasts cells incubated with myxothiazol.**

C2C12 cells incubated with myxothiazol showed an elongated mitochondrial network compared to the control cells. These results demonstrate that myxothiazol by increasing Mfn2, Mfn1 and Opa1 protein levels, and decreasing Drp1 levels is able to promote the elongation of mitochondria.

10.10. Myxothiazol effects in MEFwt cells

The effect of myxothiazol was analysed in Mouse Embryonic Fibroblasts (MEF). MEFwt cells were seeded in a 6-well plate (90,000 cells/well) and the next day the cells were incubated with myxothiazol at 2 µM for 12 h. Opa1, Drp1 and β-actin protein levels were analysed by western blot (Figure 62).

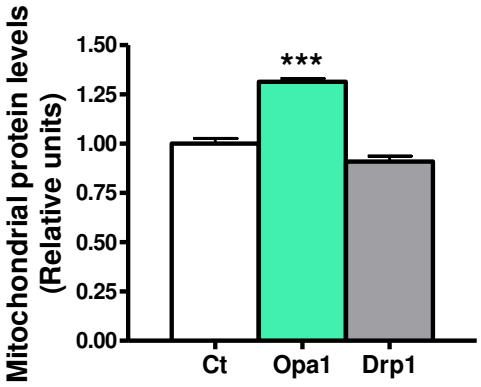

Figure 62. **Mitochondrial protein levels in MEFwt cells incubated with myxothiazol.** Opa1, Drp1 and β-actin protein levels in total lysates from MEFwt cells incubated with myxothiazol at 2 µM for 12 h were analysed by western blot. Quantification by densitometry was performed for mitochondrial proteins in MEFwt cells using β-actin as a control. Data represents mean ± SEM expressed relative to the control (Ct) group of one representative experiment. ***P < 0.001. One independent assay was performed per triplicate in MEFwt cells (n = 1).

Myxothiazol produced a 1.3-fold increase in Opa1 expression in MEFwt cells. We need to analyse the levels of mitochondrial proteins involved in fusion such as Mfn2 and Mfn1, and Drp1 fission protein.

10.11. Mitochondrial morphology in MEFwt cells

In order to elucidate the mitochondrial network of MEFwt cells, MEfwt cells stably expressing mtDsRed were seeded on coverslips in 6-well plate, and the next day were incubated with myxothiazol (2 μM) for 12 h. MEFwt cells were fixed and visualized at the spectral confocal microscopy (Figure 63). Moreover, MEFwt cells treated with myxothiazol were recorded at the spinning disk confocal microscopy. The videos are in the supplementary information.

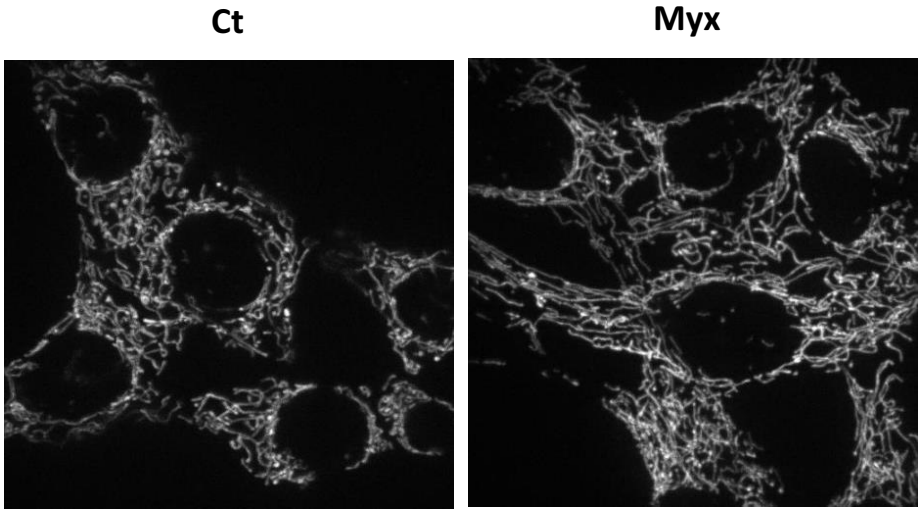

Figure 63. **Representative confocal images of mitochondrial morphology in mtDsRed expressing MEFwt cells incubated with myxothiazol.**

MEFwt cells incubated with myxothiazol showed an elongated mitochondrial network compared to the control cells, demonstrating that myxothiazol by increasing Opa1 protein levels and probably Mfn2 and Mfn1 protein levels is able to promote the elongation of mitochondria.

11. p53 activation is triggered by inhibition of pyrimidine synthesis in response to leflunomide

Linke et al.[20] described that ribonucleotide biosynthesis inhibitors, causing depletion of ribonucleotide pools, produced a p53 dependent arrest pathway. In normal fibroblasts the absence of replicative DNA synthesis results in a cell cycle arrest at the G1/S phase dependent of p53. They showed that CTP, GTP, or UTP depletion was sufficient to induce p53 arrest. Addition of external uridine, which restored nucleotides levels through salvage pathways, reversed p53 up-regulation. They suggested that p53 can maintain genetic stability by preventing DNA replication during metabolic depletion. Moreover, Khutornenko et al.[21] reported that strong p53 response is induced specifically after an inhibition of the mitochondrial cytochrome bc1 (the electron chain complex III) but not by the impairment of the ETC itself. The p53 response is triggered by the deficiency in pyrimidines that is developed through the uncoupling of complex III and inner mitochondrial membrane-bound DHODH enzyme. DHODH converts dihydroorotate to orotate using ubiquinone as a direct electron acceptor. Complex III and DHODH inhibitors, as myxothiazol and leflunomide respectively, up-regulate p53 by blocking directly or indirectly the DHODH step of pyrimidine biosynthesis.

Our hypothesis is that the depletion of pyrimidine pools, by complex III or DHODH inhibitors, would cause cell stress and trigger p53 response, which would modulate mitochondrial proteins involved in fusion and fission events and would promote mitochondrial elongation to overcome the induced stress (Figure 64).

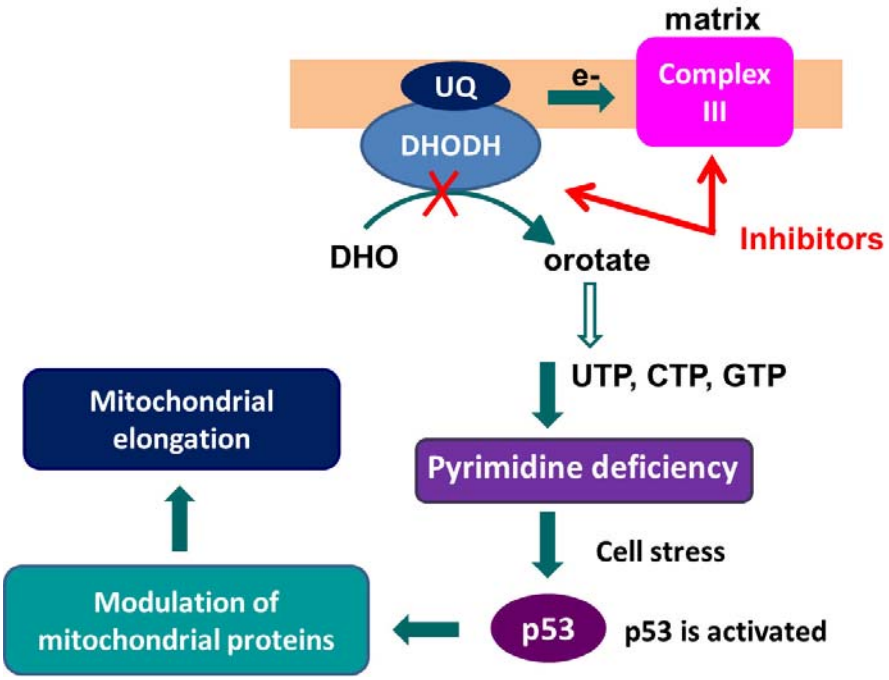

Figure 64. **Pyrimidine biosynthesis is linked to p53 pathway.**

To test these hypothesis the levels of p53 were analysed in HeLa, C2C12, MEFwt, MEF Mfn2$^{-/-}$ and MEF Mfn1$^{-/-}$ cells treated with DHODH or complex III inhibitors.

11.1. Leflunomide and Teriflunomide induce p53 expression

We have demonstrated that leflunomide and teriflunomide increase Mfn2 and Mfn1 mRNA and protein levels by inhibition of DHODH and consequently, the *de novo* synthesis of pyrimidines (See section 5 and 6). The addition of external uridine, which reverses the deficiency in pyrimidine biosynthesis, reversed the increase in Mfn2 and Mfn1 gene expression and the antiproliferative activity induced by leflunomide and teriflunomide. The next step was to measure p53 mRNA levels in HeLa, C2C12 and MEFs cells incubated with DHODH inhibitors.

11.1.1. Leflunomide and teriflunomide induce p53 expression in HeLa cells

First of all p53 mRNA and protein levels were measured in HeLa cells incubated with leflunomide and its active metabolite.

11.1.1.1. p53 mRNA levels of HeLa cells incubated with leflunomide and teriflunomide ± uridine

HeLa cells were incubated with leflunomide and teriflunomide at 50 µM ± uridine at 50 µM for 48 h and p53 mRNA levels were measured by qPCR (Figure 65).

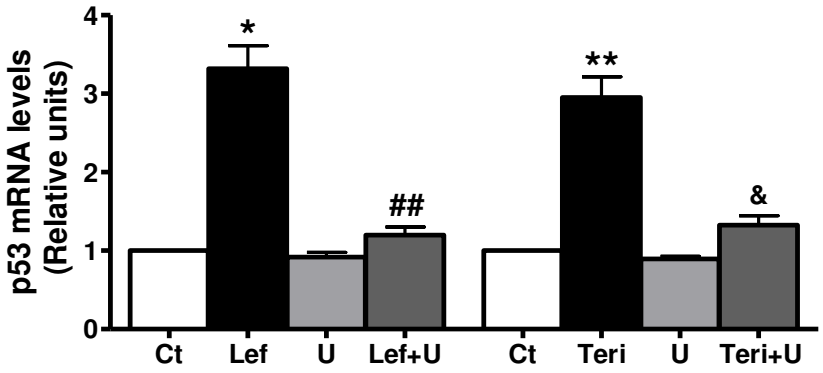

Figure 65. **Leflunomide and teriflunomide increase p53 mRNA levels and external uridine prevents p53 induction in HeLa cells.** p53 mRNA levels in HeLa cells incubated with leflunomide and teriflunomide at 50 µM ± uridine at 50 µM for 48 h were measured by qPCR. The housekeeping gene used was GAPDH. p53 and GAPDH dyes were SYBR. Data represents mean ± SEM expressed relative to control group. *P < 0.05 vs Ct, ##P < 0.01 vs Lef, &P < 0.05 vs Teri. Ct, control; Lef, leflunomide; Teri, teriflunomide; U, uridine. Four independent assays were performed per triplicate (n = 4).

Leflunomide and teriflunomide produced a 3.3- and 3-fold increase in p53 mRNA levels, respectively, and the addition of external uridine prevented p53 gene up-regulation.

Leflunomide and teriflunomide inhibited the DHODH enzyme and consequently the synthesis of pyrimidines, and induced p53 gene expression. External uridine, which reversed the deficiency in pyrimidine biosynthesis, was able to prevent p53 up-regulation.

11.1.1.2. p53 protein levels in HeLa cells incubated with leflunomide

The next step was to measure p53 protein levels to be sure that leflunomide was inducing p53 expression by depleting the synthesis of pyrimidines. HeLa cells were incubated with leflunomide at 50 µM for 48 h and p53 protein levels were analyzed by western blot (Figure 66).

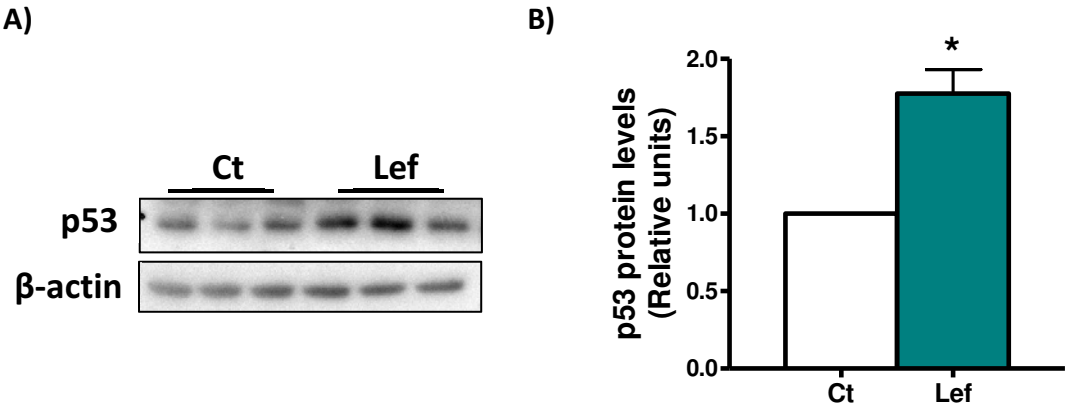

Figure 66. **Leflunomide increases p53 protein levels in HeLa cells.** The p53 and β-actin protein levels in total lysates from HeLa cells were analysed by western blot (A) and quantified by densitometry using β-actin as a control (B). Data represents mean ± SEM expressed relative to the control group. *P < 0.05 vs Ct. Ct, control; Lef, leflunomide. Four independent assays were performed per triplicate (n = 4).

Leflunomide produced a 1.8-fold increase in p53 protein levels. These results suggest that leflunomide produced the depletion of pyrimidine pools by inhibiting the DHODH enzyme and induced p53 accumulation in HeLa cells.

11.1.2. Leflunomide induces p53 expression in C2C12 cells

In order to elucidate the mechanism of action of leflunomide C2C12 cells were incubated with leflunomide at 50 µM ± uridine at 250 µM for 48 h and p53 proteins levels were analysed by western blot (Figure 67).

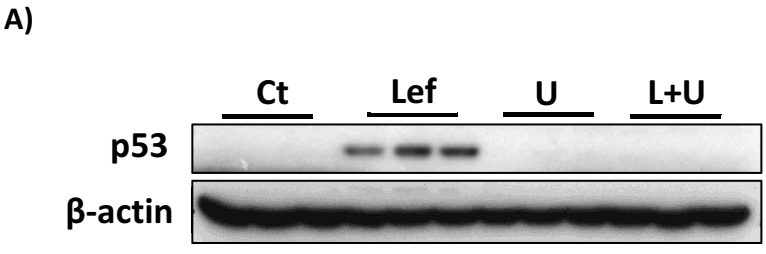

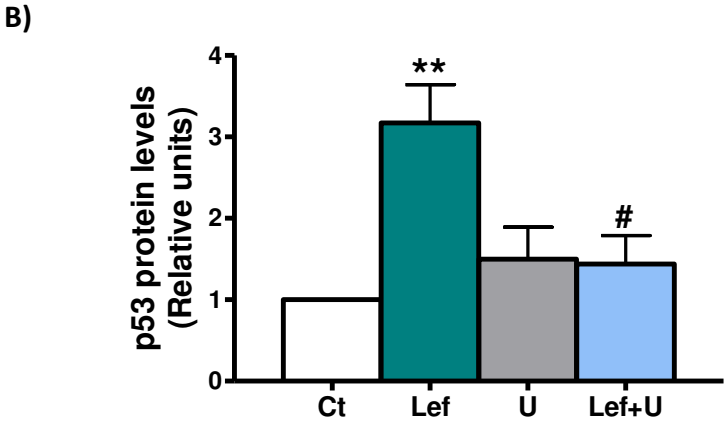

Figure 67. **Leflunomide increases p53 protein levels and external uridine prevents the p53 induction in C2C12 cells.** The p53 and β-actin protein levels in total lysates from C2C12 cells were analysed by western blot (A) and quantified by densitometry using β-actin as a control (B). Data represents mean ± SEM expressed relative to the control group. **P < 0.01 vs Ct, #P < 0.05 vs Lef. Ct, control; Lef, leflunomide: U, uridine. Five independent assays were performed per triplicate (n = 5).

Leflunomide induced p53 protein expression in 3.2-fold increase and supplementation with uridine prevented the p53 induction. These results indicate that leflunomide-induced activation of p53 is driven by the deficiency in pyrimidines.

Once we have showed that p53 increases in response to leflunomide in HeLa and C2C12 cells, the next step was to test whether this effect was conserved in MEFwt and MEFs deficient in Mfn1 (Mfn1$^{-/-}$) and Mfn2 (Mfn2$^{-/-}$) cells.

11.1.3. Leflunomide induces p53 expression in MEF wt, MEF Mfn2$^{-/-}$ and MEF Mfn1$^{-/-}$ cells

MEFwt and MEFs deficient in Mfn1 (Mfn1$^{-/-}$) and Mfn2 (Mfn2$^{-/-}$) cells were incubated with leflunomide at 50 µM ± uridine at 250 µM for 48 h (Figure 68).

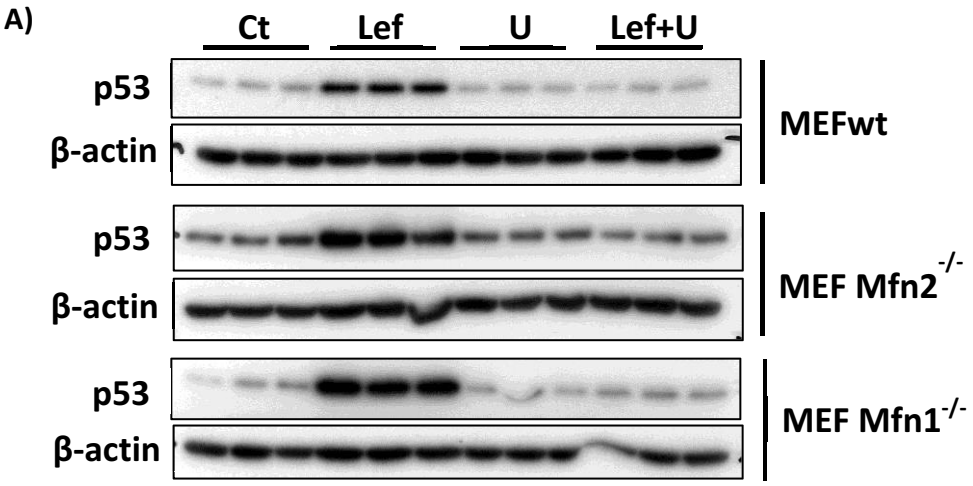

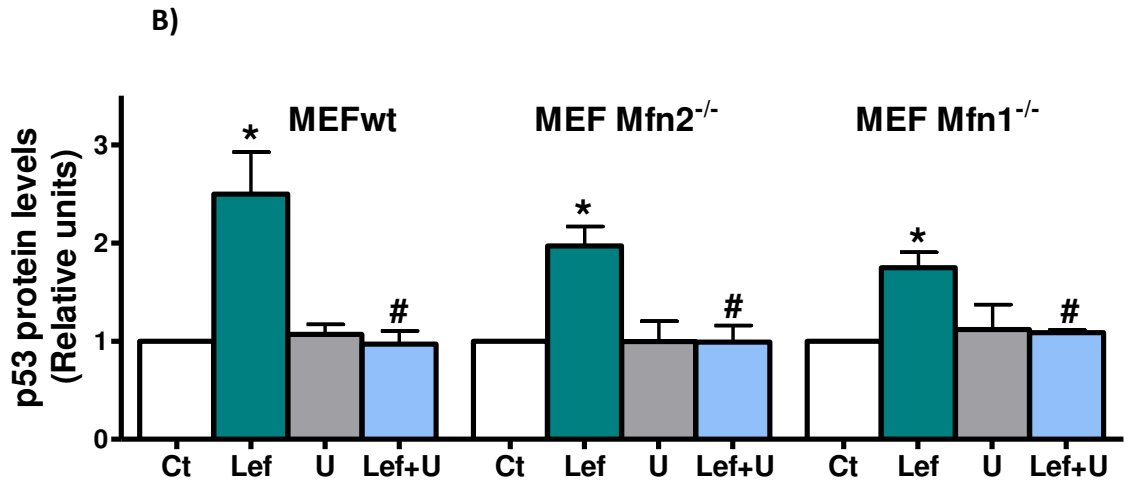

Figure 68. **Leflunomide increases p53 protein levels and external uridine prevents p53 induction in MEFwt, MEF Mfn1$^{-/-}$, and MEF Mfn2$^{-/-}$ cells.** The p53 and β-actin protein levels in total lysates from MEFs cells were analysed by western blot (A) and quantified by densitometry using β-actin as a control (B). Data represents mean ± SEM expressed relative to the control group. *P < 0.05 vs Ct, #P < 0.05 vs Lef. Ct, control; Lef, leflunomide: U, uridine. Four independent assays were performed per triplicate (n = 4).

Leflunomide induced p53 protein expression in all MEFs cells and supplementation with uridine prevented the p53 induction.

These results suggest that leflunomide up-regulated mitochondrial fusion proteins and promoted the elongation of mitochondria by p53 induction, which is driven by the deficiency of pyrimidines.

11.2. Myxothiazol induces p53 expression

It has been demonstrated that myxothiazol increases Mfn2 and Mfn1 expression in HeLa and C2C12 cells by decreasing the intracellular levels of pyrimidines through complex III inhibition (See section 10). Then, the next step was to test the effect of myxothiazol in p53 expression.

11.2.1 Myxothiazol induces p53 expression in HeLa cells

p53 mRNA and protein levels were measured in HeLa cells incubated with myxothiazol and uridine.

11.2.1.1. p53 mRNA levels of HeLa cells incubated with myxothiazol ± uridine

Hela cells were incubated with myxothiazol at 2 µM ± uridine at 50 µM for 24 h and p53 mRNA levels were measured by qPCR (Figure 69).

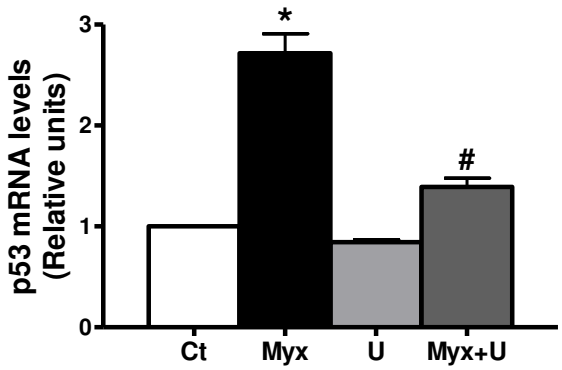

Figure 69. **Myxothiazol increases p53 mRNA levels and external uridine prevents p53 induction in HeLa cells.** p53 mRNA levels in HeLa cells incubated with myxothiazol at 2 µM ± uridine at 50 µM for 24 h were measured by qPCR. The housekeeping gene used was GAPDH. Both probes, p53 and GAPDH, were SYBR. Data represents mean ± SEM expressed relative to control group. *P < 0.05 vs Ct, #P < 0.05 vs Myx. Ct, control; Myx, myxothiazol; U, uridine. Three independent assays were performed per triplicate (n = 3).

Myxothiazol increased p53 mRNA in 2.7-fold increase by depletion of pyrimidine synthesis. External uridine, which reversed the deficiency in pyrimidine biosynthesis, was able to prevent p53 up-regulation.

11.2.1.2. p53 protein levels in HeLa cells incubated with myxothiazol

HeLa cells were incubated with myxothiazol at 2 µM ± uridine at 250 µM for 24 h and p53 protein levels were analyzed by western blot (Figure 70).

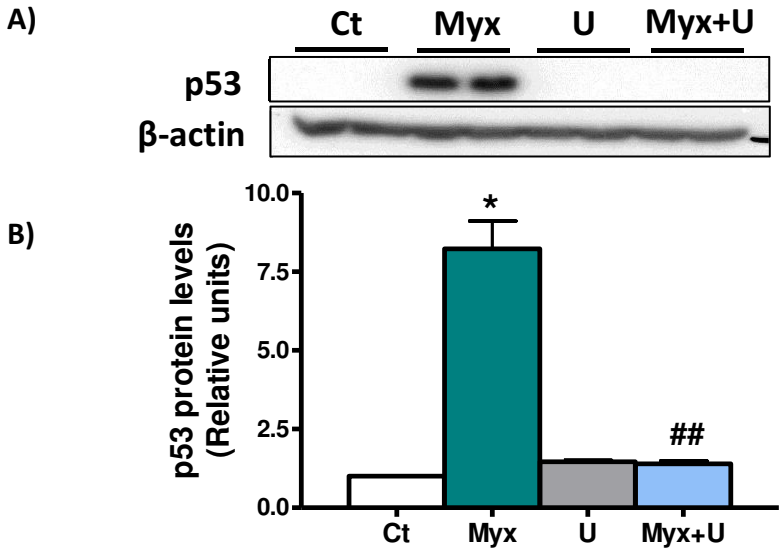

Figure 70. **Myxothiazol increases p53 protein levels, and external uridine prevents p53 up-regulation in HeLa cells.** The p53 and β-actin protein levels in total lysates from HeLa cells were analysed by western blot (A) and quantified by densitometry using β-actin as a control (B). Data represents mean ± SEM expressed relative to the control group. *P < 0.05 vs Ct, ##P < 0.01 vs Myx. Ct, control; Myx, myxothiazol; U, uridine. Three independent assays were performed per duplicate (n = 3).

Myxothiazol induced p53 protein levels in 8.2-fold increase and addition of external uridine was able to prevent the p53 up-regulation. These results indicate that myxothiazol-induced activation of p53 is driven by the deficiency in pyrimidines.

11.2.2. Myxothiazol induces p53 expression in C2C12 cells

C2C12 cells were incubated with myxothiazol at 2 µM for 12 h and p53 protein levels were analysed by western blot (Figure 71).

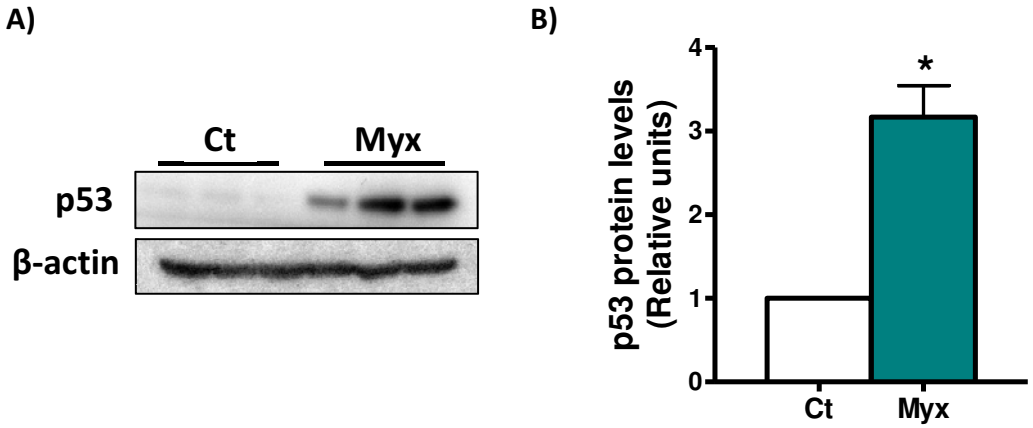

Figure 71. **Myxothiazol increases p53 protein levels in C2C12 cells.** The p53 and β-actin protein levels in total lysates from C2C12 cells were analysed by western blot (A) and quantified by densitometry using β-actin as a control (B). Data represents mean ± SEM expressed relative to the control group. *P < 0.05 vs Ct. Ct, control; Myx, myxothiazol. Three independent assays were performed per triplicate (n = 3).

Once we have confirmed that p53 is implicated in the mechanism of action of myxothiazol in HeLa and C2C12 cells, the results suggest that myxothiazol inhibits the synthesis of pyrimidine through complex III inhibition and up-regulates mitochondrial fusion proteins by inducing p53 in HeLa and C2C12 cells.

12. Leflunomide and myxothiazol activate p53 through phosphorylation of Ser15

The p53 tumor suppressor protein plays a major role in cellular response to DNA damage and to depletion of ribonucleotide pools[20]. Activation of p53 can lead to either cell cycle arrest and DNA repair or apoptosis[22]. In normal cells a p53 protein level is maintained through a controlled degradation in 26S and 20S proteasomes[23,24]. MDM2 and other E3-ligases[25] inhibits p53 accumulation by targeting it for ubiquitination and 26S proteasomal degradation[26,27], and the process is interrupted by stresses, through phosphorylation of p53 at its N termini or through overexpression of the $p14^{ARF}$ inhibitor protein[28]. A reduced interaction between p53 and its negative regulator, the oncoprotein MDM2[29], is achieved by phosphorylating p53 at Ser15 and Ser20. Phosphorylation impairs the ability of MDM2 to bind p53, promoting both the accumulation and activation of p53[29,30].

In HeLa and C2C12 cells we found strong stimulation of Ser15 phosphorylation after treatment with leflunomide and myxothiazol.

12.1. p53 protein is activated through phosphorylation of Ser15 by leflunomide and myxothiazol in HeLa cells

To confirm that the depletion of pyrimidines pools induced p53 expression by phosphorylation of Ser15, ρ-p53 protein levels were measured in HeLa cells incubated with leflunomide at 50 µM for 48 h ± uridine at 50 µM by western blot (Figure 72).

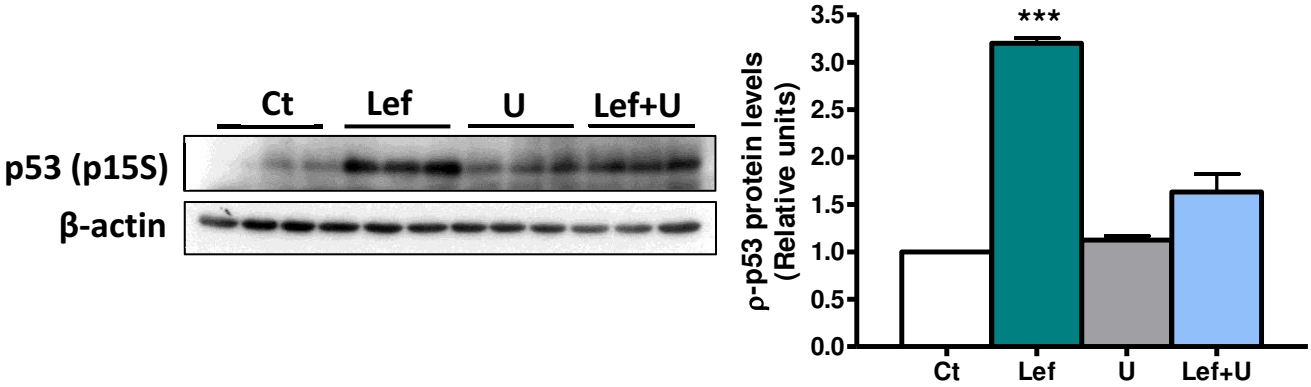

***Figure 72.* ρ-p53 levels in HeLa cells incubated with leflunomide.** The ρ-p53 and β-actin protein levels in total lysates from HeLa cells were analysed by western blot (A) and quantified by densitometry using β-actin as a control (B). Data represents mean ± SEM expressed relative to the control (Ct) group. **P < 0.01 vs Ct. Ct, control; Lef, leflunomide; U, uridine. Two independent assays were performed per triplicate (n = 3).

Leflunomide induced a 3.2-fold increase in ρ-p53 protein levels, and the addition of external uridine, which reversed the deficiency in pyrimidine biosynthesis, was able to

prevent p53 phosphorylation. These results suggest that inhibition of biosynthesis of pyrimidines by leflunomide, which inhibited the DHODH enzyme, triggered p53 response by phosphorylation of Ser15 in HeLa cells.

Then, HeLa cells were incubated with myxothiazol at 2µM ± uridine at 250 µM for 24 h and ρ-p53 protein levels were analysed and quantified by western blot (Figure 73).

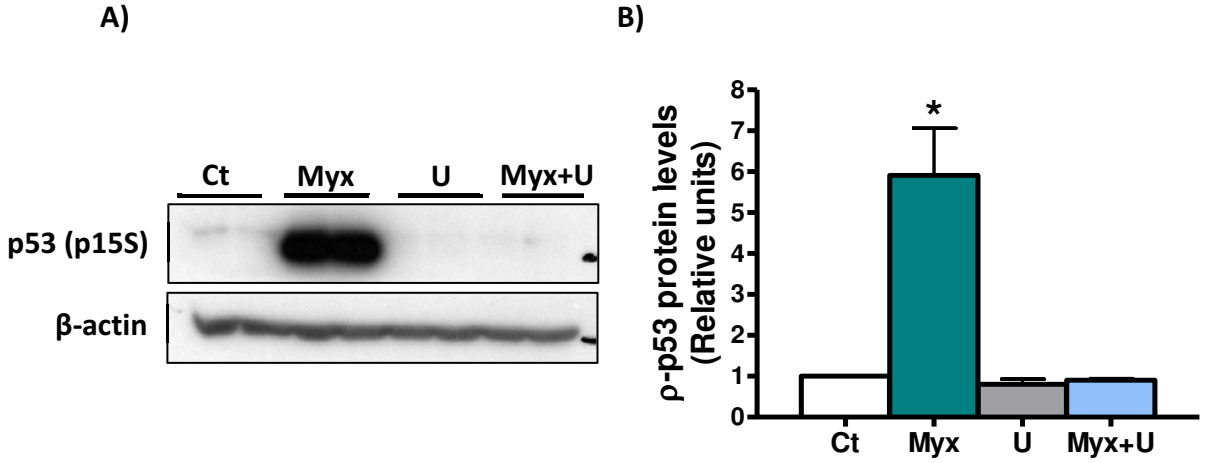

***Figure 73.* ρ-p53 levels in HeLa cells incubated with myxothiazol.** The ρ-p53 and β-actin protein levels in total lysates from HeLa cells were analysed by western blot (A) and quantified by densitometry using β-actin as a control (B). Data represents mean ± SEM expressed relative to the control (Ct) group. *P < 0.05 vs Ct. Ct, control; Myx, myxothiazol; U, uridine. Four independent assays were performed per duplicate (n = 4).

Myxothiazol induced ρ-p53 protein levels in 5.9-fold increase and the addition of external uridine, which reversed the deficiency in pyrimidine biosynthesis, was able to prevent p53 phosphorylation. These results confirm that inhibition of biosynthesis of pyrimidines by myxothiazol, which blocked complex III and indirectly inhibits the DHODH enzyme, triggers p53 response by phosphorylation of Ser15 in HeLa cells.

12.2. p53 protein is activated through phosphorylation of Ser15 by leflunomide and myxothiazol in C2C12 cells

To confirm the results obtained in section 12.1 the same experiments were performed in C2C12. C2C12 cells were incubated with leflunomide at 50 µM ± uridine at 250 µM for 48 h and ρ-p53 and β-actin protein levels were analysed and quantified by western blot (Figure 74).

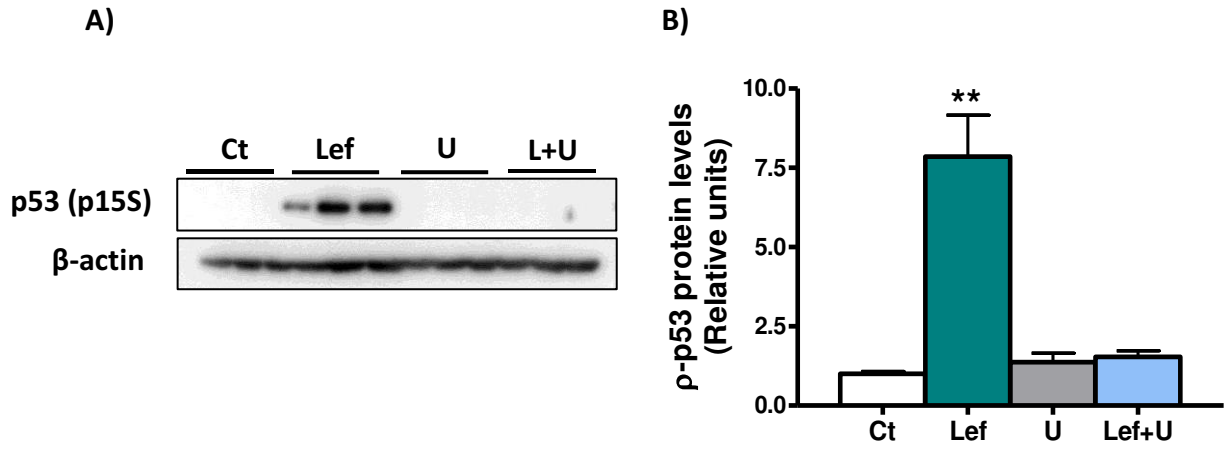

***Figure 74.* ρ-p53 levels in C2C12 cells incubated with leflunomide.** The ρ-p53 and β-actin protein levels in total lysates from C2C12 cells were analysed by western blot (A) and quantified by densitometry using β-actin as a control (B). Data represents mean ± SEM expressed relative to the control (Ct) group of one representative experiment. **P < 0.01 vs Ct. Ct, control; Lef, leflunomide; U, uridine. Two independent assays were performed per triplicate (n = 2).

Leflunomide induced ρ-p53 protein levels in 7.9-fold increase and the addition of external uridine, which reversed the deficiency in pyrimidine biosynthesis, was able to prevent p53 phosphorylation. These results confirm that leflunomide by inhibiting the DHODH enzyme and consequently the *de novo* synthesis of pyrimidines, activated p53 accumulation by phosphorylation of Ser15 in C2C12 cells.

Once it was confirmed that the depletion of pyrimidines pools caused p53 activation by phosphorylation of Ser15, we wanted to be sure that myxothiazol by inhibiting complex III was also activating p53 through Ser15 phosphorylation in C2C12.

C2C12 cells were incubated with myxothiazol at 2 µM for 12 h and ρ-p53 and β-actin protein levels were analysed and quantified by western blot (Figure 75).

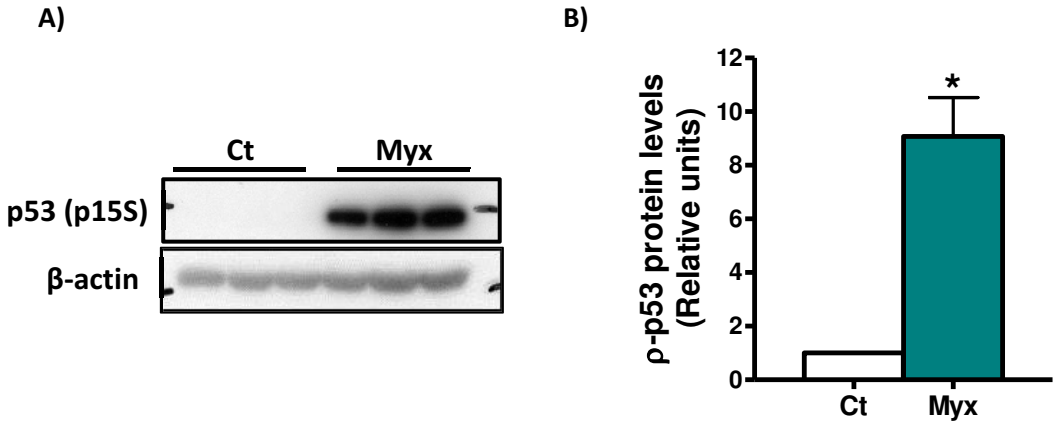

***Figure 75.* ρ-p53 levels in C2C12 incubated with myxothiazol.** The ρ-p53 and β-actin protein levels in total lysates from C2C12 cells were analysed by western blot (A) and quantified by densitometry using β-actin as a control (B). Data represents mean ± SEM expressed relative to the control (Ct) group. *P < 0.05 vs Ct. Ct, control; Lef, leflunomide. Three independent assays were performed per triplicate (n = 3).

Myxothiazol induced ρ-p53 protein levels in 9.1-fold increase. These results confirm that myxothiazol by inhibiting complex III and indirectly DHODH, and consequently the *de novo* synthesis of pyrimidines, activated p53 accumulation by phosphorylation of Ser15 in C2C12 cells.

13. Pyrimidine biosynthesis links mitochondrial elongation to the p53 pathway

The results from section 11 and 12 suggests that the depletion of pyrimidines pools, by DHODH or complex III inhibitors, up-regulates mitochondrial fusion proteins and promotes the elongation of mitochondria through p53 induction by phosphorylation of Ser15. Thus, to assess whether p53 status affected mitochondrial gene and proteins expression U87MG (TP53 wild-type) and T98G (TP53 mutant, M237I) human glioma cell lines were obtained from Avelina Tortosa group (Institut d'Investigació Biomèdica de Bellvitge-Universitat de Barcelona).

13.1. U87MG and T98G human glioma cell lines

U87MG cells that express p53 wild-type were incubated with leflunomide at 50 µM for 48, 72 and 96 h and Mfn2, Mfn1, Opa1, Drp1, p53, β-actin and porin proteins levels were assessed by western blot assay (Figure 76).

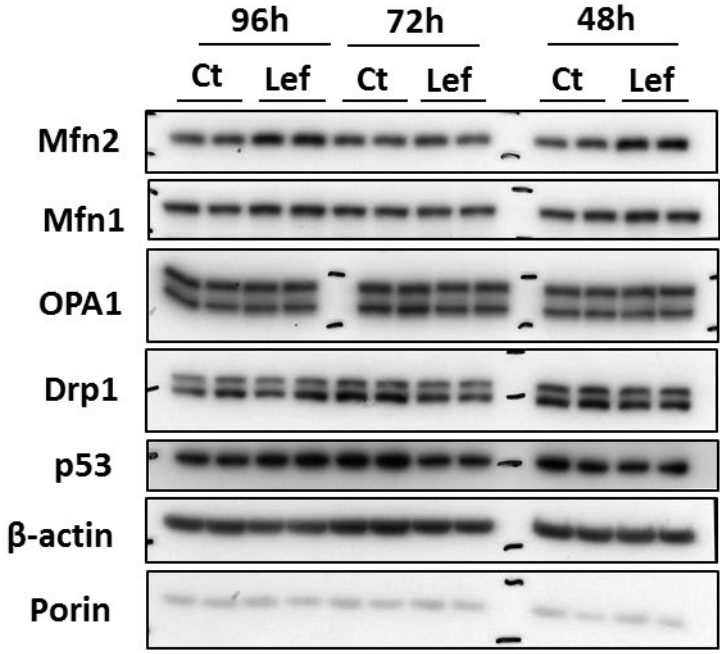

Figure 76. **Mitochondrial proteins levels in U87MG cells incubated with leflunomide.** The Mfn2, Mfn1, Opa1, Drp1, p53, β-actin and porin protein levels in total lysates from U87MG cells were analysed by western blot.

Leflunomide at 48 and 96 h was able to increase Mfn2 and Mfn1 protein levels. No changes were observed for Opa1 protein levels, and Drp1 decreased at 72 h. p53 protein levels were increased at 96 h of incubation with leflunomide.

Then, T98G cells that have a single mutation in the codon position 237, a methionine (ATG) in wild-type cells is mutated by a isoleucine (ATA), were incubated with leflunomide at

50 µM for 48 h and Mfn2, p53 and β-actin protein levels were assessed by western blot (Figure 77).

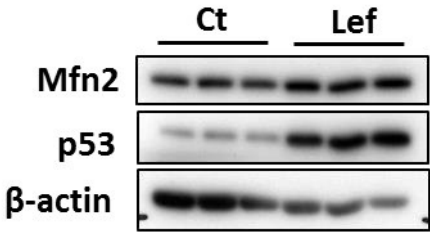

Figure 77. **Mfn2 and p53 protein levels in T98G cells incubated with leflunomide.** The Mfn2, p53 and β-actin protein levels in total lysates from T98G cells were analysed by western blot.

Leflunomide increased Mfn2 and p53 protein levels indicating that the mutation in T98G cells did not prevent the up-regulation in p53 protein levels.

13.2. p53 overexpression in HeLa cells

Other attempts to assess whether p53 functionally regulates mitochondrial genes involved in mitochondrial dynamics were performed. HeLa cells were transient transfected with either a p53 expression vector (CMVp53) or an empty negative control vector (pcDNA3.1) (See section 3 in materials and methods).

The transfection efficiency was measured by FACS, and the maximum efficiency achieved was 60%. Once the cells were transfected, they were incubated with leflunomide at 50 µM for 48 h. Then, Mfn2 and p53 mRNA levels were measured by qPCR.

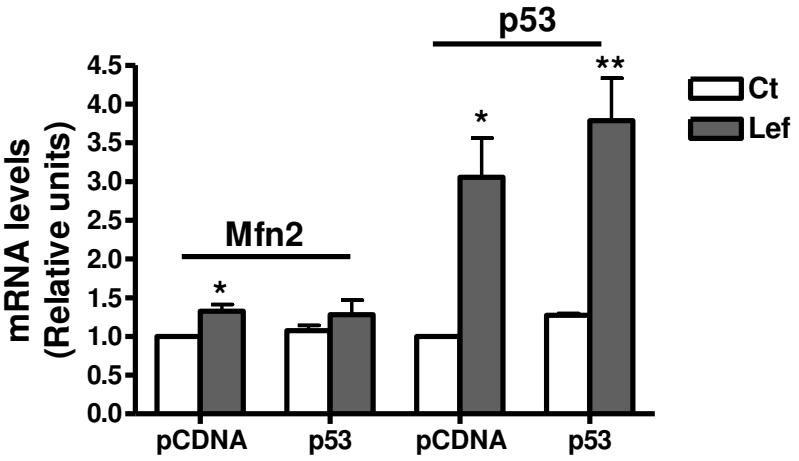

Figure 78. **Mfn2 and p53 mRNA levels in HeLa cells transient transfected with p53 expression vector.** Mfn2 and p53 mRNA levels in HeLa cells incubated with leflunomide at 50 µM for 48 h were measured by qPCR. The housekeeping gene used was GAPDH. All the dyes, Mfn2, p53 and GAPDH, were SYBR. Data represents mean ± SEM expressed relative to control group. *P < 0.05 vs Ct, **P < 0.01 vs Ct. Ct, control; Lef, leflunomide. Three independent assays were performed per triplicate (n = 3).

Only a small increase in p53 mRNA levels was achieved when HeLa cells were transfected with p53 expression vector. This increase was not sufficient to confirm if the levels of the Mfn2 mRNA parallel changed with p53 mRNA expression.

13.3. Effect of p53 gene silencing in HeLa cells

To further address whether p53 was involved in the mechanism of action of leflunomide, we decided to silence p53 gene to down-regulate p53 expression. HeLa cells were transient transfected overnight with either a p53 siRNA (human specific) or a control siRNA (fluorescein conjugate) to measure transfection efficiency. The next day the medium was renewed and the cells were incubated with leflunomide at 50 µM for 48 h.

The transfection efficiency was measured by FACS, and the efficiency achieved was 90%. Once the cells were transfected, they were incubated with leflunomide at 50 µM for 48 h. Then, p53 and Mfn2 mRNA levels were measured by qPCR (Figure 79).

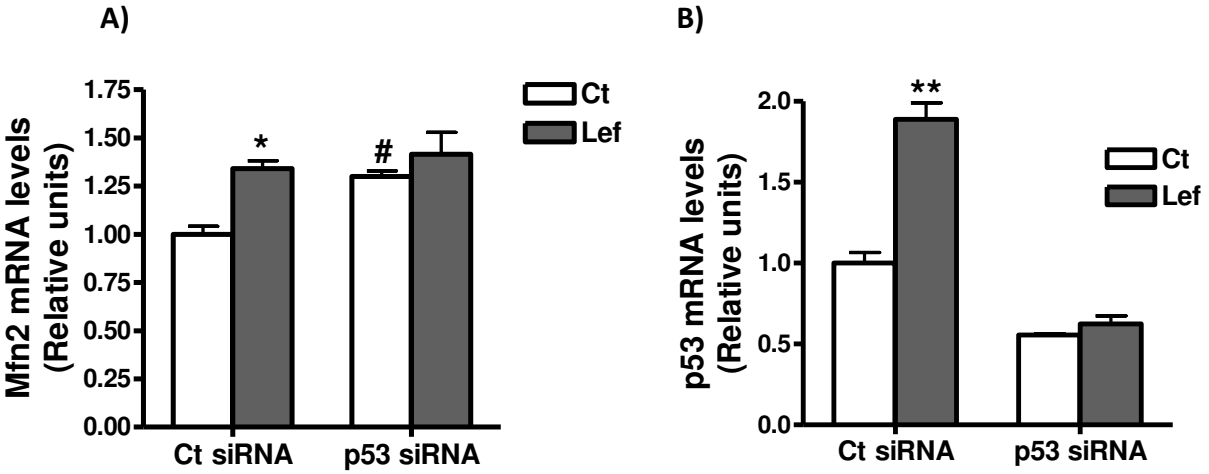

Figure 79. **p53 and Mfn2 mRNA levels in HeLa cells transient transfected with control and p53 siRNA. A)** p53 and **B)** Mfn2 mRNA levels in HeLa cells, transient transfected with control and p53 siRNA, were incubated with leflunomide at 50 µM for 48 h were measured by qPCR. The housekeeping gene used was GAPDH. All the dyes, Mfn2, p53 and GAPDH, were SYBR. Data represents mean ± SEM expressed relative to control group of one experiment. *P < 0.05 vs Ct, **P < 0.01 vs Ct, #P< 0.05 vs Ct siRNA. Ct, control; Lef, leflunomide. One independent assay was performed per triplicate (n = 1).

First of all, p53 mRNA levels were determined to be sure that p53, in HeLa cells transfected with p53 siRNA, was silenced. Leflunomide produced a 1.9-fold increase in p53 protein levels in HeLa cells transfected with control siRNA. However, p53 mRNA levels in HeLa p53 knockdown cells incubated or not with leflunomide were down-regulated compared to control siRNA levels. This results confirmed p53 repression. The levels of Mfn2 mRNA in HeLa cells transfected with control siRNA and incubated with leflunomide were 40% higher than the control ones. HeLa cells transfected with p53 siRNA showed up-regulation of the basal levels of Mfn2 gene expression compared to the control ones. Although the basal levels were increased, leflunomide was not able to increase Mfn2 gene expression.

The next step was to check p53 protein levels in HeLa cells transient transfected with p53 siRNA to be sure that p53 is down-regulated. HeLa cells were transient transfected overnight with either a p53 siRNA or a control siRNA. The next day the medium was renewed and the cells were allowed to grow for 24 h (Figure 80).

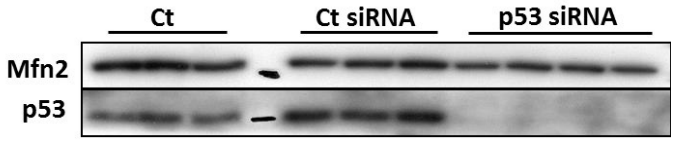

Figure 80. **Mfn2 and p53 levels in HeLa cells transient transfected with p53 and control siRNA.** The Mfn2 and p53 protein levels in total lysates from HeLa cells were analysed by western blot.

p53 protein levels were not observed in HeLa cells transfected with p53 siRNA. In this case the levels of Mfn2 gene expression were down-regulated in comparison with HeLa cells transfected with control siRNA.

To evaluate whether the changes in mitochondrial proteins involved in mitochondrial dynamics were dependent of p53, HeLa cells were transfected with p53 and control siRNAs and incubated with leflunomide for 48 h. Mfn2, Mfn1, p53 protein levels were analysed by western blot (Figure 81).

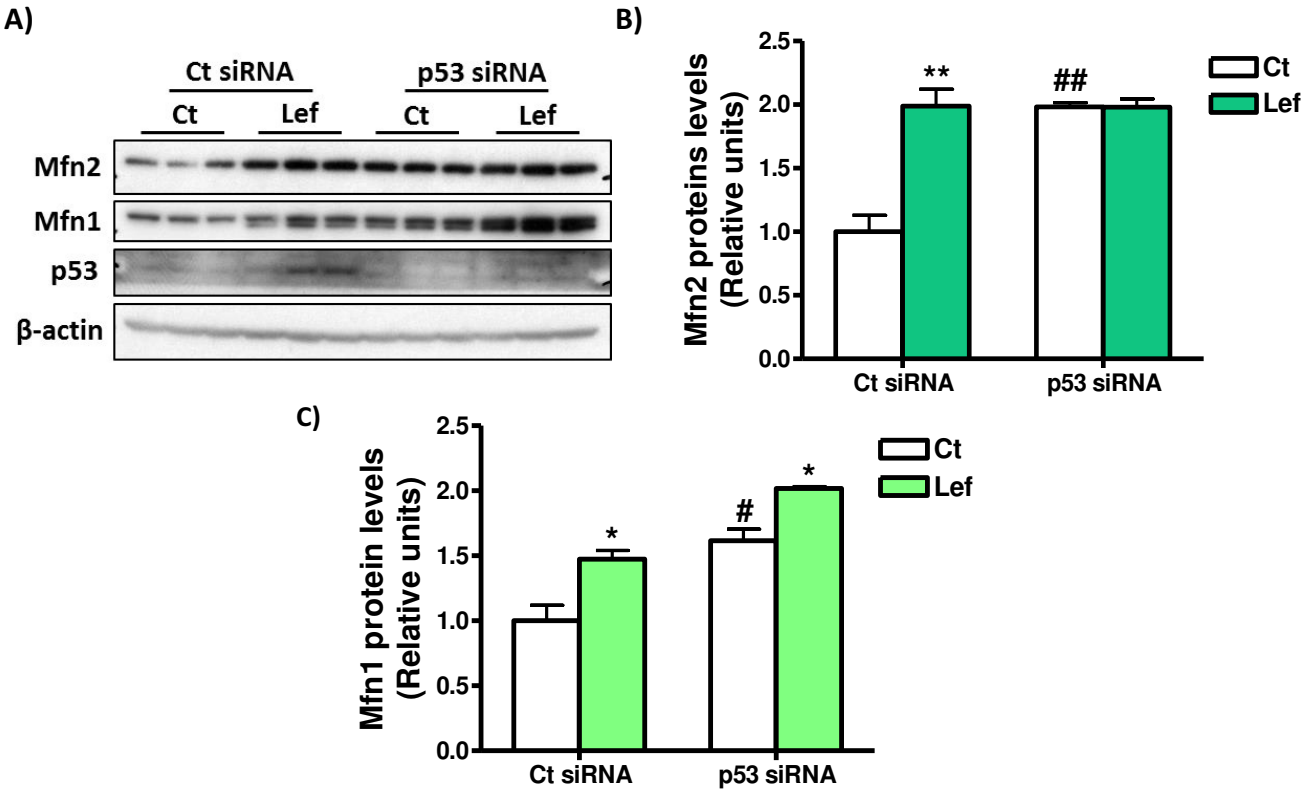

Figure 81. **Mfn2, Mfn1 and p53 levels in HeLa cells transient transfected with p53 and control siRNA.** The Mfn2, Mfn1 and p53 protein levels in total lysates from HeLa cells were analysed by western blot (A) and Mfn2 (B) and Mfn1 (C) were quantified by densitometry using β-actin as a control (B). Data represents mean ± SEM expressed relative to the control group of one representative experiment. *P < 0.05 vs Ct, **P < 0.01 vs Ct, #P <

0.05 vs Ct siRNA, ##P < 0.01 vs Ct siRNA. Ct, control; Lef, leflunomide. Two independent assays were performed per triplicate (n = 2).

Mfn2 increased two-fold in HeLa cells transfected with control siRNA in response to leflunomide. However, HeLa cells transfected with p53 siRNA showed up-regulation of the basal levels of Mfn2 protein compared to the control siRNA. Although the basal levels were increased, leflunomide was not able to increase Mfn2 expression. Moreover, Mfn1 augmented 1.5-fold in control and in HeLa cells silenced for p53 treated with leflunomide. In addition, the basal levels of Mfn1 in HeLa cells transfected with p53 siRNA were also up-regulated. These results suggested that p53 down-regulation increases the basal levels of Mfn2 and Mfn1 in HeLa cells.

13.4. Effect of p53 gene silencing in C2C12 cells

To further explore whether the changes in mitochondrial proteins involved in mitochondrial dynamics were dependent of p53 in C2C12 cells, the cells were transfected with p53 and control siRNA and incubated with leflunomide for 48 h. Mfn2, Mfn1, Drp1 and p53 protein levels were analysed by western blot (Figure 82).

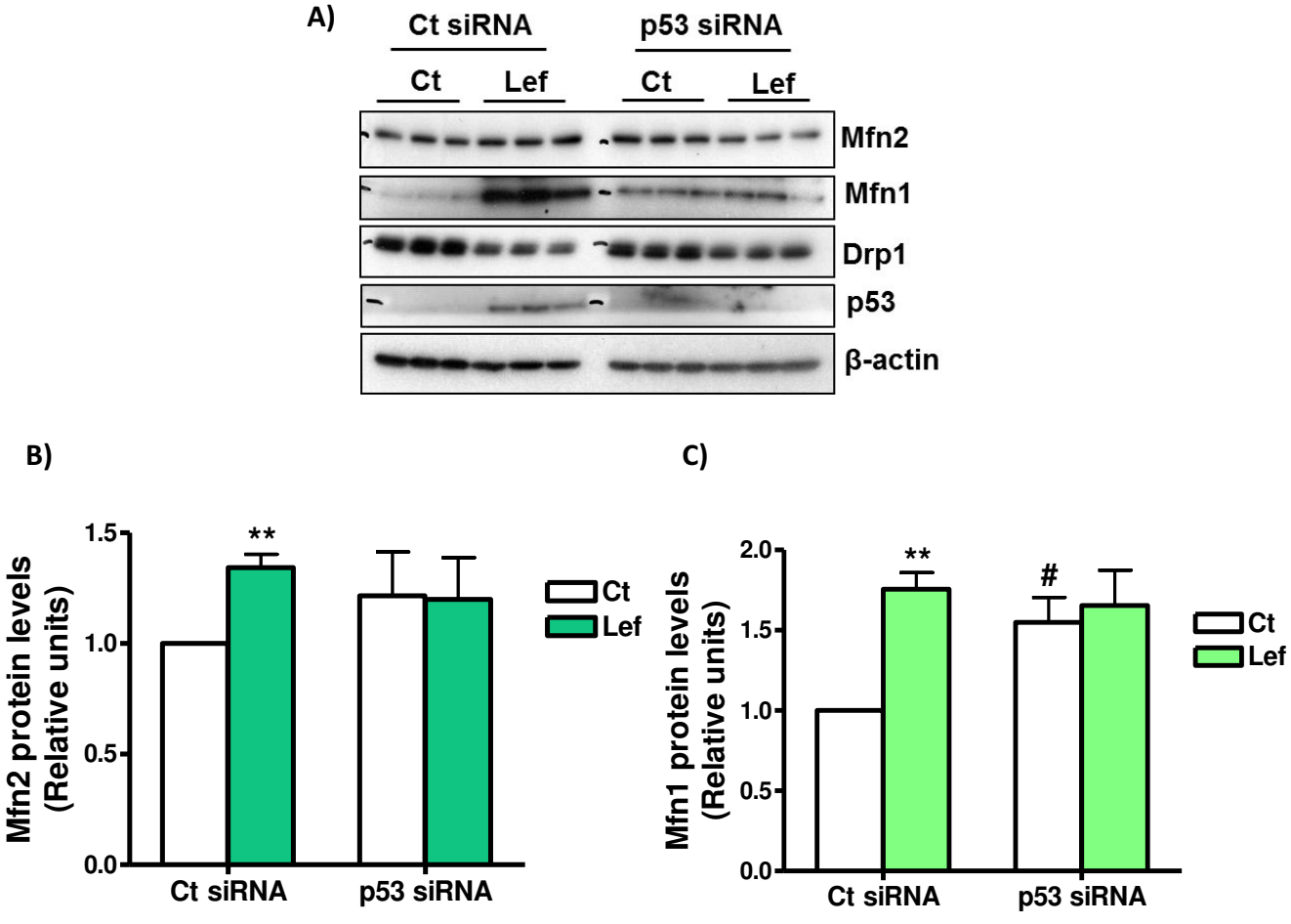

D)

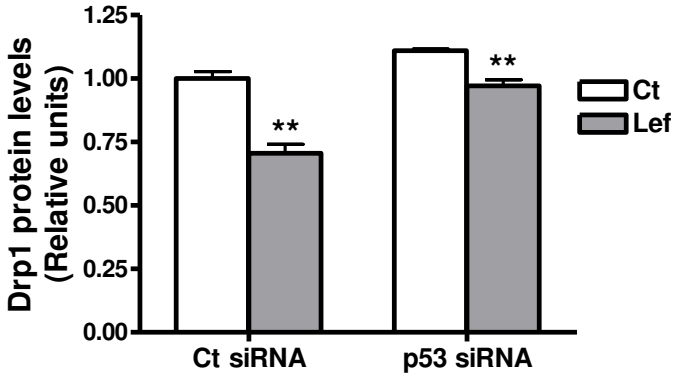

Figure 82. **Mfn2, Mfn1, Drp1 and p53 levels in C2C12 cells transient transfected with p53 and control siRNA.** The Mfn2, Mfn1, Drp1 and p53 protein levels in total lysates from C2C12 cells were analysed by western blot (A) and Mfn2 (B), Mfn1 (C), Drp1 (D) were quantified by densitometry using β-actin as a control. Data represents mean ± SEM expressed relative to the control group. **P < 0.01 vs Ct, #P < vs Ct siRNA. Ct, control; Lef, leflunomide. Three independent assays were performed per triplicate (n = 3).

Mfn2 and Mfn1 increased 1.4- and 1.8-fold, respectively, in C2C12 cells transfected with control siRNA with leflunomide. However, C2C12 cells silenced for p53 and treated with leflunomide did not show up-regulation of Mfn2 or Mfn1. In addition, the basal levels of Mfn1 protein in C2C12 p53 knockdown cells were up-regulated compared to the control as in HeLa cells. Drp1 was 30% reduced in C2C12 transfected with control siRNA with leflunomide and 15% reduced in C2C12 p53 knockdown cells treated with leflunomide. These results suggest that p53 down-regulation increases the basal levels of Mfn1. Moreover, p53 down-regulation blocked leflunomide-dependent Mfn2 and Mfn1 up-regulation in C2C12 cells.

REFERENCES

1 Bach, D. *et al.* Expression of Mfn2, the Charcot-Marie-Tooth neuropathy type 2A gene, in human skeletal muscle: effects of type 2 diabetes, obesity, weight loss, and the regulatory role of tumor necrosis factor alpha and interleukin-6. *Diabetes* **54**, 2685-2693, doi:54/9/2685 [pii] (2005).

2 Sebastian, D. *et al.* Mitofusin 2 (Mfn2) links mitochondrial and endoplasmic reticulum function with insulin signaling and is essential for normal glucose homeostasis. *Proc Natl Acad Sci U S A* **109**, 5523-5528, doi:10.1073/pnas.1108220109 (2012).

3 Soriano, F. X. *et al.* Evidence for a mitochondrial regulatory pathway defined by peroxisome proliferator-activated receptor-gamma coactivator-1 alpha, estrogen-related receptor-alpha, and mitofusin 2. *Diabetes* **55**, 1783-1791, doi:10.2337/db05-0509 (2006).

4 Heitman, L. H. *et al.* False positives in a reporter gene assay: identification and synthesis of substituted N-pyridin-2-ylbenzamides as competitive inhibitors of firefly luciferase. *J Med Chem* **51**, 4724-4729, doi:10.1021/jm8004509 (2008).

5 Auld, D. S. *et al.* Characterization of chemical libraries for luciferase inhibitory activity. *J Med Chem* **51**, 2372-2386, doi:10.1021/jm701302v (2008).

6 Auld, D. S., Thorne, N., Nguyen, D. T. & Inglese, J. A specific mechanism for nonspecific activation in reporter-gene assays. *ACS Chem Biol* **3**, 463-470, doi:10.1021/cb8000793 (2008).

7 Fox, R. I. *et al.* Mechanism of action for leflunomide in rheumatoid arthritis. *Clin Immunol* **93**, 198-208, doi:10.1006/clim.1999.4777S1521-6616(99)94777-0 [pii] (1999).

8 Cherwinski, H. M. *et al.* The immunosuppressant leflunomide inhibits lymphocyte proliferation by inhibiting pyrimidine biosynthesis. *J Pharmacol Exp Ther* **275**, 1043-1049 (1995).

9 Zielinski, T., Zeitter, D., Muller, S. & Bartlett, R. R. Leflunomide, a reversible inhibitor of pyrimidine biosynthesis? *Inflammation research : official journal of the European Histamine Research Society ... [et al.]* **44 Suppl 2**, S207-208 (1995).

10 Schwartsmann, G. P., G.J.; Laurensse, E.; De Wall, F.C.; Pinedo, H.M. Schedule-dependency of growth-inhibitory and antipyrimidine effects. *Biochem. Pharmacol.* **37**, 3257-3266 (1988).

11 Weber, G. Biochemical strategy of cancer cells and the design of chemotherapy: G. H. A. Clowes Memorial Lecture. *Cancer Res* **43**, 3466-3492 (1983).

12 Bach, D. *et al.* Mitofusin-2 determines mitochondrial network architecture and mitochondrial metabolism. A novel regulatory mechanism altered in obesity. *J Biol Chem* **278**, 17190-17197, doi:10.1074/jbc.M212754200M212754200 [pii] (2003).

13 Malka, F. *et al.* Separate fusion of outer and inner mitochondrial membranes. *EMBO Rep* **6**, 853-859, doi:10.1038/sj.embor.7400488 (2005).

14 Chen, H. *et al.* Mitofusins Mfn1 and Mfn2 coordinately regulate mitochondrial fusion and are essential for embryonic development. *J Cell Biol* **160**, 189-200, doi:10.1083/jcb.200211046 (2003).

15 Tondera, D. *et al.* SLP-2 is required for stress-induced mitochondrial hyperfusion. *EMBO J* **28**, 1589-1600, doi:10.1038/emboj.2009.89emboj200989 [pii] (2009).

16 Wong, E. D. *et al.* The intramitochondrial dynamin-related GTPase, Mgm1p, is a component of a protein complex that mediates mitochondrial fusion. *J Cell Biol* **160**, 303-311, doi:10.1083/jcb.200209015 (2003).

17 Duvezin-Caubet, S. *et al.* Proteolytic processing of OPA1 links mitochondrial dysfunction to alterations in mitochondrial morphology. *J Biol Chem* **281**, 37972-37979, doi:10.1074/jbc.M606059200 (2006).

18 Ishihara, N., Fujita, Y., Oka, T. & Mihara, K. Regulation of mitochondrial morphology through proteolytic cleavage of OPA1. *EMBO J* **25**, 2966-2977, doi:10.1038/sj.emboj.7601184 (2006).

19 Griparic, L., Kanazawa, T. & van der Bliek, A. M. Regulation of the mitochondrial dynamin-like protein Opa1 by proteolytic cleavage. *J Cell Biol* **178**, 757-764, doi:10.1083/jcb.200704112 (2007).
20 Linke, S. P., Clarkin, K. C., Di Leonardo, A., Tsou, A. & Wahl, G. M. A reversible, p53-dependent G0/G1 cell cycle arrest induced by ribonucleotide depletion in the absence of detectable DNA damage. *Genes & development* **10**, 934-947 (1996).
21 Khutornenko, A. A. *et al.* Pyrimidine biosynthesis links mitochondrial respiration to the p53 pathway. *Proc Natl Acad Sci U S A* **107**, 12828-12833, doi:10.1073/pnas.0910885107 (2010).
22 Levine, A. J. p53, the cellular gatekeeper for growth and division. *Cell* **88**, 323-331 (1997).
23 Tsvetkov, P., Reuven, N. & Shaul, Y. Ubiquitin-independent p53 proteasomal degradation. *Cell Death Differ* **17**, 103-108, doi:10.1038/cdd.2009.67 (2010).
24 Chumakov, P. M. Versatile functions of p53 protein in multicellular organisms. *Biochemistry (Mosc)* **72**, 1399-1421 (2007).
25 Brooks, C. L. & Gu, W. p53 ubiquitination: Mdm2 and beyond. *Mol Cell* **21**, 307-315, doi:10.1016/j.molcel.2006.01.020 (2006).
26 Chehab, N. H., Malikzay, A., Stavridi, E. S. & Halazonetis, T. D. Phosphorylation of Ser-20 mediates stabilization of human p53 in response to DNA damage. *Proc Natl Acad Sci U S A* **96**, 13777-13782 (1999).
27 Honda, R., Tanaka, H. & Yasuda, H. Oncoprotein MDM2 is a ubiquitin ligase E3 for tumor suppressor p53. *FEBS Lett* **420**, 25-27 (1997).
28 Sherr, C. J. & Weber, J. D. The ARF/p53 pathway. *Current opinion in genetics & development* **10**, 94-99 (2000).
29 Shieh, S. Y., Ikeda, M., Taya, Y. & Prives, C. DNA damage-induced phosphorylation of p53 alleviates inhibition by MDM2. *Cell* **91**, 325-334 (1997).
30 Tibbetts, R. S. *et al.* A role for ATR in the DNA damage-induced phosphorylation of p53. *Genes & development* **13**, 152-157 (1999).

DISCUSSION

DISCUSSION

Mitochondria produce most of the cellular ATP, and are involved in many other cellular functions such as Ca^{2+} signaling, cellular differentiation, apoptosis, substrates oxidation, as well as, the control of the cell cycle and cell growth . The correct function of mitochondria is ensured by fusion and fission processes, which are known as mitochondrial dynamics. Mitochondrial fusion controls mitochondrial metabolism and calcium flux, whereas mitochondrial fission facilitates apoptosis to damaged mitochondria. Metabolic disorders such as type 2 diabetes or obesity showed Mfn2 down regulation in muscle[1], and several human diseases are caused by mutations in genes involved in mitochondrial dynamics, such as Charcot-Marie-Tooth syndrome and autosomal dominant optic atrophy caused by functional loss of Mfn2 and Opa1. In addition, cardiomyopathies are the result of an imbalance in mitochondrial dynamics[2]. Thus, modification of mitochondrial dynamics by modulating proteins involved in fusion and fission events has emerged as a novel pharmacological strategy.

The main objective of this chapter was to identify a compound with capacity to enhance human Mfn2 expression for the treatment of diseases associated with decrease in Mfn2 protein expression, such as Charcot Marie Tooth type 2A neuropathy, as well as, metabolic disorders such as type 2 diabetes or obesity[1,3].

1. Identification of a positive modulator of Mfn2 expression

To achieve our goal, HeLa cells, stably expressing luciferase under the control of 2 kb of human Mfn2 promoter, were incubated with a FDA-approved library of 1,120 compounds (Prestwick Chemical Library). The Prestwick Chemical Library® is composed by 90% of marketed drugs and 10% of bioactive alkaloids or related substances showing high chemical and pharmacological diversity, as well as, bioavailability and safety in humans. Prestwick chemical library was chosen to reduce low quality hits and the cost of the initial screening, guaranteeing hits that can accelerate the drug discovery process due to its known bioavailability and toxicity studies that have proven usefulness in humans. These drugs can be immediately tested in patients for other uses that have not been previously described. The HTS was carried out and a small compound called leflunomide was identified as a potent transcriptional activator of the Mfn2 promoter. Importantly, leflunomide increased Mfn2 mRNA and protein levels in HeLa and C2C12 cells, validating its activity as an activator of Mfn2 expression.

Leflunomide (Arava) is indicated for the treatment of active Rheumatoid Arthritis (RA) as a disease-modifying antirheumatic drug (DMARD), and was launched in United States in 1998[4]. Leflunomide once administrated is rapidly converted to an active metabolite

(A771726), also known as teriflunomide. In addition, teriflunomide also increased transcriptional activity of the Mfn2 promoter and Mfn2 mRNA levels in HeLa cells suggesting that teriflunomide exhibited the same activity as leflunomide.

Leflunomide secondary effects were evaluated after 10 years of licensing[5]. Leflunomide treatment presented gastrointestinal common adverse effects such as diarrhoea, dyspepsia, nausea/vomiting, abdominal pain, oral ulcers, as well as, abnormal liver function tests, drug eruptions, alopecia, infections, weight loss and hypertension. Although leflunomide was effective for the treatment of active RA, had diverse secondary effects and therefore was discarded for the treatment of diseases related with alterations in Mfn2 expression due to the difficulty to be approved by the U.S. Food and Drug Administration (FDA) and the European Medicines Agency (EMA). However, we decided to further study the effects and the mechanism of action of this compound in different cell lines.

2. Leflunomide promotes mitochondrial elongation

Interestingly, leflunomide and teriflunomide induced the gene expression of both Mfn2 and Mfn1, whereas no changes were observed in Opa1 and Drp1 mRNA. Furthermore, leflunomide induced the expression of the mitochondrial fusion proteins Mfn2 and Mfn1 and repressed the mitochondrial fission protein Drp1 in HeLa and C2C12 cells. Nonetheless, Opa1 protein levels slight decreased in HeLa cells and no changes were observed in C2C12 cells, suggesting that leflunomide does not modulate Opa1 expression. The up-regulation of Mfns and the decrease of Drp1 proteins suggested a displacement of the balance of mitochondrial dynamics towards mitochondrial fusion.

Our results show that leflunomide treatment of HeLa and C2C12 cells triggers mitochondrial network elongation. In addition, leflunomide is able to increase Mfn2, Mfn1 and Opa1 protein levels in MEFwt, MEF Mfn2$^{-/-}$ and MEF Mfn1$^{-/-}$ cells. Our data suggest that induced mitochondrial fusion by leflunomide is dependent on both the outer and inner mitochondrial membranes in MEFs cells. The increase of Mfn1 protein level is higher than Mfn2 in MEFwt cells, suggesting that Mfn1 may have a marked role in mitochondrial elongation. Opa1 and Drp1 modulation in MEFwt cells differs from the previous results in HeLa and C2C12 cells, indicating that leflunomide-modulated activity is conditioned by the type of cells used. Therefore, we can assume that leflunomide always increases Mfn2 and Mfn1 proteins, which are involved in fusion events, and Opa1 and Drp1 modulation is dependent on the cell type.

Mitochondria can rapidly change their morphology by mitochondrial dynamics in response to many stress conditions. Guillery et al.[6] showed that mitochondria dysfunction

results in mitochondria fragmentation. Primary fibroblast cells were treated with OXPHOS inhibitors such as piericidin A, antimycin A, potassium cyanide, and oligomycin that inhibit respiratory complexes I, III, IV, and V respectively. All OXPHOS inhibitors induced mild mitochondrial fragmentation, decreasing the proportion of cells with elongated mitochondria and increasing the proportion of cells with an intermediate mitochondrial morphology. Moreover, shorter mitochondria and a decrease in fusion activity have been described in metabolic stress during hypoxia-reoxygenation in H9c2 cells[7]. On the other hand, recent publications have reported the effect of some compounds promoting mitochondrial elongation. Yue et al. identified a diterpenoid derivative 15-oxospiramilactone (S3) that inhibits a mitochondria-localized deubiquitinase USP30 producing mitochondrial fusion through increasing ubiquitination of Mfns in MEF cells lacking Mfn1 or Mfn2. Moreover, knockdown of USP30 in MEF cells lacking Mfn1 or Mfn2 resulted in mitochondrial elongation[8,9]. Wang et al. identified a small molecule with the ability to rescue mitochondrial fragmentation in Mfn1 or Mfn2 KO MEFs cells, although did not change mitochondrial morphology in MEFwt cells. Moreover, mitochondrial elongation has been reported in HeLa and MRC5 fibroblasts cells enforced to produce ATP through OXPHOS by growing the cells in galactose grown medium for several days[10]. In addition, mitochondrial elongation can be modulated by nutrient starvation, and is dependent on the type and the severity of the starvation stress, as well as, on the fusion mitochondrial proteins Mfn1 and Opa1[11]. Specifically, Tondera[12] and colleagues elucidated that cell stress induce mitochondrial elongation. Cells exposed to selective stresses such as UV irradiation, actinomycin D and mRNA translation inhibition (cycloheximide) that down-regulates protein synthesis produce mitochondria hyperfusion forming highly interconnected network. Moreover, they described that stress-induced mitochondrial hyperfusion (SIMH) is independent of Mfn2, although requires Mfn1 and L-Opa1 proteins, and is dependent on the presence of stomatin-like protein2 (SLP2). The examples reviewed here demonstrate that treatment with uncouplers, OXPHOS inhibitors or exposure to nutrient excess produce uncoupled respiration and is associated with mitochondrial fragmentation and inhibition of fusion, whereas the opposite situation, starvation or acute “proteostatic” stress is associated with mitochondrial elongation and inhibition of fission[13].

MEFwt cells incubated with leflunomide caused mitochondrial elongation in almost all the cells. Leflunomide treatment of MEF Mfn2$^{-/-}$ increased from 8% up to 53% the cells containing elongated mitochondrial network (tubules longer than 9 μM) and decreased from 82% to 41% the cells containing ovals and short tubules. Leflunomide treatment of MEF Mfn1$^{-/-}$ did not increase as much as MEF Mfn2$^{-/-}$ the cells containing elongated mitochondria. However, cells containing short mitochondria increased from 12% up to 34% (mitochondrial tubules ranged from several microns to 5 μm), and decreased from 88% to 63% the cells containing fragmented mitochondria. Mfn1 and Mfn2 deficient MEFs cells incubated with leflunomide were able to display the networks of longer extended tubules compared with the control ones. Moreover, MEF Mfn2$^{-/-}$ cells incubated with leflunomide showed long

extended tubules similar to wild-type cells incubated with leflunomide. Our data suggest that mitochondrial elongation is more dependent of Mfn1 than Mfn2 due to the higher mitochondrial elongation of MEF Mfn2$^{-/-}$ compared to MEF Mfn1$^{-/-}$ cells. Our findings differ from previous reports describing that stress-induced mitochondrial hyperfusion is independent of Mfn2[12]. However, our results agree with the results provided by Chen et al[14] showing that overexpression of Mfn1 in Mfn2-deficient cells rescued the mitochondrial morphology in 75-80%. In contrast, overexpression of Mfn2 in Mfn1-deficient cells restored mitochondrial tubules in 25%, indicating that mitochondrial elongation is more dependent of Mfn1 than Mfn2. Moreover, the mitochondrial fusion depends on the functional GTP-binding domain of Mfns. Ishihara et al[15]. described that purified recombinant Mfn1 exhibited higher GTPase activity than Mfn2. These findings were further confirmed by Cipolat et al[16]. suggesting the role of Mfn1 but not Mfn2 in Opa1-mediated mitochondrial fusion.

Several authors have reported that mitochondrial fusion is abolished by dissipation of the inner membrane potential by using the carbonyl cyanide m-chlorophenyl hydrazone (cccp), a protonophore that dissipates the inner membrane potential in cells[17,18]. In addition, they describe that mitochondrial fusion by overexpressing Mfn1 required inner membrane potential in HeLa cells[18]. Guillery et al[6]. reported that cccp treatment caused complete fragmentation, and showed that the dissipation of the mitochondrial membrane potential is a much potent inhibitor than OXPHOS inhibitors of mitochondrial membrane fusion in primary fibroblasts. Moreover, a small subset of mitochondria lose their membrane potential in MEF lacking Mfn1 or Mfn2, being more noticeable for Mfn1 knockout cells[19]. Our findings show that leflunomide increases the expression of Mfn2 and Mfn1, promotes mitochondrial elongation and increases mitochondrial membrane potential in C2C12, MEFwt, MEF Mfn2$^{-/-}$ and MEF Mfn1$^{-/-}$ cells. These results suggest that there is a positive relation between fusion and mitochondrial membrane potential.

3. Leflunomide links pyrimidine synthesis and mitochondrial morphology

It has been described that leflunomide inhibits dihydroorotate dehydrogenase (DHODH), an enzyme that catalyses the fourth step in the *de novo* biosynthesis of pyrimidines. Leflunomide inhibits DHODH by binding to the ubiquinone binding channel, and prevents the production of the pyrimidine ribonucleotide uridine monophosphate (UMP)[4]. UMP is a source for pyrimidine nucleotides, which are essential for cellular metabolism and cell growth. DHODH inhibition causes depletion of ribonucleotides pools and produces cell stress and cell cycle arrest[4,20-22].

Leflunomide and teriflunomide showed anti-proliferative effects through inhibition of DHODH, and consequently the *de novo* synthesis of pyrimidines is decreased in HeLa, C2C12, MEFwt, MEF Mfn2$^{-/-}$ and MEF Mfn1$^{-/-}$ cells. External uridine can be taken up by the cells and

enter the metabolic pathway to restore pyrimidine nucleotides levels by the salvage pathway. This is achieved by conversion of uridine to UMP by uridine kinase[23]. The addition of external uridine reverses the deficiency in pyrimidine biosynthesis[4] and antagonises the ability of leflunomide and teriflunomide to inhibit cell proliferation in HeLa and C2C12 cells. However, only a partial recovery of the antiproliferative effects by uridine in MEFwt, MEF $Mfn2^{-/-}$ and MEF $Mfn1^{-/-}$ cells treated with leflunomide is achieved. These results seem to indicate that MEFs cells are more sensitive to depletion of pyrimidine synthesis than HeLa or C2C12 cells.

Moreover, Mfn2 and Mfn1 gene expression were measured in HeLa cells treated with leflunomide and teriflunomide with or without the presence of uridine. In addition to the effects on proliferation, addition of external uridine prevented the increase in Mfn2 and Mfn1 mRNA in HeLa cells. Moreover, uridine was able to prevent Mfns proteins up-regulation in C2C12 cells. These results suggest that the leflunomide induced up-regulation of Mfn2 and Mfn1 and mitochondrial elongation, through DHODH inhibition, was dependent on pyrimidine synthesis. Therefore, by studying this compound, we have found an important and unknown connection between pyrimidine metabolism and mitochondrial morphology.
This connection is further supported by Tufi et al.[24]. Recently, they have reported that the activation of the nucleotide salvage pathway (deoxynucleoside kinase) occurs in PINK1 mutant flies, which may be an adaptive mechanism to ameliorate mitochondrial function.

4. Mechanism of action of complex III inhibitors

DHODH is an enzyme located in the inner mitochondrial membrane and catalyses oxidation of dihydroorotate into orotate using ubiquinone as co-substrate electron acceptor. In this reaction ubiquinone is converted to ubiquinol, which is a substrate for Complex III in the respiratory chain. Thus, the novo synthesis of pyrimidine nucleotides is coupled to the mitochondrial respiratory chain (RC) via DHODH. It has been reported that DHODH depletion partially inhibits complex III, decreases the mitochondrial membrane potential and increases ROS generation.[25] Respiratory chain dysfunction using specific inhibitors of complex III, as myxothiazol and antimycin A, impairs pyrimidine synthesis by indirect inhibition of DHODH. Myxothiazol and antimycin A produced an increase in Mfn2 mRNA and protein levels in HeLa cells, and showed anti-proliferative effects through inhibition of complex III, and consequently the *de novo* synthesis of pyrimidines in C2C12 cells. The addition of external uridine, which reverses the deficiency in pyrimidine biosynthesis, reversed the increase in Mfn2 gene expression induced by complex III inhibitors, further supporting the idea that the signal that triggers the increase in Mfns is the deficiency in pyrimidines and not the inhibition of the enzyme DHODH or alterations in respiration.

Myxothiazol up-regulated Mfn1 expression, down-regulated Opa1 expression and no changes were observed for Drp1 in HeLa cells. Moreover, myxothiazol was validated in C2C12 showing an increase in mitochondrial fusion proteins (Mfn2, Mfn1 and Opa1), and a decrease in fission protein Drp1. These results suggested a displacement of the balance between mitochondrial fusion and fission towards mitochondrial fusion. C2C12 and MEFwt cells treated with leflunomide showed an elongated mitochondrial network compared to the control cells. Our results demonstrate that myxothiazol by causing a deficiency in pyrimidines through complex III inhibition, up-regulates Mfn2 and Mfn1 fusion proteins and promotes elongation of mitochondria network as leflunomide. These results concur with Tondera[12] and colleagues, which reported that cell stress induces mitochondrial elongation.

Antimycin A treatment of cells produced a shift from long (L) isoforms bands to short (S) isoforms bands of Opa1, whereas no detectable changes were observed for Mfn1, and Drp1 bands. The L-isoforms activate mitochondrial fusion by interacting with Mfns; the S-isoforms arrest fusion and generate mitochondrial fragments[26-28]. Apoptosis causes Opa1 release into the cytosol, the L-isoforms are proteolytically processed to the S-isoforms and mitochondria are fragmented[28]. HeLa cells treated with antimycin A showed mitochondrial fragmentation. This result suggested that antimycin A accelerates the proteolytic processing of Opa1 L-isoforms to S-isoforms, and mitochondrial fragmentation is triggered by Opa1 inactivation. Our finding agreed with the results reported by Guillery et al.[6] showing that OXPHOS inhibitors induced mild mitochondrial fragmentation.

The electron transport chain (ETC) is the major generator of superoxide species within mitochondria[29]. The ETC is composed of four multi-protein complexes (I–IV) embedded in the inner membrane. Complexes I and II oxidize NADH and FADH2 respectively through transferring the resulting electrons to ubiquinone, which is converted to ubiquinol that carries electrons to Complex III. Complex III transports the electrons across the intermembrane space to cytochrome c, which brings electrons to complex IV. Complex IV then uses the electrons to reduce oxygen to water.

Complexes I and II generate ROS within the mitochondrial matrix while complex III generates ROS into either the matrix or the intermembrane space[30,31,32]. Superoxide generated in the intermembrane space can escape into the cytoplasm through voltage-dependent anion channels[33]. ROS induces cellular machinery dysfunction, and can lead to mitochondrial damage and apoptosis[34,35]. We will focus in the mitochondrial complex III, which generates superoxide during the ubiquinone (Q)-cycle[34,36].

The bc1 complex has a dimeric structure[37] incorporating 4 metal centers in each monomer (hemes bH and bL in cytochrome (cyt) b, heme c1 in cyt c1, and a [2Fe–2S] cluster in the iron–sulfur protein (ISP)), which provide electron transfer chains connecting two quinone processing sites, and three additional catalytic interfaces. The Q-cycle[37] involves the

transfer of two electrons to ubiquinone from complex I and complex II resulting in the reduction of ubiquinone to ubiquinol (QH2). The oxidation of QH2 occurs at the Qo-site, where the two electrons are diverted down two different chains. The first electron goes down the high-potential chain to the Reiske iron-sulfur center protein (RISP). This electron is then transferred to cytochrome c1 and subsequently to cytochrome c. Removal of one electron from ubiquinol results in the unstable radical ubisemiquinone (SQ•) at the Qo-site. Ubisemiquinone can donate its unpaired electron to oxygen to generate superoxide anion, the precursor of reactive oxygen species (ROS). However, under most circumstances the unpaired electron of ubisemiquinone is transferred to the low potential chain hemes groups of cytochrome b (Heme bL and Heme bH). Heme bL is located closer to the intermembrane space and has a lower affinity for electrons than heme bH which is located closer to the matrix side. Ubisemiquinone transfers its electron to bL (Qo-site) to form ubiquinone. Heme bL in turn donates an electron to heme bH (Qi-site), which subsequently reduces another molecule of ubiquinone, forming ubisemiquinone. Because reduction of Q at the Qi-site requires two electrons, the complete Qcycle has to occur twice. After a second round of the Q-cycle, two molecules of ubiquinol have been oxidized on the intermembrane side of the inner membrane, two molecules of cytochrome c have been reduced, and one molecule of ubiquinone has been reduced on the matrix side of the inner membrane (Figure 83).

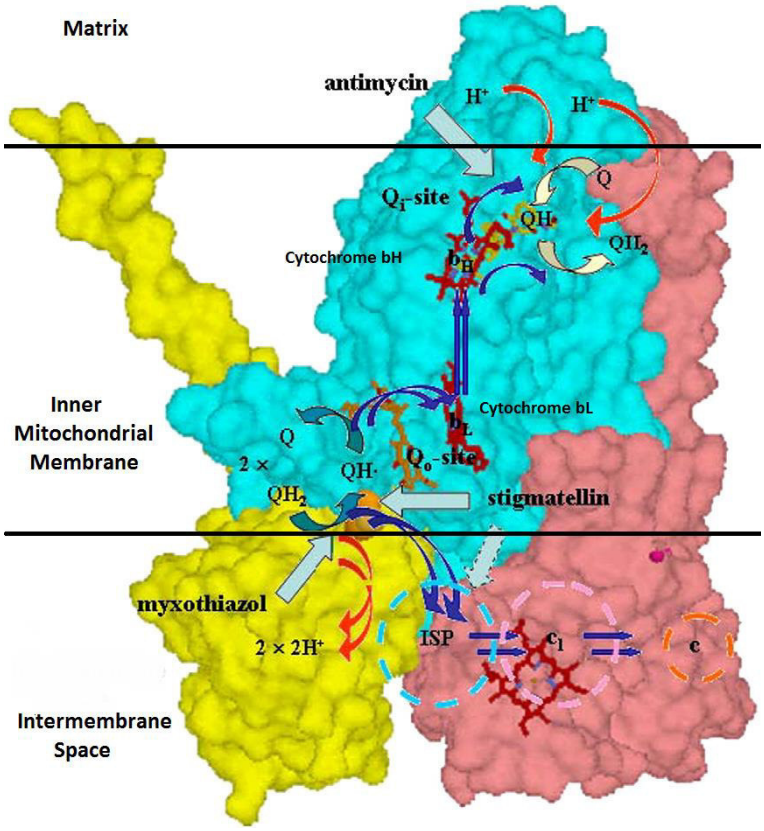

Figure 83. **Mechanism of action of complex III inhibitors.** Adapted from Crofts et al. Biochimica et Biophysica Acta, 2008.

Much of this information has been achieved using specific complex III mitochondrial inhibitors. Muller et al.[31] reported that complex III produces superoxide formation at both sides of the inner mitochondrial membrane. In fact, superoxide anion formation by ubisemiquinone can be prevented by inhibiting electron flux to iron-sulfur protein, cytochrome c1 or cytochrome c. Stigmatellin is an inhibitor that prevents the oxidation of ubiquinol to ubisemiquinone by inhibiting electron flux to the iron sulfur protein[31,34].

The different results obtained for myxothiazol and antimycin A regarding mitochondrial filament elongation can be explained by the different mechanism of action of both compounds by inhibiting complex III. Antimycin A, a Qi site inhibitor, binds to the ubiquinone reduction site in the bc1 complex and prevents the oxidation of heme bH[38]. Antimycin A increases the steady state concentration of ubisemiquinone (SQ•), resulting in an increase in the production of superoxide anion formation within the Q-cycle[39,40]. Myxothiazol, a Qo site inhibitor, prevents ubiquinol oxidation in the bc1 complex, and it is supposed to be a superoxide formation inhibitor. Viola et al[41]. described that myxothiazol or stigmatellin (Qo inhibitors) attenuate the increase in superoxide after transient exposure of cardiac myocytes to hydrogen peroxide. However, antimycin A that inhibits the electron flow at the Qi site, which resides downstream from the Qo site, did not alter the increase in superoxide. These data suggest that the Qo site is the predominant source of superoxide generation[41]. However, there is some controversy over whether myxothiazol induces or inhibits ROS production. Muller et al. and Sun et al. described that myxothiazol allows superoxide anion formation at lower rate than antimycin A[34,42].

Further studies are needed to have more information about the mechanism of action of myxothiazol. For instance, we should measure ROS production in cells incubated with myxothiazol and antimycin A to know if myxothiazol is acting as an inducer or an inhibitor of ROS. Nevertheless, we can be sure that antimycin A produce more superoxide anions than myxothiazol. Han et al. described that antimycin A damages mitochondria, causes ROS production, and induces S phase arrest in HeLa cells[43,44], and recently Xu et al. reported that antimycin A can induce apoptosis through ROS and Ca^{2+} in PC12 cell line[45]. Moreover, Guillery et colleagues[6] described that antimycin A produces mild mitochondrial fragmentation in human skin fibroblasts, which agree with our results. With all these considerations in mind we can suggest that antimycin A by inhibiting complex III causes a strong cellular stress, produces superoxide anions and triggers Opa1 inactivation causing mitochondrial fragmentation and apoptosis. Moreover, myxothiazol inhibits complex III causing a modest stress to the cells, which induced mitochondrial elongation as a cellular response. However, myxothiazol causes mitochondrial fragmentation at 24 h, in C2C12 cells, indicating that higher or continuous cellular stress promotes cellular apoptosis causing mitochondrial fragmentation (data not shown).

We conclude that leflunomide and myxothiazol by depleting the synthesis of pyrimidines promote mitochondrial elongation and uncovered a novel regulatory mechanism of mitochondrial fusion.

5. Leflunomide and myxothiazol promote mitochondrial elongation through p53 activation

Linke et al.[46] reported that ribonucleotide biosynthesis inhibitors, causing depletion of ribonucleotide pools, produced a p53-dependent Go/G1 arrest pathway in normal fibroblasts. The addition of external uridine that restored nucleotides levels reversed p53 up-regulation. In the present PhD thesis we have not analysed the cell cycle when using DHODH and complex III inhibitors. However, the number of cells was quantified, showing that the cells incubated with leflunomide, teriflunomide, myxothiazol and antimycin A undergo cell cycle arrest due to the depletion of pyrimidine synthesis. Moreover, the cell cycle arrest induced in HeLa and C2C12 cells by treatment with leflunomide and teriflunomide was prevented by cotreatment with the salvage metabolite uridine.

Kulawiec et al.[47] described that p53 functions as a checkpoint protein when mitochondria is damaged by mtOXPHOS inhibitors. To maintain the functional state of mitochondria the mito-checkpoint may induce cell death when mitochondrial damage is severe or it may delay cell proliferation when mitochondria is under stress conditions, similar to what occurs in response to DNA damage[48]. Moreover, Khutornenko et al.[49] reported that pyrimidine deficiency triggers a strong p53 response through a specific inhibition of the mitochondrial cytochrome bc1 (the electron chain complex III). We showed that leflunomide and teriflunomide by directly inhibiting the DHODH step of pyrimidine synthesis up-regulated p53 mRNA levels in HeLa cells. Subsequent uridine addition, which reversed the deficiency in pyrimidine biosynthesis, prevented p53 mRNA levels induction. Moreover, leflunomide increases p53 protein levels in HeLa, C2C12, MEFwt, MEF Mfn1$^{-/-}$ and MEF Mfn2$^{-/-}$ cells and the addition of uridine prevented p53 up-regulation, confirming that the mechanism of action of leflunomide was the same in MEFwt and MEFs deficient in Mfn1 or Mfn2 cells. Myxothiazol also confirmed the link between p53 and the deficiency of pyrimidines. Myxothiazol induced p53 mRNA and protein levels and cotreatment with external uridine was able to prevent the p53 up-regulation in HeLa cells.

In response to stress signals the levels of p53 protein are rapidly increased and p53 activity is augmented after phosphorylation at the Ser 15 residue[50] resulting in the up-regulation of downstream genes. Moreover, stress signals reduced interaction between p53 and its negative regulator, the oncoprotein Mdm2[51], by phosphorylating p53 at Ser15 and Ser20. Phosphorylation impairs the ability of MDM2 to bind p53, promoting both the accumulation and activation of p53[51,52]. Our results confirmed that leflunomide and

myxothiazol by causing a pyrimidine deficiency produced a cell stress response. Consequently, p53 was phosphorylated at Ser15 producing p53 activation and accumulation in HeLa and C2C12 cells. Subsequent uridine addition, which reversed the cell stress by restoring pyrimidine nucleotides levels, prevented the phosphorylation of p53 at Ser15.

Our results indicate that the deficiency in pyrimidines, through DHODH or complex III inhibitors, causes a stress signal that triggers p53 activation by phosphorylating p53 at Ser15, and produces accumulation and activation of p53 in HeLa and C2C12 cells.

Wang et al. described[53,54] that Mfn2 is a target gene of p53. They reported that there is a p53 binding site in the Mfn2 promoter and showed that p53 induces Mfn2 gene expression in HepG2 and Hep3B cells. In order to confirm the role of p53 we wanted to demonstrate that the depletion of pyrimidine pools, by complex III or DHODH inhibitors, would cause cell stress and trigger p53 response. p53 would modulate mitochondrial proteins involved in fusion and fission events and would promote mitochondrial elongation to overcome the induced stress. For these reasons, and to assess whether p53 status affected mitochondrial gene and proteins expression U87MG (TP53 wild-type) and T98G (TP53 mutant, M237I) human glioma cell lines were incubated with leflunomide. Leflunomide was able to increase Mfn2 and p53 levels in both cell lines, indicating that the mutation in T98G cells did not prevent the up-regulation in p53 protein levels. T98G cells have been pondered as a p53 mutated cell line[55]. However, in a catalogue of somatic mutations in cancer (COSMIC)[56] T98G cells have been pondered as a wild type cell line. Thus, there is a controversy whether T98G cells are considered a p53 mutated cell line or not, and in consequence, we can not drew solid conclusions on the relationship between p53 and Mfn2.

In a second approach, knockdown of p53 expression was done. In HeLa cells transfected with control siRNA and incubated with leflunomide Mfn2 mRNA and protein levels were up-regulated. However, HeLa p53 knockdown cells treated with leflunomide did not show increase in Mfn2 mRNA and protein levels, although the basal levels of Mfn2 were up-regulated. Moreover, Mfn1 up-regulation was not prevented in HeLa p53 knockdown cells incubated with leflunomide, and Mfn1 basal levels were also increased. These results suggested that p53 down-regulation increases the basal levels of Mfn2 and Mfn1 in HeLa cells. In addition, Mfns were up-regulated in C2C12 cells transfected with control siRNA and treated with leflunomide. Nevertheless, C2C12 p53 knockdown cells were not able to increase Mfns levels in response to leflunomide, despite Mfn1 basal levels were up-regulated as in HeLa cells. Drp1 was 30% reduced in C2C12 transfected with control siRNA with leflunomide and 15% reduced in C2C12 p53 knockdown. These results indicate that p53 down-regulation is able to block leflunomide induced up-regulation of Mfn2 and Mfn1 expression, and partially blocks Drp1 down-regulation in leflunomide-treated C2C12 cells, although the basal levels of Mfn1 in p53 knockdown C2C12 cells increases. Based on the fact

that these studies were performed in confluent cells, and it has been reported that cellular growth rate and density-dependent inhibition of growth is dependent of the status of p53 expression[57], we think that p53 knockdown confluent cells can activate downstream genes to compensate the absence of p53. Therefore, further studies are required in non-confluent p53-deficient HeLa cells. It is of interest to notice that HeLa cells transfected for 24h with siRNA for p53, which did not reach confluence, did not show an increase for Mfn2 basal levels compared with control ones (See figure 80 in results and discussion).

In addition to its transcriptional function, p53 has distinct and direct roles in mitochondria and plays two different pathways, survival or death. p53 has been linked to mitochondrial function regulating apoptosis/necrosis, autophagy/mitophagy, and mitochondrial quality control[58]. Therefore, it is possible that p53 can also control mitochondria by controlling mitochondrial dynamics.

We conclude that the depletion of pyrimidine pools, by complex III or DHODH inhibitors, causes cell stress, and triggers p53 accumulation and activation by p53 phosphorylation at Ser15 causing cell cycle arrest. We suggest that up-regulation of Mfns and down-regulation of Drp1 is triggered by p53. The modulation of mitochondrial proteins involved in fusion and fission events promotes mitochondrial elongation to confer stress resistance on cells. The addition of external uridine is able to block the antiproliferative effects and the up-regulation of p53 and Mfns proteins caused by leflunomide and myxothiazol. Therefore, we propose that mitochondrial elongation represents an adaptive response against stress (Figure 84).

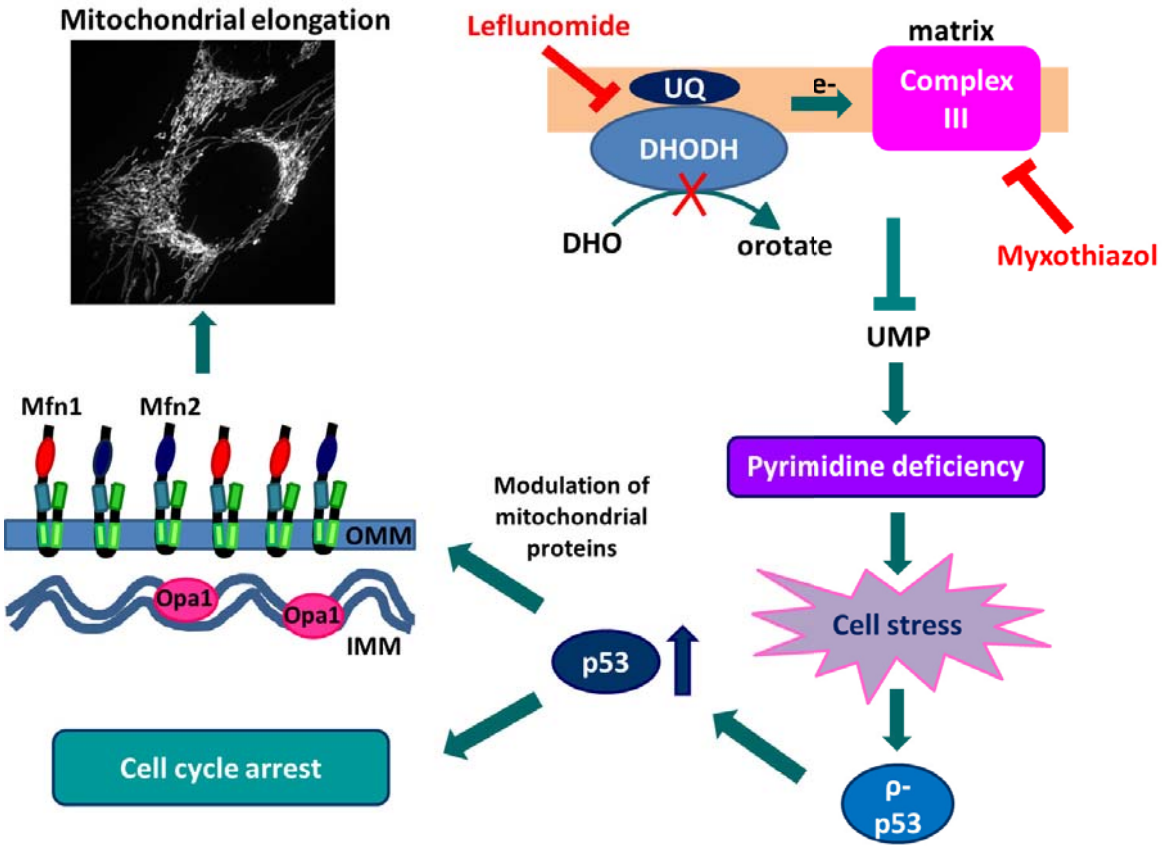

Figure 84. **Leflunomide and myxothiazol promotes mitochondrial elongation through p53 activation**

To confirm these results we need to perform further experiments in p53 knockout cells to be sure that p53 status modulates mitochondrial proteins involved in mitochondrial dynamics. Moreover, we want to know if cells lacking p53 have Mfns protein basal levels up-regulated as an adaptive response.

REFERENCES

1 Bach, D. *et al.* Expression of Mfn2, the Charcot-Marie-Tooth neuropathy type 2A gene, in human skeletal muscle: effects of type 2 diabetes, obesity, weight loss, and the regulatory role of tumor necrosis factor alpha and interleukin-6. *Diabetes* **54**, 2685-2693, doi:54/9/2685 [pii] (2005).

2 Hwang, S. J. & Kim, W. Mitochondrial Dynamics in the Heart as a Novel Therapeutic Target for Cardioprotection. *Chonnam medical journal* **49**, 101-107, doi:10.4068/cmj.2013.49.3.101 (2013).

3 Babbar, M. & Sheikh, M. S. Metabolic Stress and Disorders Related to Alterations in Mitochondrial Fission or Fusion. *Molecular and cellular pharmacology* **5**, 109-133 (2013).

4 Fox, R. I. *et al.* Mechanism of action for leflunomide in rheumatoid arthritis. *Clin Immunol* **93**, 198-208, doi:10.1006/clim.1999.4777S1521-6616(99)94777-0 [pii] (1999).

5 Alcorn, N., Saunders, S. & Madhok, R. Benefit-risk assessment of leflunomide: an appraisal of leflunomide in rheumatoid arthritis 10 years after licensing. *Drug safety : an international journal of medical toxicology and drug experience* **32**, 1123-1134, doi:10.2165/11316650-000000000-00000 (2009).

6 Guillery, O. *et al.* Modulation of mitochondrial morphology by bioenergetics defects in primary human fibroblasts. *Neuromuscular disorders : NMD* **18**, 319-330, doi:10.1016/j.nmd.2007.12.008 (2008).

7 Liu, X. & Hajnoczky, G. Altered fusion dynamics underlie unique morphological changes in mitochondria during hypoxia-reoxygenation stress. *Cell Death Differ* **18**, 1561-1572, doi:10.1038/cdd.2011.13 (2011).

8 Yue, W. *et al.* A small natural molecule promotes mitochondrial fusion through inhibition of the deubiquitinase USP30. *Cell Res*, doi:10.1038/cr.2014.20 (2014).

9 Nakamura, N. & Hirose, S. Regulation of mitochondrial morphology by USP30, a deubiquitinating enzyme present in the mitochondrial outer membrane. *Molecular biology of the cell* **19**, 1903-1911, doi:10.1091/mbc.E07-11-1103 (2008).

10 Rossignol, R. *et al.* Energy substrate modulates mitochondrial structure and oxidative capacity in cancer cells. *Cancer Res* **64**, 985-993 (2004).

11 Rambold, A. S., Kostelecky, B., Elia, N. & Lippincott-Schwartz, J. Tubular network formation protects mitochondria from autophagosomal degradation during nutrient starvation. *Proc Natl Acad Sci U S A* **108**, 10190-10195, doi:10.1073/pnas.1107402108 (2011).

12 Tondera, D. *et al.* SLP-2 is required for stress-induced mitochondrial hyperfusion. *EMBO J* **28**, 1589-1600, doi:10.1038/emboj.2009.89emboj200989 [pii] (2009).

13 Liesa, M. & Shirihai, O. S. Mitochondrial dynamics in the regulation of nutrient utilization and energy expenditure. *Cell Metab* **17**, 491-506, doi:10.1016/j.cmet.2013.03.002 (2013).

14 Chen, H. *et al.* Mitofusins Mfn1 and Mfn2 coordinately regulate mitochondrial fusion and are essential for embryonic development. *J Cell Biol* **160**, 189-200, doi:10.1083/jcb.200211046 (2003).

15 Ishihara, N., Eura, Y. & Mihara, K. Mitofusin 1 and 2 play distinct roles in mitochondrial fusion reactions via GTPase activity. *J Cell Sci* **117**, 6535-6546, doi:10.1242/jcs.01565 (2004).

16 Cipolat, S., Martins de Brito, O., Dal Zilio, B. & Scorrano, L. OPA1 requires mitofusin 1 to promote mitochondrial fusion. *Proc Natl Acad Sci U S A* **101**, 15927-15932, doi:10.1073/pnas.0407043101 (2004).

17 Ishihara, N., Jofuku, A., Eura, Y. & Mihara, K. Regulation of mitochondrial morphology by membrane potential, and DRP1-dependent division and FZO1-dependent fusion reaction in mammalian cells. *Biochem Biophys Res Commun* **301**, 891-898 (2003).

18 Legros, F., Lombes, A., Frachon, P. & Rojo, M. Mitochondrial fusion in human cells is efficient, requires the inner membrane potential, and is mediated by mitofusins. *Molecular biology of the cell* **13**, 4343-4354, doi:10.1091/mbc.E02-06-0330 (2002).

19 Chen, H., Chomyn, A. & Chan, D. C. Disruption of fusion results in mitochondrial heterogeneity and dysfunction. *J Biol Chem* **280**, 26185-26192, doi:10.1074/jbc.M503062200 (2005).
20 Cherwinski, H. M. *et al.* Leflunomide interferes with pyrimidine nucleotide biosynthesis. *Inflammation research : official journal of the European Histamine Research Society ... [et al.]* **44**, 317-322 (1995).
21 Zielinski, T., Zeitter, D., Muller, S. & Bartlett, R. R. Leflunomide, a reversible inhibitor of pyrimidine biosynthesis? *Inflammation research : official journal of the European Histamine Research Society ... [et al.]* **44 Suppl 2**, S207-208 (1995).
22 Herrmann, M. L., Schleyerbach, R. & Kirschbaum, B. J. Leflunomide: an immunomodulatory drug for the treatment of rheumatoid arthritis and other autoimmune diseases. *Immunopharmacology* **47**, 273-289 (2000).
23 Schwartsmann, G. P., G.J.; Laurensse, E.; De Wall, F.C.; Pinedo, H.M. Schedule-dependency of growth-inhibitory and antipyrimidine effects. *Biochem. Pharmacol.* **37**, 3257-3266 (1988).
24 Tufi, R. *et al.* Enhancing nucleotide metabolism protects against mitochondrial dysfunction and neurodegeneration in a PINK1 model of Parkinson's disease. *Nat Cell Biol* **16**, 157-166, doi:10.1038/ncb2901 (2014).
25 Fang, J. *et al.* Dihydro-orotate dehydrogenase is physically associated with the respiratory complex and its loss leads to mitochondrial dysfunction. *Biosci Rep* **33**, doi:10.1042/BSR20120097 (2013).
26 Duvezin-Caubet, S. *et al.* Proteolytic processing of OPA1 links mitochondrial dysfunction to alterations in mitochondrial morphology. *J Biol Chem* **281**, 37972-37979, doi:10.1074/jbc.M606059200 (2006).
27 Ishihara, N., Fujita, Y., Oka, T. & Mihara, K. Regulation of mitochondrial morphology through proteolytic cleavage of OPA1. *EMBO J* **25**, 2966-2977, doi:10.1038/sj.emboj.7601184 (2006).
28 Griparic, L., Kanazawa, T. & van der Bliek, A. M. Regulation of the mitochondrial dynamin-like protein Opa1 by proteolytic cleavage. *J Cell Biol* **178**, 757-764, doi:10.1083/jcb.200704112 (2007).
29 Turrens, J. F. Mitochondrial formation of reactive oxygen species. *J Physiol* **552**, 335-344, doi:10.1113/jphysiol.2003.049478 (2003).
30 Brand, M. D. The sites and topology of mitochondrial superoxide production. *Experimental gerontology* **45**, 466-472, doi:10.1016/j.exger.2010.01.003 (2010).
31 Muller, F. L., Liu, Y. & Van Remmen, H. Complex III releases superoxide to both sides of the inner mitochondrial membrane. *J Biol Chem* **279**, 49064-49073, doi:10.1074/jbc.M407715200 (2004).
32 Murphy, M. P. How mitochondria produce reactive oxygen species. *Biochem J* **417**, 1-13, doi:10.1042/BJ20081386 (2009).
33 Han, D., Antunes, F., Canali, R., Rettori, D. & Cadenas, E. Voltage-dependent anion channels control the release of the superoxide anion from mitochondria to cytosol. *J Biol Chem* **278**, 5557-5563, doi:10.1074/jbc.M210269200 (2003).
34 Sun, J. & Trumpower, B. L. Superoxide anion generation by the cytochrome bc1 complex. *Arch Biochem Biophys* **419**, 198-206 (2003).
35 Raha, S. & Robinson, B. H. Mitochondria, oxygen free radicals, and apoptosis. *American journal of medical genetics* **106**, 62-70, doi:10.1002/ajmg.1398 (2001).
36 Chandel, N. S. Mitochondrial complex III: an essential component of universal oxygen sensing machinery? *Respiratory physiology & neurobiology* **174**, 175-181, doi:10.1016/j.resp.2010.08.004 (2010).
37 Crofts, A. R. *et al.* The Q-cycle reviewed: How well does a monomeric mechanism of the bc(1) complex account for the function of a dimeric complex? *Biochim Biophys Acta* **1777**, 1001-1019, doi:10.1016/j.bbabio.2008.04.037 (2008).

38 Turrens, J. F., Alexandre, A. & Lehninger, A. L. Ubisemiquinone is the electron donor for superoxide formation by complex III of heart mitochondria. *Arch Biochem Biophys* **237**, 408-414 (1985).

39 Chen, Q., Vazquez, E. J., Moghaddas, S., Hoppel, C. L. & Lesnefsky, E. J. Production of reactive oxygen species by mitochondria: central role of complex III. *J Biol Chem* **278**, 36027-36031, doi:10.1074/jbc.M304854200 (2003).

40 Gille, L. & Nohl, H. The ubiquinol/bc1 redox couple regulates mitochondrial oxygen radical formation. *Arch Biochem Biophys* **388**, 34-38, doi:10.1006/abbi.2000.2257 (2001).

41 Viola, H. M. & Hool, L. C. Qo site of mitochondrial complex III is the source of increased superoxide after transient exposure to hydrogen peroxide. *J Mol Cell Cardiol* **49**, 875-885, doi:10.1016/j.yjmcc.2010.07.015 (2010).

42 Muller, F. L., Roberts, A. G., Bowman, M. K. & Kramer, D. M. Architecture of the Qo site of the cytochrome bc1 complex probed by superoxide production. *Biochemistry* **42**, 6493-6499, doi:10.1021/bi0342160 (2003).

43 Han, Y. H., Kim, S. H., Kim, S. Z. & Park, W. H. Antimycin A as a mitochondria damage agent induces an S phase arrest of the cell cycle in HeLa cells. *Life Sci* **83**, 346-355, doi:10.1016/j.lfs.2008.06.023 (2008).

44 Han, Y. H., Kim, S. H., Kim, S. Z. & Park, W. H. Intracellular GSH levels rather than ROS levels are tightly related to AMA-induced HeLa cell death. *Chem Biol Interact* **171**, 67-78, doi:10.1016/j.cbi.2007.08.011 (2008).

45 Xu, L., Xu, J., Liu, S. & Yang, Z. Induction of apoptosis by antimycin A in differentiated PC12 cell line. *Journal of applied toxicology : JAT*, doi:10.1002/jat.2890 (2013).

46 Linke, S. P., Clarkin, K. C., Di Leonardo, A., Tsou, A. & Wahl, G. M. A reversible, p53-dependent G0/G1 cell cycle arrest induced by ribonucleotide depletion in the absence of detectable DNA damage. *Genes & development* **10**, 934-947 (1996).

47 Kulawiec, M., Ayyasamy, V. & Singh, K. K. p53 regulates mtDNA copy number and mitocheckpoint pathway. *Journal of carcinogenesis* **8**, 8, doi:10.4103/1477-3163.50893 (2009).

48 Riley, T., Sontag, E., Chen, P. & Levine, A. Transcriptional control of human p53-regulated genes. *Nature reviews. Molecular cell biology* **9**, 402-412, doi:10.1038/nrm2395 (2008).

49 Khutornenko, A. A. *et al.* Pyrimidine biosynthesis links mitochondrial respiration to the p53 pathway. *Proc Natl Acad Sci U S A* **107**, 12828-12833, doi:10.1073/pnas.0910885107 (2010).

50 Buschmann, T. *et al.* Jun NH2-terminal kinase phosphorylation of p53 on Thr-81 is important for p53 stabilization and transcriptional activities in response to stress. *Mol Cell Biol* **21**, 2743-2754, doi:10.1128/MCB.21.8.2743-2754.2001 (2001).

51 Shieh, S. Y., Ikeda, M., Taya, Y. & Prives, C. DNA damage-induced phosphorylation of p53 alleviates inhibition by MDM2. *Cell* **91**, 325-334 (1997).

52 Tibbetts, R. S. *et al.* A role for ATR in the DNA damage-induced phosphorylation of p53. *Genes & development* **13**, 152-157 (1999).

53 Wang, W. *et al.* Mitofusin-2 is a novel direct target of p53. *Biochem Biophys Res Commun* **400**, 587-592, doi:10.1016/j.bbrc.2010.08.108 (2010).

54 Wang, W. *et al.* Hepatitis B virus X protein inhibits p53-mediated upregulation of mitofusin-2 in hepatocellular carcinoma cells. *Biochem Biophys Res Commun* **421**, 355-360, doi:10.1016/j.bbrc.2012.04.015 (2012).

55 Pena-Rico, M. A. *et al.* TP53 induced glycolysis and apoptosis regulator (TIGAR) knockdown results in radiosensitization of glioma cells. *Radiotherapy and oncology : journal of the European Society for Therapeutic Radiology and Oncology* **101**, 132-139, doi:10.1016/j.radonc.2011.07.002 (2011).

56 *COSMIC: Catalogue Of Somatic Mutations In Cancer*.

57 Meerson, A., Milyavsky, M. & Rotter, V. p53 mediates density-dependent growth arrest. *FEBS Lett* **559**, 152-158, doi:10.1016/S0014-5793(04)00027-4 (2004).

58 Wang, D. B., Kinoshita, C., Kinoshita, Y. & Morrison, R. S. p53 and mitochondrial function in neurons. *Biochim Biophys Acta*, doi:10.1016/j.bbadis.2013.12.015 (2014).

CONCLUSIONS

CONCLUSIONS

The principal conclusions that turn out from chapter 2 are:

1. A cell-based assay method to screen positive modulators of Mfn2 has been established in the laboratory. Mfn2P 14 clone cell line that stably expresses luciferase under the control of 2 kb (region -1982/+54) of the human Mfn2 promoter was generated. This is a rapid, efficient, sensitive and reproducible method to screen possible activators of Mfn2 promoter in HTS assays.

2. Leflunomide was identified as a positive hit from the HTS of the Prestwick Chemical Library, and was validated as a positive modulator of Mfn2 expression. Moreover, teriflunomide, the active metabolite of leflunomide, was also validated as a positive modulator of Mfn2 gene expression.

3. Leflunomide causes mitochondrial elongation in HeLa, C2C12 and MEFwt cells by modulating mitochondrial membrane proteins involved in mitochondrial dynamics such as Mfn2, Mfn1, Opa1 and Drp1. Our data indicate that mitochondrial elongation caused by leflunomide depends on both Mfn1 and Mfn2 mitochondrial outer membrane proteins.

4. Leflunomide and teriflunomide inhibit dihydroorotate dehydrogenase (DHODH), and consequently the *de novo* synthesis of pyrimidines. The addition of external uridine reverses the deficiency in pyrimidine synthesis, and blocks the alterations in mitochondrial fusion protein expression. These results suggest that mitochondrial elongation represents an adaptive response against cell stress induced by inhibition of pyrimidine biosynthesis.

5. Myxothiazol, a complex III inhibitor, also causes a deficiency in pyrimidines by indirect inhibition of DHODH. Moreover, myxothiazol promotes mitochondrial elongation in HeLa, C2C12, and MEFwt cells by increasing Mfn2, Mfn1 and Opa1 mitochondrial fusion proteins and decreasing the fission protein Drp1. These results confirm that mitochondria elongate in response to cell stress induced by inhibition of pyrimidine biosynthesis.

6. The mechanism by which leflunomide, teriflunomide and myxothiazol enhance Mfn2 and Mfn1 expression may depend on p53 activation. These compounds inhibit the *de novo* synthesis of pyrimidines and cause cell stress producing activation and accumulation of p53, which causes cell cycle arrest. Subsequent uridine addition, restoring pyrimidine nucleotides levels, prevented phosphorylation of p53 at Ser15 and p53 up-regulation. We suggest that p53 promotes mitochondrial elongation to confer resistance to cell stress.

MATERIALS AND METHODS

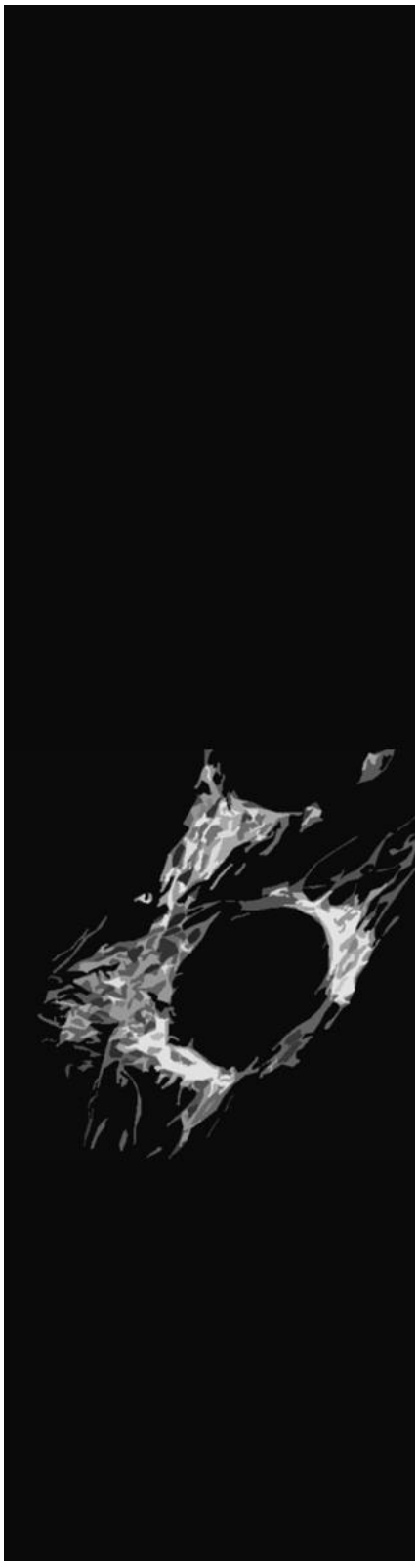

MATERIALS AND METHODS

1. Instrumentation

1.1. General basic instrumentation

Instrument	Model
Cell Incubator	Thermo Electron Corporation, Model 3121, Forma Series II, Water Jacketed CO_2 Incubator, HEPA class 100 filter
Laminar flow hood	Telstar, BIO II A Cabina de seguridad biológica
Centrifuge	Beckman Coulter Allegra^{TM} 21 Centrifuge
Orbital shakers	Heidolph instruments, Unimax 1010
Thermomixer	Eppendorf, Thermomixer confort
Microscopy	Nikon Eclipse TS 100
Centrifuge	Eppendorf, Centriguge 5415 R, centrifuge 5415 D
Spectrophotometer	Thermo scientific, NanoDrop 2000, UV-Vis sphectrophotometer
Luminometer	Berthold Techonologies, Lumat LB 9507
Thermocycler qPCR	Applied Biosystems, Abi-Prism 7900 HT

Table3. **General basic instrumentation**

2. Cell Culture

Cultured cells are kept in the most favourable conditions and are grown under sterile conditions to maintain a healthy state and to minimize risk contamination. The common contaminants are bacteria, mycoplasma and fungi, which can alter the physiology of cells. Consequently, cells manipulation has been performed in a laminar flow hood, which prior to and after use must be kept under UV irradiation for 15 minutes and cleaned with 70% ethanol to preserve sterile conditions. Working hands cannot pass over cells or culture solutions. All reagents, solutions, fungible material and equipment that come in contact with the cells must be sterile. They can be sterilized using autoclave 20 minutes at 120 ^{o}C, UV irradiation or 70% ethanol. The cell culture material such as flask, culture plates and plastic pippetes, as well as, solutions (culture media) have been purchased as sterile material. Once the experiment ends, all biologic materials should be properly handled: cells are killed with bleach and the material used and the hood again sterilized.

2.1. Cell lines

Immortalized cells, also known as transformed cells, continue to grow and divide indefinitely in vitro for as long as the correct culture conditions are maintained. All the cells used in the present thesis if is not specified were grown in Dulbecco Modified Eagle's Medium (DMEM, Ref 41966, Gibco, Invitrogen) with 10% Fetal Bovine Serum (FBS, Gibco, Ref 10270-106), 25 mM of HEPES (Panreac), 100 U/mL and 100 µg/mL of penicillin/streptomycin (Ref 15140-122, Gibco, Invitrogen) respectively, at 37 ^{o}C in a humidified atmosphere of 5% CO_2/95% air to maintain the pH of the medium. The medium is renewed three times per week. Since these cells show highly proliferating rates, the cultures might be subcultured at least twice a week.

2.1.1. HeLa cells

HeLa cells are the oldest and most commonly used immortal human cell line, derived from cervical cancer cells from Henrietta Lacks. The cells were propagated by George Otto Gey shortly before Lacks died of her cancer in 1951. Henrietta Lacks (HeLa) cells are human epithelial cells from a cervical carcinoma transformed by human papillomavirus 18 (HPV18)[1].This was the first human cell line to prove successful in vitro. HeLa cells are adherent cells (they stick to surface) that maintain contact inhibition *in vitro*. They spread out across the culture flask and when two adjacent cells touch each other, this contact signals allows them to stop growing. HeLa cells have been used until 25 passes.

2.1.2. HeLa Mfn2P clones

In the laboratory several human cell clones that stably express luciferase under the control of 2 kb (region -1982/+54) of the human Mfn2 promoter were generated by Dr. David Sebastián. These clones were grown in the medium described above and 7.5 ml Geneticin 50 mg/mL (Gibco, Ref. 10131-027) were added in the medium to select the clones that integrate the construct containing the Mfn2 promoter, the luciferase reporter gene and a selection marker. HeLa M2P clones cells have been used until 30 passes.

2.1.3. HeLa cells expressing mtDsRed

HeLa mtDsRed were generated from HeLa stably expressing mitochondrial matrix-targeted DsRed (mtDsRed) protein. mtDsRed is directed towards mitochondrial matrix as a result of an importing mitochondrial sequence of complex IV subunit, human Cox8a to N-terminal (mtDsRed). HeLa mtDsRed cells have been used until 25 passes.

2.1.4. C2C12 cells

C2C12 cells were generated by Blau and collaborators[2] from mouse myoblasts C2 generated by Yaffe and Saxel[3]. C2C12 cells are available in the American Type Culture Collection (ATCC). C2C12 cells have the capacity to differentiate to muscular cells or multinucleated myotubes. C2C12 cells have been used until 20 passes.

2.1.5. C2C12 cells expressing mtDsRed

C2C12 mtDsRed were generated in our lab by Dr. Marc Liesa from C2C12 stably expressing mtDsRed dye using lentivirus transduction (MOI = 200 TU/cell). mtDsRed is directed towards mitochondrial matrix as a result of an importing mitochondrial sequence of complex IV subunit, human Cox8a to N-terminal (mtDsRed). C2C12 mtDsRed cells have been used until 25 passes.

2.1.6. MEFs, Mfn1 KO and Mfn2 KO MEFs cells

Mouse embryonic fibroblasts (MEFs), Mfn1 KO and Mfn2 KO MEFs were a gift from D.C. Chan (Division of Biology, California Institute of Technology, UA). MEFs, Mfn1 KO and Mfn2 KO MEFs cells have been used until 30 passes.

2.1.7. MEFs, Mfn1 KO and Mfn2 KO MEFs cells expressing mtDsRed

MEFs, Mfn1 KO and Mfn2 KO MEFs cells expressing mtDsRed were generated by Dr. Juan Pablo Muñoz from MEFs, Mfn1 KO and Mfn2 KO MEFs cells stably expressing mtDsRed. mtDsRed is directed towards mitochondrial matrix as a result of an importing mitochondrial sequence of complex IV subunit, human Cox8a to N-terminal (mtDsRed). MEFs, Mfn1 KO and Mfn2 KO MEFs cells expressing mtDsRed have been used until 35 passes.

2.1.8. U87MG and T98G myoblastoma cell lines

U87MG (TP53 wild-type) and T98G (TP53 mutant, M237I) human glioma cell lines were obtained from the Dr. Avelina Tortosa group (Unitat de Fisiologia, Dept. Ciències Fisiològiques II and Department IMQ, Campus de Ciències de la Salut) and cultured with DMEM with 10% fetal calf serum (FCS) supplemented with L-glutamine (2 mM) and penicillin–streptomycin (100 U/ml–100 lg/ml) in a humidified atmosphere of 5% CO_2/95% air to maintain the pH of the medium.

2.2 Culture media

DMEM (Gibco-Invitogen) with 4.5 g/L of D-glucose, L-glutamine and pyruvate have been used as basal medium for cultured cells in the present thesis. The culture media must be kept at 4 ^{o}C until the expiration date. Once supplied with additional components, media should not be stored for more than one month at 4 ^{o}C, since the components can precipitate or degrade.

The medium for cell growth is prepared with 10% of FBS (Gibco), 25 mM of HEPES (Panreac) and penicillin/streptomycin (Invitrogen) at 100 U/mL / 100 µg/mL, respectively. FBS provides to the medium a high content of embryonic growth promoting factors that are necessary for cellular proliferation. FBS must be inactivated prior to use, the treatment is performed at 56 ^{o}C for 30 minutes. FBS must be kept at -20 ^{o}C. HEPES (4-(2-hydroxyethyl)-1-piperazineethanesulfonic acid) 1.25 M pH 7.4 is used as buffering agent in cell culture media, providing a buffer solution additional to the bicarbonate of the medium. HEPES must be keep at -20 ^{o}C. Penicillin and streptomycin are two different types of antibiotics that prevent bacterial growth and minimize culture contamination. Penicillin inhibits the synthesis of the bacterial growth and streptomycin inhibits bacterial protein synthesis. Both antibiotics must be keep at -20 ^{o}C.

Culture media needs to be replaced often, the frequency increases with the cell metabolic rate. Normally culture media is supplied with a pH indicator that change color media from red to yellow when the media needs to be refreshed. Pre-heating (37 ^{o}C) the media and other solutions before use is recommended to minimize the exposure of cells to stressful conditions.

2.3. Maintenance and subculture

The number of cells growing in a common space cannot exceed a certain maximum, which is determined by the confluence on the surface. Once the maximum limit is reached, the culture must be divided by splitting. This process is known as subculturing or passaging, the medium is removed and the cells are transferred from the previous cell plate into a new cell plate with fresh growth medium, enabling the further propagation of the cell line.

Cells are seeded on 10 cm dishes and attached to the surface through several proteins belonging to the cellular membrane. Maintenance cultures are normally plated at low confluences, with 10% being the minimal percentage recommended. Once cells reach a threshold confluence (90 %), the culture needs to be subcultured by splitting and seeding into a new dish:

1. Cell culture medium and trypsin are pre-warmed at 37 ^{o}C bath.

2. Cell culture media is removed and discarded from the culture plate.

3. Cells are washed using phosphate buffered saline (PBS) (approximately 5 mL per 10 cm cell culture dish). The wash solution is added to the side of the cell plate gently, to avoid cell layer disturbing.

Note: The wash step removes any traces of serum, calcium, and magnesium that would inhibit the action of the trypsin reagent.

4. The wash solution is removed and discarded from the culture plate.

5. Trypsin is added to the side of the flask (1 mL per 10 cm cell culture dish) and must cover the entire cell layer. Trypsin is a serine protease that disrupts the proteins bonding the cultured cells to the dish.

6. The culture plate is incubated at 37 ^{o}C for 3 minutes in the incubator.

7. Once the cells have been detached, 10 mL of pre-warmed growth medium is added to the cell plate. The medium is dispersed by pipetting over the cell layer surface several times to homogenize.

8. Transfer the cells to a 15 mL conical tube and centrifuge then at 2000 rpm for 3 minutes.

Note: this step is only needed in cell lines that are slightly sensitive to trypsin. In other cases, the dilution with the media is enough.

9. The supernatant is removed and the cell pellet is resuspended in 10 mL of pre-warmed complete growth medium. 12 µL of cell suspension are removed for counting.

10. The cells are counted in a Neubauer chamber.

11. The cell suspension is diluted to the seeding density desired. The seeding density is a function of the time and amounts in which cells are needed.

12. Finally the cells are returned to the incubator.

2.4. Freezing and defrosting

Both freezing and thawing out procedures must be carefully performed to minimize the risk of cellular death. The best method for cryopreserving cultured cells is storing them in liquid nitrogen in complete medium in the presence of a cryoprotective agent, such as dimethylsulfoxide (DMSO). Cryoprotective agents reduce the freezing point of the medium and also allow a slower cooling rate, greatly reducing the risk of ice crystal formation, which can damage cells and cause cell death. The cultured cells must be freezed at a high

concentration and at as low a passage number as possible to have sufficient stock and preserve their original characteristics, respectively. The cells must be 90% confluence in the culture plate and viable before freezing.

Procedure for freezing cells:

1. The cells are detached from the culture plate using trypsin as it has been described in procedure 1.3.

2. Once the cells have been detached, 10 mL of pre-warmed growth medium is added to the cell plate. The medium is dispersed by pipetting over the cell layer surface several times to homogenize.

3. The cells are transferred to a 15 mL conical tube and centrifuged at 1300 rpm for 5 minutes at RT.

4. The supernatant is removed without disturbing the cell pellet, and then the cell pellet is resuspended in 5 mL of complete growth medium with 10% DMSO sterile (v:v). The exposure of the cells to the solution of DMSO at room temperature should be kept to a minimum for toxic reasons.

5. The cell suspension is dispensed in 5 aliquots of 1 mL into sterile cryogenic storage vials, which are on ice.

6. The cells are frozen at -80°C in the freezer for 24 hours.

7. The next day the cells are immersed in the liquid nitrogen tank. The cells can be stored in liquid nitrogen for years.

Defrosting must be rapidly performed to minimize the exposure of cells to DMSO at RT to minimize the risk of cellular death.

Procedure for defrosting cells:

1. Cell culture medium is pre-warmed at 37 ^{o}C bath.

2. The cryogenic storage vial is taken from the liquid nitrogen tank and defrosted in a 37 ^{o}C bath for 1 minute.

3. The cell suspension is then diluted in a 15 mL conical tube containing 10 mL of pre-warmed fresh complete growth medium, homogenized and centrifuged at 1300 rpm for 5 minutes at RT.

4. The supernatant is removed without disturbing the cell pellet to eliminate DMSO, and then the cell pellet is resuspended in 10 mL of pre-warmed fresh complete growth medium.

5. Finally, the cells are plated in 10 cm cell culture dish.

2.5. Cell counting

The cells are counted using a Neubauer chamber. The two semi-reflective rectangles are the counting chambers. Each chamber is engraved with a laser-etched grid of perpendicular lines. The device is carefully crafted so that the area bounded by the lines is 1 mm^2, and the depth of the chamber is 0.1 mm, making possible to count the number of cells in a specific volume of fluid, and thereby calculate the concentration of cells in the mixture the sample come from.

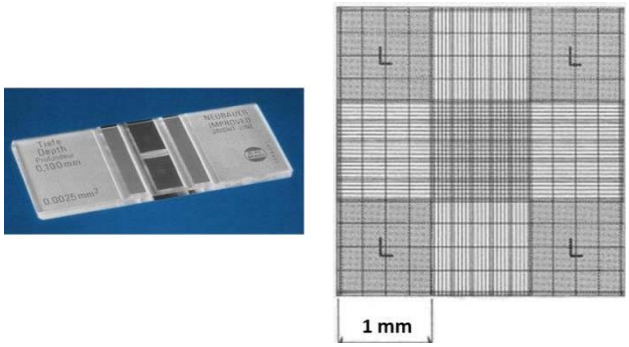

***Figure 85*. Neubauer chamber**

Procedure for counting cells in a Neubauer chamber:

1. Once the cells have been detached using trypsin, 10 mL of pre-warmed growth medium is added to the cell plate, and the cell suspension is homogenized (proceed with steps 1 to 7 from the procedure 1.3).

2. The cell suspension (12 µL) is applied between the coverslip 24 x 50 mm (Menzel-Glaser) and the Neubauer chamber (Neubauer improved de Brand Gmbh). The cell suspension is applied to the edge of the coverslip to be sucked into the void by capillary action which completely fills the chamber with the sample.

3. The number of cells in the chamber can be determined by direct counting using a microscope (Nikon Eclipse TS100). The Neubauer chamber contains 4 squares (1 x 1 mm). The number of cells per each square is counted and the average of the 4 squares is calculated.

4. To calculate the number of cells per mL of cell suspension, the average value is multiplied per 10^4.

2.6. Mycoplasma test

In addition to bacterial and fungal contaminations, which are easily detectable and treatable, other types of contamination can critically affect the culture without being readily apparent. Mycoplasma cell culture contamination is very common; it can produce abnormal behavior of the cells such as decrease of the cell culture growth rates, loss of cell adhesion, decrease in the transfection efficiency, as well as, DNA, RNA and protein synthesis alteration. To confirm the type of contamination and the species of parasite involved, several commercially available tests are used. In the present thesis periodic controls have been performed to discard mycoplasma contamination using the EZ-PCR Mycoplasma Test Kit (biological industries Co.), which is based on PCR amplification of the mycoplasma genome. It contains primers with broad range that allow the detection of twelve mycoplasma species. A sample of 1 mL of culture media that has been in contact with the cells for 48 hours is used as a template for the reaction. If the result is positive the cells are eliminated or treated with plasmocin kit.

2.7. Cell decontamination

Plasmocin™ (InvivoGen) is a mycoplasma removal agent, and is used to treat cell lines infected by mycoplasma. Plasmocin™ is a well-established antimycoplasma reagent; it contains two bactericidal components strongly active against mycoplasmas that allow their elimination in only 2 weeks. The first component acts on the protein synthesis machinery while the second acts on the DNA replication. These two specific and separate targets are found only in mycoplasmas and many other bacteria and are completely absent in eukaryotic cells. Plasmocin™ is active on both free mycoplasmas and intracellular forms, and there are two types of plasmocin, one is the treatment and the other one is prophylactic, the last one can be used as a routine addition in liquid media to prevent mycoplasma contamination.
Typically, Plasmocin™ Treatment is used for 2 weeks at 25 µg/mL and can be used in combination with penicillin and streptomycin.

Procedure for cell decontamination:

1. The cells are subcultured into medium containing 25 µg/ml of Plasmocin™ Treatment (see procedure 1.3).

2. The culture medium is removed and replaced with fresh Plasmocin™ Treatment containing medium every 3-4 days for 2 weeks. At high concentrations of Plasmocin™, slowdown of cell growth rate may be observed.

Note: If 25 µg/mL of Plasmocin™ is toxic for the cells, the concentration of Plasmocin™ can be reduced to 12.5 µg/ml and the cells are treated for an additional week.

3. Test for the presence of mycoplasma by a conventional PCR method or using a cell based assay. If mycoplasmas are still present following treatment, increase the concentration of plasmocin to 37.5 µg/mL for one week.
4. For the maintenance of a mycoplasma free culture, Plasmocin™ Prophylactic is used at a concentration of 5 µg/mL.
Plasmocin™ treatment is shipped at room temperature and should be stored at 4°C or -20°C.

2.8. Number of cells for each experiment

Each cell line was seeded with an initial different number of cells to obtain a final confluence of 100% at the end of the experiment to perform transcriptional activity, qPCR, western blot and cell counting. Microscopy was performed at 50 % of cell confluence.

Cells	HeLa M2P14	HeLa	C2C12	MEFwt	MEF Mfn2$^{-/-}$	MEF Mfn1$^{-/-}$	T98G	U87MG
Transcriptional activity (24-well plate)	90.000	-	-	-	-	-	-	-
mRNA (12-well plate)	-	70.000	45.000	-	-	-	-	-
Western and MMP (6-well plate)	-	140.000	90.000	90.000	80.000	80.000	140.000	140.000
Cell counting (12-well plate)	-	70.000	-	35.000	35.000	35.000		
Microscopy (6-well plate)	-	50.000	40.000	35.000	35.000	35.000	-	-
Oxygen consumption	-	-	15.000	15.000	15.000	15.000	-	-

Table 4. **Number of cells for each experiment**

3. Cell treatments

Cultured cells are exposed to a wide variety of compounds to study and evaluate their diverse responses such as to elucidate a signal transduction and biological pathways, to find specific molecules for therapeutic use. In the present thesis we will focus in transfection and direct uptake of the molecules.

3.1. Transient transfection

The DNA transient transfection is used to study the function of a protein in a cell line. There are several reagents to accomplish DNA transient transfection such as polyethylenimine (PEI), lipofectamine and metafectene. In the present thesis PEI was used to DNA transient transfection.

jetPEI™ is a powerful transfection reagent that ensures effective and reproducible transfection with low toxicity[4]. jetPEI™ compacts DNA into positively charged particles capable of interacting with anionic proteoglycans at the cell surface and entering cells by endocytosis[5]. It possesses the unique property of acting as a "proton sponge" that buffers the endosomal pH and protects DNA from degradation.

The overexpressed protein by transfection is usually encoded within episomal DNAs, which can be produced via maxi or minprep. Maxipreps are recommended for transfections since provide highly concentrated and purified DNA solutions.

The method applied in this thesis to quantify the transfection efficiency relies on the use of a plasmid codifying the Green Fluorescent Protein (GFP). Cells are co-transfected with GFP DNA and the DNA of the studied protein in a ratio (1:9) (v:v). The transfection percentage is determined quantifying the amounts of GFP transfected using flow cytometer (FACS). Since the amounts of the protein of study exceed the amounts of GFP, it is assumed that all GFP cells also contain the studied protein. Thus, the percentage of GFP can be considered the percentage of the studied protein. It is essential to include non-transfected cells as a negative control for FACS cytometry.

The most important thing in transient transfection is to find the best conditions to obtain the highest transfection efficiency. A control DNA, a sterile solution of NaCl (150 mM) to dilute PEI and DNA, and GFP DNA are needed for transfection. Initially four different concentrations of DNA (studied protein) are tested: 0.5, 1, 3 and 6 µg using the same ratio of PEI/DNA 4:1 (v:v). Once the amount of DNA is optimized, four different ratios of PEI/DNA are tested: 3:1 (v:v), 4:1 (v:v), 6:1 (v:v) and 8:1 (v:v). The condition giving the highest transfection efficiency is chosen for further experiments (3 µg DNA + 6:1 PEI/DNA). It is important that

further transfections are performed in the same manner to reproduce the same transfection efficiencies.

Procedure for DNA transient transfection:

1. Cells are plated at 20% of confluence in a 6-well plate (100,000 cells/well).

2. The next day 3 µg of DNA + 0.3 µg of GFP are diluted into 260 µL 150 mM NaCl in 2 mL eppendorf. To perform the experiment a DNA control is also used and each different condition is carried out per triplicate.

Note: Transient transfection requires two controls, one control is for FACS (cells without GFP), and the other control is for the experiment (DNA control).

3. 18 µL of PEI are added (PEI/DNA 6:1 v:v) per well.

4. DNA/NaCl/PEI is mixed per inversion for 30 seconds.

5. The mixture is incubated for 15 minutes at room temperature.

6. The medium from the cell plate is renewed for fresh complete growth medium.

7. The mixture is mixed again per inversion for 30 seconds.

8. The mixture (280 µL) is added into the medium to each 6-well plate. The mixture is homogenized by gently swirling the plate.

9. The mixture is incubated with the cells for 24h at 37 ^{o}C in a humidified atmosphere of 5% CO_2/95% air. Since it always necessary to control transfection efficiency, a small percentage of cells must be reserved for the flow cytometer assays.

10. The cells are washed twice with PBS and fresh media is added. Once the cells are transfected they are ready to perform the experiment.

In the thesis two plasmids were used in HeLa cells: a p53 expression vector (CMVp53) and an empty negative control vector (pcDNA3.1). CMVp53 expresses human p53, human p53 cDNA was cloned in the pCMV-Neo-Bam vector. CMVp53 was a gift from Dra. Pilar Ruiz-Lozano (University of Stanford (School of Medicine).

3.1.1. Definition of N/P (PEI/DNA) ratio

Efficient cell entry requires cationic particles. The ionic balance of jetPEI™ cations and DNA anions should be in favor of the cations. The *N/P ratio* is a measure of the ionic balance of the complexes. It refers to the number of nitrogen residues of jetPEI™ per DNA phosphate. Approximately one in three nitrogen atom of PEI is a cation, so electroneutrality

of jetPEI™ /DNA complexes is reached for N/P = 2 - 3. In practice, the best transfection results are obtained for N/P = 5 - 10. The amount of jetPEI™ solution to be mixed with DNA in order to obtain a desired N/P ratio can be calculated using the following formula:

µL of jetPEI™ to be used = µg of DNA x N/P ratio

3.2. Determination of transfection efficiency by FACS

Flow cytometry is based in laser technology employed in cell counting and cell sorting. Fluorescence-activated cell sorting (FACS) is a specialized type of flow cytometry, providing fast and quantitative fluorescent signals from individual cells, as well as, physical separation of cells of particular interest into two containers, one cell at a time, based upon the specific light scattering and fluorescent characteristics of each cell. In our case FACS quantifies GFP and fluorescein conjugate transfection. The GFP and fluorescein proteins emit fluorescence when it is excited at a certain wavelength, so GFP and fluorescein positive cells can be distinguished from the negative cells. Thus, each cell population (transfected, non-transfected, or dead) can be distinguished and counted.

The transfection is performed for 24h. The cells reserved for FACS are washed and trypsinized (200 µL). Once the cells are disattached 1 mL of fresh medium is added. The cells are homogenized by pipetting and transferred to an eppendorf of 2 mL. Homogenization step is important because FACS does not count aggregates and can be obstructed by their presence. It is essential to include non-transfected cells as a negative control for FACS cytometry.

All FACS determination for the present thesis were performed using the “Centres Científics i Teconlògics de la Universitat de Barcelona” (CCiTUB).

3.3. Stable transfections

Transiently-transfected cells with DNAs containing neomycin resistance gene (neo) can be stably transfected. Therefore, the steps needed to generate a stable cell line begin identically as transient transfection (Section 3.1). After 24 hours of transfection, geneticin is added to the culture media at the selected concentration. Geneticin interferes with the function of 80S ribosomes and protein synthesis in eukaryotic cells. Resistance to geneticin is conferred by the Neomycin resistance gene (*neo*) from Tn5 encoding an aminoglycoside 3‘-phosphotransferase, APH 3‘ II. Using the specified selection pressure, only neomycin positive cells are selected, while the rest are killed.

Stable transfections in the present thesis were performed using two circular DNA: one plasmid contained the promoter of Mfn2 with the luciferase reporter gene and

neomycin resistance gene (pGL3-Mfn2Prom), and the other plasmid contained GFP expression vector, which served as a control of the transfection efficiency.

The only difference between transient and stable transfection is the amount of cells required and the type of plates needed. There should be enough cellular material to plate several dilutions of transfected cells. In addition, a no transfected cell plate is used to control the effectiveness of geneticin.

Procedure to generate stable transfected cells:

First of all several conditions were tested to obtain the highest transfection efficiency using 6-well plates:

1. First of all HeLa cells are co-transfected with the plasmid pGL3-Mfn2Prom (Section 4.2) and GFP vector in 6-well plate following the procedure detailed in section 3.1. The plasmid pGL3-Mfn2Prom is transfected using 4 different amounts: 3, 6, 9 and 15 µg to find the best conditions to obtain the highest transfection efficiency. PEI is added in a ratio PEI/DNA 4:1 (v:v). Duplicates are performed for each condition.

2. After 24 h of incubation with the transfection media the cells are washed and trypsinized to measure the transfection efficiency by FACS. The best results were obtained using 3 and 6 µg of plasmid pGL3-Mfn2Prom.

3. The cells are seeded in a 24-well plate to measure the transcriptional activity of the Mfn2 promoter performing the luciferase assay (See section 6). The highest luminescence was obtained for the cells transfected with 3 and 6 µg of pGL3-Mfn2Prom. Luciferase activity results agreed with the results obtained from FACS.

Once we have determined the best conditions the process was performed again using 10 cm cell culture plates:

4. HeLa cells are again seeded in 10 cm cell culture plates (600,000 cells/plate).

5. The next day HeLa cells are co-transfected with the plasmid pGL3-Mfn2Prom (10 and 20 µg) and GFP vector in 10 cm plate, and PEI is added in a ratio PEI/DNA 4:1 (v:v).

6. After 24 h of incubation the cells are washed and the transfection efficiency is measured by FACS. High transfection efficiency was obtained for both conditions.

7. The cells are seeded in 24-well plate to measure the transcriptional activity performing the luciferase assay (See section 6), and highest luminescence values were also obtained for both conditions. 10 µg of pGL3-Mfn2Prom was selected for further experiments in 10 cm plate.

8. HeLa cells are incubated at different concentrations of geneticin (100, 250, 500, 750 and 1.000 µg/mL) to know the lethal dose. The cells died at 750 µg/mL, and this concentration was used to select the clones.

9. HeLa cells are seeded in 10 cm plates (600,000 cells/plate) and the next day are transfected with the plasmid pGL3-Mfn2Prom (10 µg) and GFP vector, and PEI is added in a ratio PEI/DNA 4:1 (v:v).

10. After 24 h, the transfection media is removed and the cells are trypsinized, counted and seeded in 15 cm plates at very low confluences: 1,000, 5,000, 10,000 cells/plate, since the main objective is to isolate the cells enough to obtain singles colonies. Triplicates were performed for each condition. The cells are grown in cultured medium supplemented with geneticin up to a final concentration of 750 µg/mL. A small fraction of these cells is used to control the transfection efficiency by FACS.

11. The next step is the selection of the transfected cell clones, which takes around 4 weeks. After 4 weeks, the cells are washed, and a cloning disc (size 6, from sigma) soaked with trypsin is applied directly to the select clone that is easily detectable and well isolated. After 2 minutes, the cells are disattached and transferred with the disc to a 24-well plate with medium and geneticin. 100 clones were isolated with extremely precision to be sure that different clones are not mixed. It is critical for the maintenance of the stable clones the presence of geneticin in the culture medium. If not, the selection pressure is lost, as well as the clone. Once all different clones are plated in 24-well plate, they are allowed to growth until confluence.

12. 57 clones grew and were plated in 6-well plate. The clones were allowed to growth until confluence.

13. The clones were trypsinized and seeded again in 6 and 24-well plate (2 well per clone) to generate stock and to select the most active clone by luciferase assay, respectively.

To analyze the generated clones the luciferase assay was performed and 11 clones were selected with high and low transcriptional activity of the Mfn2 promoter.

3.4 siRNA transfection

Small interfering RNA or silencing RNA (siRNA) technology is highly effective in post-transcriptional regulation. siRNA is a class of double-stranded RNA molecules, which specific knockdown the gene of interest by interfering with the expression of the specific gene with complementary nucleotide sequence, and inhibits the expression of the protein. Thus, the cellular incorporation of exogenous siRNA by transfection allows the total or partial inhibition of the targeted gene.

Specificity has to be taken in account. Blast searching of the selected siRNA sequence against EST libraries is recommended to ensure that only one gene is targeted. One of the best options is knockdown the gene using two independent siRNA duplexes to control the specificity of the silencing effect. It is necessary to demonstrate a reduction in the targeted protein by western blot or a reduction in the mRNA levels by RT-PCR when siRNA is used.

siRNA transfection can be performed using different reagents such as lipofectamine and metafectene. In the present thesis metafectene was selected because provided higher transfection efficiencies than lipofectamine. Metafectene is a polycationic transfection reagent based on liposome technology. The specifically designed molecular structure of the cationic lipid ensures easy entry of DNA/RNA into cells by condensing DNA/RNA to compact structures (DNA/RNA/lipid-complex) and endosome buffering.

In the thesis different siRNA were used: one p53 siRNA and one control siRNA (Fluorescein conjugate) were used for HeLa cells, and two p53 siRNA and one control siRNA were used for C2C12 cells. The control siRNAs will not lead to the specific degradation of any cellular messenger RNA. They serve as a negative control for experiments using targeted siRNA transfection. Moreover, the siRNA for HeLa cells is fluorescein conjugated and allows quantifying transfection efficiency by FACS. It is essential to include non transfected cells as a negative control for FACS cytometry.

siRNA	Recognized Species	Sequence (5'-3')	Storage	Source	Catalog number	$[Conc]_f$[1]
p53 siRNA	Human specific	-	-20 °C	Cell Signaling	6231	50 nM
Control siRNA	All species expected	-	-20 °C	Cell Signaling	6201	50 nM
MISSION® siRNA Universal Negative Control	Mouse specific	-	-20 °C	Sigma	Sic001	25 nM
SASI_Mm01_00080292	Mouse specific	CCACUACAAGUACAUGUGU[dT][dT]	-20 °C	Sigma	NM_011640	25 nM
		ACACAUGUACUUGUAGUGG[dT][dT]				25 nM

[1] Final concentration of the compound with the cells

SASI_Mm02_00310137	Mouse specific	CCACUACAAGUACAUGUGU[dT][dT]	-20 °C	Sigma	NM_001127233	25 nM
		ACACAUGUACUUGUAGUGG[dT][dT]				25 nM

Table 5. **small interfering RNA used for transfection**

Procedure for siRNA transfection:

1. HeLa and C2C12 cells are seeded in a 6-well culture plate in 1mL of fresh complete medium for each well, and are incubated at 37 °C in a CO_2 incubator. HeLa cells treated with control siRNA are seeded at 120.000 cells/well and HeLa cells treated with p53 siRNA are seeded at 190.000 cells/well. C2C12 cells treated with control siRNA are seeded at 40.000 cells/well and C2C12 cells treated with p53 siRNA are seeded at 55.000 cells/well. The growth rates of HeLa and C2C12 cells treated with control or p53 siRNA are different. Thus, we seeded different cell confluences to finish the experiment at 90 % of cell confluence.

2. The next day the cells are washed with PBS, and 1 mL of medium with FBS and without penicillin/streptomycin (antibiotics) is added. It has been reported that in some cases, the presence of antibiotics interferes with optimal transfection results.

3. The solutions of RNA and metafectene transfection reagent should have an ambient temperature and should be gently vortexed prior to use.

4. The following solution is prepared in a 2 mL eppendorfs: 100 µL of medium free of serum and antibiotics + 10 µL of metafectene.

5. The mixture is incubated at room temperature for 5 min.

6. 5 µL of siRNA (10 µM) are added to the mixture. The final concentration of the siRNA in the 6 well plate must be 25 or 50 nM (ratio lipid/RNA 2:1 v:v). The solutions are mixed gently by carefully pipetting several times.

7. The mixture is incubated at room temperature for 5 min. This time is required to form the RNA-lipid complex.

8. Add the RNA-lipid complexes (115 µL) to the wells with the cells and mix gently. Incubate at 37 °C in a CO_2 incubator for 24 h.

Note: Since it always necessary to control transfection efficiency, a small percentage of cells incubated with control siRNA must be reserved for the flow cytometer assays.

9. The cells are washed with PBS and complete fresh media is added. Once the cells are transfected they are ready to perform the experiment.

Optimization of the transfection protocol is recommended for each combination of siRNA and cell line used, if optimal results are desired. Every cell line has a characteristically optimal lipid/RNA ratio, and a successful transfection requires a slightly net positive charge of the METAFECTENE-RNA-complex.

3.5. Cells incubated with chemical compounds

Certain cellular functions are modifiable via chemical compounds, which can up-regulate, down-regulate or block various cellular functions. To prevent insoluble problems, all the compounds used in the thesis were dissolved in DMSO. It is important not to prepare diluted stock solutions since DMSO at high concentrations is toxic for the cells. A final DMSO percentage, without showing toxic effects, was established in the media exposed to cells to compare different conditions.

The compounds should reach the cell and be introduced without compromising cell survival. The most critical factor is the internalization of the compounds in the cells, and it depends on the size and the hydrophobicity of the compound.

Compounds must be stored in the freezer (-20 ^{o}C) to maintain their stability over long periods.

Compounds	Applications	Storage	Source	Catalog number	Purity	$[Conc]_f$[2]
9-cis-retinoic acid	Binds to RAR and RXR receptor	-20 ^{o}C	Sigma	R4643		10 µM
Antimycin A	Inhibits complex III	-20 ^{o}C	Sigma	A8674		10 µM
Butamben	Local anesthetic	-20 ^{o}C	TCI Europne nv	A0270	>99 %	50 µM
Clorgyline hydrochloride		-20 ^{o}C	Sigma	M3778		50 µM
Dimebon			Axon	1445	99.5 %	50 µM
Hesperetin		-20 ^{o}C	Sigma	H4125	95 %	50 µM
Indoprofen		-20 ^{o}C	Sigma	I3132		50 µM
Lansoprazole		-20 ^{o}C	Sigma	L8533		10 µM

[2] Final concentration of the compound with the cells

Leflunomide	Inhibits DHODH	-20 °C	Sigma	L5025		50 µM
Myxothiazol	Inhibits complex III	-20 °C	Sigma	T5580		2 µM
Nabumetone		-20 °C	Sigma	N6142		50 µM
Parbendazole		-20 °C	Carbone Scientific	CC09_004810-1	99.2 %	10 µM
Phenezopyridine hydrochloride		-20 °C	ABCR GmbH		98 %	10 µM
Resveratrol		-20 °C	TCI Europne nv	R0071	>98 %	50 µM
Teriflunomide (A77 1726)	Inhibits DHODH	-20 °C	Bio Trend	BG0506	99.4 %	50 µM
Thiabendazole		-20 °C	TCI Europne nv	T0830	98 %	50 µM

***Table 6*. Compounds used in the present thesis**

4. DNA protocols

4.1 General considerations

The manipulation of nucleic acids and bacteria must be performed using sterile material to avoid DNAses, RNAses, other bacteria and exogenous DNA contamination. The material can be sterilized using autoclave 20 minutes at 120 °C and 1 atmosphere of pressure. Bacteria manipulation must be handled in proximity to a flame source, which provides a sterile atmosphere working area minimizing the contamination risk. The working bench surface and the micropipettes should be carefully cleaned with 100% ethanol, and all solutions and reagents must be prepared with ultra-pure water (Mili Q from Millipore) and then further sterilized by autoclaving or filtered by 0.22 µm diameter filters.

DNA samples must be kept on ice when preparing an experiment, and never vortex genomic DNA. Genomic DNA is stored at 2-8 °C; storage at -15 to -25 °C can cause shearing of the DNA. Plasmid DNA can be stored at 2-8 °C for short term storage or in aliquots at -15 to -25 °C for long term storage.

4.2. Firefly Luciferase Reporter Vectors

The pGL3-Promoter vector includes the synthetic *luc+* genes, and a multiple cloning region. In our lab Mfn2 promoter was cloned in SacI-SmaI in pGL3-Promoter vector (pGL3-Mfn2Prom). However, to generate stable cells lines a mammalian selectable marker gene was needed.

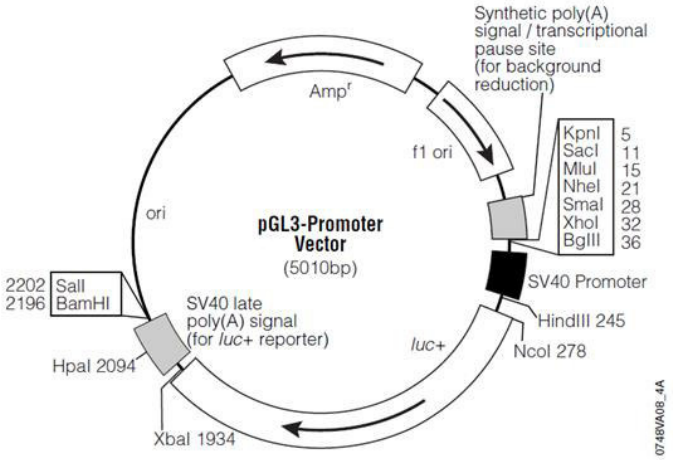

***Figure 86*. pGL3-Promoter Vecor**

The pGL4 Luciferase Reporter Vectors are the next generation of reporter gene vectors optimized for expression in mammalian cells. The pGL4.17[luc2/Neo] vector includes the synthetic firefly *luc2* (*Photinus pyralis*) genes, which have been codon optimized for more efficient expression in mammalian cells, a multiple cloning region, and a mammalian selectable marker (Neo). The reporter genes including the ampicillin (Amp^r) gene and the mammalian selectable marker gene neomycin (Neo^r), have been engineered to reduce the number of consensus transcription factor binding sites, reducing background and the risk of anomalous transcription.

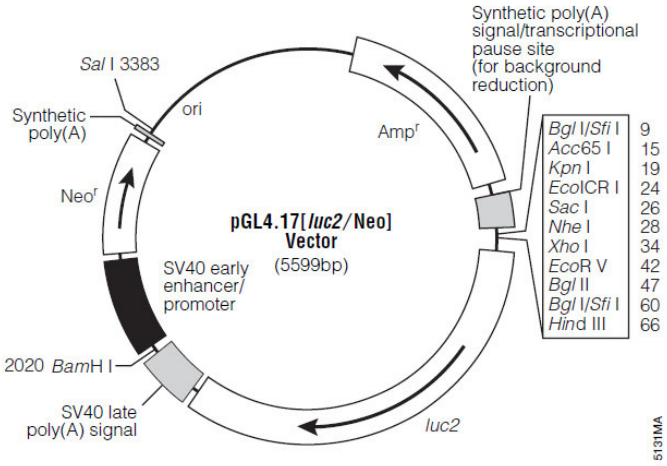

***Figure 87*. pGL4.17[luc2/Neo] Vector**

Thus, we wanted to clone the Mfn2 promoter in pGL4.17[luc2/Neo]. However it was no possible because some multiple cloning regions were deleted in our pGL3 containing the Mfn2 promoter. So, we decided to clone the mammalian selectable marker gene neomycin into pGL3-Mfn2P. So, the selectable marker neomycin gene was extracted from pGL4 using *Bam*H I and *Sal* I restriction enzymes and was cloned into pGL3-Mfn2Prom.

4.3. Bacterial transformation by heat shock and plasmid purification

Plasmids are circular DNA molecules that can be introduced in host cells (bacteria) by transformation without being degraded. Once cells are transformed, a selective pressure is applied to exclusively allow the growth of cells containing the desired plasmid. Generally, plasmids are provided with selective markers (such as antibiotic resistance), which permit cell growth when antibiotic is added in the growth media.

Bacteria containing the plasmid will replicate in the normal way, generating multiples copies of itself by several cycles of cell division and replication. Finally, a bacterial colony that contains billions of copies of the plasmid is generated. This process, which is called transformation is used for the maintenance and amplification of plasmid DNA, and rely on the use of a bacterial host.

The host bacteria used in this thesis were the *E. coli* DH5α Dam^-/DMc^- and XL1-Blue strains. Both types of competent cells were obtained via a procedure whereby bacteria are treated with a calcium chloride solution to alter the bacterial wall and therefore facilitate the entry of exogenous DNA. The competent cells, as well as, the growth medium for bacteria (LB liquid and LB-agar plates with the desired antibiotics) were routinely generated by the technical lab assistance. Once the bacterial strains acquire their 'competence' state, they are ready to be transformed by the DNA of interest. The host bacteria cells must be stored at -80 ^oC.

In the present thesis bacterial transformation have been achieved by heat shock, which is the procedure most commonly used.

Procedure for bacterial transformation by heat shock:

1. An Eppendorf containing 100 µL of competent cells are defrosted on ice.

2. The plasmid (50-100 ng) is added to bacteria and is kept on ice for 30 min. This step allows the DNA attachment to the bacterial surface.

3. The mixture is incubated at 42 ^oC for 90 s and then is placed on ice for 10 min. This step enhances cell recovery after the heat shock.

4. 1 mL of LB medium is added and the mixture is incubated at 37 ^{o}C for 1 h with shaking. In this point, bacteria containing the plasmid will start to express the antibiotic resistance codified by the plasmid which allows their selection. In this thesis ampicillin (100 μg/mL) was used as antibiotic.

5. 100 μL of the cellular suspension is seeded in a LB-agar plate with the selected antibiotic (for bacterial selection), and the plate is incubated at 37 ^{o}C for 16 h. The bacterial colonies appear between 12 and 18 h.

6. One colony is selected from the LB-agar plate and the colony is grown in LB liquid medium with the selective marker (antibiotic) for 16 h at 37 ^{o}C with shaking.

7. Plasmids are purified from this bacterial culture suspensions using different commercial kits depending on the quantity and quality of the DNA required:
· Small (5-15 μg): Qiaprep Miniprep.
· Medium (300-500 μg): Qiagen Plasmid Maxi Kit.
· High (7-10 mg): Qiagen Plasmid Giga Kit.
The procedure is indicated in the manual of each kit.

4.4. Cloning of DNA

Restriction enzymes cut up the DNA at certain sites, rendering new shorter fragments, and the DNA target must be endowed with a restriction site recognized by the chosen enzyme in order to be removed. To digest DNAs by these enzymatic activities, one should follow the guidelines set forth by the supplier. Each restriction enzyme has one optimal action buffer (indicated as 100%) and several others in which the efficiency is variable (from 25 to 75%).

In single digestions (one enzyme), the optimum buffer should provide the maximal efficiency for the enzyme selected. In complex digestions (double or triple) the chosen buffer should provide the optimal efficiency relative to all the enzymes used. However, in many cases the buffers used for different enzymes are completely incompatible. Therefore, the digestion should be performed in a step-wise manner: the DNA is digested first by one enzyme, and then purified from the reaction buffer (DNA columns, or by extraction from agarose gels). Once purified, the subsequent digestions can proceed. Although some enzymes have specific temperatures, most of them work at 37 ^{o}C.

The cloning of DNA is performed with 1 μg of DNA for 1 hour of digestion (1U/μg) at the optimal enzyme temperature. Sometimes, higher amounts of enzyme are used (2-4U/μg) to optimize digestion, though these should never exceed a certain percentage of the final reaction volume. Enzymes are commonly supplied in glycerol (cryoprotector)-containing buffers (50%) to greater preserve longer their stability. However, excessive amounts of

glycerol can inhibit the reaction progress. Therefore, the amount of enzyme should not surpass 10% of the final digestion mix volume.

4.5. Agarose gel and electrophoresis

The migration rate of different DNA fragments in an agarose gel is inversely proportional to its molecular weight logarithm. Thus, small DNA fragments go across large lengths, and large DNA fragments go across short lengths.

The percentage of agarose used in the gel is dependent of the size of DNA fragments; as the percentage of agarose increases the pores are smaller. Thus, large DNA fragments need low agarose percentages (around 0.4-1 %), and small DNA fragments need high agarose percentages (around 1.5-3 %). To prepare agarose gel TAE 50x buffer is used (Tris base 40 mM, acetic acid 20 mM and EDTA 1 mM, pH 8.5), and 1 µL of ethidium bromide (400 µg/ µL) is added in the agarose gel (50 mL) before solidification because intercalates with DNA emitting fluorescence when is exposed to ultraviolet (UV) light. The samples are mixed with loading buffer 5x (40mM EDTA, 0.1 % SDDS, 30 % Ficoll-400, 0.2 BBF) and H_2O to dilute the mixture up to 1x. DNA molecular weight ladder is used in electrophoresis, which is run at constant voltage (90 v) for 1 % agarose gels, and at 70 v for 3% agarose gels.

Once the desired fragments are separated and visualized, they must be isolated.

4.6. Isolating DNA fragments

Once the DNA linear fragments are obtained they must be purified for further use. In the present thesis the illustra GFX PCR DNA and Gel Band Purification Kit was used for the purification and concentration of DNA from agarose gel bands. Before starting the isolation of DNA from agarose gel, kit solutions must be prepared in advance.

Protocol for purification of DNA from TAE agarose gels:

1. DNase-free 1.5 mL microcentrifuge tube is weighted.

2. Using ultraviolet light (365 nm) and minimal exposure time, the agarose band containing the sample of interest is cut out, and placed into a DNase-free 1.5 mL microcentrifuge tube.

3. Weigh the microcentrifuge tube plus agarose band and calculate the weight of the agarose slice.

4. 10 µL of capture buffer type 3 are added for each 10 mg of gel slice, mixed by inversion and incubated at 60 °C for 15–30 minutes until the agarose is completely dissolved. The tube is mixed by inversion every 3 minutes.

5. Once the agarose has completely dissolved, the Capture buffer type 3-sample mix must be yellow or pale orange in color. One GFX icroSpin column is placed into one Collection tube for all the samples.

6. Capture buffer type 3- sample mix is centrifuged briefly to collect the liquid at the bottom of the tube.

7. 800 µL of Capture buffer type 3- sample mix are transferred onto the assembled GFX MicroSpin column and Collection tube, and incubated at room temperature for 1 minute.

8. The assembled column and Collection tube is centrifuged at 16 000 × g for 30 seconds.

9. The flow through is discarded by emptying the Collection tube, and the GFX MicroSpin column is placed back inside the Collection tube.

10. Sample Binding steps 7 to 9 are repeated as necessary until all sample is loaded.

11. 500 µL of Wash buffer type 1 are added to the GFX MicroSpin column, and is centrifuged at 16 000 × g for 30 seconds.

15. The Collection tube is discarded and the GFX MicroSpin column is transferred to a fresh DNase-free 1.5 mL microcentrifuge tube.

16. 10–50 µL Elution buffer type 4 or type 6 are added to the center of the membrane in the assembled GFX MicroSpin column and sample Collection tube and are incubated at room temperature for 1 minute.

18. The assembled column and sample Collection tube is centrifuged at 16 000 × g for 1 minute to recover the purified DNA.

19. The purified DNA is stored at -20 °C.

4.7. Ligation

Once insert DNA and vector DNA are obtained after digestion with restriction enzymes, and purification from agarose gel, they are mixed in a test tube in order to allow the ends to join to each other and form recombinant DNA.

When insert and vector DNA show compatible ends, such as two blunted ends, or two equal protruding ends, the populations are mixed and the DNA fragments from the two

sources can be directly ligated by the addition of *DNA ligase*, which create phosphodiester bonds at the joined ends to make a continuous DNA molecule.

One of the problems is that the end of a DNA molecule can rejoin rather than form recombinant DNA. The possibility of self-ligation can be avoided using alkaline phosphatase enzyme activity, which dephosphorylates the ends of the DNA molecules providing DNA molecules unable to bind themselves again. Although this treatment is optional, it is highly recommended.

Several commercially available ligases exist and the ligation procedures should be adapted to the enzyme requirements indicated by the supplier. The standard ligation method used in the present thesis is described below:

1 The fragments to join (Insert/vector) are mixed in a molar ratio 8 insert/1 vector.

2. The amounts of indicated Ligase buffer (1 to 5 µL) are added. The amount of buffer required depends on the concentration of the stock supplied. Ligation buffers are highly enriched in salts so they must be properly dissolved prior to use.

3. 1 µL of T4 DNA ligase and H_2O MiliQ are added to the mix and the ligation is performed at RT for 15 min. Then, the samples are kept at 4 ^{o}C until transformation step.

4. The ligation product is transformed in competent cells.

5. RNA protocols

5.1 General considerations

Working with RNA is more demanding than working with DNA, because of the chemical instability of the RNA and the ubiquitous presence of RNases especially on the skin and ambient dust. RNA work requires extreme caution since RNases enzymes potentially degrade any kind of RNA. Any work with RNA samples must be performed under strict conditions using gloves and sterile material. The working bench surface and the micropipettes should be carefully cleaned with 100% ethanol, and all solutions and reagents must be prepared with ultra-pure water (MiliQ from Millipore) to avoid RNases and contamination.

5.2 RNA purification

The method selected to purify RNA is the RNAeasy Mini Kit Quiagen, for the reason that is less time consuming that other standard procedures, and avoids the use of toxic

substances such as phenol and chloroform. RNAeasy Mini Kit Quiagen purifies total RNA by specific binding to silica column providing RNA of good quality.

Procedure for RNA purification:

1. The cells are seeded in 24-well plate (90,000 cells/well) in 500 µL of fresh complete medium for each well, and are incubated at 37 °C in a in a humidified atmosphere of 5% CO_2/95% air. The RNA extraction was performed 72 h later.

2. The cells are lysed in 350 µL RLT buffer + DTT (2M) (20 µl/mL buffer RLT) and transferred to a 1.5 mL eppendorf.

3. The cells are homogenized with a syringe (10 passes). At this point the pellet can be freezed at -70 ^{o}C and keeped for several weeks.

4. 350 µL of 70 % ethanol is added and mixed by pipetting.

5. The 700 µL of the sample are transferred (including any precipitate formed) to an RNeasy spin column, and centrifuged for 15 s at 8,000 x g. The flow-through is discarded.

Note: if performing optional on column DNase digestion follow subprotocol A. DNase is used to eliminate genomic DNA.

6. 700 µL of buffer RW1 are added to the RNeasy spin column and centrifuged for 15 s at 8,000 x g to wash the spin column membrane. The flow-through is discarded.

7. 500 µL of buffer RPE are added to the RNeasy spin column and centrifuged for 15 s at 8,000 x g to wash the spin column membrane. (Ensure that ethanol is added to this buffer). The flow-through is discarded.

8. 500 µL of buffer RPE are added to the column and centrifuged for 2 min at 8,000 x g to wash the column.

9. Optional: the RNeasy spin column can be placed in a new 2 mL collection tube and the old collection tube with flow-through is discarded. The column is centrifuged for 1 min at maximum speed.

10. The RNeasy spin column is placed in a new 1.5 mL collection tube. 30 µL of pre-warmed RNase-free water at 70 ^{o}C are added directly to the SPIN column membrane, leaved 1 min at RT, and centrifuge for 1 min at 8,000 x g to elute RNA. This step can be repeated with the eluate to increase the recovery of RNA. RNA samples are kept at -80 ^{o}C.

Subprotocol A:

The lyophilized DNase I is dissolved in 550 µL of the RNase free water provided, and mixed gently by inverting the vial and do not vortex. Procedure for DNAse digestion:

Once the samples are loaded onto the RNeasy spin column, instead of performing the first wash step, the steps A1-A4 below are folowed:

A1. 350 µL of buffer RW1 are added to the RNeasy spin column and centrifuged for 15 s at 8000 x *g* to wash the spin column membrane. The flow-through is discarded.

A2. 10 µL of DNase I stock solution are added to 70 µL of buffer RDD. The solution is mixed by gently inverting the tube, and centrifuge briefly to collect residual liquid from the sides of the tube.

Note: DNase I is especially sensitive to physical denaturation. Mixing should only be carried out by gently inverting the tube. Do not vortex.

A3. DNase I incubation mix (80 µL) is added directly to the RNeasy spin column membrane, and placed on the bench top (20-30 °C) for 15 min.

A4. 350 µL of buffer RW1 are added to the RNeasy spin column, and centrifuged for 15 s at ≥8000 x *g*. The flow-through is discarded, and the protocol is continued with the first buffer RPE wash step in the relevant protocol (step 6).

5.3 RNA quantification

Once the RNA is extracted, it is necessary to check its quantity and purity, which can be evaluated by spectrophotometry. In the present thesis RNA was measured by NanoDrop 2000 UV-Vis Spectrophotometer, which provides the concentration of the RNA in ng/µL and its purity is assessed at two different ratios of absorbance.

Nucleotides, RNA and DNA absorb at 260 nm. RNA samples are measured at the ratio of absorbance at 260/280 nm to assess their purity. A ratio of 2.0 is generally accepted as “pure”, if the ratio is appreciably lower, it may indicate the presence of protein, or other contaminants that absorb strongly at or near 280 nm. The ratio 260/230 is used as a secondary measure of nucleic acid purity. The 260/230 values for “pure” nucleic acid are often higher than the respective 260/280 values. Expected 260/230 values are commonly in the range of 2.0-2.2. If the ratio is appreciably lower than expected, it may indicate the presence of contaminants which absorb at 230 nm, such as ethanol.

5.4. Reverse transcription polymerase chain reaction (RT-PCR)

RT-PCR is used to clone expressed genes by reverse transcribing the single-stranded RNA of interest into its complementary single-stranded DNA, a process termed *reverse transcription*. Reverse transcriptase (RT) is the enzyme used to generate complementary

DNA (cDNA) from the RNA template. In the present thesis SuperScript™ II Reverse Transcriptase (RT) kit and oligo dT both from Invitrogen were used for reverse transcription. Oligo dT binds to the poly (A) tail of the different mRNA and the enzyme SuperScript synthesize the cDNA from the oligo dT, using mRNA as a template.

Procedure for RT-PCR:

1. A 20 µL reaction volume can be used for 1 ng-5 µg of total RNA. In the present thesis reverse transcription was performed for 1, 1.5 and 2 µg, depending on the RNA concentration. At a higher concentration of RNA less µg of RNA are required. Once we have decided the number of µg of RNA, we must calculate the µL of RNA and Milli Q H_2O that will be used for each sample. The total volume (µL RNA + µL Milli Q H_2O) must be 10 µL.

2. Eppendorfs are marked with the sample name, and the calculated H_2O for each sample is added to each eppendorf.

3. A mix of dNTP and oligodT 12-18 (500 µg/mL) in a ratio 1:1 (v:v) are prepared for all the samples, and 2 µL of the mix is added to each ependorf. The mix of dNTP (10 mM each) contains dATP, dCTP, dGTP and dTTP.

4. The RNA previously calculated is added, and the eppendorfs are placed on ice.

5. The eppendorfs are incubated at 70 ^{o}C for 5 min and quick placed on ice.

6. A mix of buffer, DTT and RNaseOUT™ is prepared:

- 4 µL First-Strand Buffer 5X
- 2 µL 0.1 M DTT
- 1 µL RNaseOUT™ (40 units/µL)

7 µL of the mix are added to each eppendorf and the contents are mixed by pipetting.

7. Eppendorfs are incubated at 42 ^{o}C for 2 min.

8. 1 µL (200 units) of SuperScript™ II RT is added to each eppendorf and mixed by pipetting gently up and down.

9. The eppendorfs are incubated at 42 °C for 50 min.

10. The reaction is inactivated by heating at 70 °C for 5 min.

11. 80 µL of RNase free H_2O are added to each eppendorf, which are stored at -20 ^{o}C.

The reverse transcription efficiency is considered as 100%.

5.5 Quantitative Polymerase Chain Reaction (qPCR)

5.5.1. Basis of the qPCR and quantification

Due to its sensitivity and dynamic range, PCR is the ideal technique to quantify nucleic acids. The polymerase chain reaction amplifies a DNA fragment from a DNA template. The fragment amplified is determined by the use of two primers that anchor to opposite DNA strands, and which are extended in different directions (towards each other). Thus, the fragment flanked by the primers is the amplified DNA. The enzymatic activity that catalyzes the synthesis of DNA from the primers is the DNA polymerase. This amplification relies on several cycles of three step-process:

1. Denaturalization (to generate single-stranded templates)
2. Primer annealing over the single-stranded templates
3. Chain extension, which is driven by the polymerase

Repeated cycles of synthesis and denaturation result in an exponential increase in the number of segments replicated. Several parameters determine the success of the reaction, such as the template (the quality of the DNA source), the primer annealing (the primers must be specific for the desired sequence) and the DNA polymerase. In conventional PCR, the amplified DNA product (amplicon) is detected in an end point analysis by visualizing the DNA product in an agarose gel after the reaction has finished.

In contrast real time PCR offers an alternative method for qualitative and quantitative analysis measuring the accumulation of PCR products during amplification with fluorescent dyes as the reaction progresses, and data is recorded.

Quantitative real time PCR (qPCR) detects a fluorescent dye and yields increased fluorescence signal with an increased amount of PCR product during the reaction. The measured fluorescence is proportional to the total amount of amplicon; the change in fluorescence over time is used to calculate the amount of amplicon produced in each cycle. Thus, real time PCR allows determining the initial number of copies of template DNA (the amplification target sequence) with accuracy and high sensitivity.

The figure below shows typical amplification curves. The number of PCR cycles is shown on the x-axis, and the fluorescence from the amplification reaction, which is proportional to the amount of amplified product, is shown on the y-axis.

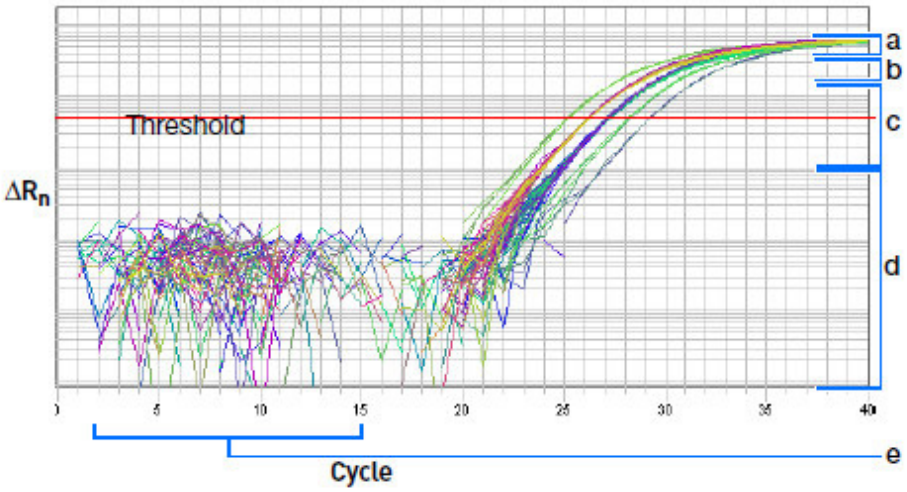

Figure 88. **Typical amplification curves of a qPCR.**

The amplification curve shows a baseline phase, which is considered as background. Then, an exponential phase starts followed by a linear phase and finally a plateau phase. During the background phase, fluorescence remains at background levels, and increases in fluorescence are not detectable (cycles 1–18) even though product accumulates exponentially (the amount of PCR product approximately doubles in each cycle). Eventually, enough amplified product accumulates to yield a detectable fluorescence signal. The threshold is determined in the exponential phase, before the linear phase to quantify the threshold cycle (C_T), the fractional cycle number at which the fluorescence passes the threshold. The level is set to be above the baseline and sufficiently low to be within the exponential growth region of the amplification curve. The threshold is the line whose intersection with the amplification plot defines the C_T. As the reaction proceeds, however, reaction components are consumed, and ultimately one or more of the components becomes limiting. At this point, the reaction slows and enters the plateau phase (cycles 32–40).

Samples with initially higher amounts of DNA molecules will require few amplifications cycles to accumulate enough product to give a fluorescence signal above background (threshold line). Thus, the sample will have a low C_T. In contrast, samples with low amounts of DNA molecules at the beginning will require more amplification for the fluorescence signal to rise above background. Thus, the reaction will have a high C_T.

In the present thesis two different methodologies have been used to detect amplified DNA: SYBER Green I and Hydrolysis Probes (Taqman).

5.5.2. Quantitative real time PCR assays formats

- **SYBR® Green** (Applied Biosystems) is used as a dye for the quantification of double stranded DNA in quantitative real time PCR. When SYBR® Green I dye intercalates into double-stranded DNA (dsDNA) molecules, its fluorescence greatly increases. The designed primers must not form dimers, in contrary the SYBR Green will intercalate in the dimers producing unspecific fluorescence. During annealing, PCR primers hybridize to the target and form small regions of dsDNA where SYBR Green I intercalates; the fluorescent signal slightly increases. In the exponential phase, more dsDNA is formed and more SYBR Green I dye can intercalate; higher fluorescence signal. At the end of the exponential phase, all DNA has become double stranded and the maximum amount of SYBR Green I is intercalated. The fluorescence is measured at the end of each elongation phase. The resulting DNA-dye-complex absorbs blue light (λ_{max} = 497 nm) and emits green light (λ_{max} = 520 nm). The SYBR® Green PCR Master Mix is a convenient premix of the components (except primers, template and water), it is supplied in a 2X concentration and contains SYBR® Green I Dye, AmpliTaq Gold® DNA Polymerase, dNTPs, and optimized buffer components to perform real-time PCR.

- **TaqMan®** (Applied Biosystems) probe contains two labels, a fluorescence reporter and a fluorescence quencher, in close proximity to each other. The reporter fluorescence signal emitted by the fluorophore when excited by the cycler's light source via Fluorescence Resonance Energy Transfer (FRET) is suppressed when the quencher dye is closed enough to the reporter dye. As long as the fluorophore and the quencher are in proximity, quenching inhibits any fluorescence signals. The 3' end of the Hydrolysis probe is dephosphorylated, so it cannot be extended during PCR.

  In the annealing phase of PCR, primers and probes specifically anneal to the target sequence. As the DNA polymerase extends the primer and synthesizes the nascent strand encounters the probe. The polymerase cleaves the probe that has annealed to the template with its inherent 5' nuclease activity, displaces the probe fragments from the target, and carries on the polymerization of the new amplicon. Cleavage of the probe releases the fluorophore from it and breaks the close proximity to the quencher, thus relieving the quenching effect and allowing fluorescence of the fluorophore. Hence, fluorescence detected in the quantitative real time PCR is directly proportional to the fluorophore released and the amount of DNA template present in the PCR, Taqman probe significantly increases the specificity of the detection. Using this method the formation of Taqman probes dimers don't effect the quantification.

In the present thesis primers and probes were purchased to Applied Biosystems (Taqman gene expression assays). 6-carboxyfluorescein (FAM) and VIC fluorophores, and the quencher tetramethylrhodamine (TAMRA) were used. Moreover, the TaqMan® Universal PCR Master Mix was purchased to perform quantitative real-time PCR. It is supplied in a 2X concentration, and contains, AmpliTaq Gold DNA Polymerase, AmpErase UNG, dNTPs with dUTP, Passive Reference dNTPs, and optimized buffer components.

5.5.3. Syber Green qPCR

Careful primer design is critical. If primer dimers or other non-specific PCR products form, they will incorporate SYBR Green dye. This may lead to inaccurate quantification, especially when detecting sequences of low abundance. Some important guidelines for designing primers for qPCR experiments follow:

1. Choose primers to give a product (amplicon) of 80-150 bp. SYBR Green dye fluorescence depends on the presence of double-stranded DNA, so products shouldn't be too short. Template regions with obvious secondary structures or long runs of the same nucleotide should be avoided when designing primers. Avoid a 3' terminal T on primers if possible, Thymidine tends to misprime more readily than other bases. 3’ terminal must contain C or G because between the nucleobases three hydrogen bonds are formed conferring more stability. The primer should contain C and G around 40-60%.

2. The optimal concentrations for the primers must be checked to perform the qPCR. A normal PCR is carried out with different primers concentrations to verify the expected band, the absence of contaminant bands and the dimers formation, and an increasing quantity of the expected product as the primers quantity is increased.

3. Check the melting temperature (Tm). Primers should anneal to DNA template at 55-60 ^{o}C, and a Tm of 52-55 ^{o}C will be sufficient.

4. If analyzing cDNA, design primers within a region of the genome that is transcribed. Coding sequence can be used, and for some studies, 5' untranslated sequences may be transcribed and can be used for qPCR. For cDNA from eukaryotes, it is also possible to design primers to span exon-exon boundaries. If this approach is used, it is worth noting that these primers may detect some splice variants but not others. The goal is to amplify cDNA but not genomic DNA.

5. BLAST the primer sequences. A similarity search of primers must be run against whole organism/non-redundant databases to determine if primers might anneal to other (unwanted) targets.

6. The primers amplification must show a gradient of a line of -3.32 among the logarithm of the ng of cDNA to amplify (axis x) and the cycles number (axis y). This value is obtained from the qPCR using successive dilutions of cDNA. A gradient of a line of -3.32 indicates that the primers have amplified a 100% of DNA copies for each cycle.

7. Run positive and negative controls with qPCR. It is important to establish that cDNA has been synthesized and gives a signal much earlier than RNA that has not been subjected to reverse transcription. Small amounts of genomic DNA can lead to results that can't be used.

5.5.4. qPCR protocol for SYBR Green

qPCR is achieved in 384-well plates with a final volume of 10 µL for each well. Each sample is measured per duplicate, and each well contains among 5 and 10 ng of cDNA. The primers are used at the optimized concentration between (150-500 nM). 5 µL of SYBR Green PCR Master Mix is added per each well and H_2O miliQ until 10 µL. The qPCR consist of a first step of 10 min at 95 ^oC and 40 cycles of two steps: one of 15 s at 95 ^oC and one min at 60 ^oC. After 40 cycles the melting step is performed by the thermocycler. During the melting step the DNA double helix is dissociated into single strands increasing the temperature gradually. The dissociation will be detected as a fluorescence decrease and it will be represented as a curve. The melting temperature is specific for each DNA molecule. Thus, if only one product has been amplified, there will be a unique curve. Sybr Green methodology have been used to determine the housekeeping levels such as GAPDH, β-actin, ARP and the target protein such as Mfn2, as well as for the mitochondrial DNA quantification using cox 2 and SdhA.

The thermocycler used in the present thesis is ABI-PRISM 7900 HT (Applied Biosystems) in the Unitat de Genòmica dels serveis cientificotècnics de la Universitat de Barcelona.

5.5.5. qPCR protocol for Taqman

All the Taqman probes used in this thesis such as Mfn2, Mfn1, Opa1 and Drp1 have been purchased in Applied Biosystems. The efficiency of the probes is 100 %, so their optimization is not necessary. The process is performed in 384-well plates with a final volume of 10 µL for each well. Each sample is measured per duplicate, and each well contains among 5 and 10 ng of cDNA. The Taqman probe is purchased at 20X and in qPCR reaction must be diluted to 1X. TaqMan Universal PCR Master Mix and H_2O miliQ are added until 10 µL. When using TaqMan probes the fluorophore must be selected in the thermocycler.

5.5.6. Housekeeping genes and negative controls

Housekeeping genes are typically constitutive genes that are required for the maintenance of basic cellular function, and are expressed in all cells of an organism at

relatively constant levels genes such as GAPDH, ARP, and β-actin. Relative quantitation of the desired gene against an internal standard (housekeeping gene) is particularly useful for gene expression measurements.

When performing qPCR is important to run positive and negative controls to be sure there is no DNA contamination. The first negative control will contain all the reagents used to perform the qPCR without cDNA to be sure that the primers and the master mix are free of contamination. The second negative control will contain all the reagents used to perform the qPCR with RNA instead of the cDNA, to be sure that the sample doesn't contain genomic DNA.

5.5.7. qPCR Quantification

In the present thesis comparative C_T method was used to quantify qPCR for both assay formats (Sybr and TaqMan). For the comparative C_T method to be valid, the efficiency of the target amplification (the gene of interest) and the efficiency of the housekeeping gene (the endogenous control) must be approximately equal.

This method compares the C_T value of one target to a housekeeping gene in a single sample:

Expression of the gene of interest against an housekeeping gene = $\mathbf{2^{-(C_T\ gen-C_T\ housekeeping)}} = \mathbf{2^{-\Delta Ct}}$

Using this method a standard curve is not needed, dilution errors made in creating the standard curve samples are eliminated, and time, money and reagents are saved.

In the present thesis different primers and probes were used (Table 7).

Assay format	Catalog number	Description	Sequence	Source
TaqMan®	Hs00966851_m1	Human Mfn1		Applied Biosystems
TaqMan®	Hs00247147_m1	Human Dnm1		Applied Biosystems
TaqMan®	Hs01047018_m1	Human Opa1		Applied Biosystems
TaqMan®	Hs00208382_m1	Human Mfn2		Applied Biosystems

SYBR® Green	hmp53rt.for	Human p53	**TGCCCAACAACACCAGCTC**	Invitrogen
SYBR® Green	hmp53rt.rev	Human p53	**CCAAGGCCTCATTCAGCTCTC**	Invitrogen
SYBR® Green	Mfn2 F (Hmfn2fulllenght_Fw)	Human Mfn2	**GACCAAGTTTGAGCAGCACACG**	Invitrogen
SYBR® Green	Mfn2 R (Hmfn2fulllenght_Rev)	Human Mfn2	**TTCACGCATTTCCTCGCAGTAA**	Invitrogen
SYBR® Green	hMfn2	Human Mfn2	**GGGGACAAGTTTGTACAAAAAAGCAGGCT T**	Invitrogen
SYBR® Green	hMfn2	Human Mfn2	**CACCATGTCCCTGCTCTTCTCTCGA**	Invitrogen
SYBR® Green	rt-hGAPDH.For	Human GAPDH	**TGCACCACCAACTGCTTA**	Invitrogen
SYBR® Green	rt-hGAPDH.Rev	Human GAPDH	**GAGGGCATGGACTGTGGTCAT**	Invitrogen
SYBR® Green	mMfn2F	Mouse Mfn2	**5’ GTAAGGGCTCGGAGAAGGTATGTG 3’**	Invitrogen
SYBR® Green	mMfn2R	Mouse Mfn2	**5’TGGCAAGAAGGGAGGCAAGTC 3’**	Invitrogen
SYBR® Green	mGAPDHF	Mouse GAPDH	**5’ CATGGCCTTCCGTGTTCCTA 3’**	Invitrogen
SYBR® Green	mGAPDHR	Mouse GAPDH	**5’ GCGGCACGTCAGATCCA 3’**	Invitrogen
SYBR® Green	mActinf	Mouse β-actin	**5' GGTCATCACTATTGGCAACGA 3'**	Invitrogen
SYBR® Green	mActinr	Mouse β-actin	**5' GTCAGCAATGCCTGGGTACA 3'**	Invitrogen

Table 7. **Probes and primers used for qPCR**

6. Transcriptional activity protocol

In the present thesis to measure the transcriptional activity Luciferase Assay System was used. Genetic reporters, such as, firefly luciferase are used commonly in cell biology to study gene expression, intracellular signal transduction, mRNA processing…

Firefly luciferase is broad used as a result of its reporter activity is available immediately upon translation, the assay is very sensitive because has the highest light efficiency in chemiluminescent reactions and there is no background luminescence in host cells, and finally the assay is rapid.

Firefly luciferase protein converts the chemical energy of luciferin oxidation through an electron transition, using ATP and Mg^{2+} as a co-substrate, to light producing oxyluciferin.

The Luciferase Assay System is generally used with a lysis buffer and Luciferase Assay Reagent (Luciferase Assay Substrate + Luciferase Assay Buffer). Lysis buffer should be stored at -20 ^{o}C and luciferase assay reagent should be stored at -20 ^{o}C for up to 1 month or at -70 ^{o}C for up to 1 year in the dark.

The Luciferase Assay Reagent and the lysis buffer must be prepared before beginning a luciferase assay.

Procedure for measuring transcriptional activity:

1. Cells are plated in a 24-well plate (50.000 cells/well) and the transcriptional activity is measured 48 h later.

2. 4 volumes of water are added to 1 volume of 5x lysis buffer, and 1x lysis buffer is equilibrated at room temperature before use.

3. The growth medium is removed from cells to be assayed and washed with PBS.

4. 75 µL of 1x lysis buffer is added to each well, the cells must be covered by the lysis buffer.

5. The cells are scraped from the well plate and all liquid is transferred to an eppendorf. The eppendorfs are placed on ice.

6. The eppendorfs are vortexed for 15 seconds, then centrifuged at 12,000 x g for 15 s at room temperature or up to 2 minutes at 4 ^{o}C. The supernatant is transferred to a new tube. At this point the supernatant (cell lysate) can be stored at -80 ^{o}C.

Note: The Luciferase Assay Reagent and samples should be at ambient temperature prior to performing a luciferase assay

7. The luminometer is programmed to perform a 2-second measurement delay followed by a 10-second measurement read for luciferase activity.

8. 10 µL of each cell lysate are transferred to a luminometer tube and 20 µL of the Luciferase Assay Reagent (luciferin) are added. The solution is mixed by pipetting 5 times.

9. The luminometer tube is placed in the luminometer and reading is initiated.

10. The cell lysate (protein) of each tube is quantified using BCA method. The results are expressed as the RLU/µg protein per each condition.

7. Protein protocols

7.1. Total protein cell extracts

1. The HeLa, C2C12 and MEFs cells are seeded in a 6-well plate (Section 2)

2. The total lysates are obtained after 48 or 72 h. The cells are washed with PBS 1x and 100 µL of cold lysis homogenization buffer is added for each well. The lysis homogenization buffer contains 50 mM TRIS, 150 mM NaCl, 1 mM EDTA, 2 mM Na_3VO_4, 20 mM PPiNa, 100 mM NaF and 1 % NP-40, and 1 complete Mini protease tablet (protease inhibitors) from Roche for 10 ml of buffer.

3. The cells are scraped and are transferred to 1.5 mL eppendorf.

4. The cells are homogenised (10 strokes) using a syringe 1 mL 25GA x 5/8in (0.5 x 16 mm) (BD Plastipak^{TM}) and centrifuged at 0.7 x g for 10 min at 4 ^{o}C to pellet cellular debris.

5. The supernatant is transferred to a new tube. At this point the supernatant (cell lysate) can be stored at -20 ^{o}C.

7.2. Protein assays and quantification

Once the cellular protein components are obtained, the next step is their quantification. In the present thesis the BCA method was used. The BCA Protein Assay Reagent (bicinchoninic acid) was purchased at Thermo scientific.

The BCA method relies on the Biuret reaction, in which proteins reacting with Cu^{2+} cations liberate Cu^{1+}, in an alkaline medium, which in turn, reacts with the bicinchoninic acid (BCA), thereby providing a highly sensitive and selective colorimetric detection because of the generation of a violet compound. Since the amount of the newly generated compound is a function of the protein amount in solution, its absorbance (spectrophotometrically measurable at 562 nm) is proportional to the sample protein concentration.

To perform protein assays accurate standard curves and calibration controls are required. In the present thesis Pierce BSA Protein Assay Standards (Thermo Scientific) was used for this purpose. These bovine serum albumin (BSA) solutions are protein

concentration reference standards for use in BCA. BSA is the universally accepted reference protein for total protein quantitation. The albumin standard is formulated at 2mg/mL in an ultrapure 0.9% sodium chloride (saline) solution.

Procedure for protein quantification using the BCA method:

1. The volumes of diluted copper-containing buffer are prepared, taking into account the amounts needed for duplicated measures of samples, standard curve and blank control (200 µL/well). BCA reagent B is diluted 50 times with BCA reagent A, and mixed for 1 min.

2. The standard curve is prepared adding different volumes of the BSA protein and a blank control (0, 2.5, 5, 10, 15, 20 µg per well) in a 96-well ELISA plate.

3. The samples (1-5 µL) are added to the 96-well ELISA plate and the diluted copper-containing buffer is added (200 µL).

4. The 96-well plate is incubated at 37 ^{o}C for 30 min to favor the reaction.

5. Finally, the plate is read at 562 nm using the software Magellan 2 in an ELISA Sunrise Remote/Touch screen (Tecan) lector.

The gradient of the straight line is calculated from the BSA standard curve and protein concentrations are determined.

7.3. Western Blot assay

The western blot is an analytical technique used to detect specific proteins in a given sample. It consists of three parts:

- Polyacrylamide gel electrophoresis to separate denatured proteins by the length of the polypeptide (protein size)

- The proteins are transferred to a membrane (typically nitrocellulose or PVDF)

- The target proteins are detected with specific antibodies

7.3.1. Electrophoresis procedure

Electrophoresis of protein samples in polyacrylamide gels is an analytical tool to separate and compare complex protein samples. Electrophoretic separations were performed in one-dimensional microgels using sodium dodecyl sulfate- Polyacrylamide gel electrophoresis (SDS-PAGE) methodology, which allows separating proteins depending on their length and mass to charge ratio.

SDS-PAGE methodology[6] utilizes the anion detergent SDS to linearize and to impart a negative charge to proteins providing denatured proteins with negative charge. Most proteins bind a uniform amount of SDS per µg of protein, which imparts a uniform charge density per unit mass. That affords the separation of proteins based on their mass.

Prior to electrophoresis, protein samples and polyacrylamide gels are prepared. Protein samples are mixed with SDS-containing loading buffers in sufficient amounts to ensure that the proteins will be properly denatured and their charges masked. The polyacrylamide gel consists of a stacking gel and a separating or resolving gel, which mainly differs in its pore size and pH. The former with a high pore size (3.3 % acrylamide and pH 6.8) allows high rates of protein migration facilitating the entry of all proteins in the resolving gel at once, whereas the latter separates the proteins based on their mass. The pore size (or acrylamide amount) of the resolving gel depends on the size of the target protein. As acrylamide concentrations increases, pore sizes decrease. To separate proteins with a molecular weight higher than 80 kDa the percentage of acrylamide used is 7.5 %, small proteins around 30 kDa the acrylamide percentage used is 15 %, and for proteins among 37 and 110 kDa 10 % polyacrylamide is used. The greater the acrylamide concentration the better the resolution of lowers molecular weight proteins, and vice versa.

Once the samples are loaded into wells in the gel, proteins are then forced to migrate in response to an electrical field towards the anode through the polyacrylamide gel matrix. The migration rate protein is determined by the gel pore size and the protein size.

In parallel to the analyzed samples, one well is reserved for a marker or ladder, a commercially available mixture of proteins having defined molecular weights and giving coloured bands to estimate the molecular mass of those proteins under study.

7.3.1.1. Gel preparation and polymerization

The electrophoresis system used in the present thesis was Mini-Protean (BioRad). All the gels were prepared with a depth of 1.5 mm. The glass-plate sandwich of the electrophoresis apparatus is prepared according to manufacturer's instructions using two clean glass plates and 1.5 mm spacer and is locked to the casting stand. The separating gel (7.5 mL) is prepared using 7.5, 10 or 15 % of acrylamide, Tris-Base 0.375 M, pH 8.8, SDS 0.1 %, ammonium persulfate (APS) 0.05 % and TEMED (BioRad) 2.2 mM, and is added among the glass-plate sandwich. Before polymerization acrylamide is a neurotoxic agent and is compulsory the use of gloves. APS and TEMED are added just before polymerization because they are the initiators and catalyst of the polymerization reaction, respectively. Once the separation gel is added in the glass-plate sandwich, isopropanol (100 µL) is added to provide a barrier to oxygen that inhibits polymerization, to avoid SDS bubbles, and to achieve a straight edge of the gel. The gel is allowed to polymerize at room temperature. Meanwhile,

the stacking gel is prepared using 3.3 % of acrylamide, Tris-HCl 0.125 M, pH 6.8, SDS 0.1 %, APS 0.1 % and TEMED 6.6 mM. Then, isopropanol is eliminated from the top of the separating gel, and 2.5 mL of the stacking gel are added. A teflon comb of 1.5 mm is inserted into the layer of the stacking gel to form the wells and polymerization is allowed at room temperature. Maximum attention is required to not trap air bubbles into the comb, which will lead to distortion in the protein bands during separation.

7.3.1.2. Protein samples preparation

Protein samples are mixed with Loading Sample Buffer (LSB) to ensure that the proteins will be properly denatured and heated for 5 min at 95 ^{o}C. The LSB 4X is composed by Tris-HCl 0.4 M, pH 6.8, glycerol 69.6 %, SDS 8 % (p/v), bromophenol blue 0.05 mg/mL (allows sample visualization), and DTT 100 mM. DTT is used to break disulphide bridges among proteins. Once the samples are boiled, the samples are centrifuged at maximum speed. Usually 40 µg of protein are loaded in each well.

7.3.1.3. Gel electrophoresis

The polymerized gel sandwich is placed in the electrophoresis system and the buffer chamber is filled with electrophoresis buffer, which contains Tris-Base 25 mM, glycine 0.19 M and SDS 0.1 %. The teflon comb is carefully removed without tearing the edges of the polyacrylamide gels. If well walls are not upright, they can be manipulated with a micropipette (10 µL). After the comb is removed, the samples and the ladder are loaded into the wells. The ladder use is the prestained SDS-PAGE standards Broad Range (BioRad). Empty wells are also loaded with loading buffer to run gels straighter, and samples are always loaded in the central wells. Finally, electrophoresis buffer is added to completely cover the platinum electrode within the upper chamber, and the electrophoresis chamber is closed and connected to the power supply. The 1.5 mm electrophoresis gel is run at a fix 25 mA/gel until the bromophenol blue dye reaches the bottom of the separating gel.

7.3.2. Transfer

In order to make the proteins accessible to antibody detection they are moved from within the gel onto a membrane made of nitrocellulose or polyvinylidene difluoride (PVDF). In the present thesis PVDF Immobilon^{TM} membranes (Millipore) were used since they have very high protein binding capacities, with good handling characteristics, and in addition, they are highly chemically inert, and effective for low-background staining. The method for transferring the proteins is called electroblotting and uses an electric current to pull proteins from the gel into the PVDF according to the charge of the protein. The proteins move from within the gel onto the membrane while maintaining the organization they had within the gel. The transfer equipment used in the present thesis was Mini Protean TransBlot Cell (BioRad), which employs a transfer tank apparatus filled with transfer buffer, in which the

gel/membrane sandwich is placed. The transfer buffer contains Tris-Base 25 mM, Glycine 0.19 M pH 8.3, and 20% of methanol.

Once electrophoresis is finished electrophoresis buffer is discarded and the glass sandwich is opened to remove the gel.

1. The gel is equilibrated in transfer buffer

2. The PVDF transfer membrane (6 x 9 cm) and the Whatman paper (7 x 9 cm) are cut. The PVDF membrane is marked at the bottom right side with a pen to know the orientation later.

3. The PVDF membrane is activated in 100% MeOH for 1 min.

4. Set up the sandwich from black (-) to red/white (+) side in transfer buffer with the following order: sponge, Whatman paper, gel (the gel is oriented that the order of the samples is well-known), the activated membrane (the written side of the membrane is collocated towards the gel), Whatman paper and sponge. All the process is performed in a tray full of transfer buffer to equilibrate all the material. Bubbles must be avoided for a correct transfer, since air bubbles prevent the transfer of proteins.

5. The sandwich is inserted in the transfer cassette into the tank with the gel on the cathode (black) side and the membrane on the anode (red) side. Proteins proceeding from an SDS-Page gel have a negative charge and will migrate towards the anode.

6. The transfer container is filled with transfer buffer and a block of ice is collocated inside the transfer container next to the sandwich to prevent overheating caused by the high current rates. The system is connected to the power supply and the transfer is performed at a constant current of 250 mA for 1 h.

7. Once the transfer was done, the power supply is disconnected and the gel and the PVDF membrane are removed from the transfer system. The membrane will be used for immunodetection, and the gel can be stained with Coomassie Brilliant Blue dye to check the uniformity and overall effectiveness of the protein transfer.

7.3.3. Immunodetection of the target protein

Once the transferred proteins are bound to the PVDF membrane surface, they are available to react with immunodetection reagents. This process consists of 4 steps: blocking, primary and secondary antibody exposure, and detection.

1. The non-specific binding sites should be blocked with a rich protein solution to avoid unspecific binding of the primary antibody to the membrane. In the present thesis the PVDF membranes were immersed in blocking solution (PBS + 0.1% Tween-20 with 5 % (p/v) of

skimmed milk) for 1 h at room temperature, and incubated with agitation on a rocking platform.

2. The membrane is incubated with the primary (specific) antibody solution (10 mL) for 16 h at 4 ^{o}C with agitation. All the primary antibodies used in the thesis were diluted in blocking solution, and their concentration was based on the information provided by the supplier. After the incubation, the membrane is washed with Tween 20 0.1 % (v/v) in PBS (3 x 10 min) at room temperature with agitation. The washes are performed to eliminate the primary antibody excess.

3. Once formed, the antibody-antigen complexes are recognized by secondary antibodies (anti- IgG) that are labeled with probes allowing their detection. All the secondary antibodies used in this thesis were labeled with peroxidase HRP (Horse Radish Peroxidase) and were purchased from Jackson. The secondary antibody solution is prepared with PBS-Tween 20 0.1 % and skimmed milk 1% (p/v). The secondary antibodies that recognize rabbit IgG (anti-rabbit) and mouse IgG (anti-mouse) were diluted in 1/10,000 and 1/25000 respectively. The membrane was incubated with the secondary antibody solution for 1 h at room temperature with agitation. Then, the membrane is washed with Tween 20 0.1 % (v/v) in PBS (3 x 10 min) at room temperature with agitation.

4. Secondary antibodies after exposure to chromogenic or luminescent substrates, serve to visualize the protein location. HRP signal is developed with ECL (Enhanced ChemioLuminiscence, Amersham Biosciences). The two reagents from the kit are mixed (1:1) and the membrane is incubated with the mix for 3 minutes. The membrane is collocated between a plastic folder in a film cassette (Wolf), drained removing the bubbles with paper tissue, and finally exposed to film in the dark room at different exposition times. The film can be exposed for a few seconds to several hours depending on the protein amounts and the primary antibody potency. The films used in the present thesis were (Amersham Biosciences) and were developed in a Hyper Processor Model AM4 (Amersham Pharmacia Biotech). The membrane can be used to detect another protein, and stored in PBS at 4 ^{o}C or discarded.

Once the film has been developed a quantitative protein analysis can be performed by densitometry. Tubulin, β-actin and porin were used to determine the proportion of protein levels referred to total mitochondrial and total mass, respectively.

In the present thesis different antibodies were used (Table 8).

Catalog number	Target protein	Source	Origen species	Dilution
ab56889	Mitofusin 2	Abcam	mouse	1/1,000
sc-50330	Mitofusin 1 (H-65)	Santa Cruz Biotechnology	rabbit	1/1,000
612606	OPA 1	BD Transduction Laboratories™	mouse	1/1,000
611112	Drp 1	BD Transduction Laboratories™	mouse	1/1,000
3491-100	Fis1	BioVision Corporate Headquarters	rabbit	1/1,000
A1978	β-actin	Sigma	mouse	1/10,000
529536	Porin	Calbiochem	mouse	1/5,000
Ab14734	VDAC1/Porin	Abcam	mouse	1/5,000
T5168	α-tubulin	Sigma	mouse	1/5,000
9282S	p53	Cell Signalling	rabbit	1/1,000
9284S	ρ-p53 (Ser15)	Cell Signalling	rabbit	1/1,000

Table 8. Antibodies used in the present thesis

7.4. Stripping

Once a membrane is blotted with specific antibodies, further incubations can be performed. Several factors determine whether or not it is necessary to eliminate the antibodies primarily bound to the membrane before the second incubation. It depends on the similarity of the molecular weight of the target proteins and the secondary antibody recognition.

Thus, if the antibodies used recognize protein sufficiently separated, or if the secondary antibody is different (anti-mouse and anti-rabbit o vice versa), blotted membranes can be directly used, since overlapping events should not occur.

In contrast, if either the molecular range or the secondary antibody producer is similar, membranes should be properly treated to detach antibodies. The stripping allows the clearance of antibodies attached to a membrane, leaving the transferred protein amounts almost intact. The stripping consists in washings of boiling H_2O (90 ^{o}C) (3 x 10 min). Once the stripping is performed, the procedure for immunodetection of the target protein is followed (Section 7.3.3.).

7.5. Densitometry analysis

Densitometry is the quantitative measurement of optical density in light-sensitive materials, such as photographic paper or photographic film, due to exposure to light. Optical density is a result of the darkness of a developed picture and in this thesis it has been used to quantify the levels of the target protein in the film obtained from the western blot. The films are scanned (HP photosmart) and the software used to quantify the protein levels is Gene Tools (SynGene). The value used in the protein quantification is the Raw Volume, which takes into account the signal intensity and the amount of the signal intensity. So, darker stretch bands will have the same value as width bands with less intensity.

8. Metabolic studies

C2C12 and MEFs cells were used in oxygen consumption studies and mitochondrial membrane potential assay.

8.1. Oxygen consumption measurements

XF24 analyzer measures the two major energy pathways of the cell: mitochondrial respiration as oxygen consumption rate (OCR) and glycolysis as extracellular acidification rate (ECAR). The former is when mitochondria use glucose or other substances to generate ATP in the presence of oxygen, whereas the latter is ATP generation through glycolysis, independent of oxygen to produce lactic acid. The XF24 analyzer simultaneously measures mitochondrial respiration and glycolysis in cells in minutes, using label-free disposable optical sensors.

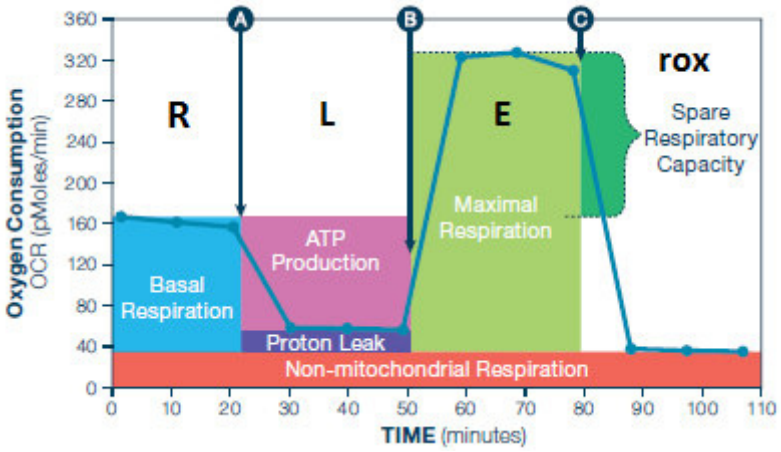

Figure 89. **Adapted from Seahorse Bioscience web page**

After measuring the basal respiration rate of C2C12 and MEFs cells, compounds modulating mitochondrial function were added sequentially into the assay medium. The

effect on oxygen consumption rates (OCR) was measured after each compound addition. (A) oligomycin was added to inhibit the ATP synthase; (B) FCCP, an uncoupler to short-circuit the proton circuit, was added to induce maximal respiration, and determine spare respiratory capacity; (C) a cocktail of antimycin A and rotenone was added to inhibit total mitochondrial respiration.

- State R (rutine): is the oxygen consumption rate of cells in basal conditions. It depends of the energy demand of the cell type and the coupling between respiration and ATP synthesis. This situation is similar to physiological conditions.
- State L (leak): is the oxygen consumption rate after the inhibition of ATP synthase (complex V) in the electron transport chain by 1 μg/mL oligomycin. The leak provides information about the oxygen consumption uncoupled to the ATP synthesis to distinguish the percentage of oxygen consumption devoted to ATP synthesis and the percentage of oxygen consumption required to overcome the natural proton leak across the inner mitochondrial membrane
- State E: is the oxygen consumption rate when the respiratory chain is decoupled from the synthesis of ATP by 1 μM FCCP addition, which induces maximal respiration. This state was used to calculate the 'spare' respiratory capacity of cells, which is defined as the quantitative difference between maximal uncontrolled OCR and the initial basal OCR.
- State rox (residual oxygen consumption): is the oxygen consumption rate when total mitochondrial respiration is inhibited by 0.1 μM antimycin A (complex III inhibitor) and 0.1 μM rotenone (complex I inhibitor). This state is used to calculate the remaining respiration caused by oxidative side reactions.

The OCRs can be expressed as mitochondrial oxygen consumption rate subtracting the oxygen consumption rate of the rox state to the other states. All substrates, uncouplers, and inhibitors were purchased from Sigma.

Procedure for oxygen consumption studies:

1. C2C12 and MEFs (MEFwt, MEF Mfn1 KO, and MEF Mfn2 KO) are plated (15.000 cells/well) in SeaHorse Bioscience XF24 plates. 4 wells without cells will be used as a negative control and as a temperature control during the experiment. The cells are incubated at 37 ^{o}C in a humidified atmosphere of 5% CO_2/95% air for 16 h.

2. The next day, the cells are treated with leflunomide at 50 μM for 48 h. Then, a Seahorse Bioscience XF24 extracellular flux analyzer is used to measure oxygen consumption.

3. The instrument is calibrated the day before the experiment, following the manufacturer's instructions. The instrument needs time to reach the optimum temperature. The calibration

plate is prepared with 1 mL/well of calibrator liquid (Seahorse Bioscience). The plate is enveloped with parafilm and incubated at 37 °C without CO_2 for 16 h.

4. On the day of the experiment, the injection ports on the sensor cartridge are loaded with 75 µL of the solutions 10X of the compounds (oligomycin, FCCP, antimycin A and rotenone) with the respiration buffer. This medium is DMEM (8,3 g/L, Sigma) supplemeted with 5,5 mM of glucose, 2 mM of GlutaMax (Gibco), 100 U/mL and 100 µg/mL of penicillin/streptomycin (Ref 15140-122, Gibco, Invitrogen), 31.6 mM NaCl and Phenol Red. The pH is adjusted at 7,4 and then, the respiration buffer is filtrated. The medium does not contain bicarbonate because it will interfere in the protons concentration measure.

5. During the sensor calibration, the medium of C2C12 and MEFs is changed for 675 µL of respiration buffer and the plates are kept in the incubator at 37 ^{o}C without CO_2 for 30-60 min.

6. The calibration plate is immediately placed into the calibrated Seahorse XF24 extracellular flux analyzer (Seahorse Bioscience). Oxygen and pH sensors are calibrated for 30 min. Then, the calibration plate is changed for the plate with the cells.

7. Plates are placed into the calibrated Seahorse XF24 extracellular flux analyzer for mitochondrial bioenergetic analysis. The instrument performed 4 measures in basal respiration (routine). Each cycle consist of 4 min of agitation, 2 min of rest, and 90 s of measure. Then, the instrument injects the oligomycin and performs 4 measures; FCCP is injected and performs 4 measures. Finally, rotenone and antimycin A are injected and 6 measures are performed. All respiration measurements are made in triplicate.

8. When the analysis is finished, the plate is removed from the instrument and the cells are lysed adding 50 µL of buffer lysis (0,1 M NaOH and 1 % SDS). The protein concentration is determined by BCA Protein Assay Reagent (Pierce).

The OCR is expressed as pmol O_2/min·µg of protein. Different ratios have been calculated from OCR values providing us information about coupling between respiratory chain and oxidative phosphorylation[7]:

- **Respiratory Control Ratio (RCR)**: is the quotient between the respiration in state E and state L (E/L) and measures the coupling between ETC and oxidative phosphorylation.

- **Phosphorylation Respiratory Control Ratio (RCR_p)**: is the quotient (R-L)/E and indicates the percentage of maximum respiratory capacity used for the cells linked to ATP synthesis.

8.2 Measurement of mitochondrial membrane potential

Measurement of mitochondrial membrane potential was performed using tetramethylrhodamine methyl ester (TMRM) from Invitrogen. TMRM is a fluorescent dye that accumulates in mitochondria in a potential-dependent manner. The TMRM emits fluorescence at 573 nm when it is excited at 540 nm. Thus, TMRM positive cells can be quantified using flow cytometry. The concentration of TMRM in the mitochondria increases proportionally to the membrane potential, and its accuracy is validated using simultaneously carbonyl cyanide m-chlorophenyl hydrazone (CCCP). CCCP is used to dissipate the mitochondrial membrane potential decreasing the TMRM incorporation and the fluorescent signal. Thus, CCCP allows determining the unspecific fluorescence signal, and is used as a blank. The stock solutions of TMRM and CCCP are prepared using DMSO, at 500 µM and 1 mM, respectively, and they are stored at -20 ^{o}C avoiding light exposure.

Procedure for measurement of mitochondrial membrane potential

1. The cells are seeded in a 6-well plate and the next day the treatment is performed.

2. Once the cells have been incubated with leflunomide for 12, 24 or 48 h, the cells are washed with PBS 1x.

3. 1 mL of growth medium ± CCCP (30 µM) is added to each 6-well plate. The cells are incubated with CCCP for 30 min at 37 ^{o}C. Duplicates are performed for each condition.

4. Then, the medium is removed and 1 mL of growth medium + TMRM (100 nM) is added to each 6-well plate. The cells are incubated 30 min at 37 ^{o}C.

5. The cells are washed twice in PBS 1x to eliminate dye excess.

6. The cells are tripsinized and diluted in 500 µL of growth medium.

7. The fluorescence emitted by the cells is analyzed by flow cytometry Coulter XL in the "Centres Científics i Teconlògics de la Universitat de Barcelona" (CCiTUB).

9. Immunochemistry of mitochondria (Immunocytochemistry)

The immunochemistry was performed using HeLa, C2C12 and MEFs cell lines that stably express mtDsRed dye.

1. The cells are seeded on round coverslips in 6-well plate and at low confluences.

2. After treatment of 12, 24 or 48 h the cells are carefully washed twice with PBS 1x.

3. The round coverslips are incubated with paraformaldehyde 4% (1 mL for each 6-well plate) for 15 min at room temperature to fix the cells. Light exposure is avoided.

4. Then, the cells are carefully washed twice with PBS 1x.

5. Hoescht is diluted 1/1000 from the stock solution (Molecular Probes) and is added (1 mL for each 6-well plate) and incubated for 10 min. Hoescht dyes the cell nucleus specifically with blue color (λ = 405 nm).

6. Then, the cells are carefully washed twice with PBS 1x.

7. Each round coverslip is washed quickly in filtered water to eliminate the salts contained in PBS 1x solution and dried with a tissue paper to eliminate water.

8. Mount the round coverslips disposing drops of 15 µL of Fluoromount® on a microscope slide. The side with cells of the coverslip must be in contact with Fluoromount.

9. The microscope slides with the round coverslips are incubated overnight at room temperature avoiding light exposure.

10. The microscope slides are stored at 4°C avoiding light exposure.

10. Microscopy

10.1. Visualization at the spectral confocal microscope

Immunofluorescence microscopy of fixed cells was performed with a Leica TCS SPE (Leica DM2500) confocal scanning microscope. The acquisition software is LAS AF version 2.4.1 and the detector is an ultra-high dynamic PMT, sequential scan. Samples were scanned using 40x/1.15 oil CS ACS APO and 63x/1.3 oil CS ACS APO objective lenses and a zoom ranging from 1 to 2.5 to analyze intracellular regions. To avoid bleed-through effects (i.e crosstalk of different fluorescence emission) in double staining experiments, each dye was scanned independently. DAPI was scanned at 405 nm diode laser and mtDsRed was scanned at 532 nm diode laser. The projection format was 512x512 or 1024x1024. Images were acquired from 10 to 20 optical sections depending on the cell type analyzed. Figures were assembled from the TIFF and LIF files using open software ImageJ.

10.2. Visualization of living cells at the spinning disk confocal microscopy

The visualization of living cells was performed in an inverted spinning disk microscope for fast acquisition and FRAPPA processes. The Olympus IX 81 confocal microscope has an incubation chamber to control temperature and CO_2. The acquisition

software is iQ1 (FastLZ) version 2.4.1 and the camera is an iXon EMCCD Andor DU-897. The spinning disk is a Yokogawa CSU-X1, and the laser illumination was used at 561 nm diode laser for mtDsRed protein.

1. The C2C12 and MEFwt cells stably expressing mtDsRed were grown on coverslips of 6-well plate, and the next day the cells were incubated with myxothiazol at 2µM for 12 h or with leflunomide at 50 µM for 48 h.

2. The coverslip that contains life cells is transferred to a metal ring (Molecular Probes), which is composed of two metal pieces. The coverslip is fixed between the two pieces and medium is added to maintain the cells alive, when adding the medium check any undesired leaking. This methodology allows observing the cells alive.

3. The incubation chamber is equilibrated at 37 ^{o}C and 5 % CO_2 control for 10 min to achieve the desired temperature for the living cells. Then the cells are focused and selected with 60x/1.42 oil Plan Apo N objective lense. The imaging should be performed quickly because the light from mercury lamp is toxic for the cells.

4. Once the area has been selected, the mitochondrial mtDsRed is excited at 561 nm at low intensity (10-20 %) due to toxicity problems. The image is amplified using the software (2x-5x) and the laser intensity is adjusted to determine the intensity of the images. The acquisition of the images can be performed at different z planes or uniquely in one plane. The images are acquired each 3 s for 20 min.

5. The software ImageJ program is used to edit the video with the images. The video was recorded in ".avi" format.

10.3. Automated fluorescence Widefield Microscopy with High Content Screening and TIRF

A fully automated inverted microscope is used for imaging wide areas, multiwell plates and multipositions of living cells. The Olympus IX 81 confocal microscope has an incubation chamber to control temperature and CO_2. The acquisition software is ScanR Acquisition and the camera is a Hamamatsu Orca-ER. The TIRF laser was used at 561 nm diode laser for mtDsRed protein.

1. MEFwt, MEF Mfn2$^{-/-}$ and MEF Mfn1$^{-/-}$ cells stably expressing mtDsRed were grown on coverslips of 6-well plate, and the next day the cells were incubated with leflunomide at 50 µM for 48 h.

2. The coverslip that contains life cells is transferred to a metal ring (Molecular Probes), which is composed of two metal pieces. The coverslip is fixed between the two pieces and

medium is added to maintain the cells alive, when adding the medium check any undesired leaking. This methodology allows observing the cells alive.

3. The incubation chamber is equilibrated at 37 ^{o}C and 5 % CO_2 control for 1 h to achieve the desired temperature for the living cells. Then the cells are focused and selected with 40x/ 0.75 UPlan FL N and a 1.6x Zoom lens was inserted in the light path. The imaging should be performed quickly because the light from mercury lamp is toxic for the cells.

4. The mtDsRed mitochondrial is excited at 561 nm at low intensity (10-20 %) due to toxicity problems. The imaging is performed automatically at the selected area and is performed at different z planes.The image is amplified using the software (2x-5x) and the laser intensity is adjusted to determine the intensity of the images. The images are acquired for 30 min. Figures were assembled from the TIFF and LIF files using open software ImageJ.

11. High Throughput Screening (HTS)

The HTS was done in collaboration with Dr. Mabel Loza at the University of Santiago de Compostela since they have operative HTS facilities (Unidad de evaluación de actividades farmacológicas de compuestos químicos (USEF)). The Prestwick Chemical Library® was used, which contains 1.120 small molecules, 90% being marketed drugs and 10% bioactive alkaloids or related substances.

The group designed and miniaturized/automatized the screening to perform a robust assay with good sensitivity and a good dynamic range to maximize reliability and reproducibility in our HTS. The HTS was executed by assaying 1.120 compounds.

The infrastructure required for carrying large-scale drug screening cascades is available and also computer software to store and analyse data. The equipment includes a Freedom Evo robot (Tecan) for handling liquids, an Aquarius robot (Tecan) for handling both 96-well and 384-well plates. Also available are Multidrop systems (TermoLab Systems), fitted to a Titan Stacker robotic arm (ThermoLab Systems) for the addition of liquid to 96-well and 384-well plates and also “Deep well” plates. A Columbus plate washer (Tecan) is also available and allows high yields in studies that require washing of excess colourants from plates (cytotoxicity, immunoenzyme assays).

11.1. Miniaturization assay

The assay for the regulation of Mfn2 gene expression was run in a miniaturized, 96-well plate format. This format requires validation and optimization of the luciferase assay

using HeLa Mfn2P 14 clone (20.000 cells/well). The cells were seeded and incubated at 37 ^{o}C in a humidified atmosphere of 5% CO_2/95% air. After 24 h the cells were incubated with RA (control activator) at 10 µM for 16 h. Then luciferase assay was performed and luminescence was measured at different times (1, 3, 4, 5, 11, 12, 13, 15, 17, and 20 min) using an integration time of 100 ms and using a Tecan Ultra Evolution detector. Miniaturization process consists in evaluate the luciferase response over time with the substrate luciferine, the signal in relation to noise (background) and the data dispersion (See section 2.1 of results and discussion).

The results obtained showed that the best condition to measure luciferase activity was 5 min after the addition of the luciferine substrate.

11.2. High Throughput Screening using Prestwick library

The compounds of the Prestwick Chemical Library® were delivered at 10 mM in DMSO (200 µL of each compound) in 96 well plates. To preserve the compounds stability the stock at 10 mM must be defrosted a maximum of two times. Thus, a diluted stock of the compounds at 1 mM in DMSO (10 µL) was prepared in 96 well plates to avoid frosting and defrosting problems. The final concentration of the compounds with the cells must be 10 µM with a maximum 1 % of DMSO to avoid toxicity problems. An intermediate 96 well plate with the compounds at 100 µM (10 % DMSO) was prepared with cell growth medium. 45 µL of cell growth medium were added in 96 well plates with a Multidrop system (TermoLab Systems), and 5 µL from the stock 96 well plate were taken and added to the intermediate plate with the Aquarius robot (Tecan) (Figure 90).

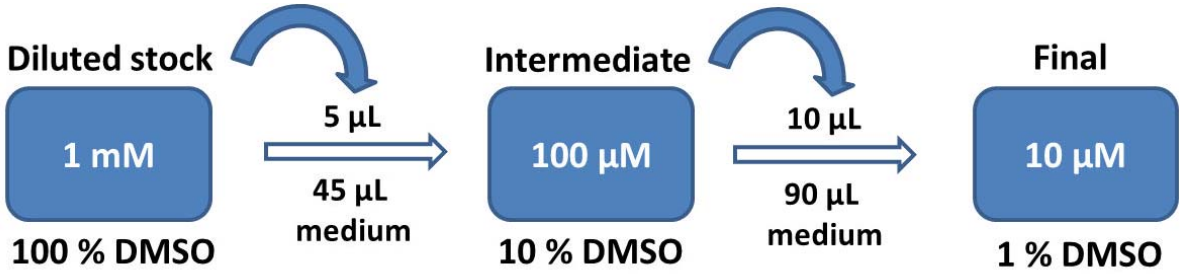

Figure 90. **Prestwick library compounds dilution to perform the HTS**

In the intermediate 96 well plate with the compounds at 100 µM, RA (100 µM) and DMSO (10 %) were added as a positive and negative controls, respectively. The RA was added manually (5 µL at 1 mM). The controls were added in the intermediate plate and not in the final plate to control the pipetting error in the Aquarius robot (Tecan). In the final plates all the pipetting was performed by the robot, so the final volumes were the same for all the wells and plates.

The intermediate plates were centrifuged for 30 s to remove the air bubbles in the wells. Then, 10 µL from each well of the intermediates plates were transferred to final plates with the Aquarius robot (Tecan). The final plates contained HeLa M2P14 cells (20.000 cells/well) with 90 µL of growth medium.

Note: The day before 14 plates of 96 wells were seeded with HeLa Mfn2M2P 14 cells (20.000 cells/well) and incubated at 37 ^{o}C in a humidified atmosphere of 5% CO_2/95% air.

Then, the cells were incubated with the compounds of the Prestwick Chemical Library® at a final concentration of 10 µM for 16 hours. Cells were incubated in parallel with RA (10 µM) and 1% DMSO (v:v). Positive and negative controls were run as an integral part of each assay to ensure the validity of the obtained results.

The next day the plates were washed with PBS1X using Columbus plate washer (Tecan), and lysis buffer (50 µL) was added with a multidrop System. The plates were shaken for 35 min. Then, 10 µL of each well plates were added in a new 96 well plates black (clear bottom) with the Aquarius robot (Tecan). Finally, luciferine was added (20 µL) to each well plates manually and the plates were shaken. Luciferase activity was measured after 5 minutes of the addition of the luciferine substrate in a Tecan Ultra Evolution detector.

The results of the screening were expressed as the activity percentage compared to 10 µM 9-RA, which has been considered as 100 % activity. Compounds showing an activity higher than 60% compared to 9-RA were considered as hits and were confirmed in an independent assay. 22 compounds were considered positive hits in the primary HTS.

A secondary screening was performed to confirm the 22 positive hits. The same process described above was performed. Finally, 12 compounds were considered possible activators of the human Mfn2 promoter (See section 2.2 of results and discussion).

11.3. Secondary screening to detect false positives

Once the HTS was done, a secondary screen using a different methodology was performed to discard compounds that generate a positive signal via other mechanisms. The objective of the secondary screening was to evaluate the direct effect of the compounds to purified luciferase activity to identify possible false positives.

The test was done in collaboration with Dr. Mabel Loza at the University of Santiago de Compostela. The kit used to perform the secondary assay was PKLight® Assay Kit (Lonza #L07-500).

Positive compounds at 10 µM final concentration (10 µL from a stock solution of 1 mM in DMSO) were added to 60 µL of the assay buffer (Imidazol 50 mM, KCl 50 mM, $MgCl_2$ 7 mM, ATP 10 µM, Tween 20 0.01 %, BSA 0.05 %, pH = 7.2). Then, 30 µL of the luciferase detection mixture was added and the mixture was incubated for 8 min at room temperature. Once the compounds were incubated the luminescence signal was measured using a lector Ultra Evolution (Tecan) using an integration time of 100 µs.

None of the evaluated compounds behaved as positive modulators of the luciferase activity (See section 2.3 of results and discussion).

REFERENCES

1 Dubbs, D. R. & Scherer, W. F. Variants of Japanese encephalitis virus cytopathic for L mouse fibroblasts and lass human epithelial cells. *Japanese journal of medical science & biology* **22**, 253-261 (1969).

2 Blau, H. M. *et al.* Plasticity of the differentiated state. *Science* **230**, 758-766 (1985).

3 Yaffe, D. & Saxel, O. Serial passaging and differentiation of myogenic cells isolated from dystrophic mouse muscle. *Nature* **270**, 725-727 (1977).

4 Boussif, O. *et al.* A versatile vector for gene and oligonucleotide transfer into cells in culture and in vivo: polyethylenimine. *Proc Natl Acad Sci U S A* **92**, 7297-7301 (1995).

5 Mislick, K. A. & Baldeschwieler, J. D. Evidence for the role of proteoglycans in cation-mediated gene transfer. *Proc Natl Acad Sci U S A* **93**, 12349-12354 (1996).

6 Laemmli, U. K. Cleavage of structural proteins during the assembly of the head of bacteriophage T4. *Nature* **227**, 680-685 (1970).

7 Hutter, E. *et al.* Senescence-associated changes in respiration and oxidative phosphorylation in primary human fibroblasts. *Biochem J* **380**, 919-928, doi:10.1042/BJ20040095 (2004).

8 Atamna, H., Paler-Martinez, A. & Ames, B. N. N-t-butyl hydroxylamine, a hydrolysis product of alpha-phenyl-N-t-butyl nitrone, is more potent in delaying senescence in human lung fibroblasts. *J Biol Chem* **275**, 6741-6748 (2000).

RESUM

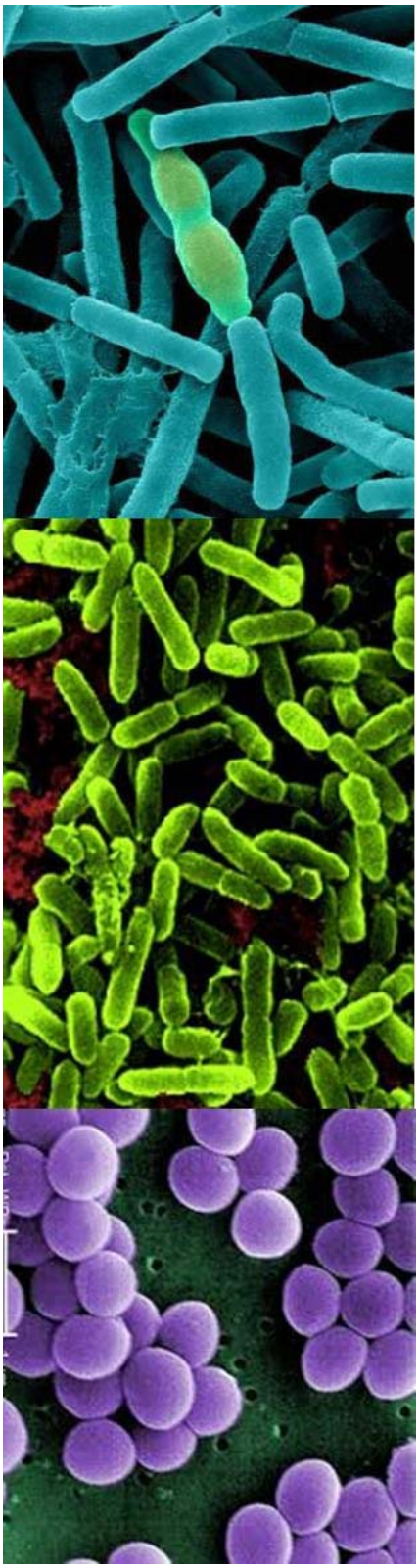

Resum

Capítol 1

Les malalties respiratòries infeccioses són malalties que afecten els conductes d'aire, els bronquis i els pulmons. Aquestes malalties oscil·len des d'infeccions agudes, com per exemple la pneumònia i la bronquitis, fins a condicions cròniques com són l'asma, la fibrosi quística i la malaltia pulmonar obstructiva crònica. Les infeccions de pulmó respiratòries són les principals causes de morbidesa i mortalitat a tot el món, amb un considerable cost humà, social i econòmic.

Les malalties respiratòries infeccioses poden ser causades per un número creixent de bacteris multi resistents als antibiòtics que existeixen actualment. Els bacteris que normalment habiten en les mucositats poden créixer fora de control i colonitzar i infectar els pulmons. Les alteracions en les mucositats tendeixen a la formació de micro-ambients bacterians coneguts com a biofilms, aquests són difícils de penetrar pels antibiòtics i les cèl·lules immunitàries. Els biofilms estan implicats en diferents infeccions patogèniques en el cos, com són les infeccions urinàries o d'orella, o poden causar greus infeccions en malalties com la fibrosi quística, la bronquièctasi i la malaltia pulmonar obstructiva crònica. Els biofilms són els responsables del 65% de totes les infeccions bacterianes.

Uns enzims indispensables pels bacteris són els enzims ribonucleòtids reductases (RNR), els quals produeixen els desoxiribonucleòtids per la síntesi d'ADN. Aquests enzims són necessaris pel creixement i per la germinació de l'espora del patogen. Hi ha tres classes d'enzims RNR, la classe I, II i III. Tots tres enzims creen un radical lliure a un residu de cisteïna, que està conservat en el lloc actiu, i així, inicien la reducció dels ribonucleòtids per a la síntesi i reparació de l'ADN. Aquestes tres classes d'enzims es diferencien en el mecanisme per generar el radical lliure, en el cofactor que necessiten, en la regulació al·lostèrica, en l'estructura quaternària i finalment en la dependència d'oxigen. Tot i aquestes diferències significatives, les tres classes d'enzims conserven l'estructura tridimensional del cor catalític i comparteixen mecanismes catalítics similars. La classe I depèn d'oxigen i només funciona en condicions aeròbiques, ja que la generació del radical tirosil necessita oxigen. La classe II és funcional en condicions aeròbiques i anaeròbiques i la classe III en condicions anaeròbiques. Una molècula capaç d'inhibir l'enzim RNR pararia el creixement del bacteri, esdevenint una estratègia terapèutica important en el tractament de les malalties respiratòries infeccioses.

Els organismes eucariòtics només codifiquen una classe de RNR, per la classe Ia. En canvi els bacteris codifiquen per més d'una classe de RNR depenent del medi on viuen. Normalment, hi ha un RNR predominant que és el responsable del creixement bacterià, i els altres RNR presents responen a altres mecanismes de regulació diferents al de la classe dominant.

L'objectiu d'aquest primer capítol està enfocat en trobar inhibidors específics dels enzims RNR de quatre línies cel·lulars de bacteris diferents: *Pseudomonas aeruginosa, Burkholderia cepacia, Staphylococcus aureus* i *Bacillus anthracis*, que són els organismes més comuns causants d'infeccions oportunistes en pacients que pateixen malalties respiratòries. *P. aeruginosa* és un dels pocs bacteris que codifiquen per les tres classes de RNR (Ia, II, i III). La classe Ia i II han estat detectades durant el creixement bacterià. *B. cenocepacia* codifica la classe RNR Ia pel creixement en condicions aeròbiques en combinació amb la classe RNR II, que és independent d'oxigen. *S. aureus* depèn de la classe RNR Ib pel creixement en condicions aeròbiques i en condicions anaeròbiques la classe III és essencial. Per últim, *B. anthracis* codifica per la classe RNR Ib en combinació amb la classe III, que només és funcional en condicions anaeròbiques. La majoria de bacteris Grams-positius depenen de la classe RNR Ib pel creixement bacterià en condicions aeròbiques. Nosaltres estem interessats a sintetitzar hidroxilamines específiques que actuïn com a radicals capturadors del radical tirosil de la classe RNR I bacteriana sense que afectin l'enzim RNR humà. Busquem inhibidors de la classe RNR I perquè vivim en condicions aeròbiques.

El primer fàrmac antiproliferatiu utilitzat per inhibir l'enzim RNR va ser la hidroxiurea, que actua com a radical capturador reduint el radical tirosil de l'enzim RNR. Torrents i *al.* van publicar un estudi on ensenyaven que el radical tirosil de l'enzim RNR Ib (NrdF) és una possible diana terapèutica per a fàrmacs amb activitat antibacteriana basada en radicals capturadors. La hidroxilamina i la *N*-metilhidroxilamina van ser identificades com a potents inhibidors pel tractament de l'àntrax, una infecció produïda per *B. anthracis.* Aquestes dues molècules inhibien el creixement del patogen a diverses ordres de magnitud de concentracions més baixes que la HU. A més a més, la *N*-metilhidroxilamina no és tòxica pels humans[8]. Per tant, els derivats de la *N*-hidroxilamina i *N*-metilhidroxilamina podrien ser utilitzats com a fàrmacs amb activitat antiproliferativa per combatre les infeccions bacterianes de pulmó.

El nostre grup amb col·laboració amb el grup del Dr. Torrents, líder de les infeccions bacterianes i teràpies antimicrobianes de l'Institut de Bioenginyeria de Catalunya (IBEC), vam enfocar la nostra recerca en desenvolupar una llibreria química basada en derivats d'àcids hidroxàmics i *N*-hidroxilamines que presentessin millors activitats antibacterianes que les descrites fins al moment, bloquejant els efectes del radical tirosil en l'enzim RNR,. L'objectiu del projecte era trobar inhibidors específics de l'enzim RNR (classe I) sense que afectin la classe Ia RNR d'humà, la qual s'expressa en cèl·lules eucariotes.

En primer lloc la síntesi dels àcids hidroxàmics es va intentar utilitzant l'estratègia en fase sòlida amb la resina 2-CTC. Es va incorporar el residu *N*-Fmoc-hidroxilamina a la resina a través d'un atac nucleòfil del grup hidroxil amb DIEA en DCM. A continuació, es va eliminar el grup Fmoc amb piperidina i DMF, i es va acoblar l'aminoàcid protegit (Fmoc-aa-OH) utilitzant el sistema TBTU-HOAt-DIEA per formar l'enllaç amida. Finalment, el grup Fmoc va

ser eliminat i l'amina lliure va ser acetilada utilitzant AcOH i DIPCDI en DCM. Un cop tenim l'àcid hidroxàmic, aquest s'escindeix de la resina amb tractament àcid utilitzant DCM-TFA 97:3 (v:v) i els protectors de la cadena lateral son eliminats amb TFA-H_2O 95:5 (v:v). Després de comprovar la puresa per HPLC-PDA i HPLC-MS l'àcid hidroxàmic és purificat per l'HPLC semi preparatiu de fase reversa (Esquema 1).

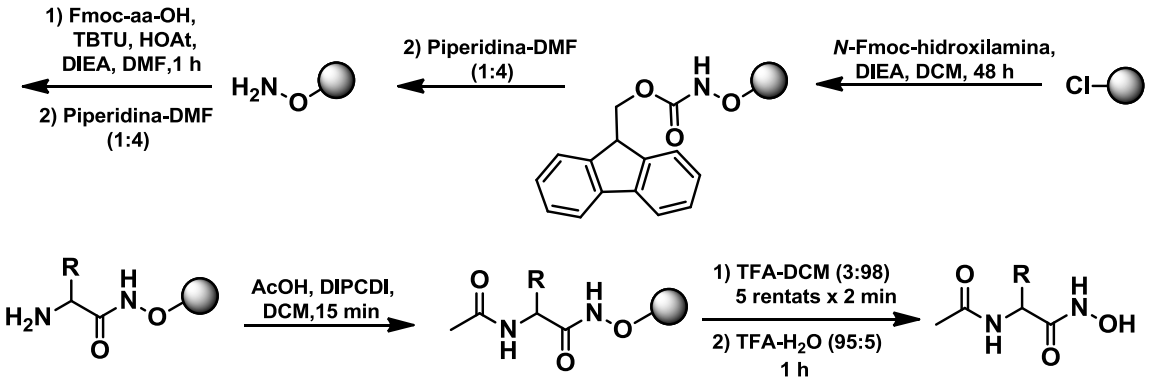

Esquema 1. Síntesi dels àcids hidroxàmics

Seguint aquest esquema sintètic, es va preparar una petita llibreria de 6 compostos. Els derivats dels àcids hidroxàmics contenien diferents aminoàcids per tal d'obtenir la mateixa estructura amb diferents cadenes laterals (Figura 1).

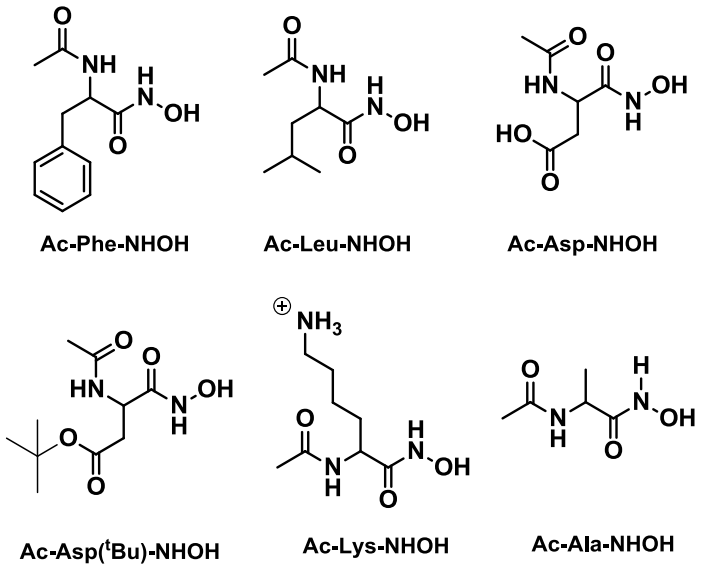

Figura 1. Llibreria d'àcids hidroxàmics sintetitzats

El procés de purificació dels àcids hidroxàmics és molt costós a causa de la petita mida i de la polaritat de les molècules. A més a més, després del pas d'acetilació s'obtenen productes secundaris que són difícils de separar. Tots aquests problemes fan que el rendiment de la síntesi sigui molt baix i s'obtingui molt poca quantitat del producte. Per això, aquesta estratègia va ser descartada. Tot i això, els productes dels quals es va obtenir més quantitat, Ac-Asp-NHOH i Ac-Ala-NHOH, van ser provats en *B. anthracis* i van donar actius.

Els compostos inhibeixen el creixement del bacteri. A més a més, l'activitat inhibidora de *B. anthracis* del Ac-Asp-NHOH és més bona que la *N*-metilhidroxilamina, utilitzada com a control positiu.

El següent pas va ser la síntesi de derivats d'hidroxilamina a partir d'amines primàries. L'oxidació d'amines primàries i secundàries dóna lloc a les hidroxilamines, que continuen tenint un parell d'electrons desaparellat i poden ser vulnerables a oxidacions. És per això, que la síntesi directa de *N*-alquilhidroxilamines a partir d'amines primàries utilitzant agents oxidants és complicada, a causa dels problemes de sobreoxidació que donen lloc als compostos nitrós i nitro.

Els mètodes més utilitzats per oxidar amines primàries a *N*-alquilhidroxilamines és utilitzant el peròxid d'hidrogen, l'àcid *m*-cloroperbenzoic (que està associat a problemes de sobreoxidació), el dimetildioxirà, l'oxone suportada sobre gel de sílice o d'alúmina o el peròxid de benzoïl. Aquest últim mètode necessita el tractament del producte intermediari, que és un *O*-acil-*N*-alquilhidroxilamina, amb àcid o base, per obtenir la hidroxilamina lliure.

Primer de tot, vam intentar oxidar les amines primàries a *N*-alquilhidroxilamines utilitzant el complex de peròxid d'hidrogen i urea i el tungstat de sodi com a catalitzador en èter. Aquest procediment va ser utilitzat per amines primàries diferents i únicament es va obtenir el producte de partida. En un cas, quan la reacció es va deixar tota la nit reaccionant, l'amina primària s'havia sobreoxidat donant com a producte el grup nitrós. Per tant, es va decidir utilitzar un altre procediment.

A continuació, vam utilitzar l'oxone, que està compost per $2KHSO_5 \cdot 1KHSO_4 \cdot 1K_2SO_4$, com a agent oxidant. L'oxone suportada sobre gel de sílice oxida amines primàries a hidroxilamines amb dissolvent o sense utilitzant el microones. Aquesta reacció es va portar a terme amb oxone suportada sobre gel de sílice, sense dissolvent i al microones a diferents temps. Utilitzant aquestes condicions, únicament es va obtenir el reactiu de partida. En canvi, en utilitzar oxone suportada sobre gel de sílice en benzè a reflux a 80 °C o en un sistema bifàsic (H_2O/DCM) a temperatura ambient, obteníem el material de partida, mescles de productes que contenien la hidroxilamina i subproductes més oxidats (nitrós i nitro) o únicament els productes sobreoxidats. La mescla de compostos no es podia separar del compost desitjat i es va decidir provar un altre procediment.

Finalment, vam decidir utilitzar el peròxid de benzoïl com a agent oxidant. Les amines primàries reaccionen amb el peròxid de benzoïl en DCM donant lloc a l'intermedi *O*-acil-*N*-alquil hidroxilamina, que per hidròlisi en condicions àcides o bàsiques dóna lloc a la hidroxilamina desitjada. Inicialment, en portar a terme la reacció, únicament obteníem el producte secundari, que és la benzilamida. Però, en utilitzar el peròxid de benzoïl en una solució aquosa saturada de K_2CO_3 vam aconseguir obtenir el producte desitjat en rendiments

baixos. Es van provar diferents condicions per augmentar el rendiment de la reacció, com per exemple, es va provar la base LiOH, es va augmentar i disminuir la temperatura, es van provar diferents dissolvents en condicions bàsiques o neutres, es va provar una solució tampó i es van variar els equivalents de peròxid de benzoïl. Finalment, les millor condicions van ser les següents: utilitzar la solució aquosa de K_2CO_3 en ACN (1:1) (v:v) a 4 °C, o utilitzar una solució tampó a pH 10.5 en DCM a 4 °C, encara que els rendiments continuaven sent baixos. Els productes secundaris obtinguts van ser incorporats a la llibreria, ja que és una pràctica habitual en la recerca de la química mèdica (Figura 2).

Un cop havíem obtingut el producte intermedi *O*-acil-*N*-alquil hidroxilamina, el següent pas era la hidròlisi en condicions àcides o bàsiques. Primer vam provar la hidròlisi en HCl en THF a 100 °C, i únicament obteníem el 4-clorobutan-1-ol, que és el producte obtingut degut a l'addició del Cl^- en el THF. Per tant, vam decidir canviar el dissolvent i utilitzar ISP a 83 °C i vam obtenir una mescla de productes. Finalment es va fer la hidròlisi en DCM a temperatura ambient i es va obtenir la hidroxilamina lliure però amb uns rendiments molt baixos. Degut als problemes obtinguts en condicions àcides, vam provar de fer la hidròlisi en condicions bàsiques utilitzant una solució aquosa de LiOH. Utilitzant aquestes condicions també obteníem una mescla de productes; el producte desitjat, la imina i un producte d'addició. El que creiem que passa és que en obtenir la hidroxilamina i la imina, la *N*-alquilhidroxilamina actua com a nucleòfil i ataca al carboni del grup imina generant un producte d'addició (Esquema 2). Els productes obtinguts eren molt difícils de separar.

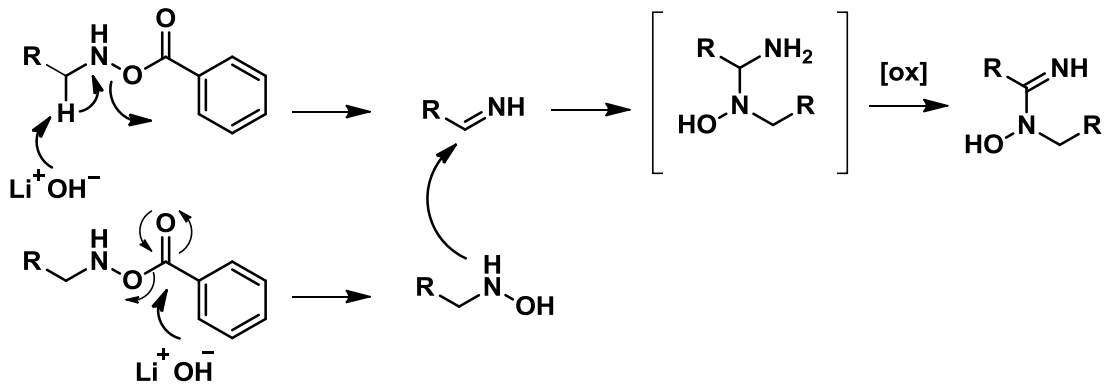

Esquema 2. Hidròlisi en condicions bàsiques utilitzant LiOH

Finalment vam decidir canviar l'estratègia per obtenir les *N*-alquilhidroxilamines i utilitzar l'aminació reductiva, on el grup carbonil es converteix en una amina a través d'una imina intermediària. El producte de partida són els aldehids, que es tracten amb una solució de liti perclorat-dietil èter (LPDE) 5.0 M amb *O*-trimetilsililhidroxilamina i s'agita durant 10 min. A continuació, s'afegeix el clorur de trimetilsilil i després de 10 min s'addiciona el complex de borà/TEA i es deixa reaccionar durant 1-2 h, obtenint la *N*-alquil-*O*-trimetilsililhidroxilamina. Per obtenir la hidroxilamina lliure s'addiciona una solució aquosa de $NaHCO_3$ saturat. En portar a terme la reacció es van obtenir uns rendiments molt baixos.

Per això, les condicions de la reacció van ser optimitzades, augmentant el nombre d'equivalents dels reactius i el temps de reacció, per millorar el rendiment de la reacció. Finalment, tota la síntesi de *N*-hidroxilamines es va realitzar deixant reaccionar l'aldehid (1eq), l'*O*-trimetilsililhidroxilamina (1.5 eq) i el clorur de trimetilsilil (1.5 eq) durant 8 h, i un cop s'addicionava el complex de borà/TEA (1.5 eq) la reacció es deixava reaccionant tota la nit.

Es va sintetitzar una petita llibreria de *N*-alquilhidroxilamines i també es van comprar altres compostos que estaven disponibles comercialment, com per exemple la *N*-tert-butilhidroxilamina, la *N*-benzilhidroxilamina i la *N*-ciclohexilhidroxilamina. A més a més, en fer la reacció, dues oximes intermediàries no es van reduir per culpa d'un efecte de conjugació entre l'anell aromàtic i el doble enllaç de l'oxima. La síntesi optimitzada de les *N*-alquilhidroxilamines i oximes va donar uns rendiments entre el 10 i el 70 %. Aquestes oximes juntament amb una altra disponible comercialment, l'etil (2*Z*)-ciano(hidroxiimino)etanoat, van ser introduïdes a la llibreria. També la *N,N*-dietillhidroxilamina, HOAt i HOBt, que són amines secundàries, i *N*-hidroxibutiramide, un àcid hidroxàmic, van ser comprats i introduïts a la llibreria (Figura 2). Tots aquests compostos donaran informació addicional sobre si les oximes, les amines secundàries, les amides i els àcids hidroxàmics poden inhibir o no l'enzim RNR, o pel contrari, si l'activitat inhibitòria de l'enzim RNR serà específic de les amines primàries.

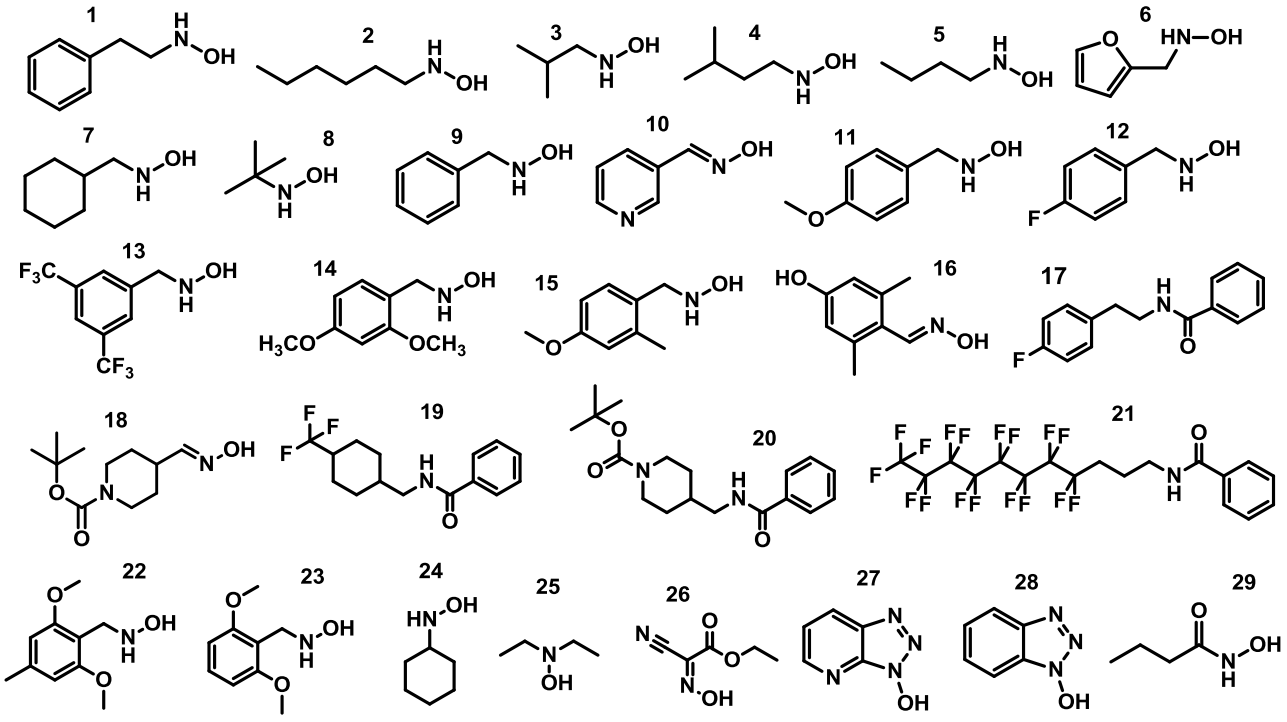

Figura 2. Llibreria d'hidroxilamines primàries, hidroxilamines secundàries, oximes, amides i àcids hidroxàmics.

La llibreria composta per àcids hidroxàmics (RCONHOH), *N*-hidroxilamines (RNHOH), oximes (RHC=NOH), hidroxilamines secundàries (RNR'OH) i amides (RNHCOR') va ser

avaluada en quatre línies bacterianes diferents: *P. aeruginosa*, *S. aureus*, *B. cenocepacia* i *B. anthracis*; que són els patògens més comuns causants d'infeccions oportunistes en pacients que pateixen malalties respiratòries.

L'avaluació biològica dels compostos va ser realitzada pel grup de l'Eduard Torrents de l'IBEC. Primer de tot, es va determinar la mínima concentració inhibitòria (MIC) dels compostos en les quatre línies de cèl·lules en cultiu líquid. Es van identificar diversos compostos amb activitat antibacteriana. Els compostos més prometedors són els compostos 1, 7, 12, 13, 14 i 16, ja que tots ells presenten activitat antiproliferativa en *B. anthracis*, *S. aureus* i *P. aeruginosa*. El compost 15 presenta activitat antiproliferativa en *B. anthracis* i *P. aeruginosa*. En canvi, cap dels compostos sintetitzats són actius en *B. cenocepacia*. Tots els compostos que presenten activitat antibacteriana són hidroxilamines primàries, només el compost 16, que és una oxima, presenta la mateixa activitat.

A més a més, alguns dels compostos van ser avaluats en la seva capacitat d'inhibir la formació de biofilm. En aquest cas els compostos 1, 7, 12 i 14 van ser incubats en *P. aeruginosa* i els compostos 7, 12 i 14 amb *S. aureus* durant 48 h a diferents concentracions. Tots els compostos a 0.0625 mM inhibien la formació de *P. aeruginosa* i *S. aureus* biofilm en un 99 %, i a concentracions superiors la inhibició era total. Un cop sabíem que els compostos podien inhibir la formació de biofilm, també volíem saber si podien inhibir el biofilm un cop ja estava format. Per això, primer de tot es va procedir a la formació de biofilm de *P. aeruginosa* i *S. aureus*. Un cop els biofilms estaven format es van afegir els compostos a diferents concentracions i a diferents temps d'incubació. El compost 7 a 0.125 mM durant 48 h era capaç d'inhibir el biofilm de *P. aeruginosa.* Els compostos 1 i 13 presentaven activitat per inhibir el biofilm format de *S. aureus*. Com més augmentava la concentració i el temps d'incubació més gran era la seva activitat de reduir el biofilm format.

Finalment, es va avaluar la citotoxicitat dels compostos que presentaven activitat antibacteriana, ja que volíem estar segurs que aquests compostos inhibien l'enzim RNR bacterià i no l'humà. Per tant, la línia cel·lular de macròfags murin J774 va ser incubada amb els compostos a diferents concentracions durant 24 i 48 h a 37 °C en una atmosfera humida al 5 % CO_2. A continuació, es va determinar la viabilitat cel·lular mitjançant un assaig colorimètric (MTT) (Taula 1).

Compound	**Cytoxicity (IC_{50}) mM**
1	**1.89**
2	**>4**
7	**1.33**
12	**1.30**
13	**2.07**
14	**2.27**

15	**2.18**
16	**>4**
19	**>4**
M-HA	**3.2**

Taula 1. Avaluació citotòxica dels compostos en una línia cel·lular de macròfags

Les concentracions citotòxiques són més altes que les concentracions que presenten activitat inhibidora de la formació de biofilm o inhibició del biofilm format. Per tant, aquests inhibidors amb activitat antibacteriana podran ser utilitzats com a medicaments en malalties respiratòries infeccioses cròniques com són la fibrosi quística, la malaltia pulmonar obstructiva crònica, bronquièctasis, granulomatosa crònica, i també en pacients que pateixen immunodeficiència o cremades cròniques.

Capítol 2

La mitofusina 2 (Mfn2) és una proteïna mitocondrial que participa en la fusió mitocondrial i regula el metabolisme mitocondrial. El grup del Dr. Antonio Zorzano ha demostrat que la proteïna Mfn2 està disminuïda en el múscul de pacients que pateixen obesitat o diabetis de tipus 2, i recentment han demostrat que la deficiència de Mfn2 en fetge o múscul produeix intolerància a la glucosa i resistència a la insulina en ratolins. Per tant, activadors de l'expressió de Mfn2 es podrien utilitzar terapèuticament pel tractament de la diabetis de tipus 2 i l'obesitat.

L'objectiu d'aquest segon capítol s'ha enfocat en trobar activadors específics de l'expressió de Mfn2 portant a terme un cribratge d'alt rendiment amb una llibreria de compostos. Els possibles activadors han de ser validats a nivell cel·lular i el seu mecanisme d'acció ha de ser identificat.

Per portar a terme aquest objectiu, es van generar diferents clons de cèl·lules HeLa que expressen de forma estable la proteïna luciferasa sota el control de 2 Kb (regió -1982/+54) del promotor humà de Mfn2. Es van generar 57 clons i es va dur a terme l'assaig luciferasa. A continuació, es van seleccionar 10 clons representatius de tots els clons generats, amb una activitat transcripcional del promotor humà de Mfn2 de rang alt i baix.

El promotor humà de Mfn2 respon a l'àcid 9-cis-retinoic (9-RA), el qual s'utilitza com a control positiu, ja que genera la proteïna luciferasa. Per validar els 10 clons seleccionats, aquests es van incubar amb 9-RA i es va mesurar la seva activitat transcripcional. Tots els clons tractats amb 9-RA mostraven una activitat transcripcional més gran respecte al control. Els clons 3, 14 i 19 van ser seleccionats, ja que eren els clons que presentaven una activitat transcripcional més gran respecte el control quan eren incubats amb 9-RA. A més,

aquests tres clons van ser transfectats amb un plasmid que codifica per PGC-1β, que és un coactivador de receptors nuclears que controla la transcripció de Mfn2, mitjançant la coactivació del receptor nuclear ERRα. El clon 14 va ser l'únic que augmentava l'activitat transcripcional del promotor de Mfn2 al ser transfectat amb PGC-1β. Per tant el clon 14 (Mfn2P 14) va ser seleccionat per portar a terme el cribratge d'alt rendiment amb la llibreria Prestwick. Aquesta llibreria conté 1120 compostos que estan aprovats per l'agència Food and Drug Administration (FDA).

El cribratge d'alt rendiment es va realitzar amb la col·laboració de la Dra. Mabel Loza a la Unitat d'avaluació d'activitats farmacològiques de compostos químics (USEF) a la Universitat de Santiago de Compostel·la. Per dur a terme el cribratge d'alt rendiment, primer de tot es va miniaturitzar el sistema per poder realitzar el cribratge en plaques de 96 pous. L'assaig luciferasa es va validar i optimitzar en plaques de 96 pous utilitzant les cèl·lules Mfn2P 14. El senyal de la luciferasa mitjançant el seu substrat, la luciferina, va ser avaluat amb el temps. A més a més, també es va avaluar el soroll de fons i la dispersió de dades. Es va decidir mesurar l'activitat luciferasa 5 min després de l'addició de la luciferina, ja que eren les condicions que proporcionaven els millors resultats per mesurar l'activitat luciferasa.

Les cèl·lules Mfn2P 14 van ser sembrades en plaques de 96 pous (20.000 cèl/pou) i l'endemà van ser incubades amb els compostos (10 μM) durant 16 h. A més a més, es va utilitzar 9-RA (10 μM) com a control positiu i 1% de DMSO, utilitzat com a vehicle pels compostos, com a control negatiu. Es va definir com a possible activador del promotor de Mfn2 aquells compostos que tinguessin una activitat luciferasa més gran del 60% respecte el 9-RA, el qual es va considerar que tenia una activitat del 100%. Els possibles activadors obtinguts del primer cribratge van ser confirmats en un assaig independent, i finalment 12 compostos van ser seleccionats com a possibles activadors del promotor humà de Mfn2.

Aquests possibles 12 activadors del promotor de Mfn2 es van comprar comercialment i es van repetir els assaigs luciferasa per triplicat en plaques de 24 pous (90.000 cel/pou) al nostre laboratori. Set dels dotze compostos van ser seleccionats, ja que donaven millor activitat transcripcional i reproductibilitat. A continuació, es van fer les corbes dosi resposta dels compostos en les cèl·lules Mfn2P 14 i es va obtenir la concentració òptima per obtenir la màxima activitat transcripcional del promotor de Mfn2.

Per validar els compostos a nivell cel·lular els set compostos seleccionats van ser incubats amb les concentracions òptimes en cèl·lules HeLa, les quals contenen el promotor de Mfn2 endogen. Seguidament, es van mesurar els nivells d'ARN missatger i de proteïna Mfn2. Únicament el compost 6, anomenat leflunomida, va ser capaç d'incrementar els nivells d'expressió de Mfn2. Es va tornar a intentar optimitzar la concentració de leflunomida i les cèl·lules HeLa van ser incubades a diferents concentracions de leflunomida a diferents

temps. Els nivells d'ARN missatger de Mfn2 van ser mesurats i les millors condicions que proporcionaven els millors resultats eren utilitzant la leflunomida a 50 µM durant 48 h.

La leflunomida, que comercialment és coneguda com a Arava, és un medicament utilitzat per l'artritis reumatoide que va ser comercialitzat als Estats Units el 1998. La leflunomida quan és ingerida es converteix en teriflunomida, que és el metabòlit actiu. Aquesta reacció té lloc en el plasma i la mucosa intestinal (Esquema 1).

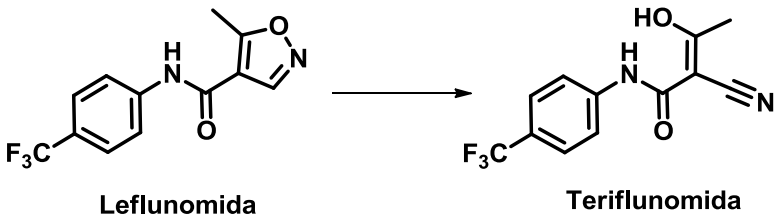

Leflunomida Teriflunomida

Esquema 1. La leflunomida es converteix en teriflunomida en el cos.

Per tant, volíem estar segurs que la teriflunomida presentava la mateixa activitat que la leflunomida. La teriflunomida va ser capaç d'incrementar els nivells d'activitat transcripcional del promotor de Mfn2 i, a més a més, també incrementava els nivells d'ARN missatger de Mfn2 en cèl·lules HeLa. Tenint en compte aquests resultats, es va concloure que la teriflunomida presentava la mateixa activitat que la leflunomida i es va seguir treballant amb la leflunomida.

La leflunomida havia estat validada en cèl·lules HeLa, però per estar segurs de la seva activitat va ser validada en les cèl·lules C2C12, on també va incrementar els nivells d'ARN missatger i de proteïna de Mfn2.

La leflunomida ha estat descrita com un inhibidor específic de l'enzim dihidroorotat deshidrogenasa (DHODH). Aquest enzim catalitza la quarta reacció de la síntesi *de novo* de pirimidines. L'enzim DHODH està localitzat a la membrana mitocondrial interna i catalitza l'oxidació del dihidroorotat a orotat utilitzant ubiquinona com a acceptor d'electrons. La leflunomida inhibeix l'enzim unint-se en el lloc d'unió de la ubiquinona, i d'aquesta manera evita la producció de la uridina monofosfat (UMP). A partir de l'UMP deriven altres nucleòtids del grup pirimidina, els quals són precursors importants utilitzats en ADN (timina i citosina), en ARN (uracil i citosina), en glicoproteïnes i en la biosíntesi de fosfolípids. Les bases pirimidíniques són essencials pel metabolisme i el creixement cel·lular.

La leflunomida i la teriflunomida produeixen efectes antiproliferatius en les cèl·lules HeLa i C2C12 a través de la inhibició de l'enzim DHODH, que causa la disminució de la síntesi de pirimidines. L'addició d'uridina, que en les cèl·lules és metabolitzada a uridina monofosfat (UMP), la qual és un prerequisit per a la formació de pirimidines difosfat i

trifosfat, reverteix la deficiència de la síntesi de pirimidines. Per tant, la uridina evita l'efecte antiproliferatiu provocat per la leflunomida i el seu metabòlit actiu (Figura 1).

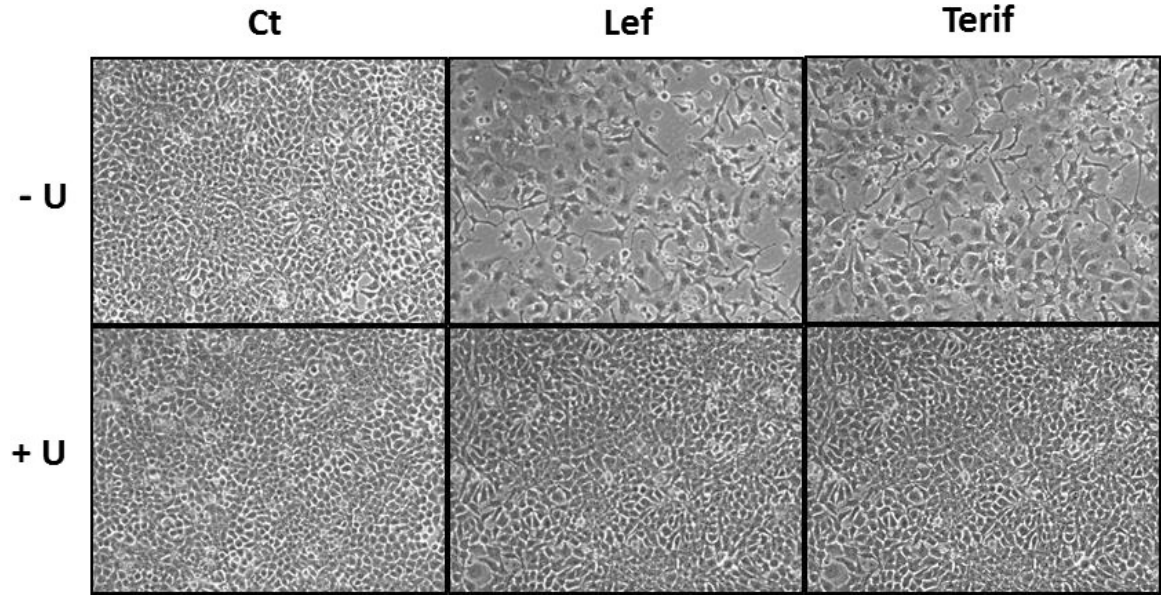

Figura 1. La uridina bloqueja l'efecte antiproliferatiu induït per la leflunomida i la teriflunomida en les cèl·lules HeLa.

A més, l'addició d'uridina en cèl·lules HeLa tractades amb leflunomida o teriflunomida bloqueja l'increment dels nivells d'ARN missatger de Mfn2. Aquests resultats suggereixen que l'augment de Mfn2 és provocat per la deficiència en la síntesi de pirimidines, indicant que el mecanisme d'acció d'aquests compostos està relacionat amb la inhibició de l'enzim DHODH.

Per tal d'elucidar l'efecte de la leflunomida en la fusió i la fissió mitocondrial, altres proteïnes de membrana mitocondrial involucrades en fusió, com per exemple la proteïna Mfn1 i Opa1, i involucrades en fissió, com per exemple Drp1 i Fis 1, van ser mesurades.

La leflunomida i la teriflunomida augmenten els nivells d'ARN missatger de Mfn1, però no es veuen canvis en els nivells d'ARN missatger d'Opa1 i de Drp1. L'addició d'uridina reverteix l'increment de Mfn2. A més, la leflunomida indueix l'expressió de la proteïna Mfn1 i disminueix la proteïna Drp1 en les cèl·lules HeLa i C2C12. Opa1 disminueix en les cèl·lules HeLa, encara que aquesta disminució no és evident en les cèl·lules C2C12, i no es veuen canvis en els nivells de proteïna de Fis1. L'addició d'uridina en les cèl·lules C2C12 tractades amb leflunomida evita l'increment de les proteïnes Mfn2 i Mfn1. Aquests resultats suggereixen que la leflunomida o teriflunomida, causen una deficiència en la síntesi de pirimidines a través de la inhibició de l'enzim DHODH, i augmenten l'expressió de les proteïnes Mfn2 i Mfn1. L'addició d'uridina, que reverteix la deficiència de pirimidines, evita l'augment de les mitofusines. Aquests resultats suggereixen un desplaçament del balanç entre fusió i fissió cap a fusió mitocondrial induint un increment de la longitud dels filaments mitocondrials quan les cèl·lules estan exposades a una deficiència de pirimidines.

Per observar els filaments mitocondrials de les cèl·lules es van utilitzar les cèl·lules HeLa i C2C12 que expressen de forma estable la proteïna mtDsRed, les quals van ser incubades amb leflunomida. Les cèl·lules HeLa van ser fixades i visualitzades al microscopi confocal. En canvi, les cèl·lules C2C12 van ser visualitzades *in vivo* utilitzant el microscopi confocal "spinning disk" (Figura 2).

A) Cèl·lules HeLa

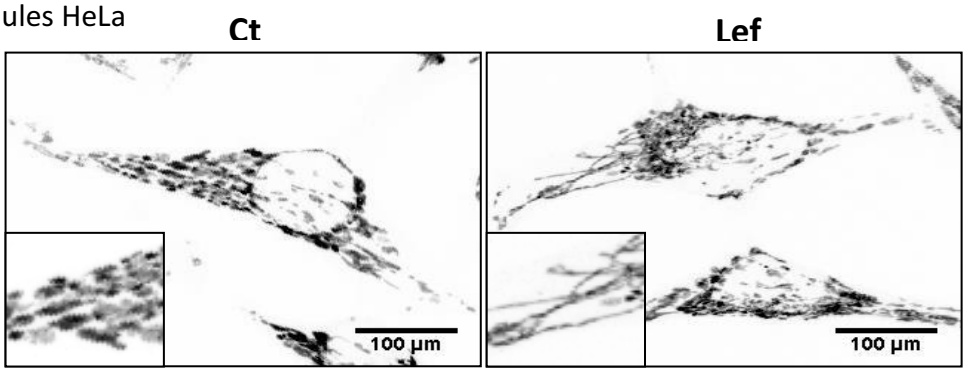

B) Cèl·lules C2C12

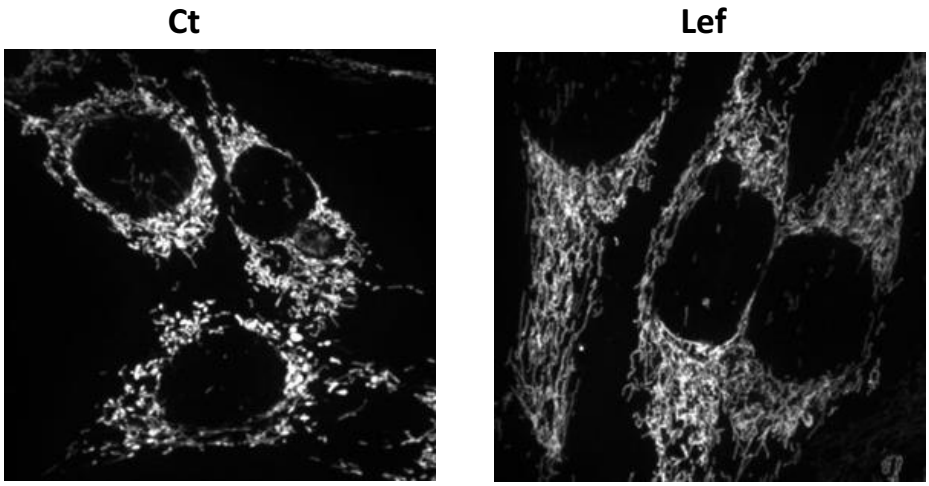

Figura 2. Imatges representatives de la morfologia mitocondrial en cèl·lules HeLa i C2C12 que expressen de forma estable la proteïna mtDsRed incubades amb leflunomida.

La leflunomida indueix un increment de la longitud dels filaments mitocondrials en les cèl·lules HeLa i C2C12. Aquesta elongació de la xarxa mitocondrial s'explica per una marcada inducció dels nivells de proteïna de fusió mitocondrial Mfn2 i Mfn1, i una disminució dels nivells de la proteïna de fissió Drp1.

Un cop sabem que la leflunomida modula les proteïnes mitocondrials involucrades en la dinàmica mitocondrial produint l'elongació de les mitocòndries, també volíem saber si afectava la funció mitocondrial en les cèl·lules C2C12. Per això es va mesurar el potencial de membrana i el consum d'oxigen. La leflunomida augmenta el potencial de membrana, i reprimeix de forma moderada la respiració mitocondrial màxima, després d'afegir FCCP (Figura 3).

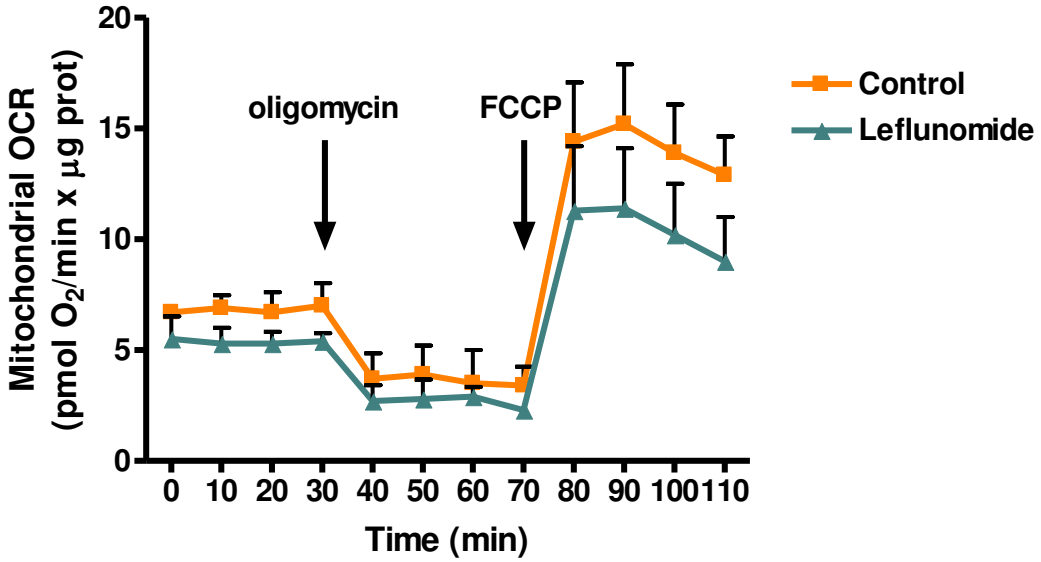

Figura 3. El consum d'oxigen mitocondrial (OCR) va ser mesurat en les cèl·lules C2C12 incubades amb leflunomida.

La fusió mitocondrial consisteix en dos processos on la membrana interna i l'externa es fusionen de forma separada. El mecanisme de fusió depèn de les proteïnes de membrana mitocondrials externes, que són la Mfn2 i la Mfn1, i de la proteïna de membrana mitocondrial interna Opa1. Nosaltres volíem saber si l'efecte de la leflunomida depenia dels components claus de la maquinària de fusió mitocondrial, per això, es van utilitzar les cèl·lules MEFwt, MEF Mfn2$^{-/-}$ i MEF Mfn1$^{-/-}$. La leflunomida incrementa els nivells de Mfn2, Mfn1 i Opa1 en totes les cèl·lules MEFs i no es veuen canvis en els nivells de proteïna de Drp1. A més a més, es va procedir a l'observació dels filaments mitocondrials en aquestes cèl·lules. Per dur a terme la visualització, es van utilitzar les cèl·lules MEFwt, MEF Mfn2$^{-/-}$ i MEF Mfn1$^{-/-}$ que expressen de forma estable la proteïna mtDsRed i es van visualitzar *in vivo* en el microscopi confocal spinning disk o en el microscopi confocal ScanR/TIRF.

Les cèl·lules MEFwt presenten dues morfologies mitocondrials diferents. La classe majoritària està caracteritzada per una xarxa d'extensos túbuls distribuïts al voltant del nucli, sense o amb poques mitocòndries esfèriques, mentre que la classe minoritària conté mitocòndries esfèriques. La leflunomida causa un allargament de les mitocòndries en la majoria de les cèl·lules, i el nombre de mitocòndries fragmentades disminueix (veure figura 4).

La pèrdua de Mfn1 o Mfn2 en les cèl·lules MEFwt provoca fragmentació mitocondrial. La diferència entre la pèrdua de Mfn1 i Mfn2, és que la pèrdua de Mfn1 provoca una fragmentació més gran produint petites esferes mitocondrials de mida uniforme, mentre que, la pèrdua de Mfn2 produeix esferes de mides variables i túbuls mitocondrials.

Les cèl·lules MEF deficients en Mfn2 tenen tres tipus de poblacions diferenciades: cèl·lules amb mitocòndries esfèriques (10%), cèl·lules amb mitocòndries esfèriques i túbuls d'una llargada màxima de 9 µm (82%) i cèl·lules amb una xarxa mitocondrial allargada que conté túbuls més llargs de 9 µM (8 %). La leflunomida incrementa el número de cèl·lules que contenen una xarxa mitocondrial allargada del 8 al 53 % de la població (veure figura 4).

Les cèl·lules MEF deficients en Mfn1 també presenten tres tipus de poblacions diferents: les cèl·lules amb mitocòndries esfèriques (88 %), les cèl·lules amb túbuls curts d'una llargada màxima de 5 µm (12 %) i una població molt més petita (1 %) que conté túbuls mitocondrials d'una llargada màxima de 5 µm. La leflunomida augmenta el número de cèl·lules que contenen els túbuls mitocondrials curts del 12 al 34 %, però no és capaç d'allargar els túbuls mitocondrials en les cèl·lules MEF Mfn1$^{-/-}$ tant com en les MEF Mfn2$^{-/-}$ (Figura 4).

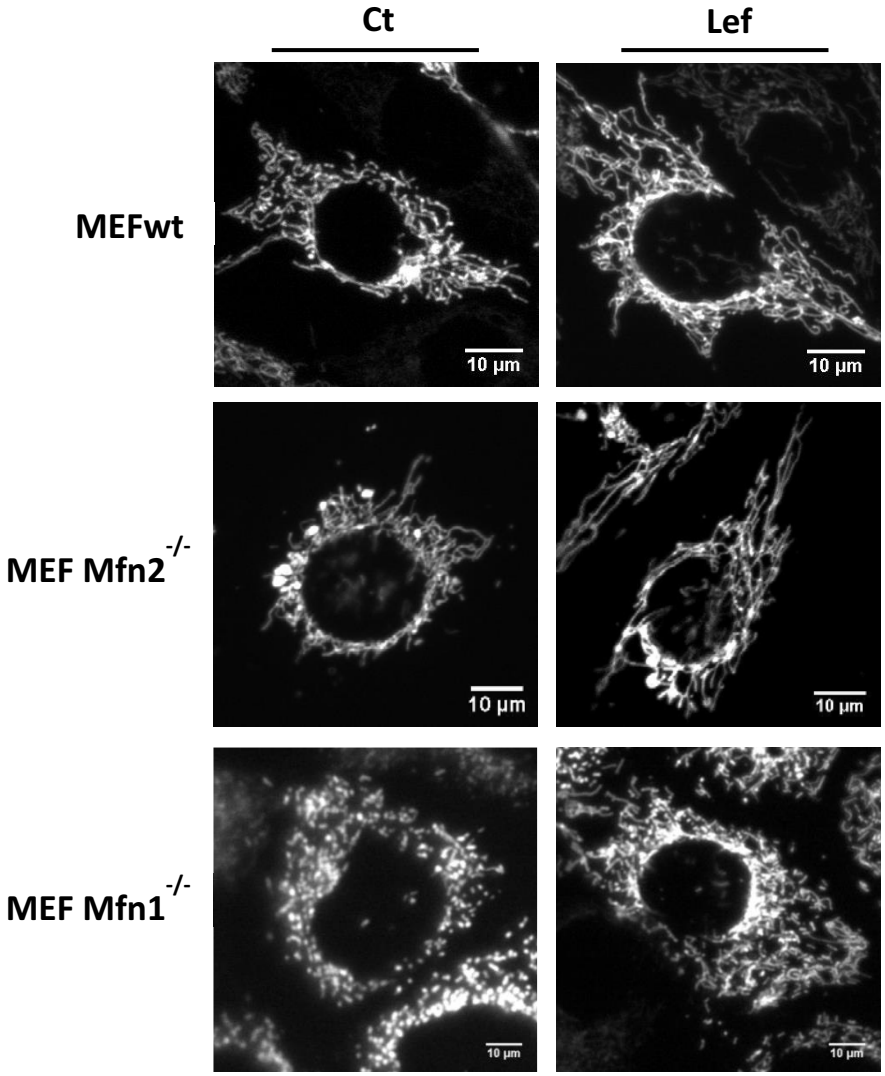

Figura 4. Imatges representatives de la morfologia mitocondrial en cèl·lules MEFwt, MEF Mfn2$^{-/-}$ i MEF Mfn1$^{-/-}$ que expressen de forma estable la proteïna mtDsRed incubades amb leflunomida.

La leflunomida promou l'allargament de les mitocòndries en totes les cèl·lules MEFs, encara que, l'elongació mitocondrial depèn més de Mfn1 que de Mfn2 a causa de l'allargament més gran de les cèl·lules MEF Mfn2$^{-/-}$ comparat amb les cèl·lules MEF Mfn1$^{-/-}$. Aquest resultat indica que Mfn1 exerceix un rol més important en l'elongació mitocondrial.

La leflunomida produeix efectes antiproliferatius en les cèl·lules MEFwt, MEF Mfn2$^{-/-}$ i MEF Mfn1$^{-/-}$ a través de la inhibició de l'enzim DHODH, que causa la disminució de la síntesi de pirimidines. L'addició d'uridina, que en les cèl·lules és metabolitzada a uridina monofosfat (UMP), reverteix la deficiència de la síntesi de pirimidines i evita parcialment l'efecte antiproliferatiu provocat per la leflunomida, ja que la recuperació no és total com en el cas de les cèl·lules HeLa i C2C12. Aquests resultats suggereixen que les cèl·lules MEFs són més sensibles a la deficiència de pirimidines que les cèl·lules HeLa o C2C12.

A continuació, la funció mitocondrial en les cèl·lules MEFwt, MEF Mfn2$^{-/-}$ i MEF Mfn1$^{-/-}$ va ser mesurada, ja que volíem saber si els efectes de la leflunomida en la funció mitocondrial depenia de l'expressió de Mfn2 o de Mfn1. La leflunomida augmenta el potencial de membrana en totes les cèl·lules MEFs i reprimeix la respiració mitocondrial en les cèl·lules MEFs, més que en les cèl·lules C2C12. En les cèl·lules MEFs s'observa menys consum d'oxigen en la situació de rutina, en la situació de leak i també en la capacitat respiratòria màxima. A més a més, a partir dels valors de consum d'oxigen mitocondrial es van calcular els "Flux Control Ratios", que ens donen informació sobre el grau d'acoblament de la cadena respiratòria i la fosforilació oxidativa. La Respiratory Control Ratio (RCR = E/L) té tendència a augmentar en les cèl·lules MEFwt i MEF Mfn1$^{-/-}$ tractades amb leflunomida, indicant que la cadena de transport electrònic i la fosforilació oxidativa estan més acoblades. En canvi, la "Phosphorylation Respiratory Control Ratio" (RCR_p = (R-L)/E) té tendència a disminuir en les cèl·lules MEFs incubades amb leflunomida, indicant que el percentatge de la capacitat respiratòria màxima que utilitzen les cèl·lules lligat a la producció d'ATP és inferior.

Anteriorment s'ha explicat que l'enzim DHODH, localitzat en la membrana mitocondrial interna, catalitza la quarta reacció de la síntesi de pirimidines, que consisteix en l'oxidació del dihidroorotat en orotat utilitzant la ubiquinona com a cosubstrat i acceptor d'electrons. Seguidament, la ubiquinona al acceptar el parell d'electrons és convertida en ubiquinol, que és el substrat del complex III de la cadena respiratòria. Per tant, la síntesi *de novo* de pirimidines està acoblada a la cadena respiratòria mitocondrial. Per això, creiem que la disfunció de la cadena respiratòria a través del complex IIII, inhibiria indirectament l'enzim DHODH causant una deficiència de la síntesi de pirimidines, i com a conseqüència produiria un allargament de les mitocòndries igual que passa amb el compost leflunomida. Per comprovar aquesta hipòtesi, dos inhibidors específics del complex III, mixotiazol i antimicina A, van ser emprats.

Primer de tot es van fer estudis de concentració i de temps d'incubació pels dos compostos, per obtenir la concentració òptima que produeix el màxim increment en els nivells d'ARN missatger de Mfn2 en cèl·lules HeLa. Les millors condicions obtingudes per mixotiazol són una concentració de 2 µM i un temps d'incubació de 24 h i per antimicina A la concentració òptima és 10 µM i un temps d'incubació de 24 h en cèl·lules HeLa. Aquestes condicions van ser validades, ja que augmentaven els nivells de proteïna de Mfn2 en cèl·lules HeLa.

D'altra banda, els compostos produeixen efectes antiproliferatius en les cèl·lules HeLa i C2C12. Així, estem segurs que els inhibidors de complex III, indirectament inhibint l'enzim DHODH, inhibeixen també la síntesi de pirimidines.

A més, es van mesurar els nivells d'ARN missatger de Mfn2, Mfn1, Opa1 i Drp1 de les cèl·lules HeLa tractades amb mixotiazol o antimicina A en presència o absència d'uridina. L 'addició d'uridina evita l'increment d'expressió gènica de Mfn2 induïda per mixotiazol i antimicin A. Aquests resultats confirmen que l'augment d'expressió de Mfn2 és desencadenada per la deficiència de pirimidines. Mixotiazol tendeix a augmentar els nivells d'ARN missatger de Mfn1 i a disminuir els d'Opa1, mentre que els nivells de Drp1 no varien. L'antimicina A tendeix a augmentar els nivells d'ARN missatger de Mfn1 i de Drp1, mentre que els nivells d'Opa1 no varien. En ambdós casos, l'addició d'uridina reverteix aquestes tendències.

El següent pas va ser analitzar els nivells de les proteïnes mitocondrials involucrades en els mecanismes de fusió i fissió en cèl·lules HeLa. Així es va trobar que mixotiazol incrementava els nivells de proteïna de Mfn1, i disminuïa els d'Opa1, mentre que Drp1 no variava. Aquests resultats suggereixen que mixotiazol podria induir l'allargament de les mitocòndries, ja que augmenta els nivells de les proteïnes Mfn2 i Mfn1. En canvi, antimicina A presenta una tendència a disminuir els nivells de proteïna de Drp1, però Mfn1 no varia. Els nivells d'Opa1 no varien però sí que s'observa una variació de les bandes. Opa1 és una proteïna mitocondrial interna que participa en la fusió de la membrana interna de les mitocòndries i presenta 8 isoformes diferents. Les isoformes llargues activen la fusió mitocondrial interaccionant amb les mitofusines, i les isoformes curtes detenen la fusió i generen fragments mitocondrials. L'apoptosi provoca que Opa1 s'alliberi en el citosol, on les isoformes llargues són proteolíticament processades a isoformes curtes i les mitocòndries són fragmentades. L'antimicin A produeix un canvi de les isoformes d'Opa1, passant de les formes llargues a les curtes. Aquests resultats suggereixen que l'antimicina A provoca fragmentació mitocondrial.

Per observar els filaments mitocondrials de les cèl·lules es van utilitzar les cèl·lules HeLa mtDsRed, les quals van ser incubades amb mixotiazol i antimicin A. Les cèl·lules HeLa mtDsRed van ser fixades i visualitzades al microscopi confocal (Figura 5).

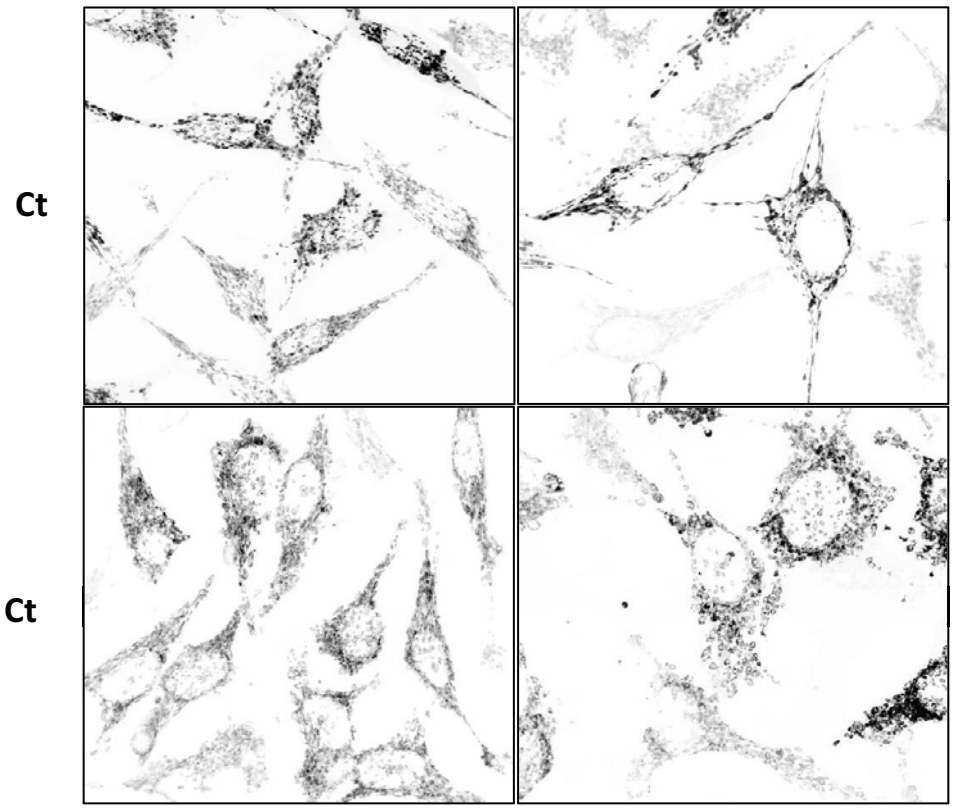

Figura 5. Imatges representatives de la morfologia mitocondrial en cèl·lules HeLa mtDsRed incubades amb mixotiazol i antimicin A.

Les cèl·lules HeLa mtDsRed incubades amb mixotiazol mostren una xarxa mitocondrial allargada comparades amb les cèl·lules control. Aquests resultats demostren que el mixotiazol incrementa l'expressió de les mitofusines i promou l'elongació de les mitocòndries. Al contrari, antimicina A causa fragmentació mitocondrial. Aquests resultats suggereixen que l'antimicina A accelera el procés proteolític de les isoformes llargues d'Opa1 a les isoformes curtes, inactivant Opa1 i produint fragmentació mitocondrial. Per tant, es va decidir descartar l'antimicina A i continuar amb mixotiazol.

El mixotiazol va ser validat en una altra línia cel·lular, en les cèl·lules C2C12. Però en aquest cas per obtenir un increment dels nivells de proteïna de Mfn2, mixotiazol s'havia d'incubar a una concentració 2 µM durant 12 h. Les cèl·lules C2C12 incubades amb mixotiazol durant 24 h presentaven apoptosis i fragmentació mitocondrial. Mixotiazol augmenta els nivells de les proteïnes Mfn2, Mfn1 i Opa1, les quals estan involucrades en fusió mitocondrial. En canvi, disminueix els nivells de proteïna Drp1, que està involucrada en fissió mitocondrial. La visualització de les cèl·lules C2C12 mtDsRed es va realitzar *in vivo* (Figura 6).

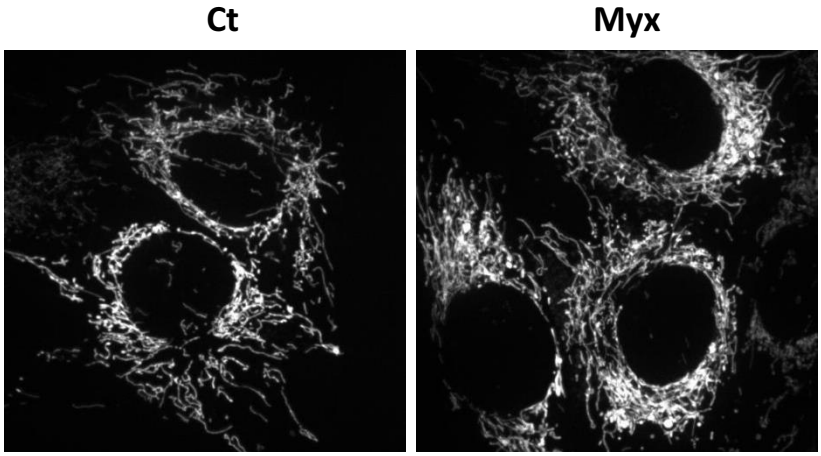

Figura 6. Imatges representatives de la morfologia mitocondrial en cèl·lules C2C12 mtDsRed incubades amb mixotiazol.

Les mitocòndries de les cèl·lules C2C12 mtDsRed incubades amb mixotiazol estan allargades respecte al control. A més, la morfologia mitocondrial de les cèl·lules MEFwt mtDsRed incubades amb mixotiazol a 2 µM durant 12 h també va ser visualitzada (Figura 7).

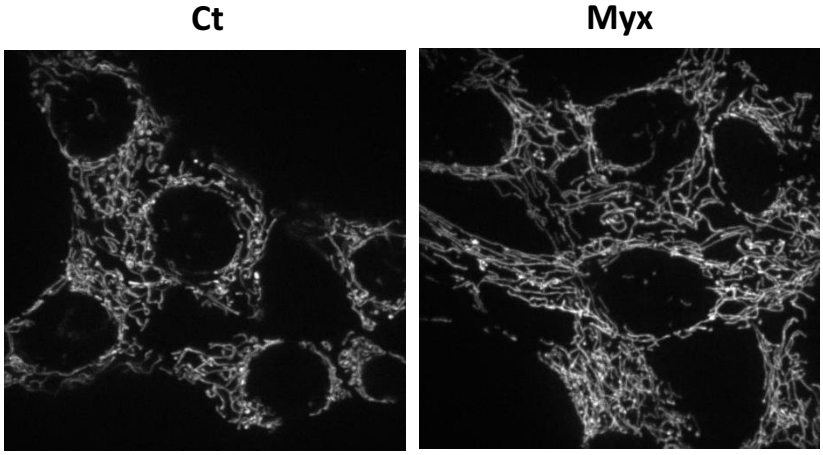

Figura 7. Imatges representatives de la morfologia mitocondrial en cèl·lules MEFwt mtDsRed incubades amb mixotiazol.

Les cèl·lules MEFwt mtDsRed incubades amb mixotiazol mostren una xarxa mitocondrial allargada comparada amb les cèl·lules control. Aquests resultats demostren que el mixotiazol incrementa l'expressió de les mitofusines i promou l'elongació de les mitocòndries en les cèl·lules HeLa, C2C12 i MEFwt.

Per tant, podem concloure que el mixotiazol i la leflunomida inhibint la síntesi de pirimidines, modulen les proteïnes mitocondrials involucrades en la dinàmica mitocondrial i promouen l'elongació mitocondrial.

Els inhibidors de la síntesi de pirimidines produeixen un bloqueig de la via depenent de p53. Ha estat descrit que l'absència de la síntesi d'ADN en fibroblast produeix una parada del cicle cel·lular a la fase G1/S depenent de p53. La disminució de CTP, GTP, o UTP és

suficient per produir una parada del cicle, depenent de p53. L'addició d'uridina, impedeix l'increment de l'expressió de p53. S'ha suggerit que p53 pot mantenir l'estabilitat genètica prevenint la replicació d'ADN durant la deficiència de pirimidines. A més a més, s'ha descrit que la inhibició específica del complex III de la cadena respiratòria, però no la inhibició de la cadena respiratòria *per se*, produeix una inducció de p53. Així doncs, el desacoblament produït entre l'enzim DHODH i el complex III produeix una resposta de p53. La nostra hipòtesi és que la deficiència de pirimidines, per causa dels inhibidors de l'enzim DHODH o del complex III, causa estrès cel·lular i desencadena l'activació de p53. p53 modularia les proteïnes mitocondrials involucrades en fusió i fissió i promouria l'elongació de les mitocòndries com a resposta a aquest estrès (Figura 8).

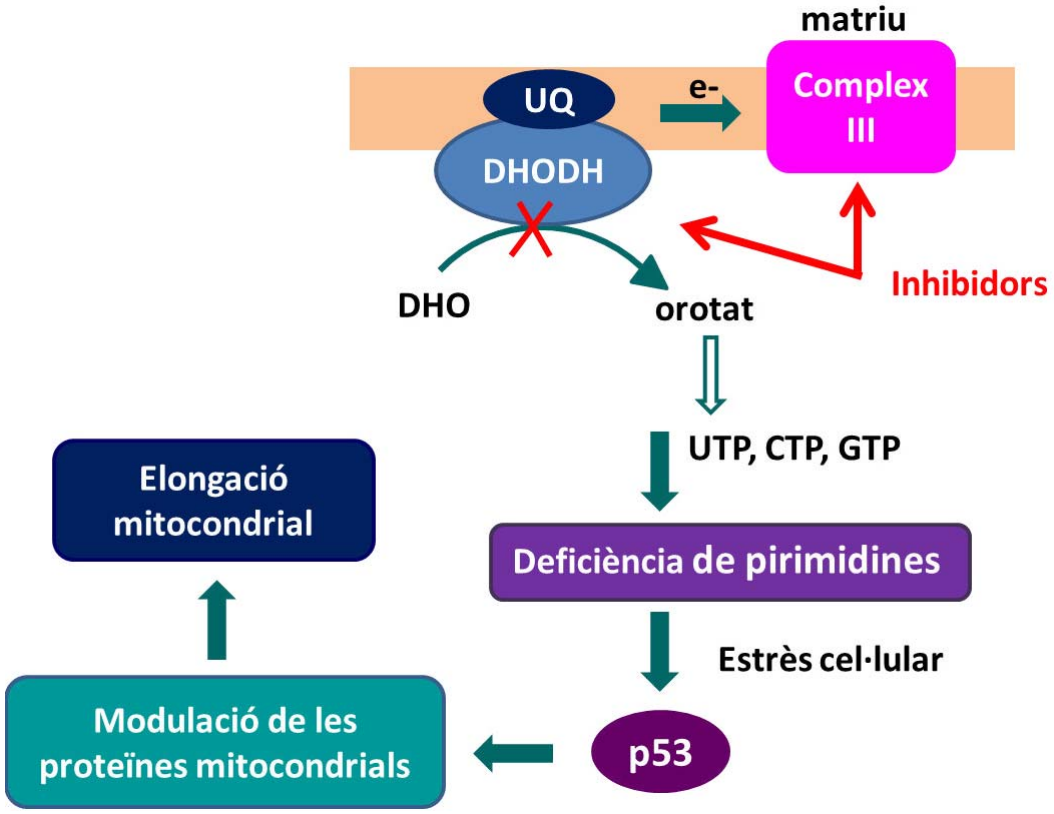

Figura 8. La síntesi de pirimidines està vinculat a la via de p53

La leflunomida i la teriflunomida disminueixen la síntesi de pirimidines inhibint l'enzim DHODH i augmenten l'expressió gènica de p53. L'addició d'uridina, que reverteix la deficiència de pirimidines, impedeix l'augment d'ARN missatger de p53. A més a més, la leflunomida augmenta els nivells de la proteïna p53 en cèl·lules HeLa. L'increment de p53 també va ser confirmat en les cèl·lules C2C12 incubades amb leflunomida, i l'addició d'uridina evitava aquest increment. Per tant, la deficiència de pirimidines causa un augment de l'expressió de p53 que pot ser impedit per l'addició d'uridina, que restableix els nivells de les pirimidines. D'altra banda volíem saber si aquest efecte també es produïa en les cèl·lules MEFwt i en les cèl·lules MEF deficients de Mfn2 o de Mfn1. Totes les cèl·lules MEFs presenten un augment dels nivells de proteïna de p53 quan són incubades amb leflunomida, el qual és impedit per l'addició externa d'uridina.

El mixotiazol, que disminueix la síntesi de pirimidines a través de la inhibició del complex III de la cadena respiratòria, també augmenta els nivells d'expressió de p53 en cèl·lules HeLa tant els nivells d'ARN missatger com els de proteïna. L'addició d'uridina externa impedeix l'augment de l'expressió de p53. A més, l'increment de l'expressió de p53 per causa de mixotiazol també va ser validat en les cèl·lules C2C12.

Per tant, podem concloure que la deficiència de pirimidines, a causa dels inhibidors de l'enzim DHODH o del complex III, leflunomida i mixotiazol, respectivament, indueixen l'increment de l'expressió de p53.

La proteïna p53 juga un paper molt important en resposta al dany de l'ADN i a la deficiència de pirimidines, ja que l'activació de p53 pot concloure en parada de cicle cel·lular i reparació de l'ADN o en apoptosis. Els nivells de p53 estan controlats a través de la degradació del proteasoma. La MDM2 i altres lligases E3 inhibeixen l'acumulació de p53, marcant p53 amb ubiqüitina per la seva posterior degradació pel proteasoma 26S. Aquest procés pot ser aturat per estrès, a través de la fosforilació de p53, o a través del increment de la proteïna inhibidora $p14^{ARF}$. La fosforilació de p53 a la Ser15 o a la Ser20 disminueix la interacció entre p53 i el seu regulador negatiu, MDM2, atès que impedeix l'habilitat de MDM2 d'unir-se a p53, promovent l'activació i l'acumulació de p53.

Tant les cèl·lules HeLa com les cèl·lules C2C12 presenten una forta activació de la Ser15 de p53 en tractar-les amb leflunomida o amb mixotiazol. A més a més, l'addició d'uridina que reverteix la deficiència en pirimidines és capaç d'inhibir l'activació de p53 a través de la Ser15. Per tant, podem concloure que la leflunomida i el mixotiazol promouen l'activació i l'acumulació de p53 a través de la fosforilació de la Ser15.

Per estar segurs que p53 regula els gens mitocondrials involucrats en la dinàmica mitocondrial les cèl·lules HeLa van ser transfectades temporalment amb un vector d'expressió de p53 (CMVp53) o amb un vector buit utilitzat com a control negatiu (pcDNA3.1). Aquests experiments no van funcionar, ja que es va aconseguir molt poc increment de p53.

Seguidament, es va reprimir l'expressió de p53 utilitzant els ARN d'interferència (siRNA). Les cèl·lules HeLa van ser transfectades amb el siRNA de p53 (específic d'humà) i el siRNA control que conté un conjugat de fluoresceïna per mesurar l'eficiència de la transfecció. A continuació, les cèl·lules van ser incubades amb leflunomida. Primer de tot es van mesurar els nivells d'ARN missatger de p53 per estar segurs que els siRNA havien funcionat. Es veia una disminució de l'expressió gènica de p53 en les cèl·lules on p53 estava reprimida, i a més a més, leflunomida no tenia cap efecte en aquestes cèl·lules. Els nivells d'ARN missatger de Mfn2 en les cèl·lules HeLa control incubades amb leflunomida augmentaven. En canvi, en les cèl·lules on p53 està reprimida els nivells basals d'ARN

missatger de Mfn2 estaven augmentats respecte a les cèl·lules control, però leflunomida no era capaç d'augmentar l'expressió gènica de Mfn2 en aquestes cèl·lules.

El següent pas va ser transfectar les cèl·lules HeLa amb el siRNA de p53 i mesurar els nivells de la proteïna p53, per estar segurs de la seva reducció (Figura 9). En les cèl·lules on p53 estava reprimida no es va observar senyal de p53 i a més a més els nivells de proteïna de Mfn2 estaven reduïts respecte al control.

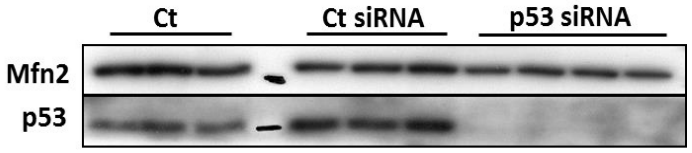

Figura 9. Els nivells de les proteïnes Mfn2 i p53 en les cèl·lules HeLa transfectades temporalment amb el siRNA control i de p53.

A continuació les cèl·lules HeLa van ser transfectades amb el siRNA control i de p53 i incubades amb leflunomida. Les proteïnes Mfn2, Mfn1 i p53 augmenten en les cèl·lules HeLa control incubades amb leflunomida. En canvi, en les cèl·lules HeLa on p53 està reprimida i incubades amb leflunomida, no es veu senyal de p53 i no es veu augment de Mfn2, però sí que augmenta Mfn1. Els nivells basals de les proteïnes Mfn2 i Mfn1 estan augmentats respecte a les cèl·lules HeLa control, igual que passa amb els nivells d'ARN missatger de Mfn2. Aquests resultats suggereixen que la reducció de p53 augmenta els nivells basals de Mfn2 i Mfn1 en les cèl·lules HeLa com a mecanisme d'adaptació. Aquest mateix experiment es va realitzar en les cèl·lules C2C12 (Figura 10). Les proteïnes Mfn2, Mfn1 i p53 augmenten i Drp1 disminueix en les cèl·lules C2C12 control incubades amb leflunomida. En canvi, en les cèl·lules C2C12 on p53 està reprimida incubades amb leflunomida, no es veu senyal de p53 i no es veu augment de Mfn2, ni de Mfn1, encara que els nivells basals de Mfn1 estan augmentats respecte a les cèl·lules C2C12 control. A més a més la disminució de Drp1 és inferior en aquestes cèl·lules respecte al control. Aquests resultats suggereixen que la reducció de p53 en les cèl·lules C2C12 augmenta els nivells basals de Mfn1 com a mecanisme d'adaptació.

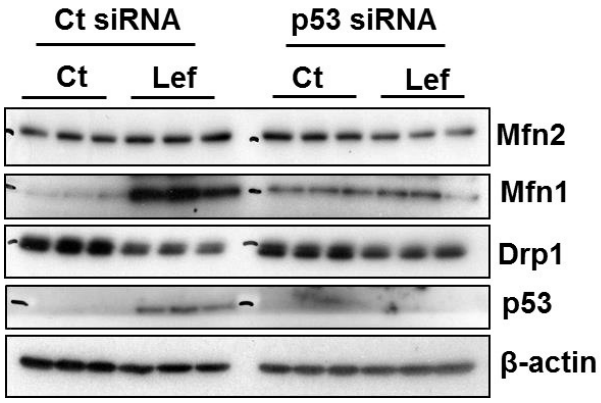

Figura 10. Els nivells de Mfn2, Mfn1, Drp1 i p53 van ser determinats en les cèl·lules C2C12 transfectades temporalment amb el siRNA control i de p53.

Tenint en compte aquests resultats, podem suggerir que el mecanisme d'acció a través del qual la leflunomida és capaç d'incrementar els nivells d'expressió de les mitofusines és a través de p53, ja que la reducció de p53 bloqueja l'increment de les proteïnes Mfn2 i Mfn1 en resposta a leflunomida.

A manera de conclusió, podem dir que la disminució de la síntesi de pirimidines a través de la inhibició del complex III o de l'enzim DHODH, causa estrès cel·lular i produeix l'activació i l'acumulació de p53 a través de la fosforilació de la Ser15, produint una parada del cicle cel·lular. Nosaltres suggerim que p53 indueix l'augment de l'expressió de les mitofusines i la disminució de Drp1, provocant l'elongació de les mitocòndries. L'allargament de la xarxa mitocondrial proporciona més resistència a les cèl·lules que pateixen un estrès cel·lular. L'addició d'uridina reverteix la deficiència de la síntesi de pirimidines, impedint l'efecte antiproliferatiu, i l'augment de p53 i de les Mfns en les cèl·lules tractades amb leflunomida. Per tant, l'elongació mitocondrial és una resposta adaptativa a l'estrès cel·lular que pateixen les cèl·lules per causa de la leflunomida o el mixotiazol (Figura 11).

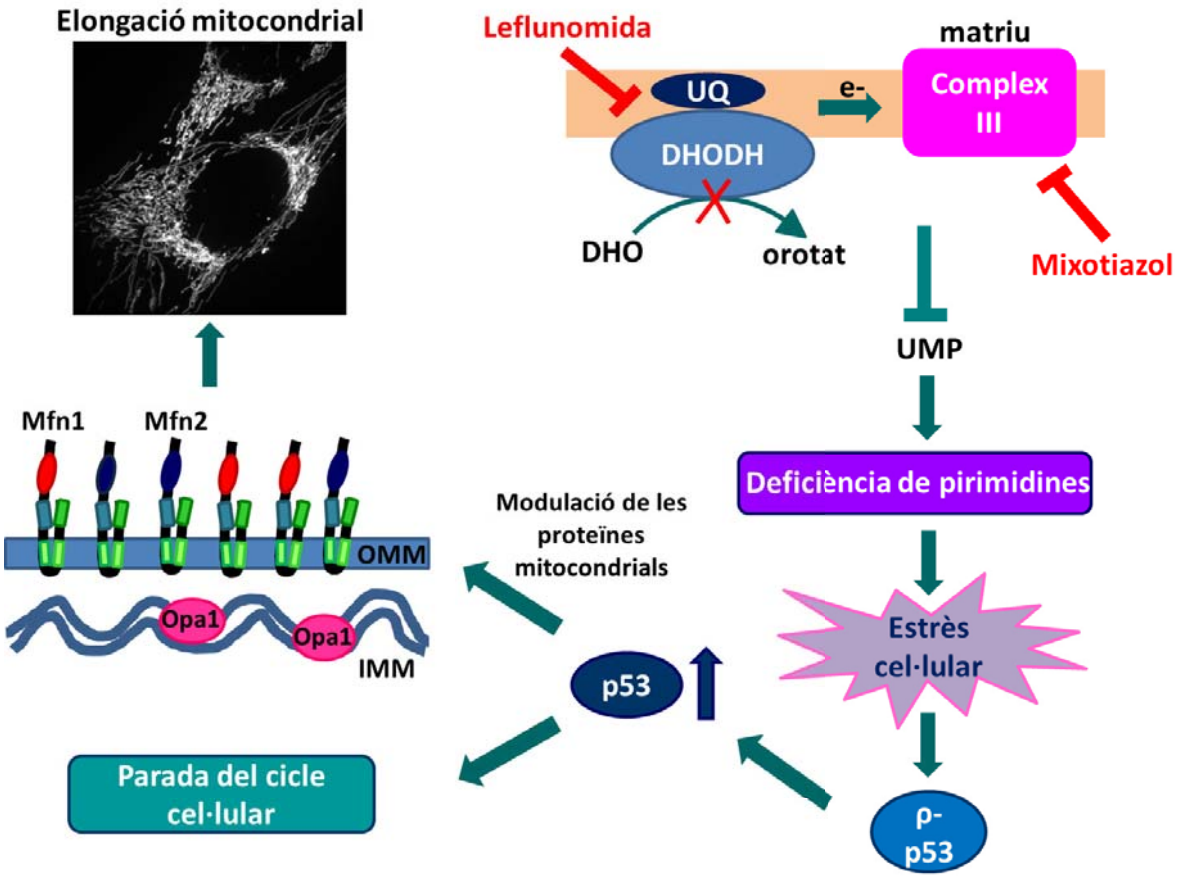

Figura 11. Leflunomida i mixotiazol produeixen elongació mitocondrial a través de l'activació de p53.